



# Adama Science and Technology University (ASTU)



**Proceedings of the 2<sup>nd</sup> International Research Symposium**

“Ensuring Sustainable Development through Research in Science and Technology”

Volume 2, No. 2, 2017

June 8-10/2017

## Members of the Organizing Committee

Dr. Shiferaw Fayissa

Dr. Jeylan Aman

Dr. Teshome Abdo

Dr. Enyew Amare

Dr. Alemu Disassa

Dr. Zelalem Birru

Dr. Mekonnen Ayana

Mr. Girma Debele

Prof. Honggyul Paik

Mr. Tesfay G/Michael

Dr. Kassaye Gutema

Mr. Girma Megerssa

Dr. Legese Lemecha

Plenary speaker (Prof. Endashaw Bekele)

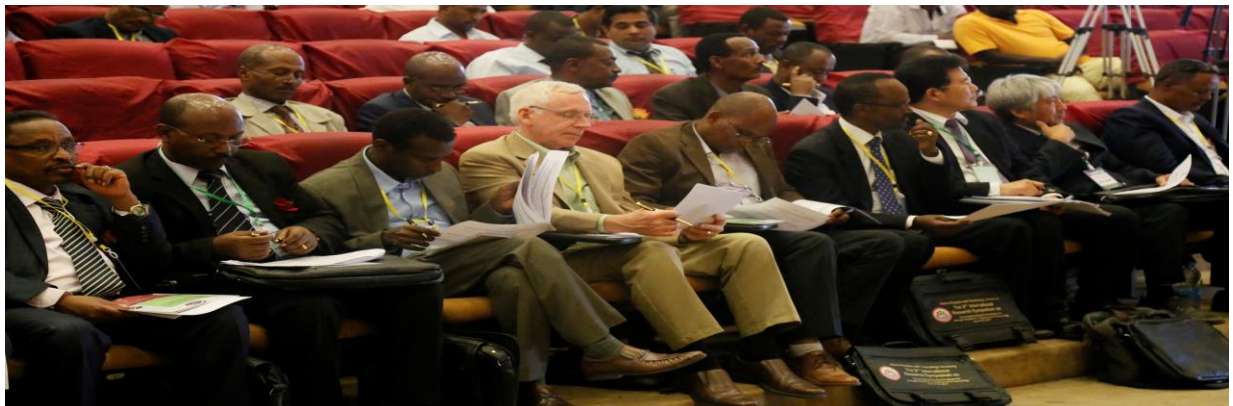


## TABLE OF CONTENT

<b>Phytochemical Analysis of Selected Medicinal Plants of Ethiopia</b> Milkyas Endale, .....	1
<b>Molecular-chemical study on the effect of recycling coffee pulp waste in soil C conservation</b> Eshetu Bekele, Christel Baum and Peter Leinweber.....	14
<b>Optimization of Dilute Sulphuric acid hydrolysis of sugarcane bagasse for enhanced xylose recovery using RSM</b> Belachew Zegale, Vijayan and S. Moholkar*.....	46
<b>Excitation Wavelength Dependence of UV and green emissions of ZnO-MgO nano Composite</b> <sup>1</sup> Ramachandra Reddy, <sup>2</sup> Abebe Belay, <sup>3</sup> K.Sowrybabu.....	60
<b>IN VITRO Screening of Sugarcane (<i>Saccharum officinarum</i> L.) Genotypes for Salt Tolerance</b> Mebrahtom Ftwi <sup>1</sup> , Firew Mekbib <sup>2</sup> And Eyasu Abraha <sup>3</sup> .....	68
<b>Vomer nasal Receptors Gene Characterization by using Molecular Techniques in Pig</b> Hunduma Dinka <sup>1</sup> and Chankyu Park <sup>2</sup> .....	92
<b>Genetic Diversity and Population structure Analysis in finger millet (<i>Eleusine coracana</i> (L.) Gaertn) Genotypes Using Inter Simple Sequence Repeat Marker in Ethiopia</b> Haftom Brhane <sup>1</sup> , Teklehaimanot Haileselassie <sup>2</sup> and Kassahun Tesfaye <sup>3</sup> .....	106
<b>Integration of Remote Sensing and Hydraulic Models to Identify Flood Prone Areas in Woybo River Catchment, South Western Ethiopia</b> <i>Aschalew Fekadu</i> <sup>1,*</sup> , <i>Daniel Teka</i> <sup>2</sup> , <i>Kassa Teka</i> <sup>2</sup> .....	119
<b>Generating Groundwater Quality Spatial Distribution Models and Investigating its Suitability for Irrigation Use based on GIS and Geospatial Technology: The case of Upper Geba Catchment, Northern Ethiopia</b> Amanuel Gidey.....	135
<b>Stabilization of Soft Soils for Pavement Application Using RBI Grade-81</b> Tariku Asfaw Tedla.....	146
<b>Estimation of Future Annual Daily Peak Stream Flow and Flood Frequency based on changes in air temperature and precipitation. A case study at Gilgel Abay River</b>	

<b>basin, Upper Blue Nile, Ethiopia</b> AregaMulu <sup>1</sup> and G.S.Dwarakish <sup>2</sup> .....	159
<b>Evaluating Implementation of Adama City Land Use Plan Using Conformance- Based Approach</b> DejeneTeseemaBulti.....	181
<b>Performance of Anaerobic Sequencing Batch Reactor for the Treatment of Tannery Wastewater and Climate Change Mitigation</b> Andualem Mekonnen <sup>1*</sup> and Seyoum Leta <sup>2**</sup> and Karoli Nicholas Njau <sup>3</sup> .....	200
<b>Bio-enzymes for Road Construction and Mentenance: an Innovative Approach</b> Eshetu Mekonnen.....	211
<b>Development of Innovative Integrated Treatment System for the Treatment of High Strength industrial Wastewater, in Ethiopia</b> Tadesse Alemu <sup>12</sup> , Eshetu Lemma <sup>2</sup> , Andualem Mekonen <sup>2</sup> & Seyoum Leta <sup>2</sup> .....	223
<b>Computer-Aided Colonic Polyp Detection Using Convolutional Neural Networks</b> Kinde A. Fante.....	234
<b>Software Complexity Prediction Model: a Combined Machine Learning Approach</b> <i>Ermiyas Birihanu and Tibebe Beshah</i> .....	248
<b>Potential Co-Targets of Isoniazid Identified through Proteome Interactome Network Analysis</b> Tilahun Melak, Sunita Gakkhar.....	265
<b>Demystifying the Nile Water Discourse</b> Wuhibegezer Ferede*.....	281
<b>Does Innovation improve the productivity of firms in least developed countries? Evidence from Ethiopia's Enterprise Survey</b> Abdi Yuya Ahmad.....	298
<b>Production and Characterization of Biodiesel from <i>Citrullus colocynthis</i> Seed oil</b> Solomon Girmay , Hizkeal Tsade.....	326
<b>Investigation on Pollution Caused by Gasoline &amp; Diesel Fueled Vehicles a Case of Adama Town</b> Solomon Neway <sup>1</sup> , Ramesh Babu Nallamothu <sup>2</sup> .....	343
<b>Productivity Improvement by using Statistical Process Control Tools:</b>	

---

Case Study at Adama Garment Industry

---

Yeshareg Diresa<sup>1</sup>, Ajit Pal Singh<sup>2</sup>.....354

**Exploring the Industrial Characteristics of Tef [*Eragrostis tef*(Zucc.)  
Trotter]: An Engineering Approach**

Workineh Abebe .....372

**Conducting polymer and polymer/carbon nanotube composites for  
electrochemical determination of biologically active compounds**

Alemnew Geto<sup>a,b\*</sup>, Merid Tessema<sup>a</sup> and Shimelis Admassie<sup>a</sup>.....384

**Prosopis Juliflora Pods Mash for Biofuel Energy Production: an Opportunity  
from the Invasive Species**

Mebrahtu Haile<sup>\*1</sup> Hadgu Hishe<sup>1</sup>, Desta Gebremedhin<sup>2</sup>.....400

**Microstructures and Electrical Properties of B-Site Modified Bismuth Sodium  
Titanate Ferroelectric-Ceramic**

<sup>1</sup>Enyew Amare, <sup>2</sup>A.V. PRASAD RAO.....416

## Preface

The transformation of a nation can basically be achieved through the advancement of science & technology. Ethiopia has long recognized the role of science and technology in bringing about sustainable development. The country has envisioned transforming itself into a middle-income country in 2025. To this end, the country has exerted relentless efforts to materialize science and technology in the country. Thus, it has made science and technology the pillar of its top priorities in the transformation of the economy.

As one of the universities mandated to spearhead the transformation process, Adama Science & Technology University, is looking forward to excel in science and technology. Its goal is to develop highly qualified, capable, competent, and innovative human resource in the field of science and technology so as to transfer relevant scientific knowledge and skills required for nation building. The university is also committed to conducting need-based problem-solving researches for alleviating the problems of the region and the country at large. To this end, the university is working in collaboration with industries in its vicinity whereby its staff members are contributing a great deal in alleviating problems. Moreover, ASTU has set Centers of excellence as a platform where academia can meet stakeholders.

ASTU's development into a full-fledged science and technology university has helped it to forge strong linkage, cooperation, and partnership with various national and international universities, development sectors, stakeholders, and relevant personalities. To show case its all-round efforts, ASTU has organized an international symposium titled "Ensuring Sustainable Development through research in Science & Technology". This broad agenda is seen as a part of the national plan of transformation of the country. Thus, this symposium aims to further strengthen the contribution of ASTU in development endeavors of the country at large.

## Phytochemical Analysis of Selected Medicinal Plants of Ethiopia

Milkyas Endale (PhD)

Adam Science and Technology University, School of Applied Natural Science, Applied Chemistry Program,

P.O.Box 1888, Adama, Ethiopia, Email: [milkyasendale@yahoo.com](mailto:milkyasendale@yahoo.com), Cell Phone: +251934208852

### Abstract

There are 6500 species of higher plants in Ethiopia making the country one of the most diverse floristic regions in the world. The greater concentrations of these medicinal plants are found in southern and south western parts of the country. Nevertheless, there are limited ethnobotanical information and knowledge on the chemical constituents of these medicinal plants. In an ongoing project to identify the phytochemical constituents of medicinal plants of Ethiopia, a comprehensive phytochemical analysis was conducted on *Zanthoxylum chalybeum*, *Aloe gilbertii*, *Millettia ferruginea*, *Tephrosia vogelli*, *Senna didymobotrya* and *Clerodendrum myricoides*. The roots of various plant parts were extracted with  $\text{CH}_2\text{Cl}_2:\text{CH}_3\text{OH}$  (1:1) and  $\text{CH}_3\text{OH}$  (100%). Phytochemical screening tests of the root extracts of these plants were done accompanied by complete isolation and spectroscopic (UV-Vis, IR, NMR; 1D and 2D) characterization of secondary metabolites. Various class of compounds were identified including a coniferyl alcohol derivative (**1**) and alkaloid (**2**) from roots of *Z. chalybeum*, flavonoids (**3,4**) from roots of *T. vogelli*, anthraquinone (**5**) from roots of *A. gilbertii*, flavonoids (**6,7**) from roots of *M. ferruginea*, phenylanthraquinone (**8**) and stilbene derivative (**9**) from roots of *S. didymobotrya* and phenylpropanoid glycosides (**10,11**) from roots of *C. myricoides*. Of these, a coniferyl alcohol derivative (**1**) and a phenylpropanoid glycoside (**10**) were identified for the first time in nature and a knipholone derivative (**12**) was identified from the roots of *Aloe gilbertii* for the first time. The structures of these compounds were determined using spectroscopic techniques (UV-Vis, IR,  $^1\text{H}$  NMR,  $^{13}\text{C}$  NMR, DEPT-135, COSY, gHSQC and gHMBC).

**Key words:** *Zanthoxylum chalybeum*, *Aloe gilbertii*, *Millettia ferruginea*, *Tephrosia vogelli*, *Senna didymobotrya*, *Clerodendrum myricoides*

## 1. Introduction

Medicinal plants, since times of immemorial, have been used in virtually all cultures as a source of medicine. Plants are efficient in developing chemical control agents for various pathogens and a significant part of pharmaceutical medicine is based on compounds isolated from plants [1]. *Clerodendrum myricoides* (Verbenaceae, fig. 1) is one of the traditional medicinal plants in Ethiopia known by the name 'Marasissa' (Afaan Oromoo), 'Algga' (Dawiro)[2] and 'Misirich' (Amharic)[3]. In Ethiopia, *C. myricoides* is widely distributed in the flora of Tigray, Gonder, Wollo, Shewa, Arsi, Welega, Illu Abba Boor, Kefa, Gamo Gofa, Sidamo and Harerge [4]. The bark of *C. myricoides* is used to treat abdominal pains and malaria [4] whereas the roots and leaves of *C. myricoides* are used to treat gonorrhoea, rabies, measles, glandular TB, eye disease, malaria, hemorrhoids, asthma and as aphrodisiac [4,5].

*Senna didymobotrya* is useful for the treatment of fungal, bacterial infections, hypertension, hemorrhoids, sickle cell anemia, inflammation of fallopian tubes, backache, stimulate lactation and to induce uterine contraction [6]. *Aloe gilbertii*(fig 3) leaves and root parts have been used for treatment of malaria and wound [7]. *Tephrosiapurpurea*(fig 2), an important plant of the genus is used as tonic, laxative, antivenom, antiulcer, antidiarrheal and in leprosy [8,9]. *Millettia ferruginea*(fig 4) fruits powder prepared with butter are topically applied to treat skin infection [10] and fruits powder mixed with honey is taken orally for amoeba and treating 'mujele' (chigger) with fruit paste mixed with butter [11]. *Zanthoxylum chalybeum*(fig 5) is used to treat both human and livestock ailments [12].



**Fig.1.** *Clerodendrum myricoides* (picture taken by Habdolo.E, Dec, 2014)



**Fig 2.** Picture of *Tephrosia vogelii* (Picture taken by Dagne, March 12, 2014)



**Fig 3.** Picture of *A. gilbetii* species taken by Nebiyu C., Dec., 2014)



**Fig 4:** *Millettia ferruginea* (picture taken by Birhanu Eribo Dec., 2013)



**Fig 5.** *Zanthoxylum chalybeum* (Ga'da) [picture taken by Mathewos A., Dec, 2014]

## 2. Materials and Methods

### 2.1 General experimental materials

UV-Vis spectrum was measured with GENESY's spectrometer (200-400nm) in methanol at room temperature. Infrared (KBr pellet) spectrum was recorded on Perk-Elmer BX infrared spectrometer in the range 400-4000 $\text{cm}^{-1}$ . Nuclear Magnetic Resonance (NMR) analysis was recorded on a Bruker avance 400MHz spectrometer with tetramethylsilane as internal standard.

Structural assignments were done on the basis of 1D NMR ( $^1\text{H}$  NMR,  $^{13}\text{C}$  NMR, DEPT-135) and 2D NMR (COSY, gHMQC, gHMBC) spectra. Thin Layer Chromatography (TLC) was done using silica gel 60 F254. Column chromatography was performed on silica gel 60 (60-100 mesh).

## 2.2 Plant material

The roots of *Clerodendrum myricoides* was collected on October 2014, from Oromia Region, Arisi zone, Shashemene area located 248km from Addis Ababa. The roots of *Zanthoxylum chalybeum* were collected from Almura area, Sidama zone, Hawassa town in February 2014. The root of *Senna didymobotrya* was collected in the natural forest around Hawassa Town, November, 2014. The roots of *Tephrosia vogelli*, was collected from Wondo Genet, which is found in Sidama Zone, SNNPR regional state in December 2013. The roots of *Aloe gilbertii Reynolds* were collected in February 2013 from Alamura hill, in sidama Zone of SNNPR, Ethiopia. All plant materials collected were identified and authenticated by botanist Reta Regasa, Department of Biology, Hawassa College of Teachers Education. Specimen was deposited at the herbarium of Hawassa College of Teacher Education, Hawassa, Ethiopia.

## 2.3 Extraction and Isolation

The collected root specimens were dried and grounded into fine powder with the help of mortar and pestle. The grounded roots (500g) were extracted by cold percolation with  $\text{CH}_2\text{Cl}_2/\text{CH}_3\text{OH}$  (1:1) three times for 24hrs while shaking at speed of 230r/min and temperature controlled at  $28.0^\circ\text{C}$ . The marc left was further extracted with methanol (100%) as above. The extract was concentrated using rotary evaporator ( $40^\circ\text{C}$ ) and gave yield of 46.8g (9.36%) for *C.myricoides*, 40g (10%) for *T.vogelli*, 59g (11.8%) for *M.ferruginea*, 69.8 g (13.41%) for *S.didymobotrya* and 49.2g (9.84%) for *A. gilbertii*. The crude extract obtained was screened for the presence of various class of secondary metabolites following the standard protocols [13,14]. Separation of the dried roots extract was done using silica gel column chromatography with increasing gradient of ethyl acetate in *n*-hexane as eluent.

## 2.4 Phytochemical Screening test

Phytochemical screening test was carried out on the crude extract of CH<sub>2</sub>Cl<sub>2</sub>:CH<sub>3</sub>OH (1:1) using standard procedures [13,14] to identify the type of secondary metabolites present in crude extract.

#### **2.4.1 Test for alkaloids**

1mL of 1% HCl was added to 3mL of the test extract in a test tube. The mixture was heated for 20min, cooled and filtered. Then 1mL of the filtrate was tested with 0.5mL Wagner's, Hager's and Mayer's reagents. Formation of reddish brown precipitate for Dragendorff's and Wagner's reagents, yellow precipitate for Hager's and cream precipitate for Mayer's indicated the presence of alkaloids [13,14].

#### **2.4.2 Test for flavonoids**

Flavonoids were determined by Mg-HCl reduction test. A piece of magnesium ribbon (powder) and 3 drops of conc. hydrochloric acid were added to 3mL of the test extract. A red coloration indicated the presence of flavonoids. Five milliliters of dilute ammonia solution was added to 5mL of the aqueous filtrate of extract followed by the addition of 1mL concentrated H<sub>2</sub>SO<sub>4</sub>. A yellow coloration indicated the presence of flavonoids. The yellow color disappeared on standing [13, 14].

#### **2.4.3 Test for terpenoids (Salkowski test)**

About 5mL of the extract was mixed with 2mL of chloroform and 3mL of concentrated H<sub>2</sub>SO<sub>4</sub> was added. A reddish brown coloration at the interface confirmed the presence of terpenes [13, 14].

#### **2.4.4 Test for tannins**

About 0.2g of the dried powdered samples was boiled in 10mL of distilled water in a test tube and then filtered. Addition of 0.1% FeCl<sub>3</sub> solution resulted in a characteristic blue, blue-black, green or blue-green color which confirmed the presence of tannins [13,14].

#### **2.4.5 Test for saponins**

About 0.2g of powdered sample extract was boiled in 2mL of distilled water on a water bath and filtered. A fraction of aqueous filtrate about 1mL was mixed with 2mL of distilled water and shaken vigorously to form a stable persistent froth. The frothing was mixed with three drops of olive oil and shaken vigorously. Formation of an emulsion confirms the presence of saponins [13, 14].

### 3. Results and Discussion

Phytochemical screening tests of the crude CH<sub>2</sub>Cl<sub>2</sub>/CH<sub>3</sub>OH (1:1) revealed the presence of various secondary metabolites in the crude extracts as summarized in Table 1.

**Table 1:** Phytochemical screening test results of the crude Dichloromethane/Methanol (1:1) extract of five plants

Plant Constituent	Reagent used	Present(+) /Absent(-)	Plant
<b>Alkaloids</b>	Dragendroff's reagent	+	<i>A.gilbertii</i> , <i>T.vogelii</i> <i>Z.chalybeum</i> <i>M. ferruginea</i>
<b>Alkaloids</b>	Dragendroff's reagent	-	<i>C. myricoides</i> <i>S. didymobotrya</i>
<b>Tannins</b>	FeCl <sub>3</sub>	+	<i>C. myricoides</i> <i>Z. chalybeum</i> <i>T. vogelii</i> <i>S. didymobotrya</i> <i>M. ferruginea</i>
<b>Tannins</b>	FeCl <sub>3</sub>	-	<i>A.gilbertii</i>
<b>Anthraquinones</b>	HCl + CHCl <sub>3</sub> + NH <sub>3</sub>	-	<i>C. myricoides</i> <i>T. vogelii</i> <i>Z.chalybeum</i>
<b>Anthraquinones</b>	HCl + CHCl <sub>3</sub> + NH <sub>3</sub>	+	<i>A.gilbertii</i> <i>S. didymobotrya</i> <i>M. ferruginea</i>
<b>Saponins</b>	Warming in water bath	+	<i>C. myricoides</i> <i>S. didymobotrya</i> <i>T. vogelii</i> <i>M. ferruginea</i>
<b>Saponins</b>	Warming in water bath	-	<i>A. gilbertii</i> <i>Z.chalybeum</i>
<b>Terpenoides</b>	Chloroform and Conc. Sulphuric acid	+	<i>C. myricoides</i> <i>S. didymobotrya</i> <i>T. vogelii</i> <i>Z.chalybeum</i>

<b>Terpenoides</b>	Chloroform and Conc. Sulphuric acid	-	<i>A. gilbertii</i> <i>M. ferruginea</i>
<b>Flavonoides</b>	Dilute ammonia solution + dil. HCl	+	<i>C myricoides</i> <i>S. didymobotrya</i> <i>T. vogelii</i> <i>Z.chalybeum</i> <i>A. gilbertii</i> <i>M. ferruginea</i>
<b>Flavonoids</b>	Dilute ammonia solution + dil. HCl	-	None

Silical gel column chromatography separation (increasing gradient of ethyl acetate in *n*-hexane as eluent) afforded as a coniferyl alcohol derivative (**1**) and alkaloid (**2**) from roots of *Z. chalybeum*, flavonoids (**3,4**) from roots of *T.vogelli*, anthraquinone (**5**) and a knipholone derivative (**12**) from roots of *A.gilbertii*, flavonoids (**6,7**) from roots of *M.ferruginea*, phenylanthraquinone (**8**) and stilbene derivative (**9**) from roots of *S. didymobotrya* and phenylpropanoid glycosides (**10,11**) from roots of *C. myricoides*. The structures of these compounds were identified by exhaustive spectroscopic analysis (UV-Vis, IR, <sup>1</sup>H NMR, <sup>13</sup>C NMR, DEPT-135, COSY, gHSQC and gHMBC) [15-17].

As an example, here we present how characterization of compound **6** was done. The compound was obtained as white crystalline solid (7mg) from the dichloromethane/methanol (1:1). The UV-Vis spectrum in H<sub>2</sub>O showed maximum absorption band at λ<sub>max</sub>; 263nm indicating the presence of π-π\* transition in conjugated system of C=C double bond. The IR spectrum exhibited strong absorption band of conjugated carbonyl at 1641cm<sup>-1</sup>, and medium absorption around 1600cm<sup>-1</sup> and 1470cm<sup>-1</sup> suggesting the presence of aromatic system. The <sup>1</sup>H NMR spectrum suggested the presence of two methyls at δ 1.56 (6H, s), two methoxy at δ 3.96 (3H, s) and δ 3.92 (3H, s), methine proton singlet at δ 7.81, H-2 (1H, s), three doublet protons at δ 7.1 H-2' (1H, d), δ 6.83, H-5' (1H, d) and δ 6.76, H4'' (1H, d) and a double doublets at δ 6.96, H-6' (1H, dd) in aromatic region and one doublet at δ 5.70, H-3'' (1H, d) in sp<sup>2</sup> system and one methylene dioxy (-OCH<sub>2</sub>O-) protons at δ 6.00, H-2''' (2H, s) as shown in the Table 2.

The <sup>13</sup>C NMR spectrum coupled with DEPT-135 showed twenty two carbons attributed to one carbonyl carbon at δ 175.4, six oxygenated quaternary aromatic carbons at δ 140.1, 147.6, 147.6, 149.2, 151.2 and 153.1, one olefinic quaternary carbon at δ 125.4, three quaternary aromatic carbons at δ 125.7, 113.2 and 106.2; three methine carbons in aromatic region at δ 122.6, 110.1,

108.3, one oxygenated olefinic methine carbons at  $\delta$  150.4, two olefinic methine carbons at  $\delta$  129.4 and 115.1, one oxygenated quaternary aliphatic carbon at  $\delta$  78.2, two methoxy carbons at  $\delta$  62.3 and 61.5, one methylene dioxy (OCH<sub>2</sub>O) at  $\delta$  101.1 and two methyl carbons at  $\delta$  28.1 (Table 2). The peaks at  $\delta$  62.25 and 61.49 suggest the existence of methoxy group attached to aromatic sp<sup>2</sup> system. The peak at  $\delta$  101.1 suggests the existence of oxymethylene group.

The UV-Vis ( $\lambda_{\max} = 263\text{nm}$ ) spectrum coupled with the <sup>1</sup>H NMR chemical shifts at  $\delta$  7.81, (1H, s, H-2) and <sup>13</sup>C NMR chemical shifts at  $\delta$  150.4 (C-2),  $\delta$  125.4 (C-3) and  $\delta$  175.4 (C-4) suggest isoflavone skeleton for this compound. Moreover, the HMQC spectrum which showed correlation between methine protons at  $\delta$  7.81, 7.1, 6.96, 6.83, 6.76, 6.00 and 5.70 correlate with the carbons at  $\delta$  150.4, 110.1, 108.3, 122.6, 129.2, 101.1, and 115.1, respectively, as shown in the Table 2. From the <sup>1</sup>H-<sup>1</sup>H COSY spectrum evidence, the doublet protons at  $\delta$  6.76 (H-4'', d, J= 8.0) and the doublet protons at  $\delta$  5.70 (H-3'', d, J= 8.0) couple each other suggesting that the two protons are on the adjacent sp<sup>2</sup> carbon atoms. HMBC spectrum (Table 2) revealed that protons H-2 ( $\delta$  7.81, s) and H-2' ( $\delta$  7.1, d, J= 2.4) correlate with the same quaternary carbon at  $\delta$  125.7 (C-1') in support of isoflavone skeleton.

Additional correlations observed between the protons H-2' ( $\delta$  7.1, d, J= 2.4), H-6' ( $\delta$  6.96, dd, J= 2.4, 7.8), H-5' ( $\delta$  6.83, d, J= 7.8) and H-6'' ( $\delta$  6.00, s, 2H) with the same oxygenated quaternary aromatic carbon C-3' ( $\delta$  147.6) coupled with the correlation of protons H-6' ( $\delta$  6.96, d, J= 2.4, 7.8), H-5' ( $\delta$  6.83, d, J= 7.8) and methylene dioxy protons (H-6'',  $\delta$  6.00, s, 2H) suggest that the oxymethylene is connected at C-3' and C-4' and ring B have an ABX spin pattern. HMBC correlations between proton H-3'' ( $\delta$  5.70, d, J= 8.0) and H-4'' ( $\delta$  6.76, d, J= 8.0) with the oxygenated aliphatic quaternary carbon C-2'' ( $\delta$  78.2) and coupled with correlation of proton H-4'' ( $\delta$  6.76, d, J= 8.0) with that of quaternary carbon C-8a at  $\delta$  153.0 suggest that the pyran ring is connected to ring A. Finally, from the HMBC spectrum correlation observed between H-4'' ( $\delta$  6.76, d, J= 8.0) with that of oxygenated quaternary carbons C-8a ( $\delta$  153.1) and C-7 ( $\delta$  149.2) support unequivocal placement of the two methoxy groups at C-5 ( $\delta$  151.17) and C-6 ( $\delta$  140.06) positions of ring A. Thus, all spectral data were in good concurrence with those reported in the literature (Dagne *et al.* 1989) and this compound was previously reported from the ethanolic extract of the stem bark of the same species and the trivial name was given as 5-methoxy durmillone (**6**, Figure 3) (Dagne *et al.*, 1989). Now the compound was isolated from the roots with full NMR (1 and 2D) data is presented by this work.

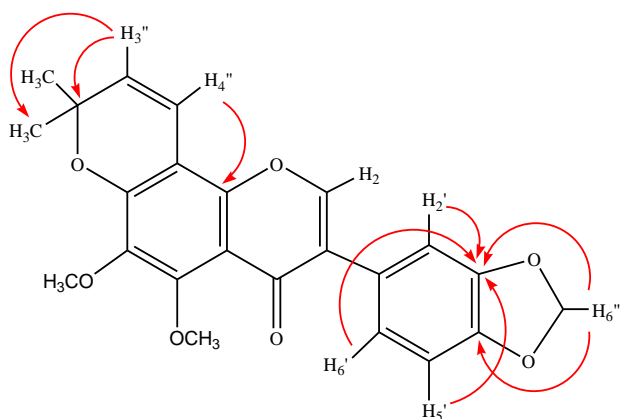


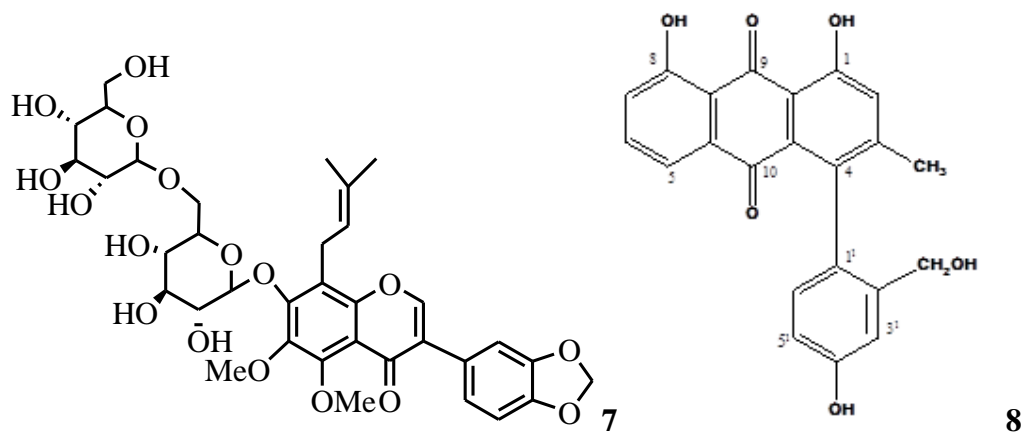
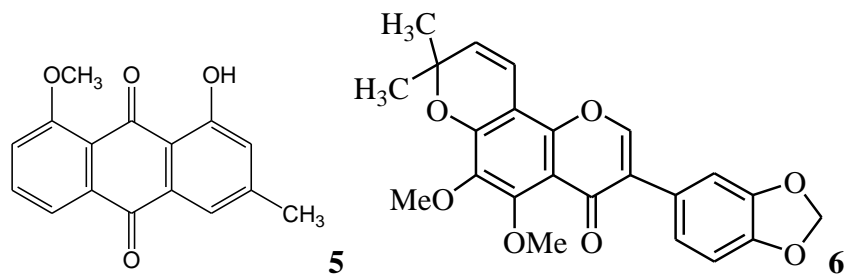
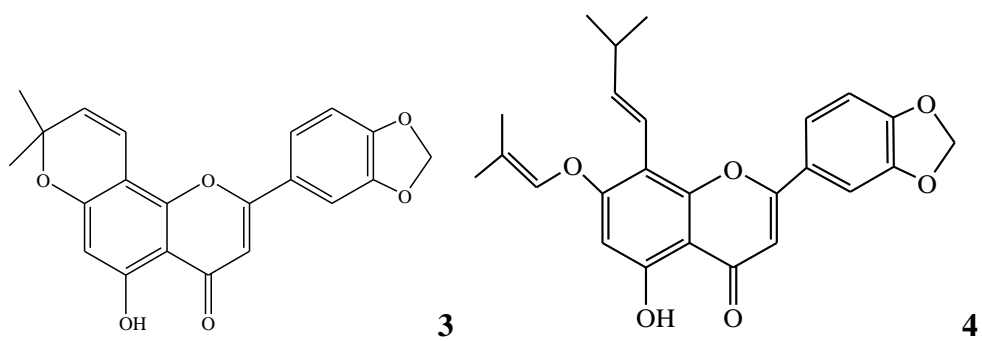
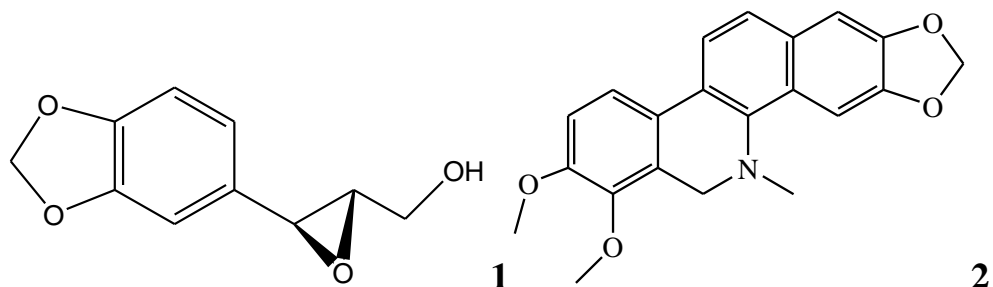
Fig 3: Important HMBC correlations of 5-methoxydurmillone (6)

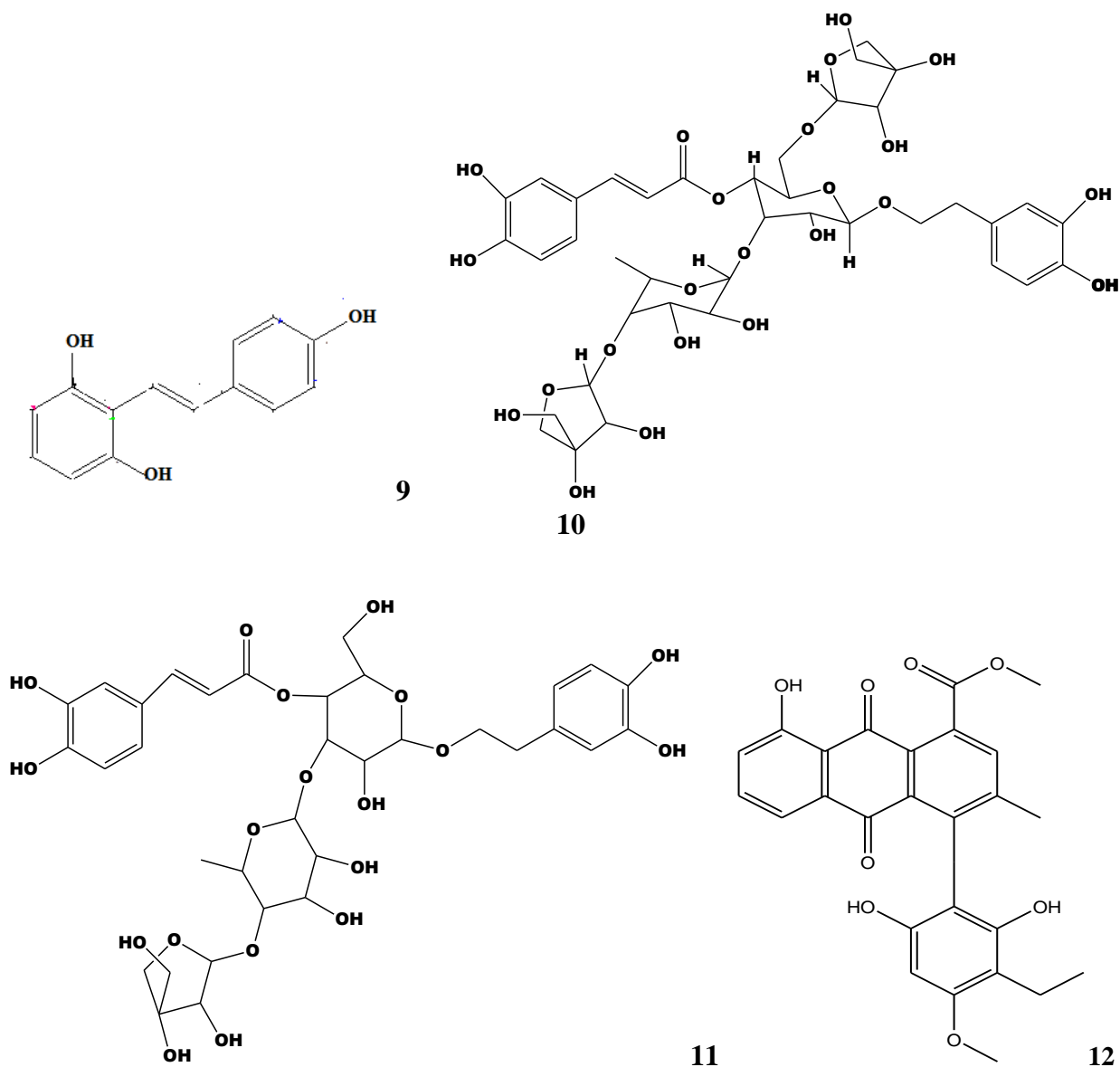
Table 2: Complete NMR data of 5-methoxydurmillone (6) (chemical shift ( $\delta$ ) is given in ppm) (400MHz, CDCl<sub>3</sub>)

Position	<sup>13</sup> CNMR data of compound 1 (ppm)	<sup>1</sup> HNMR data of compound 1 (ppm)	of <sup>1</sup> H- <sup>1</sup> H correlation n	HMBC		Reported <sup>13</sup> CNMR*	Reported <sup>1</sup> HMR*
				<sup>2</sup> J	<sup>3</sup> J		
C-2	150.4	7.81 (H-2, s)			C-1', 4, 5	150.2	7.81
C-3	125.4					125.3	
C-4	175.0					175.0	
C-4a	106.7					106.5	
C <sub>5</sub>	151.2					151.0	
C <sub>6</sub>	140.1					140.0	
C <sub>7</sub>	149.2					149.1	
C <sub>8</sub>	113.2					113.1	
C <sub>8a</sub>	153.0					153.0	
C <sub>1'</sub>	125.7					125.6	
C <sub>2'</sub>	110.1	7.10 (H-2', d, J= 2.4)			C-3''	110.0	7.08
C <sub>3'</sub>	147.6					147.5	
C <sub>4'</sub>	147.6					147.5	
C <sub>5'</sub>	108.3	6.83 (H-5', d, J= 7.8)			C-3'	108.2	6.85
C <sub>6'</sub>	122.6	6.96 (H-6', dd, J= 2.4, 7,8)			C-1' C-6, C-2'	122.5	6.93
C <sub>2''</sub>	78.2					68.1	
C <sub>3''</sub>	115.1	5.70 (H-3'', d, J= 8.0)	H-7 ↔ H-5		C-2'', C-3, C-7	114.9	5.68
C <sub>4''</sub>	129.2	6.76 (H-4'', d, J= 8.0)	H-5 ↔ H-7		C-8, 2''-CH <sub>3</sub>	129.0	6.76
2''-CH <sub>3</sub>	28.1	1.56 (H-5'', s)				28.0	1.55

<b>O-CH<sub>2</sub>-O</b>	101.1	6.00 (H-6'', s)	100.0	5.98
<b>5-OCH<sub>3</sub></b>	62.2	3.96 (H-7'', s)	62.1	3.96
<b>6-OCH<sub>3</sub></b>	61.5	3.92 (H-8'', s)	61.3	3.90

\*Dagne et al., 1989





#### 4. Conclusion

In order to promote Ethiopian herbal drugs and traditional use of medicinal plants, there is an urgent need to evaluate the therapeutic potentials of the drugs as per the WHO guidelines. Bioactive extracts should be validated and standardized on the basis of phytochemical constituents. Despite the rich biodiversity of Ethiopian flora, there is limited information about the type of secondary metabolites present in most of these plants and their biological activity. In an ongoing project to analyze the chemical constituents of medicinal plants of Ethiopia, we have studied over fifteen plants in past four years. This paper highlighted a summary of the phytochemical analysis works we have carried out on six plants; *Zanthoxylum*

*chalybeum*, *Aloe gilbertii*, *Millettia ferruginea*, *Tephrosia vogelli*, *Senna didymobotrya*, and *Clerodendrum myricoides*. Currently the project has also continued to search for bioactive chemical constituents from other medicinal plants such as the genus *Balanaitis*, *Acanthus*, *Euphorbia* etc. Comprehensive phytochemical screening tests were done on the root extracts ( $\text{CH}_2\text{Cl}_2/\text{CH}_3\text{OH}$ , 1:1 and  $\text{CH}_3\text{OH}$ , 100%) of these plants accompanied by fractionation with silica gel column chromatography and spectroscopic analysis of the pure compounds. From these six plants, twelve secondary metabolites (**1-11**) were fully characterized. To the best of our knowledge, a coniferyl alcohol derivative (**1**) and a phenylpropanoid glycoside (**9**) were identified for the first time in nature and a knipholone derivative (**12**) was isolated for the first time from the roots of *Aloe gilbertii*. This work is one of the few attempts to phytochemically analyze the polar extracts of these plants and further work is recommended on polar extracts of the root, stem bark and leaf of these plants so as to identify more novel and bioactive secondary metabolites in support of their traditional use.

### **Acknowledgement**

We are grateful to botanist Reta Regassa, Department of Biology, Hawassa Teacher's College for plant identification. Hawassa University, School of Graduate Studies is duly acknowledged for offering the postgraduate opportunity to my previous students; Mathewos Anza, Dagne Addisu, Iserael Alemeyahu, Habdolo Esatu and Berhanu Eribo who participated in the research project. We are thankful to Department of Chemistry, Addis Ababa University for allowing us to use their NMR, UV-Vis and IR instruments.

## 5. References

1. Abebe D., (1986). Traditional medicine in Ethiopia: the attempts being made to promote it for effective and better utilization SINET, 9: 61-69
2. Mathewos A, Sebsebe D and Zemedede A. (2013). Ethnobotany of Medicinal Plants in Loma and Gena Bosa Districts (Woredas) of Dawro Zone, Southern Ethiopia. *J. Herb. Med.*, 2(9):195.
3. Desta B., (1994). Ethiopian traditional herbal drugs. Part III: anti-fertility activity of 70 medicinal plants. *Journal of Ethnopharmacology*, 3:199-209.
4. Persson E., (2006). Clerodendrum. Flora of Ethiopia and Eritrea. In: Hedberg. I, Emsermu. K, Edwards. S and Sebsebe. D (eds.), *Gentianaceae to cyclocheilaceae*. Addis Ababa, Ethiopia; Uppsala, Sweden, 525-526.
5. Abebe D., Debella A., Urga K., (2003). Medicinal plants and other useful plants of Ethiopia. *Ethiopian Health and Research Institute*, 262-265.
6. Ngule C.M., Anthoney S.T., Jackie O., (2013). Phytochemical and bioactivity evaluation of *Senna didymobotrya* Fresen Irwin used by the Nandi community in Kenya.
7. Dagne E., Bisrat, D., Viljoen, A., Van Wyk, B.E. (2000). Chemistry of *Aloe* species. *Current Organic Chemistry* 4(10): 1055-1078.
8. Qureshi R., Bhatti G.R., Memon R.A., (2010). Ethnomedicinal uses of herbs from northern part of NARA desert, Pakistan. *Pak. J. Bot* 42, 839-851.
9. Virupanagouda P.P., Shivakumar H., Nanjappaiah H.M., Navanath K., Mohan C., Pandarinath. T., (2011). Phytopharmacology of *Tephrosia purpurea* Linn: An Overview. *Pharmacologyonline*, 3:1112-1140.
10. Fisseha M., Sebsebe D., Tilahun T., (2009). An ethnobotanical study of medicinal plants in Vonago Woreda. SNNPR. Ethiopia. *J. Ethnobiol. Ethnomed.* 5:25-30.
11. Tilahun T., Minitse G., (2007). Ethnobotanical study of medicinal plants used by people in Zegie Peninsula. Northwestern Ethiopia. *J. Ethnobiol. Ethnomed.* 3:12-16.
12. Regassa R., (2013). Assessment of indigenous knowledge of medicinal plant practice and mode of service delivery in Hawassa city, southern Ethiopia. *J. Med. Plants Res.*, 7(9): 517-535.
13. Pradeep A., Dinesh M., Govindaraj A., Vinothkumar D., Ramesh B. (2014). Phytochemical analysis of some important medicinal plants. *Int J Biol Pharm Res*; 5: 48-50.

14. Saleem M., Karim M., Qadir M.I., Ahmed B., Rafiq M., Ahmad B. (2014). *In vitro* antibacterial activity and phytochemical analysis of hexane extract of *Vicia sativa*. *Bangladesh J Pharmacol.*9: 189-193.
15. Mathewos A. Erimias H., Sisay T., Fikre M., Milkyas E., (2014), A coniferyl alcohol derivative from the roots of *Zanthoxylum chalybeum*, *Journal of Coastal Life Medicine* 2(12): 970-974.
16. Iserael A., Sisay T., Fikre M., Milkyas E., (2015). Phenylanthraquinone and stilbene derivatives from roots of *Senna didymobotrya*, *Journal of Medicinal Plants Research*, Manuscript submitted.
17. Habdolo E., Iserael A., Ermias H., Sisay T., Fikre M., Milkyas E., (2015), Phenylpropanoid glycosides from roots of *Clerodendrum myricoides*, *Americal Journal of essential oils and Natural Products*, Manuscript submitted.

## **Molecular-chemical study on the effect of recycling coffee pulp waste in soil C conservation**

<sup>1</sup>Eshetu Bekele,

Adama Science and Technology University: School of Applied natural Sciences,  
Applied Chemistry Program, P.O.Box 1888

<sup>2</sup>Christel Baum and <sup>2</sup>PeterLeinweber

Rostock University- Rostock, Germany

### ***Abstract***

*Organic waste recycling in agriculture through composting has been considered as an environmentally favorable strategy to make use of the increasing amount of organic wastes and foster soil organic matter (SOM) stabilization and C sequestration. Therefore, this study investigated the C mineralization and SOM molecular modification of a typical tropical soil amended with regional compost of different maturity. Compost samples were produced from coffee pulp alone and/or co-composted with fruit and vegetable waste in a method of small heap composting and the samples were collected in three different phases of composting. Both the fresh waste and compost samples were analyzed for their physicochemical and biological properties. These samples were added to a tropical Nitisol at the rate of 48 t ha<sup>-1</sup> and a control was set up without amendment. The CO<sub>2</sub>-C respired was determined during 98 days of incubation and the incubated samples were taken at the start and end of incubation for molecular-chemical analysis by Pyrolysis-Field Ionization Mass Spectrometry (Py-FIMS). The CO<sub>2</sub>-C respired was best explained by a first order plus linear model. A soil amended with a compost taken at the thermophilic phase attained the lowest overall organic C loss. In general, the Py-FIMS revealed a significant enrichment of stable N-compounds during the incubation in all amended soils compared to the control. Furthermore, among the compost-soil mixtures, Py-FIMS indicated significantly higher increases in the proportions of carbohydrates, peptides and phenols/lignin monomers at the expense of fatty acids and sterols in soil amended with composts from the thermophilic phase. Thermal volatilization curves of Py-FIMS indicated enrichments of stable N-compounds and peptides in compost amended soil. This was a result of enhanced decomposition and stabilization of decomposition products by physical protection through association with clay and soil aggregates. In summary, application of compost shortly after reaching the high temperature phase was shown to be more efficient in organic C sequestration in a clay-rich tropical agricultural soil than application at the later stages that may led to the losses of carbohydrates and N-compounds rather than the formation of stable compounds.*

## **Introduction**

Organic waste recycling in agriculture through composting is increasing as an environmentally sustainable waste management strategy (Favoino and Hogg, 2008). It improves the soil fertility as compost increases the soil organic matter (SOM) content (Ceccanti *et al.*, 2007; Eshetu *et al.*, 2007) and modifies the chemical, physical and biological properties of SOM (Nardi *et al.*, 2004; Adani *et al.*, 2007; Lima *et al.*, 2009). Moreover, the added compost can lead to significant changes in the composition of SOM and minimize carbon (C) mineralization from the soil (Mondini *et al.*, 2007; Sanchez-Monedero *et al.*, 2008; Gillis and Price, 2011; Eshetu *et al.*, 2012). This will have a global implication as it is in line with the Kyoto protocol (1997) that aims at reducing greenhouse gas emissions through C sequestration in soils. Some authors suggested a significant impact of land application of organic residues to meet the emission reduction target agreed under the Kyoto protocol (Lal, 1999; Smith *et al.*, 2001). The strategy has more implications in tropical regions like Ethiopia where the degradation of SOM has been accelerated by the high temperature and a wide set of soil fertility issues (Davidson *et al.*, 2003). Moreover, tropical soils have lost a significant part of their original SOM pool, and therefore, have a capacity to sequester C by adopting recommended management practices. For these soils the estimated annual C sequestration potential is 0.34 to 0.52 Pg. (Lal, 2002).

Coffee (*Coffea arabica L.*) is one of the abundant agricultural products generates expressive amounts of agricultural residues during processing (Murthy *et al.*, 2012). Ethiopia is the third coffee producer country in the world with a production accounting for 61% of the annual commodity exports (Gezahegne *et al.*, 2011). At present considerable amounts of coffee processing by-products like coffee pulp (40% of the wet weight) are generated and mainly dumped to water bodies, unsanitary landfills and partly applied to agricultural fields without pre-treatment. This causes freshwater eutrophication, health problems, adverse effects on soil properties such as induced anaerobic conditions and release of phytotoxic compounds impairing plant growth as well as offensive odour and greenhouse gases generation when collected, transported and disposed (Gezahegne *et al.*, 2011; Negassa *et al.*, 2011). Moreover, a further increase of the amount of agro-industrial by-products can be assumed by the current development plan of Ethiopia. This triggers the need to find a sink for this growing amount of waste and at the same time opens up the chance for recycling the waste as compost for the improvement of soil fertility and the sequestration of C in soil. However, composting of organic

waste has to be optimized to avoid adverse effects to plant growth and minimize overall C losses in the transformation process.

Aerobic incubation experiments were used to measure organic matter decomposition or soil C sequestration potential in compost-fertilized, inorganic fertilized or non-amended soils (Bernal *et al.*, 1998; Mondini *et al.*, 2007). Moreover, better understanding of the decomposition dynamics need fitting the resulting carbon dioxide (CO<sub>2</sub>) release data to different kinetic models used to describe the mineralization of organic waste. Incubation of different waste mixtures (prepared with sewage sludges, manures, city refuse, cotton waste, olive-mill wastewater, and sweet sorghum bagasse) after they had been composted for various periods with soil revealed decreases in CO<sub>2</sub> evolution with longer composting duration (Bernal *et al.* 1998). Moreover, Mondini *et al.* (2007), Sanchez-Monedero *et al.* (2008) and Adani *et al.* (2009) evaluated the significance of adding compost of diverse origin in improving the soil C sequestration. All reported compost application increased the amount of stable compound retained in the soil and minimize the overall C loss. However, the majority of this information has been generated in temperate soils and little information is available on C mineralization of typical tropical soils amended with regional composts of different stability. The molecular-chemical composition of those compost-soil-mixtures has never been studied.

Pyrolysis–field ionization mass spectrometry (Py-FIMS) was used to characterize organic matter in sewage farm soils (Leinweber *et al.* 1996), in different stages of biowaste composting (Smidt *et al.*, 2005), and to study long-term compost effects on the molecular composition of SOM (Eshetu *et al.*, 2012). Recently Py-FIMS was used to characterize the organic matter composition of fresh agro-industrial wastes (including coffee pulp) and significant correlations between the organic composition and soil biochemical properties after application were reported (Negassa *et al.* 2011). However, neither Py-FIMS nor another highly sensitive speciation method has been applied so far to disclose effects of differently stabilized composts on C transformations in tropical soils.

Therefore, the objectives of the study were (1) to investigate how the CO<sub>2</sub>-respiration from a tropical Nitisol was altered following the application of differently stabilized composts, and (2) to evaluate effects of the differently stabilized composts on the molecular composition of SOM and its short-term modification during an incubation experiment. The overall objective was to

find out which compost is favorable to improve the soil fertility by sequestration of C in the soil based on a low CO<sub>2</sub>-release to the atmosphere.

## Materials and methods

### Soil and composting samples

The soil was sampled from a coffee plantation farm located in the southwestern highlands of Ethiopia and belonged to the major Soil Unit “Nitosol” (FAO, 1998). The sampling area is situated 36°36'E longitude and 7°56'N latitude (**Figure 2.1**). The elevation varies between 1533-1548 m a.s.l. Mean maximum and minimum temperature range from 26 to 30 °C and 11 to 14 °C, respectively, and the mean of precipitation ranges from 1131 to 1150 mm. Thus, the climate may be described as warm tropical. A total of 50 subsamples were taken from a total area of 5.91 h, traversed in a zig-zag pattern, from soil depth of 0–30 cm using a GPS and an Auger. The subsamples were well mixed in a plastic container and then a representative sample of 3 kg was placed in a labeled plastic bag. This soil sample was air-dried and milled to pass through a 2-mm-sieve. Its main characteristics were 84 % clay, 14 % silt and 1 % sand, pH (CaCl<sub>2</sub>) 5.2, electrical conductivity 2.39 mS (cm)<sup>-1</sup>, 3.9 % C<sub>org</sub>, 0.3% N<sub>t</sub>, C/N ratio of 12.0, and 0.1% S.

Composts were produced from 8 m<sup>3</sup> fruit and vegetable waste (dominated by fruit), 1600 kg wet coffee pulp waste and 300 kg garden trimmings (dry leaves, and young tree branches) in a method of small heap composting. Heaps were piled in a bamboo box of dimensions 1.5 m (l) × 1.0 m (w) × 0.8 m (h)). The platform used has been considered as pilot compost production unit by the Addis Ababa city council environmental protection authority, Ethiopia.

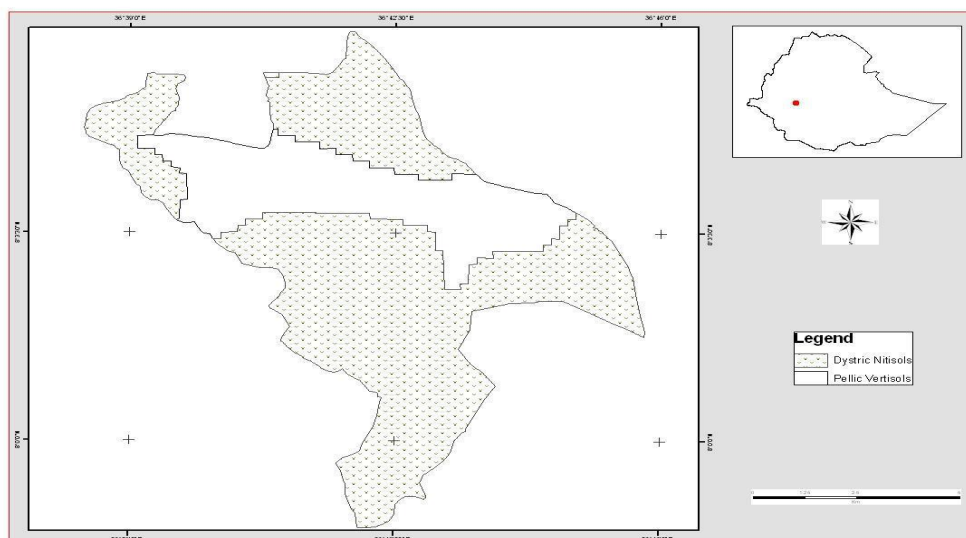


**Figure 2.1.**Map of Ethiopia showing area of study and soil type

The regional climate is tropical, with average temperatures between 15 °C and 25 °C. Three piles were constructed for experimental purposes with three replicates each and monitored as treatment COM1 (composed of coffee pulp waste), COM2 (fruit and vegetable waste), and COM4 (coffee pulp waste with fruit and vegetable waste in which the ratio was 50:50 by volume). The same quantity of soil was added as additional source of microbial colonization and garden trimmings to improve the structure. The experiment lasted from November 2010 to February 2011. The piles were manually turned each week during the active phase which lasts approximately 13 to 30 days, and then in a 15-days-interval during the maturation phase. Depending on the situation the piles were watered so as to maintain the moisture above 40%. Temperatures were measured daily for the first two weeks and in a three-days-interval during the next period always in the early morning using digital thermometers (0.5 and 1.0 m in length) at 2 different points of the heaps (25 and 60 cm depth). The composting was considered to be finished when the temperature of the mixture remained stable and near ambient (about 21 °C).

Representative compost samples (about 1 kg) were taken by mixing nine subsamples from different levels of the section in the pile along the whole profile at different phases of the composting, day 8 (thermophilic phase = T), day 24/36 (mesophilic phase = M, depending on the duration each treatment lasted in this phase), and 89/119 (final compost = F, depending on the duration each treatment lasted in this phase). In this way composts of different degree of stability were obtained from three different composting piles. The samples were air dried and ground to pass through a 0.5 mm sieve. The main properties of the composts are shown in **Table 1**.

### **Phytotoxicity test of compost samples**

Raw coffee pulp waste (RCPW) and composts sampled at the end of the thermophilic phase (COM1-T, COM2-T, COM4-T), mesophilic phase (COM1-M, COM2-T, COM4-M) and final compost (COM1-F, COM2-F, COM4-F) were investigated for possible phytotoxic effects. A germination test was carried out using garden cress (*Lepidium sativum*) and radish (*Raphanus sativus*) seeds as suggested by (Zucconi et al., 1985). In brief, Whatman filter papers were placed in a 145/20 mm disposable petri dish. The filter paper was wetted with 5 ml of filtered compost-water-extract. The extract was prepared by putting 10 g of compost sample (dry weight) in a 200 ml flask filled with 100 ml of distilled water and shaking at 125 rpm for 16 hours at room

temperature using an electric shaker. Then, 50 seeds of radish and cress were placed on the wetted paper. Distilled water was used as a control. The petri dish was covered and then kept in the oven at 25 °C. At day 3 and 6 germinated seeds were counted and root length was measured for cress and radish, respectively. Germination percentages ( $G \% = (\text{No of seed germinated in each extract} / \text{No of seed germinated in control}) \times 100$ ) and root growth percentage ( $RG \% = (\text{mean root length in each extract} / \text{mean root length in control}) \times 100$ ) was determined. The germination index (GI %), which is sensitive for phytotoxicity, was then calculated as ( $GI \% = (G \% \times RG \% ) / 100$ ) (Zucconi et al., 1985). Each treatment was replicated four times.

### **Aerobic incubation and respiration measurement**

10 g dry weight of sieved soil samples (<2 mm) were thoroughly mixed with 200 mg organic amendment (at desired application rates  $48 \text{ t ha}^{-1}$ ) and placed in 100 ml incubation vessels in five replicates each. They were monitored as treatments S+RCPW, S+COM1-T, S+COM1-M, S+COM1-F, S+COM2-T, S+COM2-M, S+COM2-F, S+COM4-T, S+COM4-M and S+COM4-F. Soil controls were run without any amendment. Distilled water (1 to 5 ml) was added to the soil-compost-mixtures to keep the moisture at 60 % of water-holding capacity. The incubation vessels were placed in a glass container containing 25 ml of 0.05 M NaOH and made air tight with a film plaster. To maintain sufficient  $O_2$  in the vessels they were opened several times in the first week and for two hours per day during the following weeks. Empty vessels were used as blanks. The  $CO_2$  evolved was measured by titration of the NaOH solution with 0.05 M HCl after the carbonate was precipitated by adding excess 0.05 M  $BaCl_2$  in 24- hour-intervals. The incubation was carried out in a temperature-controlled incubator at 25°C for 98 days. Subsamples (2 g) were taken destructively from each treatment at the start (day 1) and end (day 98) of incubation for chemical and mass spectrometric analyses. Percent increase and decrease in soil organic C as a result of added composts and subsequent mineralization were computed using a mathematical formula: % increase  $C_{org} = (C_t / C_s ) \times 100 - 100$ , % decrease  $C_{org} = (100 - (C_a / C_b) \times$

Where  $C_t$  is total organic C of the compost-soil mixture,  $C_s$  is organic C of the control soil,  $C_b$  is organic C at the end of incubation, and  $C_a$  is organic C at the start of incubation.

### **Chemical analyses: basic data and molecular-chemical characterization**

The soil samples were analyzed for pH, EC in 0.01 M CaCl<sub>2</sub> suspensions (1:2.5 w/v) and composting samples were analyzed for pH, EC in H<sub>2</sub>O suspensions (1:10 w/v). Whereas the concentrations of total organic carbon (C<sub>org</sub>), total nitrogen (N<sub>t</sub>) and total sulfur (S<sub>t</sub>) were determined for both soil and compost samples using a CNS analyzer (Vario EL III; Elementar Analysensysteme, Hanau, Germany).

For Py-FIMS analyses composting pile COM4 was selected because this treatment reached stability in a shorter time period than the other treatments and high analyses costs restricted the number of samples that could be measured. About 3 mg of the air dried, ground and homogenized soil samples amended with differently stabilized COM4 were thermally degraded in the ion source (emitter: 4.7 kV, counter electrode -5.5 kV) of a double-focusing Finnigan MAT 95 mass spectrometer. All samples were heated in a vacuum of 10<sup>-4</sup> Pa from 50 °C to 700°C in temperature steps of 10 °C over a time period of 18 minutes. Between magnetic scans the emitter was flash-heated to avoid residues of pyrolysis products. About 65 magnetic scans were recorded for the mass range *m/z* 15 to 900.

Ion intensities were referred to 1 mg of the sample. For each of the single scans, the absolute and relative ion intensities of ten classes of compounds in the OM were calculated by summation of the ion intensities of indicator signals to obtain thermograms of their volatilization and averaged Py-FI mass spectra. This procedure was done for each three replicate measurements per soil sample and the results were averaged for statistical analyses.

### **Statistical analyses**

The C-losses during the incubation experiment were fitted to mathematical models using the non-linear regression procedure. Means and standard errors were calculated for chemical and phytotoxicity parameters, CO<sub>2</sub>-C volatilization data and ion intensities from Py-FIMS. Comparisons between means of ion intensities of compound classes of different treatments were done by applying One Way ANOVA test (LSD mean comparison method were used). All statistics were computed using data analysis and graphic software (Origin 8.1G).

Table 2.1. Germination index (GI) and chemical properties of row coffee pulp waste and composts of different degree of stability taken at different composting time (t). Different letters indicate that samples are significantly different ( $P < 0.05$ ) according to Fisher LSD with in a column and values followed by the same letters with in a column were not significantly different at 5% probability level.

Compost Samples	composting time (days)	pHH <sub>2</sub> O	Corg. (g kg <sup>-1</sup> )	Ntot (g kg <sup>-1</sup> )	S (g kg <sup>-1</sup> )	C/N	EC (ms cm <sup>-1</sup> )	GI (%)	
								Cress	Radish
COM1-T	8	8.81(0.03)ab	151.0(2.0)a	10.5(0.0)a	1.70(0.0)ad	14.37	1.99(1.3)a	106(8.9)a	121(8.5)a
COM1-M	36	9.29(0.03)a	149.0(4.0)a	12.7(0.5)b	2.22(0.0)b	11.72	2.13(0.0)a	109(4.6)a	120(8.4)a
COM1-F	119	9.07(0.02)ab	139.2(3.0)b	12.7(0.3)b	2.40(0.0)b	10.98	2.07(0.5)a	102(16.9)a	125(4.8)a
COM2-T	8	8.70(0.2)ab	77.0(2.5)c	6.8(0.1)c	1.35(0.0)c	11.40	1.67(0.0)b	112(8.0)a	118(5.6)a
COM2-M	24	9.15(0.08)ab	73.2(2.0)c	7.0(0.1)c	1.80(0.0)d	10.48	1.09(0.0)c	113(9.0)a	120(7.5)a
COM2-F	89	8.96(0.27)ab	73.1(1.0)c	7.3(0.1)c	1.80(0.0)d	9.98	1.33(0.0)f	115(3.5)a	132(3.9)a
COM4 –T	8	8.05(0.01)c	107.9(3.0)d	8.74(0.0)d	1.40(0.0)c	12.35	1.36(0.0)f	107(9.4)a	111(12.1)a
COM4-M	24	8.65(0.02)b	93.3(1.0)e	9.32(0.1)d	1.70(0.0)d	10.01	1.07(1.0)c	107(4.7)a	108(8.4)a
COM4-F	89	8.55(0.05)bc	91.49(3.0)e	8.99(0.0)d	1.88(0.0)d	10.18	1.11(0.0)c	108(8.8)a	115(9.3)a
RCPW	0	5.81(0.01)d	397.0(1.6)f	21.1(0.3)e	3.10(0.2)e	18.86	6.73(0.0)d	3(1.1)b	26(3.0)b

COM – compost; T – thermophilic phase; M – mesophilic phase; F – final stage; RCPW - row (fresh) coffee pulp waste

Corg: total organic carbon; Ntot: total nitrogen; C/N: carbon to nitrogen ratio; EC: electrical conductivity and standard errors in brackets.

## Results

### Germination index (GI)

In the experiment with garden cress the GI varied between 3% and 115% (**Table 2.1**). All the compost samples yielded GI greater than 100% whereas the RCPW yielded 3%. Moreover, a germination delay was observed in the treatments with fresh coffee pulp waste. In the test with radish the GI varied between 26% and 132%. Similar to the results with cress all the compost samples yielded GI greater than 100% whereas the RCPW yielded 26%. The phytotoxicity of RCPW and the sanitation effect of composting were not reflected by the Germination percentages (GP) as all samples had GP above 80% (not shown).

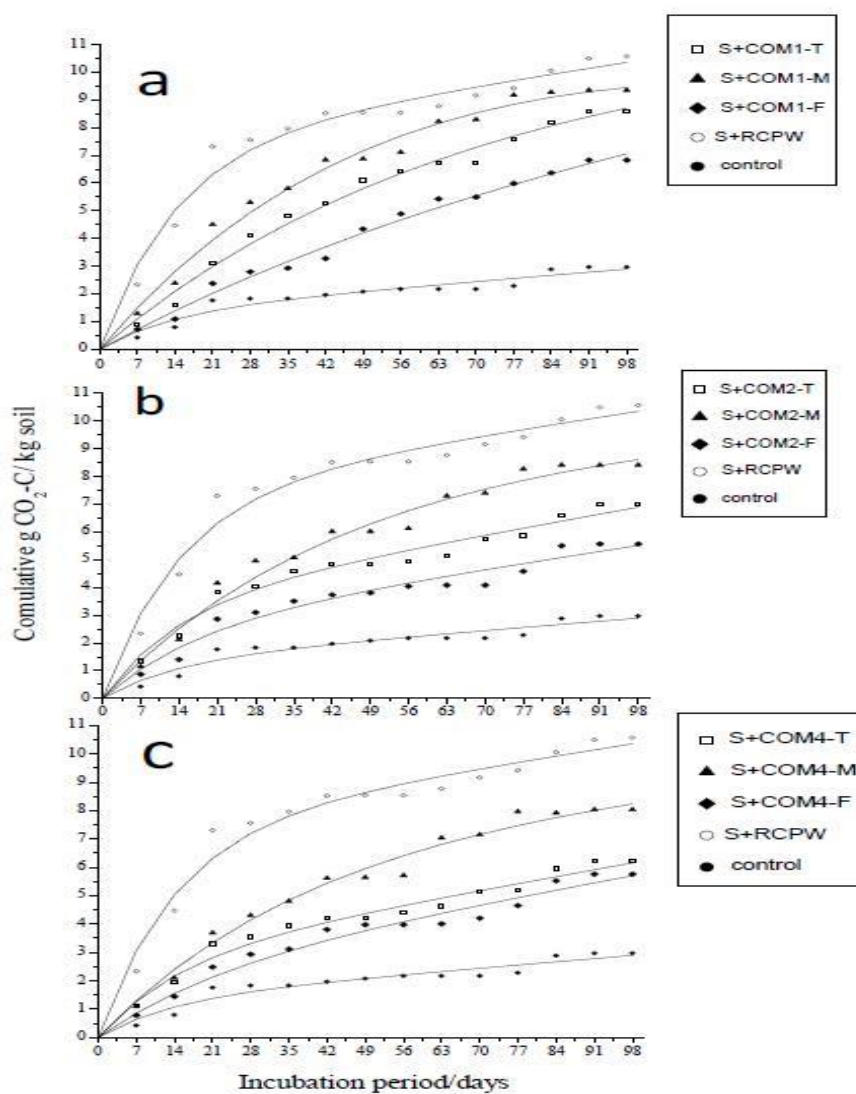
### Carbon mineralization

In all treatments the cumulative respiration curves showed two distinct phases for CO<sub>2</sub>-C evolution. An initial most intensive biological transformation phase was followed by a slower second phase (**Figure 2.2**). The maximum of CO<sub>2</sub>-C release was achieved in the first weeks of incubation in all treatments. The equation first order plus linear model gave the best fit for the cumulative CO<sub>2</sub>-C respired. The different parameters in the equation have a biological meaning,

$$C_t = C_1(1 - e^{-k_1 t}) + k_2 t$$

i.e.,  $C_t$  is the amount of organic C mineralized,  $C_1$  is the amount of the labile C ( $\text{mg g}^{-1}$ ),  $K_1$  ( $\text{day}^{-1}$ ) and  $K_2$  ( $\text{day}^{-1}$ ) are the rate constants for the mineralization of labile and recalcitrant C, respectively, and  $t$  is the incubation time in days. The CO<sub>2</sub>-C release followed the order S+RCPW > S+COM-M > S+COM-T > S+COM-F > CONTROL in all treatments. However, the cumulative CO<sub>2</sub>-C release curves of treatments S+COM4-T and S+COM4-F were not significantly different (**Figure 2.2**). In the short time of three weeks between 35 % and 69 % of the total C had been evolved. The cumulative CO<sub>2</sub>-C respired from the amended soils were varied between  $5.6 \text{ g C (kg soil)}^{-1}$  and  $10.6 \text{ g C (kg soil)}^{-1}$  at the end of the incubation (**Table 2.2**). The rate constants  $K_1$  were higher in treatment S+RCPW and lower in the control whereas the higher rate constants  $K_2$  were observed in treatment

S+COM-F. In all treatments the  $K_1$  values exceeded the  $K_2$  values (**Table 2.2**). During the whole incubation period the  $\text{CO}_2\text{-C}$  release from S+RCPW ( $10.6 \text{ g C (kg soil)}^{-1}$ ) was significantly higher than in soils amended with any of the compost materials.



;2

**Figure 2.2.** Cumulative  $\text{CO}_2\text{-C}$  release from the control, soil amended with raw coffee pulp waste (S+RCPW), and composts of different degree of stability made up of mainly composting of: a) coffee pulp waste (S+COM1-T, S+COM1-M, S+COM1-F); b) fruit and vegetable waste (S+COM2-T, S+COM2-M, S+COM2-F); and c) equal proportion of coffee pulp waste with fruit and vegetable waste (S+COM4-T, S+COM4-M, S+COM4-F).

**Table 2.2.** Carbon mineralized (g C kg<sup>-1</sup>soil), total amount (g kg<sup>-1</sup>) of selected elements, C/N ratio, percent increase in soil organic carbon (% inc. C<sub>org</sub>, percentdecrease of organic carbon (% dec. C<sub>org</sub>), the labile pool rate constant (K<sub>1</sub> (day<sup>-1</sup>) and recalcitrant pool rate constant (K<sub>2</sub> (day<sup>-1</sup>) of the control and amended soil during the incubation. Values followed by the same letters with in a column were not significantly different at 5% probability level (S+COM – soil-compost mixture; T – thermophilic phase; M – mesophilic phase; F – final stage; S+RCPW – soil-row coffee pulp waste mixture). Numbers in brackets represent standard errors.

Treatments	K <sub>1</sub>	K <sub>2</sub>	CO <sub>2</sub> -C	At day									
				At day 1					98				
				C <sub>org</sub>	N <sub>tot</sub>	S	C/N	% inc.	C <sub>org</sub>	N <sub>tot</sub>	S	C/N	% dec.
S+COM1-T	0.06	0.00	8.57(1.43)a	42.03	3.5	0.7	11.89	5.60	41.2	3.4	0.8	11.90	2.04
S+COM1-M	0.08	0.01	9.35(2.6)a	42.01	3.6	0.7	11.60	5.53	40.3	3.4	0.7	11.94	4.08
S+COM1-F	0.04	0.01	6.83(1.43)b	41.77	3.6	0.8	11.72	4.93	40.7	3.4	0.7	12.00	2.55
S+COM2-T	0.07	0.00	6.99(2.02)b	40.58	3.3	0.7	12.28	1.96	40.0	3.3	0.7	12.00	1.42
S+COM2-M	0.08	0.00	8.41(1.83)a	40.50	3.4	0.7	11.97	1.75	39.3	3.4	0.8	11.54	2.90
S+COM 2-F	0.06	0.01	5.57(1.67)c	40.46	3.4	1.3	11.78	1.66	39.2	3.3	0.7	11.91	3.05
S+COM4-T	0.07	0.00	6.22(1.2)c	41.20	3.4	0.8	12.17	3.51	40.2	3.3	0.7	12.03	2.43
S+COM4-M	0.07	0.00	8.03(2.08)a	40.93	3.4	0.7	11.96	2.82	39.3	3.4	0.8	11.63	4.09
S+COM4-F	0.05	0.00	5.76(0.85)c	40.77	3.5	0.7	11.74	2.44	39.8	3.4	0.7	11.71	2.50
S+RCPW	0.12	0.00	10.57(1.7)d	47.60	3.7	0.8	12.89	19.60	42.6	3.7	0.8	11.61	10.49
Control	0.04	0.00	2.97(1.41)e	39.80	3.3	0.7	12.15	0.00	38.3	3.2	0.7	11.82	3.66

The application of differently stabilized composts significantly affected the CO<sub>2</sub>-C release from soil (**Table 2.2**). Addition of COM4-F to soil resulted in the lowest CO<sub>2</sub>-C release (5.76 g C (kg soil<sup>-1</sup>)) followed by COM4-T (6.22 g C (kg soil<sup>-1</sup>)) and COM4-M (8.03 g C (kg soil<sup>-1</sup>)). Respiration of soils amended with differently stabilized COM1 and COM2 followed the same order. Considering the loss in percent of C<sub>org</sub> derived from the C<sub>org</sub> contents at the start and end of the incubation showed the smallest overall C loss (ranges from 1.42% to 2.43%) from the soil amended with COM-T during the incubation (**Table 2.2**).

### **Pyrolysis–field ionization mass spectrometry (Py-FIMS)**

In the Py-FIMS analyses of the control and soils amended with differently stabilized COM4 the thermograms of total ion intensity (TII) showed a reduction in intensity and a shift towards higher pyrolysis temperature during incubation. For instance the thermal evolution of molecules reached maximum intensities in the temperature 460 and 480 °C at start of the incubation and shifted to 490 and 510 °C at the end of incubation (see upper right inserts in **Figure 2.3**).

In the Py-FI mass spectra, a particular enrichment of N-compounds during the incubation in compost treated soil was reflected by *m/z* signals 67, 110 and 117 being more intense in Figure 3 b, d and f than in Figure 3 a, c and e. This difference, however, was not shown in the control (**Figure 2.3 g and h**). Comparison of mass spectra at the start and end incubation indicated increased proportions of carbohydrates (e.g. more intense *m/z* signals 84, 96, 110 in Figure 3 b, d, f and h than in **Figure 2.3 a, c, e and g**), lignin building blocks (e.g. more intense *m/z* signals 156, 168, 178, 192, 194, 202, 216 and 218 in **Figure 2.3 b, d, f and h** than in **Figure 2.3 a, c, e and g**). A decreased proportion of homologous series of free fatty acids and alkenes was indicated by *m/z* signals at 252, 266, 280, 294, 308 322, 336, and 350 (e.g. less intensive in **Figure 2.3 a, c, e and g** than in Figure 3 b, d, f and h) in all incubated treatments, but most pronounced in S+COM4-T.

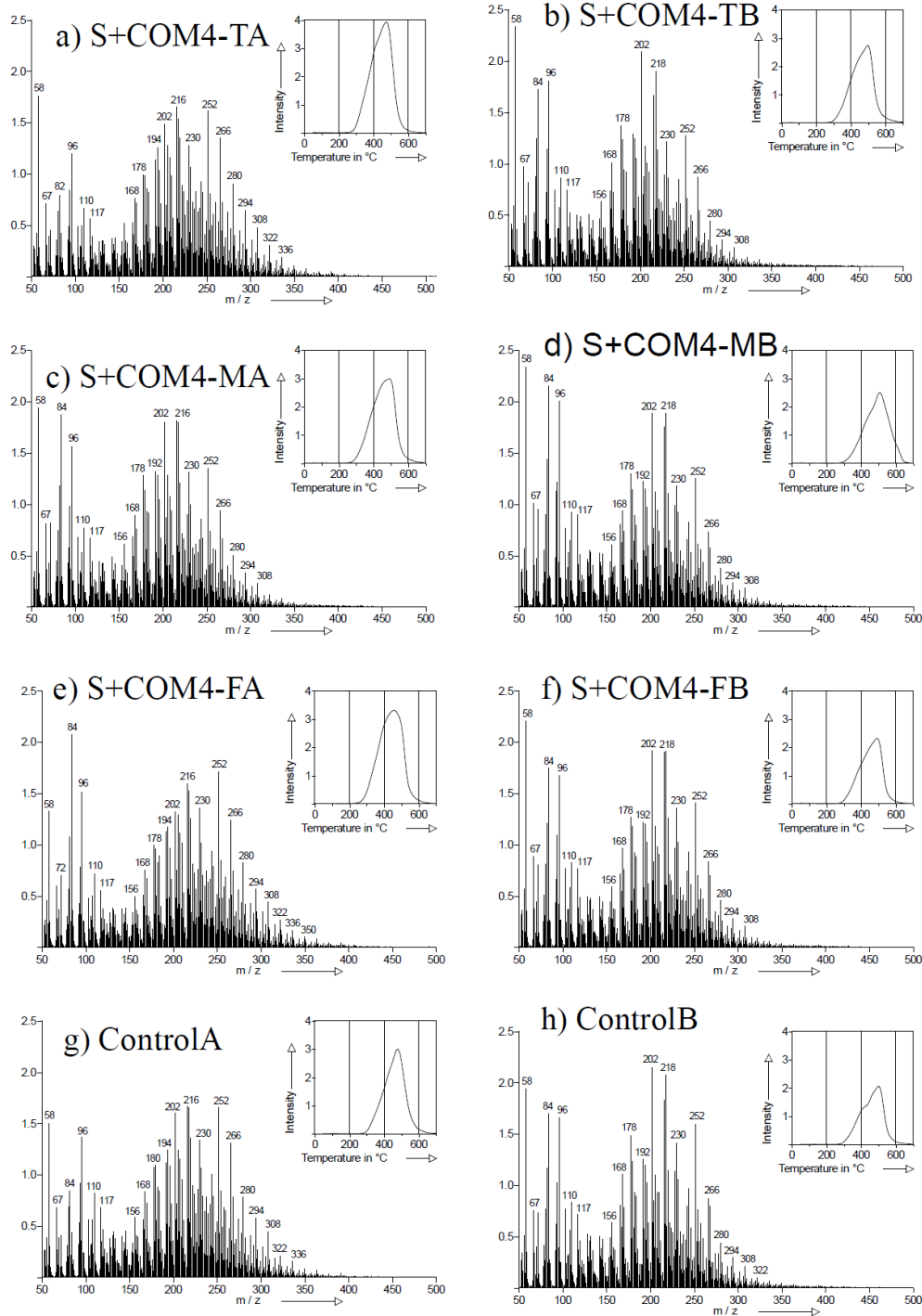


**Figure 2.3** Summed and averaged pyrolysis-field ionization mass spectra and thermograms of total ion intensity (TII) (upper right inserts) of the non-treated control soil and soil amended with different degree of stability composts (COM – compost; T–thermophilic phase; M–mesophilic phase; F– final stage); at the start of incubation (-A) and end of incubation(-B)

The TII values were significantly larger in all amended soils than in the control at start of the incubation (**Table 2.3**). However, significantly higher TII's ( $p < 0.05$ ) were recorded only in the treatment S+COM4-T than the control, both at the start and end of incubation. This well agreed with the  $C_{org}$  concentrations at the start and end of the incubation experiment (**Table 2.2**).

The relative ion intensities (% TII) of compound classes indicated a significant ( $p < 0.05$ ) enrichment of N-compounds during the incubation in all amended soils (by 39.1 % in S+COM4-T, by 28.6 % in S+COM4-M and by 40.9% in S+COM4-F). However, in the control the proportions of N-compounds did not significantly change between the start and end of incubation (**Table 2.3**). Among compost amended treatments significantly higher increases in the proportions of carbohydrates (by 65.3 %), phenols/lignin monomers (by 12.9 %) and peptides (by 43.5 %) at the expense of fatty acids and sterols were observed in the treatment S+COM4-T than in any other treatment. The compound classes phenols/lignin monomers and alkylaromatics are the major constituents of the SOM both at the start and end of incubation. The proportions of fatty acids and sterols were the smallest but an active component in the compost amended soils in which their proportion decreased largely during the incubation (**Table 2.3**). The proportions of alkylaromatics, lignin dimers and lipids did not differ among treatments, neither at the start nor at the end of incubation.

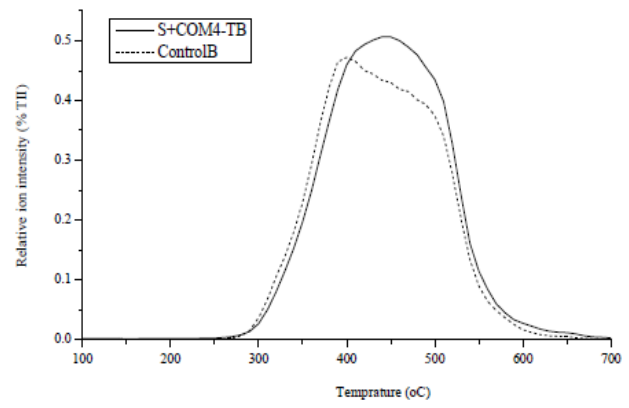
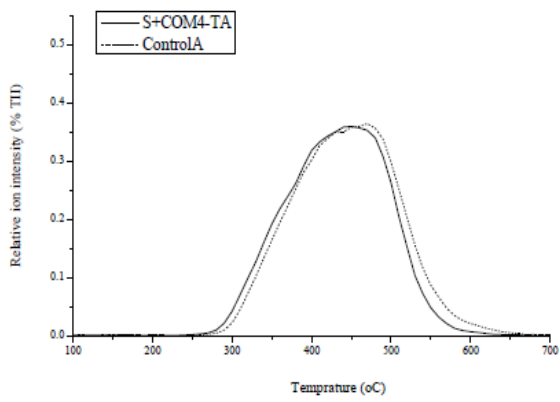
**Table 2.3** Total ion intensity (TII), volatile matters (VM %) and relative abundance (% TII) of principal classes of compounds from incubated samples at the start of incubation (---A) and end of incubation (----B). Values followed by the same letters within a column and column without letters were not significantly different at 5% probability level.

Treatment	TII	CARB	PHLM	LDIM	LIPID	ALKY	NCOMP	STER	PEPT	SUBE	FATTY	VM (%)
S+COM4-T												
A	60.0(1.5)a	4.9(0.1)a	12.4(0.3)e	7.7(0.3)	3.1(0.3)	15.6(0.2)	4.6(0.1)a	0.3(0.1)a	6.2(0.1)a	0.0(0.0)	0.3(0.1)a	21.7(1.3)
S+COM4-T												
B	41.5(2.2)b	8.1(0.1)b	14.0(0.1)f	8.1(0.1)	2.8(0.1)	15.1(0.1)	6.4(0.1)b	0.1(0.0)b	8.9(0.1)bc	0.0(0.0)	0.0(0.0)b	23.7(0.5)
S+COM4-M												
A	49.7(4.3)b	7.8(0.1)b	13.5(0.3)f	8.0(0.1)	3.1(0.1)	15.5(0.3)	5.6(0.1)c	0.2(0.0)ab	8.3(0.1)d	0.0(0.0)	0.1(0.0)b	20.0(1.9)
S+COM4-M												
B	41.2(7.2)b	9.2(0.5)c	13.6(0.5)f	8.3(0.3)	2.8(0.4)	14.9(0.4)	7.2(0.2)d	0.1(0.0)b	9.4(0.4)c	0.0(0.0)	0.0(0.0)b	19.8(1.2)
S+COM4-F												
A	57.2(2.1)a	7.5(0.1)b	12.2(0.3)e	8.0(0.0)	3.5(0.1)	15.5(0.2)	4.4(0.1)a	0.3(0.0)a	7.4(0.0)e	0.0(0.0)	0.4(0.0)a	24.0(2.1)
										0.0(0.0)	0.1(0.0)b	
S+COM4-F B	35.1(0.7)bc	7.8(0.2)b	13.5(0.2)f	8.3(0.0)	3.2(0.2)	15.1(0.3)	6.2(0.1)b	0.1(0.0)b	8.7(0.1)bd			23.4(0.5)
Control A	42.9(0.5)b	5.4(0.1)d	13.1(0.1)f	8.3(0.0)	3.8(0.2)	15.6(0.1)	5.1(0.2)c	0.2(0.0)a	6.4(0.2)a	0.0(0.0)	0.1(0.0)b	18.8(0.1)
Control B	30.6(1.0)c	7.7(0.3)b	14.0(0.4)f	8.5(0.1)	3.4(0.1)	15.0(0.3)	5.6(0.1)c	0.2(0.1)ab	8.3(0.2)d	0.0(0.0)	0.1(0.0)b	23.3(0.7)

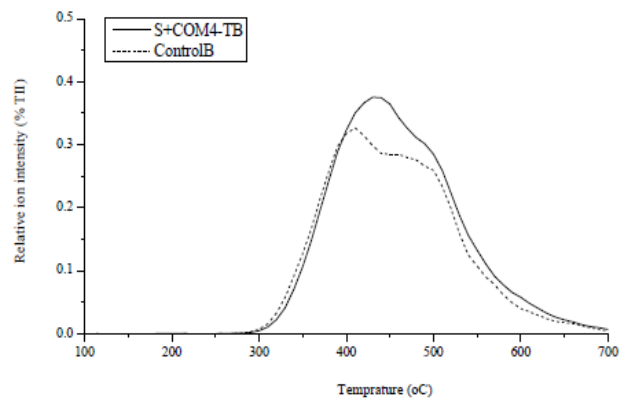
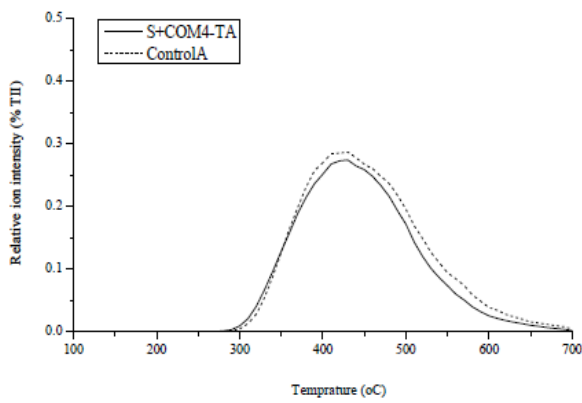
CARB: carbohydrates, PHLM: phenols/lignin monomers, LIPID: lipids, NCOMP: N-compounds, ALKY: alkylaromatics, LDIM: lignindimers, STER: sterols.

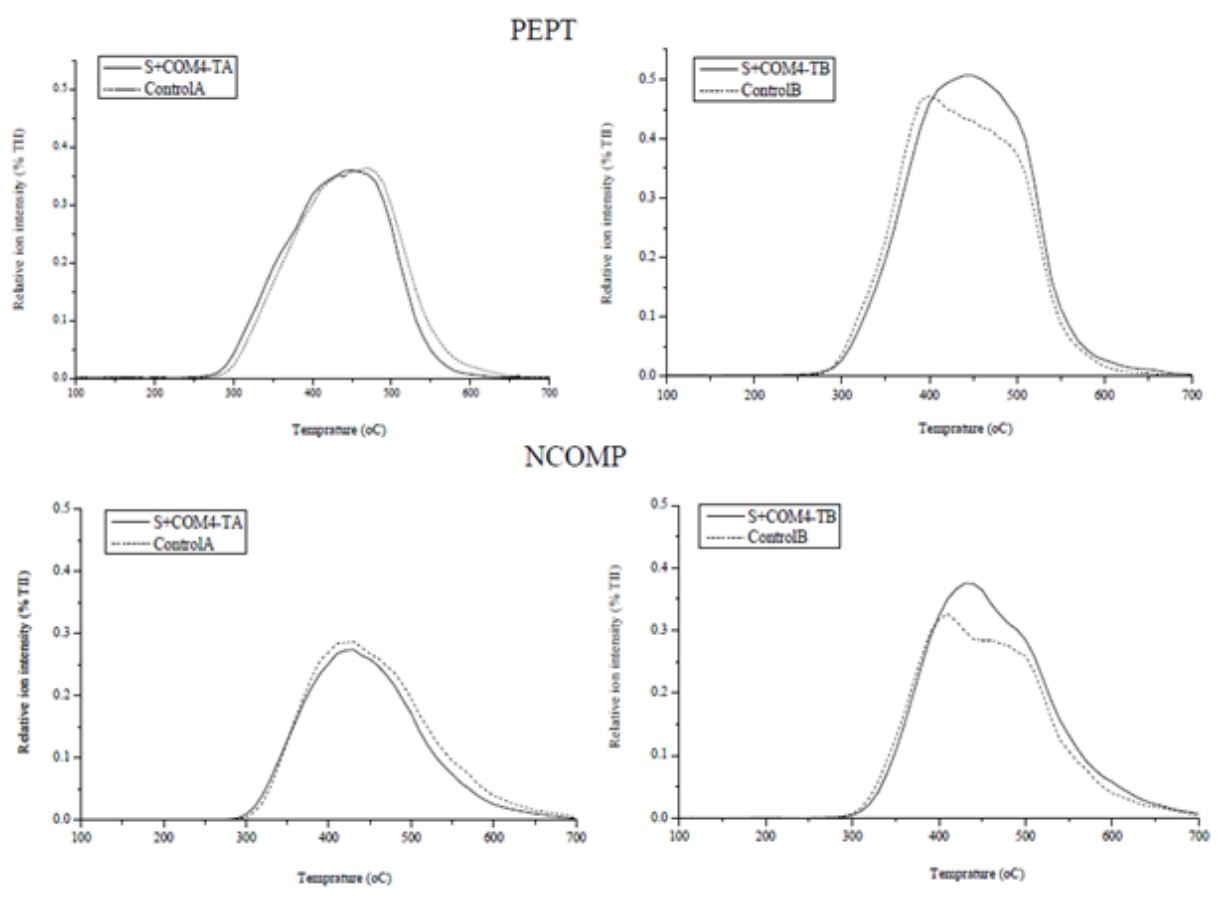
PEPT: peptides, SUBE: suberin, FATTY: *n*-Fatty Acids (*n*-C16 to *n*-C34) and standard errors in brackets, S- soil, COM – compost, T – thermophilic phase; M – mesophilic phase; F – final stage; RCPW - row (fresh) coffee pulp waste.

PEPT

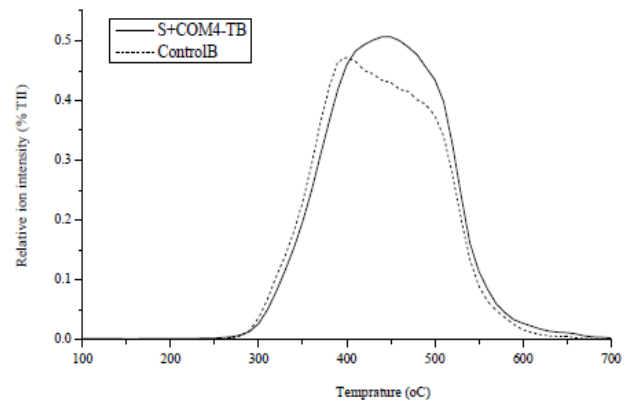
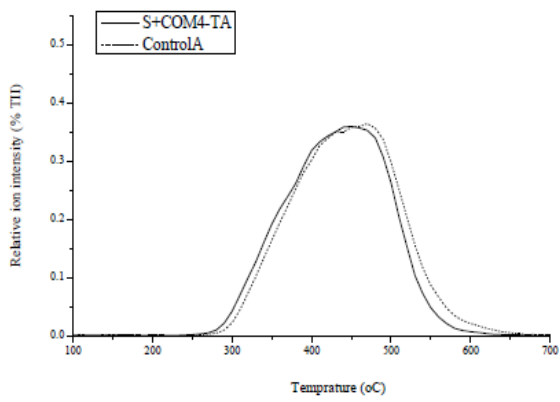


NCOMP

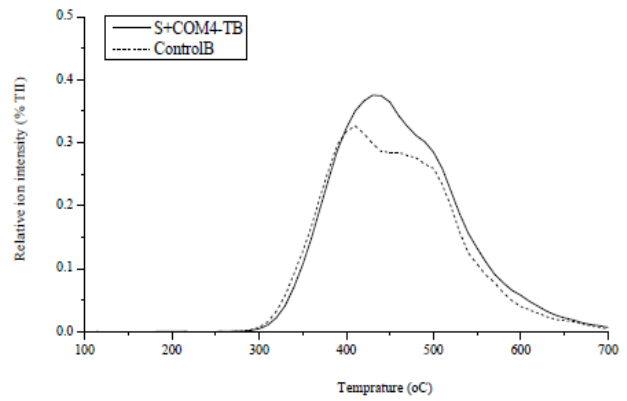
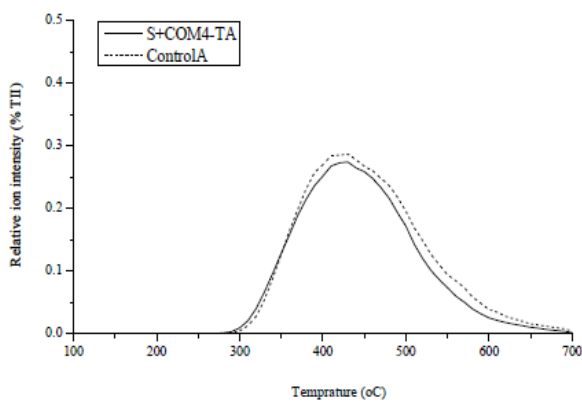




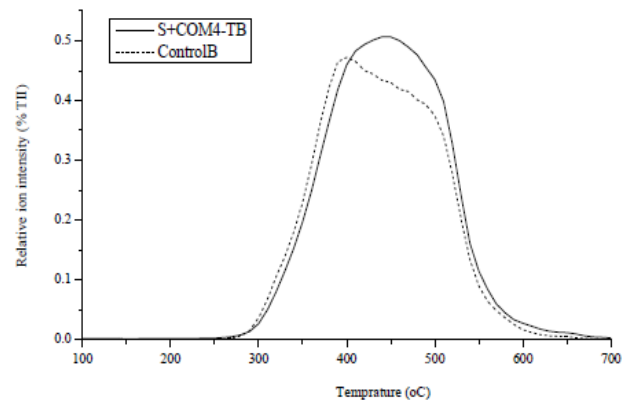
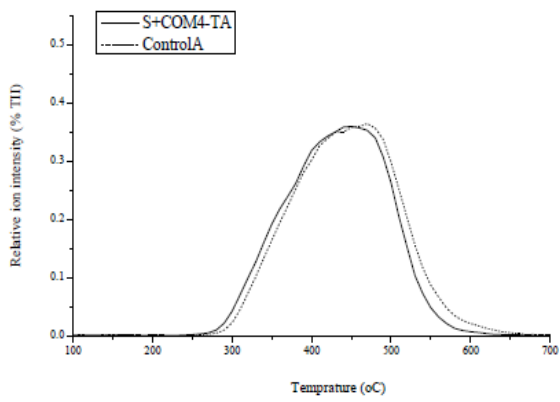
PEPT



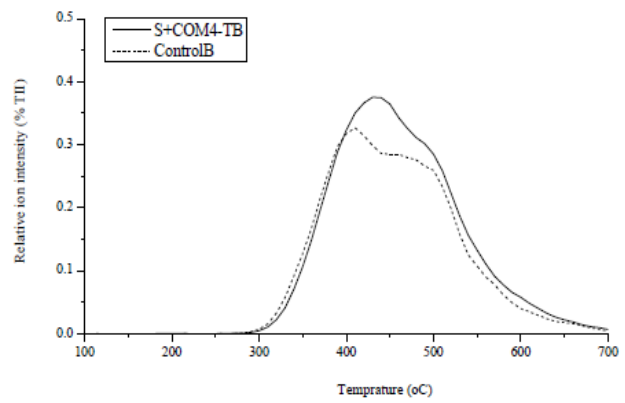
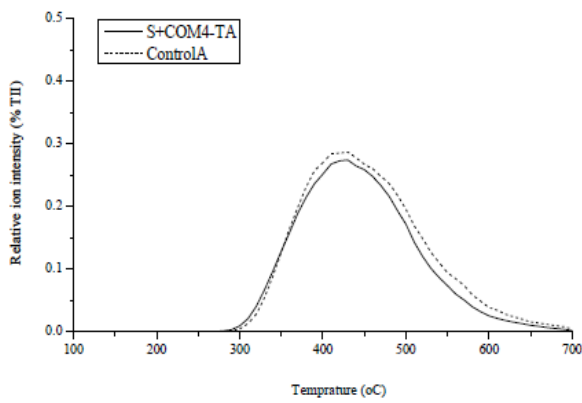
NCOMP

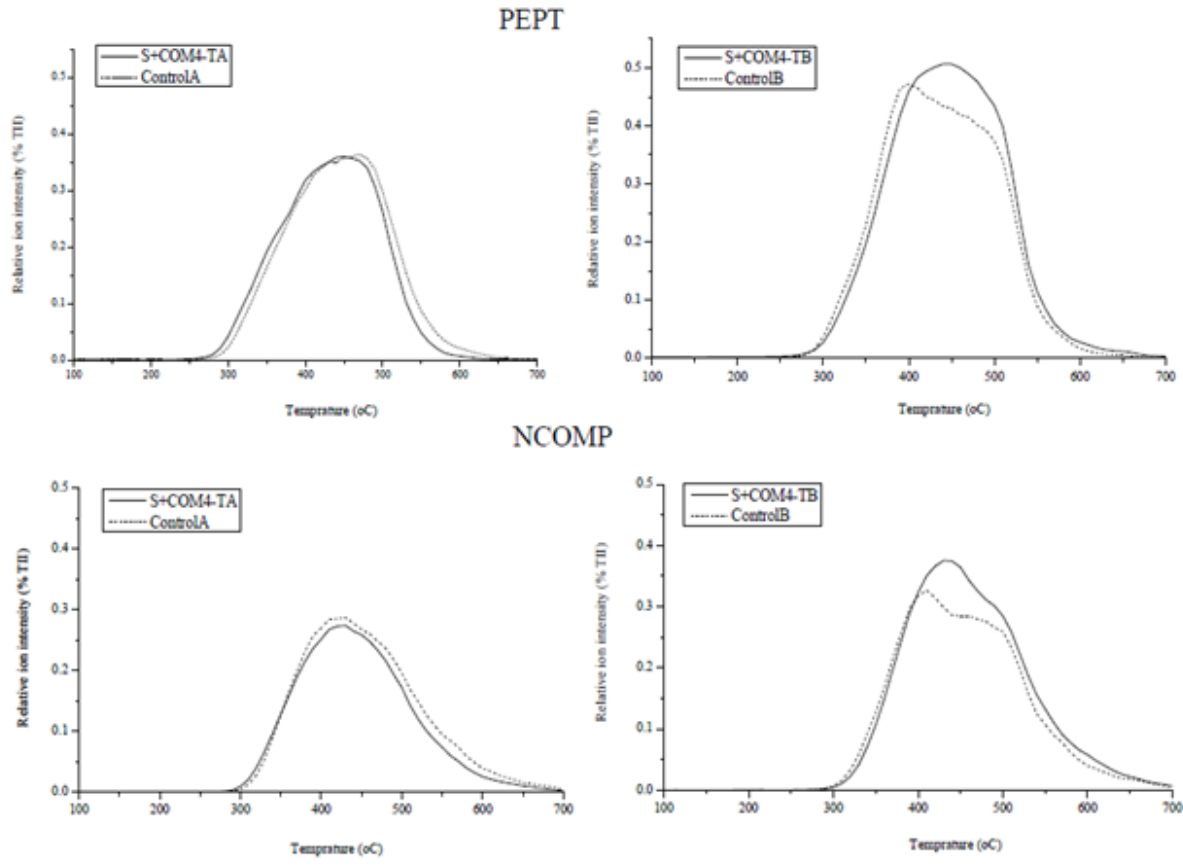


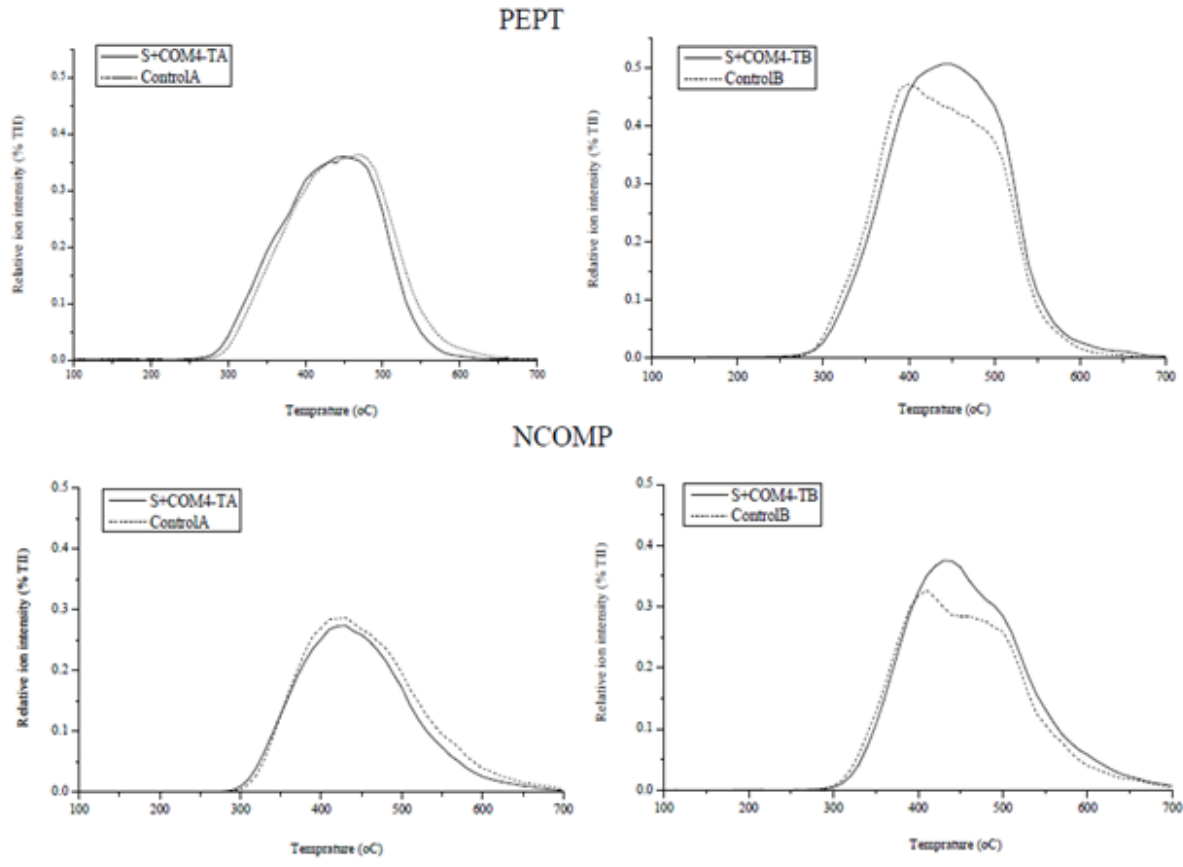
PEPT



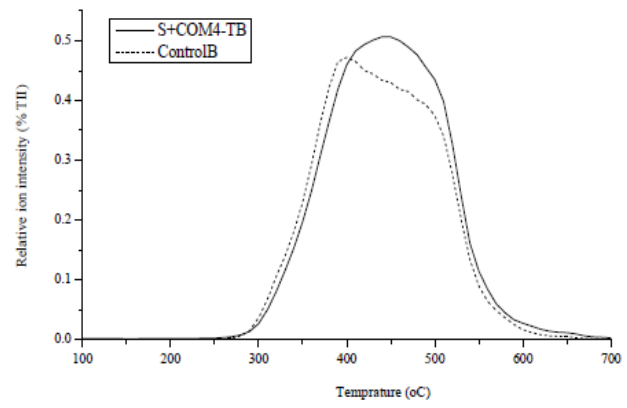
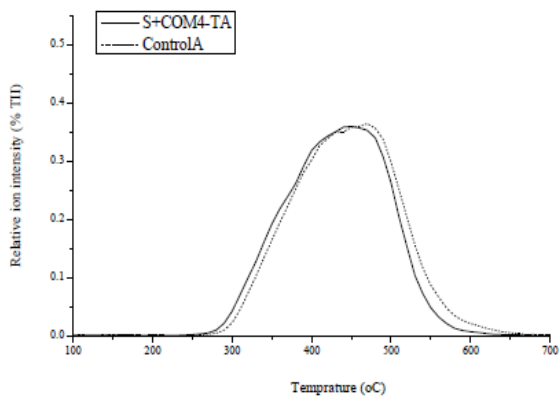
NCOMP



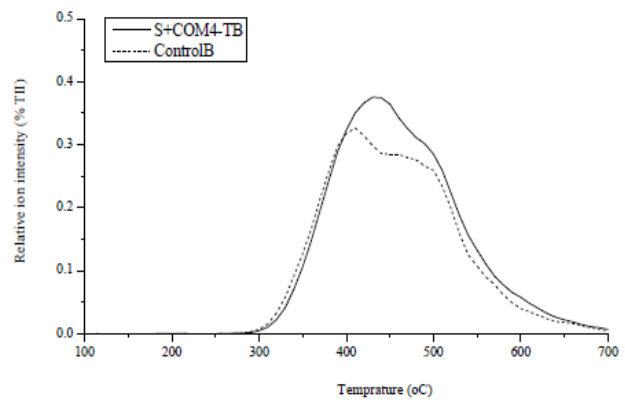
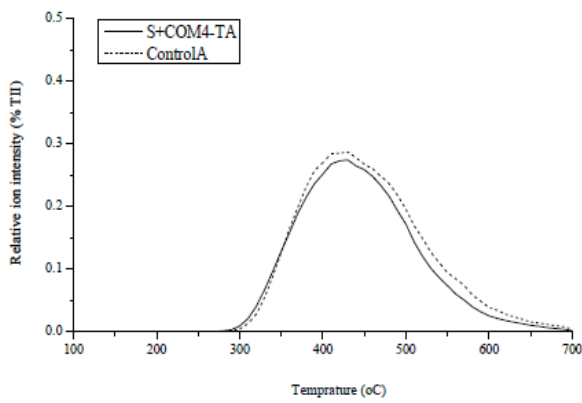




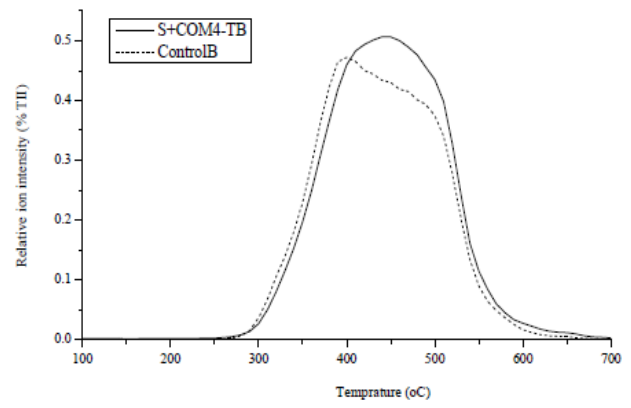
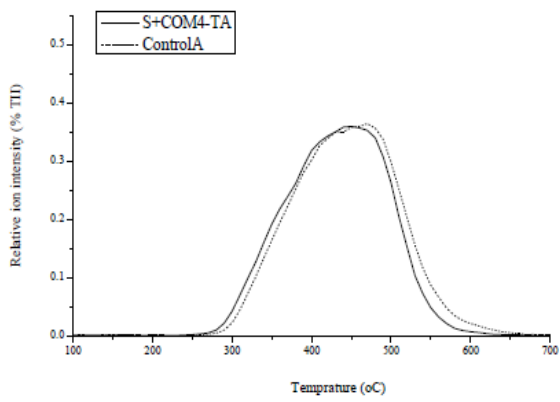
PEPT



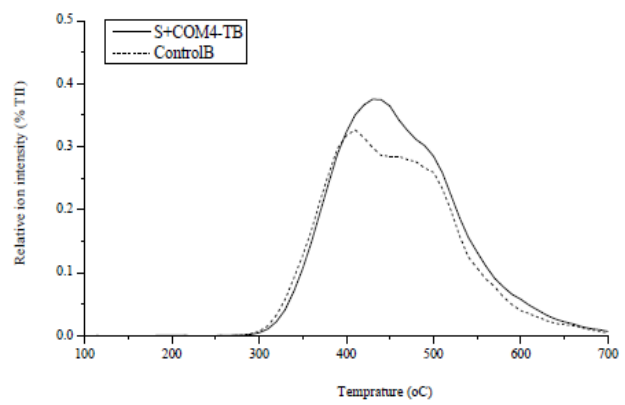
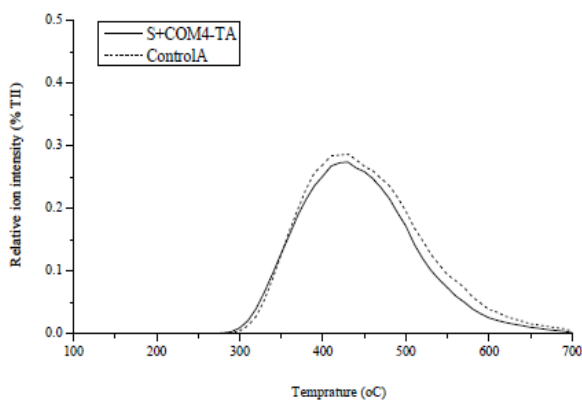
NCOMP



PEPT



NCOMP



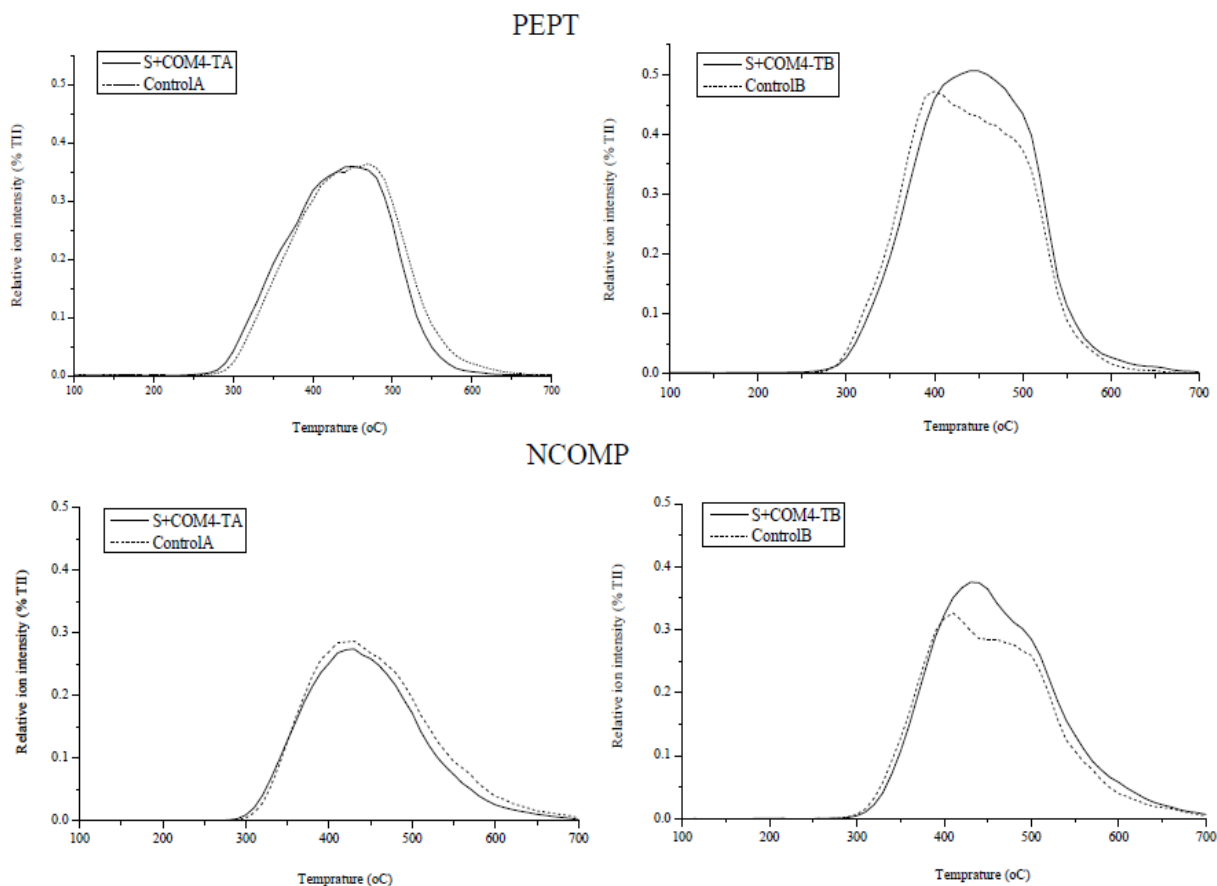


**Figure 2.4** Thermograms for the evolution of peptides (PEPT) and mainly heterocyclic N-compounds (NCOMP) from non-treated control soil (Control) and soil amended with thermophilic compost (S+COMP4-T) at the start of incubation (Control A, S+COMP4-TA) and end of incubation (Control B, S+COMP4-TB).

The temperature-resolved volatilization curves for N-compounds and peptides showed a clear difference in thermal stability between S+COMP4-T and the control during the incubation (**Figure 2.4**). At start of the incubation the thermograms for these two compound classes indicated no change in the thermal stability between treatments S+COMP4-T and the control. At the end of incubation, however, clear shifts of peaks to higher pyrolysis temperature were observed in S+COMP4-T when compared with the control.

## Discussion

### Phytotoxicity of starting material and composts

The low GI of 3% with cress and 26% with radish measured for the RCPW indicates its high phytotoxicity (Zucconi *et al.*, 1985; Lasaridi *et al.*, 2006). Moreover, the germination delay observed in this treatments can be attributed to the high salt content (electrical conductivity =  $6.73 \text{ mS cm}^{-1}$ ) of the sample (Lasaridi *et al.*, 2006). A GI < 50 % means high phytotoxicity, values between 50 and 80% a moderate phytotoxicity and values > 80% no phytotoxicity (Zucconi *et al.*, 1985). Therefore, the GI > 80% in all compost samples indicated that phytotoxicity of the raw material disappeared during the composting. The observed values of GIs greater than 100% in all composting samples agreed with (Lasaridi *et al.*, 2006) who found a range of GIs between 25% and 151% in a study with 28 composts and cress seeds. This indicates the promotion of the germination by compost samples (Paradelo *et al.*, 2008). A Gp of >80% for radish in all samples including the RCPW indicates a lower sensitivity of this seedling against the RCPW.

### Organic matter mineralization

The observed pattern in CO<sub>2</sub>-C release agreed with the model used by Gillis and Price (2011). They compared four different models to describe the mineralization dynamics from soil amended with alkaline treated municipal biosolids. The first rapid phase corresponded to the fast microbial decomposition of labile compounds (Bernal *et al.*, 1998; Ceccanti *et al.*, 2007). The second slower phase corresponded to the slow decomposition of resistant organic compounds. The CO<sub>2</sub>-C release from RCPW and compost-amended soils above that from the untreated control soil can be explained by the addition of labile C sources. This agrees with Pascual *et al.* (1998) and Mondini *et al.* (2007) who reported increased respiration of soils after amendment with organicwaste of diverse origins and stability from 7<sup>th</sup> to 30<sup>th</sup> day of incubation. Similarly, the observed difference in the CO<sub>2</sub>-C release between the RCPW and compost amended soils resulted mostly from the first three weeks of decomposition. In the later incubation period a faster degradation of organic compounds was observed in soil amended with

COMP-F ( $K_2=0.008$ ) than in RCPW and soil amended with COM-T ( $K_2=0.001$ ) (**Table 2.2**).

The variation in the  $CO_2$ -C release among the soils amended with differently stabilized composts despite of similar initial  $C_{org}$  contents and C/N ratios indicated a C immobilization. This immobilization was stronger in the soil amended with COM-T than in the soil amended with COM-M. This confirms Sanchez-Monedero *et al.* (2008) who observed that the degree of stabilization of added compost materials must not necessarily agree with the efficiency in C conservation. Moreover, some authors found an inverse relationship between the  $CO_2$ -C release and the degree of transformation/stabilization of compost materials added (Pascual *et al.*, 1998; Bernal *et al.*, 1998; Mondini *et al.*, 2007). One explanation for the partial disagreement of our data for respiration and stabilization with the above three references might be the quantity of added labile components with COM-T. This quantity might have been too low to promote the microbial decomposition significantly in the initial phase of incubation (Smidt *et al.*, 2005). Another explanation is the stabilization of C by clay-organic matter associations (Bolan *et al.*, 2012). Moreover, the lowest  $C_{org}$  loss (ranges from 1.4% and 2.4%) in the soil amended with COM-T indicated the suitability of composts from an early composting phase. This confirms that composts with a short composting period can be optimal for C sequestration in soil (Mondini *et al.*, 2007; Gillis and Price, 2011).

### **Changes in SOM composition**

The larger TII in the compost-amended treatments than in the control at the start of incubation coincided with the  $C_{org}$  concentrations in the treatments. It is explained by the additional organic matter from the composts (Leinweber and Schulten, 1993; Sorge *et al.*, 1993). However, the larger TII in S+COM4-T than in any other treatment at the end of incubation proved selective preservation of compounds that were possibly mineralized in samples with longer composting time. The best explanation for such a selective protection is the binding of organic matter at clay surfaces, and a consecutive aggregation of clay-organic matter complexes (Schulten *et al.*, 1993; Bustamante *et al.*, 2010; Bolan *et al.*, 2012).

The signal patterns of Py-FI mass spectra indicated the clearest impact of compost application by increasing proportions of N-compounds at the expense of fattyacids and sterols (**Figure 2.2, Table 2.3**). The stabilization of N-compounds in compost amended soils compared to the controls was also reflected by changes in the thermal volatilization of this compound class after 98 days of incubation (**Figure 2.3**). This suggests that the organic matter in compost-amended soils was relatively enriched in heterocyclic N-compounds which obviously resisted microbial decomposition. This indicates a residual relative enrichment of rather stabile compounds during the decomposition (Janssen 1996; Schulten and Schnitzer, 1997; Bustamante *et al.*, 2010). This explanation agrees with Stewart *et al.* (2011), who described enrichments of heterocyclic N-compounds in SOM also beneath forest trees. In the same line, enrichments of N-compounds were detected at the end of composting by Py-FIMS and FT-IR spectroscopy (Smidt *et al.* 2005). However, these N-compounds were completely decomposed in re-circulated leachates in larger scale lysimeters (Franke *et al.*, 2007), likely caused by the lack of sorptive surfaces. This indirectly points to the importance of the sorptive surfaces of the clay minerals in the present experiment.

The temperature-resolved Py-FIMS showed that thermally stable carbohydrates, phenols/lignin monomers, and peptides were more enriched during the incubation of S+COM4-T than in any other compost amended treatment. This indicates that these compound classes were microbially synthesized during incubation or selectively preserved. The pronounced enrichment of phenols/lignin monomers agreed with Leifeld *et al.* (2002) who stated that composition of SOM after compost amendment changed mainly by increases in the proportion of lignins. The stronger decrease in the lignin content in a soil amended with final compost than with early compost (treatment S+COM4-T) underlined the advantage of the early compost. Moreover, significantly increased carbohydrate proportions in the variant S+COM4-T during the incubation proved selective carbohydrate preservation. This agrees with findings of Chefetz *et al.* (1996) that progressive compost maturity reflected a decrease of the carbohydrate content. In agreement with Spaccini and Piccolo (2009) and Smidt *et al.* (2005), we found a progressive association of bio-labile peptides during composting.

### **Explanation of the organic matter mineralization by changes in the molecular composition of SOM**

Computing the percentage decrease of ion intensities in the temperature range  $<400\text{ }^{\circ}\text{C}$  (**Figure 2.3**) as indicator of thermally labile compounds during incubation revealed the largest decrease by 49% in S+COM4-M, followed by 35% in S+COM4-T, 28% in S+COM4-F whereas no decrease was observed in the control. This result is consistent with the order in  $\text{CO}_2\text{-C}$  release during the incubation experiment (**Figure 2.2**). Moreover, the changes in TII values ( $10^6$  counts  $\text{mg}^{-1}$ ) of the compound classes (not shown) confirmed the respired  $\text{CO}_2\text{-C}$  mainly resulted from reduced ion intensities of phenols/lignin monomers, lignin dimers, lipids, alkylaromatics, fatty acids and sterols during incubation for 98 days. On the other hand thermally stable compounds ( $>400^{\circ}\text{C}$  according to Kalbitz *et al.*, 2003) relatively increased by 12% in S+COM4-M, 16% in S+COM4-T and S+COM4-F but only by 1% in the control. Moreover, computing the relative increase in thermally stable carbohydrates (volatilized  $>400^{\circ}\text{C}$ ), N-compounds (volatilized  $>380^{\circ}\text{C}$ ) and peptides (volatilized  $>350\text{-}400^{\circ}\text{C}$ ) confirmed that addition of composts particularly from the end of the thermophilic phase to soil significantly enriched the SOM during incubation by stabilized compounds of microbial and plant origin.

The decrease in TII mainly in the temperature range below  $400^{\circ}\text{C}$  (thermally labile compounds) in the compost amended soils only implied that a large portion of labile components of the compost material itself was transformed or degraded during the incubation process. This supports the idea that decomposition of the added composts in soil goes along with humification in the composts themselves (Leifeld *et al.*, 2002). Here we show that this decomposition process is accompanied by the pronounced development of thermally stable carbohydrates, phenols/lignin monomers, and peptides of plant and microbial origin if the composts from the early phase of composting were applied. This was really a positive contribution of adding compost to SOM composition in the clay dominated Nitisol because this was not observed following NPK fertilization of soil (Leinweber *et al.*, 2008) and matured compost application in sandy soil (González-Vila *et al.*, 1999).

## **Conclusions**

1. The combination of laboratory incubation and Py-FIMS for the first time provided compelling evidence for effects of the compost stability on C mineralization and the molecular composition SOM when composts were applied to a typical clay-rich tropical soil.
2. The combined results revealed that it would be sufficient to end up the composting of coffee pulp and fruit waste immediately after a short thermophilic phase as its application better conserved the C (a) during composting and (b) during transformations in the soil.
3. Application of compost from the early phase of composting may result in a quicker mineralization of biologically labile organic matter from the compost and a better enrichment of SOM with stable compounds of plant and microbial origin such as carbohydrates, phenols/lignin monomers and peptides at the expense of free fatty acids and sterols compared to mature compost. This may have considerable economic implications as composting of coffee pulp in heaps may take 6 to 8 months to reach the mature stage.
4. Therefore, the application of compost from the early composting phase can be recommended not only as a soil amendment but also as a measure to mitigate CO<sub>2</sub>-enrichment in the atmosphere. Forthcoming studies will be directed to disclose in more detail the stabilization mechanism of biologically labile, compost-derived organic molecules in tropical and other soils.

## References

- Adani, F., Genevini, P., Ricca, G., Tambone, F. and Montoneri, E. 2007. Modification of soil humic matter after 4 years of compost application. *Waste Manage.*, 27: 319–324.
- Bernal, M. P., Sa´nchez-Monedero, M. A., Paredes, C. and Roig, A. 1998. Carbon mineralization from organic wastes at different composting stages during incubation with soil. *Agri.Ecosyst.Environ.*, 69: 175–189.
- Bolan, N. S., Kunhikrishnan, A., Choppala, G. K., Thangarajan, R. and Chung, J. W. 2012. Stabilization of carbon in composts and biochars in relation to carbon sequestration and soil fertility. *Sci.totalEnviron.*, 1(424): 264-270
- Bustamante, M. A., Said-Pullicino, D., Paredes, C., Cecilia, J. A. and Moral, R. 2010. Influences of winery–distillery waste compost stability and soil type on soil carbon dynamics in amended soils. *Waste Manage.*, 30(10): 1966-1975.
- Ceccanti, B., Masciandaro, G. and Macci, C. 2007. Pyrolysis-gas chromatography to evaluate the organic matter quality of a mulched soil. *Soil Till. Res.*, 97: 71–78.
- Chefetz, B., Hatcher, P.G., Hadar, Y. and Chen, Y. 1996. Chemical and biological characterization of organic matter during composting of municipal solid waste. *J. Environ. Qual.* 25: 776–785
- Davidson, O., Halsnaes, K., Huq, S., Kok, M., Metz, B., Sokona, Y. and Verhagen, J. 2003. The development and climate nexus: the case of sub-Saharan Africa. *Climate Policy*, 31: 97-113.
- Eshetu, B., Jandl G. and Leinweber, P. 2012. Compost Changed Soil Organic Matter Molecular Composition: A Study by Py-GC/MS and Py-FIMS. *Compost Sci. Util.*, 20: 230-238.
- Favoino, E. and Hogg, D., 2008. The potential role of compost in reducing greenhouse gases. *WasteManage. Res.*, 26: 61–69.
- Franke, M., Jandl, G. and Leinweber, P. 2006. Organic compounds in re-circulated leachates of aerobic biological treated municipal solid waste. *Biodegradation*, 17: 473–485.
- Franke, M., Jandl, G. and Leinweber, P. 2007. Analytical pyrolysis of re-circulated leachates: Towards an improved municipal waste treatment. *J. Anal. Appl. Pyrol.*, 79: 16–23.
- Gezahegne, B., Fikre, L. and Mulatu, W. 2011. Exploring the suitability of coffee pulp compost as growth media substitute in greenhouse production. *Int. J. Agri. Res.*, 6(3): 255-267
- Gillis, J. D. and Price, G. W. 2011. Comparison of novel model to three conventional models describing carbon mineralization from soil amended with organic residues. *Geoderma*, 160: 304-310.
- González-Vila, F. J., Almendros, G. and Madrid, F. 1999. Molecular alterations of organic fractions from urban waste in the course of composting and their further transformation in amended soil. *Sci. Total Environ.*, 236: 215–229.
- Janssen, B. H. 1996. Nitrogen mineralization in relation to C:N ratio and decomposability of organic materials. *Plant Soil*, 181: 39–45
- Kalbitz, K., et al. 2003. Changes in properties of soil-derived dissolved organic matter induced by biodegradation. *Soil Biol. Biochem.*, 35: 1129–1142.
- Lal, R. 1999. Soil management and restoration for C sequestration to mitigate the accelerated greenhouse effect. *Prog. Environ. Sci.*, 1, 307–326.

- Lal, R., 2002. The potential of soils of the tropics to sequester carbon and mitigate the greenhouse effect. *Adv. Agron.*, 74: 155–192.
- Lasaridi, K., Protopapa, I., Kotsou, M., Pilidis, G., Manios, T. and Kyriakou, A. 2006. Quality assessment of composts in the Greek market: The need for standards and quality assurance. *J. Environ. Manag.*, 80: 58-65.
- Leifeld, J., Siebert, S. and Kögel-Knabner, I. 2002. Changes in the chemical composition of soil organic matter after application of compost. *Eur. J. Soil Sci.*, 53: 299–309
- Leinweber, P., Blumenstein, O. and Schulten, H.-R. 1996. Organic matter composition in sewage farm soils: Investigations by <sup>13</sup>C-NMR and pyrolysis-field ionization mass spectrometry. *Eur. J. Soil Sci.*, 47: 71-80.
- Leinweber, P., Jandl, G., Baum, C., Eckhardt, K.-U., Kandeler, E., 2008. Stability and composition of soil organic matter control respiration and soil enzyme activities. *Soil Biol. and Biochem.*, 40:1496-1505.
- Leinweber, P. and Schulten, H.-R. 1993. Dynamics of soil organic matter studied by pyrolysis-field ionization mass Spectrometry. *J. Anal. Appl. Pyrol.*, 25: 123-136.
- Lima, G., Diana L. D., Santos, M. S., Scherer, W. H., Schneider, J. R., Duarte, C. A., Santos, B. H. E. and Esteves, I. V. 2009. Effects of organic and inorganic amendments on soil organic matter properties. *Geoderma*, 150: 38-45.
- Mondini, C., Cayuela, M. L., Sinicco, T., Cordaro, F., Roig, A. and Sánchez-Monedero, M. A. 2007. Greenhouse gas emissions and carbon sink capacity of amended soils evaluated under laboratory conditions. *Soil Biol. Biochem.*, 39: 1366-1374.
- Murthy, P. S. Manjunatha, M. R., Sulochannama G. and Naidu, M. M. 2012 Extraction, Characterization and Bioactivity of Coffee Anthocyanins. *Eur. J. Biol. Sci.*, 4: 13-19.
- Nardi, S., Morari, F., Berti, A., Tosoni, M. and Giardini, L. 2004. Soil organic matter properties after 40 years of different use of organic and mineral fertilizers. *Eur. J. Agron.*, 21: 357–367.
- Negassa, W., Baum, C. and Leinweber, P. 2011. Soil amendment with agro-industrial products: Molecular-chemical compositions and effects on soil biochemical activities and phosphorus fractions. *J. Plant Nutr. Soil Sci.*, 174: 113-120.
- Paradelo, R., Moldes, A. B., Rodríguez, M. and Barral, M. T. 2008. Relationship between heavy metals and phytotoxicity in composts. *Cienc. Tecnología Aliment.*, 6: 143-151.
- Pascual, J. A., Hernandez, C., García C. and Ayuso, M. 1998. Carbon mineralization in arid soil amended with organic wastes of varying degrees of stability. *Communications in Soil Science and Plant Analysis*, 29: 835–846.
- Sánchez-Monedero, M. A., Cayuela, M. L., Mondini, C., Serramia, N. and Roig, A. 2008. Potential of olive mill wastes for soil carbon sequestration. *Waste manage.* 28: 767-773.
- Smidt, E., Eckhardt, K.-U., Lechner, P., Schulten, H.-R. and Leinweber, P. 2005. Characterization of different decomposition stages of biowaste using FT-IR spectroscopy and pyrolysis-field ionization mass spectrometry. *Biodegradation*, 16: 67–79
- Smith, P., Powlson, D.S., Smith, J. U., Falloon, P., Coleman, K., 2001. Meeting Europe's climate change commitments: quantitative estimates of the potential for carbon mitigation by agriculture. *Global Change Biol.*, 6: 525–539.

- Sorge, C., Müller, R., Leinweber, P. and Schulten, H.-R. 1993. Pyrolysis-mass spectrometry of whole soils, soil particle-size fractions, litter materials and humic substances: Statistical evaluation of sample weight, residue, volatile matter and total ion intensity. *Fresenius J. Anal. Chem.*, 346: 687-703.
- Schulten H.-R. and Schnitzer, M. 1997. The chemistry of soil organic nitrogen - a review". *Biol. FertilSoils*, 26: 1–15.
- Schulten, H.-R., Leinweber P. and Sorge, C. 1993. Composition of organic matter in particle size fractions of an agricultural soil. *J. Soil Sci.*, 44: 677–691.
- Spaccini, R. and Piccolo, A. 2009. Molecular characteristics of humic acids extracted from compost at increasing maturity stages. *Soil Biol. Biochem.*, 41: 1164–1172
- Stewart, C. E., Neff, J. C., Amatangelo, K. L. and Vitousek, P. M. 2011. Vegetation Effects on soil organic matter chemistry of Aggregate Fractions in a Hawaiian Forest. *Ecosystems*, 14: 382–397.
- Zucconi, F.; A. Monaco; and M. Forte (1985). Phytotoxins during the stabilization of organic matter. In: Gasser J. K. R. (Editor), *Composting of Agricultural and other Wastes*, Elsevier Applied Science Publication, New York, NY, U.S.A., pp. 73-86.

## Optimization of dilute sulphuric acid hydrolysis of sugarcane bagasse for enhanced xylose recovery using RSM

Belachew Zegale, Vijayanand S. Moholkar\*

Department of Chemical Engineering, Indian Institute of Technology Guwahati, Guwahati 781  
039, Assam, India

\*Corresponding author. Tel: +91 9954709058, E. mail: [vmoholkar@iitg.ernet.in](mailto:vmoholkar@iitg.ernet.in)

### Abstract

Lignocellulosic materials are an abundant and inexpensive source of sugars for the production of biofuels and value-added chemicals and hence sugarcane bagasse is among the lignocellulosic materials for the synthesis of biofuels and value-added products such as xylitol. This study evaluated first the compositional characterization of sugarcane bagasse and then Box Behnken design (BBD) with response surface methodology was adopted to optimize the parameters (temperature, acid concentration and hydrolysis time) of dilute sulphuric acid hydrolysis of sugarcane bagasse in order to get a xylose rich hemicellulosic hydrolysate and their subsequent conversion into value-added products via microbial fermentation. The optimum conditions for dilute sulphuric acid hydrolysis found were a temperature of 120°C, 2% (v/v)  $H_2SO_4$  concentration and hydrolysis time of 33 min. Under these optimal conditions a hemicellulosic hydrolysate with xylose concentration of 8.49 g/L, corresponding to the yield of 84.9% by weight of the hemicellulosic fraction of sugarcane bagasse was obtained. The results of validation experiment under the optimum conditions agreed well with model predictions. Finally the monomer sugar and inhibitory compounds under optimal conditions of dilute sulphuric acid hydrolysis of sugarcane bagasse was characterized and found as: glucose (2.46 g/L), xylose (8.68 g/L), arabinose (1.25 g/L), acetic acid (1.02 g/L), furfural (0.365 g/L), and 5-HMF (0.214 g/L).

**Keywords:** Sugarcane bagasse, Dilute acid hydrolysis, Box Behnken design (BBD), Xylose

### 1. Introduction

Researchers have been devoted to study the production of chemicals and biofuels originated from lignocellulosic materials due to environmental changes and depletion of fossil fuels [1]. Lignocellulosic materials are an abundant and inexpensive source of sugars for the

production of biofuels and value-added chemicals and hence sugarcane bagasse is among the lignocellulosic materials for the synthesis of biofuels and value-added products such as xylitol[2].

Like other lignocellulosic materials the main components of sugarcane bagasse are cellulose, hemicellulose, and lignin. Apart from this, it also consists of ash, extractives and others. Among these constituents, hemicellulose is of particular interest because of its unique properties and composition. Last two decades of research has observed the technological development for the hemicellulose depolymerization into its monomeric constituents, mainly xylose, and their subsequent conversion into value-added products via microbial fermentation[3].

Dilute acid hydrolysis has been widely used for pretreatment of lignocellulosic biomass. This is due high hydrolysis rate, specific towards hemicellulose, and more economical than enzymatic, concentrated acid and base pretreatment[4]. The yield of fermentable sugars during acid hydrolysis is affected by various factors such as hydrolysis time, solid to liquid ratio, hydrolysis temperature, acid concentration, etc. Dilute sulphuric acid hydrolysis is the most commonly and effective pretreatment process for sugarcane bagasse[5] but other reagents such as hydrochloric, nitric and phosphoric acids can also be used.

The conventional method of optimization involves varying one factor at a time and keeping the others constant. This is often useful but does not explain the effect of interaction between the various factors under consideration. Response surface methodology is an empirical statistical technique adopted for multiple regression analysis of quantitative data obtained from statistically designed experiments by solving the multivariate equations simultaneously[6].

The aim of this study was first to characterize the composition of sugarcane bagasse and then to optimize the effect of dilute sulphuric acid hydrolysis conditions: acid concentration (acid load), hydrolysis temperature, and hydrolysis time and the interaction among these factors on the hydrolysis of sugarcane bagasse to extract xylose for the biosynthesis of xylitol. The study was not only to optimize the parameters of acid hydrolysis but also to characterize the sugar monomers and inhibitory compounds at the optimum conditions. A three variable Box Behnken design was adopted to design the acid hydrolysis experiments.

## **2. Materials and methods**

### **2.1. Materials**

Sugarcane bagasse obtained from local area in Guwahati, Assam (India) was dried cut into small pieces, ground, sieved to 0.6 mm sizes using 25 BSS mesh screen, and then stored in a zipped lock plastic bag at ambient temperature until use. All chemicals for compositional characterization, acid hydrolysis pretreatment of sugarcane bagasse and analytical instruments are of analytical grade (Merck, Germany and Himedia, India).

### **2.2. Compositional characterization of sugarcane bagasse**

#### **2.2.1. Determination of extractives**

The amount of extractives in sugarcane bagasse was estimated by using Soxhlet extraction apparatus through extraction thimbles. Acetone 60 mL for 1 g of oven dried bagasse was used as the solvent for extraction, and the temperature was held at 70°C for a 4 h run period on the heating mantle. The sample was air dried for few minutes at room temperature. It was then dried at 105°C in an oven until a constant weight was obtained and then cooled in a desiccator. The % (w/w) of the extractives content was evaluated as the difference in weight between the raw extractive-laden bagasse and extractive-free bagasse [7, 8].

#### **2.2.2. Hemicellulose analysis**

1 g of extracted dried bagasse was transferred into a 250 mL Erlenmeyer flask. 150 mL of 0.5M NaOH was added. The mixture was boiled for 3.5 h with distilled water so as to increase the heating effect and minimize lime scales that can come from tap water. It was filtered after cooling through vacuum filtration and washed until neutral pH. The residue was dried to a constant weight at 105°C in an oven. The difference between the sample weight before and after this treatment was the hemicellulose content (% w/w) of oven dried bagasse [7-10].

#### **2.2.3. Lignin analysis**

0.3 g of dried extracted bagasse was weighed in glass test tubes and 3 mL of 72% (w/w) H<sub>2</sub>SO<sub>4</sub> was added. The sample was kept at room temperature for 2 h with carefully shaking at 30 min

intervals to allow for complete hydrolysis. After the initial hydrolysis, 84 mL of distilled water was added in order to get 4% (w/w) H<sub>2</sub>SO<sub>4</sub> solution. The second step of hydrolysis was made to occur in an autoclave for 1 h at 121°C. The mixture was then cooled at room temperature. Hydrolyzates were filtered through vacuum filtration. The acid insoluble lignin was determined by drying the residues at 105°C and cooled in a desiccator. The acid soluble lignin fraction was determined by measuring the absorbance of the acid hydrolyzed samples at 278 nm. The lignin content (%w/w) was calculated as the summation of acid insoluble lignin and acid soluble lignin[7, 11].

#### **2.2.4. Cellulose**

The cellulose content (%w/w) was calculated by difference, assuming that extractives, hemicellulose, lignin, and cellulose are the only components of the entire bagasse.

### **2.3. Acid hydrolysis of sugarcane bagasse**

Sugarcane bagasse was treated with dilute sulphuric acid to hydrolyze hemicellulose. The bagasse samples were treated with 0.5–3.5% (v/v) H<sub>2</sub>SO<sub>4</sub>, temperature range of 100–130°C and reaction time of 10–40 min at a solid to liquid ratio of 1:30 (w/v). Experiments were carried out in an autoclave at 15 lbs pressure. Each sample was immediately cooled in an ice bath to stop the hydrolysis reaction.

### **2.4. Analytical methods**

After dilute sulphuric acid hydrolysis the hydrolysate was centrifuged at 6000 rpm for 10 min and then filtered in a vacuum filter (0.45µm membrane filter). The sugar concentrations (glucose, xylose, and arabinose) and acetic acid were determined by HPLC (Perkin) using a Hiplax-H column, 0.005M H<sub>2</sub>SO<sub>4</sub> as mobile phase, refractive index detector and flow rate of 0.6 ml/min at a temperature of 60°C. The inhibitory compounds (furfural and 5-HMF) were determined by Shimadzu HPLC using a C-18 column, mobile phase acetonitrile:water (20:80)% and UV detector at 280 nm.

## 2.5. Experimental design

For optimization of dilute sulphuric acid hydrolysis conditions for enhanced xylose extraction from sugarcane bagasse a three variable (temperature, concentration of H<sub>2</sub>SO<sub>4</sub>, and hydrolysis time) Box Behnken design (BBD) with three replicates at the center point was performed. The coded and actual levels of the variables are summarized in table 1.

**Table 1 Coded and actual levels of the variables for Box-Behnken design.**

Independent variables	Symbols	Coded and actual levels		
		-1	0	+1
Temperature (°C)	X <sub>1</sub>	100	115	130
Hydrolysis time (min)	X <sub>2</sub>	10	25	40
Acid load (Concentration of H <sub>2</sub> SO <sub>4</sub> % (v/v))	X <sub>3</sub>	0.5	2	3.5

Table 2 Box-Behnken design with experimental and predicted responses of dependent variable (xylose concentration g/L).

Run no.	Temperature (°C)	Hydrolysis time (min)	Acid load % (v/v)	Xylose (g/L)	
	X <sub>1</sub>	X <sub>2</sub>	X <sub>3</sub>	Experimental	Predicted
1	-1	-1	0	2.19	2.36
2	+1	-1	0	7.21	7.08
3	-1	+1	0	5.63	5.76
4	+1	+1	0	7.64	7.50
5	-1	0	-1	1.15	1.10
6	+1	0	-1	6.65	6.91
7	-1	0	+1	5.97	5.73
8	+1	0	+1	6.32	6.38
9	0	-1	-1	3.29	3.18
10	0	+1	-1	7.01	6.93
11	0	-1	+1	6.99	7.07
12	0	+1	+1	7.02	7.13
13	0	0	0	7.93	7.92
14	0	0	0	8.27	7.92
15	0	0	0	7.56	7.92

The experimental design consisted of 15 runs including three center points. The experimental data for xylose extraction was fitted using a second order polynomial function model:

$$Y = \beta_0 + \sum \beta_i X_i + \sum \beta_{ii} X_i^2 + \sum \beta_{ij} X_{ij} \quad (1)$$

Where: Y is the response;  $\beta_0$  a constant;  $\beta_i$  the linear coefficients;  $\beta_{ii}$  the squared coefficients; and  $\beta_{ij}$  the interaction coefficients.

The design and levels of variables with experimental and predicted xylose concentration from the dilute sulphuric acid hydrolysis of sugarcane bagasse are summarized in table 2. MINITAB statistical software 17.1 (Trial Version) was used for the analysis and optimization of the experimental data. Analysis of variance (ANOVA) was performed in order to evaluate the statistical significance of the model.

### **3. Results and discussion**

#### **3.1. Compositional characterization of sugarcane bagasse**

The compositional analysis of sugarcane bagasse is shown in table 3 with a comparison of results obtained in the present work to the literature values for the same biomass species. The composition of sugarcane bagasse in the present study was cellulose (40.27%), hemicellulose (30.13%), lignin (27.14%) and extractives (2.46%) on dry basis. Adeeyo [7] studied the compositional characterization of Nigerian sugarcane bagasse by the same method as we used in this study. The result of their research work was cellulose (35.28%), hemicellulose (33.28%), lignin (25.20%), extractives (2.14%) and 4.1% ash. Timung [12] obtained the chemical composition of Indian sugarcane bagasse as cellulose (40.15%), hemicellulose (22.78%), lignin (20.81%) using TGA method and extractives 0.9, 6.5 and 7.7% with hexane, ethanol and water as a solvent for extraction respectively.

The results of this study are comparable to other results done by various researchers as shown in table 3. The composition of sugarcane bagasse varies depending on the plant genetics, growth conditions, age and processing conditions, geographical locations, methods (procedures) developed for analysis, the type of solvents used in the compositional analysis [7, 13].

Table 3 Composition of sugarcane bagasse on dry basis (% w/w)

Cellulose (%)	Hemicellulose (%)	Lignin (%)	Extractives (%)	Ash (%)	Reference
40.27	30.13	27.14	2.46	-	Present study
35.28±1.2	33.28±0.8	25.20±1.1	2.14±0.6	4.1±0.3	[7]
40.15 ± 0.3	22.78 ± 0.2	20.81± 0.2	15.1	-	[12]
39	26.2	24	-	-	[14]
43	31	11	9	6	[15]

### 3.2. Optimization of dilute sulphuric acid hydrolysis of sugarcane bagasse

The second order polynomial model equation for the fitted data using coded values of independent variables and concentration of xylose as a response variable is:

$$\text{Xylose (g/L)} = 7.92 + 1.615X_1 + 0.956X_2 + 1.021X_3 - 1.646X_1^2 - 0.599X_2^2 - 1.244X_3^2 - 0.745X_1X_2 - 1.290X_1X_3 - 0.922X_2X_3 \quad (2)$$

Box Behnken design (BBD) with the experimental and predicted xylose concentration is shown in table 2. The p-value, t-value, linear, quadratic and interaction coefficients for the second order polynomial model are given in table 4. Analysis of variance (ANOVA) for the fitted quadratic model is shown in table 5. The model summary for regression coefficients ( $R^2 = 99.2\%$ , adjusted  $R^2 = 97.8\%$  and predicted  $R^2 = 92.8\%$ ) show that the quadratic model fits to the experimental data.

The t-test, F-values and p-values show relative significance of independent variables of quadratic polynomial model coefficients. A large t-stat value and p-value  $< 0.05$  indicates significance of the coefficient and the corresponding independent variable. Relative F-values of linear, interaction and quadratic coefficient indicate the significance of the individual effect of the independent variable and the magnitude of interaction between them.

From the ANOVA results shown in table 5, the F-value for the model, linear, quadratic, and interaction coefficients are 70.39, 120.47, 50.19, and 40.50 respectively. P-values for all the linear, interaction and square coefficients are < 0.05, which indicate that all variables have significant effect on dilute sulphuric acid hydrolysis of sugarcane bagasse. The Lack of Fit with F-value and p-value of 0.67 and 0.645 respectively indicates that Lack of Fit is not significant as compared to the pure error or in other words the model was significant.

Table 4 Model coefficients, t- and p-values for second order regression model

Term	Coefficient	t-value	p-value
Constant ( $\beta_0$ )	7.92	43.15	0.000
<b>Linear coefficients</b>			
Temperature ( $X_1$ )	1.615	14.37	0.000
Time ( $X_2$ )	0.956	8.51	0.000
Acid load ( $X_3$ )	1.021	9.09	0.000
<b>Quadratic coefficients</b>			
Temperature ( $X_1^2$ )	-1.646	-9.95	0.000
Time ( $X_2^2$ )	-0.599	-3.62	0.015
Acid load ( $X_3^2$ )	-1.244	-7.52	0.001
<b>Interaction coefficients</b>			
Temperature x Time ( $X_1X_2$ )	-0.745	-4.69	0.005
Temperature x Acid load ( $X_1X_3$ )	-1.290	-8.12	0.000
Time x Acid load ( $X_2X_3$ )	-0.922	-5.80	0.002

Table 5 ANOVA for quadratic model

Source	DF	SS	MS	F-value	p-value
Model	9	64.022	7.113	70.39	0.000
Linear	3	36.525	12.175	120.47	0.000
Quadratic	3	15.217	5.072	50.19	0.000
Interaction	3	12.280	4.093	40.50	0.001
Error	5	0.505	0.101		
Lack-of-Fit	3	0.253	0.084	0.670	0.645
Pure error	2	0.2522	0.1261		
Total	14	64.527			

DF is the degree of freedom; SS is the sum of squares; MS is the mean square; significant p values,  $p \leq 0.05$ ;  $R^2 = 0.992$ ; predicted  $R^2 = 0.928$ ; adjusted  $R^2 = 0.978$ .

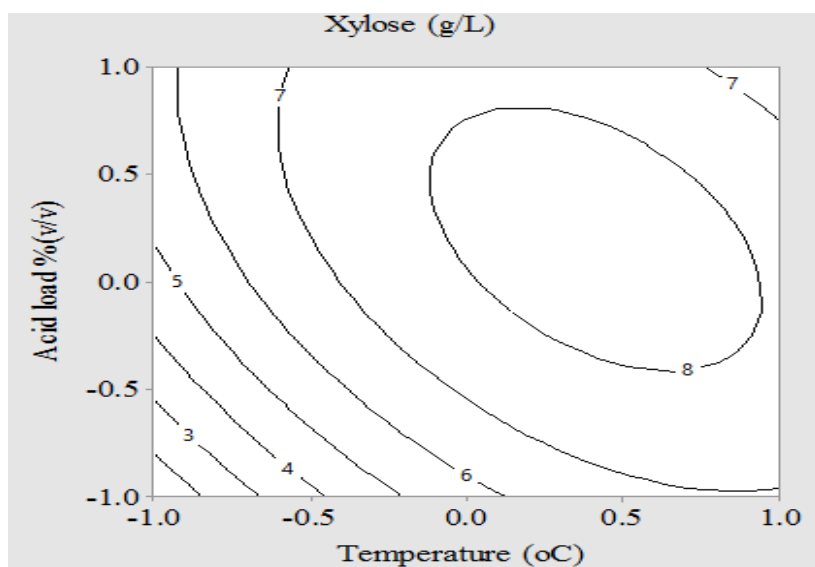
The contour plots xylose concentration (g/L) in the dilute sulphuric acid hydrolysis of sugarcane bagasse as a function of any two independent variables is shown in fig. 1. The contour plots; which are graphical representation of regression model equation 2; represent infinitive number of combinations of two test variables, with the third variable maintained at its zero (center point) level.

The contours were plotted to observe the interaction of two independent variables. An elliptical contour plot is obtained by the interaction of temperature with acid load fig. 1A indicating a strong interaction between the parameters. An elliptical nature contour plots are obtained in fig. 1B (temperature vs time) and fig. 1C (time vs acid load) indicating significant interaction between the variables. It is also confirmed by the t- and p-values of their interaction coefficients.

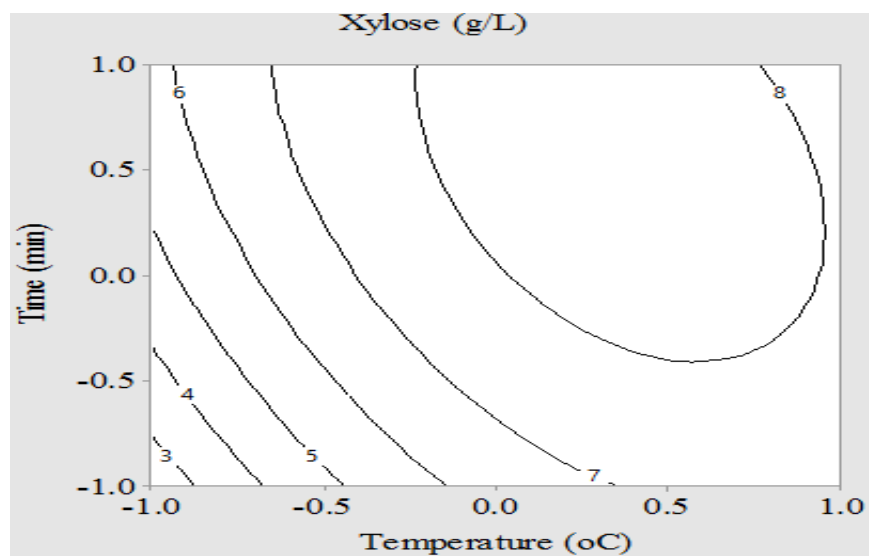
The maximum xylose concentration (8.27 g/L) was obtained at the center points i.e. 2% (v/v) H<sub>2</sub>SO<sub>4</sub> concentration, temperature of 115°C and 25 min (experiment run no. 14). The corresponding minimum xylose concentration (1.15 g/L) was obtained at 0.5% (v/v) H<sub>2</sub>SO<sub>4</sub> concentration, temperature of 100°C and 25 min (experiment run no. 5). This indicates that at lower temperature and acid concentration the xylose extraction was also lower. At higher temperature, lowering of the xylose concentration might be due to formation of by-products from the hydrolyzed xylose whereas the lower temperature was not sufficient enough to hydrolyzed sugarcane bagasse.

The optimum conditions for dilute sulphuric acid hydrolysis of sugarcane bagasse for maximum xylose concentration (8.49 g/L) with a corresponding yield of 84.9% by weight of hemicellulose under this model were 2% (v/v) H<sub>2</sub>SO<sub>4</sub> concentration, temperature of 120°C and hydrolysis time of 33 min. Other researchers have been studied that the optimal acid hydrolysis conditions for maximum xylose concentration (6.09 g/L) at a temperature of 120°C, 2.5% (w/v) H<sub>2</sub>SO<sub>4</sub> concentration and hydrolysis time of 90 min for corn stover [16]. Moutta [17] studied optimization of sugarcane leaves hydrolysis and obtained a maximum xylose concentration of (56.5 g/L) under the hydrolysis conditions of 2.9% (w/v) H<sub>2</sub>SO<sub>4</sub>, temperature (130°C), solid to liquid ratio (1:4) and hydrolysis time of 30 min and the researchers observed that a considerable inhibitory by-products were formed at this optimal conditions. Laopaiboon [2] obtained xylose concentrations (10.12, 6.48, 8.87 and 8.44 g/L) with H<sub>2</sub>SO<sub>4</sub> concentration (0.5, 2, 3, and 5%

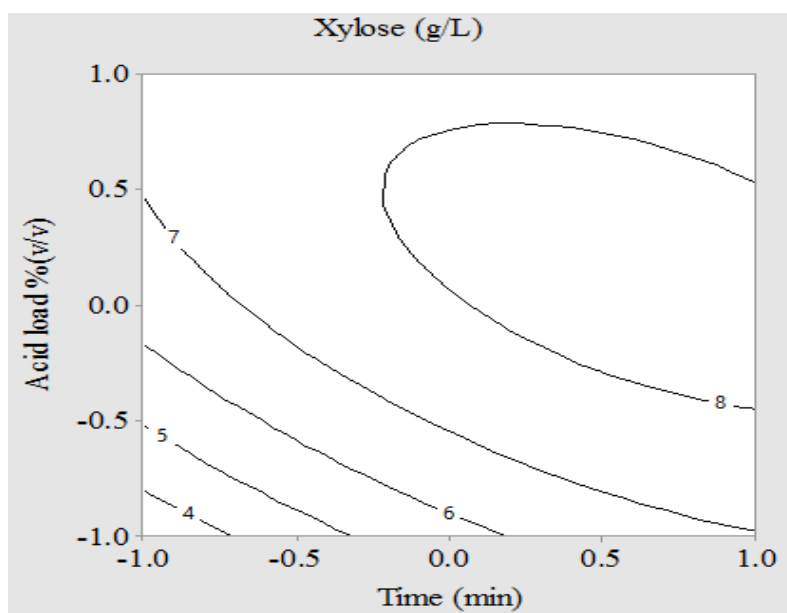
(v/v)) and hydrolysis time of (4, 2, 2 and 1 h) respectively at a temperature of 120°C from sugarcane bagasse.



(A)



(B)



(C)

Figure 1 Contour plots showing the interaction between two independent variables during dilute acid hydrolysis of sugarcane bagasse. (A) Interaction between temperature and acid load; (B) interaction between temperature and time; (C) interaction between time and acid load. The values of variables are shown in coded units.

### 3.3. Characterization of sugarcane bagasse hemicellulosic hydrolyzate

After completion of dilute sulphuric acid hydrolysis of sugarcane bagasse under optimum conditions, the hydrolyzate medium was analyzed for the presence of various sugar monomers and inhibitory compounds (Fig. 2). It was observed that the optimum conditions of acid hydrolysis allowed reaching a xylose concentration of 8.68 g/L corresponding to a yield of 86.8% by weight of hemicellulose fraction of sugarcane bagasse. However, the inhibitory compounds furfural and 5-HMF were also generated in a significant amount in dilute sulphuric acid catalyzed hydrolysis process of sugarcane bagasse which directly affect the fermentation efficiency of microorganisms used in the downstream process. Therefore, detoxification of these inhibitors should be considered during fermentation of the hydrolysate.

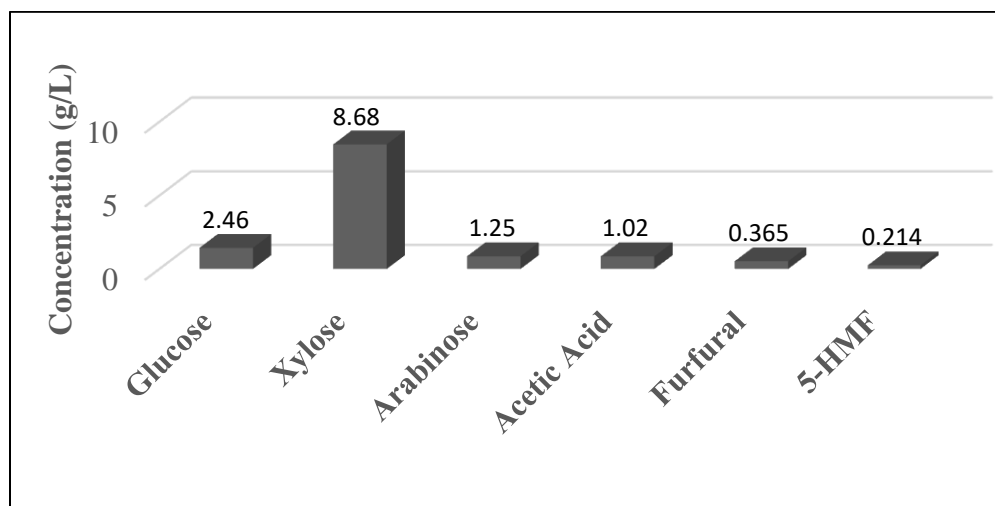


Fig. 2 Characterization of hemicellulosic hydrolyzate obtained by dilute sulphuric acid hydrolysis of sugarcane bagasse at the optimum conditions

#### 4. Conclusion

Under the optimum conditions for dilute sulphuric acid hydrolysis (a temperature of 120°C, 2% (v/v) H<sub>2</sub>SO<sub>4</sub> acid concentration and hydrolysis time of 33 min) we found a hemicellulosic hydrolysate with xylose concentration of 8.49 g/L, corresponding to the yield of 84.9% by weight of the hemicellulosic fraction of sugarcane bagasse. The results showed that sugarcane bagasse is a good potential lignocellulosic biomass for the production of biofuels and value added-chemicals.

The inhibitory compounds furfural and 5-HMF were also generate in a significant amount in experiments under optimized dilute sulphuric acid catalyzed hydrolysis process of sugarcane bagasse which directly affect the fermentation efficiency of microorganisms used in the downstream process. Therefore, detoxification of these inhibitors should be considered during fermentation of the hydrolysate.

## References

1. Himmel, M.E., et al., *Biomass recalcitrance: engineering plants and enzymes for biofuels production*. science, 2007. **315**(5813): p. 804-807.
2. Laopaiboon, P., et al., *Acid hydrolysis of sugarcane bagasse for lactic acid production*. Bioresource Technology, 2010. **101**(3): p. 1036-1043.
3. Harmsen, P., et al., *Literature review of physical and chemical pretreatment processes for lignocellulosic biomass*. Energy Research Centre of the Netherlands, 2010: p. 10-13.
4. Hosseini, S.A., et al., *Multiscale Modeling of Hydrothermal Pretreatment: From Hemicellulose Hydrolysis to Biomass Size Optimization*. Energy & Fuels, 2010. **24**(9): p. 4673-4680.
5. Lavarack, B., G. Griffin, and D. Rodman, *The acid hydrolysis of sugarcane bagasse hemicellulose to produce xylose, arabinose, glucose and other products*. Biomass and Bioenergy, 2002. **23**(5): p. 367-380.
6. Khuri, A. and J. Cornell. *Determining optimum conditions*. Response surface design and analyses 1987; 149-205].
7. Adeeyo, O., O.M. Oresegun, and T.E. Oladimeji, *Compositional analysis of lignocellulosic materials: Evaluation of an economically viable method suitable for woody and non-woody biomass*. American Journal of Engineering Research (AJER), 2015. **4**(4): p. 14-19.
8. Di Blasi, C., et al., *Product distribution from pyrolysis of wood and agricultural residues*. Industrial & Engineering Chemistry Research, 1999. **38**(6): p. 2216-2224.
9. Ayeni, A., et al., *Hydrogen peroxide and lime based oxidative pretreatment of wood waste to enhance enzymatic hydrolysis for a biorefinery: Process parameters optimization using response surface methodology*. Fuel, 2013. **106**: p. 187-194.
10. Ayeni, A., et al., *Optimization of pretreatment conditions using full factorial design and enzymatic convertibility of shea tree sawdust*. biomass and bioenergy, 2013. **48**: p. 130-138.
11. Sluiter, A., et al., *Determination of structural carbohydrates and lignin in biomass*. Laboratory analytical procedure, 2008. **1617**.

12. Timung, R., et al., *Effect of subsequent dilute acid and enzymatic hydrolysis on reducing sugar production from sugarcane bagasse and spent citronella biomass*. Journal of Energy, 2016. **2016**.
13. Rafiqul, I. and A.M. Sakinah, *Processes for the production of xylitol—a review*. Food Reviews International, 2013. **29**(2): p. 127-156.
14. Aguilar, R., et al., *Kinetic study of the acid hydrolysis of sugar cane bagasse*. Journal of Food Engineering, 2002. **55**(4): p. 309-318.
15. Martin, C., H.B. Klinke, and A.B. Thomsen, *Wet oxidation as a pretreatment method for enhancing the enzymatic convertibility of sugarcane bagasse*. Enzyme and Microbial Technology, 2007. **40**(3): p. 426-432.
16. Hong, E., et al., *Optimization of dilute sulfuric acid pretreatment of corn stover for enhanced xylose recovery and xylitol production*. Biotechnology and Bioprocess Engineering, 2016. **21**(5): p. 612-619.
17. Moutta, R., et al., *Statistical optimization of sugarcane leaves hydrolysis into simple sugars by dilute sulfuric acid catalyzed process*. Sugar tech, 2012. **14**(1): p. 53-60.

## Excitation wavelength dependent photoluminescence and its Origin in ZnO-MgO nanocomposite

<sup>1</sup>A. Ramachandra Reddy <sup>2</sup>Abebe Belay <sup>3</sup>Sowry Babu

<sup>1,2</sup>Adama Science & Technology University, Applied Physics Program

<sup>3</sup>A. Ramachandra Reddy

Department of Physics, National Institute of Technology Warangal, Warangal-506 004, Andhra Pradesh, India.

Email: [arcr.nitw@gmail.com](mailto:arcr.nitw@gmail.com)

### Abstract

*The excitation wavelength dependence of UV and green emissions of ZnO-MgO nanocomposite is investigated using the photoluminescence (PL) emission and excitation spectra. It is found that the position of green emission peak is independent of excitation wavelength. The analysis of PL excitation and emission spectra of samples confirmed that green emission is originated due to the transition of an electron from conduction band edge to deep trap level. It is also inferred that the green emission can be excited effectively only with the excitation wavelengths above the band gap energy. Contrary to the green emission, UV emission shifted continuously from 363 nm to 412 nm as the excitation wavelength changed from 320 nm to 370 nm. The effect of surface capping, defect concentration, quantum confinement effects on excitation wavelength dependent PL of ZnO is investigated in detail. These results confirmed that the shift of UV peak with excitation wavelength is due to the existence of intrinsic excited states above the conduction band edge of ZnO. However, the intensity of the UV emission peaks positioned at various wavelengths enhanced significantly with MgO capping.*

**Keywords:** ZnO nanocrystals; MgO; Excitation wavelength dependent Photoluminescence.

### Introduction

ZnO is one of the II-VI group semiconductors which is having a wide and direct band gap (~3.37 eV) and large exciton binding energy (~60 meV) at room temperature. Because of these unique properties, ZnO find potential applications in optical and optoelectronics area for several decades [1-2]. The emission property of ZnO plays very crucial in the above mentioned applications. The photoluminescence (PL) of ZnO generally exhibits an UV peak termed as near band edge emission (NBE) and a broad trap or deep level emission called green emission[3-4]. Unfortunately, there is no consensus on the origin of the green luminescence (GL) of ZnO. The PL of ZnO shows peculiar behavior at nano-dimensions. One of the most interesting features of these nanostructures is quantum confinement [5]. Another phenomenon is excitation wavelength dependence of ZnO nano structures [3, 6-11]. Djuricic *et al.* investigated the effect of excitation

wavelength on green, yellow and orange emissions from different ZnO nanostructures [6]. Their results demonstrated that green emission can be excited by excitation below the band edge, while the orange-red emission could be excited only by excitation above the band edge. Later, Irimpan *et al.* found that shift of the emission peak of ZnO from 345 nm to 475 nm with change of excitation wavelength from 230 to 355 nm [7]. Such kind of excitation wavelength dependence was attributed to the solvation and energy transfer. Zeng *et al.* also studied the excitation wavelength dependence of blue and green emissions from ZnO nanoparticles and concluded that green emissions can be excited only by energies larger than the bandgap energy [8]. They also found that the green emission originated from the transition from the conduction band to deep defect levels from excitation dependence PL and EPR results. Further, Zhang *et al.* studied the effect of excitation wavelength on visible emission and assigned the red shift of these peaks to quantum confinement effects [9]. Xu *et al.* also studied the excitation wavelength and size dependence of ZnO quantum dots (QD's) to clarify the transition mechanisms responsible for violet and green emissions [10]. Very recently, we found great enhancement in the UV emission intensity of ZnO nanoparticles only by changing the excitation wavelength. This is due to every PL peak corresponds to a special excitation wavelength [11]. Obviously, there has been a great deal of interest to understand the phenomenon responsible for the excitation wavelength dependent PL of ZnO.

In the present work, we have prepared ZnO nanoparticles coated with MgO to study the excitation wavelength dependence of the PL. The PL of ZnO/MgO core/shell nanocrystals showed only a sharp emission peak centered at 396 nm at 600 °C and a broad and intense green emission also developed at 900 °C. The violet emission was red shifted from 363 nm to 412 nm as the excitation wavelength changed from 320 nm to 370 nm. But the position of GL positioned at 503 nm did not change with excitation wavelength. The mechanism responsible for this anomalous behavior of ZnO/MgO core/shell nanocrystals was discussed in detail.

## **Experimental**

The ZnO/MgO core/shell nano crystals were prepared by the simple two stage method reported elsewhere [12]. First, aqueous solutions of Zn (NO<sub>3</sub>)<sub>2</sub>·6H<sub>2</sub>O and polyvinyl alcohol (PVA) in stoichiometric proportions were prepared. These two solutions were mixed together and stirred

for sufficient time. The stirring and heating continued until the gel like compound was formed. This gel type sample was dried at 150 °C for about 12 h in an oven to obtain ZnO nanoparticles in powder form. This powder was annealed at 600 °C to obtain pure ZnO nanocrystals. To prepare ZnO/MgO core/shell nanocrystals, aqueous solution of Mg (NO<sub>3</sub>)<sub>2</sub>·6H<sub>2</sub>O and NaOH were prepared to get 0.25M concentration and mixed together in the subsequent steps by stirring at 60 °C. The as prepared ZnO powder was added to this solution and stirred for four hours then aged and retrieved through filtering. The samples were thoroughly washed with water and ethanol several times. Finally, samples were annealed at a temperature of 600 °C and 900 °C to obtain ZnO/MgO core/shell nanocrystals. The samples were analyzed with High Resolution Transmission Electron Microscope. The PL spectra were acquired on Jobin Yuon spectro fluorometer equipped with 450 W Xenon arc lamp.

## Results and Discussion

Figure 1 shows the PL spectra of ZnO/MgO core/shell nanocrystals annealed at 600 °C and 900 °C. These PL spectra shows two emission peaks one in the UV region centered at 396 nm and another in the visible region termed as green emission positioned at 503 nm. In spite of the decades of research on luminescence of ZnO, the origin of green emission is still in dispute.

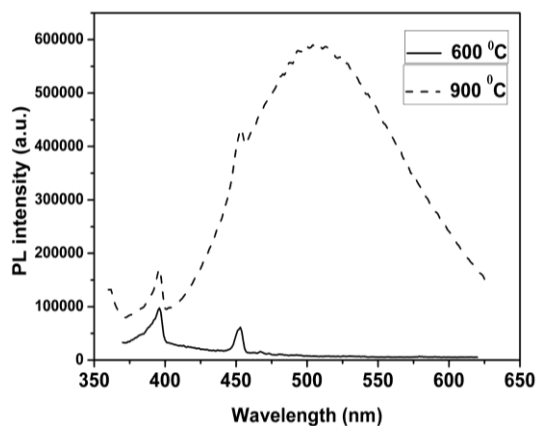
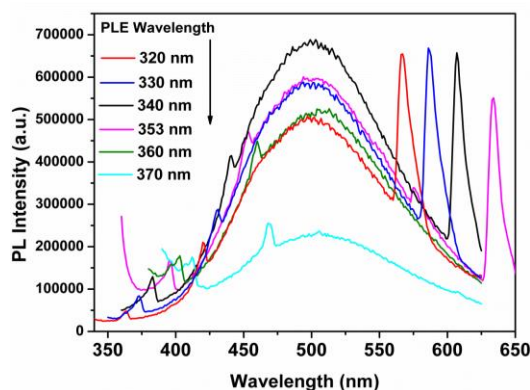


Fig. 2. PL spectra of ZnO-MgO nano composite acquired with different excitation wavelengths.

Recent studies of Zhang et al. and Xu et al. demonstrated that green emission originated due to the transition of an electron from conduction band to the deep level in amorphous ZnO films and quantum dots (QD's)[8, 10].

Fig. 1. PL spectra of ZnO-MgO nano composite annealed at 600 C and 900 C



It was found that these deep levels are caused by the oxygen vacancies in the sample. However, it is widely accepted that the broad green emission band is due to oxygen vacancies. Recently, excitation-dependent emission has become an effective approach to link the excitation and emission process and it has been employed to understand the visible emissions of ZnO [6-10]. So, the PL spectra of ZnO-MgO nanocomposites were acquired with different excitation wavelengths and are shown in Fig 2. As can be seen from the Fig.2 the change in excitation wavelength from 320 nm to 370 nm has no effect on the position of the broad green emission band centered at 503 nm. However, the intensity of the green emission first increases and reaches its maximum as the excitation wavelength increased from 320 nm to 340 nm and afterwards decreases for 353, 360 and 370 nm excitation wavelengths. Very recently, similar variation in the intensity of green emission was observed by Xu et al. in ZnO QD's with increase in excitation wavelength. But the intensity decreased abruptly for excitation wavelengths below 340 nm which corresponds to the band gap of QD's. In this study, the green emission intensity decreases gradually even for excitation wavelengths larger than band gap energy (3.51 eV or 353 nm). This indicates that the green emission can be excited effectively only by photons with energy above band gap energy ( $E_g$ ). This result is contrary to the results of Djrisic et al. they found that green emission can be excited only by the energies below the band gap energy [6]. This could be due to the assignment of different types of defects that are responsible for the green emission. To know the transition responsible for this broad green emission band, the PLE spectra were measured by monitoring the emission wavelengths at 396 nm and 503 nm. As shown in Fig. 3, the PLE spectrum acquired by monitoring the emission wavelength at 396 nm exhibited a peak at 353 nm. This peak at 353 nm corresponds to the band gap energy of ZnO nanocrystals. The PLE spectrum obtained by monitoring the emission wavelength at 503 nm showed an intense and broad peak centered at 350 nm. This indicates that the electrons excited to the same state for UV and green emissions and hence it can be concluded that green emission is originated due to the transition of an electron from conduction band to the deep level. Such a deep trap is usually known to originate from oxygen vacancy defects, which are assumed to be the most likely recombination centers involved in the green emission of ZnO [8, 10].

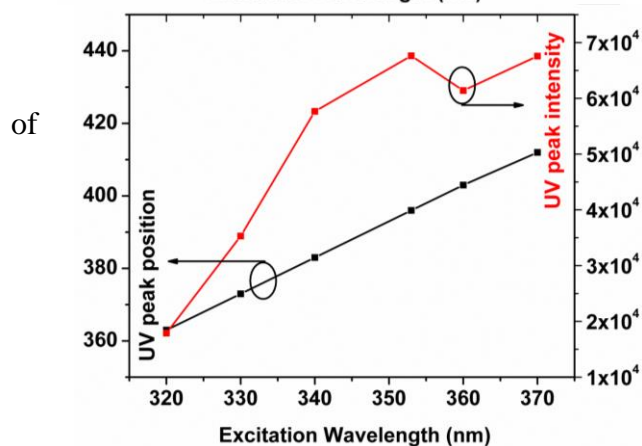
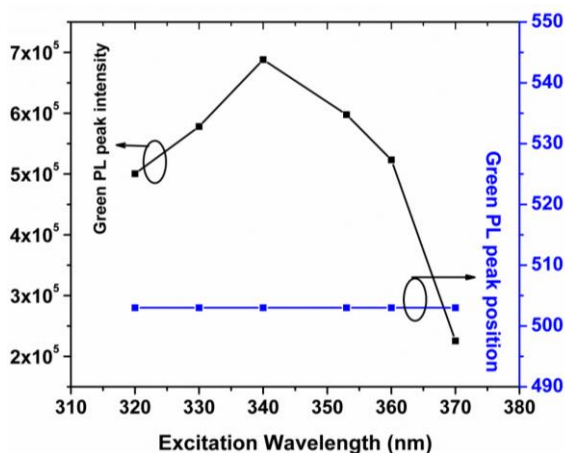


Fig. 3. Peak position and intensity variations green emission and UV emission peaks with excitation wavelengths.

Figure 2 also shows that the UV emission peak red shifted linearly as the excitation wavelength increased from 320 nm to 370 nm. It was reported that accumulation of internal strain or an increase of defect concentration caused the red shift of the emission peaks in amorphous porous anodic alumina membrane with increase of excitation wavelength [13]. To understand the effect of strain on excitation wavelength dependent UV peak, the PL spectra of ZnO/MgO core/shell nanocrystals annealed at 600 °C recorded with different excitation wavelength. It has relatively lower strain or defect concentration compared to the sample annealed at 900 °C. Figure 3 shows the variations in peak position and intensity of UV peak with increase in excitation wavelength. The UV peak red shifted linearly from 363 nm to 412 nm with increase in excitation wavelength from 320 nm to 370 nm. Such a red shift may be due to the shorter wavelength component of emission disappears with increasing excitation wavelength [10]. The shift and intensity variations are exactly similar to that are observed in the ZnO/MgO core/shell nanocrystals annealed at 900 °C.

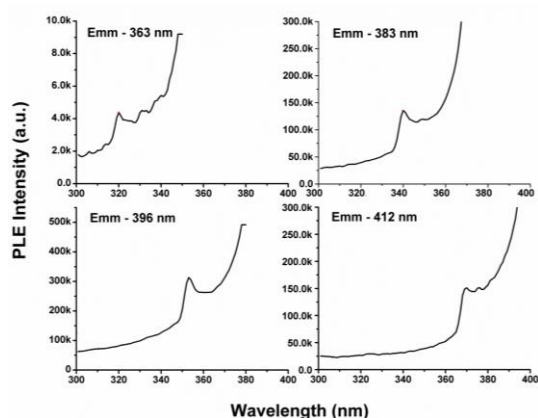


Fig. 4. PL excitation spectra of ZnO-MgO nano composite annealed at 900 C.

From these results, it can be inferred that shift of the UV emission should not be due to the internal strain or increase of defect concentration. In the view of the preparation and characterization methods of samples the excitation wavelength dependence of the PL bands cannot also be attributed to the presence of energetically different associated forms of the constituent molecules and slow rate of the excited state relaxation process [7]. Furthermore, possible reasons reported in the literature for the shift of the emission peaks are quantum confinement effect and surface capping [6, 14]. According to the HR-TEM pictures of ZnO/MgO core/shell nanocrystals, there is no large size distribution or in other words the size of the particles is nearly uniform. Figure 4 shows the PLE spectra acquired by monitoring the emission wavelengths at 363 nm, 383 nm, 396 nm and 412 nm from ZnO/MgO core/shell nanocrystals annealed at 600 °C. It is evident from this plot that the PLE peak shifted monotonously with increase of excitation wavelength. But such a huge and linear shift should not be due to the variation in the band gap caused by the size in homogeneity. Hence, we believe that excitation wavelength dependent PL is due to the surface capping of ZnO nanocrystals with MgO. To explore the effect of surface capping, the PL spectra of pristine ZnO nanocrystals were recorded with different excitation wavelengths. The shapes of the PL spectra are nearly same for excitation wavelengths 320 nm, 330 nm and 340 nm. But the shape changed abruptly for excitation wavelength of 353 nm and a sharp UV emission peak is evolved. However, very weak UV emission peaks can be seen at 363 nm for 320 nm excitation wavelength and at 383 nm for 340 nm excitation wavelength respectively. This indicates that pristine ZnO nanoparticles themselves showing the excitation wavelength dependent PL but the intensity of emission peaks is not appreciable. So, from the PL and PLE of ZnO and ZnO-MgO nanocomposites, it is easy to

understand that there exist a set of excited states even in the pristine ZnO nanoparticles above the band edge (353 nm). Further, transitions are taking place from the set of excited states which are above the band edge to the valence band. These results demonstrate that each excited has its own characteristic emission peak above the band edge. But, in the case of ZnO-MgO nanocomposite, intensity of UV peaks at 363 nm, 373 nm and 383 nm enhanced significantly. It implies that, MgO capping is enabling the more number of transitions from the excited states that are above the band edge to the valence band. As a result of it intensities of UV emission peaks positioned at 363 nm, 373 nm, 383 nm and 396 nm enhanced significantly. Finally, these results confirmed that green and UV emissions are excited effectively with the excitation energies above the band gap. This is contrary to the results of Xu et al. they observed that Green emission can be excited effectively at energies higher than the band edge and UV emission with energies below the band edge emissions.

## **Conclusions**

In summary, the effect of excitation wavelength on green and UV emissions were studied in detail using the PL emission and PL excitation spectra of ZnO and ZnO-MgO nanocomposites. It was found that (i) green emission is originated due to the transition of an electron from conduction band edge to the deep level (ii) green emission can be excited effectively only with the excitation wavelengths above the band gap energy (iii) the position of the green emission is independent of the excitation wavelength. Contrary to this, UV emission peak red shifted from 363 nm to 412 nm monotonously with increase in the excitation wavelength from 320 nm to 370 nm. This kind of shift is due to the presence of intrinsic excited states that are present in the ZnO nanoparticles above the conduction band edge. It is also observed that transitions from the excited states above the conduction band edge to valence band were enhanced significantly with ZnO-MgO nano composite.

## Reference

1. Y. Qin, X. Wang, and Z. L. Wang, *Nature (London)* 451, 809 (2008).
2. Z. L. Wang and J. Song, 242 (2006).
3. D. Bera, P.H. Holloway and H. Yang 2008 Time-evolution of photoluminescence properties of ZnO/MgO core/shell quantum dots *J. Phys. D: Appl. Phys.* 41 182002
4. A. van Dijken, E. A. Meulenkaamp, D. Vanmaekelbergh, and A. Meijerink, *J. Phys. Chem. B* 104, 1715 (2000).
5. X. L. Wu, G. G. Siu, C. L. Fu, and H. C. Ong, *Appl. Phys. Lett.* 78, 2285(2001)
6. A. B. Djurišić, Y. H. Leung, K. H. Tam, L. Ding and W. K. Ge, H. Y. Chen and S. Gwo, Green, yellow, and orange defect emission from ZnO nanostructures: Influence of excitation wavelength, *Appl. Phys. Lett.* 88, 103107 (2006)
7. Irimpan, B. Krishnan, A. Deepthy, V.P.N. Nampoori, P. Radhakrishnan, Excitation wavelength dependent fluorescence behaviour of nano colloids of ZnO, *Journal of Physics D: Applied Physics* 40(2007) 5670–5674.
8. W.C. Zhang, X.L. Wu, H.T. Chen, J. Zhu, G.S. Huang, Excitation wavelength dependence of the visible photoluminescence from amorphous ZnO granular films, *Journal of Applied Physics* 103(2008) 093718.
9. H. Zeng, G. Duan, Y. Li, S. Yang, X. Xu, W. Cai, Blue Luminescence of ZnO Nanoparticles Based on Non-Equilibrium Processes: Defect Origins and Emission Controls, *Adv. Funct. Mater.* 2010, 20, 561–572.
10. X. Xu, C. Xu, Z. Shi, C. Yang, B. Yu, J. Hu, Identification of visible emission from ZnO quantum dots: Excitation-dependence and size-dependence, *J. Appl. Phys.* 111, 083521 (2012).
11. Sowri Babu K, Ramachandra Reddy A, Sujatha Ch, Venugopal Reddy K. Optimization of UV emission intensity of ZnO nanoparticles by changing the excitation wavelength. *Materials Letters* 2013; 99: 97–100.
12. K. Sowri Babu, A. Ramachandra Reddy, K. Venugopal Reddy, Controlling the size and optical properties of ZnO nanoparticles by capping with SiO<sub>2</sub>, *Materials Research Bulletin* 49 (2014) 537–543
13. B. S. Zou, V. V. Volkov, and Z. L. Wang, *Chem. Mater.* 11, 3037 (1)

## **IN VITRO Screening of Sugarcane (*Saccharum officinarum* L.) Genotypes for Salt Tolerance**

**MEBRAHTOM FTWI<sup>1</sup>, FIREW MEKBIB<sup>2</sup> AND EYASU ABRAHA<sup>3</sup>**

<sup>1</sup>Ethiopian Sugar Corporation, Research and Training, Nazareth, Ethiopia, email: [mebreftwi@gmail.com](mailto:mebreftwi@gmail.com)

<sup>2</sup>Haramaya University, P.O Box 138 Dire Dawa, Ethiopia, email: [Firew.mekbib@gmail.com](mailto:Firew.mekbib@gmail.com)

<sup>3</sup>Tigray Agricultural Research Institute, P.O Box -492, Mekelle, Ethiopia, email: [eyasuabraham@gmail.com](mailto:eyasuabraham@gmail.com)

### **Abstract**

*Salinity is one of the main problems affecting sugarcane production in Ethiopia. This investigation was conducted to evaluate sugarcane genotypes for salinity tolerance under in vitro and field condition. Explants of three sugarcane varieties were regenerated directly and indirectly (through somaclonal variation), and evaluated for salinity tolerance based on their callus induction and shoot regeneration potential at MS supplemented with different salt concentrations (0-240 mM). The analysis of variance for percent of callus induction and shoot regeneration indicated that there was highly significant difference ( $P \leq 0.01$ ) among varieties and salt concentrations used. At root regeneration, eighteen (18) root regenerants (genotypes) were developed from salt tolerant and healthy shoot regenerants. These were further screened for salinity tolerance using root regeneration percentage, number of roots per plantlet, length of roots per plantlet, length of whole plantlet and shoot number per plantlet. Results showed variability ( $P \leq 0.01$  among regenerants significantly) and significant salt effects ( $P \leq 0.01$  while these regenerants showed inconsistent performance for root regeneration percentage, number of shoots per plantlets. Among the regenerants screened, S4SP-70-1284, S4 C0-501 and S2B-78-505 showed relatively considerable salt tolerance under in vitro and at field conditions. The cluster analysis conducted to assess the existed variability among regenerants with respect to the two regeneration pathways used demonstrated the existence of marked variability among regenerants. The improved tolerance to salinity in the selected in vitro developed regenerants would be valuable in enhancing the diversity of sugarcane varieties with high degree of salt tolerance suitable for salt prone sugarcane production areas in Ethiopia. We recommend these regenerants be used as a source of variability for future stress breeding studies and to be used as alternative varieties in the salt affected sugarcane production areas. Thus, this study is an important step forward in improving salt tolerance of sugarcane using in vitro screening techniques.*

**Key words:** Direct Regeneration, Evaluation, Genetic Variation, Indirect Regeneration, Tissue Culture

### **Introduction**

Abiotic stresses have undesirable effects on growth (Wang *et al.*, 2001), production (Rengasamy, 2010) and physiology (Cha-um *et al.*, 2012) of crops. Agronomically improved

sugarcane varieties endowed with tolerance to biotic and abiotic stresses are highly beneficial, as unfavorable environmental factors challenging cultivation and crop productivity (Suprasanna *et al.*, 2011). The complexity and polygenic nature of salinity tolerance has further limited the efforts to develop the tolerant crop varieties through conventional breeding practices (Jain 2005). Breeding of crops for salt tolerance would be the milestone to improve crops under such stresses but appropriate methods that can tackle the problems should be followed (Vasantha *et al.*, 2009). However, physiological mechanisms that determine the level of tolerance to the specific stress are complex and are controlled by polygenes and unavailable of high throughput screening methods and limited selection criteria have negatively impacted on the progress of stress tolerance breeding.

The conventional breeding programs are being used to integrate genes of interest from inter crossing genera and species into the crops to induce stress tolerance. However, in many cases, these conventional breeding methods have failed to provide desirable results (Rai *et al.*, 2011) especially in sugarcane owing to its inherent polyploidy and limited flowering rate and successful crosses. The serious obstacles to genetic improvement of salinity tolerance are the diversity of physiological mechanisms that determine the level of tolerance to salinity or drought, their multigenic nature of inheritance, the lack of appropriate screening methodology, appropriate selection criteria for evaluation of germplasm, and segregating material (Subbarao and Johansen, 1999). Moreover, Conventional methods have greatly contributed to crop improvement; however limitations such as complex genome, narrow genetic base, poor fertility, susceptibility to biotic and abiotic stresses and long duration to breed elite cultivars still impose a challenge (Suprasanna *et al.*, 2011). The time spent for this multiplication is also considered a serious economic problem, mainly in view of the higher yields that would be obtained by planting the new variety earlier on a large commercial scale is another tiresome task (Biradar *et al.*, 2009).

Currently, plant tissue culture is an optimistic tool to generate significant and useful genetic variability for stress tolerance in terms of the desired traits in short period of time. Salt stress is one of the important abiotic stresses for commercial crops and successful isolation of salt tolerant lines has been exploited using a number of plant materials (callus, suspension

cultures, somatic embryos, shoot cultures, etc.) which has been screened for variation in their ability to tolerate relatively high levels of salt in the culture media. Somaclonal variation is one of the sources of variability for salinity tolerance (Perez-Clemente *et al.*, 2012). Ample variability in salt tolerance has been observed *in vitro* in sugarcane (Raesjwari *et al.*, 2009; Mohammed *et al.*, 2011).

Salinity is the major sugarcane production constraints in Ethiopia, especially at Metahara Sugar Estate. A study made by Girma (1993) on salinity and sodicity status of the Metahara Sugar Estate showed the presence of salinity and sodicity problems in which the yield of certain fields is decreasing and a significant area of cultivated lands are abandoning, which is attributed to the expansion of saline Lake Basaka (Megersa *et al.*, 2009) and improper use of irrigation water (Tate, 2009). Despite these problems, successful research on development of sugarcane varieties tolerant to salt stress on salt affected fields have not been conducted as appropriate methodologies that help to isolate drought tolerant sugarcane varieties at field condition have not been well developed. These technical problems demand the use of tissue culture to screen and develop salt tolerant sugarcane varieties and developed regenerants under *in-vitro* condition. Therefore, the objective of this study were to screen sugarcane genotypes for salinity tolerance under *in vitro* condition, assess variability among genotypes on the basis of the two regeneration pathways used and validate their tolerance at salt affected field conditions.

## **Materials and Methods**

### **Explants Selection**

Healthy young leaf sheath explants of 4 month age cane of three commercial sugarcane varieties collected from Wonji sugarcane research center was used for indirect propagation and meristem was also used for direct propagation simultaneously. The basis for selecting these varieties to be evaluated for salt tolerance under *in vitro* condition was based on their salt tolerance background under field evaluation and local history. Accordingly, sugarcane varieties B78-505 (tolerant), SP 70-1284 (moderate) and C90-501 (susceptible) were used for this experiment. The explants were excised properly using knife and washed using drop of

tween 20 and 10%NaCl (Barakina) and drop of soup solution for 10 minutes. Then the explants were immersed in to 0.25% of redimol and bayeloton /100 ml of water for 30 minutes which is used to remove the fungal and bacterial contaminants. Then the explants were excised properly and some sheathes of the explants were pilled and immersed in to 20%of Na<sub>2</sub>OCl for 5 minutes. After rinsed by using of DH<sub>2</sub>O (deionized water) for three times, the explants were immersed in to 0.25% of HgCl<sub>2</sub> to kill microbes that were present in the explants.

### **Treatments and Culture Methods**

In the first culture (callus induction), four types of media preparations namely; (i) MS+30 gL<sup>-1</sup> sugar+4 gL<sup>-1</sup> agar+1.5 mgL<sup>-1</sup> of 2, 4-D (ii) MS+30 gL<sup>-1</sup> + sugar + 4 gL<sup>-1</sup> agar +3 mgL<sup>-1</sup> of 2, 4-D (iii) MS+30 gL<sup>-1</sup> sugar+3 mgL<sup>-1</sup> of 2, 4-D (without agar) and (iv) MS+30 gL<sup>-1</sup> sugar+4 gL<sup>-1</sup> agar+3 mgL<sup>-1</sup>BAP+3 mgL<sup>-1</sup> IBA were used. Of these different media preparations used, the media MS+30 gL<sup>-1</sup> Sugar + 4 gL<sup>-1</sup> agar+3 mgL<sup>-1</sup> of 2, 4-D was the most convenient media combination as it relatively produced good callus both in quality and quantity and embryogenic calli were established from healthy young leaf sheath explants of popular sugarcane varieties. After callus induction, the calli were cut in to small pieces and re-inoculated on callus induction medium for selection of salt tolerant calli. Embryogenic calli were identified of glossed aspect, compact, characterized by their yellow color and their globular structure, while the non-embryogenic callus are of wet aspect, translucent and of more brownish in color. In the second culture, salt tolerant calli were sub-cultured on fresh MS+30 gL<sup>-1</sup> sugar + 4 gL<sup>-1</sup> agar +1 gL<sup>-1</sup> BAP+0.5 mgL<sup>-1</sup> IBA for shoot regeneration. In the third culture, salt tolerant and healthy initiated shoots were separated and were sub-cultured again on fresh medium with ½ MS+30 gL<sup>-1</sup> sugar+4 gL<sup>-1</sup> agar+5 gL<sup>-1</sup> NAA for root development. In all culture methods used (callus induction, shoot regeneration and root regeneration mediums), MS medium was supplemented with five levels of NaCl, i.e. 0 mM, 30 mM, 100 mM, 170 mM, and 240 mM and selection was done based on lethal dosage of NaCl. For comparison purposes, plantlets were direct regenerated simultaneously using meristem culture on the same MS media but without 2, 4-D and screened for salt tolerance at the same salt regimes.

## **Experimental Design and Treatment Combination**

The experiment was a factorial experiment of two factors and arranged in Completely Randomized Design. The first factor was variety where three sugarcane varieties B78-505, SP70-1284 and CO-501 were included. The second factor was salinity where five salinity levels (0, 30, 100, 170 and 240 mM NaCl) were supplement to MS medium in all cultures. The experiment was repeated (replicated) three times for all cultures. During the field evaluation, RCBD design with two replications was used and the successfully acclimatized and *in vitro* developed genotypes and the three locally grown varieties (B78-505, SP70-1284 and CO-501) were included in the field evaluation. But SP70-1284 was the only survived local variety and the four *in vitro* developed salt tolerant genotypes were evaluated at salt affected field condition along with SP70-1284. Each genotype was planted at plot size of 16 m<sup>2</sup> (4 m x 4 m) with planting ratio of one plantlet to one double budded seed set at recommended spacing.

## **Data Collected**

Percent of Explants Inducing Callus (PEIC): Leaf sheath of 20 explants per treatment was used for callus induction and callus was induced for all varieties and data for percentage of explants inducing callus was collected for each treatment five weeks after inoculation. 40 days after inoculation, the calli were cut in to small pieces and re-inoculated on callus induction medium and calli that are white with vigorous growth were selected as salt tolerant calli for further evaluation.

Shoot Regeneration Percentage (SRP): after two consecutive subcultures, salt tolerant calli (Sixteen pieces of callus per treatment) were transferred in to shoot regeneration medium and data for shoot regeneration percentage was collected for each treatment. After shoot regeneration, salt tolerant and healthy shoots were selected from each culture, labeled and multiplied before transferred to rooting medium.

## **Shoot and Root Related Data**

After shoot multiplication, 40 healthy shoots were selected for each labeled regenerant and transferred to rooting medium containing different salt levels of 0, 30, 100 170 and 240 mM NaCl. Plantlets of different regenerants were evaluated based on their mean performance per

treatment. Data for root regeneration percentage (RRP), root number/plantlet (RNPP), root length per shoot (RLPS), average shoot number/plantlet (ASNPP) and whole plantlet length (WPL) of root regenerants screened at different levels of salt stress were recorded. Reduction%:reduction% in performance of a regenerant evaluated at salt induced selection medium relative to the performance of the same regenerant recorded at salt free selection medium. It was calculated as

$$= \frac{(\text{Values at salt free selection medium} - \text{Values at salt selection medium}) * 100}{\text{Values at salt free selection medium}}$$

Acclimatization of regenerated plants: Regenerated plants bearing well developed roots were transferred to greenhouse for acclimatization were grown in beds in greenhouse and survival % of the *in vitro* developed plantlets was recorded. After 20 days of acclimatization, the plantlets were transferred to salt affected field and evaluated for tillering capacity (tiller number), stalk population and height. Data for numbers of tillers ( $\text{ha}^{-1}$ ) were recorded four months after planting date while data for stalk population and height were recorded at 11 months after planting date.

## Data Analysis

Data were subjected to analysis of variance and interaction means were separated through Tukey's multiple mean comparison test and means of main effects were separated by LSD using the SAS software package (SAS, 2009). Data transformation was carried out prior to statistical analysis as suggested by Steel and Torrie (1981). The calculated Euclidean distance was used to construct Dendrogram based on average linkage method using MINITAB V. 17.

## RESULTS AND DISCUSSION

### Callus Induction and Shoot Regeneration of Sugarcane Varieties Evaluated at MS Medium Supplemented with Different Salt Concentrations

Analysis of variance for data collected during *in vitro* callus induction and shoot regeneration are provided in Table 1. Variety and salt effects were highly significant ( $P \leq 0.01$ ) for both percent of explants induced callus and shoot regeneration percentages. The interaction effect of variety and salt was nonsignificant ( $P > 0.05$ ) for percent of explants inducing callus while

highly significant ( $P \leq 0.05$ ) interaction was observed between varietal and salt effects for shoot regeneration percentage. Similar result was reported by Shomeili *et al.* (2011); Avinash *et al.* (2012) and Gadakh *et al.* (2015). The significance of variety and salt effects indicated varieties varied in inducing callus and regenerating shoots from callus which is dependent on salt concentration while the significance of the interaction suggested varieties showed consistent response in inducing callus across all salinity levels used. The significant effect of variety and salt interaction revealed shoot regeneration potential of varieties was inconsistent across the salt concentrations used which are in agreement with report of Begum and Islam (2015). This is because plants regenerated from organ cultures, calli, protoplasts and via somatic embryogenesis sometimes exhibit phenotypic and/or genotypic variations (Orbovic *et al.* 2008).

Table 1: Mean squares for sugarcane varieties evaluated at different levels of Salt under *in vitro* condition

Sources of Variation	DF	PEIC (%)	SRP (%)
Variety	2	3409.3**	2686.9**
Salt level	4	1370.3**	1808**
Var*salt	8	147.58ns	127.27**
Error		104.32	57.22
CV		16.5	16
Mean		61.93	47.28

\*\*significant at 1%; \*significant at 5%; ns=nonsignificant; PEIC =Percent of Explants Induced Callus and SRP=Shoot Regeneration Potential

### **Effect of Variety on Callus Induction and Selection of Salt Tolerant Calli**

As the interaction effect of variety and salt stress was nonsignificant for percent of explants induced callus (Table 1), only the effect of variety and salt on percent of explants induced callus was discussed. Mean comparison presented in Table 2 indicated the higher % of explants (75.17%) induced calli were from Variety C0-501 while the % of explants induced callus in variety SP 70-1284 was lower (44%), suggesting callus induction was genotype dependent which is consistent with reports of Gandonou *et al.* (2005) where the varieties included in their study showed different callus inducing ability. The high potential in embryogenic callus induction of C0-501 and B78-505 lead us to suggest these varieties to be

used as good model sugarcane varieties for future studies of physiological mechanisms associated with *in vitro* salt tolerance in sugarcane and *in vitro* selection salt tolerant lines.

Regarding to the effect of salt on callus induction, 74.44%, 71.83, 64.77%, 53% and 45% of explants induced calli at 0, 30, 100, 170 and 240 mM NaCl selection mediums respectively. This declining trend in callus induction of the explants with increasing salt concentration of MS medium highlighted the higher salt concentration reduced the callus inducing ability of the varieties. In the present study, however, salt tolerant, healthy and vigorous calli (Fig. 1 a, b, c) were identified from all varieties at 170 mM NaCl selection medium and were selected for further evaluation. Our result was similar to reports of Patade and Suprasanna (2009) where salt tolerant calli were isolated at MS medium supplemented with 171.5 mM NaCl. Results of the present study are in close agreement with those reported by Gandonou *et al.* (2005), Kenganal *et al.* (2008); Patade and Suprasanna (2009); Shomeili *et al.* (2011); and Gadakh *et al.* (2015). But opposite results were reported by Gandonou *et al.* (2006), Ashraf *et al.* (2007) and Karpeet *et al.* (2012) where salt tolerant calli were identified on MS medium supplemented with 68, 100 and 100 mM NaCl respectively. Moreover, morphological and color changes were observed among the calli of all varieties treated with 240 mM NaCl (Fig. 1 d, e, f) and growth of calli sharply reduced which is consistent with reports of Patade and Suprasanna (2009) in which all calli exhibited morphological and color changes at 256.7 mM NaCl.

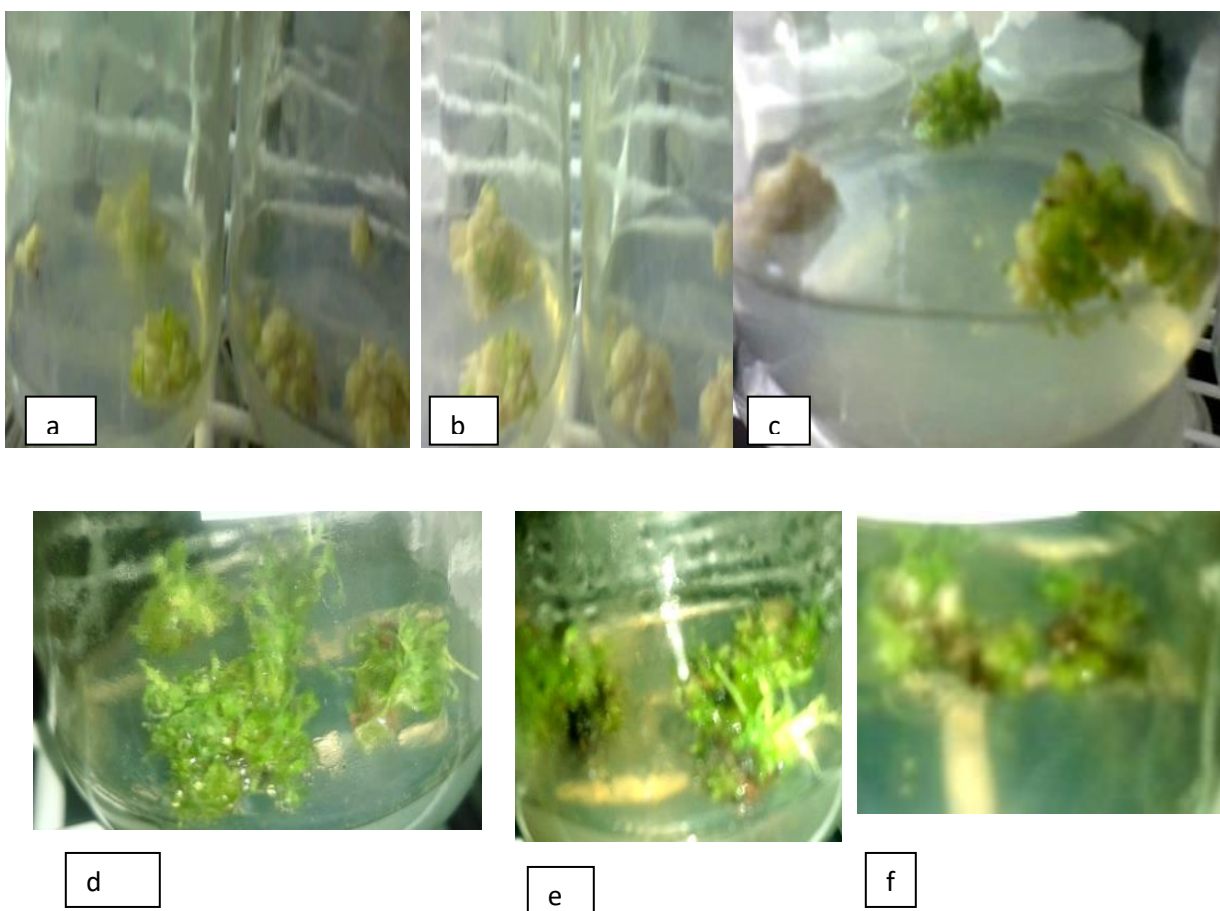


Figure 1: Callus induction of (a) B78-505, (b) CO-501 and (c) SP70-1284 selected on MS medium with 70 Mm 100 Mm and 100 mM respectively (d) shoots regenerated from varietyB78-505 at 170 mM, (e) shoots regenerated from callus cultures of variety CO-501 at 100 mM and (f) shoots regenerated from callus cultures of variety SP 70-1284 at 30 mM.

This result is in agreement with reports of Karpeet *et al.* (2012) where salt tolerant calli were found on up to 100 Mm salt in MS medium but opposite with results reported by (Suprasanna, 2009) in which tolerant calli were isolated at MS medium supplemented with 171.5 Mm salt level. Moreover, there has been observed that some morphological changes among the callus cultures (Fig. 1) similar to the results reported by Gandonou *et al.* (2005) but no color change (browning) was observed which is in contrary with finding reported by Munir and Aftab (2013). On the contrary, the number of explants induced callus in variety SP 70-1284 were relatively low (44%) and low in quality (Fig. 1f). In the absence of salt stress (0 Mm), higher

number of explants from all varieties induce callus (74.44%) while it was low (45%) when the salt stress level was increased to the higher level (240 mM).

Table 2: Variety and salt effects on percent of explants callus induced callus (PEIC)

Varieties	PEIC (%)
B78-505	67.82a
SP70-1284	44.80b
C90-501	75.17a
LSD <sub>0.05</sub>	7.64
<b>Salt levels</b>	
0	74.444a
30 mM	71.833a
100 mM	64.778a
170 mM	53b
240 mM	45b
LSD <sub>0.05</sub>	9.86

\*Means with same letters are not statistically significant at  $\alpha=0.05$ ; PEIC =Percent of Explants Induced Callus

### **Variety and Salt Effects on Shoot Regeneration and Selection of Salt Tolerant Shoot Regenerants**

In the absence of salt (0 mM NaCl), 78.67% of callus cultures of variety B78-505 regenerated healthy shoots which is significantly higher than shoots regenerated from callus cultures of other varieties while lower % (55%) of callus cultures from variety SP70-1284 regenerated shoots (Table 3). The result suggests varieties varied in their ability in regenerating shoots from salt tolerant calli evaluated at salt free MS shoot regeneration medium. At 100 mM NaCl selection medium, the higher % of callus cultures (60.34%) regenerated shoots were from variety C0-501 where lower % of callus cultures (45.30%) from variety B78-505 regenerated shoots. Moreover, 56, 39 and 53.50 % of callus cultures from varieties B78-505, SP70-1284 and C0-501 respectively regenerated healthy and vigorous shoots at 170 mM NaCl selection medium where salt tolerant shoot regenerants were identified. However, 38.72, 23.6 and 14.34% of callus cultures that regenerated shoots at 240 mM NaCl were from varieties B78-505, CO-501 and SP70-1284 respectively. But most of the regenerated shoots were not healthy enough to be transferred in to rooting medium for further evaluation, indicating this level of salt stress adversely affected shoot regeneration even from salt tolerant calli.

Table 3. Interaction effects of variety and salt on shoot regeneration percentage (%)

Sugar cane Varieties	Salt Levels (0-240 Mm)				
	0 mM	30 mM	100 mM	170 mM	240 mM
B78-505	78.67 <sup>a</sup>	64 <sup>ab</sup>	45.30 <sup>de</sup>	56 <sup>bc</sup>	38.72 <sup>ef</sup>
SP70-1284	55b <sup>c</sup>	44.65 <sup>ef</sup>	51.66 <sup>bc</sup>	39 <sup>ef</sup>	23.60 <sup>fg</sup>
C90-501	65 <sup>ab</sup>	51.66 <sup>bcd</sup>	60.34 <sup>b</sup>	53.50 <sup>c</sup>	14.34 <sup>g</sup>

\* Lsmeans with same letters are not statistically significant based on Tukey's multiple comparison tests at  $\alpha=0.05$

### Root Regeneration and Selection of Salt Tolerant Root Regenerants

The analysis of Variance root characters are presented in Table 4 indicated that both regenerant and salt effects were highly significant ( $P \leq 0.01$ ) for all roots and shoot related traits of plantlets studied. It suggested significant variability has been existed among the *in vitro* regenerated regenerants under the different salt concentrations used that brought significant effects on these traits. During *in vitro* selection in the root regeneration medium, the interaction between regenerant and salt effects was highly significant ( $P \leq 0.01$ ) for all traits studied. The result suggests regenerants showed variable performances in responses to changing salt concentrations. On the contrary, the interaction was nonsignificant for the average number of roots and shoots/plantlet; an indication of consistent salt tolerance with increasing salt concentration.

Table 4: Mean Squares for root sugarcane regenerants evaluated at different levels of salt under *in vitro* condition

Sources of Variation	DF	RRP (%)	RNPP	RLPS (cm)	WPH (cm)	SNPP
Salt level	4	0.008ns	0.12*	0.26*	40.88*	0.55**
Regenerant	17	0.09**	0.03**	0.08**	0.09**	0.33**
Regenerant *salt	68	0.05**	0.033*	0.04**	0.15**	0.03ns
Error	178	0.012	0.013	0.010	0.0029	0.011
CV (%)		6.59	13	16	5.38	15.8

\*\*=highly significant at 1%; \*= significant at 5%; RNPP =Root number per culture; RRP=Root Regeneration Potential; RLPS=Root length/shoot; WPH=whole Plantlet height; SNPP= Shoot Number/Plant

### Effect of PEG on Root Regeneration Performance of Genotypes

The regenerants were screened for salinity tolerance using root regeneration percentage, number of roots per plantlet, length of roots per plantlet, length of whole plantlet and shoot number per plantlet and these traits were highly significantly ( $P \leq 0.01$ ) dependent on regenerant and salt effects.

Table 5: Means of root and shoot number/plantlet for sugarcane regenerants evaluated at different NaCl concentrations

Code	Regenerants	Root number per plantlet
1	S1SP-70-1284	8.81 <sup>abcdef</sup>
2	S2SP-70-1284	9.21 <sup>abc</sup>
3	S3SP-70-1284	8.57 <sup>abcdef</sup>
4	S4SP-70-1284	9.35 <sup>ab</sup>
5	S5SP-70-1284	8.89 <sup>abcd</sup>
6	S1B-78-505	9.68 <sup>a</sup>
7	S2B-78-505	8.76 <sup>abcdef</sup>
8	S3B-78-505	9.14 <sup>abcd</sup>
9	S4B-78-505	8.4 <sup>cdef</sup>
10	S5B-78-505	7.79 <sup>def</sup>
11	S1C0-501	7.77 <sup>efg</sup>
12	S2C0-501	8.62 <sup>abcdef</sup>
13	S3C0-501	7.78 <sup>efg</sup>
14	S4 C0-501	9.81 <sup>a</sup>
15	S5 C0-501	7.49 <sup>fg</sup>
16	MB-78-505	7.86 <sup>cdef</sup>
17	MSP-701284	6.46 <sup>g</sup>
18	MC0-501	7.46 <sup>gf</sup>
LSD <sub>0.05</sub>		1.3576
Salt Levels		
1	0 mM	11.48 <sup>a</sup>
2	30 mM	10.66 <sup>b</sup>
3	100 mM	7.88 <sup>c</sup>
4	170 mM	6.58 <sup>d</sup>
5	240 mM	5.57 <sup>e</sup>
LSD <sub>0.05</sub>		0.7155

\*Means followed by the same letters in a column are not statistically significant at  $\alpha=0.05$

Data of root related traits recorded during rooting regeneration were also subjected to analysis of variance. As the effect of the interaction effect between regenerant and salt for average root number per plantlet was nonsignificant ( $P>0.05$ ) (Table 4), only the main effects (regenerant and salt) were discussed. Regenerants namely, S4SP-70-1284, S2B-78-505, S4 C0-501 and S3B-78-505 showed higher root and shoot number per plantlet and are salt tolerant (Table 6.5). At 0 mM NaCl, regenerants produced higher numbers of roots (11) and shoots (6) per plantlet but adversely decreased when salt concentration of MS medium was increased to 240 mM level of NaCl where 51% and 48% of reduction was observed root and shoot numbers per plantlet respectively. The trend suggests the selected regenerants were tolerant at 240 mM level of NaCl.

Regenerants were for salinity tolerance screened at each level of salt concentrations (0, 30, 100, 170 and 240 Mm) using root regeneration%, whole plantlet length, root length per plantlet and shoot number/plantlet (Table 6) as the interaction between regenerant and salt effects was significant for these root characters (Table 4). The screening results indicated regenerants namely; S4 C0-501, S3B-78-505, S5SP-70-1284, S4SP-70-1284 and S3C0-501 showed better root regeneration percentage at 240 mM NaCl selection medium. These regenerants were more tolerant than the other regenerants with lowest reduction% of 13.23, 21.98, 11.4, 15.65 and 17.6 respectively as compared with the performance of these regenerants at salt free (0 mM) selection medium. Regenerants S4SP-70-1284, S4 C0-501, S3SP-70-1284, S4B-78-505, S5B-78-505 and S2SP-70-1284 showed better growth in plantlet length at 240 mM NaCl selection medium and relatively better tolerance with lowest reduction in growth of 9.49, 16.44, 16.08, 26.89, 27.03 and 27.46% respectively relative to their growth observed at salt free (0 mM) selection medium.

Moreover, regenerants S4SP-70-1284, S4 C0-501, S3B-78-505, S2SP-70-1284 and S2B-78-505 showed better root growth at 240 mM NaCl selection medium with a minimum reduction of 2.89, 12.4, 18.5, 16.1 and 28.6% respectively when compared to the root growth observed at salt free (0 mM) selection medium. Generally, from the *in vitro* salt tolerance screening results for plantlets (regenerants), sugarcane regenerants S4-SP70-1284, S4-CO-501, S4-B78-505, S3B-78-505 and S2-B78-505 showed relatively better tolerance to salt effect for all traits

considered. Their tolerance to salt was ascribed in relation to all direct and indirect regenerated plantlets (regenerants) at 240 mM NaCl which is opposite to reports of Begum and Islam (2015) where more variability for salt tolerance was obtained at 150 mM NaCl selection medium. Therefore, this salt level can be selected as a basis for screening and the mean performance of the regenerants during *in vitro* screening for salt tolerance. Moreover, it was observed that the effect of salinity on growth of direct regenerated plantlets was varietal dependent and consistent with the salt tolerance background of the varieties. On the contrary, the salt tolerance trend plantlets regenerated indirectly (regenerated from callus) was not variety dependent at all salt regimes and showed better tolerance to salt effect; these regenerants responded to salt effects regardless of the background of the respective source varieties which is an indication of the existence of variability as a result of use of indirect regeneration. Munir and Aftab (2013) found similar results where roots attributes regenerated from callus were genotype independent.

The above results highlighted a variability created among the varieties and regenerated variants with respect to salinity tolerance, the variants accumulate more variability for the stress. This result was in favor of the findings reported by Begum and Islam (2015). The analysis of variance showed that there was ample genetic variability among the varieties, indicating the explants of the varieties used had different callusing nature and shoot regeneration potential. The significance of salt effect indicated that the different concentrations of salt used brought distinct tolerance difference among the explants of different varieties. Moreover, the highly significant effect of the interaction (Except for callus induction%) revealing that the varietal and salinity effects were inter dependent on each other with respect to the traits studied under *in vitro* condition which is in agreement with results found by Mohamed *et al.* (2011) in which the subclonal variants of intergeneric hybrids showed significant differences for various characters. Both direct and indirect regenerated Plantlets (regenerants) were screened for salinity tolerance using data for root regeneration%, average root per plantlet, shoot number per plantlet, whole plantlet length and numbers of shoots per plantlet.

Table 6: Means of direct (16-18) and indirect (1-15) regenerated plantlets screened for root regeneration percentage (RRP), whole plantlet length (WPL) and shoot number/plantlet (SNPP) in response to different levels of salt concentrations

Code	Regenerant *Salt	Root Regeneration Percentage						Whole Plantlet Length					
		0 mM	30 mM	100 mM	170 mM	240 mM	R240 (%)	0 mM	30 mM	100 mM	170 mM	240 mM	R240 (%)
1	S1SP-70-1284	64.87 <sup>a-f</sup>	43.9 <sup>a-f</sup>	65.03 <sup>a-f</sup>	27.97 <sup>f</sup>	37.5 <sup>b-f</sup>	42.19	15.71 <sup>ab</sup>	13.31 <sup>a-h</sup>	14.91 <sup>a-e</sup>	8.84 <sup>a-h</sup>	9.63 <sup>a-h</sup>	38.7
2	S2SP-70-1284	54.77 <sup>a-f</sup>	58.1 <sup>a-f</sup>	58.4 <sup>a-f</sup>	38.07 <sup>b-f</sup>	26.9 <sup>f</sup>	50.89	14.75 <sup>a-f</sup>	12.64 <sup>a-h</sup>	11.47 <sup>a-h</sup>	10.7 <sup>a-h</sup>	10.7 <sup>a-h</sup>	27.46
3	S3SP-70-1284	74.43 <sup>abc</sup>	42.7 <sup>a-f</sup>	57.03 <sup>a-f</sup>	28.9 <sup>ef</sup>	35.73 <sup>cdef</sup>	52	11.44 <sup>a-h</sup>	13.25 <sup>a-h</sup>	13.63 <sup>a-g</sup>	11.5 <sup>a-h</sup>	9.6 <sup>a-h</sup>	16.08
4	S4SP-70-1284	53.03 <sup>a-f</sup>	45.8 <sup>a-f</sup>	44.7 <sup>a-f</sup>	50 <sup>a-f</sup>	44.73 <sup>a-f</sup>	15.65	15.8 <sup>a</sup>	14.74 <sup>a-f</sup>	8.237 <sup>a-h</sup>	14.8 <sup>a-f</sup>	14.3 <sup>a-f</sup>	9.494
5	S5SP-70-1284	48 <sup>a-f</sup>	60.83 <sup>a-f</sup>	40.43 <sup>a-f</sup>	31.37 <sup>ef</sup>	42.53 <sup>a-f</sup>	11.4	14.44 <sup>a-f</sup>	15.14 <sup>a-e</sup>	12.3 <sup>a-h</sup>	7.49 <sup>efgh</sup>	9.55 <sup>a-h</sup>	33.86
6	S1B-78-505	75.43 <sup>ab</sup>	60.17 <sup>a-f</sup>	72.6 <sup>abc</sup>	55.73 <sup>a-f</sup>	34.07 <sup>b-f</sup>	54.83	11.51 <sup>a-h</sup>	14.16 <sup>a-f</sup>	7.84 <sup>c-h</sup>	8.87 <sup>a-h</sup>	5.97 <sup>gh</sup>	48.13
7	S2B-78-505	79.77 <sup>a</sup>	79.13 <sup>a</sup>	50.8 <sup>a-f</sup>	40.67 <sup>a-f</sup>	54.37 <sup>a-f</sup>	31.84	15.38 <sup>abc</sup>	13.54 <sup>a-g</sup>	15.34 <sup>abcd</sup>	12.1 <sup>a-h</sup>	10.8 <sup>a-h</sup>	29.78
8	S3B-78-505	55.63 <sup>a-f</sup>	67.97 <sup>a-e</sup>	57.5 <sup>a-f</sup>	41.8 <sup>a-f</sup>	43.4 <sup>def</sup>	21.98	13.77 <sup>a-f</sup>	11.68 <sup>a-g</sup>	14.63 <sup>a-f</sup>	9.58 <sup>a-h</sup>	9.07 <sup>a-h</sup>	34.13
9	S4B-78-505	51.43 <sup>a-f</sup>	37.67 <sup>b-e</sup>	55.27 <sup>a-f</sup>	40.93 <sup>a-f</sup>	32.5 <sup>def</sup>	36.81	10.56 <sup>a-h</sup>	11.41 <sup>a-h</sup>	10.35 <sup>a-h</sup>	8.57 <sup>a-h</sup>	7.72 <sup>c-h</sup>	26.89
10	S5B-78-505	60.47 <sup>a-f</sup>	62.1 <sup>a-f</sup>	44.73 <sup>a-f</sup>	46.43 <sup>a-f</sup>	38.3 <sup>b-f</sup>	36.66	10.84 <sup>a-h</sup>	13.87 <sup>a-f</sup>	13.61 <sup>a-g</sup>	11.7 <sup>a-h</sup>	7.91 <sup>c-h</sup>	27.03
11	S1C0-501	49.47 <sup>a-f</sup>	37.33 <sup>b-e</sup>	46.77 <sup>a-f</sup>	40.9 <sup>a-f</sup>	37.5 <sup>b-f</sup>	24.2	11.83 <sup>a-h</sup>	12.85 <sup>a-h</sup>	13.66 <sup>a-g</sup>	10.2 <sup>a-h</sup>	7.8 <sup>c-h</sup>	34.07
12	S2C0-501	67.77 <sup>a-e</sup>	56.13 <sup>a-f</sup>	38.93 <sup>b-f</sup>	39 <sup>b-f</sup>	36.57 <sup>b-f</sup>	46.04	13.13 <sup>a-h</sup>	14.26 <sup>a-f</sup>	8.49 <sup>a-h</sup>	9.53 <sup>a-h</sup>	7.61 <sup>d-h</sup>	42.04
13	S3C0-501	47.57 <sup>a-f</sup>	58.1 <sup>a-f</sup>	64.53 <sup>a-f</sup>	46.57 <sup>a-f</sup>	39.2 <sup>b-f</sup>	17.6	12.28 <sup>a-h</sup>	13.48 <sup>a-g</sup>	8.673 <sup>a-h</sup>	11 <sup>a-h</sup>	7.61 <sup>d-h</sup>	38.03
14	S4 C0-501	59.93 <sup>a-f</sup>	34.9 <sup>cdef</sup>	48.87 <sup>a-f</sup>	54.53 <sup>a-f</sup>	52 <sup>a-f</sup>	13.23	14.84 <sup>abc</sup>	12.78 <sup>a-h</sup>	13.107 <sup>a-h</sup>	13.7 <sup>a-f</sup>	12.4 <sup>a-h</sup>	16.44
15	S5 C0-501	52.23 <sup>a-f</sup>	35.23 <sup>cdef</sup>	35 <sup>cdef</sup>	46.1 <sup>a-f</sup>	33.27 <sup>def</sup>	36.3	12.37 <sup>a-h</sup>	7.447 <sup>efgh</sup>	7.97 <sup>b-h</sup>	7.07 <sup>fgh</sup>	5.67 <sup>h</sup>	54.16
16	MB-78-505	46.8 <sup>a-f</sup>	47.8 <sup>a-f</sup>	35 <sup>cdef</sup>	35 <sup>cdef</sup>	35 <sup>cdef</sup>	40.48	10.38 <sup>a-h</sup>	10.63 <sup>a-h</sup>	12.5 <sup>a-h</sup>	7.7 <sup>d-h</sup>	6.33 <sup>gh</sup>	39.02
17	MSP-701284	56.17 <sup>a-f</sup>	56.67 <sup>a-f</sup>	36 <sup>b-f</sup>	36 <sup>b-f</sup>	36 <sup>b-f</sup>	35.91	10.9 <sup>a-h</sup>	12.5 <sup>a-h</sup>	12.9 <sup>a-h</sup>	5 <sup>h</sup>	5.64 <sup>h</sup>	48.26

18	MC0-901	47.83 <sup>a-f</sup>	48 <sup>a-f</sup>	32 <sup>ef</sup>	42 <sup>a-f</sup>	32 <sup>ef</sup>	44.67	10.2 <sup>a-h</sup>	11.53 <sup>a-h</sup>	13.47 <sup>a-g</sup>	7.93 <sup>c-h</sup>	5.43 <sup>h</sup>	46.76
Plantlet Root Length							R240	SNPP					
1	S1SP-70-1284	7.5 <sup>a</sup>	5.07 <sup>a-g</sup>	5.83 <sup>a-g</sup>	4.13 <sup>a-g</sup>	2.6 <sup>fg</sup>	65.3	6.94 <sup>abcd</sup>	5.45 <sup>a-e</sup>	6.36 <sup>a-e</sup>	5.04 <sup>a-e</sup>	4.02 <sup>a-e</sup>	42.07
2	S2SP-70-1284	5.6 <sup>a-g</sup>	4.57 <sup>a-g</sup>	4.57 <sup>a-g</sup>	5.43 <sup>a-g</sup>	4.7 <sup>a-g</sup>	16.1	7.82 <sup>a</sup>	5.53 <sup>a-e</sup>	5.61 <sup>a-e</sup>	5.37 <sup>a-e</sup>	3.13 <sup>e</sup>	59.97
3	S3SP-70-1284	5.33 <sup>a-g</sup>	5.57 <sup>a-g</sup>	3.8 <sup>a-g</sup>	4.77 <sup>a-g</sup>	3.5 <sup>b-g</sup>	34.3	6.18 <sup>a-e</sup>	5.59 <sup>a-e</sup>	5.7 <sup>a-e</sup>	5.28 <sup>a-e</sup>	4.42 <sup>a-e</sup>	28.48
4	S4SP-70-1284	7.27 <sup>abcd</sup>	4.57 <sup>a-g</sup>	4.9 <sup>a-g</sup>	6.44 <sup>a-g</sup>	7.1 <sup>abc</sup>	2.89	5.24 <sup>a-e</sup>	5.63 <sup>a-e</sup>	6.0 <sup>a-e</sup>	4.34 <sup>a-e</sup>	6.3 <sup>abc</sup>	-20.2
5	S5SP-70-1284	6.37 <sup>a-f</sup>	3.07 <sup>defg</sup>	2.47 <sup>g</sup>	2.43 <sup>g</sup>	2.51 <sup>fg</sup>	60.6	7.70 <sup>ab</sup>	6.51 <sup>a-e</sup>	4.82 <sup>a-e</sup>	4.81 <sup>a-e</sup>	6.82 <sup>abc</sup>	11.43
6	S1B-78-505	7.67 <sup>a</sup>	5.77 <sup>a-g</sup>	4.42 <sup>a-g</sup>	4 <sup>a-g</sup>	3.9 <sup>a-g</sup>	49.2	7.12 <sup>abcd</sup>	5.73 <sup>a-e</sup>	5.82 <sup>a-e</sup>	4.11 <sup>a-e</sup>	3.82 <sup>de</sup>	46.35
7	S2B-78-505	7 <sup>abc</sup>	5.8 <sup>a-g</sup>	5.6 <sup>a-g</sup>	4.57 <sup>a-g</sup>	5 <sup>a-g</sup>	28.6	7.23 <sup>abcd</sup>	5.86 <sup>a-e</sup>	6.51 <sup>a-e</sup>	4.52 <sup>a-e</sup>	3.92 <sup>a-e</sup>	45.78
8	S3B-78-505	6.17 <sup>a-g</sup>	5.67 <sup>a-g</sup>	2.87 <sup>defg</sup>	7.05 <sup>ab</sup>	5.03 <sup>a-g</sup>	18.5	7.56 <sup>abc</sup>	5.83 <sup>a-e</sup>	5.76 <sup>a-e</sup>	4.69 <sup>a-e</sup>	4.22 <sup>a-e</sup>	44.18
9	S4B-78-505	6.67 <sup>abcd</sup>	4.71 <sup>a-g</sup>	5.13 <sup>a-g</sup>	5.67 <sup>a-g</sup>	3.53 <sup>b-g</sup>	47.1	5.09 <sup>a-e</sup>	5.38 <sup>a-e</sup>	4.45 <sup>a-e</sup>	3.75 <sup>a-e</sup>	6.97 <sup>abcd</sup>	-36.9
10	S5B-78-505	4.3 <sup>a-g</sup>	4.07 <sup>a-g</sup>	5.53 <sup>a-g</sup>	3.07 <sup>d-g</sup>	2.67 <sup>fg</sup>	37.9	5.96 <sup>a-e</sup>	4.89 <sup>a-e</sup>	3.6 <sup>cde</sup>	3.94 <sup>a-e</sup>	4.08 <sup>a-e</sup>	31.54
11	S1C0-501	5.1 <sup>a-g</sup>	5 <sup>a-g</sup>	3.4 <sup>b-g</sup>	5.92 <sup>a-g</sup>	2.6 <sup>fg</sup>	49	5.88 <sup>a-e</sup>	6.19 <sup>a-e</sup>	6.08 <sup>a-e</sup>	5.31 <sup>a-e</sup>	4.67 <sup>a-e</sup>	20.58
12	S2C0-501	4.7 <sup>a-g</sup>	5.27 <sup>a-g</sup>	3.37 <sup>b-g</sup>	5.77 <sup>a-g</sup>	2.57 <sup>fg</sup>	45.3	5.40 <sup>a-e</sup>	6.28 <sup>a-e</sup>	4.75 <sup>a-e</sup>	5.73 <sup>a-e</sup>	4.12 <sup>a-e</sup>	23.7
13	S3C0-501	5.57 <sup>a-g</sup>	5.07 <sup>a-g</sup>	3.83 <sup>a-g</sup>	6.57 <sup>a-d</sup>	2.5 <sup>fg</sup>	55.1	6.44 <sup>a-e</sup>	4.75 <sup>a-e</sup>	4.23 <sup>a-e</sup>	4.36 <sup>a-e</sup>	3.86 <sup>a-e</sup>	40.06
14	S4 C0-501	6.72 <sup>a-g</sup>	5.57 <sup>a-b</sup>	2.79 <sup>efg</sup>	6.7 <sup>abcd</sup>	5.89 <sup>a-g</sup>	12.4	7.73 <sup>a</sup>	4.29 <sup>a-e</sup>	4.03 <sup>a-e</sup>	4.06 <sup>bcde</sup>	7.07 <sup>abcd</sup>	8.538
15	S5 C0-501	4.33 <sup>a-g</sup>	3.07 <sup>defg</sup>	2.87 <sup>defg</sup>	2.5 <sup>fg</sup>	2.72 <sup>efg</sup>	37.2	5.92 <sup>a-e</sup>	5.41 <sup>a-e</sup>	5.19 <sup>a-e</sup>	3.77 <sup>bcde</sup>	3.84 <sup>de</sup>	35.14
16	MB-78-505	4.47 <sup>a-g</sup>	3.92 <sup>a-g</sup>	2.87 <sup>g</sup>	4.02 <sup>a-g</sup>	2.6 <sup>efg</sup>	41.8	3.57 <sup>bcde</sup>	3.64 <sup>a-e</sup>	4.27 <sup>a-e</sup>	2.82 <sup>f</sup>	2.92 <sup>f</sup>	18.21
17	MSP-701284	5.37 <sup>a-g</sup>	3.43 <sup>b-g</sup>	4.28 <sup>defg</sup>	4.86 <sup>a-g</sup>	2.61 <sup>efg</sup>	51.4	3.04 <sup>e</sup>	3.07 <sup>e</sup>	2.76 <sup>f</sup>	3.67 <sup>a-e</sup>	2.7 <sup>f</sup>	11.18
18	MC0-501	3.9 <sup>a-g</sup>	2.96 <sup>defg</sup>	2.47	3.26 <sup>b-g</sup>	2.17 <sup>fg</sup>	44.4	2.63 <sup>f</sup>	1.3 <sup>f</sup>	3.16 <sup>e</sup>	2.73 <sup>f</sup>	2.24 <sup>f</sup>	14.83

\* Different letters within a specific column represent significant difference based on Tukey's multiple comparison tests at  $\alpha=0.05$ ; M=mother plant; R240=Reduction% at 240 mM NaCl selection medium relative to 0 mM (salt free) selection medium; negative values of R240 indicate increments

## Clustering of *in Vitro* Developed Sugarcane Regenerants

Root and shoot related data of 18 regenerants which were indirectly (1-15) and directly (16-18) regenerated under *in vitro* condition were used for cluster analysis (Table 7). Clustering of 18 regenerants of sugarcane was computed by Euclidean distance measure based on average linkage method and the dendrogram constructed clustered regenerants in to 6 clusters. In between Euclidean distance of 3.04-3.4, the dendrogram was divided in to two major clusters where the salt tolerant regenerants 4, 8, 14 and 7 were separated from the others (Fig. 2).

Table 7. Mean Values of Regenerants developed through indirect (1-15) and direct (16-18) Regeneration used for Cluster Analysis

Regeneration	Code	Indirect Regeneration					
		RRP (%)	RNPP	RLPS (cm)	WPH (cm)	SNPP	Genetic Distance
S1SP-70-1284	1	27.95	10.57	5.03	8.84	4.02	1.44
S2SP-70-1284	2	38	9.94	4.53	5.7	3.13	1.63
S3SP-70-1284	3	28.9	8.96	4.59	7.11	4.42	1.44
S4SP-70-1284	4	70	11.14	5.14	9.11	6.3	0.96
S5SP-70-1284	5	31.36	10.19	3.3	7.49	6.82	0.96
S1B-78-505	6	55.7	9.42	5.15	6.09	3.82	1.63
S2B-78-505	7	40.66	12.09	5.39	12.12	3.92	3.04
S3B-78-505	8	84.1	10.86	5.36	9.58	4.22	0.96
S4B-78-505	9	60.93	8.47	4.3	8.57	6.97	1.67
S5B-78-505	10	46.44	10.39	3.93	8.87	4.08	0.72
S1C0-501	11	40.9	11.61	4.4	4.9	4.67	0.77
S2C0-501	12	43.33	10.7	4.33	9.52	4.12	0.72
S3C0-501	13	46.56	11.15	4.71	5.8	3.86	0.77
S4 C0-501	14	84.1	8.54	4.33	12.51	7.07	2.59
S5 C0-501	15	46	10.07	3.1	7.07	3.84	0.96
Direct regeneration							
MB78-505	16	44.7	13.89	4.62	7.16	3.92	0.65
MSP-70-1284	17	43.7	14	4.86	6	4	0.65
MCO-501	18	44	13	3.56	6	4	1.90

\* RNPC=Root number per culture; RRP=Root Regeneration Percentage; RLPS=Root length/Plantlet; WPH=whole Plantlet length; SNPP=Shoot number per plantlet; M=mother plant

Moreover, the dendrogram was divided in six clusters within Euclidean distance range of 2.2-3.04 where regenerants developed *via* direct regeneration (16-17) classified in separate cluster. The separation of the salt tolerant regenerants suggested these regenerants accumulate variability with respect to salt tolerance which is similar to the results reported by Patade *et al.* (2006). Generally, the cluster analysis efficiently displayed the variability among the regenerants on the basis of the regeneration pathways used and salt tolerance. Result presented in table 6.8 revealed clusters IV and V showed higher means for all root characters studied than the others while cluster I recorded the lowest mean. The result suggested the clusters were productive and each contained single regenerants and the clustering of the regenerants was on the basis of the mean.

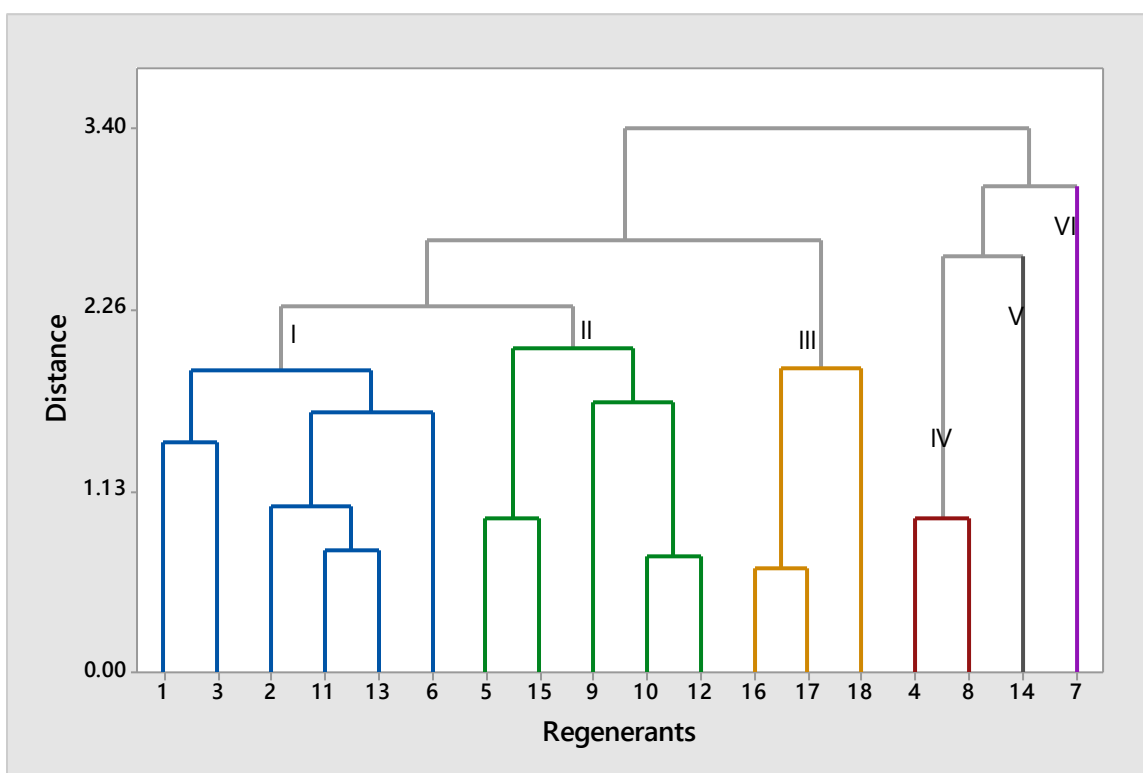


Figure 6.2: Dendrogram of 18 sugarcane Regenerants based on Euclidean Distance

### Acclimatization of in Vtro Developed Genotypes at Greenhouse Condition

20 days after the regenerants were transferred to greenhouse, survival% of regenerant was calculated (Table 8). Regenerants namely, S5SP-70-1284, S3B-78-505, S5B-78-505 and S5 C0-501 were weak during transferring to greenhouse and not survived (0%). On the contrary, the other Regenerants showed survival % from 53.3 (MSP-70-1284) to 96.9% (S1C0-501). Those

regenerants which showed relatively good tolerance to salt stress under *in vitro* condition were also well survived at greenhouse and field conditions.

Table 8. Survival rate (%) of sugarcane regenerants under greenhouse condition

Name	Number of plantlets	Plantlets survived	% of survival
S1SP-70-1284	12	9	75
S2SP-70-1284	10	8	80
S3SP-70-1284	10	7	70
S4SP-70-1284	13	9	69
S5SP-70-1284	2	0	0
S1B-78-505	30	27	90
S2B-78-505	40	36	90
S3B-78-505	5	0	0
S4B-78-505	10	9	90
S5B-78-505	4	0	0
S1C0-501	32	31	96.9
S2C0-501	32	30	93.8
S3C0-501	29	26	89.7
S4 C0-501	20	16	80
S5 C0-501	3	0	0
MB78-505	10	7	70
MSP-70-1284	15	8	53.3
MCO-501	18	12	66.7

### **Performance of *In Vitro* Regenerated Genotypes at Salt Affected Field Conditions**

After the greenhouse acclimatization was completed, the genotypes were transferred to saline field for further field validation along with the locally grown varieties C0-501, B78-505 and SP-70-1284. However, only SP-70-1284 was survived and the salt tolerant genotypes were evaluated against this variety. Based on the field evaluation at Tendaho Sugar Project, regenerants S4 C0-501 (Fig. 3a), S4SP-70-1284 (Fig. 3b), and S2B-78-505 (Fig. 3c) showed good performances in tillering capacity and vigor in growth. All of the *in vitro* developed genotypes were better than the locally grown variety in numbers of tillers ( $\text{ha}^{-1}$ ), stalk population ( $\text{ha}^{-1}$ ) and plant height than the locally grown variety, S4SP-70-1284 (Table 9). However, only genotypes S4 C0-501 and S4SP-70-1284 were significantly better than the locally grown variety. Moreover, the genotypes

showed high vigor in growth and tillering capacity as shown in Fig. 3 a, b, c. These regenerants were salt tolerant under *in vitro* condition (Table 6), suggesting the salinity tolerance accumulated under *in vitro* condition was realized at field condition. This shows the reliability of the experiment and this kind of studies should be encouraged in stress screening research. Similar field validation studies using morphological traits reported by Shah *et al.* (2004); Patel (2007); and Gadakh *et al.* (2015) identified superior somaclones over donor parents.

Table 8: performance of sugarcane genotypes at salt affected field condition

Genotype name	Mean performance		
	Number of tillers (ha <sup>-1</sup> )	stalk height (m)	stalk population (ha <sup>-1</sup> )
S4 C0-901	214406a	1.78 <sup>a</sup>	150594 <sup>a</sup>
S4SP-70-1284	198038 <sup>a</sup>	1.73 <sup>a</sup>	111132 <sup>ab</sup>
S2B-78-505	117704 <sup>b</sup>	1.34 <sup>b</sup>	107331 <sup>b</sup>
S3B-78-505	36180 <sup>c</sup>	1.3b	102082 <sup>b</sup>
SP-70-1284	116516 <sup>b</sup>	1.31 <sup>b</sup>	58818 <sup>c</sup>
LSD <sub>0.05</sub>	80335	0.30	43263
Mean	136568.8	1.62	125285

\*Means with the same letter in a column are not significantly different

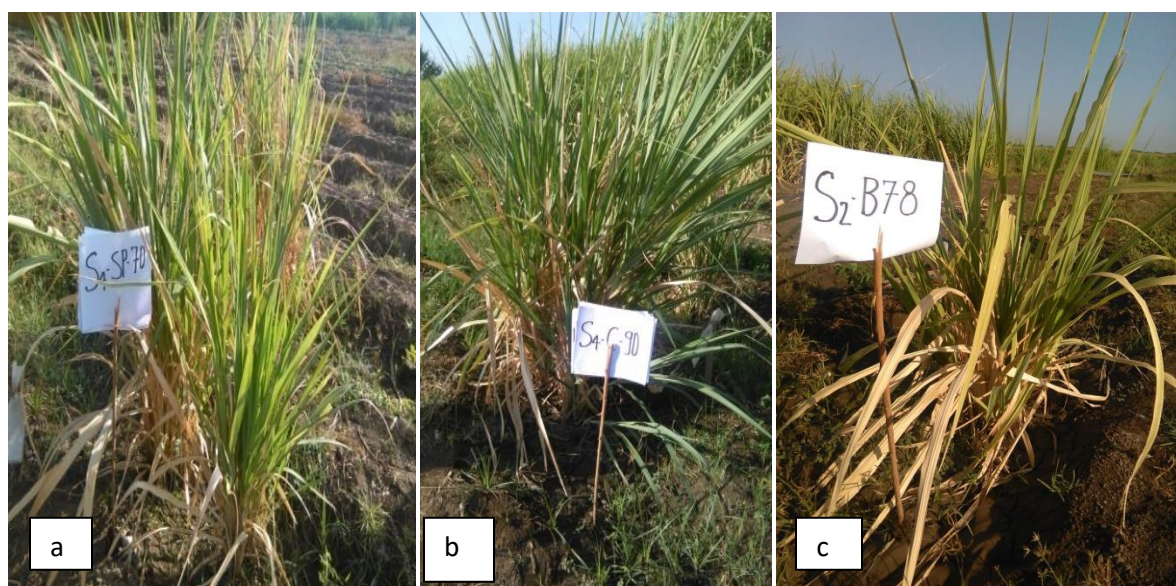


Figure 3: Field Performance of Salt Tolerant Sugarcane Regenerants (a, b, c) at Tendaho Sugar Project

## CONCLUSION

The investigation conducted to screen sugarcane varieties and *in vitro* developed regenerants for salinity tolerance under *in vitro* condition is successful in detecting variability among varieties and the developed regenerants with respect salt tolerance, and isolating salt tolerant regenerants. Among the regenerants screened, regenerants namely; S4SP-70-1284, S4 C0-501 and S2B-78-505 showed considerable tolerance for salt stress under *in vitro*, greenhouse and field conditions.

The cluster analysis conducted to assess the existed variability among regenerants, demonstrated the existence of ample genetic variability among regenerants. The dendrogram separated those regenerants developed through direct regeneration from those regenerants developed through indirect regeneration and was capable of separating the regenerants based on their tolerance to salinity. The improved tolerance to salinity observed in the *in vitro* developed and selected regenerants would be valuable in enhancing the diversity of sugarcane varieties with high degree of salt tolerance suitable for salt affected sugarcane production areas in Ethiopia.

## Reference

- Arzani, A. 2008.Improving salinity tolerance in crop plants: A biotechnological view.*In Vitro Cell Development Biololgy Plant*, 44:373-383.
- Ashraf, M., Rahmatullah, K.S, Tahi, M.A., Sarwar, A. and Ali, L. 2007. Differential Salt Tolerance of Sugarcane Genotypes.Directorate of Land Reclamation, Irrigation & Power Department, Punjab, Pakistan. *Pakistan Journal Agriculture science*, 44(1):85-89
- Avinash, L., Prashant, N. and Bharose, A.A. 2012. College of Agricultural Biotechnology Marathwada Krishi Vidyapeeth Latur, India.*In vitro* Screening of Sugarcane CultivarCo 86032 for Salinity Tolerance.*Journal Sugar Research*, 2(1): 25-31.
- Begum, M.S, Kohinoor, T. and Islam, MDO.2015.Selection of salt tolerant somaclones for development of salt stress tolerant varieties.*Plant* 3(4): 37-46.
- Cha-um, S., Chuencharoen, S., Mongkolsiriwatana, C., Ashraf, M. and Kirdmanee, C. 2012. Screening sugarcane (*Saccharum sp.*) genotypes for salt tolerance using multivariate cluster analysis. National Center for Genetic Engineering and Biotechnology.*Plant Cell, Tissue Organ Culture*, 110 (2): 23-33.
- Garcia A.A., Kido, E.A, Meza, A.N, Souza, H.M.B., Pinto, L.R, Pastina, M.M., Leite, C.S., Silva, D., Ulian,. ED., Figueira, A. and Souza, AP. 2006. Development of an integrated genetic map of a sugarcane (*Saccharum spp.*) commercial cross; based on maximum likelihood approach for estimation of linkage and linkage phases. *Theoretical Applied Genetics*, 112: 298-314.

- Girma, A. 1993. Assessment of salinity effect and sodicity status of Metahara Sugar Estate. MSc Thesis. Alemaya University, College of Agriculture, Ethiopia.
- Gandonou, C.H., Errabini, T., Abrinii, J., Idaomar, M., Chibi, F. and Skali, S.N, 2005. Effect of genotype on callus induction and plant regeneration from leaf explants of sugarcane. *African Journal Biotechnology*, 4(11): 1250-1255.
- Gower, J.C. 1971. A general coefficient of similarity and some of its properties. *Biometrics* 27: 857-871.
- Hadi, M.Z. and Bridgen, M.P. 1996. Somaclonal variation as a tool to develop pest resistant plants of *Torenia fournieri* 'Compacta Blue'. *Plant Cell Tiss Org Cult*, 46: 43-50
- Larkin, P.J. and Scowcroft, W.R. 1981. Somaclonal variation – a novel source of variability from cell cultures for plant improvement. *Theoretical Applied Genetics*, 60: 197-214.
- Mahmoud, S., Majid, N., Mosa, M and Hamid, R. 2011. Evaluation of sugarcane (*Saccharum officinarum* L.) somaclonals tolerance to salinity via *in vitro* and *in vivo* culture. *African Journal Biotechnology*, 10: 9337-9343.
- Maas, E.V. 1986. Salt tolerance in plants. *Applied Agriculture Research*, 1: 12–26.
- Megersa, O., Willibald, L. and Josef, F. 2009. Effect of Lake Basaka expansion on the sustainability of Matahara SE in the Awash River basin, Ethiopia. Water, sanitation and hygiene: sustainable development and multisectoral approaches. 34th WEDC International Conference, Addis Ababa, Ethiopia.
- Munir, N. and Aftab, F. 2013. Effect of salt stress on callus morphology and growth of sugarcane callus cultures. Department of biotechnology, Lahore College for Women University, Lahore. *Pakistan Journal Science*, 65(4): 473-477.
- Naidoo, S., Van, R.A. and Parmmenter, N.W. 2004. Quantifying the effect of soil salinity on the physiology of three South African sugarcane varieties. Council for Scientific and Industrial Research, South Africa. *Proceeding South African Sugar Technology Association*, 78:1-19
- Orbovic, V., Calovic, M., Vilorio Z., Nielsen B., Gmitter F., Castle W., Grosser J. 2008. Analysis of genetic variability in various tissue culture-derived lemon plant populations using RAPD and flow cytometry. *Euphytica*, 161 329–335.
- Patade, V.Y., Suprasanna, P., Bapat, V.A. and Kulkarni, U.G. 2006. Selection for abiotic (salinity and drought) stress tolerance and molecular characterization of tolerant lines in sugarcane. *Bhabha Atomic Research Centre Newsletters*, 27:244-257
- Patade, V.P. and Suprasanna, P. 2009. An *in vitro* radiation induced mutagenesis selection system for salinity tolerance in sugarcane. Functional Plant Biology Section, Nuclear Agriculture and Biotechnology Division, Bhabha. *Sugar Technology* DOI: 10.1007/s12355-009-0042-4.
- Patel, S. R. (2007) Induction of variability through callus culture in sugarcane (*Saccharum officinarum* L.) variety CoN 95132. Ph.D. thesis submitted to N.A.U., Navsari.

- Perez-Clemente, R.M. and Gomez- Cadenas, A. 2012. *In vitro* tissue culture, a tool for the study and breeding of plants subjected to abiotic stress conditions. Department of Agricultural Sciences. Universidad Jaime I, Spain. *Recent Advances in Plant in Vitro Culture*, DOI: 10.5772/50671
- Rajeswari, S., Krishnamurthi, M., Shinisekar, S., Prem, A.S. and Thirugnana, K.S. 2009. Performance of somaclones developed from intergeneric hybrids of sugarcane. *Sugar Technology*, 11:258-261.
- Rengasamy, P. 2010. Soil Processes affecting crop production in salt affected soil. School of agriculture, food and wine, university of Adelaide, Australia. *Functional plant biology*, 37 (7): 613-620.
- Shah, J.K., Khan, M.A., Ahmad, H.K., Khan, R.D. and Zafar, Y. 2004. Somaclonal variation in sugarcane through tissue culture and subsequent screening for salt tolerance. *Asian Journal of Plant Science*, 3: 330-334.
- Statistical Analysis System Institute. 2009. *SAS Users Guide*; Version 9.2. SAS Ins. Inc. Cary North Carolina, USA.
- Steel, R. G. D. and Torrie, J. H. 1981. In: Principles and procedures of statistics. McGraw Hill International Book Company, London (2nd Edition). pp: 254-238.
- Subbarao, G.V. and Johanssen, C. 1999. Strategies and scope for improving salinity tolerance in crop plants In: *Advanced Life Support Systems Group*. John F. Kennedy Space Center Kennedy Space Center, Florida.
- Tate, B. 2009. Re-evaluation of the plantation soils at Metahara Sugar Factory, Ethiopia.
- Vasanth, S., Venkataramana, P.N., Gururaja, R. and Gomathi, R. 2009. Long term salinity effect on growth, photosynthesis and osmotic characteristics in sugarcane. *Biological Life Science*, 12(1): 5-8.
- Wagih, M.E., Aal A and Musa, Y. 2003. Regeneration and evaluation of sugarcane somaclonal variants for drought tolerance. *Sugarcane Technology*, 2:35-40.

## Vomeronal Receptors Gene Characterization by Using Molecular Techniques in Pig

Hunduma Dinka<sup>1</sup> and Chankyu Park<sup>2</sup>

<sup>1</sup>Centers of Excellence, Adama Science and Technology University, Adama, Ethiopia.P.O.Box  
1888

E-mail: [dinkahu@gmail.com](mailto:dinkahu@gmail.com). Phone number: +251 (09) 24543160.

<sup>2</sup>Department of Animal Biotechnology, Konkuk University, Gwangjin-gu, Seoul, South Korea.

### *Abstract*

*In mammals, sensory neurons at the vomeronasal organ express three different types of vomeronasal receptor families [VIR, V2R, and formyl peptide-like receptors (FPR)]. Despite the detailed characterization of the vomeronasal receptors gene, such as VIR and V2R, across several mammalian genomes, including mouse, rat, dog, human, cattle, goat, sheep, little is known about these in domestic pigs. Therefore, in this study, we analyzed the gene repertoire, tissue expression pattern of vomeronasal receptors and its gene expression regulation pattern in pigs. We identified a total of 25 VIR genes consisting of 10 functional genes, 3 pseudogenes, and 12 partial genes, while functional V2R and FPR genes were not present in the pig genome. Functional pig VIRs were located on chromosomes 6 and 1 with 7 and 3 genes, respectively, and were classified into three subfamilies: D, F, and J. By using direct high resolution sequencing-based typing of all functional VIRs, a total of 24 SNPs were identified. The average Ka/Ks ratio and Neutrality Index (NI) in VIRs were 0.304 and 1.471, respectively, both indicating that pig VIRs are largely shaped by strong purifying selection. A high expression level of VIRs was detected in the vomeronasal organ (VNO) and testes, while a low expression level of VIRs was observed in all other tissues examined. To understand its gene expression regulation pattern we conducted bioinformatics in silico analysis for the promoter region of pig VIRs and identified five motifs (MV1, MV2, MV3, MV4 and MV5) that are shared by at least 50% of the pig VIR promoter input sequences from both strands. Among the five motifs, we identified MV2 as a common promoter motif shared by all (100%) pig VIR promoters. For further analysis, to better characterize and get deeper biological insight associated with MV2, we compared it to the known motif databases (such as JASPAR) to see if they are similar to a known regulatory motif (transcription factor). Hence, we revealed that MV2 serves as binding site mainly for BetaBetaAlpha-zinc finger (BTB-ZF) transcription factor gene family to regulate expression of pig VIR genes. Moreover, we showed that pig VIR promoters are CpG islands poor that might indicate the mechanisms of their gene expression regulation pattern is in tissue specific manner. In a nutshell, our results showed that pigs could serve as an interesting large animal model system to study pheromone-related neurobiology because of their genetic simplicity.*

**Keywords:** vomeronasal receptors, motif, transcription factor, CpG island.

## **2. Introduction**

Chemodetection is achieved in mammals by olfaction (detection of odorants and pheromones) and gustatory perception (taste), enabling animals to sense chemicals and identify chemical cues from the environment. In mammals, olfaction is mediated by two distinct organs that are located in the nasal cavity: the main olfactory epithelium (MOE) that binds mainly volatile odorants responsible for the conscious perception of odors, and the vomeronasal organ (VNO) that binds pheromones responsible for various behavioral and neuroendocrine responses between individuals of the same species (Dulac and Axel, 1995).

In mammals, sensory neurons at the VNO express three different types of vomeronasal receptor families [V1R, V2R, and formyl peptide-like receptors (FPR)], belonging to seven trans-membrane G-protein coupled receptors (GPCR), which differ in their expression pattern and gene structure (Rouquier and Giorgi, 2007; Herrada and Dulac, 1997; Ryba and Tirindelli, 1997). The importance of pigs in agriculture as a source of food and their role as biomedical models due to their anatomical and physiological similarities to humans has brought a keen interest in the detailed understanding of the pig genome (Prather *et al.*, 2008). Despite the detailed characterization of the repertoires of VRs, such as V1R and V2R, across several mammalian genomes, including mouse, rat, dog and cattle, human, goat and sheep, little is known about these in domestic pigs. On the other hand analysis for some V1R and OR promoter regions of mouse found motifs that are common to a large number of these promoters (Michaloski *et al.*, 2011) revealing BTB-ZF transcription factor gene family for both genes and found to express in vomeronasal and olfactory neurons indicating that it is likely to play a role in gene regulation in these neurons but no reports has been made in domestic pigs. Therefore, in this study, we analyzed the gene repertoire and expression pattern of VRs, and their gene expression regulation pattern in domestic pigs. Our results contribute towards the understanding of the machinery responsible for pheromone detection and its influence on pig behavior because pigs serve as an interesting large animal model system to study pheromone-related neurobiology due to their genetic simplicity.

## **2. Materials and methods**

### ***2.1. Animals and DNA isolation***

Ear tissues from two unrelated individuals for each pig breed including: Yorkshire, Berkshire, Duroc, Landrace, and Korean native pig (KNP) were used. Genomic DNA isolation was done using phenol/chloroform extraction method (Sambrook and Russell, 2001).

### ***2.2. Identification of vomeronasal receptor related sequences in the pig genome***

Identification of V1R sequences in the pig genome was carried out as described by Young et al. (2005). Briefly, we downloaded available protein sequences (n = 4117) consisting of 3453 V1R, 606 V2R, and 58 FPR from the NCBI database. The sequences were filtered for any duplicated or unrelated sequences by manual examination, and resulted in 3453 unique candidate sequences. These, 3453, sequences were used for tBLASTn analysis against the current pig genome assembly (*Sus scrofa* 10.2) with a cut-off e-value  $10^{-5}$ . Candidate sequences were considered “functional V1Rs” if they were at least 300 amino acid long without any interrupting stop codons and/or frame shifts within the open reading frames (ORFs). Candidate sequences were considered “V1R pseudogenes” if they were at least 300-amino acid long but contained stop codons or frame shifts within the ORFs, while candidate sequences were considered “partial V1Rs” if they were more than 100 but less than 300-amino acid long and matched the sequences of the known V1Rs.

### ***2.3. Phylogenetic analysis and subfamily classification of porcine V1Rs***

To construct phylogenetic tree in addition to the 13 V1R sequences of the pig, at least one representative sequence from each mice subfamily (n = 105) were used from previous studies (Grus *et al.*, 2005; Dong *et al.*, 2012; Young *et al.*, 2010; Rodriguez and Mombaerts, 2002; Rodriguez *et al.*, 2002). The nucleotide sequences were aligned together with gap opening penalty and gap extension penalty of 10 and 0.2, respectively, using ClustalW, and an unrooted consensus phylogenetic tree with 1,000 bootstrap replications was constructed using MEGA 6 (Tamura *et al.*, 2013).

### ***2.4. Genomic PCR and direct sequencing-based genotyping of ten functional V1Rs***

PCR primers for amplification and sequencing of 10 functional V1R loci were designed using CLC Genomics Workbench v. 3.6.5 (<http://clcbio.com>, CLC bio, Aarhus, Denmark). Amplification of V1Rs was performed in a 20- $\mu$ L reaction containing 50 to 100 ng of

genomic DNA, 0.5  $\mu$ M specific primers, 200  $\mu$ M dNTPs, PCR buffer [10 mM Tris (pH 8.3), 50 mM KCl, and 1.5 mM MgCl], and 0.5 U of Taq™ DNA polymerase (JMR Holdings, Kent, UK) using a Thermocycler 3000 (Biometra, Gottingen, Germany). The PCR conditions consisted of an initial denaturing temperature of 95 °C for 5 min, followed by 35 cycles of a three-step process of 45 s at 94°C, 45 s at a specific annealing temperature, and 2 min extension time at 72 °C for each primer, followed by a final incubation at 72°C for 10 min. The PCR products were checked by electrophoresis on a 1.5% agarose gel in 1× TAE buffer for 30 min at 100 V. The gel was stained with ethidium bromide and visualized under UV light. After doing the necessary steps on the PCR products we did direct sequencing using an automated DNA analyzer (3730XL, Applied Biosystem, Foster City, CA).

### ***2.5. Evolutionary Analysis of VIRs***

The rates of synonymous(Ks) and non-synonymous (Ka) substitutions were computed using the CLC Genomics Workbench v. 3.6.5 (<http://clcbio.com>, CLC bio, Aarhus, Denmark). Ka/Ks ratio, the average rates of non-synonymous (Ka) over synonymous substitutions (Ka) per site. Both independence for evolutionary changes and MacDonald-Kreiman tests to determine whether selection has acted on a particular gene to compute neutrality index (NI) were carried out using DnaSP v5 (Librado and Rozas, 2009).

### ***2.6. Analysis of VIR expression using semi-quantitative Reverse transcription (RT)-PCR***

Total RNA was extracted from seven tissues, including the vomeronasal organ, spleen, testis, main olfactory epithelium, lung, small intestine, and tongue, using Trizol (Invitrogen, Carlsbad, California) reagent according to the manufacturer's protocol. For the detection of the expression of VIRs, locus specific primers were designed for each VIR. An equal amount of cDNA was used as a template in all reactions and PCR amplifications was carried out with the following conditions: an initial denaturation for 5 min at 95 °C, followed by 28 cycles of 45 s at 94 °C, 30 s at 60 °C and 20 s at 72 °C, followed by a final incubation at 72 °C for 10 min. PCR products were analyzed by electrophoresis on a 1.5% agarose gel in 1× TAE buffer for 30 min at 100 V. The gel was stained with ethidium bromide and visualized under UV light.

### **2.7. Identification of Transcription Start Sites (TSSs) and determination of promoter regions for pig VIR genes**

To determine their respective TSSs for the ten pig VIR intact coding sequences, 1 kb sequences upstream of the start codon were excised from each gene. We used the Neural Network Promoter Prediction (NNPP version 2.2) tool set with the minimum standard predictive score (between 0 and 1) cutoff value of 0.8 for eukaryote (Reese, 2001). Therefore, as previously done for mice VIR gene promoter regions determination (Michaloski *et al.*, 2011) we defined promoter regions for pig VIR genes as 1 kb region upstream of each TSSs.

### **2.8. Identification of common motifs and transcription factors among porcine VIR promoter regions**

All the identified pig VIR promoter sequences were analyzed using the MEME version 4.10.0 searches, via the web server hosted by the National Biomedical Computation Resource (<http://meme.nbcr.net>) (Bailey and Elkan, 1994), and TOMTOM web server to look for common motifs and transcription factors that regulate the expression of VIR genes, respectively.

### **2.9. Search for CpG islands in pig VIR promoter regions**

We used two algorithms to search for CpG islands. First, we used the stringent search criteria in the Takai and Jones (Takai and Jones, 2002) algorithm: GC content  $\geq 55\%$ , ObsCpG/ExpCpG  $\geq 0.65$ , and length  $\geq 500$  bp. Secondly, we used the CLC Genomics Workbench ver. 3.6.5 (<http://clcbio.com>, CLC bio, Aarhus, Denmark) for searching the restriction enzyme *MspI* cutting sites (fragment sizes between 40-220bps).

## **3. Results**

### **3.1. Identification of vomeronasal receptor genes in the pig genome**

Based on the Genome BLAST search, we identified 25 VIR corresponding regions consisting of 10 (40.0%) functional genes with intact ORFs, 3 (12.0%) pseudogenes, and 12 (48.0%) partial genes in the pig genome (Table 1). However, we were unable to identify intact V2R and FPR sequences in the pig genome. Therefore, we focused on the analysis of VIRs as vomeronasal receptors in the pig genome. All of the intact or near intact VIRs were located on chromosomes 1, 2, and 6 with three, one, and nine genes, respectively, showing that chromosome 6 contains the largest number of VIRs in the pig genome. Two and one

V1R pseudogenes were identified from chromosomes 6 and 2, respectively (Table 1). These results indicate that the number of vomeronasal receptor genes is relatively small in pigs compared to other mammals, including other artiodactyl species such as cattle.

Table 1. Description of vomeronasal receptor type 1 (V1R) genes and their locations in the pig genome.

Gene ID	Gene name	Chromosome	Genome coordinate <sup>a</sup>		Length (bp)
LOC102167894	<i>sVIRD4</i>	6	54822222	54823184	963
LOC100626136	<i>sVIRF5</i>	6	52278473	52279411	939
LOC100738896	<i>sVIRD3</i>	6	55086207	55087136	930
LOC100738814	<i>sVIRD1</i>	6	55063285	55064214	930
LOC100624632	<i>sVIRF3</i>	6	52191360	52192292	933
LOC100622750	<i>sVIRJ1</i>	6	49351197	49352129	933
LOC100622109	<i>sVIRF4</i>	1	308988718	308989659	942
LOC100520313	<i>sVIRD2</i>	6	55135499	55136446	948
LOC100520712	<i>sVIRF2</i>	1	308948105	308949046	942
NC_010443	<i>sVIRF1</i>	1	308980430	308981437	1008
NC_010448.3	<i>sVIRD1p</i>	6	54925326	54924379	948
LOC102164459	<i>sVIRJ1p</i>	2	159906829	159905930	900
NC_010448	<i>sVIRD2p</i>	6	55175118	55174213	906

<sup>a</sup>Genome assembly, *Sus scrofa* 10.2

### 3.2. Assigning locus names to the V1Rs in pigs

For those genes as part of large gene families, it is important to establish the locus names according to the systematic nomenclature for accurate genome annotation or biological study, which will enable to understand the gene family function. The subfamily names of pig V1Rs were assigned according to the results of the clustering analysis, which compared them to known V1R subfamilies in mice which harbors numerous V1Rs (Rodriguez *et al.*, 2002) (Fig. 1). The letters “s” and “p” were used to represent *Sus scrofa* and pseudogenes at the beginning and at the end of the names, respectively (Table 1).

Next, we analyzed the genetic relationships among all identified pig V1Rs, including functional genes and pseudogenes. These formed three distinct clusters, which is consistent

with the results from figure 1. Although the number of genes was largest for the D subfamily, the genetic diversity within gene subfamilies was largest for the F subfamily.

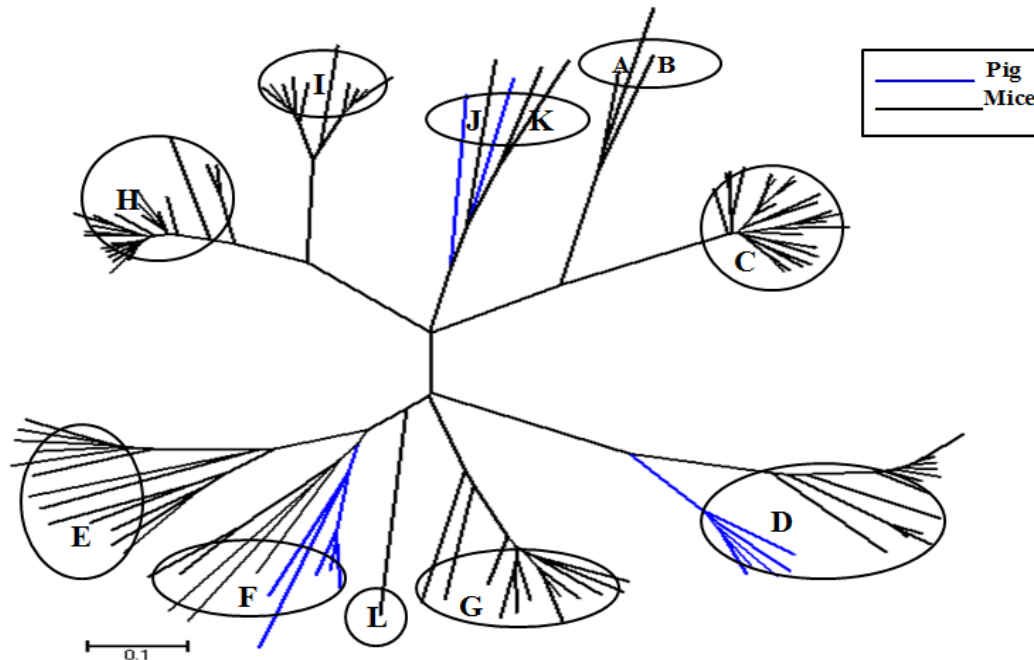


Fig. 1. Phylogenetic tree of pig and mice V1Rs. An unrooted tree representing 13 pig and 105 mice V1R nucleotide sequences, showing that the pig V1Rs cluster within the D, F and J subfamilies of the known mice V1Rs. The scale bar indicates 0.1 amino acid substitutions per site.

### 3.3. Allelic diversity in porcine V1Rs

In addition to the subfamily variation of V1Rs, we investigated the allelic variation of V1Rs by analyzing the nucleotide sequences of the entire coding region of ten functional V1Rs from a panel of ten animals of five different pig breeds, including Yorkshire, Berkshire, Duroc, Landrace, and Korean native pigs. The largest number of SNPs ( $n = 12$ ) was detected in Duroc and Yorkshire breeds, and the lowest ( $n = 6$ ) in Berkshire pigs. Consistent with the number of SNPs for each breed, the number of non-synonymous SNPs was the highest (35.29%) in Duroc, whereas Berkshire pigs had the lowest (11.76%). The number of SNPs in each V1R ranged from zero for *sVIRF5* and *sVIRJ1*, to 6 and 8 for *sVIRF1* and *sVIRF4*, respectively (Table 2), and 58% of the SNPs were synonymous. Considering that there were 24 SNPs in the 10 V1Rs within a 1 kb coding region, the average number of SNPs for pig V1Rs was approximately one SNP per 0.4 kb.

Table 2. Nucleotide polymorphisms identified in the coding region of pig vomeronasal receptors type 1 (V1Rs).

Locus name	Number of SNPs		
	Total	Nonsynonymous	Synonymous
<i>sVIRF1</i>	6	2	4
<i>sVIRF2</i>	1	1	0
<i>sVIRF3</i>	2	1	1
<i>sVIRF4</i>	8	2	6
<i>sVIRF5</i>	0	0	0
<i>sVIRJ1</i>	0	0	0
<i>sVIRD1</i>	1	0	1
<i>sVIRD2</i>	2	2	0
<i>sVIRD3</i>	2	1	1
<i>sVIRD4</i>	2	1	1
Total	24	10	14 (58%)

Note: Single nucleotide polymorphisms (SNPs) were deposited in the SNP database of the GenBank under the accession numbers described under materials and methods.

### 3.4. Evolution of porcine V1Rs

The ratio between non-synonymous ( $K_a$ ) and synonymous mutations ( $K_s$ ) was calculated to have an insight on the evolution of V1Rs (Table 3). We found that 85.75% of pig V1Rs have been subjected to purifying selection ( $K_a/K_s = 0.130\sim 0.708$ ) and only a single V1R, *sVIRJ1*, showed positive selection with  $K_a/K_s = 1.182$ . The average  $K_a/K_s$  ratio for V1R was 0.304, indicating that the evolution of pig V1Rs is largely shaped by strong purifying selection through the removal of alleles that are deleterious, resulting in stabilizing selection in the phenotypic outcomes. Inferences on selection using the McDonald-Kreitman test showed that pig V1Rs have been subjected to purifying selection (the average neutrality index (NI) = 1.471, Table 3) confirming the results of the average  $K_a/K_s$  ratio.

Table 3. Analysis of evolutionary forces on vomeronasal receptors in pigs based on the analysis of nucleotide polymorphisms in ten functional V1R loci in pigs

Locus name	Ks	Ka	Ka/Ks	NI*
<i>sVIRJ1</i>	0.00088	0.00104	1.182	1.591
<i>sVIRF1</i>	0.01098	0.00143	0.130	1.201
<i>sVIRF2</i>	0	0.00028	-	1.331
<i>sVIRF3</i>	0.00211	0.00066	0.313	1.981
<i>sVIRF4</i>	0.01123	0.00386	0.344	1.146
<i>sVIRF5</i>	0.00079	0.00026	0.329	1.589
<i>sVIRD1</i>	0.00042	0	0	0.966
<i>sVIRD2</i>	0	0.00027	-	1.802
<i>sVIRD3</i>	0.00227	0.00055	0.242	-
<i>sVIRD4</i>	0.00216	0.00153	0.708	1.631
Average	0.003084	0.000938889	0.304	1.471

Note: A total of 24 nucleotide polymorphic sites from 10 pigs of 5 different breeds were analyzed.\*NI, Neutrality index.

### 3.5. The expression pattern of V1Rs in pigs

The expression of pig V1Rs was evaluated using semi-quantitative RT-PCR in seven pig tissues, including the vomeronasal organ (VNO), spleen, testis, main olfactory epithelium, lung, small intestine, and tongue. All of the 10 functional sV1Rs were expressed in the VNO (Fig. 2) at varying degrees. The expression level was relatively strong for *sVIRF1*, *sVIRF3*, *sVIRF4*, *sVIRD3*, *sVIRD2*, and *sVIRD4* when compared to the rest. In addition, a low level expression of sV1Rs was detected in the lung after 28 PCR amplification cycles and no expression was detected using these PCR conditions in other tissues, including spleen, tongue, main olfactory epithelium, and small intestine. However, we were able to detect V1R specific bands in all tissues examined after 35 PCR amplification cycles, suggesting that all tissues examined had low expression levels of V1Rs. The level of expression and the expression pattern were almost identical for all 10 V1Rs, and only the results for *sVIRF3* are shown in Fig. 2 as an example.

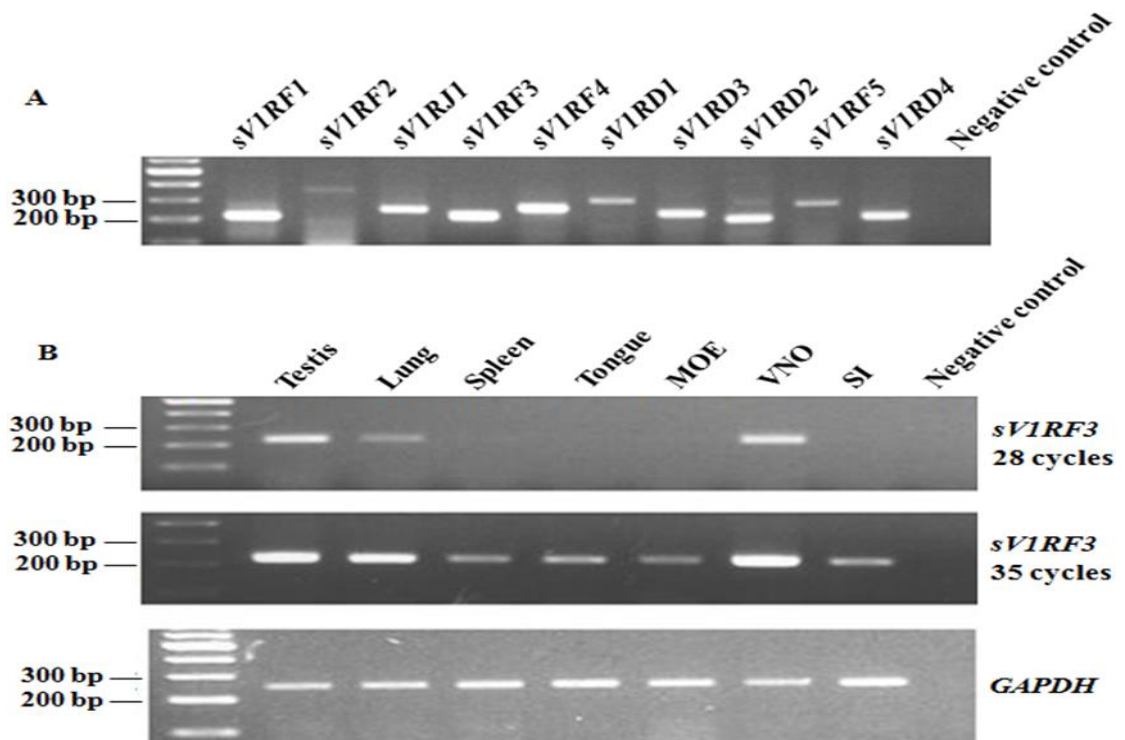


Fig. 2. Expression pattern of ten functional pig V1Rs in various tissues. (A) The expression of different pig V1Rs in the vomeronasal organ (VNO). Lane 1, size marker; lanes 2 to 11, pig V1Rs; lane 12, negative control in which *sVIRF3* primers were used for a PCR reaction without cDNA templates. (B) The expression pattern of *sVIRF3* in different pig tissues after 28 and 35 cycles of PCR amplification each. Lane 1, molecular marker; lanes 2 to 8, different tissues, lane 9, negative control in which *sVIRF3* primers were used for a PCR reaction without cDNA templates. *GAPDH* was used as the control for comparing the expression levels of *sVIRF3* among different tissues.

### 3.6. Identification of Transcription Start Sites (TSSs)

We first predicted TSSs for each of the 10 functional V1R genes and to make our prediction more reliable for genes containing more than one TSS, TSS of the highest prediction score was considered and identified as the correct TSSs. Consequently, as previously done for the determination of V1R gene promoters in mice (Michaloski *et al.*, 2011) we defined promoter candidate regions for pig V1R genes as 1 kb regions upstream of each TSS and used them for further analysis. We also revealed that the locations for 70% of the TSSs are within -500 bp relative to the start codon.

### 3.7. Common motifs and associated transcription factors in the promoter regions of pig VIRs

Because promoter regions of VIRs are likely to contain conserved motifs which are binding sites for transcription factors (Das and Dai, 2007), we tried to identify motifs that are common to most of pig VIR promoter sequences using the MEME Suite web server. Accordingly, we found five motifs that are shared by at least 50% of the pig VIR promoter input sequences (Table 4).

**Table 4. Identified common motifs in pig VIR promoter regions.**

Discovered motif	Number (%) of VIR promoters containing each one of the motifs	E-value*	Motif width	Total no. of binding sites
MV1	5 (50%)	1.1e-023	50	5
MV2	10 (100%)	2.4e-023	41	10
MV3	7 (70%)	2.5e-019	47	7
MV4	5 (50%)	3.2e-014	49	5
MV5	5 (50%)	9.9e-012	50	5

\* Probability of finding an equally well-conserved motif in random sequences.

We presented the relative location and spatial distribution of these motifs in the promoter regions: majority of them are concentrated between -600 and +1 bp of the TSSs (Fig. 3). It is also interesting to notice that motifs are almost equally distributed on both positive and negative strands with 17 and 15, respectively.

To determine motifs which are functionally important, we chose motifs which were shared by majority of promoter regions of pig VIR gene. Accordingly, we revealed MV2 as the common promoter motif for all (100%) pig VIR genes that serves as binding sites for transcription factors involved in the expression regulation of these genes.

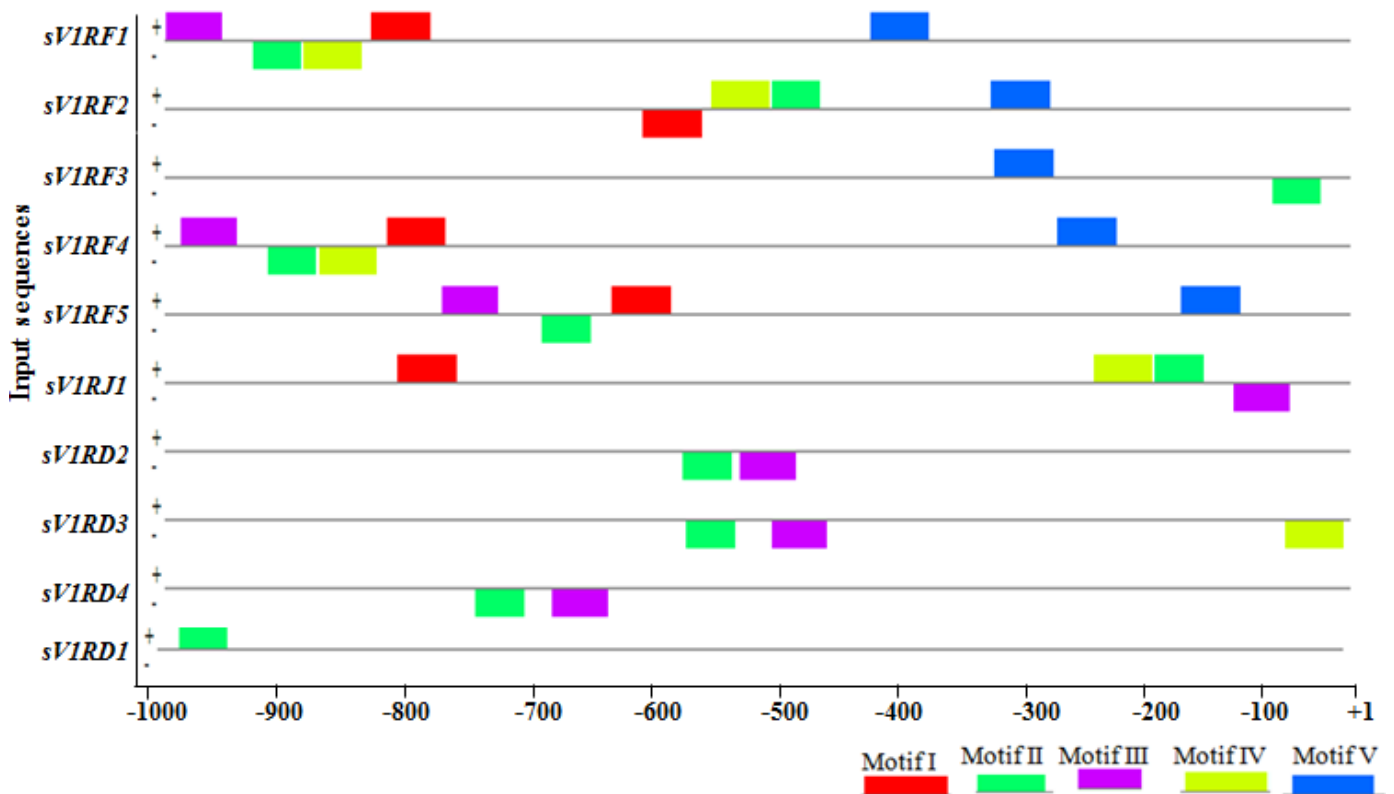


Fig. 3. Block diagrams showing the relative positions of motifs in different V1R subfamily sequences relative to TSSs. The nucleotide positions are indicated at the bottom of the graph from +1 (beginning of TSSs) to the upstream 1000 (-1000) bp.

Furthermore, we performed additional analyses to get more insights on the MV2 motif of pig V1R genes. We compared MV2 to registered motifs in publically available databases such as JASPAR to see if they are similar to known regulatory motifs for transcription factor by using the TOMTOM web application (Gupta *et al.*, 2007). As a result, MV2 matched with 15 out of 205 known motifs found in JASPAR vertebrates' motif databases. On the basis of their statistical significance values, we selected top 10 matched motifs. From our analysis result, we found six BetaBetaAlpha-zinc finger (BTB-ZF), three Hormone-nuclear Receptor (HNR) and one Helix-Loop-Helix (HLH) transcription factor families which are binding candidates for MV2 motif. Our result also show that MV2, has the highest resemblance with the binding motif for BTB-ZF genes, which is also a known transcription factor family for mouse V1R and OR gene regulations (Michaloski *et al.*, 2011). Therefore, the MV2 motif could also serve as a binding site for the BTB-ZF transcription factor gene family in pigs to regulate the expression of pig V1R genes.

### 3.8. Investigation for CpG islands (CGIs) in pig V1R promoter regions

To further explore the regulatory elements that are involved in 10 V1R genes, we conducted *in silico* analysis to investigate for CpG islands in its promoter and gene body regions using Takai and Jones' algorithm (Takai and Jones, 2002). Accordingly, we were unable to find any CpG islands from either promoter or gene body regions of pig V1R genes.

Using the second approach to evaluate the presence of CpG in the pig V1Rs, we performed the *in silico* digestion for the ten pig V1R sequences using restriction enzyme *MspI*. Accordingly, we only found CpG islands from the *sVIRJ1* gene that contains three fragment sizes: 74, 75 and 201bps in its promoter region and 93, 163 and 203bps in its gene body region. However, there were no CpG island specific sequences in other nine V1Rs in pigs, indicating that pig V1R is poor in CpG islands.

## 4. Discussion

In the present study we carried out a genome level analysis of vomeronasal receptors in the pig genome through the analysis of the current pig genome assembly. We showed that only V1Rs are functional in pigs among the three types of pheromone receptors, V1Rs, V2Rs, and FPR. We also showed that the genetic diversity of vomeronasal receptors has been under strong purifying selection and that are expressed at a low level in all tissues examined, except for the high expression of V1Rs in the VNO and testes. Our results contribute towards the understanding of the machinery responsible for pheromone detection and its influence on pig behavior because pigs could serve as an interesting large animal model system to study pheromone-related neurobiology due to their genetic simplicity as described in this study.

## References

- Bailey LT, Elkan C: "Fitting a mixture model by expectation maximization to discover motifs in biopolymers", *Proceedings of the Second International Conference on Intelligent Systems for Molecular Biology*, 1994:28-36, AAAI Press, Menlo Park, California.
- Dong D, Jin K, Wu X, Zhong Y: CRDB: Database of chemosensory receptor gene families in vertebrate. *PLoS One* 2012, **7**:e31540.
- Dulac C, Axel R: A novel family of genes encoding putative pheromone receptors in mammals. *Cell* 1995, **83**:195–206.
- Grus WE, Shi P, Zhang YP, Zhang J: Dramatic variation of the vomeronasal pheromone receptor gene repertoire among five orders of placental and marsupial mammals. *Proc. Natl Acad. Sci. USA* 2005, **102**:5767–5772.
- Gupta S, Stamatoyannopoulos JA, Timothy B, William SN: "Quantifying similarity between motifs", *Genome Biology* 2007, **8**:R24.

- Herrada G, Dulac C: A novel family of putative pheromone receptors in mammals with a topographically organized and sexually dimorphic distribution. *Cell* 1997, **90**:763–773.
- Librado P, Rozas J: DnaSP v5: A software for comprehensive analysis of DNA polymorphism data. *Bioinformatics* 2009, **25**:1451-1452.
- Michaloski JS, Galante PA, Nagai MH, Armelin-Correa L, Chien MS, Matsunami H, Malnic B: Common promoter elements in odorant and vomeronasal receptor genes. *PLoS ONE* 2011, **6**:e29065.
- Prather RS, Shen M, Dai Y: Genetically modified pigs for medicine and agriculture. *Biotechnol. Genet. Eng. Rev.* 2008, **25**:245–246.
- Reese MG: Application of a time-delay neural network to promoter annotation in the *Drosophila melanogaster* genome". *Comput Chem* 2001, **26**: 51-56.
- Rodriguez I, Del Punta K, Rothman A, Ishii T, Mombaerts P: Multiple new and isolated families within the mouse superfamily of V1r vomeronasal receptors. *Nat Neurosci.* 2002, **5**:134–140.
- Rodriguez I, Mombaerts P: Novel human vomeronasal receptor-like genes reveal species-specific families. *Curr Biol.* 2002, **12**:409–411.
- Rouquier S, Giorgi D: Olfactory gene repertoires in mammals. *Mutat. Res.* 2007, **616**:95-102.
- Ryba NJ, Tirindelli R: A new multigene family of putative pheromone receptors. *Neuron* 1997, **19**:371–379.
- Sambrook J, Russell DW: *Molecular cloning: A Laboratory Manual*. 3rd edn. Cold Spring Harbor Laboratory Press, Cold Spring Harbor; New York, 2001.
- Takai D, Jones PA: Comprehensive analysis of CpG islands in human chromosomes 21 and 22. *Proc Natl Acad Sci USA* 2002, **99**:3740-3745.
- Tamura K, Stecher G, Peterson D, Filipowski A, Kumar S: MEGA6: Molecular Evolutionary Genetics Analysis version 6.0. *Mol. Biol. Evol.* 2013, **30**: 2725-2729.
- Young JM, Kambere M, Trask BJ, Lane RP: Divergent V1R repertoires in five species: amplification in rodents, decimation in primates, and a surprisingly small repertoire in dogs. *Genome Res.* 2005, **15**:231–240.
- Young JM, Massa HF, Hsu L, Trask BJ: Extreme variability among mammalian V1R gene families. *Genome Res.* 2010, **20**:10–18.

## Genetic Diversity and Population Structure Analysis in Finger Millet (*Eleusine coracana* (L.) Gaertn) Genotypes Using Inter Simple Sequence Repeat Marker in Ethiopia

Haftom Brhane<sup>1</sup>, Teklehaimanot Haileselassie<sup>2</sup> and Kassahun Tesfaye<sup>3</sup>

<sup>1</sup> Department of Biology, Haramaya University, Ethiopia Email: [haftom1@gmail.com](mailto:haftom1@gmail.com)

<sup>2</sup> Institute of Biotechnology, AAU, Addis Ababa, Ethiopia Email: [tekle1961@yahoo.com](mailto:tekle1961@yahoo.com)

<sup>3</sup> Institute of Biotechnology, AAU, Addis Ababa, Ethiopia Email: [kassahuntesfaye@yahoo.com](mailto:kassahuntesfaye@yahoo.com)

### Abstract

*In Ethiopia the ever increasing of population need to supply enough and balanced diets. Uses of integrated conventional and molecular agricultural technologies are the pertinent way to achieve sustainable and stable agriculture development in Ethiopia. Among the crops in Ethiopia, Finger millet is one of the crop which is cultivated in stress environments particularly drought areas which reduced starvation. In other hands, it is affected by diseases like head blast. Hence to reduced production constraints which influences finger millet productivity and production; studies on genetic diversity, population structure and screening of unique markers for desirable traits in finger millet genotypes are determinant issues. Therefore this research was conducted to investigate level of genetic diversity in 80 finger millet accessions using ISSR markers. The study was done in Genetics and molecular laboratory in Addis Ababa University. DNA was extracted from a bulk of three plants of leaf per accession using a modified Cetyl trimethyl ammonium bromide CTAB method. Six/or seven ISSR primers amplified a total of 45 clear and reproducible bands. Six ISSR primers amplified a total of 45 clear and reproducible bands. The total genetic diversity (H) and Shannon's diversity information index (I) for the entire populations was 0.28 and 0.41, respectively. Analysis of molecular variance in both grouping and without grouping revealed larger genetic diversity within the populations (58.54%) than among populations (41.45%). The total genetic diversity 5.88 % was attributed to populations within groups, 38.33 % to among groups and 55.79 % to differences within populations. Both unweighted pair- group method with arithmetic average dendrograms and a neighbor joining trees were constructed for the individuals and populations using Jaccard's similarity coefficient. Most accessions from all populations tended to form their own cluster, while only few of the individuals were distributed all over the tree. Generally, the result of the present study confirmed the presence of genetically diversified accessions that can be used to improve the productivity, conservation and sustainable use. For further improvement of the crop quantitative trait locus analysis should be studied. In this study the genetic diversity analysis of *Eleusine coracana* accessions was done using ISSR markers. Therefore, further study with accessions from different agro-ecology using different molecular markers such as SSRs as well may be needed to confirm the result of the present study as a single molecular marker cannot fulfill all of the desirable properties of molecular markers.*

**Keywords:** Finger millet; genetic diversity; gene flow

## 1. Introduction

Finger millet (*Eleusine coracana L.*) is extensively cultivated in the tropical and sub-tropical regions of Africa and India. It is known to save the lives of poor farmers from starvation at times of severe drought (Kotschi, 2006). It adapt to a wide range of environments and grown mainly by subsistence farmers which serves as a food security crop because of its high nutritional value; longer shelf life and requires low agricultural inputs (Dida *et al.*, 2007).

Ethiopia is one of the major finger millet producing country next to Uganda, India, Nepal and China. It is also native to the highlands of the country. Finger millet plays an important role in Ethiopia both the dietary needs and incomes of many rural households like other African countries due to its richness in fiber, iron and calcium (Bezaweletaw 2011).

Molecular markers have the distinct advantages of being independent of climatic variables and very numerous. ISSR-PCR is one of the most convenient and popular method to identify intraspecific genetic polymorphism (Zietkiewicz *et al.*, 1994). ISSR markers could be good tools to assess the genetic diversity and relationship at inter and intra population level. Even though finger millet is an important crop used for food security, its integrated use of agricultural technologies to boost productivity and production is lower compare to other major crops (sources). Therefore, it is vital to investigate the level of genetic diversity of finger millet genotypes and populations structures which were collected from different regions in Ethiopia, Zimbabwe and India using ISSR markers. The study provides information on the overall genetic variability in finger millet genotypes which assist in the identification and selection of unique genetic markers that used for further breeding program.

## 2. Materials and Methods

### 2.1. Description of Study Area and Experimental materials

The study was conducted at Genetics and molecular laboratory in Addis Ababa University in 2015 year. Eighty finger millet genotypes were collected from different regions of Ethiopia, Zimbabwe and India (69, 6 and 5 genotypes), respectively, which obtained in Ethiopian Institute of Biodiversity. Eighty finger millet genotypes were grown in Addis Ababa University green house for six weeks. Six ISSR primers (UBC810, UBC811, UBC848, UBC866, UBC873 and UBC880) were used to explore genetic diversity of these finger millet genotypes.

## **2.2. Experimental Procedures and Techniques**

### **2.2.1. DNA Extraction**

Eighty genotypes collected from different regions of Ethiopia, Zimbabwe, and India obtained from Ethiopian Institute of Biodiversity were germinated in green house for six weeks. Total genomic DNA was extracted following protocol of Borsch et al.(2003). Dried leaf samples were bulked and ground with Mix and Mill grinding machine MM 400 and the quality and amount of genomic DNA was tested using NanoDrop (NanoDrop™2000/2000c) spectrophotometer and 1 % agarose. Working solution was made by diluting the genomic DNA in a 1:5 ratio, stored at -20°C until PCR reaction started.

### **2.2.2. ISSR-PCR amplification and gel electrophoresis**

Three genotypes were selected from each population with 1:5 dilutions to screen primers for their amplification, polymorphism and reproducible bands. A total of six out of seven polymorphic and reproducible ISSR primers were selected after testing and screenings. Polymerase chain reaction (PCR) amplifications were performed in Biometra 2003 T3 Thermo cycler programmed to run the following temperature profile: a preheating and initial denaturation for 4 minutes at 94°C, then 15 seconds denaturation at 94°C, 1 minute primer annealing at 45°C/48°C/55°C (based on primers used), 1.30 minutes extension at 72°C for 40 cycles and the final extension for 7 minutes at 72°C with holding temperature at 4°C. Each PCR reaction of ISSR markers had a final reaction volume of 25 µl, containing 1 µl dNTPs, 2.5 µl PCR buffer, 3 µl MgCl<sub>2</sub>, 0.4 µl primer, 0.4 µl Taq polymerase and 10-50 ng template DNA. A negative control, in which the template DNA was replaced by double distilled water, and also included in each round of reactions to check for absence/presence of contamination. The PCR products were stored at 4 °C until loading on the gel for electrophoresis. Amplification products were separated by electrophoresis in 1.67 % (w/v) agarose gels. A total of 8 µl PCR product of each sample and 6x loading dye was loaded on to the ISSR gel. Fifteen wells comb was used for each ISSR gel slab. The first lane was loaded with 100 bp ladder by loading 2 µl (peq gold range mix) with loading dye in that well as a size standard and the last lane was control (without DNA template). The ISSR electrophoreses were done for about 3 hours at constant voltage of 100 V. After electrophoresis, the gels were stained in 50 µl (10 mg/ml) ethidium bromide mixed with 450 ml distilled water for 30 minutes and destained with distilled water for 30 minutes then banding patterns were visualized under UV light and photograph using canon camera in the Biometra Biodoc Analyzer (Biosens SC750) and documented for band scoring and analysis.

### 2.2.3. Data recording and statistical analysis

Inter simple sequence repeat (ISSR) markers were treated as dominant markers and each locus was considered as a bi-allelic locus with one amplifiable and one null allele. Band scoring was done manually for each primer based on presence (1) and absence (0) or ambiguous (?), and each band was regarded as a locus. POPGENE version 1.32 software (Yeh *et al.*, 1999) was used to calculate genetic diversity for each population as number of polymorphic loci, percent polymorphism, gene diversity ( $h$ ) and Shannon–Weaver diversity index ( $I$ ). Analysis of molecular variance (AMOVA) was used to calculate variation among and within population using Arlequin version 3.01 (Excoffier *et al.*, 2006).

NTSYS- pc version 2.02 (Rohlf, 2000) and Free Tree 0.9.1.50 (Pavlicek *et al.*, 1999) software's were used to calculate Jaccard's similarity coefficient which is calculated using the following formula:-

$$S_{ij} = \frac{a}{a+b+c}$$

Where, 'a' is the total number of bands shared between individuals  $i$  and  $j$ , 'b' is the total number of bands present in individual  $i$  but not in individual  $j$  and 'c' is the total number of bands present in individual  $j$  but not in individual  $i$ .

The unweighted pair group method with arithmetic average (UPGMA) (Sneath and Sokal, 1973) was used in order to determine the genetic relationship among accessions and generates phenogram using NTSYS- pc version 2.02 (Rohlf 2000). The neighbor joining (NJ) method (Saitou and Nei, 1987; Studier and Keppler, 1988) was used to compare individual accessions and evaluate patterns of accession clustering using Free Tree 0.9.1.50 Software (Pavlicek *et al.*, 1999).

A principal coordinated (PCOA) analysis was performed based on Jaccard's coefficient (Jaccard 1908) to further examine the patterns of variation among individual samples. The calculation of Jaccard's coefficient was made with PAST soft ware version 1.18 (Hammer *et al.*, 2001). The first three axes were later used to plot with STATISTICA version 6.0 software (Hammer *et al.*, 2001; Statistica soft, Inc.2001).

## 3. Result and Discussion

### 3.1. ISSR Primers and Their Banding Patterns

Pre-screening of primers was performed to test the polymorphism and reproducibility of the primers. Among the seven primers tested initially, six of them gave clear, reproducible and

polymorphic bands were selected as informative markers. The fragment size amplified with these primers was in the range of 200 to 1500 base pair. A total of 45 fragments were amplified by the six ISSR primers of which 35 were polymorphic and the remaining 10 fragments were monomorphic. The highest number of bands was amplified by primer UBC-880 and UBC 866, while the lowest number was amplified with UBC-811 (Table 1).

**Table 1.**List of ISSR primers used with their repeat motifs, amplification fragment size, number of scorable bands and amplification pattern data

No.	Primers		Amplified Fragment size (bp)	NSB	Amplification pattern
	Name	Sequence			
1	UBC 810	(GA)8C	300-1000	7	Very Good
2	UBC 811	(GA)8T	400-1000	4	Very Good
3	UBC 848	(CA)6RG	200-1000	5	Excellent
4	UBC 866	(CTC)6	300-1500	10	Excellent
5	UBC 873	(GACA)4	300-1500	9	Excellent
6	UBC 880	(GGAGA)3	200-1000	10	Excellent

*Key: Single-letter abbreviations for mixed base positions: R = (A, G), NSB: number of scorable bands*

### **3.2. Polymorphism Bands and Genetic Diversity in Finger Millet Genotypes**

The number of polymorphic loci ranges from 2 for UBC-811 to 9 for UBC-880, where they are SSR with di- and penta- nucleotide repeat motif, respectively, (Table 2). Penta-nucleotide primer (UBC 880) generated high number of percent polymorphism compared to the di-, tri-, and tetra-nucleotide, UBC-811 was showed the least polymorphism with 50.0%, while UBC-880 was showed the highest polymorphism with 90.0% polymorphism. The overall gene diversity (h) by the six primers was 0.28, while Shannon's information index was 0.41. The highest gene diversity (h) 0.37 and Shannon's information index (0.54) were obtained from UBC- primer 880, while the least gene diversity of (0.17) and Shannon's information index of (0.25) from UBC-811. Moreover, the choice of appropriate primer motifs in ISSR fingerprint is essential to detect high polymorphism and to reveal relationships within and

among populations. The abundance and distribution of SSRs in the genomes of finger millet could be another factor that determines the levels of polymorphism.

This study was showed high percentage of polymorphism (77.78%) using six ISSR primers According to (Bezaweletaw 2011) study 72.35 % percentage of polymorphism in 66 finger millet genotypes from Ethiopia and Eritrea using RAPD markers, (Fakrudin *et al.*, 2004) study 85.82 % percentage of polymorphism in 32 germplasms from Indian using ISSR or other markers, and (Salimath *et al.*, 1995) report 26 % percentage of polymorphism in 17 finger millet genotypes from Africa, Asia and Brazil using ISSR. Inclusion of large number of finger millet accessions from diverse ecological condition and large geographical range such as Ethiopia, Zimbabwe and India contributes for high percentage of polymorphism.

Among all the populations, Gojam population was showed higher percentage of polymorphism with 55.56%, while the least percent was detected from Omo population with 13.33%. Generally, Amhara region finger millet population has highest percent of polymorphism (60.0%) than other region populations (24.44 - 51.11%) (Table 2). The highest gene diversity ( $h$ ) 0.19 and Shannon's information index (0.29) were obtained from Gojam, Wellega, Awi and Zimbabwe populations, while Omo population showed the least gene diversity of (0.05) and Shannon's information index of (0.07). Generally, Amhara region finger millet populations have highest variability (0.35), while the least was obtained from SNNP (0.15) (Table 2). This result Implies Amhara region farmers are active in finger millet seed exchange with other regions via market channels and also through seed dispersal.

**Table 2. Number of polymorphic loci (NPL), percent polymorphism (PP) and genetic diversity (h) and Shannon information index (I) of finger millet genotypes with each population using primers**

<b>All primers</b>				
	<b>NPL</b>	<b>PPL</b>	<b>h</b>	<b>I</b>
Gojam	25	55.56%	0.19 ± 0.20	0.28 ± 0.29
Gondar	18	40.00%	0.17 ± 0.21	0.24 ± 0.30
Awi	20	44.44%	0.19 ± 0.22	0.28 ± 0.31
Wellega	21	46.67%	0.19 ± 0.21	0.28 ± 0.31
Ilu Ababora	7	15.56%	0.06 ± 0.15	0.08 ± 0.21
Adwa	11	24.44%	0.10 ± 0.19	0.15 ± 0.27
Shire	8	17.78%	0.06 ± 0.14	0.09 ± 0.21
Hadiya	10	22.22%	0.10 ± 0.19	0.14 ± 0.28
Omo	6	13.33%	0.05 ± 0.14	0.07 ± 0.20
India	9	20.00%	0.09 ± 0.18	0.12 ± 0.26
Zimbabwe	20	44.44%	0.19 ± 0.23	0.28 ± 0.32
Overall	35	77.78%	0.28 ± 0.19	0.41 ± 0.26
<b>Groups</b>				
Oromia	21	46.67 %	0.19 ± 0.21	0.28 ± 0.31
Amhara	27	60.00 %	0.24 ± 0.21	0.35 ± 0.30
Tigray	13	28.89 %	0.11 ± 0.19	0.17 ± 0.27
SNNP	11	24.44 %	0.10 ± 0.19	0.15 ± 0.28
Exotic	23	51.11 %	0.21 ± 0.22	0.30 ± 0.31
Overall	35	77.78 %	0.29 ± 0.19	0.43 ± 0.26
<b>Individual primer</b>				
810	6	77.78%	0.31 ± 0.18	0.46 ± 0.25
811	2	50.00%	0.17 ± 0.22	0.25 ± 0.32
848	4	80.00%	0.29 ± 0.18	0.43 ± 0.26
866	7	70.00%	0.18 ± 0.19	0.29 ± 0.27
873	8	88.89%	0.30 ± 0.17	0.46 ± 0.24
880	9	90.00%	0.37 ± 0.16	0.54 ± 0.22
Overall	35	77.78%	0.28 ± 0.19	0.41 ± 0.26

### 3.3. Analysis of Molecular Variance (AMOVA) in Finger millet

There were highly significant genetic differences ( $p \leq 0.001$ ) between the five groups as well as between twelve Populations of finger millet genotypes. AMOVA showed that higher percent of variation (58.54%) is attributed to within population variation, while 41.45 % is due to the among population variation. On the other hand, of the total genetic diversity 5.88 % was attributed to populations within groups, 38.33% to among groups and 55.79% to differences within populations, which implies high genetic exchange or gene flows among populations by the dispersal of the seeds and seed exchange via market channels. Similarly, Tsehay (2012) reported that high variation (90.59%) attributed to the within species, while the remaining variation (9.41%) was due to among species variation.

Table 3. AMOVA of finger millet populations, A; without grouping. B; with groups

Source of variation	d.f.	Sum of squares	Variance component	Percentage of variation	Fixation Indice (FST)	P-value
Among populations	10	187.56	2.49	41.45	0.41	P<0.001
Within populations	63	204.28	3.52	58.54	-	P<0.001
Total	73	391.84	6.01	-	-	
Among geographic groups	4	153.75	2.42	38.33		P<0.001
Among populations with in geographic groups	6	33.81	0.37	5.88	0.44	P<0.001
Within populations	63	204.28	3.52	55.79	-	P<0.001
Total	73	391.84	6.31	-	-	-

### 3.4. Clustering analysis

Unweighted pair group method with arithmetic mean (UPGMA) and NJ analysis was carried out to construct dendrogram for the 12 populations and 80 individuals based on 45 PCR bands amplified by six ISSR primers. In Figure1, there was clear-cut clustering of populations. Besides this, individual based NJ (Figure 2) and PCOA (Figure 3) clustering of an overall analysis showed strong clustering of individuals with respect to their population except few intermixed populations. The present study was in agreement with the finding of

(Fakrudin *et al.* 2004) who found a clear apportionment of finger millet accessions in concordance with geographical origin using RAPD marker, while in contrast with (Bezawletaw, 2011) reported no clear-cut clustering of accessions to their geographic origin. Though the accessions evaluated in this study mainly represented landraces from different geographical regions of Ethiopia, the analysis of UPGMA tree showed a clear-cut pattern of variation in relation to geographical region, which could be due to domestication and cultivation of finger millet that might be development of local landraces limited in a particular location and with limited gene flow.

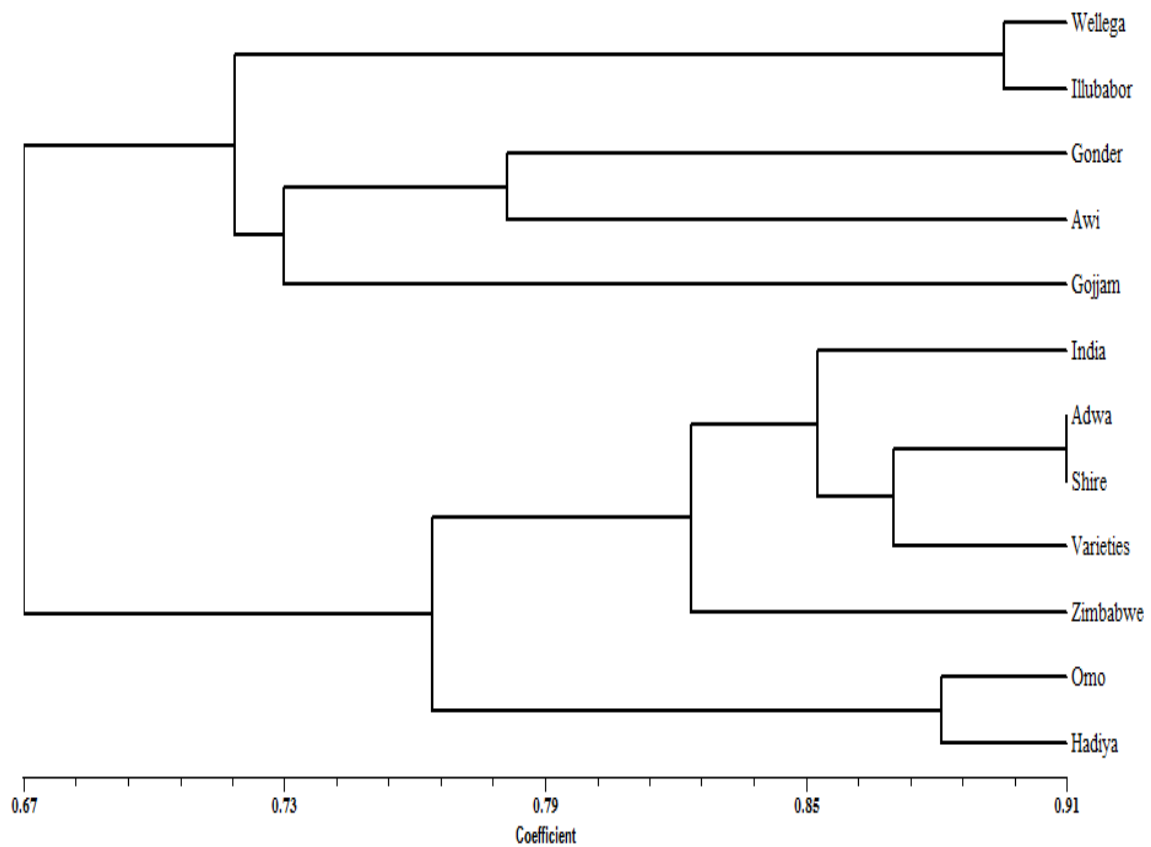
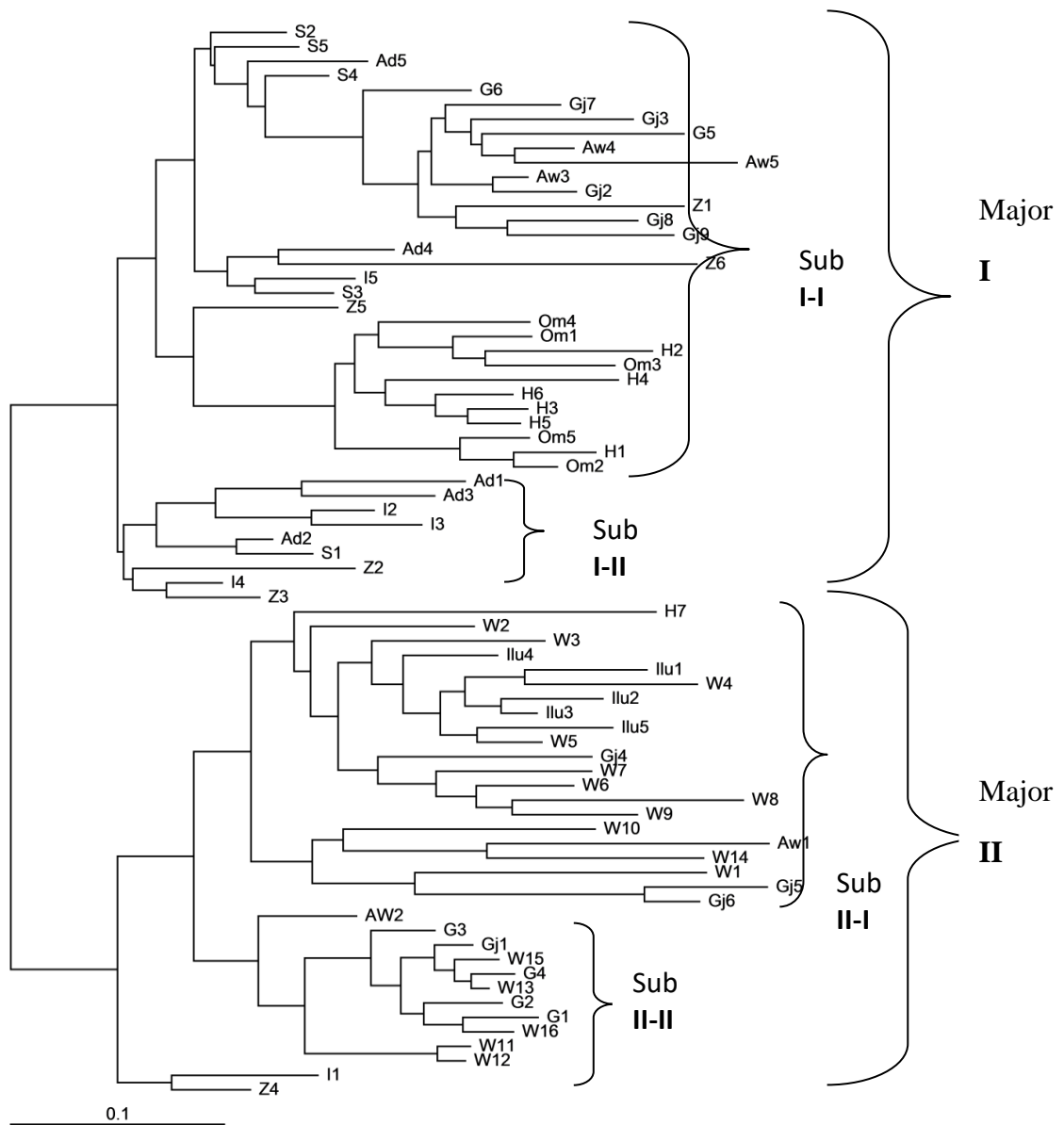


Figure1. Clustering of 12 populations using 80 finger millet genotypes/or 45 bands based on UPGMA analysis methods using six ISSR primers.



**Key:**

*W1-16= Wellega      Aw1-5=Aw1      S1-5= Shire      Gj1-9= Gojam*  
*Ilu1-5= Ilu Ababora      I1-5= India      O1-5= Omo      Ad1-5=Adwa*  
*G1-6= Gondar      Z1-5= Zimbabwe      H1-7= Hadiya*

Figure 2. Neighbor-joining analysis of 80 individuals based on 45 PCR bands amplified by five primers.

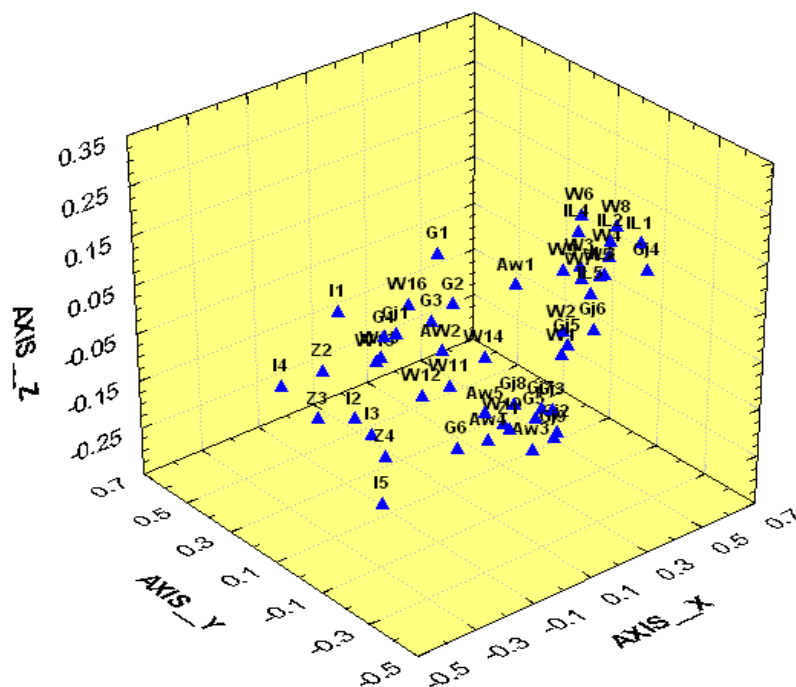


Figure 3. Three-dimensional (3D) plot obtained from principal coordinate analysis of 80 *E. coracana* accessions using six ISSR primers with Jaccard's coefficient similarity.

#### 4. CONCLUSIONS

The genetic diversity data generated by six ISSR primers revealed that high genetic diversity exists in finger milletgermplasms. The assessed genetic diversity level varied among populations, which could be due to different environmental conditions in which they are growing, naturally distributed and human selection pressure. Moreover, Gojam and Wellega populations showed relatively high genetic diversity than others. The AMOVA analysis showed that, high genetic variation within populations than among populations shows the existence of high gene flow and low genetic differentiation among populations. The UPGMA cluster analysis supported the grouping of accessions to the defined geographical location and the respective population in the analysis of the total accessions. The findings of this study indicate that ISSR markers could be good tools to assess the genetic diversity and relationship at inter and intra population level of finger millet.

#### 5. Acknowledgments

The researcher would like to thank Ethiopian Institute of Biodiversity (Addis Ababa, Ethiopia) for kindly providing seeds with their passport data.

## References

- Bisht, M. and Mukai, Y. 2001. "Genomic in situ hybridization identifies genome donor of finger millet (*Eleusine coracana*). *Theoretical and Applied Genetics* 102:825-832.
- Borsch, T., Hilu, K.W., Quandt, D., Wilde, V., Neinhuis, C. and Barthlott, W. 2003. Noncoding plastid *trnT-trnF* sequences reveal a well resolved phylogeny of basal angiosperms. *J. Evol. Biol.* 16: 558–576.
- Dida, M.M., Srinivasachary, R.S., Bennetzen, J.L, Gale, M.D. and Devos, K.M. 2007. The genetic map of finger millet, *Eleusine coracana*. *Theor Appl Genet.* 114: 321–332.
- Excoffier, L., Laval, G. and Schneider, S. 2006. *An Integrated Software Package for Population Genetics Data Analysis. Computational and Molecular Population Genetics Lab (CMPG)*, Institute of Zoology, University of Berne, Switzerland.
- Fakrudin, B. Kulkarni, R.S., Shashidhar, H.E and Hittalmani, S. 2004. Genetic diversity assessment of finger millet, *Eleusine coracana* (Gaertn), germplasm through RAPD analysis. *Plant Gen. Res. Newslet.* 138: 50-54.
- Hammer, O., Harper, D.T. and Ryan, P.D. 2001. PAST: Paleontological statistics software package for education and data analysis. *Palaeontologia electronic* 4:9, [http://palaeo-electronica.org/2001\\_1/past/issue1-01.htm](http://palaeo-electronica.org/2001_1/past/issue1-01.htm).
- Jaccard, P. 1908. Nouvelles recherches Sur la distribution florale. *Bull. Soc. Vaud. Sci. Nat.* 44: 223-270.
- Kebere Bezawetaw 2011. Genetic diversity of finger millet [*Eleusine coracana*.(L) Gaertn] landraces characterized by Random Amplified Polymorphic DNA Analysis. *Innov. Syst. Design Eng.* 2: 2222-2871.
- Kotschi, J. 2006. Coping with Climate Change, and the Role of Agrobiodiversity. Conference on International Agricultural Research for Development. Tropentag 2006 University of Bonn. October 11-13, 2006.
- Pavlicek, A., Hrda, S. and Flegr, J. 1999. Free-tree-software program for construction of phylogenetic trees on the basis of distance data and bootstrap/jackknife analysis of the tree robustness. Application in the RAPD analysis of genus *Frenkelia*. *Folia Biol. (Praha)*. 45: 97-99.
- Rohlf, F.J. 2000. *NTSYS-pc ver 2.11T. Exter Software*, Setauket, New York.
- Saitou, N. and Nei, M. 1987. The neighbor-joining method: A new method for reconstructing phylogenetic trees. *Mol. Biol. Evol.* 4: 406-425.
- Salimath, S.S., de Oliveira, A.C., Godwin, I.D. and Bennetzen, J.L. 1995. Assessment of genome origins and genetic diversity in the genus *Eleusine* with DNA markers. *Genome* 38: 757–763.
- Sneath, P. and Sokal, R. 1973. *Numerical taxonomy*. Freeman, Sanfrancisco.
- Statistica Stat Soft, Inc. 2001. STATISTICA (data analysis software system) Version 6.0. [www.statsoft.com](http://www.statsoft.com).
- Studier, J. A. and Keppler, K. L. (1988). A note on the neighbor-joining algorithm of Saitou and Nei. *Mol. Biol. Evol.* 5: 729-731.

- Tsehay, S. 2012. Genetic diversity and relationships among cultivated and wild *Eleusine* species collected from Ethiopia as revealed by ISSR Marker. MSc thesis, Addis Ababa University, Ethiopia.
- Yeh, F., Yang, R. and Boyle, T. 1999. Population genetic analysis of co-dominant markers and qualitative traits. *Belgian J. Bot.* 129: 157.
- Zietkiewicz, E., Rafalski, A. and Labuda, D. 1994. Genome fingerprinting by simple sequence repeat (SSR)-anchored polymerase chain reaction amplification. *Genomics* 20: 176-183.

## **Integration of Remote Sensing and Hydraulic Models to Identify Flood Prone Areas in Woybo River Catchment, South Western Ethiopia**

**Aschalew Fekadu<sup>1,\*</sup>, Daniel Teka<sup>2</sup>, Kassa Teka<sup>2</sup>**

<sup>1</sup>Department of Natural Resource Management, Institute of Geo-information and Earth Observation Sciences (I-GEOS), Mekelle University

<sup>2</sup>Department of Land Resources Management and Environmental Protection, Mekelle University \*e-mail: [mmbalm11@gmail.com](mailto:mmbalm11@gmail.com), Tel: +251-9-47990159

### **Abstract**

*Flooding is one of the major challenges globally threatening human life and affecting agricultural lands. In Ethiopia there are limited research efforts that address challenges related to flooding through integrated approach of satellite imageries and hydraulic models. In this study, integration of Remote Sensing (RS) and one-dimensional (1-D) HEC-RAS model was used in Woybo River catchment, South Western Ethiopia. The Required data set, a remotely sensed land sat 7 image of march 2013 with a spatial resolution of 30m, were downloaded from united states geological survey. These images were classified into different land cover types so as to use them for estimating the roughness coefficient of the various cover types. Daily peak rainfall data were collected from two metrological stations (1990 – 2013) to estimate design rainfall and runoff corresponding to 5, 10, 25, 50, 100 and 200 return period. Steady flow analysis was carried out in HEC-RAS to evaluate the flooding risk zones along the river. The result showed that the estimated design rainfall corresponding to these return periods is 63.2, 70.87, 80.57, 87.77, 94.91 and 102.02 mm and estimated runoff corresponding to these return periods is 378, 461, 568, 650.5, 733, and 817m<sup>3</sup>/sec. Up to 1987 ha of land can be inundated through a runoff having a 200 yr. return period. The study showed that flood prone areas were at the lower reach along the River extending to 50m from the river banks. The results were verified using ground-based assessment corresponding to the various return periods. The result demonstrates that integration of RS and hydraulic models can suitably be used to identify flood prone areas and to assist early warning systems related to flooding.*

**Keywords:** Remote Sensing, Design rainfall; Design runoff; HEC-RAS

### **INTRODUCTION**

Fluctuations in seasonal rainfall and amount resulted from Climate change have major impact on flooding which led to a common occurrence and largely distributed natural hazard in the world, (Jelínek et al., 2007; Cook and Merwade, 2009). These hazards include destruction of agricultural soils and devastation of different installations, (Shu et al., 1993; Rakhi et al., 2008). According to Abhas and Jessica, (2012), flood affected about 178 million people

worldwide in 2010 alone with a total financial loss exceeding \$40 billion. It is reported as the second major natural hazard next to drought in Ethiopia, (IFRC, 2010). According to the EM-DAT 2008 report, major floods in Ethiopia (1999 -2009) affected about 1,108,604 people. This is mainly linked to the national topography of the highland mountains and lowland plains with natural drainage systems formed by the principal river basins, (Zewde, 2004; NMA, 2013). The country receives about 80% of the rains in the rainy season (June and September) in which the major perennial rivers as well as their numerous tributaries form the country's drainage systems carry their peak discharges, (DPPA, 2006). Other drivers of increased flooding impacts are the increased population size lead to increased demand for land for agriculture which again direct to forest degradation and encroachment of people to settle in close proximity to the flood prone areas (Semu, 2007; Bishaw, 2012). Regardless of the challenges of flooding hazard in the country in general and the study area in particular, the use of scientific approach to identify flood prone areas and estimate the rainfall and run-off amount and intensity were not common. Hence, identifying flood prone area is very essential for planning and focused development functions. Numerous flood hazard assessment studies conducted in the world indicated that Integration of technologies GIS (Geographic Information System), Remote Sensing (RS) and one-dimensional (1-D) HEC-RAS model is efficient in simulating, identifying and analyzing flood events in a geo spatial environment (Sam and Shamsi, 2002). In this connection, (Collins Fosu, et al., 2007; Asgar et al., 2013; Okirya, 2012) in their studies found that Geographic Information System coupled with HEC-RAS and remotely sensed data is essential in flood plain delineation and hazard mapping. Also (Getahun and Gebre, 2015), used integration of GIS and one dimensional hydraulic models for Flood Hazard Assessment of the Awash River Basin in Ethiopia from stream flow data. Since this study area is un-gauged and data scarce catchment the study, therefore, aimed at introducing the use of GIS and RS as well as hydrologic models to map the spatial distribution of flood hazard areas from daily peak rainfall data so as to help planners and implementers prioritize their planning and decision making.

## **MATERIAL AND METHODS**

### **Description of the study area**

The study was conducted at Woybo river catchment. It is located in North East of Omo Gibe basin in South western, Ethiopia at  $6^{\circ} 55' 20''$  N to  $7^{\circ} 2' 40''$  N and  $37^{\circ} 51' 40''$  to  $37^{\circ} 31' 0''$  E, Fig. 1 The catchment area is  $561.26 \text{ km}^2$ .

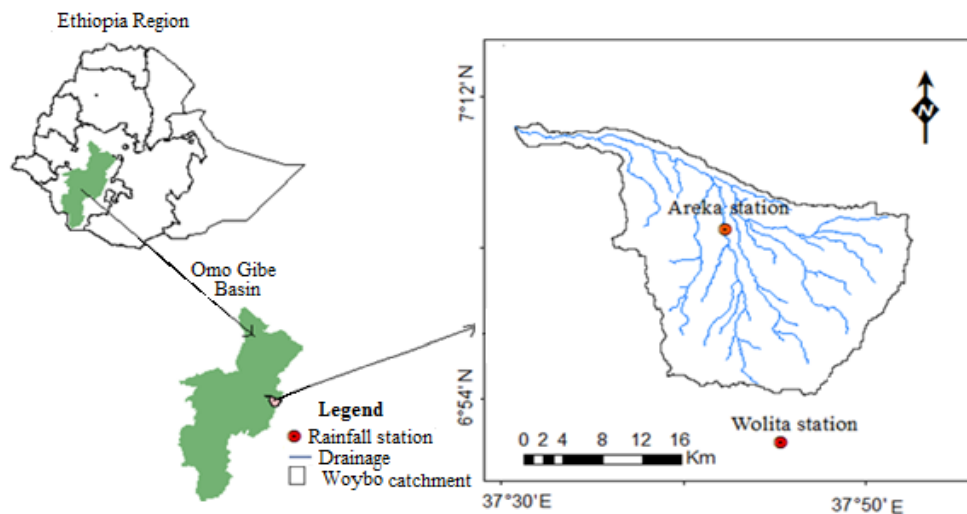


Figure 1. Location of Woybo River catchment(own processing)

The topography of Woybo river catchment is very steep in upper reaches and sudden in lower reaches, The altitude ranges from 768 to 2946 M.a.s.l. The soil types in the area are important as they control the amount of water that can infiltrate into the soil, and hence the amount of water which becomes runoff, (Teka, 2014). The major soil reference groups in Woybo river catchment are Dystric Nitosols (55.3%), Pellic Vertisols (31.94%), Chromic Luvisols (10.54%) and Eutric Cambisols (1.69%). The study area **has tropical climate regime**. Monthly average temperature varies between **21.5 °C in Mar to 17.8 °C in July**. **The monthly average relative humidity (RH) falls in the range of 44.61 -76.65% while the average sunshine hours for almost 8 months of the year is about 80%, and falls to below 50% during monsoon**. The rainfall distribution of the study area is largely controlled by the south - north movement of the Inter Tropical Convergence Zone (ITCZ) (Mathewos 2013). The study area is characterized by bimodal rain fall type, short rainy season, which extends between March to May and locally known as “Belg” receives 28% (338.4 mm) and the long rainy season and locally known as “Kiremt”, which extends from June up to October receive 62% (847.9 mm). The average annual rainfall of the study period (1990 to 2013) is 1366 mm.

## Methodology

In this study several models and software are used. The Storm water Management and Design Aid (SMADA) distribution model was used for the frequency analysis of the daily rainfall data so as to estimate the rainfall with a given return period. The surface runoff was estimated using SCS-CN method and the peak runoff was estimated using SCS-CN composite hydrographs. HEC-Geo-RAS and HEC RAS were used to analyze the flood prone areas. The methods followed in this study are schematically represented in Figure 2.

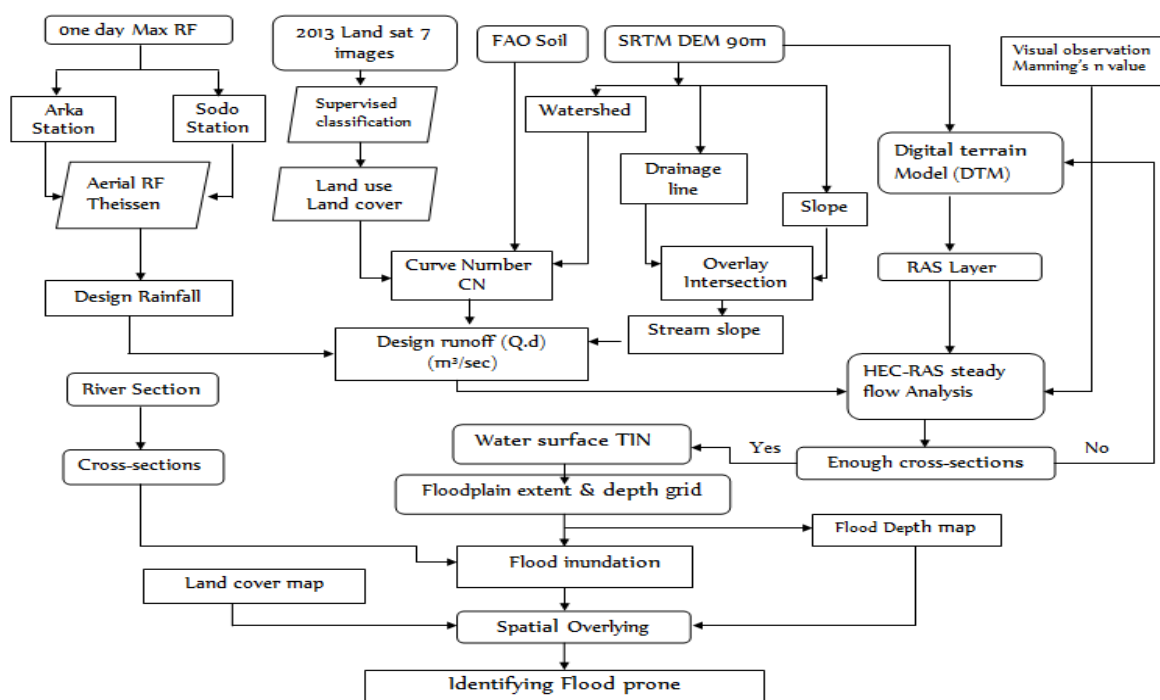


Figure2.Flow chart for flood prone area identification

## Land Cover Classification and Mapping

Prior to image classification, actual field observation was held and a total of seven land cover classes which include cropland, forest, shrubs and bush land, grazing land, bare lands, woodland and Built-up were selected. Land sat 7 imagery (path 169 and row 55) for the year 2013 (March) was used to classify the current land cover types. The land cover classification was done in ERDAS 9.2 software. In the pre-processing of image classification extraction and image staking was done using band combinations in Arc-GIS to



and 200 years return periods: Normal, 2 parameter log normal, parameter log normal, person distribution, person type III, and Gambel in combination with Weibull plotting position. The DISTRIB 2.0 component in SMADA (Storm Water Design Aid) software was used to conduct the daily rainfall frequency analysis.

### **Testing the goodness of fit of probability distribution**

The best probability distribution function was determined by comparing Chi-square values obtained from each distribution and selecting the function that gave smallest chi-square value (Agrawal et al., 1988), and mean square errors RMSE (Ahmad, 2012). The chi-square test is given as:

$$X^2 = \sum_{i=1}^k \frac{(O_i - E_i)^2}{E_i} \dots \dots \dots \text{(Eq 2)}$$

Where,  $O_{ii}$  is the observed rainfall,  $E_{ii}$  is the expected rainfall and will have chi-square distribution with  $(N - k - 1)$  degree of freedom (d.f.).

$$X^2 = \frac{1}{N} \sum_{i=1}^N (P_i - O_i)^2 \dots \dots \dots \text{(Eq 3)}$$

Where P is the predicted value, O is the observed value and N is the number of data.

### **Hydrological soil group**

Soils are classified into four HSG's (A, B, C, and D) according to their minimum infiltration rate. The different soil textures of Woybo river catchment were obtained from the digital soil and terrain database of east Africa FAO 1997. Based on the rules of hydrologic soil group classifications developed by the US Natural Resource Conservation Service (NRCS), the hydrologic soil map of Woybo river catchment was generated.

### **The Curve Number (CN)**

The Curve Number (CN) for the catchment was created by intersecting two shape files; the soil hydrologic group map and the land cover map. From standard SCS-CN look up Table the correct curve numbers were assigned for all the combinations. The weighted hydrologic curve number was determined for the whole catchment area based on the three antecedent moisture conditions (Equation 4).

$$CN = \left( \sum \frac{CN_i \times A_i}{A} \right) \dots \dots \dots \text{(Eq 4)}$$

Where: CN = weighted curve number, CN<sub>i</sub> = curve number from 1 to any no. N, A<sub>i</sub> = area with curve number CN<sub>i</sub>, A = the total area of the Woybo river catchment.

### **Design Peak run off estimation**

SCS-CN model was used to estimate the Rainfall-runoff depth and runoff rate is estimated using composite hydrograph method (Teka, 2014).

$$Q = \frac{(P-0.2)^2}{P+0.8S} (p>0.2S) \dots \dots \dots (Eq 5)$$

Where, S is Woybo river catchment storage (in mm); Q is the actual direct runoff (in mm); and p is the total rainfall (in mm).

The equation has one variable p and parameter s. s is related to curve number (CN) by:

$$S = \frac{25400}{CN} - 254 \dots \dots \dots (Eq 6)$$

### **Hydraulic models used for data Analysis**

The current study used HEC-Geo-RAS 10 and HEC-RAS 4.1 models. A HEC-Geo RAS model was used to create RAS Layers under GIS environment and provide the interface between the systems, and HEC-RAS model. HEC-GeoRAS generates stream centerline, flow path center lines, main channel banks, and cross-section cut Lines (Masoud et al., 2013) using Digital Terrain Model (DTM). HEC-RAS provides the geometric simulation of the river to calculate water surface profiles.

### **Steady Flow analysis**

HEC-RAS model perform steady and unsteady flow analysis. In this study steady Flow analysis was used since it assumed flow is steady in each river reach i.e. the model not considers flood duration as a factor (Ripendra, 2003). To calculate water surface profiles in HEC-RAS, the output from HEC-Geo RAS was used. The Manning roughness coefficient, 'n' value of different land resulted from field visit and calibration was inputted to HEC-RAS manning's n value table, designed runoff of six return periods as 2, 10, 25, 50, 100 year and 200 year different periods, was inputted in steady flow data and Reach boundary conditions of Upper most cross section River Station of each streams was taken as upper stream boundary. Critical depth for the rest upstream and downstream was also inputted in this window. By running Sub critical steady flow analysis, water surface profiles were calculated.

Then HEC-RAS data are exported to Arc GIS for flood inundation mapping and flood prone area identification. Finally a total of 11 Ground truth points were collected from 5 frequently affected kebele (Adila, Areka town 04, Chama hemibecho, Matala hemibecho and Werimuma) of the river catchment for model validation.

## **Results & Discussion**

### **Land cover classification**

The land cover classification showed that crop and bush and shrubs land covered for (60.70%) and (26.07% of the study area) respectively while forest, built up, wood, bare and grazing lands accounted to about (4.27%), (0.11%), (0.77%), (1.52%) and (6.52%) respectively. The results of classification accuracy were found to be 90.47% and 0.876 Overall Kappa Statistics.

### **Design daily maximum rainfall**

The estimated daily maximum design rainfall corresponding to 5, 10, 25, 50, 100, and 200 year return period is indicated in Table-1.

Table 1: Predicted Design peak Rainfall using six PD

Plotting Position	Error measure	Probability Distributions					
		Normal	2 para Log normal	Person Type III	Log person Type III	3 para Log normal	Gambel
Weibul	RMSE	4.48	3.67	3.30	3.42	3.31	<b>3.11</b>
	Chi-square	0.21	0.33	0.36	0.49	0.39	<b>0.12</b>
Return period (year)		<b>Estimated Design Rainfall (mm)</b>					
	5	63.32	62.62	60.44	61.39	61.74	<b>63.20</b>
	10	68.58	69.05	68.57	68.32	68.84	<b>70.87</b>
	25	74.19	76.62	79.47	77.27	77.86	<b>80.57</b>
	50	77.82	81.95	87.86	84.10	84.62	<b>87.77</b>
	100	81.08	87.05	96.37	91.07	91.41	<b>94.91</b>
	200	84.06	92.00	105.02	98.25	98.29	<b>102.02</b>

Chi-square values varied from 0.12 to 0.49 for the six PDFs. Least Chi-square values are

observed in Gumbel Type I distribution for prediction of design rainfall. The chi-square values for normal, log-normal, 2 parameter log normal, Pearson type-III, log-Pearson type-III, 3 parameter log normal and Gumbel distributions are 0.21, 0.33, 0.489, 0.365, 0.39 and 0.124. Moreover, the RMSE is estimated to be 4.48, 3.67, 3.297, 3.416, 3.313 and 3.105 respectively were estimated for the return periods. As Gumbel combined with Weibull provides minimum Chi-square value and RMSE, the design rainfall is selected as 63.20, 70.87, 80.57, 87.77, 94.91, and 102 mm for 5, 10, 25, 50, 100 and 200 years return periods. This finding is in agreement with the research results of Bishaw (2012), ICIMOD (2007) and Mandal et al. (2013) who reported that Gumbel's method is the best fit. Other studies documented that PDF other than Gumbel are best estimates for the daily maximum rainfall estimation. For example Singh et al. (2012) and Mandal et al. (2013) showed that log-Pearson type-III is the best probability distribution.

### **Design runoff**

The maximum retention from the SCS-CN is estimated as 24.43mm. The daily runoff depths are 63.20, 70.80, 80.57, 87.77, 94.91 and 102.02 mm. This corresponds to a peak runoff rate

of which were used to estimate the design runoff in  $\text{m}^3/\text{se}$  using SCS-CN composite hydrographs for different return periods are 378, 461, 568, 650.5, 733, and 817. The design runoff analyzed in all (23) reach of the river catchment showed that the average runoff volume contributed by thus river reaches is  $413.2 \text{ m}^3/\text{sec}$  4% of the total. Generally, design runoff analyzed from these reaches of the river catchment showed that upper reaches generate an average runoff of  $5879.53 \text{ m}^3/\text{second}$  (58.6% runoff contribution) and lower reach's generate  $4155 \text{ m}^3/\text{second}$  (41.4% runoff contribution) of the entire river catchment.

### **HEC-RAS Steady flow**

#### **Cross-section**

Cross sectional graph given below elucidates the capacity of the natural drainage system to pass the volume of water generated by rainfall in different return periods. The X axis show the Cross sectional distance in meter and the Y axis represents the water elevation of 5, 10, 25, 50, 100 and 200 years return periods in meter.

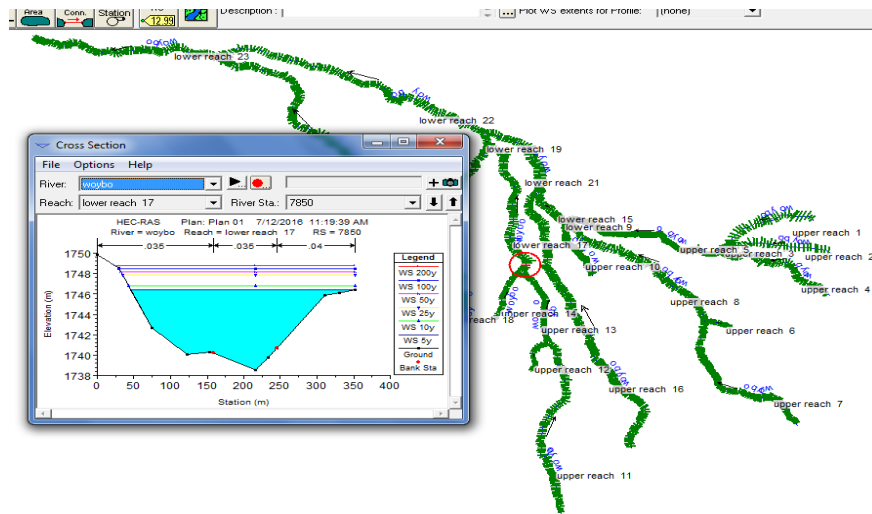


Figure 3. Cross sections map of lower reach 17

The result showed that some cross sections are narrow and runoff can out-flow the river Cross section. As can be seen from Fig. 3, at the lower river reach (Reach 17, river station 7850), even the 5 year return period flood can overpass the river section and can inundate the surrounding area.

### Longitudinal profile

Similarly the runoff carrying capacity as can be seen through the longitudinal profiles at each river Cross section shows that selected river sections are small to carry the runoff corresponding to various return periods. As can be seen on Fig. 4, at river reach 17, the 5 year return period runoff can over flow the river reach. This finding is in agreement with (parviz, 2013), which reported that with increasing return period water elevation in the longitudinal profile will be increased too. Also Steady analysis result rating curve showed direct relationship between design runoff and water surface elevation.

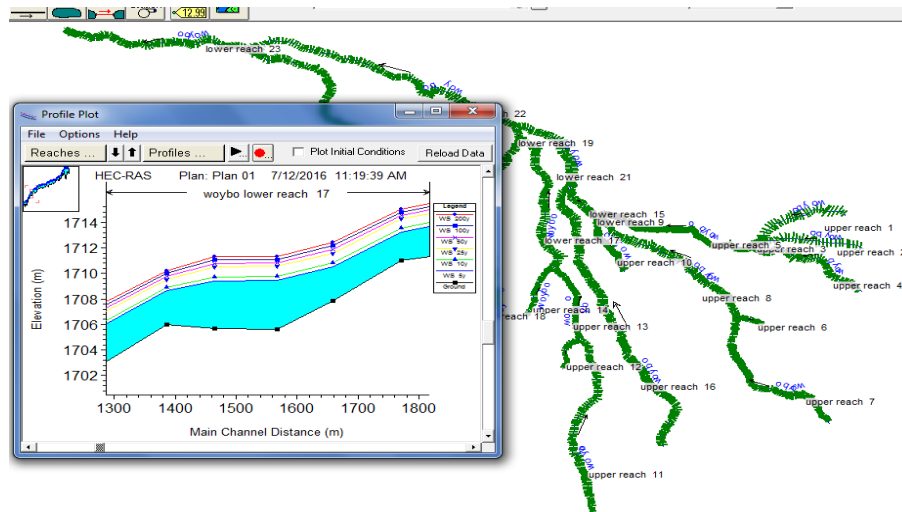


Figure 4. Longitudinal profiles of Woybo River lower reach 17 of different year floods.

### Flood Prone area

The result of flood delineation showed that area inundated by flood in the 5, 10, 25, 50, 100 and 200-years return periods floods is 1727, 1788, 1859.6, 1905.6, 1949.6 and 1987 hectare respectively. The result of flood delineation areas in the sub-catchments of the river showed that the maximum and minimum average flood inundation areas for the different return periods are 196.84 hectare and 0.0012 hectare respectively. The average flood area inundation by thus sub catchments is 80.24 hectare. The result also indicated that flood area inundation increased with increasing design runoff. Furthermore water depth increased with the increased flooding intensity. It was also observed that 11 sub-catchments (75.55% of the catchment area) show inundation area above the average. The result also showed total design runoff from the river catchment at different return periods are 6104.8, 7463.9, 9136.6, 10388, 1115.5 and 12780.6 m<sup>3</sup>/second respectively which inundated 1727, 1788, 1859, 1905, 1950 and 1987 hectare of the river catchment respectively.

The classification of flood depth areas indicate that 31%, 34%, 38%, 40%, 43% & 45% of the total flooded areas has water depths greater than 3 m. The total area under the water depth of 2-3 m was 23%, 23%, 23%, 22%, 20% and 20% respectively. The total area under the water depth of more than 3.0 m increased considerably with an increase in the intensity of flooding. For the 5 year return period, it is observed that the inundated area by flood depth of < 2, 2-3, and >3 meter are 795, 542.6 and 390 hectare respectively. Whereas for the 10 year return

period the inundated areas are 760, 407 and 621. For the 25 year return period, the inundated areas are 736, 422.8 and 702. For the 50 year return period, the inundated areas are 716.4, 425 and 765 hectare. For the 100 year returned period, the inundated areas are 708.6, 398.2 and 843 hectare and for the 200 year return period, they are 690, 390 and 900 hectare respectively. These results indicated that flood hazard increased with increased return period. The flood inundation and depth map were overlaid in land cover map as shown in Fig. 5.

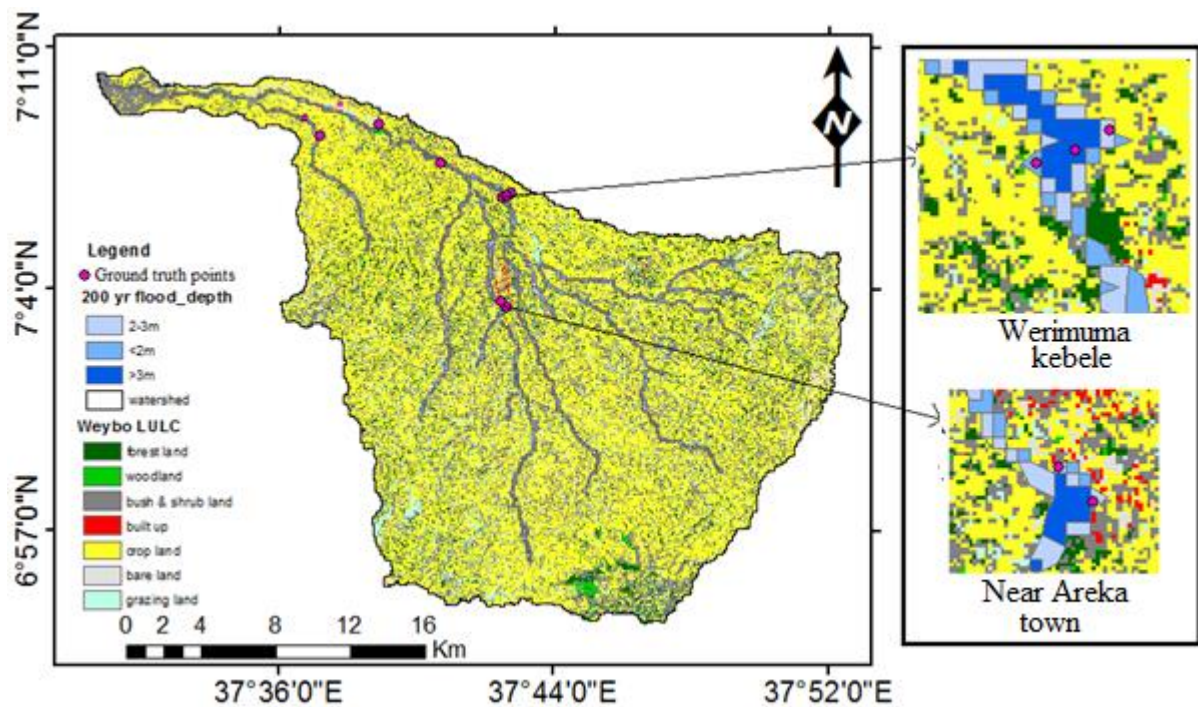


Figure 5. Flood prone areas of Woybo River catchment for the 2000 year return period

The result of spatial overlay Figure 5, showed that the lower reach areas especially crop land and villages located near the river side area (within 50m) are flood prone and affected more by 50, 100 and 200 return period flood. Flood inundation map overlay in elevation map show that the prone areas lies in elevation range between 1500 to 1800 M.a.s.l. Similarly Manandhar (2010) stated that large percentage (> 40 %) of vulnerable area lied on sand area followed by vulnerable area lied in forest and cultivation area. Okirya (2012) found that Sironko river middle reach and some villages located in the flood plain would be affected more especially with the 50, 100, 250, and 500 year floods.

## **Conclusions & Recommendations**

This research demonstrates that the integration of RS and GIS with one dimensional hydraulic model like HEC-RAS can provide reliable results to map out flood prone areas in Ethiopian catchments. Gumbel distribution matched with Weibull plotting Positions is a better predictor of design runoff for Woybo river catchment. Estimation of design Rainfall runoff using SCS hydrograph model can provide reliable estimates of peak runoff for delineating flood prone areas. Woybo upper reach 11 has the maximum runoff value of 8.02% contribution to the entire river catchment where as Woybo upper reach 6 has the minimum runoff contributions only 2%. Assessment of flood inundated area using HEC-RAS using current land use for different return periods of 5, 10, 25, 50, 100 and 200 showed small difference for the Woybo river catchment. The flood prone area was lies along the river side's crop area which is more fertile and productive area. About 39% of the areas under flooding have water depth above 3m. Area located near the river side would be affected more especially with the 50, 100, and 200 year floods. The identified flood-prone areas validation showed good result. However, further studies should be conducted with more rain fall station data for the period of 500 and 1000 return period.

## **REFERENCES**

- Abhas, k. Robin, B. & Jessica, L. (2012). Cities and flooding. Integrated urban flooding risk management for the 21<sup>st</sup> centry. p 21/638
- Abubaker, H. M. A. Elhag, A. M. H, & Salih, A . M. (2013). Accuracy Assessment of Land Use & Land Cover Classification in Shomadi area Upper Nile, South Sudan". International Journal of Scientific and Research Publications, ISSN 2250-3153 Vol. 3 (3).
- Ahmad, S. Chong, S. Nor, A. & Faustian, A. (2012). Determination of the Best Probability Plotting Position for Predicting Parameters of the Weibull Distribution: International Journal of Applied Science and Technology. Vol. 2 No. 3
- Asgar, S. H. Alireza, P. & Majid, R. (2013). Flood Zoning in Rural Watersheds by GIS and HECGEO-RAS in North western Iran. Greener Journal of Science, ISSN: 2276-7835 Vol. 3.
- Agarwal, M.C. Katiyar, V. S. & Babu, R. (1988). Probability analysis of annual maximum daily rainfall of U. P., Himalaya. Indian Journal of Soil Conservation 16(1, 35-42).

- Bhim, S. & Deepak, R. (2012). Probability analysis for estimation of annual one day maximum rainfall of Jhalarapatan area. India. Mpuat College of Horticulture and Forestry.
- Bishaw, K. (2012). Application of GIS and Remote Sensing Techniques for Flood Hazard and Risk Assessment: in Dugeda Bora Woreda of Oromiya Regional State, Ethiopia.
- Cook, A. & Mervade, V. (2009). Effect of topographic data, geometric configuration and modeling approach on flood inundation mapping. *Journal of hydrolog*, Vol(377).
- CollinsFosu, A. A. (2012, May). River inundation and hazard mapping a case study of Susan River Kumasi. Paper presented at the meeting of Global Geospatial Conference, Canada.
- Daniel, A. D. (2007). Assessment of flood risk in Dire Dawa town, Eastern Ethiopia, using GIS. Department of Earth Science, Addis Ababa University Ethiopia.
- DPPA. (2006). Joint Government and Humanitarian Partners Flash Flood Disaster in Ethiopia. Addis Ababa, Ethiopia.
- Getahun, Y. S. & Gebre, S. L. (2015). Flood Hazard Assessment and Mapping of Flood Inundation Area of the Awash River Basin in Ethiopia using GIS and HEC-GeoRAS/HEC-RAS Model. *Journal of Civil & Environmental Engineering*.
- Hasmadi, M. (2008). Satellite Data Classification Accuracy Assessment Based From Reference Dataset. *International Journal of Environmental, Ecological, Geological and Mining Engineering*. Vol: 2, 18.
- IFRC. (2010). Ethiopia: Response to seasonal floods. International Federation of Red Cross and Red Crescen.
- ICIMOD & UNESCO., 2007 Preparing for Flood Disaster Mapping and Assessing Hazard in the Ratu Watershed, Nepal Kathmandu, p. 33.
- Jelínek, R. Wood, M. Hervás, J. (2007). Risk Mapping of Flood Hazards in New Member States. European Commission Joint Research Centre.
- Manisha, B. P. (2012). Image Classification Tool for Land Use / Land Cover Analysis: A Comparative Study of Maximum Likelihood and Minimum Distance Method. *International Journal of Geology, Earth and Environmental Science* Vol. 2 (3), 2277-2081(Online).

- Mandal, K. G. Padhi, J. Kumar, A. D. K. Sahoo, P. Majhi, S. Ghosh, R. K. Mohanty, M. R. (2013). Analyzing Rainfall Events and Soil Characteristics for Water Resources Management in a Canal Irrigated Area, *Journal of Water Resources and Ocean Science*. Vol. 2, No. 1.
- Manandhar, B. (2010). Flood Plain Analysis and Risk Assessment of Lothar Khola. Tribhuvan University, Institute of Forestry, department of Watershed Management, Nepal.
- Masoud, B. M. Farzad, H. & Seyyed, M. T. (2013). Flood Management of Sistan River using Levee. *Journal of Academic and Applied Studies*. ISSN1925-931X, Vol. 3(10).
- Mathewos, M. B. (2013). Modeling Rainfall-Runoff using SWAT model in the Woybo River Catchment of south western Ethiopia. Department of Geo-information and Earth Observation Sciences for Natural Resource Management, Mekelle University
- NMA., 2013. Flood alert. National Meteorology Agency. Addis Ababa Ethiopia.
- Okirya, M. Albert, R. & Janka, O. (2012). Application of HEC HMS/RAS and GIS tools in flood. *Global journal of engineering, design and technology*, ISSN 2319 – 7293 Vol. 1(2), 20.
- Parviz, K. & Mohammad, H. Q. (2013). Efficiency of Hydraulic Models for Flood Zoning Using GIS (Case Study: Ay-Doghmush River Basin). *Life Science Journal* 2013; 10(2)
- Ripendra, A. (2003). Floodplain Analysis and Risk Assessment of Lakhandei River. Applied Research Grants Program for Disaster Risk Reduction (Rounds I and II).
- RAY, S. M. (2012). Simulation of runoff and flood inundation in kosi river basin using hydrological models, ANN, Remote sensing and GIS, Nepal(Unpublished master's thesis). Department of Civil Engineering National Institute of Technology, Nepal.
- Sam U. Shamsi., 2002. GIS Applications in Floodplain Management. In: 22nd Annual ESRI International User Conference, July 8–12, San Diego, CA: ESRI.
- Semu. A. M. (2007). Flood Forecasting and Early Warning System (FFEWS) an Alternative Technology for Flood Management System and Damage Reduction in Ethiopia: A Concept Note. Catchment and Lake Research. Arba Minch University, School of Graduate Studies
- Shu, L. & Finlayson, B. (1993). Flood management on the lower Yellow River hydrological and Geo-morphological perspective. *Sedimentary Geology*, Vol (85), pp285- 296.

Teka, Daniel. (2014). Multi-scale analysis of surface runoff and water harvesting dams in a semi-arid region: a case study in Tigray (Ethiopia). Earth and Life Institute Centre de recherche sur la Terre et le climat Georges Lemaitre, University catholique de Louvain.

Zewde. Z. M. (2004). Development of Flood Forecasting Model in Middle Awash River Basin of Ethiopia. MEE09204.

**Generating Groundwater Quality Spatial Distribution Models and Investigating its Suitability for Irrigation Use based on GIS and Geospatial Technology: The case of Upper Geba Catchment, Northern Ethiopia**

**Amanuel Gidey**

Email: [amanuelgw19@gmail.com](mailto:amanuelgw19@gmail.com)/[amanuelgw@yahoo.com](mailto:amanuelgw@yahoo.com), Cell phone number:  
+251914751663/+251914014247

Mekelle University Institute of Geo-Information and Earth observation Sciences, Mekelle,  
Tigray, Ethiopia.

***Abstract***

*The existing water resources in the study area was adversely affected due to rapid growth of population density, fast expansion of urbanization, industrialization, overexploitation, very poor management of wastes and watershed management these leads to decline the water resource quality as well as irrigation production rate and food security. Agricultural irrigation with poor water quality causes unsuitable to the plant growth, soil structure and affecting its fertility rate. To overcome these sever environmental problems, a systematic evaluation and investigation on water quality using GIS and geospatial techniques. The main goal of this research work was mapping spatial distribution and investigating on the current situation of water resources on its quality and suitability by measuring level of suitability to irrigation use based on salinity, sodicity, bicarbonate and specific ion toxicity hazards. To diagnosis the laboratory data AAS, UV, Titration and Calculation methods was used. GIS and geostatistical methods like kriging, IDW, spline, semivariogram model types and weighted overlay techniques have been used for data processing and analysis. RMSE, MSE, RMSSE, ASE and comparison on measured values versus predicted values was used for accuracy assessment. According salinity result, 71.43 % doubtful water class, 14.29 % good water class, 11.43 % unsuitable water class and 2.86 % suitable water class to irrigational use. Hence, the result revealed that 71.43 % of the water samples of the study area were hardly suitable for irrigational purpose. Based on SAR and RSC values, the result revealed suitable water to irrigational use. The overall view of the water quality and its suitability of the present study showed that most of the area having a good irrigation water quality, but also determined unsuitable water samples in the catchment like salinity hazard, high pH, hardness and toxicity problems. This study confirms an organized and effective water resource evaluation based on GIS and geospatial analysis is a key factor for water resource quality and suitability to improve agricultural production and food security. Therefore, this paper recommends, there must be adequate protection of water resources with best watershed management to achieve a full yield irrigation production, to improve food security and to sustain it for long period of time, to avoid the possibility of increasing environmental problems in the future generation.*

**Key words:** Groundwater, GIS, Spatial Distribution, Elala Catchment

## **INTRODUCTION**

Groundwater quality estimation in developing countries has become a critical subject due to surface water shortages. Generating groundwater quality spatial distribution map and investigation its suitability for irrigation use is an important for groundwater vulnerability analysis and vital for groundwater planners and decision makers. Groundwater quality mapping is one of the major methods, which provide information about groundwater suitability for irrigation purpose. Water quality is the process to determine the chemical, physical and biological characteristics of water, usually with respect to its suitability for a particular purpose (FAO, 1998). High quality crops can be produced only by using high-quality irrigation water keeping other inputs optimal. The quality of water plays a prominent role in promoting both the standard of agricultural production, environmental health and human health protection assessment. Irrigation water quality problems are very complex. They include salinity hazard, permeability hazard, toxicity hazard, and miscellaneous problems. Each of these problems may affect crop singly or in a combination of two or more (Ayres & Westcot, 1985).

GIS is a powerful tool to determine groundwater quality, its suitability and to develop solutions for water resources vulnerability and agricultural sustainable development. Geographic information system (GIS) has emerged as a powerful tool for storing, analyzing, and displaying spatial data and using these data for decision making in several areas including engineering and environmental fields (Stafford, 1991); (Goodchild, 1993); (Burrough & McDonnell, 1998; Lo & Yeung, 2003)). GIS is utilized to locate groundwater quality zones suitable for different usages such as irrigation and domestic (Yammani, 2007). The main goal of this research work was mapping groundwater spatial distribution and investigating on the current situation of water resources on its quality and suitability by measuring level of suitability to irrigation use based on salinity, sodicity, bicarbonate and specific ion toxicity hazards. The knowledge of groundwater spatial distribution and irrigation water quality determination is critical to understand what types of management changes are necessary for long term and short term productivity; particularly for agricultural crops that are highly sensitive to changes in quality as well as it is vital information for planners, managers and decision makers.

## **MATERIALS AND METHODS**

### Description of the study area

This study was conducted in Upper Geba Catchment in the case of Elala watershed found in Northern part of Ethiopia around Mekelle city. According to Ethiopian temperature zoning, the catchment is located under the semiarid agro ecological zone. The area coverage of the catchment is about 341 km<sup>2</sup> with shape length of the longest river flow path about 131 km long. Elala catchment geographical located between 13°35'22.2" to 13°29'34.0"N latitude and 39°22'36.8" to 39°42'33.5"E longitude with 1,730 meter minimum elevation and 2,718 meter maximum elevation (Figure 1).

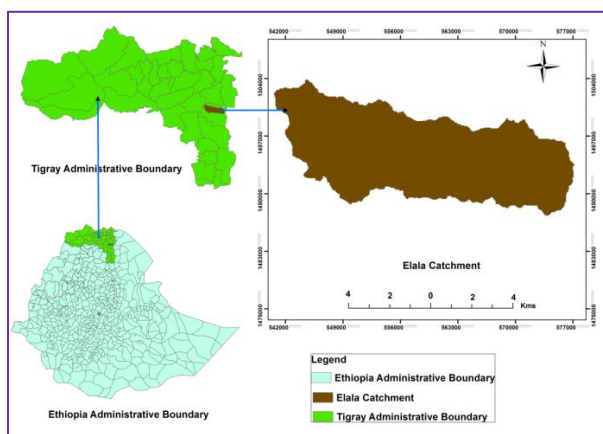


Figure 1: Study area location map of the catchment

### **Methodology**

In order to evaluate the groundwater quality for irrigation use in Elala Catchment, 35 surveyed water samples were collected from open hand dug wells, boreholes and springs during year 2015/ and 2016. The co-ordinates and its elevation of the sampling location of the water samples were collected using Garmin hand held Global Positioning System (GPS) during field surveying. The water samples were collected using 1 liter capacity vials or plastic bottles, first I had been cleaned the vials by tap water next by distil water finally rinsed out three to four times with sampling water. Then the vials were filled up to the brim and immediately sealed to avoid exposure to air and labeled for identification and brought to the laboratory. AAS Method, UV Method, Titration Method, different Calculation Methods and different software packages were used to analyze these physicochemical groundwater quality parameters. The water quality induces were calculated using the following methods and others.

$$\text{Percentage sodium (\% Na)} = \frac{(Na + K) * 100}{(Ca + Mg + Na + K)} \quad (1)$$

$$\text{Residual sodium carbonate (RSC)} = [HCO_3 + CO_3] - [Ca + Mg] \quad (2)$$

$$\text{Sodium adsorption ratio (SAR)} = Na^+ / [(Ca^{2+} + Mg^{2+})/2]^{0.5} \quad (3)$$

For reliability checking Duplicated and Electro Neutrality Methods was done.

$$\text{Electroneutrality} = \frac{\sum \text{Cations} - \sum \text{Anions}}{\sum \text{Cations} + \sum \text{Anions}} * 100 \quad (4)$$

Arc GIS software packages version 10 is used to map the groundwater quality spatial distribution and to analyze the data. For analyzing the chemical aspects of groundwater in the study area, observation open hand dug wells, boreholes and springs have been selected for investigation. Water quality data used in the analysis include pH, Electrical Conductivity (EC), Total alkalinity, Total Dissolved Solids (TDS), RSC,%Na, Total Hardness (TH), calcium, sodium, magnesium, potassium, bicarbonate, Sodium Adsorption Ratio (SAR),carbonate, chloride, and sulphate. Suitability of groundwater quality for irrigation purpose in the present study were evaluated based on its salinity hazard, Sodicity hazard, Bicarbonate hazard, Specific Ion Toxicity hazard and Other Miscellaneous problems. Geo-statistical analysis was applied first to fully explore the data in which the histogram, normality, trend of data, semivariogram cloud and cross covariance cloud of the raw data were observed. The spatial interpolation technique was done using kriging, IDW and spline (RBF) as well as normal QQPlot, histogram, log transformation and trend removal also applied to test the data. Transformations were used to make the data normally distributed and satisfy the assumption of equal variability for the data. In Arc GIS Geostatistical Analyst, the histogram and normal QQPlots were used to see what transformations were needed to make the data more normally distributed. The ME, MSE, RMSE, MSE, ASE and RMSSE have been used for model validation and accurate assessment. Meaning prediction performances were assessed by crossvalidation. For a model that provides accurate predictions, the standardized meanerror should be close to 0, the root-mean-square error andaverage standard error should be as small as possibleand the root-meansquare standardized error should be close to 1.

## **Result and Discussion**

### **Irrigation water Quality**

The concentration and composition of total dissolved components in groundwater regulates its quality for irrigation purpose. The characteristics of irrigation groundwater quality that appear to be most important in determining its quality are: (1) salinity hazard (total concentration of soluble salts and EC), (2) sodicity hazard (relative proportion of sodium to other cations), (3) bicarbonate hazard, and (4) specific ions toxicity hazard (concentration of sodium, Chloride, and boron or other elements that may be toxic (Staff, 1954) ).

### **Salinity hazard**

The effect of groundwater salinity hazard for irrigation use determined by total dissolved solids (TDS) and electrical conductivity (EC). Groundwater with 100-250  $\mu\text{S/cm}$  electrical conductivity (EC) is excellent for irrigation with low salinity water, groundwater with 250-750  $\mu\text{S/cm}$  is satisfactory for irrigation, groundwater with in the range of 750 to 2,250  $\mu\text{S/cm}$  with high salinity and widely used, and satisfactory crop growth is obtained under good management and favorable drainage conditions, but saline conditions will develop if leaching and drainage are inadequate. Groundwater with  $>2,250 \mu\text{S/cm}$  are very high salinity water (Wilcox, 1955) and (FAO, 1985 and 1989). Out of the analyzed thirty five water samples, one sample has EC between 100-250  $\mu\text{S/cm}$ , five samples have electrical conductivity between 250-750  $\mu\text{S/cm}$ , twenty five samples have an electrical conductivity values between 750-2,250  $\mu\text{S/cm}$  and the remaining four samples have an electrical conductivity greater than 2,250  $\mu\text{S/cm}$ . According salinity result, 71.43 % doubtful water class, 14.29 % good water class, 11.43 % unsuitable water class and 2.86 % excellent water class to irrigational use. Hence, the EC result in Elala catchment revealed that 71.43 % of the water samples of the study area were hardly suitable for irrigational purpose. Water with high salinity from 750-2,250  $\mu\text{S/cm}$  may require slight leaching; but it is permissible under normal irrigation practices except in soils of extremely low permeability. To achieve a full yield potential using this water classification, gradually increasing care in selection of vegetation crop and good management alternatives are required. Water classified under very high salinity may develop and to use such types of water needs very high care and management with treatment because to use such type water for irrigation use is severe or unsuitable to grow vegetation crop. Based on TDS value, water containing less than 450  $\text{mg/l}$  consider as high

suitable water class, from 450 to 750 mg/l grouped as good water class, between 750 to 2000 mg/l consider as permissible water class, but water containing more than 2000 mg/l of TDS concentration value classified as unsuitable water class to irrigational use (Balachandar, Sundararaj, Rutharvel Murthy, & Kumaraswamy, 2010). Most of the water samples in the catchment according to TDS concentration values were within the prescribed limit suitable and permissible except in GWSN13, GWSN24 and GWSN29 that have been TDS concentration value above the desirable limit to irrigation use. The result of TDS values indicated that 17.94 % of the water samples from the total sample were classified under highly suitable water class (S1) to irrigation, 20.51 % moderately suitable water class (S2), 53.84 % permissible water class (S3), 7.69 % unsuitable water class (N) to irrigational use from the total water samples of the catchment.

### **Sodicity Hazard**

Sodium adsorption ratio measures the proportion of sodium relative to the combined concentrations of calcium and magnesium. The danger of high concentration amount of sodium in irrigation groundwater is determined by sodium adsorption ratio (SAR). SAR indicates the effect of relative cation concentration on sodium accumulation in the soil. Water having a high SAR leads to a breakdown in the physical structure of the soil. Sodium is adsorbed and becomes attached to the soil particle. The soil then becomes hard and compact when dry and increasingly impermeable to water penetration. SAR is an important parameter for the determination of the suitability of irrigation water because it is responsible for sodium hazard. The water having SAR less than or equal to 10 are said to be irrigation water with low sodicity, groundwater having 10 up to 18 are medium sodium hazard for irrigation use, groundwater within the range 18 to 26 are high sodium concentration that is doubtful for plant growth and groundwater for irrigation with equal or greater than 26 SAR values are said to be with very high sodium concentration and unsuitable for irrigation use (Wilcox, 1955). Regarding on sodium absorption ratios for water samples of the catchment were classified under low sodicity class 1 its concentration values were less < 10 meq/l, indicated low sodicity water class for irrigation use and also could be observed from Wilcox diagram plot for sodicity hazard water quality model see Figure 2. Based on SAR, most of the water samples of the catchment fall in low SAR value

category to irrigation use by (Sultana, Haque, & Elahi, 2009,)in Muktagacha Upazila in Bangladesh had been also reported the same this result.

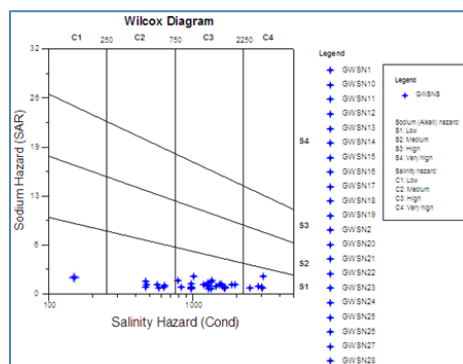


Figure 2 Wilcox Diagram plot for irrigation Water Classification (based on Salinity hazard (EC) and Sodicity hazard (SAR))

### Bicarbonate Hazard

Bicarbonate hazard was analyzed in terms of residual sodium carbonate (RSC). Water having high concentration of bicarbonates, there is a tendency for calcium and magnesium to precipitate as the water in the soil becomes more concentrated. Irrigation water with Residual Sodium Carbonate of less than 1.25 meq/l is considered as good quality water for irrigation use, RSC between 1.25 to 2.50 meq/l is classified under doubtful and irrigation water with its RSC more than 2.50 are classified as unsuitable water for irrigation use (Eaton, 1950 ) and (USDA, 1914, 1954)). RSC > 2.5 meq/l leads to salt build up which may hinder the aeration and water movement by clogging the soil pores and lead to degradation of the physical condition of the soil. During the present study all the water samples in Elala Catchment have its residual sodium carbonate  $\leq$  1.25 meq/l. This is safe to irrigation use for all crops without any restriction regarding the guideline. In Jaffna Peninsula in Sri Lanka by (Sutharsiny, Pathmarajah, Thushyanthy, & Meththika, 2012) and in Maniyad Reservoir of Parala Village in INDIA by (Aher & Deshpande, 2011) also done the similar this result.

### Specific Ions Toxicity Hazard

A toxicity problem is different from the salinity and the permeability problems, in that toxicity occurs within the crop itself as a result of the uptake and accumulation of certain constituents from the irrigation water. Certain ions from water or soil accumulate in sensitive crops to

concentrations high enough to cause crop damage and reduced yields. Toxicity normally results when the toxic ions are taken up with the soil water and accumulate in the leaves during water transpiration to an extent that can damage the plant. The usual toxic ions in irrigation water are chloride, sodium, boron and others. During field surveying I have seen specific ion toxicity problems see Figure 3.



Figure 3 Specific Ions Toxicity hazard (Na and Cl)

### Geospatial Modeling for Groundwater Spatial Distribution

The major cation of the groundwater samples in Elala catchment were in the order of  $\text{Ca}^{2+} > \text{Na}^+ > \text{Mg}^{2+} > \text{K}^+$ . Among the major cations, calcium was the most dominant element in Elala catchment and its concentration varies from 56 to 226 mg/l. The cation concentration of  $\text{Na}^+$ ,  $\text{Mg}^{2+}$ , and  $\text{K}^+$  in mg/l ranges between 26.4 to 128.8, 21 to 66.8, and 2.1 to 5.8 mg/l respectively. The spatial distribution map of the major cations had been obtained and presented in Figure 4. From the spatial distribution map of the major cations, it was observed that generally an increasing concentration distribution of the major cations from eastern to western part of the catchment, especially around Mekelle city there was high concentration of sodium, potassium and magnesium distribution.

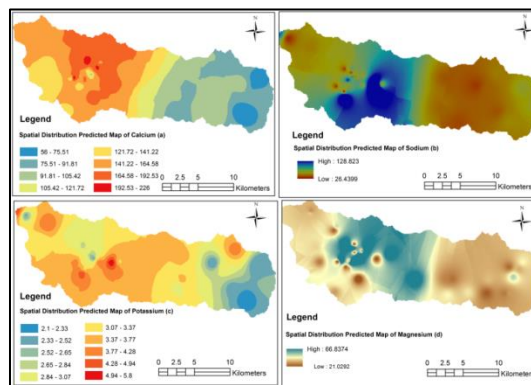


Figure 4 Groundwater Spatial Distribution Maps of Ca, Na, K and Mg

The dominance of the major anion in the study area of groundwater samples in the catchment were in the order of  $\text{HCO}_3^- > \text{Cl}^- > \text{SO}_4^{2-} > \text{NO}_3^- > \text{CO}_3^{2-}$ . Bicarbonate was the most dominant anion in the groundwater samples in the catchment. The predominant anions in the catchment were bicarbonates and chloride. The anionic concentration of  $\text{HCO}_3^-$ ,  $\text{Cl}^-$ ,  $\text{SO}_4^{2-}$  and  $\text{CO}_3^{2-}$  mg/l ranges between 127.0 to 397.0, 29.0 to 154.7, 22 to 97.9 and 1.0 to 4.0 in mg/l, respectively. Figure 5 indicates the spatial distribution map of the major anions in Elala catchment, from the spatial distribution map of major anions there were an increasing concentration distribution from the upper scenario towards the down scenario of the catchment especially at central scenario there were high chloride concentration spatial distribution in the study area.

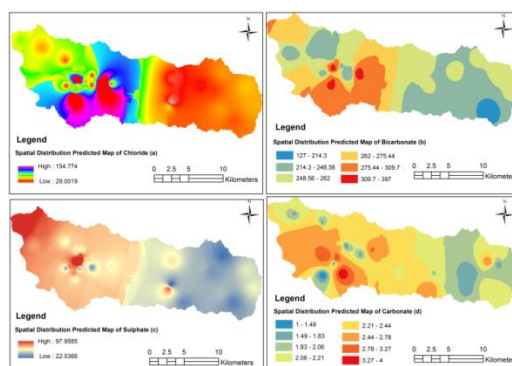


Figure 5 Groundwater Spatial Distribution Maps of  $\text{Cl}^-$ ,  $\text{HCO}_3^-$ ,  $\text{SO}_4^{2-}$  and  $\text{CO}_3^{2-}$

The pH and K (potassium) have been taken as an example for cross validation of the water quality parameters of the catchment.

## Conclusion

The overall view of the water quality and its suitability of the present study showed that most of the area having a good irrigation water quality, but also we have determined unsuitable like salinity hazard, hardness, high pH and toxicity problems of water samples in the catchment. So as population density increase, factory and industry formulated as well as expansion of urban area occurs gradual increase of water quality pollutants due to anthropogenic effects may cause water quality problem hence necessary measures are to be taken to control it. Therefore, this paper recommends, there must be adequate protection of water resources with best watershed management to achieve a full yield irrigation production, to improve food security and to sustain

it for long period of time, to avoid the possibility of increasing environmental problems in the future generation.

## **Reference**

- Aher, K.R., & Deshpande, S M. (2011). Assessment of Water Quality of the Maniyad Reservoir of Parala Village , district Aurangabad : Suitability for Multipurpose Usage. *I(3)*, 6-17.
- Ayres, R.S., & Westcot, D. W. (1985). Water Quality for Agriculture. FAO Irrigation and Drainage Paper No. 29. Food and Agriculture Organization of the United Nations, Rome. pp. 1-117.
- Balachandar, D., Sundararaj, P., Rutharvel Murthy, K., & Kumaraswamy, K. (2010). An Investigation of Groundwater Quality and Its Suitability to Irrigated Agriculture in Coimbatore District, Tamil Nadu, India A GIS Approach. *International Journal of Environmental Sciences, I* 176-190.
- Burrough, PA., & McDonnell, RA. (1998). Principles of Geographical Information Systems Oxford: Oxford University Pressp. 333.
- Eaton. (1950 ). Significance of Carbonate in Irrigation Water. *Soil Sci.* 67:112-133.
- FAO. (1985 and 1989). Water quality for agriculture. FAO irrigation and drainage paper 29 Rev. 1, Food and Agriculture Organization of the United Nations, Rome, Italy.
- FAO. (1998). Water Quality for Agriculture, (Irrigation and Drainage). *Guideline no.29*.
- Goodchild, MF. (1993). The state of GIS for environmental problemsolving. In M. F. Goodchild, B. O. Parks, & L. T. Steyart (Eds.), *Environ. Modeling GIS, New York: Oxford University Press* pp. 8–15.
- Lo, CP., & Yeung, AKW. (2003). Concepts and techniques of geographic information systems New Delhi: Prentice-Hall of India Pvt. Ltd, p.492.
- United States Salinity Laboratory Staff. (1954). Diagnosis and Improvement of Saline and Alkali Soils, U.S.D.A., Agricultural Handbook No. 60pp.
- Stafford, DB. (1991). Civil engineering applications of remote sensing and geographic information systems. *New York: ASCE*.

- Sultana, N., Haque, M., and, & Elahi, S. (2009,). Evaluation of surface irrigation water quality in Muktagacha Upazila of Bangladesh. *Songklanakarin Journal of science and technology*, 31, 229\_235.
- Sutharsiny, A, Pathmarajah, S, Thushyanthy, M, & Meththika, V. (2012). Characterization of Irrigation Water Quality of Chunnakam Aquifer in Jaffna Peninsula. *23(3)*, 237-248.
- USDA. (1914). US Department of Agriculture. Washington. *Bulletin No. 197*.
- USDA. (1954). U.S. Salinity Lab. Staff., Diagnosis and improvement of saline and alkali soils *Hand book-60*, p. 160.
- Wilcox, L.V. (1955). Classification and use of irrigation waters. *U.S. Dept. Agri., Cir, 969*, 19pp.
- Yammani, S. (2007). Groundwater quality suitable zones identification: application of GIS, Chittoor area, Andhra Pradesh, India. *Environ. Geol.*, 53(1): 201–210.

## **Stabilization of Soft Soils for Pavement Application Using RBI Grade-81**

**Tariku Asfaw Tedla**

Department of Civil Engineering Defense University, College of Engineering Bishoftu

### ***Abstract***

*The present computation study focuses on the stabilization of high plasticity soils especially for road application using RBI grade-81 chemical. The quality of subgrade plays an important role in designing a long lasting pavement. A pavement constructed over a weak subgrade soil is unable to sustain traffic load, and therefore, may cause early failure before its design life. Generally, stabilization of soil is recommended to improve its engineering property and reducing traffic jams in big cities (import and export soils). There are limited data available on the long term performance of these materials for Ethiopian scenario. Hence, a detailed research is required before these materials can be used in a regular practice for construction of roads in Ethiopia. Soft soil or high expansive soil collected for this study. The soft soil was stabilized with different percentages of RBI (i.e., 2, 4, 6, and 8%). All the samples used in this study were in the laboratory according to the available standard procedures by ASTM and based on the different literature review. Preliminary tests, performance tests, SEM, chemical and mineralogical composition were conducted on the stabilized and un-stabilized soils. There is considerable change in the virgin soft soils with increase use of RBI admixture, for instance 8% of RBI chemical increases 16 times CBR values and 4 times UCS values when compare to virgin clay soil. In addition, PI of soil decrease with addition of RBI, hence making this additive to be suitable for construction of pavements.*

**Key words**-Soft soil, Soil stabilization, Preliminary tests, Performance tests, RBI grade-81

### **1. Introduction**

Subgrade layer is the lowest layer in the pavement structure; receive the stresses from the layers above generally, subgrade consists of various locally available soil materials that sometimes might be soft and wet that cannot have sufficient strength to support pavement loading. Poor sub grade soil having very less strength value replaced by high quality material. This research deals with instead of replacing enhance in various properties of sub grade soil by using soil

stabilization RBI. Stabilization is done to improve engineering property of subgrade soil. A stabilized soil can be much stronger as compared to untreated soil, and many studies have shown that stabilization of a soil is a better technique to reduce thickness of a pavement and to increase its service life.

There are many traditional additives available in market for stabilization According to a study by (Brooks .R, 2011); (Kolias S., 2005) and (Solanki, 2014) on fly ash, lime, and cement have noted that generally improving the structures of pavement performance and quality of the road.

The motivation to promote these additives is to help constructing durable and long lasting pavements in Ethiopia. Use of these accredited materials for construction of pavements is not popular in Ethiopia as it is expected. There are limited data available on the long term performance of these materials for Ethiopian scenario. Hence, a detailed research is required before these materials can be used in a regular practice for construction of roads in Ethiopia.

All performance tests after prepared the samples were cured for 7 days prior to testing. The moulded samples were placed in airtight plastic wrapper, and kept in a 100% humid room in before applying tests.

## **2. Material and methodology**

High plasticity soil or very soft soil is collected for this study. The soil was collected below 1.5 meter from the ground surface.

RBI Grade 81 is an odourless, light brown powder and nontoxic material that is composed of a number of naturally occurring compounds. It consists of pH (12.5) and bulk density 700 Kg/m<sup>3</sup>.

The soft soil was stabilized with different percentages of RBI (i.e., 2, 4, 6, and 8%). All the samples used in this study were in the laboratory according to the available standard procedures by ASTM and based on the different literature review.

Preliminary tests like consistency, specific gravity, California bearing ratio (CBR), unconfined compressive strength (UCS) and performance tests such as indirect tensile strength (ITS), durability, Scanning Electron Microscopy (SEM), and X-Ray fluorescence (XRF) carry out for this research. Geotechnical properties of untreated soft soils reported in the Table 1.

Table 1. Index Properties of untreated soil

Soil Properties	Result
LL (%)	65
PL (%)	42
PI (%)	23
Specific gravity	2.56
Gravel (%)	1.47
Sand (%)	20.05
Below #200(%)	78.49
Silt fraction (%)	52.92
Clay fraction (%)	25.57
MDD (Kg/m <sup>3</sup> )	1626
OMC (%)	20.5
CBR (%)	2.3
UCS (KPa)	391
ITS (KPa)	28
AASHTO soil classification	A-7-5
Rating as a sub grade	Poor soil

### 3. Results and Discussion

#### 3.1 Effect on Atterberg Limit

As ASTM D4318 standard test methods for liquid limit, plastic limit and plasticity index of soil before and after treated show in Table 2. The liquid limit behaviour of RBI treated soil decreases as the admixture content increasing finally results reduction of plasticity index.

Table 2. Atterberg limit test

RBI (%)	Result of atterberg limit		
	LL (%)	PL (%)	PI (%)
Raw soil	65	42	23
2	62	44	18
4	60	46	14
6	57	47	10
8	55	48	7

### 3.2 Effect on Moisture-Density Relation

As RBI percentages increase the values of optimum moisture content (OMC) content increases linearly and maximum dry density (MDD) slightly decreases. Generally RBI chemical almost half unit weight density of raw soil. A variation of MDD and OMC at different percentages of RBI shown on Table 3 and Fig. 1. These findings are in consistent with the results reported by (Arun, 2013) and (Roy, 2014).

Table 3. OMC and MDD at different percentage of RBI

RBI-81(%)	OMC(%)	MDD(kg/m <sup>3</sup> )
Raw soil	20.50	1626
2	22.48	1610
4	23.20	1593
6	23.60	1558
8	24.00	1521

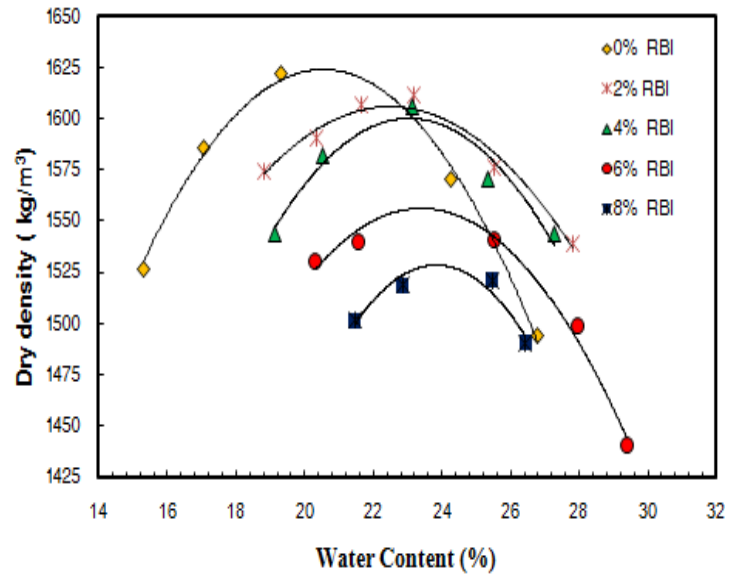


Fig. 1 Relationship between dry density and moisture content at different percentages of RBI

### 3.3 Effect on California Bearing Ratio

California bearing ratio samples were compacted accordance with modified proctor compaction. After preparing sample as per procedure placed on suitable carriers in the moist chamber for 7 days and 96 hours soaking. CBR values rapidly increase with the increase of RBI. The results have been shown in Table 4.

Table 4. CBR test for raw soil and stabilized soil samples

RBI(%)	CBR values	CBR values relative to raw
Raw soil	2.3	-
2	9	291
4	17.9	678
6	25.4	1004
8	35.6	1448

### 3.4 Effect on Unconfined Compressive Strength

Accordance with ASTM D 2166 standard procedure, after curing period the samples tested. General trends of increasing unconfined compressive strength with increasing RBI Content were observed as shown in Fig.2. Also, the unconfined compressive strength data are given in Table 5. The treated soil sample was increases on stress soil sample after failure under UCS machine shown on Fig. 3.

Table 5. Unconfined compressive strength values at various percentage of RBI

RBI(%)	Max stress (KPa)	Failure Strain (%)
Raw soil	391	5.7
2	484	5.1
4	583	4.4
6	684	3.8
8	771	3.2

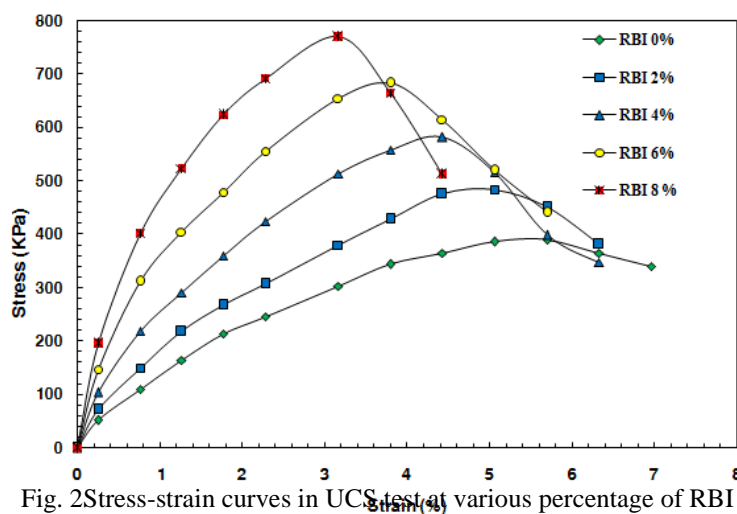


Fig. 2 Stress-strain curves in UCS test at various percentage of RBI

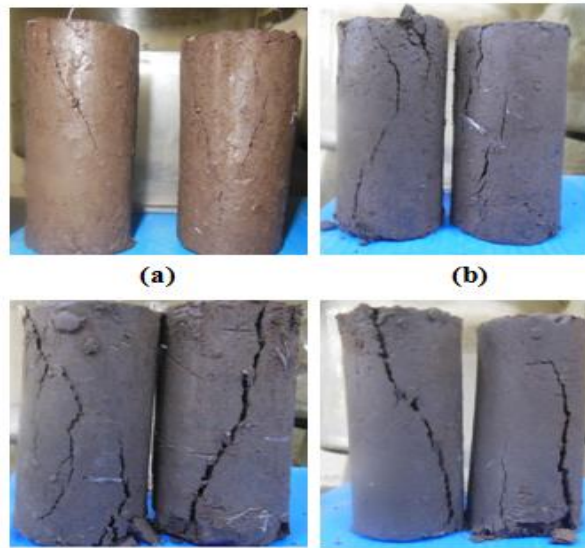


Fig. 3 UCS specimens after failure (a) 2% RBI (b) 4% RBI (c) 6% RBI and (d) 8% RBI

### 3.5 Effect on Indirect Tensile Strength

Due to the effect of repetitions of wheel loads, component layers of the pavement are stressed due to tension and as a result tensile crack is developed. Tensile stress may also be developed due to differential ground movement. The reason for differential ground movement is seasonal variation and temperature gradient (Bandyopadhyay, 2013).

As ASTM D 6931 test method is used to determine the indirect tensile of soil-RBI by using of cylindrical specimens diameter 101.6 mm were prepared, with different percentage of RBI mixing with soil for each percentage prepared samples. The value of ITS shown in Table 6 and the soil sample molded after failure under ITS machine shown on Fig. 4.

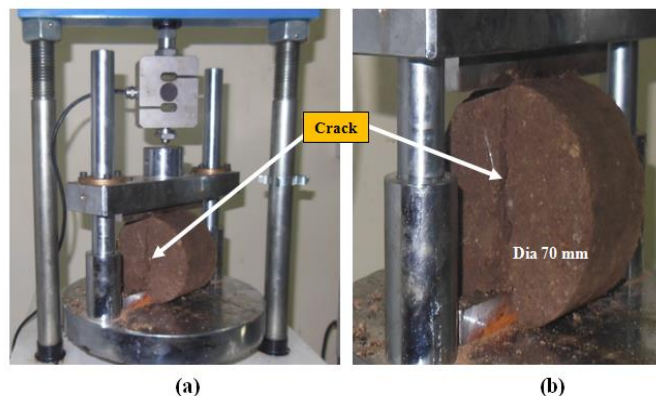


Fig. 4(a) Indirect Tensile Strength instrument (b) Specimen after failure

Table 6. Indirect Tensile Strength values at various percentages of RBI

<b>RBI (%)</b>	<b>Max load (kN)</b>	<b>Average height (mm)</b>	<b>IDT ( kPa )</b>
0	0.31	70.05	28
2	0.51	70.10	46
4	0.77	70.60	68
6	1.04	70.64	93
8	1.58	71.09	140

### **3.6 Effect on Durability Test**

The durability test was performed in accordance with ASTM D 559. The soil sample shall be prepared in accordance with the procedure of proctor test briefly, this test consisted of exposing the stabilized soil specimens to 12 cycles and each cycle consisted of wetting and dry. After 7 days curing period the specimens were submerged in potable water at room temperature for a period of 5 hours and then removed. The specimens were then placed in an oven maintained at temperature 71°C for 42 hours. After the specified time the samples were removed from oven and allowed to cool for one hour. Each specimen is placed on a scale and brushed at 1.4 kgf pressure using a wire brush, so that the total surface area is brushed twice, (total of 18 strokes on the sides and four on each end). After brushing, the specimens are weighed, measured, and their condition evaluated and recorded.

After the 12 cycles, specimens were dried to a constant weight at a temperature of 110°C and weighed to determine the oven-dry weight of the specimens. The data were used to calculate the volume and moisture changes of specimen (1 and 2) and losses of specimen (3 and 4).

Specimens are considered to have passed the test when there is, 2% change in volume (sample 1&2) and are considered to have passed the weight-loss criterion if it is, 10%. The ASTM D559 procedure does not provide any guidelines for the loss criteria of soil type A-7-5 and RBI, only guided for cement additives, the resistance of wet and dry values shown in Table 7.

fig. 5

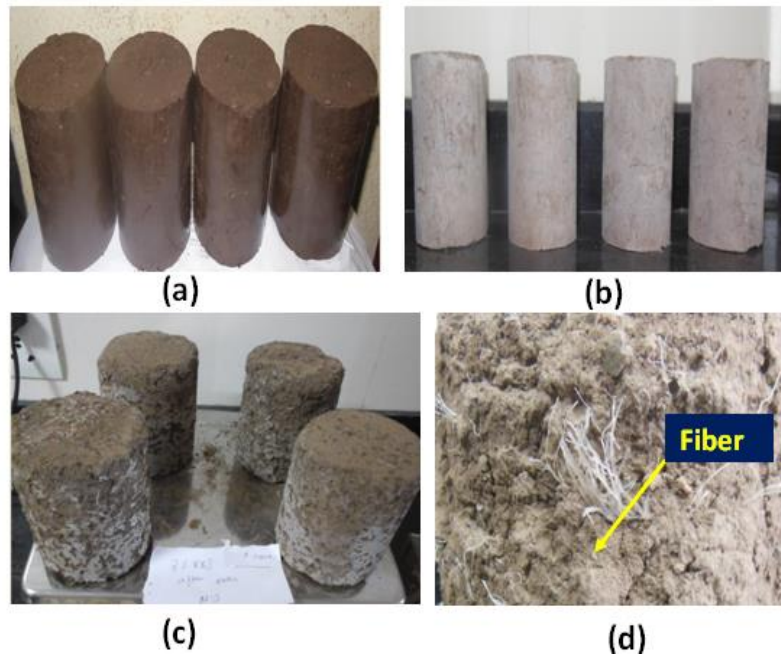


Table 7. Durability at various percentages of RBI

RBI (%)	Performance	Status
Raw soil	Fail	Failed at 1 <sup>st</sup> cycle
2	Fail	Failed at 2 <sup>nd</sup> cycle
4	Fail	Failed at 4 <sup>th</sup> cycle
6	Fail	Failed at 8 <sup>th</sup> cycle
8	Pass	Resist at 12 <sup>th</sup> cycle

Fig. 5 Processes of durability (a) at the time of molding (b) after oven drying 6<sup>th</sup> cycle @8(%) RBI, (c) after oven drying 12<sup>th</sup> cycle @8(%) RBI and (d) typical photograph of a soil specimen surface area with RBI Fiber. Except 8% RBI stabilized soil samples other percentages could not withstand the wet and dry cycle (durability) test. All the samples failed at 2, 4 and 6 percentages of RBI below 12 cycles. At 8 % RBI volume and weight change, 2.15% and 10.88% respectively

The maximum limit of volume change for cement stabilized soil is reported as 2% (Arun, 2013) and (Khattak, 2006). Since RBI-81 is a relative new stabilizer, limiting volume change value is not known, hence samples with volume change of 2.15% is considered pass.

### **3.7 X-Ray Fluorescence (XRF)**

The soil samples prepare for XRF test after 7 days of curing period. 4 gram soil sample and 1gram microcrystal cellulose and isopropyl alcohol were mixed toughly and the mixture was keep below an IR lamp for slow drying .Cellulose has excellent self-binding properties with adequate grinding abrasiveness during short to moderate grinding cycle without degradation from heat.

A small aluminum dish upper diameter 40mm and bottom diameter 33 mm and height is 12 mm was taken and 2/3 of the dish was filled with the mixture of 70% methyl cellulose and 30% paraffin wax followed by filling up the dried sample. The sample was compressed with the help of hydraulic jack by applying 15T load, for 1 minute. The prepared XRF sample soil is shown in Fig.6.

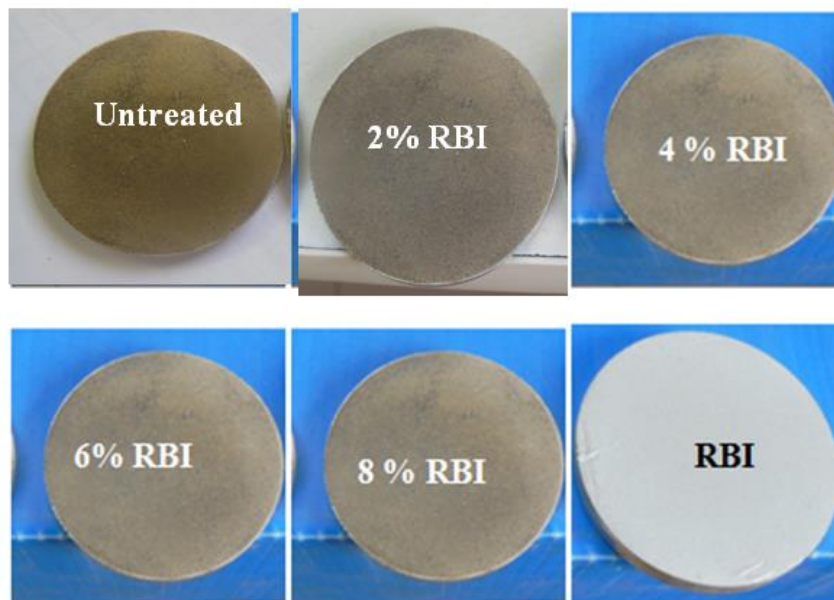


Fig. 6 X-Ray fluorescence test samples soil at different percentages of RBI , raw soil and RBI powder.

Calcium oxide (CaO) raw soil increase as the admixture RBI content increasing, CaO improves the strength of clayey soils for secure subgrade soil; improve their removes water from the soil or mud through its reactivity with the calcium ions and form a solid platform. The results are plasticity reduction, reduction in moisture-holding capacity (drying), swell reduction, improved stability. The calcium oxide results in pozzolanic reactions which results in higher load-bearing capacity of the subgrade, and decrease plasticity index (Griffin, 2014).The soil samples before and after treated chemical composition result shown on Table 8.

Table 8. Chemical compound of RBI, raw soil and stabilized soil samples

Chemical compound	RBI <sub>powder</sub> (%)	Percentage of RBI				
		Raw soil	2	4	6	8
Al <sub>2</sub> O <sub>3</sub>	5.7	9.2	8.7	8.4	7.6	7.1
SiO <sub>2</sub>	14.3	38.3	36.8	30.1	28.4	26.4
CaO	58.8	3.9	7.4	9.5	10.1	11.0
Fe <sub>2</sub> O <sub>3</sub>	1.5	6.6	6.4	6.3	6.0	6.0
MgO	1.42	1.42	1.317	1.45	1.07	1.28

### 3.8 Scanning Electron Microscopy

Scanning electron microscope is a technique to visualize changes on microstructures or fabric of stabilized soils. Observations were performed on stabilized soils after 7 days of curing. Examination of SEM images of RBI reveals different sizes, non-uniformed shapes and fibrous particles and smooth texture. The SEM images of raw soil samples show different sizes, non-uniformed and irregular shapes, rough texture, pores and cracks, weakly bonded structure and open texture as shown in Fig.7. After stabilization of soils with RBI, the existing gap in raw soils filled with RBI and the improved soil seem more dense structure and solid particles with less voids. The finding is in agreement with the work of conducted by (Brooks .R, 2011).

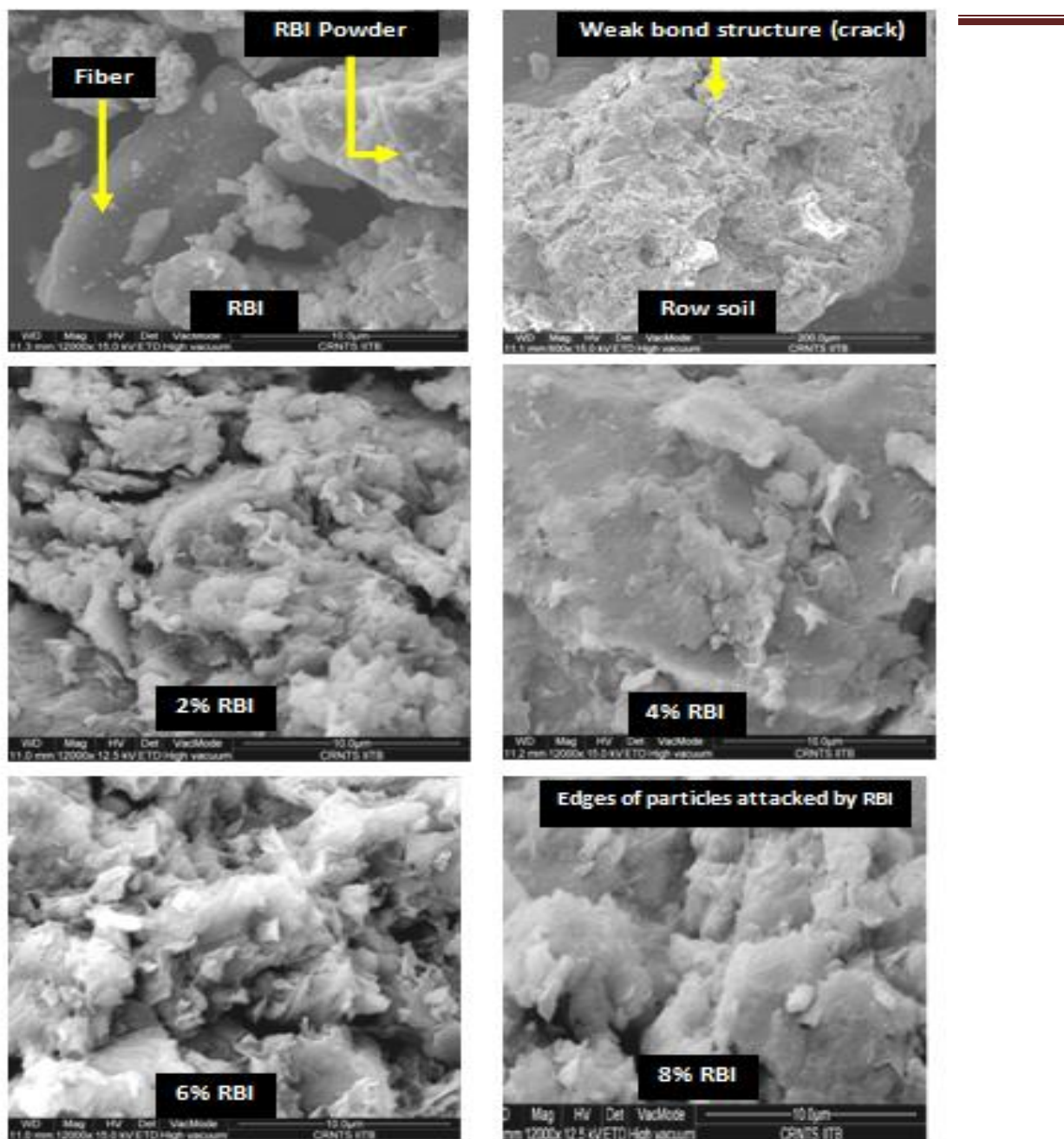


Fig. 7 SEM image of raw soil, RBI and at different percentages of RBI.

#### **4. Conclusion**

The following conclusions can be drawn from the results and discussion presented in this report.

- The plasticity index (PI) of soft soil decreases with an increase in RBI. For soft soil or expansive raw soil, PI decreases from 23% to 7% (stabilized soil) after addition of 8% RBI. It is seen that the addition of RBI is significantly effective for soft soil.
- The CBR value of soft soils increases with an increase in RBI-81 content. For instance, addition of 8% of RBI to soft soil increases CBR value to 35.6% (1448% increase with respect to raw soil). The increase in CBR value is an indication of higher compressive strength of a soil, and hence a better for construction of pavements.
- Additions of RBI to the soft soil increase the unconfined compressive strength. The percentage of failure strain decreases with addition of RBI, this indicating a brittle behaviour of stabilized soils.
- The tensile strength determined from IDT value increases with addition of RBI for the raw soil. For instance, IDT value of soft soil increases from 28 kPa (raw soil) to 245 kPa with addition of 8% RBI. The results indicate that addition of RBI to soft soils is beneficial to increase their tensile strength.
- Untreated specimens failed as soon as they were introduced to the first stage of durability cycle except 8% modified RBI-81; all the samples of raw soil, 2, 4 and 6 percentages of RBI sample soil failed before 12 cycles. Considering durability criteria, a minimum of 8% RBI for soft soil is sufficient to sustain wet and dry cycles for long term pavement performance.
- The calcium oxide content of expansive soils was estimated from XRF technique was found to be as 3.9%. The CaO content of the soil increases with addition of RBI. This is because of the fact that RBI is rich in CaO. A higher percentage of CaO helps in pozzolanic reaction and hence provides higher load-bearing capacity and reduced plasticity index of soils.
- The SEM images of raw soil samples after stabilization of soils with RBI, the existing gap in raw soils filled and the soil seems more dense structure and solid particles with less voids.
- Based on the different laboratory performance tests, it can be concluded that RBI can be considered as a potential stabilizers for clay soil. It helps to improve compressive strength,

and tensile. In addition, PI of soil decrease with addition of RBI, hence making this additive to be suitable for construction of pavements.

### **Acknowledgement**

The author is grateful to the Alchemist Technology Limited, India for supplying RBI-81 stabilizer used in this study and I would like to express my deep sense of gratitude to Prof. Dharamveer Sing.

### **References**

1. Arun, U. K. (2013). "Effect of Purity of Lime on Strength and Durability of Soil-Lime mixes No. 8 August 2013. *A Review of Road And Road Transport Development Vol. 41 ISSN 0376-7256* , pp.42-49.
2. Bandyopadhyay, K. A. (2013). Split Tensile Strength Test Of Lime and Cement Stabilized Fly Ash. *Indian highways A Review of Road And Road Transport Development, Vol. 41 No. 12 December 2013 ISSN 0376-7256* , pp. 96-102.
3. Brooks .R, U. (2011). Geotechnical Properties of Problem Soils Stabilized with Fly Ash and Limestone Dust in Philadelphia. *Journal of Materials in Civil Engineering ASCE* , 711-716.
4. *Griffin Soil Access online* . (2014). Retrieved May 21 02, 2014,, from Chemical Reactions in the Soil Stabilization Process Using Lime:  
[www.griffinsoil.com/ph\\_of\\_lime\\_stabilized\\_soils](http://www.griffinsoil.com/ph_of_lime_stabilized_soils).
5. Khattak, M. A. (2006). Durability and mechanistic characteristics of fiber reinforced soil-cement mixtures. *The International Journal of Pavement Engineering Vol. 7, No. 1* , pp.53-62.
6. Koliass S., R. V. (2005). Stabilisation of clayey soils with high calcium fly ash and cement . *Cement and Concrete Composites science direction* , 301-313.
7. Roy, A. (2014). Soil Stabilization using Rice Husk Ash and Cement. *International Journal of Civil Engineering Research. ISSN 2278-3652 Vol 5, No.1* , pp. 49-54.
8. Solanki, P. A. (2014). Behavior of Stabilized Subgrade Soils under Indirect Tension and Flexure. *Journal of Materials in Civil Engineering* , 833-844.

## **Estimation of Future Annual Daily Peak Stream Flow and Flood Frequency based on changes in air temperature and precipitation. A case study at GilgelAbay River basin, Upper Blue Nile, Ethiopia**

**AregaMulu<sup>1</sup> and G.S.Dwarakish<sup>2</sup>**

<sup>1</sup>Departement of Hydraulics and Water Resources Engineering, Debre Markos University,  
Ethiopia

<sup>2</sup>Department of Applied Mechanics and Hydraulics, National Institute of Technology Karnataka  
Surathkal, 575 025, Mangalore, Karnataka, India

Email: [muluarega21@gmail.com](mailto:muluarega21@gmail.com)  
[dwaraki.gs@gmail.com](mailto:dwaraki.gs@gmail.com)

### **Abstract**

*Flood is the most chronic and hazardous phenomena all over the world. It occurs when the volume of water exceeds the embankment of the river and causes loss of human life, natural resources as well as infrastructures. Therefore; to design safe and economical hydraulic structures, such as bridges and culverts, it is important to find out the magnitude of annual daily peak stream flow with a specified Annual Exceedance Probabilities (AEPs). Annual daily precipitation and air temperature are projected to increase during the end of 21<sup>st</sup> century. Therefore; it is important for engineers and resource managers to understand how annual daily peak stream flow will change in the future in this area. Hence, the main objective of this study is to estimate future annual daily peak streamflow and flood frequency at the end of the 21<sup>st</sup> century at GilgelAbay river basin, Upper Blue Nile, Ethiopia on the basis of projected changes in precipitation and air temperature by using Precipitation Runoff Modeling System (PRMS). PRMS is a deterministic, distributed-parameter modeling system, it computationally incorporates multiple components of the hydrologic cycle as understood through known empirical relations in hydrologic science. System inputs are precipitation, air temperature, and solar radiation. Future annual daily peak stream flow and flood frequency values of historical climate (temperature and precipitation) in the basin was adjusted on the basis of changes that are projected at the end of 21<sup>st</sup> century at GilgelAbay River Basin. These adjusted air temperature and precipitation formed nine combinations (including no change scenarios). These adjusted climate changes were from GCM outputs which were statistically downscaled and used as input to PRMS model. Hence, annual daily peak stream flow and flood frequency were estimated using*

*PRMS and Hodge-Lehman estimator. This indicated that as temperature increases, annual daily peak flow will decrease by large amount. If precipitation is held constant and when temperature is increased by 1.5<sup>0</sup>c and 3<sup>0</sup>c, there is 34.4% and 36.9% decrease in annual daily maximum peak stream flow with 50% AEP respectively. Since precipitation and evapotranspiration are one of the components of hydrological cycle, with no change of precipitation, if temperature increased it caused decrease of stream flow because of increase of evapotranspiration which losses water to the atmosphere. If temperature is increased by 1.5<sup>0</sup>c and 3<sup>0</sup>c and if precipitation is increased by 10%, there is a decrease of annual daily peak stream flow with 50% AEP by 23.8% and 24.9% respectively, because of increasing evapotranspiration. Large increase in annual daily peak stream flow (14.3%) with 50% AEP occurred when temperature is held constant and precipitation is increased by 10% because of precipitation contributed to stream flow is more than loses due to evapotranspiration.*

**Key words:** Peak Stream Flow, Future Flood, PRMS, AEP, River Basin

## **1. Introduction**

Flood is the frequent and costly natural disaster all over the world. It occurs when the volume of water exceeds the embankment of the river and causes loss of human life, natural resources as well as infrastructures. Information on annual daily peak stream flow and flood frequency values are required for designing hydraulic structures such as bridges, culverts, water ways, dams, and economic evaluation of flood protection projects (Subramanya, 2006). Chow (1962) stated that different methods are used for estimation of flood and flood frequency studies such as Landwehr *et al.*, (1979), Wallis and Wood (1985), Hosking and Wallis (1988), Jin and Stedinger (1989), Potter and Lettenmaier (1990), Farquharson (1992), Iacobellis and Fiorentino (2000), Martins and Stedinger (2000), and Peelet *et al.*, (2001). Most of these methods are using arbitrary formulae (imposing only a narrow set of criteria), as a result, failures of hydraulic structures such as bridges, culverts, dam, spill ways and drainage canal took place (Polemio, 2010). Therefore, proper selection of design flood value must be considered, while higher value would result in an increase in the cost of hydraulic structures, an under estimated value is likely to place the structure and population involved at some risk. This is because these methods did not consider changes on peak stream flow and flood frequency values due to changes in climate (air

temperature and precipitation) for future conditions. Past designs of hydraulic structures at GilgelAbay were predicted on the basis of few years data which predicted as magnitude and frequency of peak stream flow as which didn't change over a long period of time. These assumptions of peak flow has long been changed by changes in land use and changes in climate (Dooge, 1986) but currently it has been given more attention because of potential effects of changing climate on temperature and precipitation and resulting effect on peak stream flow (Milly et al., 2008). Therefore, it is important for engineers and resource managers to understand how peak stream flow may change in the future. Many studies found that flood risk is conditionally dependent on changes in climate and antecedent wetness condition (Pui et al., 2011). Changes in climate system can lead to changes in magnitude and frequency of hydrological extremes such as flood risk (Xu et al., 2006). These changes lead to problem on designing of hydraulic structures. Therefore, it needs revision of existing methods or developing alternative design flood estimation methods. Hence, estimating flood and flood frequency depending on future changes on climate (air temperature and precipitation) is very important for designing of hydraulic structures and flood protection structures using PRMS model (Hodgkins et al., 2013). Therefore, the objective of the present study is to estimate annual daily peak stream flow and flood frequency at the end of 21<sup>st</sup> century based on changes in air temperature and precipitation using PRMS model and Hodge Lehmann estimator.

## **2. Materials and Methodology**

### **2.1. Description of the study Area**

The research was conducted at GilgelAbay river basin which has an area of 5000 km<sup>2</sup>. Among four main tributaries of River Basin (GilgelAbay, Gumara, Megech and Rib), GilgelAbay river basin is the largest and contributes about 60% of runoff to Lake Tana. It is located at 10<sup>o</sup>56' to 11<sup>o</sup>51' N latitude and 36<sup>o</sup>44' to 37<sup>o</sup>23' E longitudes with an elevation range of 1787m to 3524m above M.S.L (Figure 2.1). The southern part of the catchment is mountainous and it has undulating topography and its periphery in the West and Southeast while the remaining part is low laying plateau with gentle slope. The geology is composed of quaternary basalts and alluviums. Most dominant soil types are clay and clayey loam soils. Agriculture 65.5%, agro-pastoral 33.4%, agro-forestry 1% and Urban 0.1% are the dominant land features; among this rainfed agriculture is dominant.

In general, as Mohammed et al., (2005) stated that the rainfall over GilgelAbay originates from moist air coming from the Atlantic and Indian oceans following the North-south movement of the Inter Tropical Convergence Zone. The study area receives 70-90% of its annual average rainfall during June to September (Kebede et al., 2006; Tarekegn and Tadege, 2005). There is a decreasing trend of rainfall from South to North with significant spatial variability, but insignificant variation of temperature throughout the year (BCEOM, 1999).

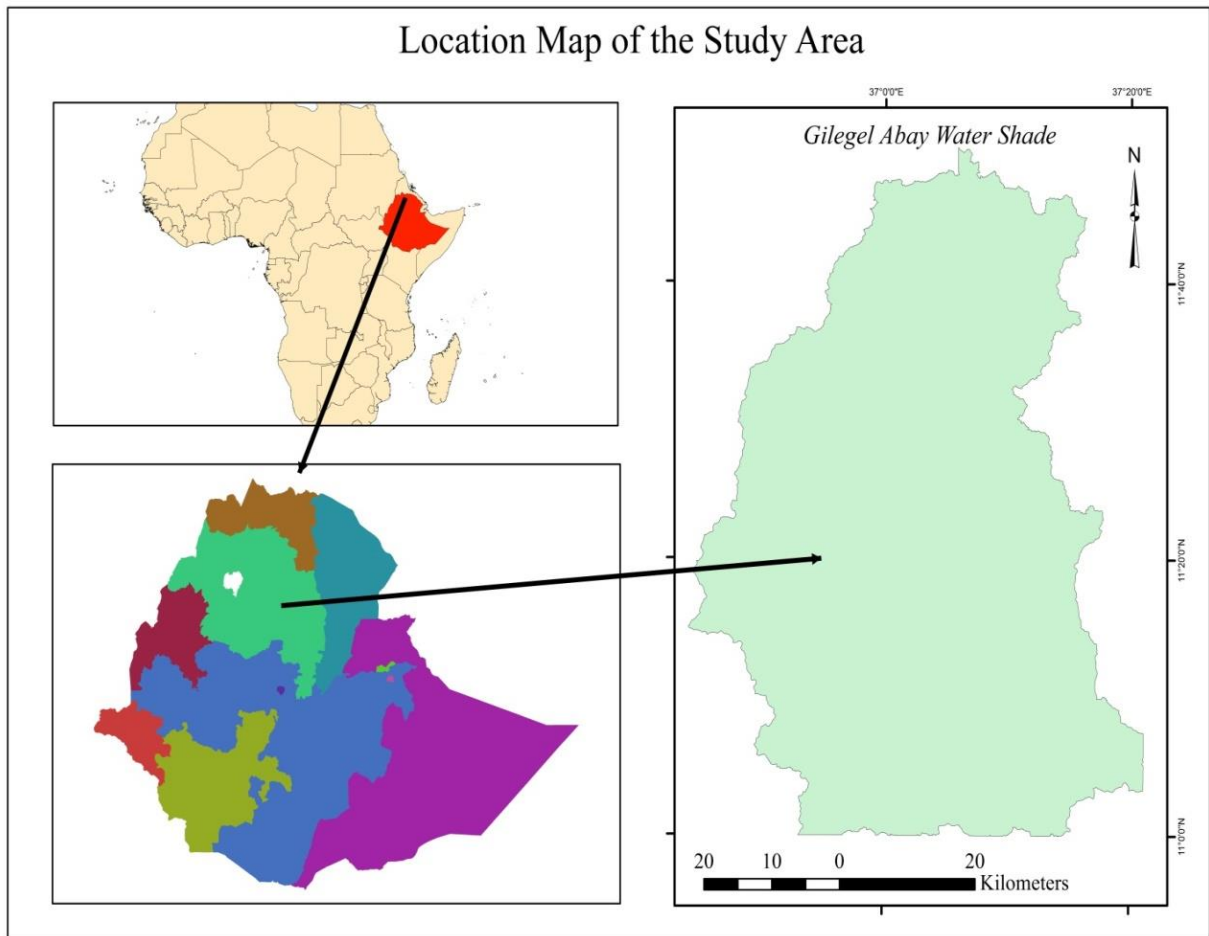


Figure.2.1. Location map of GilgelAbay River Basin, Upper Blue Nile, Ethiopia.

The parameters which are instrumental in selection of study area are its future potential for irrigation, having a lot of settlements near to the river basin, and it is the origin of Blue Nile river

basin which contributes 60% of inflow (water or sediment) to lakeTana. In addition,there is high way which crosses it.

## 2.2.Data Products Used

Table 2.1. Data products used for the present study

<b>Data types</b>	<b>Types of Data</b>	<b>period</b>	<b>Source</b>	<b>Description</b>	<b>Puepose</b>
Conventional Data	Precipitation	1993-2012	Ethiopian Metrological Agency	Daily rainfall	Hydrological analysis
	Stream flow	1993-2012	Ethiopian Minister of Water Resources	Mean daily river discharge	Hydrological analysis
	Temperature	1993-2012	Ethiopian Metrological Agency	Daily max. and min. air temperature	Hydrological analysis
	Soil data		Survey of Ethiopian soil		For additional information
Remote sensing data	Food and Agricultural Organization (FAO) soil Map	1998-2012	Food and Agricultural Organization (FAO)	Harmonized World Soil Database V 1.2	Hydrological analysis
	LU/LC, vegetation type, vegetation density	1990-2000 2001-2010	Satellite image and gridded global maps		For parameter generation
	Digital Elevation Model (DEM)	2000	SRTM image USGS	Resolution of 90m	For HRU delineation and parameter generation

Conventional data are more site-specific and accurate; but data collection is expensive, time-consuming, requiring more manpower and may not be extrapolated to a larger area. Remotely sensed data has got advantages due to repetitive and synoptic coverage of the large, inaccessible areas quickly and economically. By combining the conventional and remotely sensed data the dual advantages can be achieved. In the present study, both conventional and remotely seen data were used for estimating future annual daily peak stream flow and and flood frequency based on changes in air temperature and precipitation as given in Table 2.1.

In addition projected climate data (temperature and precipitation) from Global Circulation Model (GCM) output were used for this study. These GCM out puts were obtained from Canadian Center for Climate Modeling and Analysis (CCCMA) of third Generation Climate Model (CGCM3). These data were arranged for present period (1993-2012) as well as for future period (2080-2100) and statistically downscaled.

### **2.3. Description of the PRMS Model.**

PRMS is a modular-design, deterministic, physically based and distributed-parameter modelling system that has been developed by the US Geological Survey (USGS) to evaluate the impacts of various combinations of precipitation, climate, and land use on stream flow, sediment yield, and general basin hydrology (Leavesley et al., 1983). Basin response to normal and extreme rainfall can be simulated to evaluate changes in water-balance relationships, flow regimes, peak flood and volumes, soil-water relationships, sediment yields, and ground-water recharge. Parameter-optimization and sensitivity analysis capabilities are provided to fit selected model parameters and evaluate their individual and joint effects on model output (Leavesley et al., 1983). The modular design provides a flexible framework for continued model-system enhancement and hydrologic-modelling research and development. Required data types for daily stream flow calculations are minimum daily precipitation and daily maximum and minimum air temperature.

PRMS divides a watershed into smaller modelling subunits based on its physical characteristics of slope, aspect, elevation, vegetation type, soil type, land use, and precipitation distribution. Two levels of partitioning are available; the first divides the basin into homogeneous hydrologic response units (HRU) based on the basin characteristics. A second level of partitioning is

available for storm hydrograph simulation, in which the watershed is conceptualized as a series of interconnected flow planes and channel segments. Surface runoff is routed over the flow planes into the channel segments, and channel flow is routed through the watershed channel system.

HRU can be considered the equivalent of one flow plane, or it can be delineated into a number of flow planes. In this study, the daily mode used for modeling daily total and monthly stream flow. The model operates at daily time step whereby stream flow is computed as a mean daily flow or at the storm mode, at time intervals shorter than a day (Legesse et al., 2003). For this study the daily time scale was used to simulate stream flow at the catchment outlet.

System inputs included daily precipitation, daily minimum and maximum air temperature, and short-wave solar radiation as well as parameters generated using GIS weasel software from data\_bin. GIS weasel generated standard parameters for PRMS model from data\_bin developed from LU/LC, vegetation type, vegetation density and soil map. It made PRMS model preferable than other hydrological models such as Soil and Water Assessment Tool (SWAT). For example SWAT model used parameters generated from LU/LC and soil maps, but PRMS used Parameters generated from LU/LC, Vegetation type, vegetation density and soil map other than time series data (daily precipitation, daily minimum and maximum air temperature). Precipitation in the form of rain, snow, or a mixture of both was reduced by vegetative canopy interception; precipitation not intercepted by the canopy becomes the net precipitation through fall that was delivered to the watershed surface. Energy inputs of air temperature and solar radiation drive the processes of evaporation, transpiration and sublimation (Markstrom et al., 2015).

An area with an impervious zone (no infiltration capacity) has a maximum retention storage capacity, which must be satisfied before surface runoff occurs. In the soil zone reservoir loss of water is through evaporation and transpiration. The depth of this zone is average rooting depth of most dominant vegetables covering the soil surface. Water storage in this zone is increased by infiltration of rainfall and decreased by evapotranspiration. Maximum retention storage occurs at field capacity and minimum storage (assumed to be zero) occurs at wilting point. The soil zones are considered as two layer systems, the upper layer (recharge zone) and the lower layer

(Leavesley et al., 1983). The losses from the recharge zone are assumed to occur from evaporation and transpiration, but losses from lower zone are assumed to occur only from transpiration.

The calculation of infiltration into the soil zone depends on whether the precipitation is rain or snow. For this study area source of precipitation is rain and no snow cover. Hence, the volume infiltrating the soil zone is calculated as a function of soil characteristics, antecedent soil moisture conditions and storm size. For daily flow calculations, defining percentage of area that contributes to runoff (contributing area concept) is used to compute the volume of rain that becomes surface runoff. Daily infiltration is computed as net precipitation less surface runoff. The routing of soil water excess that percolates to the shallow ground water zones near stream channels or that moves downward from point of infiltration to some point of discharge above the water table is performed in subsurface reservoir (defined either linear or non-linear).

Recharge to the ground water reservoir takes place from the soil zone and the subsurface reservoir. The soil recharge zone takes place only when field capacity is higher in the soil zone and it has daily upper limit. Subsurface reservoir recharge is computed daily as a function of a recharge rate coefficient and the volume of water stored in the subsurface reservoir. The ground water reservoir is a linear reservoir and source of all base flow. Streamflow is the sum of the direct surface runoff, subsurface flow and base flow from each HRU (Figure 2.2).

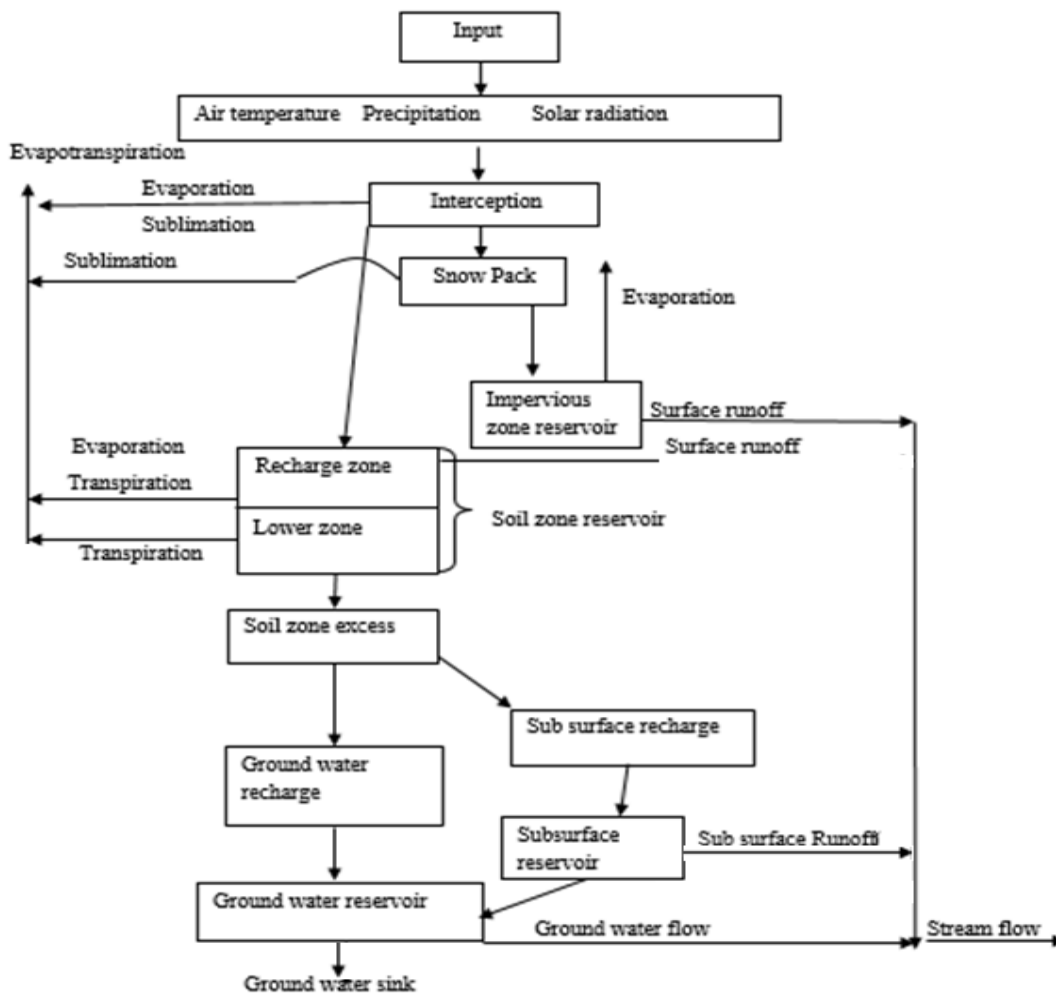


Figure.2.2.Schematicrepresentations for differentcomponentsofPRMSmodel(Source:Leavesleyetal.,1983).

The Modular Modelling System (MMS) was used to build Precipitation Runoff Modelling System (PRMS) for the study area. Distributed parameter capabilities of PRMS enabled by portioning catchment into subareas that were assumed to be homogeneous in their hydrologic response by using GIS Weasel. FAO soil map and satellite image derived land use/land cover were integrated in GIS environment. Daily precipitation data were interpolated using kring technique to obtain mean monthly and annual spatial distribution of the precipitation in the basin. Because this interpolation method is a particular type of local interpolation which is exact and more advanced geostatistical technique. In this study, simulations under different scenarios were performed in order to analyse the impacts of possible climate and land use/land cover changes on peak stream flow.

## 2.4. Model Performance Evaluation

Model performance evaluation of daily and monthly scales was evaluated using standard model efficiency (E) (Nash and Sutcliffe, 1970). Nash Sutcliffe method is widely used in evaluating hydrologic modelling. The E value varies from negative infinity to 1.0, with higher values indicating good agreement between observed and simulated values. This method of evaluation is as follows:

$$E = \frac{\sum_1^N (Q_{oi} - Q_o)^2 - \sum_1^N (Q_{oi} - Q_{si})^2}{\sum_1^N (Q_{oi} - Q_o)^2} \quad (2.1)$$

Where,

$E$  = Model goodness of fit efficiency

$Q_{oi}$  = Observed stream flow for day or month  $i$

$Q_{si}$  = Simulated stream flow for day or month  $i$

$Q_o$  = Mean observed daily or monthly stream flow

$N$  = number of samples.

## 2.5. Model Calibration and Validation

Model calibration involves the process of adjusting parameters to minimize the difference between measured and simulated values. Model validation is determining the degree to which a simulation model and its associated data are accurate representation of observed values for periods which were different from calibration period. PRMS was calibrated using Luca software (Hay and Umemoto 2006; Hay et al. 2006), a multiple-objective, stepwise, automated procedure for hydrologic model calibration and the associated graphical user interface (GUI). The Shuffled Complex Evolution global search algorithm (Duan et al. 1993; Duan et al. 1992; Duan et al. 1994) was used to calibrate PRMS. For the present work, simulation period (1993-2012) was

divided into calibration periods (1994-2005) and validation periods (2006-2012). One year period (1993) was used for initiation to minimize the effects of the user's estimate of initial value of state variables at the model start up by allowing iterations.

## **2.6. Estimation of future annual daily peak stream flow (flood) and flood frequency**

To estimate future annual daily peak stream flow and flood frequency at Gilgel Abay River Basin, the values for historical climate change (temperature and precipitation) in the basin was adjusted on the basis of changes that are projected for 21<sup>st</sup> century at Gilgel Abay River Basin. Climate change scenarios used in the assessment of future developments in complex systems that are either inherently unpredictable or have high scientific uncertainties (*IPCC*, 2007). Outputs generated from the Third Generation Global Climate Model (CGCM3) were used for this study. Because Down loading GCM out puts from Canadian Center for climate Modeling and Analysis is easily possible using any computers and it has also well arranged climate data according to simple Statistically down scaling method used for this analysis. The Special Report on Emissions scenarios (SRES) (IPCC, 2000) are grouped into four scenario families (A1, A2, B1, and B2) that explore alternative development pathways, covering a wide range of demographic, economic, and technological driving forces and resulting greenhouse gas emissions. In this study three SRES(A1B, B1, and A2) were used (Setegn et al., 2011). These scenarios were constructed to explore future developments in the global environment with special reference to the production of greenhouse and aerosol precursor emissions. Each scenario assumes a distinctly different direction for future developments. The SRES A1B emissions scenarios (a scenario in the A1 family) describes a future world of very rapid economic growth, global population that peaks in mid-century and declines thereafter, and rapid introduction of new and more efficient technologies (IPCC, 2000). The SRES A2 emissions scenarios describe a very heterogeneous world with high population growth, slow economic development, and slow technological change. B1 describes a convergent world with the same global population as in the A1 storyline but with rapid changes in economic structures toward a service and information economy, with reductions in materials intensity, and the introduction of clean and resource efficient technologies (IPCC,2000).

Precipitation changes of -10% and +10% of historical precipitations as well as temperature changes of +1.5°C and +3°C of historical temperature values from time series data were considered based on GCM outputs for selected scenarios of the region and statistically downscaled (Setegn et al., 2011; IPCC, 2000; IPCC, 2001; Legesse et al., 2003; Jones et al., 2001). The procedures which were used for statistical downscaling were as follows. The GCM output variables for present period (1993-2012) and for future period (2080-2100) were arranged and Cumulative Frequency Distributions (CFDs) for each period were identified using MATLAB program. The difference between the daily cumulative frequency distribution of a GCM output variables for a present period and a future period was calculated, and this difference was applied to an observed data to obtain changes in temperature. While for precipitation the changes were derived as ratios with respect to the present period values. Because the fractional changes in the low rainfall end of the CDF may be large, all GCM rainfall values less than 0.1 mm/day were considered to be zero, and zero values omitted for CDF calculations. The extreme of the CDFs were deliberately not sampled. The changes in the CDFs sampled at different cumulative frequencies were then linearly interpolated and extrapolated to cover the entire frequency range (0-1). Finally, the historical data were ranked and modified to reflect the changes in the GCM CDF for selected time periods. From these, temperature and precipitation values were considered for scenario simulations. Hence, to encompass the projected future changes in climate at Gilgel Abay River Basin, air temperature was adjusted by temperature values are no change (0°C), +1.5°C and +3°C changes of historical temperatures by adjusting model parameters rather than adjusting input variables, because simply adding temperature values more than 2°C from time series data is not acceptable for PRMS model. Precipitation was adjusted by two different precipitation values ranging -10% to 10% of observed precipitation by adjusting input variables (Hodgkins et al., 2013). The historical time series precipitation values were used from 1993-2012. These precipitation adjustments were made by adding or subtracting values from magnitude of historical climate changes (increasing or decreasing values). Nine combinations of adjusted values for temperature and precipitation (including no change scenarios) were used as an input to PRMS model with data files. Annual daily peak stream flow and flood frequency were calculated for each combination. The PRMS derived annual daily peak stream flow from adjusted temperature and precipitation changes were then compared to

unadjusted (historical) PRMS derived annual daily peak stream flow by using Hodge-Lehman estimator (Lehmann, 2006).

### 3. RESULTS AND DISCUSSION

#### 3.1. Model Calibration and Validation at Daily and Monthly modes

For the area of interest which has 26 HRU, PRMS model was calibrated using Luca software. This provided a good agreement between daily simulated and measured stream flow during calibration and validation periods for the study area with average E values 0.71 and 0.70 respectively. Average E values for calibration and validation of monthly scale are 0.91 and 0.90 respectively. This indicated that there is better agreement between observed and simulated stream flow in monthly scale than daily measured and simulated values at Gilgel Abay River Basin (Figures 3.1 and 3.2). It is also clear that the model can simulate stream flow in daily mode (Figures 3.3 and 3.4). Twenty years simulation (1993-2012) indicated that nearly 20,358 mm or 55% of precipitation (from the total 36,897 mm) returned to the atmosphere as ET and the remaining 16,538 mm or 45% of precipitation became stream flow to the river basin.

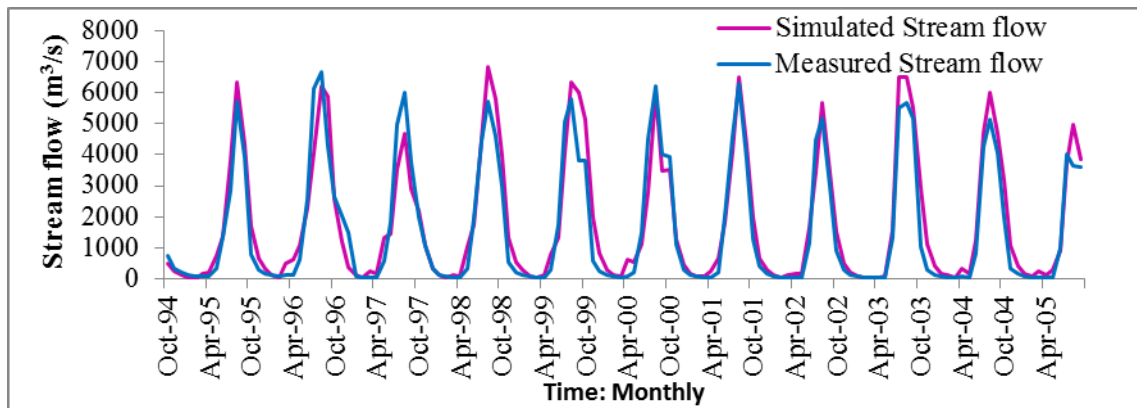


Figure 3.1. Monthly measured and simulated stream flow for calibration period (1994-2005).

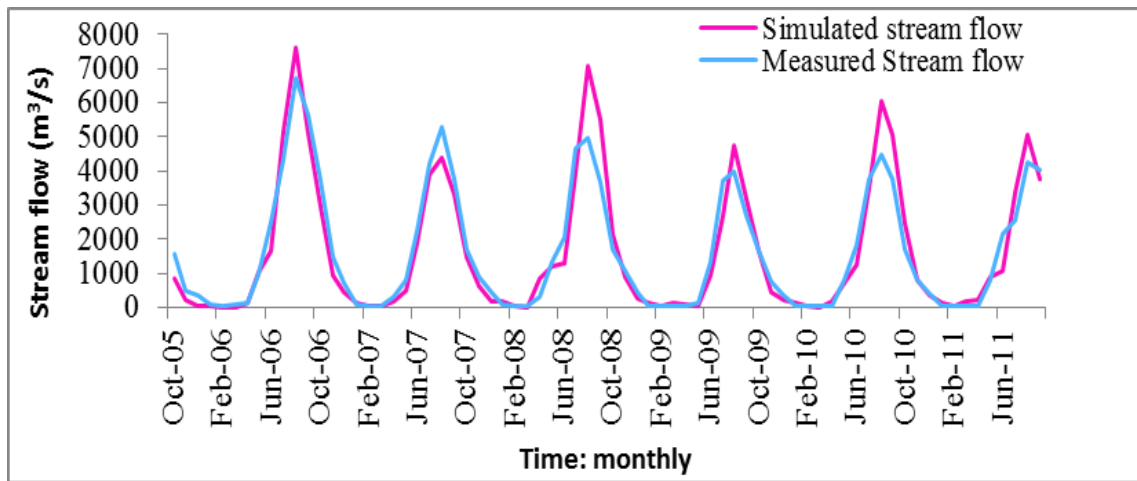


Figure 3.2. Monthly measured and simulated stream flow for calibration period (1994-2005).

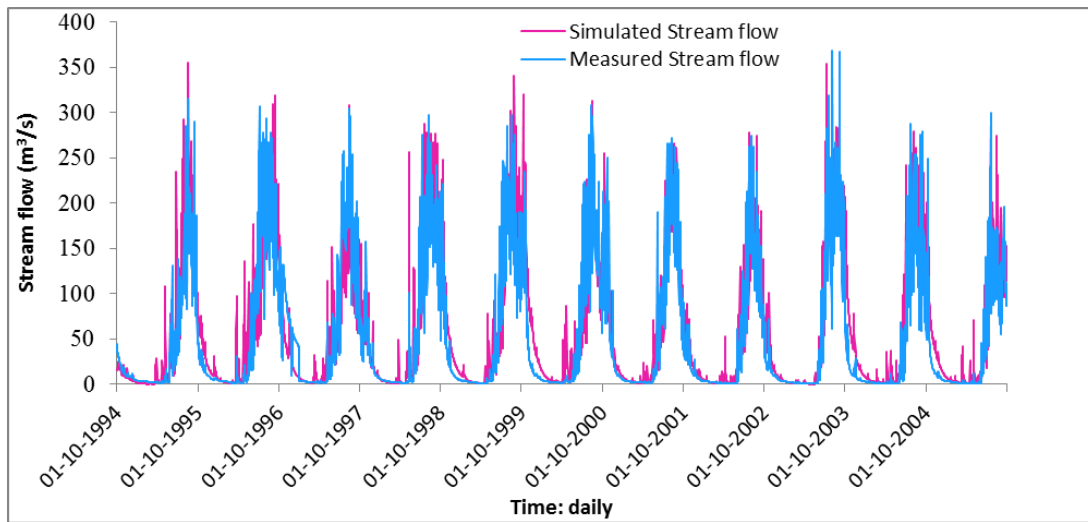


Figure 3.3. Daily measured and simulated stream flow for calibration period (1994-2005).

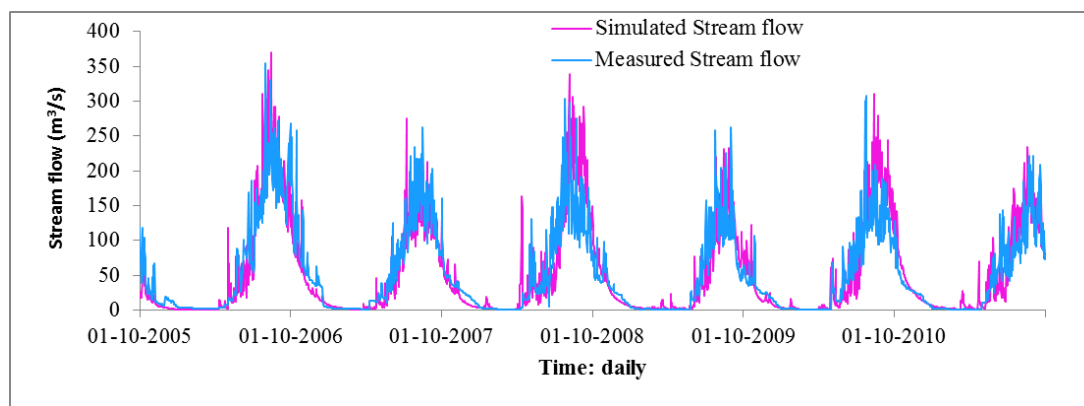


Figure 3.4. Daily measured and simulated stream flow for calibration period (1994-2005).

### 3.2. Estimation of Future annual daily Peak Stream Flow (Flood) and Changes in Flood Frequency

To estimate future annual daily peak stream flow and flood frequency at GilgelAbay River Basin, the values for historical climate changes (temperature and precipitation) in the basin was adjusted on the basis of changes that are projected for the end of 21<sup>st</sup> century at GilgelAbay River Basin. Historically PRMS modeled annual daily peak stream flow and flood frequency is also compared with observed annual daily peak stream flow and flood frequency as shown in Tables 3.1 and 3.2.

Table 3.1. Historical modelled annual daily peak flow compared with observed annual daily peak flow

Stream flow at gauging station	Period of observed record	Observed annual daily peak stream flow (m <sup>3</sup> /s)	Historical modelled annual daily peak stream flow (m <sup>3</sup> /s)	Percentage difference
Gilgel Abay	1993-2012	368.4	375.7	1.9

Hodges-Lehmann estimator was used to compare modelled versus observed peak stream flow and flood frequencies. The difference between modelled annual daily peak flow and observed annual daily peak flow is small (1.9%) as shown in Table 3.1. This indicated that there is good agreement between modelled and observed annual daily peak stream flow.

### **3.3.Flood Frequency Analysis for Historical Modeled and Observed Annual Daily Peak Stream Flow**

Historical PRMS modelled and observed annual daily peak stream flow is compared with 50% and 1% Annual Exceedance Probabilities (AEPs) (equivalent to 2 years and 100 years recurrence interval respectively). Based on selected AEPs (on basis of observed data and most published materials), percentage differences of observed and modelled annual daily peak stream flow are 1.8% and 8.3% for 50% and 1% AEPs respectively and are provided in Table 3.2.

Table 3.2. Differences between historical modelled peak flow with 50% and 1% annual exceedance probabilities (AEPs) and observed peak flow with 50% and 1% AEPs.

Stream flow at gauging station	Years of record	Annual exceedance probability (percentage)	Observed annual daily peak stream flow (m <sup>3</sup> /s)	Historical modelled annual daily peak stream flow (m <sup>3</sup> /s)	Percentage difference
Gilgel Abay	20	50	270	274.9	1.8
Gilgel Abay	20	1	482.6	522.5	8.3

### **3.4.Future annual daily Peak Stream Flow Changes on the Basis of Changes in Air Temperature and Precipitation**

Nine combinations of adjusted values of temperature and precipitation (including no change scenarios) were used as inputs to PRMS model, and annual daily peak stream flow were calculated for each combination. The PRMS derived annual daily peak stream flow from the adjusted temperature and precipitation changes were compared to unadjusted (historical) PRMS derived peak stream flow (Table 3.3). Annual daily Peak stream flow increased for combinations of no temperature change with +10% precipitation change (positive value). Because stream flow is a function of precipitation that is an increase in precipitation increased stream flow more than loses due to constant value of temperature which causes increase of

evapotranspiration. As it is indicated in Figure 2.2 precipitation and temperature are two basic factors for increasing and decreasing of stream flow. On the other hand annual daily peak stream flow decreased for combinations +1.5<sup>0</sup>c temperature change with -10% precipitation change, +1.5<sup>0</sup>c temperature change with no precipitation change and +1.5<sup>0</sup>c with +10% precipitation change (negative values). The reason for these results may be an increase in temperature will result in high value of evapotranspiration than precipitation that results to decrease of stream flow. This indicated that as temperature increases annual daily peak flow will decrease by large amount due to high value of evapotranspiration at the end of 21<sup>st</sup> century. If precipitation is held constant there is a decrease in annual daily peak stream flow when temperature is increased by 1.5<sup>0</sup>c and 3<sup>0</sup>c (30.4% and 32.6% respectively) because of high value of evapotranspiration which losses water to the atmosphere rather than making precipitation values to stream flow. If temperature is held constant there is an increase in annual daily peak stream flow of 10.2% when precipitation is increased by 10%. This is due to high contribution of precipitation to stream flow than contribution of temperature to evapotranspiration. This means precipitation in the form of rain or snow infiltrates in to the soil and contributes more for surface runoff, subsurface runoff and baseflow than losses to the atmosphere as evapotranspiration. But there is a decrease by 19.5% in annual daily peak stream flow when precipitation is decreased by 10% of historical values of precipitation. This is because temperature change has more effect on stream flow than precipitation change. This changes in temperature caused high value of evapotranspiration which will reduce runoff. Generally, this result indicated that there is a decrease in annual daily peak stream flow when temperature is increased by 1.5<sup>0</sup>c and 3<sup>0</sup>c of historical time series data.

Table 3.3. Percentage changes of annual daily maximum peak flow changes based on changes in precipitation and air temperature.

Precipitation change	Temperature change		
	No change	+1.5 <sup>0</sup> c	+3 <sup>0</sup> c
-10 % change	-19.5	-41.2	-41.5
No change	0.0	-30.4	-32.6
+10 % change	10.2	-16.5	-18.1

### **3.5.Future Flood Frequency Analysis on the Basis of Changes in Air Temperature and Precipitation**

Future flood frequency at Gilgel Abay River basin estimated based up on adjusted temperature and precipitation changes and tabulated in Tables 3.4 and 3.5. Fifty percent and one percent annual exceedance probability annual daily peak stream flow (equivalent to 2 year and 100 year recurrence interval peak stream flow, respectively) are calculated for Gilgel Abay River basin using PRMS and Hodges-Lehmann estimator. Percent changes for adjusted modeled AEP annual daily peak stream flow from the adjusted changes in temperature and precipitation are compared with unadjusted (historical) modelled AEP annual daily peak stream flow (Tables 3.4 and 3.5). Changes in percent of annual daily peak stream flow with 50% AEP (Table 3.4) and changes in percent of annual daily peak stream flow with 1% AEP (Table 3.5) are similar to changes in annual daily peak stream flow described in Table 3.3, except variation in magnitude of changes. These percent change values are future annual daily peak flow and flood frequency values at the end of 21<sup>st</sup> century compared to unadjusted (historical) modelled annual daily peak flow and flood frequency. This indicated that as temperature increases, annual daily peakstream flow will decrease by large amount. This may be due to an increase of evapotranspiration which loses water to the atmosphere from water bodies and through plant surfaces. If precipitation is held constant and when temperature is increased by 1.5<sup>0</sup>c and 3<sup>0</sup>c, there is 34.4% and 36.9% decrease in annual daily peak stream flow with 50% AEP respectively. Since precipitation and evapotranspiration are one of the components of hydrological cycle, with no change of precipitation, if temperature increased, it caused decrease of stream flow because of increase of evapotranspiration. If temperature is increased by 1.5<sup>0</sup>c and 3<sup>0</sup>c and precipitation is increased by 10%, there is a decrease of annual daily peak stream flow with 50% AEP by 23.8% and 24.9% respectively, because of increasing evapotranspiration. Large increase in annual daily peak stream flow (14.3%) with 50% AEP occurred when temperature is held constant and precipitation is increased by 10%. This is because precipitation which will contribute to stream flow is more than loses due to evapotranspiration.

Table 3.4. Fifty percent annual exceedance probability peak flow changes based on changes in precipitation and air temperature

Precipitation change	Temperature change		
	No change	+1.5 <sup>0</sup> c	+3 <sup>0</sup> c
-10 % change	-18.3	-43.8	-44.1
No change	0.0	-34.4	-36.9
+10 % change	14.3	-23.8	-24.9

Table 3.5. One percent annual exceedance probability peak flow changes based on changes in precipitation and air temperature

Precipitation change	Temperature change		
	No change	+1.5 <sup>0</sup> c	+3 <sup>0</sup> c
-10 % change	-17.8	-42.4	-42.7
No change	0.0	-32.1	-34.2
+10 % change	14.3	-20.5	-21.7

#### 4. CONCLUSIONS

Future annual daily peak stream flow at 50% and 1% AEPs will increase by 14.3% of historical modeled value of stream flow at the end of 21<sup>st</sup> century at Gilgel Abay river basin when temperature is held constant and precipitation increases by 10%. This is because an increased precipitation will contribute for an increase in stream flow. On the other hand, as temperature is increases by 1.5<sup>0</sup>c and precipitation is decreased by 10%, annual daily peak stream flow at 50% AEPs will decrease by 17.8% of historical modeled value of stream flow. This may be due to high value of evapotranspiration which will decrease runoff. This indicated that during designing of Hydraulic structures and economic evaluation of flood protection projects, considering changes in magnitude and frequency of annual daily peak stream flow in the future based on changes in climate (precipitation and air temperature) is very essential for minimizing failures in hydraulic structures. This is also important for resource managers to have an information to protect resources from risk.

## **Acknowledgements**

The authors would like to acknowledge the financial support of Ethiopia Government for this research work under Ph.D. program for Arega Mulu. We also would like to thank Dr. Dagnachew Legess, Dr. Shushma B., Dr. Vincent F, Mr. Superno G., Dr. Roland J. Viger, Dr. Steven L. Markstrom, Dr. R. Steven Regan, Dr. Lauren E. Hay and other USGS modeling scientists for their endless assistance and help for our work. Finally, we would like to thank reviewers for their constructive and appreciable comments.

## **REFERENCES**

- BCEOM, (1999). Abay River Basin integrated master plan, main report. Ministry of Water Resources, Addis Ababa. 71-83.
- Dooge, J.C.I., (1986). Looking for hydrologic laws: *Water Resources Research*. 22, 465–585.
- Duan, Q.Y., Sorooshian, S, Gupta, V, (1992). Effective and efficient global optimization for conceptual rainfall-runoff models. *Water Resources*. 28, 1015–1031.
- Duan, Q.Y., Gupta, V. K., Sorooshian, S., (1993). Shuffled complex evolution approach for effective and efficient global minimization. *Journal of Optimization Theory Application*. 76, 501–521.
- Duan, Q.Y., Sorooshian, S. Gupta, V. K., (1994). Optimal use of the SCE-UA global optimization method for calibrating watershed models. *Journal of Hydrology*. 158 (3–4), 265–284.
- Farquharson, J. R., (1992). Regional flood frequency analysis in arid and semi-arid areas. *Journal of Hydrology*. 138, 487–501.
- IPCC, (2001). *Climate Change 2001. The Scientific Basis. The Third Assessment Report of the Intergovernmental Panel on Climate Change*, Cambridge University Press, New York.
- Kebede, E., (2009). *Hydrological Responses to Land Cover Changes in Gilgel Abbay Catchment of Ethiopia*. ITC, Netherlands.
- Kebede, S., Travi, Y., Alemayehu, T., Marc, V., (2006). Water balance of Lake Tana and its sensitivity to fluctuations in rainfall, Blue Nile basin, Ethiopia. *Journal of Hydrology*. 316(1–4), 233–247.
- Hodgkins, G.A., Dudley, R.W., (2013). Modeled future peak stream flows in four coastal Maine Rivers, U.S. Geological Survey Scientific Investigations Report 2013–5080, 18 p.
- Hosking, J. R. M., Wallis, J. R., (1988). The effect of interstice dependence on regional flood frequency analysis. *Journal of Water Resource*. 24(4), 588–600.
- Hodges, J. L.; Lehmann, E. L., (1963). Estimation of location based on ranks. *Annals of Mathematical Statistics*. 34 (2): 598–611.

- Jin, M., Stedinger, J. R., (1989). Flood frequency analysis with regional and historical information. *Journal of WaterResources*.25(5), 925–936.
- Landwehr, J. M., Matalas, N. C., Wallis, J. R., (1979). Probability weighted moments compared with some traditional techniques of estimating Gumbel parameters and quantiles. *Journal of Water Resource*.15(6), 1055–1064.
- Leavesley, G.H., Lichty, R.W., Troutman, B.M., Saindon, L.G., (1983). *Precipitation-Runoff Modeling System: User's Manual*. US Geological Survey Water-Resources Investigations Report 83-4238, 207.
- Legesse, D., Vallet-Coulomb, C., Gasse, F., (2003). Hydrological response of a catchment to climate and land use changes in Tropical Africa: Case study South Central Ethiopia. *Journal of Hydrology*. 275(1–2), 67–85.
- Lehmann, Erich L., (2006). *Nonparametric: Statistical methods based on ranks*. New York: Springer. ISBN 978-0-387-35212-1.
- Markstrom, S.L., Regan, R.S., Hay, L.E., Viger, R.J., Webb, R.M.T., Payn, R.A., LaFontaine, J.H., (2015). PRMS-IV, the precipitation-runoff modeling system, version 4: U.S. Geological Survey Techniques and Methods, book 6, chap. B7, 158 p.
- Martins E. S., Stedinger, J. R., (2000). Generalised maximum-likelihood generalised extremevalue quantile estimators for hydrologic data. *Journal of WaterResource*.36(3), 737–744.
- Milly, P.C.D., Betancourt, J., Falkenmark, M., Hirsch, R.M., Kundzewicz, Z.W., Lettenmaier, D.P., Stouffer, R.J.,(2008). Stationarity is dead: Whither water management? *Journal of Hydrological Science*. 319, p. 573–574.
- Mohamed, Y.A., B., van den Hurk, B. H., Savenije, H. G., Bastiaanssen, W. G. M., (2005). Impact of the Sudd wetland on the Nile Hydro climatology. *Journal of Water Resources Research*.41(8), W08420.
- Nash, J.E., Sutcliffe, J.V., (1970). River flow forecasting through conceptual models. Part 1- A discussion of principles. *Journal of Hydrology*. 10, 282-290.
- Nash, LL. Gleick, P.H., (1991). Sensitivity of streamflow in the Colorado Basin to climatic changes. *Journal of Hydrology*. 125, 21-241.
- Peel, M. C., Wang, Q. J., Vogel, R. M., McMahon, T. A., (2001). The utility of L-moment ratio diagrams for selecting a regional probability distribution. *Journal of HydrologicalScience*.46(1), 147–156.
- Pegram G., Parak M., (2004). A review of the regional maximum flood and rational formula using geomorphological information and observed floods. *South Africa ISSN 0378-4738, Water SA Vol. 30 No. 3 July 2004*.
- Polemio, M., 2010. Historical floods and a recent extreme rainfall event in the Murgia Karstic environment, Southern Italy, *Z. Geomorph*, 54, Suppl> Issue 2, 195-219.
- Potter, K. W., Lettenmaier, D. P., (1990). A comparison of regional flood frequency estimation methods using resampling method. *Journal of WaterResources*.26, 415–424.

- Pui, A., Lal, A., Sharma, A., (2011). How does inter decadal pacific oscillation affect design floods in Australia? *Journal of Water Resources*.47, W05554.
- Setegn, S.G., Rayner, D., Melesse, A.M, Dargahi B., Srinivasan, R., (2011). ‘Impact of climate change on the hydro climatology of Lake Tana Basin, Ethiopia.’*Journal of water Resources*.47:13.
- Subramanya, K., (2006). ‘Engineering Hydrology.’Second Edition.Tata McGraw-Hill Publisher, New Delhi, India.
- Taddele, Y., Berndtsson, R., Setegn, S.G., (2013). “Hydrological Response to Climate Change for Gilgel AbayRiver, in the Lake Tana Basin, Upper Blue Nile Basin of Ethiopia. *Plose ONE* 8(10). E7926. Doi: 10.1371/journal. Pone.0079296.
- Tarekegn, D., Tadege, A., (2005). Assessing the impact of climate change on the water resources of the Lake Tana sub-basin using the WATBAL model.CEEPA, Republic of South Africa.
- Wallis, J. R., Wood, E. F., (1985). Relative accuracy of Log-Pearson III Procedures.*Journal of Hydraulic Engineering, ASCE*.111(7), 1043–56.
- Xu, C.Y., Gong, L., Jiang, T., Chen, D., Singh, V.P., (2006).Analysis of spatial distribution and temporal trend of reference evapotranspiration and pan evaporation in Changjiang (Yangtze River) catchment.*Journal of Hydrology*. 327 (1–2), 81–93.

## **Evaluating Implementation of Adama City Land Use Plan Using Conformance-Based Approach**

**Dejene Tesema Bulti**

Geodesy and Geomatics Engineer, Adama Science and Technology University, Adama, Ethiopia

[dejenetesema@yahoo.com](mailto:dejenetesema@yahoo.com) Tel: +251 930 070802 P.O.Box: 1888

### **Abstract**

*The fundamental goal of urban land use plan is to ensure sustainable development of urban areas. However, presently it is unclear that how well urban land use plan is being implemented after plan adoption and major factors contribute to the variation of its implementation in Adama City, Ethiopia. The research examines the extent to which Adama City Land use plan functioned from 2004 to 2014 is guided and controlled the spatial development of the City by measuring the degree to which actual land use outcomes over a ten-year period conform to the plan intention. First, existing land uses of the City are spatially mapped; and digital land use plan map is generated. Second, conforming, nonconforming, and unfulfilled developments are identified through morphological conformity assessment using spatial overlay analysis in Geographic Information System (GIS) environment. Third, two indicators on construction boundary control are used, through which the effectiveness of boundary containment, and proposed land sufficiency are explored. The findings of the study demonstrate that despite the area proposed by the plan is reasonable; the plan has met difficulties to control and guide new spatial developments of the City. The limited effectiveness is mainly attributed to residential land use followed by social service and total urban growth. Moreover, major factors associated to nonconforming developments are geographic variables, monitoring and evaluation, lack of commitment, and political influence. The study would support sustainable spatial policy and direction of spatial development with respect to sustainable urban environment and creating a balance between ecological and socio-economic needs.*

**Keywords:**-Land use planning, urban planning, conformance based approach, GIS, plan evaluation

## **1. INTRODUCTION**

The fundamental goal of urban land use plan is to ensure sustainable development of urban areas. By controlling urban expansion within the planned boundary, it will conserve ecological sensitive areas; ensure effective use of existing resources and balanced development; and support smart growth. Hence, understanding and appraisal of urban land use plan implementation determines the plans' effectiveness and success, consenting for the enhancement of plans and the planning process in subsequent planning (Oliveira and Pinho, 2009; 2010).

Plan implementation has been evaluated for decades using the most acknowledged theories: conformance-based approach and performance-based approach. Conformance-based approach highlights conformity between actual physical development and plan's intention, which fits physical-oriented plans. In this regard, plan implementation is considered as a success if actual land use outcomes fit into plan intentions (Faludi, 2000; Laurian et al., 2004a). On the other hand, performance-based approach explores how the ideas within a plan are delivered and implemented. It is well suited to evaluate strategic plans (Mastop and Faludi, 1997). A plan is considered implemented if it is used or consulted in decision-making processes, no need to be strictly adhering to the actual outcome.

Conformance-based approach has been used in variety of studies; For instance it is used in evaluation of the degree to which actual land use outcomes conforms to plan intention (Alterman and Hill, 1978; Tian and Shen, 2007; Loh, 2011; He, 2012; Ranasinghe and Silva, 2013); examination of effectiveness of urban growth boundary (Nelson and Moore, 1993; Han, 2009); and assessment of the efficiency of land use planning and plan implementation (Brody et al., 2005).

Although these studies have provided insight into the case, the process of plan implementation is rather complex that influenced by various factors, and suggests the need for more researches to develop a sufficient understanding with regard to associated factors influencing plan implementation. For this reason, evaluation of plan outcomes should be considered in a broad context, encompassing specific physical location of the area and human and socio-economic factors. On top of this, land use plan for Adama City have been prepared and implemented since 1937. The latest plan is prepared in 2004 and denoted by LUP04 in this study. It is functioned

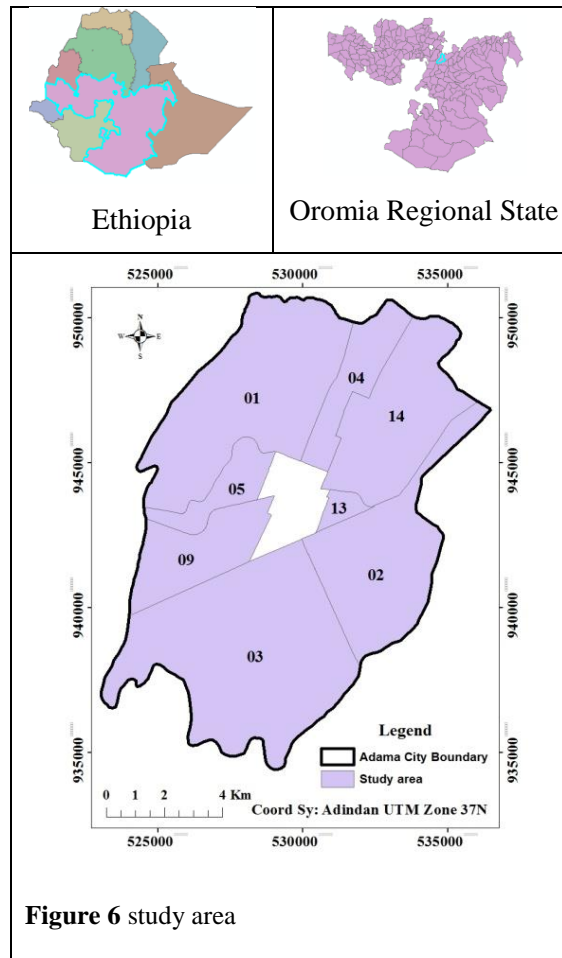
from 2004 to 2014. However, presently it is unclear that how well the plan is guided and controlled the spatial development of the City during the planning period.

Hence, this study intends to examine the extent to which LUP04 is implemented using conformance-based approach. More specifically it is carried out to (i) identify conforming and nonconforming developments (ii) identify variables related to limited implementation of LUP04 (iii) highlight major driving factors associated with nonconforming developments.

## **2. MATERIALS AND METHODS**

### **2.1. The Study Area**

Adama City is one of fast growing cities in the Ethiopia with an estimated total population of 343,212. It is located at a distance of about 96 km from capital City, Addis Ababa. The City has totally 14 smallest administrative units called Kebele. 6 Kebeles are located at the central part covering 5.8 square kilometer. They were dense mixed built up areas when LUP04 is prepared. The rest 8 kebeles are located at the periphery covering 127.9 square kilometer. Even though the LUP04 proposal covers the whole Kebeles, new expansions were mainly proposed in periphery Kebeles (figure 1) including Kebele 01, 04, 14, 13, 02, 03, 09, and 05. Hence, these Kebeles are deemed to demonstrate new developments under LUP04 control in planning period and selected for this study.



## 2.2. Data and Data Sources

Primary and secondary data used in this study were collected from different sources. Land uses as of 2004 were extracted from IKONOS satellite image and land use land cover map of the City as of 2004. Land uses as of 2014 were collected using ground surveying techniques, and digitized from digital orthophoto of the City as of 2014. Proposed land uses by the plan were extracted from structural plan map of LUP04 in GIS framework. Urban Construction Control Boundary (UCCB) was delimited through reclassification of proposed land use classes into constructible and construction forbidden areas.

### **2.3. Variables and Indicators**

The conceptual framework for the Structure Plan of LUP04 mainly focused on the following six framing elements that have direct and strong impact on the development of the City(NRSO, 2004) and explained below.

**Urban growth:** land development crucially shows the direction of urban growth. Period of land development reflects spatial organizations according to the economic situation and policies. Accordingly, the plan has proposed new expansion areas and thus redefined UCCB targeting at bringing compact development.

**Housing:**housing expansion area was proposed to accommodate fast growing population in the City. The proposal is mainly at periphery areas focusing to the northern and southern parts. Some vacant areas within the City were also proposed to be used for new housing construction.

**Social services:**location and spatial distribution of social services were proposed in such a way that to be integrated with hierarchy and size of centers to provide social services in the deprived parts of the City to ensure balanced development and to provide sufficient services.

**Manufacturing and storage:**locations of sites for manufacturing and warehouses were mainly intended to decentralize activities and minimize the need for transportation and also bring about balanced development. Moreover, the plan was aimed at relocating existing manufacturing and warehouses that create disturbance at different parts of the City.

**Road network:**development of infrastructure was the most important strategy in LUP04 to improve living environment and enhance the City competitiveness. It influences the future urban development through establishing a transport framework. Accordingly, the plan was aimed at improving the existing road network, development of streets in expansion areas through increasing length of main components of the road network proposal.

**Environment and green space:**LUP04 provided green space as an important strategy to prevent unplanned urban expansion, to protect natural setup of the City through proposal of green frames (formal green, informal green, farmland, and ground water protection area).

These elements are deemed to demonstrate the conformity of actual land use outcome with plan intention. Hence, evaluation of LUP04 implementation in terms of these variables would be interesting. Each variable was examined through Quantitative and Morphologic conformity using selected indicators (table 1)

**Table 2** Indicators of the selected variables for evaluation LUP04 implementation

<b>Variables</b>	<b>Indicators</b>	
	<b>Quantitative</b>	<b>Morphological</b>
Urban growth (total built up land)	area	Growth boundary
Housing (all types of Residential)	area	Spatial location
Social Service (Education, Health, Religion, and Cultural)	area	Spatial location
Manufacturing and storage	area	Spatial location
Road network	length	Spatial location
Environment & Green space (Farmland, Informal green, Formal green, and Ground water protection zone)	area	Spatial location

## **2.4. GIS Spatial Overlay Analysis**

Spatial Overlay analysis is a technique frequently used to process geographic information. In this research, the technique was realized through the use of ArcGIS 10.1 software package, as it can process a large amount of information at the same time and present the information in a visualized way. This makes an evaluation of LUP04 possible.

## **2.5. Conformity Assessment**

LUP04 is essentially a material-oriented blueprint plan with a clear envisaged end-state. In other words, the future is closed in the framework of the plan. Therefore, effectiveness of the plan should be measured by the level of conformity between actual land use outcomes and plan proposal from both morphological and quantitative perspective.

Hence, morphological conformity was examined through spatial overlay analysis of actual land use outcomes as of 2014, map of proposed variables in the plan, and land use as of 2004. In this regard, for every variable, three indices were defined:

- *Conforming*: If the use of land as of 2014 is the same with the variable and consistent with proposed land use
- *Unfulfillment*: If the use of a piece of land as of 2004 and 2014 are consistent, but different from plan proposal for the variable, then the plan is not yet implemented. But the plan might or might not be implemented in the future.
- *Nonconforming*: if actual land use as of 2014 is the same with the variable but different from plan proposal

The result of morphological conformity was then verified through field visit and personnel interview to pinpoint associated factors related to the implementation of the plan.

Quantitative conformity was assessed to evaluate the level of spatial extents of actual land use outcomes of each variable conform to the extent proposed by the plan. It was examined using two basic indicators: Boundary Containment Ratio (BCR) and Boundary Sufficiency Ratio (BSR) proposed by (Han et al., 2009). Figure 2 helps to illustrate these indicators

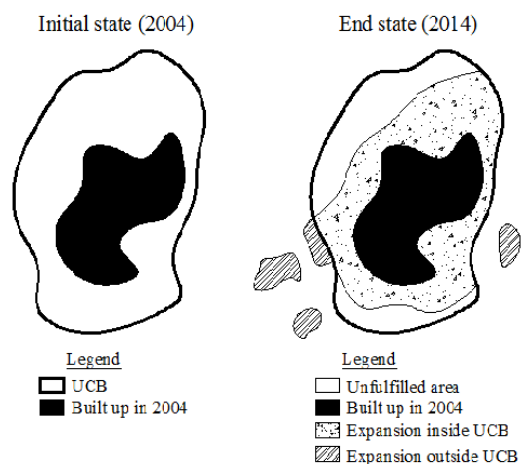


**Figure 7** Illustration of the area analysis

BCR was used to identify to what extent actual land use outcome as of 2014 deviates from intended land use in the plan. In this regard, if the plan is to be considered effective to contain

the specific variable development, less nonconforming developments should occur than conforming developments. It was measured by the ratio of “area of nonconforming developments to area of conforming development”. The higher values of BCR indicate limited implementation and vice versa.

$$BCR_i = \frac{(\text{Nonconforming area})_i}{(\text{Conforming})_i}$$

Implies

$$BCR = 0, \quad \text{complete effectiveness}$$

$$0 < BCR < 1, \quad \text{limited effectiveness}$$

$$BCR \geq 1, \quad \text{complete failure}$$

BSR was used to define the total possible increase of developed land for selected variable. In this case, in order to achieve effective containment, the area of actual total development of the variable should not be more than the area proposed for the variable. It was measured by the ratio of “total area of actual developments to area of proposed land in LUP04”. BSR is inversely proportional to sufficiency of the size of proposed land.

$$BSR_i = \frac{(\text{Total development})_i}{(\text{proposed area})_i}$$

Implies

- $BSR < 1$ , planned area is sufficient to accommodate the development
- $BSR > 1$ , planned area is insufficient to accommodate the developments.

### 3. RESULTS

- **Urban Growth**

Result of morphological conformity assessment depicted in figure 3 shows significant land developments occurring outside of UCCB. Only 1615.2ha of land is developed following the plan while 1124.6ha of land proposed at northern and southern parts of the City is not yet developed. These areas are mainly characterized by insignificant infrastructure developments. In contrary, nonconforming developments are covering 570.44 ha. Most of these developments especially at western and eastern parts located along main road and expressway are existing developments before LUP04 preparation and expanded in planning period. Other leapfrogging developments are informal developments may be related to lack of close supervision and monitoring.

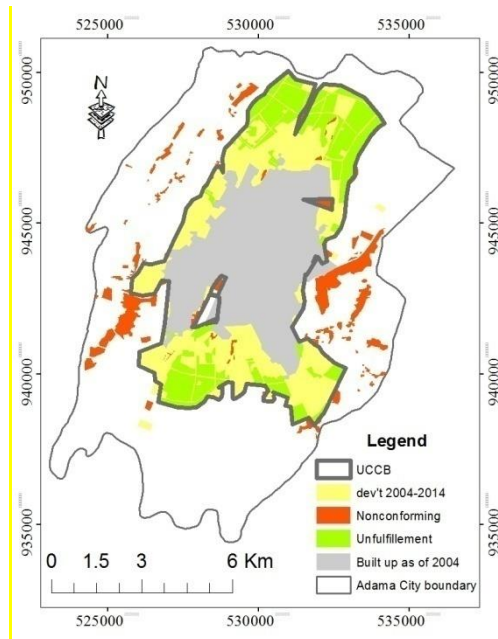


**Figure 8** spatial distribution of conforming, nonconforming, and unfulfilled total land developments

Further, computed value of BCR, 0.35, indicates that nonconforming developments have a significant share of the total growth underscoring the limitation of the plan in controlling the spatial location of new land developments. On the other hand, value of BSR, 0.21, indicates that the plan was reserved sufficient land area to accommodate all new urbanization during planning period if measured by the actual development density.

- **Road network**

Result of spatial analysis of existing road network shows that total actual length of existing road as of 2014 in study area is only 131.629km indicating 64.142km is not yet developed. Unfulfilled road development is distributed mainly at northern and southern part of the City (figure 4).

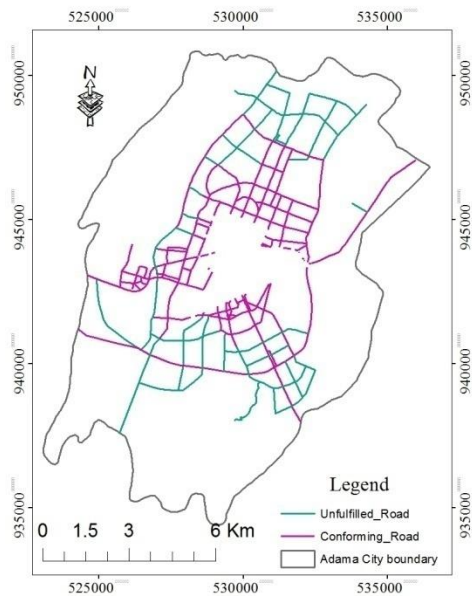


**Figure 9** spatial distribution of existing and unfulfilled road development

Further analysis suggests that principal Arterial Street is reached about 69.13 km (78.5%); minor arterial is about 33.37 km (45%); and Collector Street about 26.48 km (89.9%) of plan intention. Only 2.65 km nonconforming development is found at western part of the City. It is due to modification of expressway alignment. Computed value of BCR indicates effective implementation of the plan.

- **Housing Development**

The proposal was mainly at periphery areas focusing to the northern and southern parts. However, result depicted in figure 5 shows that significant nonconforming housing developments are occurring at different parts of the City covering 512.49ha of land. In contrary, 1019.35ha of reserved land is waiting for development.

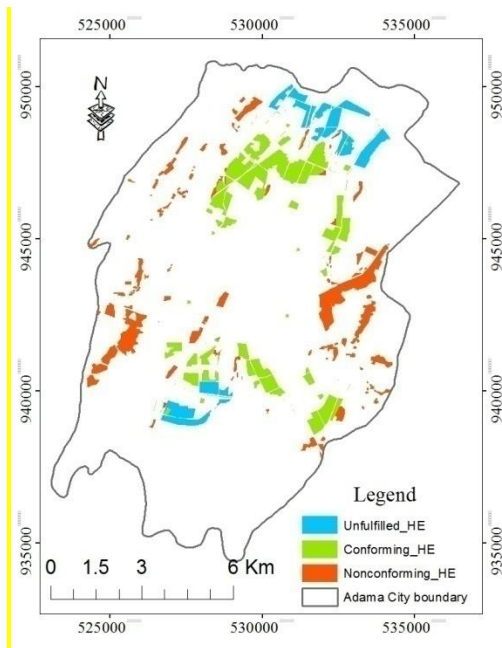


**Figure 10** spatial distribution of conforming, nonconforming, and unfulfilled housing development

Furthermore, field observation of nonconforming developments especially at western and eastern parts of the City may be related to ease transportation access. On the other hand, areas of unfulfilled development are mainly characterized by low infrastructure development and serving for farming activities.

In addition, computed value of BCR is 0.78 indicating the plan has limited effectiveness in controlling the spatial location of newly residential development. On the other hand, value of BSR is found 0.68 indicating the planned area for residential land use was much enough to encompass all new housing developments.

- **Manufacturing and Storage**

The result depicted in figure 6 shows that nonconforming developments are occurring mainly at south and southwest and west parts of the City. In contrary, majority of reserved land at southern and northern parts are not fully utilized. Further, actual land use outcome utilized by manufacturing and storage within planned area is about 277.738 ha and that of outside is found 51.615 ha. Most of these nonconforming developments are mainly warehouses existing before

LUP04 approval and proposed to be removed. Conversely, 185.78 ha of undeveloped land is due to its location at about extreme northern part of planning area. This area mainly lacks infrastructure developments and used for farming activities.

Further, computed value of BCR is 0.19 indicating the plan has limited effectiveness in controlling the spatial location of manufacturing and storage. On the other hand, value of BSR is found 0.71 indicating the Plan was designed encompassing area large enough to accommodate new developments.

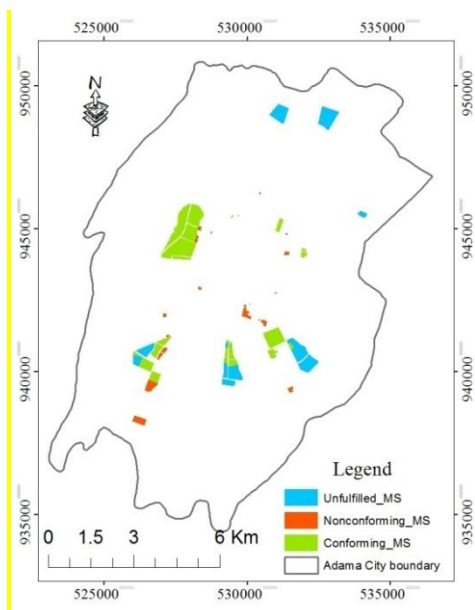


**Figure 11** spatial distribution of accordance, deviation, and unfulfilled manufacturing and storage development

## **Social Services**

The result of spatial overlay analysis (figure 7) demonstrates that a total actual social service development is found 353.9ha of which only 263.1ha is developed following the plan. The rest 90.8ha nonconforming developments are occurring at different parts of the City. In contrary 73.89 ha of proposed land at southern and northern parts of the City are waiting for development. These areas could not attract developments due to low infrastructure development in the areas and geographical location at extreme north.

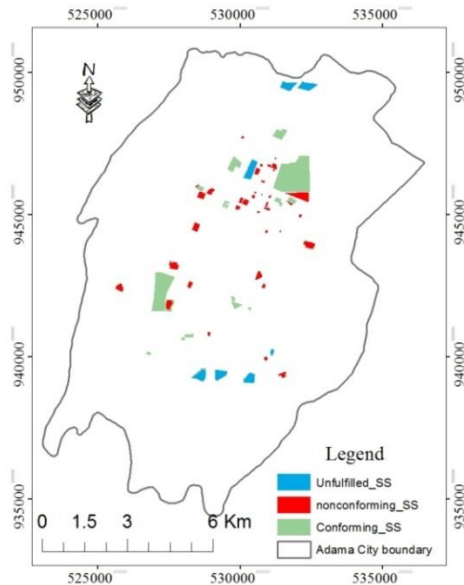


**Figure 12** Spatial distribution of accordance, deviation, and unfulfilled social service developments

Computed value of BCR is 0.35. This indicates that the plan has limited effectiveness in controlling the spatial location of newly developed social service land. Value of BSR equals 1.05 indicating the social service development a bit exceeds the proposed land area. This may be due to existing schools located in proposed mixed built up area.

- **Environment and Green Space**

However, the result of spatial overlay analysis of developments outside of UCCB and map of open space land uses depicted in figure 8 indicates that open space encroachments are composed of 412.35ha (72.3%) from farmland, 73.68ha (12.9%) from formal green, and 84.42 ha (14.8%) from informal green. In contrary, proposed farm and ground protection zone (FGWPZ) is well preserved.

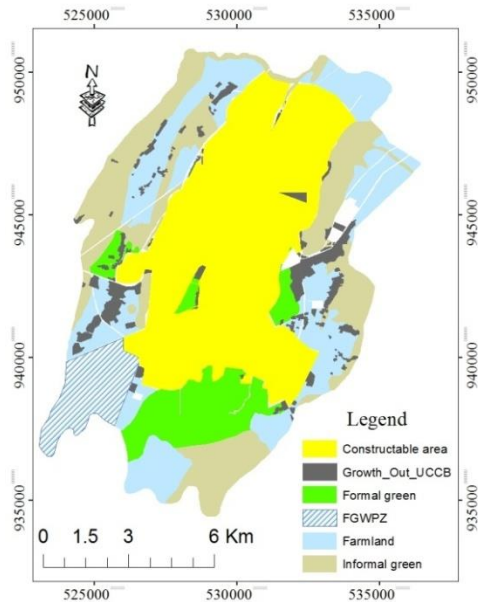


**Figure 13** spatial distribution of unplanned developments encroaching proposed green frame

Open spaces encroachment perceived in the western part is strategic site suited close to main road and office of “Aba Geda” Conference Hall Administration. Furthermore, nonconforming developments are located at the junction point of expressway and main road passing through the City at both ends. These sites are perceived suited to ease transportation access and have better infrastructures like water supply etc.

#### 4. DISCUSSIONS

This study examined implementation of LUP04 using six variables: manufacturing and storage, housing, road network, social service, urban growth, and environment and green frame. The findings demonstrate that the level of conformity is acceptable when measured by the size or quantity. In other words, the total area of increased developed land in planning period remains in the limit of the land use quota proposed by the plan. However, level of conformity is low when measured in terms of morphology indicating limitation of the plan in controlling spatial location of new developments. The limitation is high in Housing developments followed by social service and urban growth while it is relatively low in manufacturing and storage, and environment and green frame. However, the plan is effective in controlling location of road network.

Nonconforming development areas are spatial indicators of urban and suburban sprawl (Brody, 2005). Based on these evidences, it is enough to conclude that LUP04 has met difficulties to play its role in guiding and controlling spatial development of Adama City from 2004 to 2014. The limitation may be related with the following four potential factors.

- **Spatial variables (Proximity to public infrastructures)**

Proximity to likely public infrastructures and major transportation corridors significantly affects the degree of plan conformity. The spatial variables support the visual results of this study and indicate that most of nonconforming developments occurred outside of UCCB are close to major road and expressway passing in the planning area due to better transportation access. It is also perceived that other infrastructures development in these areas is relatively good. In the contrary, lack of these variables at extreme northern and southern parts of the City has retarded the development of housing, social services, and manufacturing and storage limiting the intended direction of growth.

- **Monitoring and evaluation**

Nonconforming developments indentified in this study might be occurred due to lack of supervision and monitoring in a timely manner. Technically, through regular monitoring and evaluation of implementation of the plan, it would be possible to identify unplanned developments and take measures to stop the construction in a timely manner. In addition to this, despite the developments outreach the plan intention, proposed area has not been fully urbanized. On the other hand, most of reserved land for new development at extreme northern and southern parts of the City is already supplied to developers before 3years of end of planning period. However, it is not developed within the time limit given by City Administration usually six months. Through close monitoring and supervision it would be transferred to potential developers and ensure balanced development in planning period.

- **Lack of commitment**

Illegal and informal developments in 2004 were not considered during plan preparation and they would be removed gradually in planning period. However, in practices, the City Administration has not removed many of these developments. Instead, spatial expansion occurred around them.

Even the City Administration recognized some of the developments that outreached UCCB. On top of this due to lack of commitment of officials, existing land use during plan preparation and proposed land use change by the plan were not implemented. It explains why the majority of illegal developments and most of residential and warehouse developments as of 2004 existed in 2014.

- **Political factor**

Of all the reasons, unsupported political leadership is perhaps the most essential reason that led to the deviation between plan and outcome. Because LUP04 is mainly a ‘government-led’ plan, the extent of support from regional government will thus largely decide the extent of implementation success of the plan. In Adama, socio-political acceptance and economic development is given the first priority. Hence, in most cases City Administration chose to secure political acceptance and support development rather than control. With this aim, political leaders in the City Administration, Mayor and its advisory team (cabinet) would place their primary focus on economic development and political security, since both are the principal criterion when regional government assesses their political achievements. Hence, the success of investments in Adama made the City Administration believed that attracting developers through land supply was an effective way to maintain a rapid economic growth.

Therefore, when development projects come to Adama, the City Administration and regional government would satisfy the site selection proposed by developers as much as possible even areas out of UCCB were chosen. Especially ones with large economic added-value showed their interests in the City, investors were almost free to select any sites they needed regardless of the limit of UCCB. In order to retain the investment, City Administration ultimately accepts their applications. This explains why nonconforming land developments occurred out of UCCB at the western part of the City is high standard hotels. Hence, political context in Adama has not created a supporting implementation environment for the plan.

## **5. CONCLUSIONS AND RECOMMENDATIONS**

### **5.1. Conclusions**

By spatial mapping of actual land use under LUP04 control and measuring the degree of plan conformance, this research evaluates the effectiveness of the plan implementation. The value of the study can be explained in different ways. First, the variables used in this study: manufacturing and storage, housing, road network, social service, total land growth, and environment and green frame are highlighted the level of conformity between actual land use outcomes and plan intention. Second, morphological conformity assessment using GIS spatial overlay analysis provides spatial extent and distribution of conforming and nonconforming developments. This can be important information to be considered in the next planning course. And also keeping a plan on track and ensuring effective implementation of unfulfilled planned areas. Moreover, it can help planners recognize where there is nonconformity or significant deviation from original plan intention that may adversely influence urban environments. It serves as a monitoring tool with which to guide the direction of plan implementation, to adjust course to updated information, or to plan a new heading before negative outcomes become irreversible. Third, quantitative conformity assessment using BCR and BSR is highlighted the level of effectiveness of the plan in guiding and controlling spatial development of the City. This provides insight into land use plan implementation as sufficient plan design only by itself will not insure plan implementation. Fourth, the findings of the study provide a better understanding of the major factors contributing to nonconforming development and sprawling growth in Adama City. Identification of why development occurs in unintended areas can help the government to design spatial policies to the context to improve plan implementation, to mitigate sprawling development patterns, and to conserve environment. Most importantly, the techniques used in the study could facilitate an adaptive approach to evaluate land use plan of other urban centers in the country.

### **5.2. Recommendations**

Although this study provides important information on the implementation of Adama City Land use plan and major influencing factors, the results should be considered only an initial step towards understanding the links between urban land use plan and its implementation. Hence,

further researches are needed on several fronts. First, only one approach is outlined to examine the implementation of urban plans, which by itself is not sufficient. Other evaluation techniques must be used, and plan implementation should be evaluated with the use of multiple approaches of analysis. In addition, the study has examined Adama City Land use plan of single planning period. Future research should analyze plans in different planning periods to identify the trend of effectiveness of plans prepared and implemented in different planning periods. It is recommended that level of implementation urban land use plans in more urban centers in Ethiopia should be examined. Comparative analyses would provide an increased understanding of the effectiveness of spatial planning and plan conformity in the country. Finally, it is recommended that regional and National land-use policies should be considered more effectively in order to isolate the effects of growth-management tools on land use plan implementation.

#### **Conflict of interest**

On behalf of all authors, the corresponding author states that there is no conflict of interest.

#### **ACKNOWLEDGEMENTS**

This research is granted by Adama Science and Technology University. The findings and opinions reported are those of the author and are not necessarily endorsed by the funding organization.

#### **REFERENCES**

- Alterman R and Hill M. (1978). Implementation of Urban Land Use Plans. *Journal of the American Institute of Planners* , 274-285.
- Brody S D, Highfield W E, Thornton S. (2005). Planning at the urban fringe: an examination of the factors influencing nonconforming development patterns in southern Florida. *Environment and Planning B: Planning and Design*, 33 , 75-96.
- Faludi, A. (2000). The performance of spatial planning. *Planning Practice & Research*, 15 , 299-318.
- Han H, LAI S, Dang A, Tan Z, WU C. (2009). Effectiveness of urban construction boundaries in Beijing: an assessment. *Journal of Zhejiang University Science, A* , 1285-1295.

- Han, H. Y. (2014). *Theories and Applications of Urban Growth Boundary*. Beijing: China Architecture & Building Press.
- He, J. (2012). Implementation of the Shanghai Master Plan. *AESOP 26th Annual Congress*, (pp. 1-26). METU, Ankara.
- Laurian L, Day M, Backhurst M, Berke P, Ericksen N, Crawford J, Dixon J, Chapman S. (2004a). What drives plan implementation? Plans, planning agencies and developers. *Journal of Environmental Planning and Management*, 47, 555-577.
- Loh C G. (2011). Assessing and interpreting nonconformance in land-use planning implementation. *Planning Practice & Research*, 26, 271-287.
- Mastop H and Faludi A. (1997). Evaluation of strategic plans: the performance principle. *Environment and Planning B: Planning and Design*, 24, 815-832.
- National Regional State of Oromia (NRSO). (2004). *Adama Master Plan Revision Project: Synthesized Structural Plan Report*. Adama, Ethiopia.
- Nelson A C and Moore T. (1993). Assessing urban growth management: The case of Portland, Oregon, the USA's largest urban growth boundary. *Land Use Policy*, 10(4), 293-302.
- Oliveira V and Pinho P. (2009). Evaluating plans, processes and results. *Planning Theory & Practice* 10(1), 35-63.
- Oliveira V and Pinho P. (2010). Evaluation in urban planning: Advances and prospects. *Journal of Planning Literature*, 24(4), 343-361.
- Ranasinghe P and Silva L. (2013). An evaluation of the outcomes of the urban development plans with special reference to Moratuwa urban development plan. *The second world construction symposium: socio economic sustainability in construction*, (pp. 22-32).
- Tian L and Shen T. (2007). Evaluation of Plan Implementation in the Transitional China: a Case of Guangzhou City Master Plan. *43rd ISOCARP Congress*.

## Performance of Anaerobic Sequencing Batch Reactor for the Treatment of Tannery Wastewater and Climate Change Mitigation

Andualem Mekonnen<sup>1\*</sup> and Seyoum Leta<sup>2\*\*</sup> and Karoli Nicholas Njau<sup>3</sup>

<sup>1,2</sup> Center for Environmental Science, College of Natural Science, Addis Ababa University, P.O.Box 33348,

Addis Ababa Ethiopia\*E-mail: [andumk21@gmail.com](mailto:andumk21@gmail.com) \*\* E-mail: [letaseyoum@yahoo.com](mailto:letaseyoum@yahoo.com)

<sup>3</sup>The Nelson Mandela African Institute of Science and Technology, P.O. Box 447 Arusha, Tanzania.Email;

[knjau30@yahoo.com](mailto:knjau30@yahoo.com)\*Corresponding Author

### Abstract

*The objective of this study was to develop and optimize a pilot scale anaerobic sequencing batch reactor (ASBR) for the treatment, biogas production and greenhouse gas emission reduction from tannery wastewater. A pilot scale ASBR was developed and integrated with aerobic SBR and constructed wetland at Modjo tannery, Ethiopia. The performance of the pilot scale ASBR was evaluated at the OLRs of 1.03, 1.23, 1.52 and 2.21 kg m<sup>-3</sup>.d<sup>-1</sup> under mesophilic condition (31<sup>0</sup>c). The removal efficiencies of COD and methane yield in the pilot scale ASBR were in the range of 69 – 85% and 0.17±0.2 - 0.30±0.02m<sup>3</sup>/kg COD removed, respectively. The optimum COD removal and methane yield were obtained at OLR of 1.03kg m<sup>-3</sup>.d<sup>-1</sup> (HRT of 4 days) in the stepwise feeding mode. At this OLR, the volumetric methane production will be 148,190m<sup>3</sup> per year when the digester will be operated at full scale level. This will replace 52% of the diesel oil consumption in the factory. The total amount of GHG emission reduction from the factory is estimated to be 3032 ton CO<sub>2</sub>-eq per year. In the kinetics studies, modified Stover-Kincannon and second-order models were found to be the most appropriate model for ASBR treating tannery wastewater (R<sup>2</sup>=0.99) than first order model (R<sup>2</sup>=0.83). The saturation value constant and maximum COD removal rate found in Stover-Kincannon model were 5.57 and 5.56 kg of COD m<sup>-3</sup>.d<sup>-1</sup>, respectively. Generally, the results of this study showed that ASBR is efficient on generating biogas and reducing greenhouse gas emission while treating high strength wastewater such as tannery.*

*Keywords: ASBR, GHG, methane yield, Stover-Kincannon and tannery wastewater*

### 1. Introduction

Tanning industries is almost a wet process that uses about 30-40 L of water/kg of hides or skin processed and also discharges about 90% of the consumed water as wastewater (IFC, 2007). The wastewaters, which are discharged without proper treatment, would contaminate surface and ground water as well as soils.

Currently, there are more than 30 tanneries under operation in Ethiopia. These tanning industries generate  $11,312\text{m}^3$  wastewater per day and disposed to the surrounding water bodies without proper treatments (LIDI, 2010). However, it is characterized by a high load of pollutants which require proper treatment before it would be discharged into the receiving water body. The treatment systems adopted by most industries are frequently considered as regulatory obligation that increase capital and operational costs and ultimately yield negative economic returns. Compliance to environmental legislations should not necessary lead to the creation of additional costs. It should instead provide a secondary source of income. Anaerobic treatment is considered as sustainable method of reducing pollution from domestic, agricultural and industrial operations (Seghezzo et al., 1998; William and David, 1999). It consumes little energy as no aeration is needed and produces renewable energy in the form biogas and nutrient rich digestate (Kaparaju and Rintala, 2011). Moreover, the anaerobic technology provides the opportunity for greenhouse gases emission reduction and global warming mitigation though substitution of fossil fuel for energy production and chemical fertilizer (Pathak et al., 2009). The ASBR (Anaerobic Sequencing Batch Reactor) operates in a cyclic batch mode with four distinct phases per cycle. The four phases are: filling, reacting, settling and release (Timur and Oèzturkm, 1999; Zhang *et al.*, 1997). The ASBR systems has been successfully applied in laboratory and pilot scales for treatment of high strength wastewaters including landfill leachate, slaughterhouse wastewater, municipal sludge and dairy wastewaters, brewery wastewater (Xiangwen *et al.*, 2008). Therefore, this study aimed to investigate the biogas production and greenhouse gas emission reduction potential of the pilot anaerobic sequencing batch reactor from tannery wastewater. The COD removal efficiency, biogas production and methane yield of the ASBR were investigated at different at various  $\text{OLR}_s$ .

## **2. Materials and Methods**

### **2.1. Experimental setup**

The pilot-scale Anaerobic SBR was constructed using concrete materials in a cylindrical in shape with a dimension of 4 meter in height and 4 meter in diameter. Figure 1 shows the schematic diagram of the pilot scale ASBR and the accessories. The total volume was  $100\text{m}^3$  of this  $80\text{m}^3$  as working volume and the remaining volume for head space. The internal part of the digester was insulated with plastic foam and covered with geo-membrane. Stainless steel tubes were installed 30cm above the bottom of the digester surface for the circulation of hot water. Mixing of the digester system was performed with wastewater circulation between ASBR and mixing chamber.

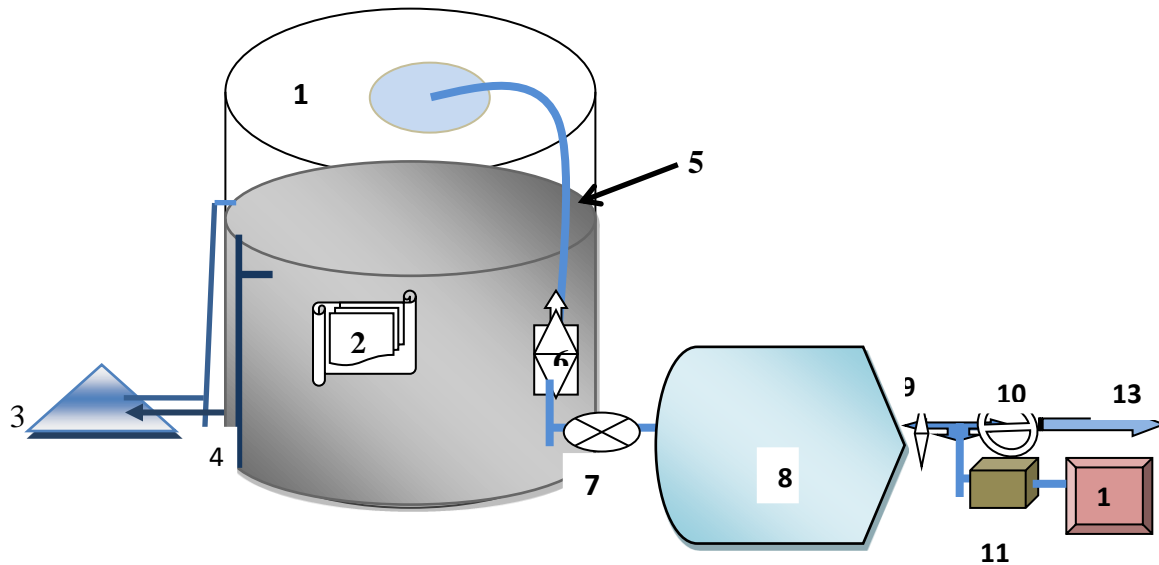


Figure 1: Schematic diagram of the pilot scale ASBR and all the installed accessories.

ASBR(1); Control panel (2); Mixing chamber (3); Feeding pipe (4); Gas pipe (5); Gas flow meter (6); Moisture trap unit (7); Biogas storage bag (8); Gas valve (9); Gas blower (10); Sulfur scrubber (11); Generator (12) and gas line to the kitchen (13).

The performance of the pilot scale ASBR was evaluated at four different OLRs (1.03, 1.23, 1.52 and  $2.21 \text{ kg} \cdot \text{m}^{-3} \cdot \text{d}^{-1}$ ) with corresponding retention time of 4, 3.5, 3 and 2 days, respectively.

### 2.3. Physico-chemical Analysis

The characteristics of influent and effluents were characterized in terms of COD, TN,  $\text{NH}_4^+\text{-N}$ ,  $\text{NO}_3^-\text{-N}$ ,  $\text{S}^{2-}$ ,  $\text{SO}_4^{2-}$ , TP and  $\text{PO}_4^{3-}$  colorimetrically using spectrophotometer (DR/2010 HACH, Loveland, USA) according to HACH instructions. pH of tannery wastewater was measured using a pH meter (CON, 2700). TDS, EC and Salinity were measured using TDS/EC/Salinity meter.  $\text{RE}(\%) = 100 * \left( \frac{S_{In} - S_{out}}{S_{In}} \right)$

### 2.4. Data Analysis

The data was entered to Microsoft EXCEL spread sheets and the mean and standard deviation was analyzed. The graphs were drawn using OriginPro 8.0 software. The analysis of variance and comparison of means were performed using SPSS package version 22. The comparison between mean was performed at 5% level of significance.

## 4. Results and discussion

### 4.1. Characteristics of raw tannery wastewater

Tannery wastewater is characterized mostly in terms of the levels of pH, salinity, organic matter (COD), nitrogenous compounds (TN,  $\text{NH}_4^+$ ), suspended solids (SS) and total dissolved solids (TDS), chromium and sulfides (Jahan *et al.*, 2014). The mean characteristics of raw wastewaters used in the study are presented in Table 1.

Table 3: Characteristics of tannery wastewater used at five different OLR

Parameters	Phase I	Phase II	Phase III	Phase IV
pH	9.64 ±0.46	9.20 ±0.33	9.28 ± 0.311	9.09±0.49
E.C. (mS)	8.76±0.40	8.46±0.39	8.08±0.38	8.43±0.72
TDS (g/l)	7.49±0.36	7.24±0.44	6.81±0.42	7.26±0.68
Salinity (g/l)	9.26±0.57	9.19±0.38	8.91±0.33	9.07±0.71
COD (mg/l)	4221±359	4265± 215	4586± 292	4458± 396
TN (mg/l)	451±47.5	517±112	492.5±89.9	458±58.6
$\text{NH}_4^+$ -N (mg/l)	231±45	270±66	255±58	248±44.46
Total phosphorus,(mg/l)	22.2±6.8	18 ±4.5	19.3 ±4.16	23.5 ±6.5
Sulfide (mg/l)	93±22.27	126±38.9	123.5±33.8	117.5±29.4
Sulfate (mg/l)	470±75.	390±76.9	520±99.13	469±69

The wastewater characterized as it was alkaline with pH value ranging from 9.09±0.49 to 9.64±0.46. It contains also high level of electrical conductivity (8.08±0.38 to 8.76±0.34mS), total dissolved solids (6.81±0.42 to 7.49±0.36g/l) and salinity content (8.77±0.72 to 9.26±0.51g/l). This due to the chemicals used in the soaking and beam house operation. It contained high organic matter and nitrogenous compounds with COD ranges from 4221±359 to 4586± 292mg/l. The influent had high total nitrogen (TN),  $\text{NH}_4^+$ -N and sulfate values ranging from 451±47.5 to 517±112 mg/l, 231±45 to 270±66 mg/land, 390±76.9 to 520±99.13mg/l, respectively; likewise, sulfide and phosphate concentrations were ranging from 92.9±23.27 to 127±43.3mg/l and 18±4.5 to 23.5±6.5mg/l, respectively.

## 4.2. Performance of the ASBR

The COD removal efficiency and biogas production, methane yield and content of the ASBR are summarized in Table 2. During the first phase of the operation, the COD removal efficiency varied in the range of 78 -84%. The average COD removal efficiency and mass removal rate in the single feeding mode were  $81\pm 2\%$  and  $791\pm 149.5\text{mg/l}$ , respectively.

Table 2. Summary in the performance of anaerobic sequencing batch reactor

Parameters	Phase I	Phase II	Phase III	Phase IV
OLR, $\text{kg.m}^{-3}.\text{day}^{-1}$	$1.03\pm 0.09$	$1.23\pm 0.06$	$1.52\pm 0.1$	$2.21\pm 0.23$
HRT, day	4	3.5	3	2
COD removal, %	$81\pm 2.1$	$79\pm 2.3$	$76\pm 1.6$	$69\pm 1.7$
COD out, mg/l	$791\pm 149.5$	$898.9\pm 122$	$1101.4\pm 123$	$1358.3\pm 170$
Biogas production, $\text{m}^3.\text{day}^{-1}$	$26.2\pm 1.6$	$28.1\pm 1.8$	$31.8\pm 2.7$	$36.7\pm 2.8$
Methane, %	$70\pm 1.6$	$68\pm 1.7$	$64\pm 3.0$	$55\pm 1.9$

In the second phase, the COD removal efficiency was varied in the range of 76 - 83% with average removal efficiency of  $79\pm 2.3\%$  while the average concentration of COD was  $898.9\pm 122\text{mg/l}$  in the final effluent. In the third phase, the average COD removal efficiency was decreased to 74-79% with average COD concentration of  $1101.4\pm 123\text{mg/l}$ . In the final phase, the COD removal efficiency was varied between 67 and 72%. The average removal COD removal efficiency and effluent concentration were  $69\pm 1.7\%$  with  $1358.3\pm 170\text{mg/l}$ , respectively. The anaerobic digester showed significant variation in COD removal efficiency with variation of organic loading rate (ANOVA,  $P < 0.05$ ). The results of this study indicate that COD removal efficiency was highest in the first phase of operation and lowest in the final phase of operation. The final phase showed residual COD 31% from the influent.

## 3.4. Biogas production and methane yield

The variations of volumetric biogas generation and methane yield during all the experimental phases are illustrated in Table 3. At the OLR of  $1.03 \text{ kg m}^{-3}\text{d}^{-1}$  (phase I), significantly higher biogas generation was observed in the step feeding than the onetime feeding ( $p < 0.05$ ). The average methane and carbon dioxide content were  $70 \pm 1.6\%$  and  $24\pm 2.1\%$  in one time feeding and  $70 \pm 2.7\%$  and  $22.8 \pm 2.2\%$  in the step feeding methods, respectively (Table 2).

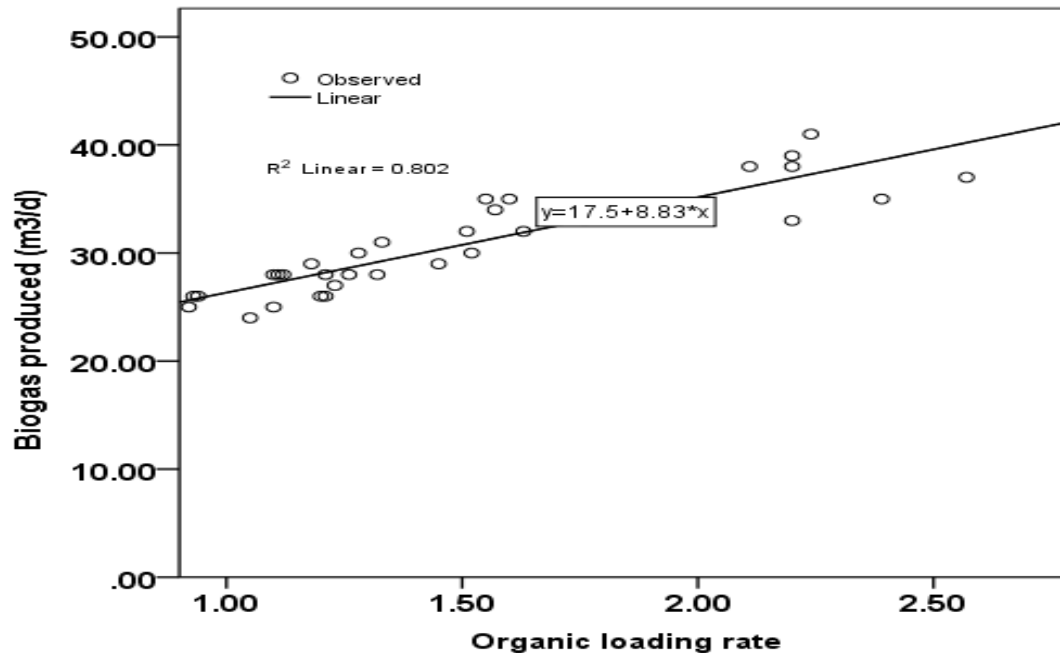


Figure 2: Biogas production with variation of OLR

Like biogas production, higher methane yield was recorded in the step feeding ( $0.30 \pm 0.02 \text{ m}^3 \text{ CH}_4$  per kg COD per day) method than one time feeding method ( $0.28 \pm 0.02 \text{ m}^3 \text{ CH}_4$  per kg COD per day). When the OLR increased to  $1.23 \text{ kg m}^{-3} \text{ d}^{-1}$  (phase II), the biogas production showed slight increment with an average methane and carbon dioxide content of  $68 \pm 1.7\%$  and  $24.2 \pm 2\%$ , respectively. On the other hand, the methane yield was significantly reduced from  $0.30 \pm 0.02$  to  $0.25 \pm 0.01 \text{ m}^3 \text{ CH}_4$  per kg COD per day. The biogas production was significantly increased when OLR rise from  $1.23$  to  $1.52 \text{ kg m}^{-3} \text{ d}^{-1}$  ( $p < 0.05$ ) while the methane yield was significantly reduced from  $0.25 \pm 0.01$  to  $0.22 \pm 0.01 \text{ m}^3 \text{ CH}_4$  per kg COD per day ( $p < 0.05$ ) and average methane content dropped to  $64 \pm 3.0\%$ . When the OLR was increased from  $1.52$  to  $2.21 \text{ kg m}^{-3} \text{ d}^{-1}$ , the biogas production was significantly higher than all the other loading rates ( $p < 0.05$ ). The results of this study showed that the biogas generation was low at the beginning of the experiment due to low OLR and then increased with increasing organic loading rate. This was due to the maximum utilization substrate in the anaerobic reactor (Kavitha and Murugesan, 2007). Biogas production was significantly strongly associated with increasing of organic loading rate ( $p < 0.05$ ; Pearson correlation = 0.97). Fig.2 also shows the linear relationship between biogas production rate per day and organic loading rate with regression coefficient of  $R^2 = 0.80$ . This shows that 20% of the total variations were not explained in the regression model.

The variation of amount COD converted to methane at different organic loading rates is shown in Fig.3. At the OLR of  $1.03 \text{ kg m}^{-3}\text{d}^{-1}$  (phase I), the amount of added and removed COD converted to methane in one time feeding mode were  $64.2\pm 5.4$  and  $79.2\pm 5.4\%$ , respectively (Table 3). The amount of both added COD ( $70.0\pm 4.5\%$ ) and removed COD converted ( $83.3\pm 3.6\%$ ) to methane in the step feeding mode were significantly higher than one time feeding methods ( $p < 0.05$ ). The remaining 16.7% of the removed COD might be partly changed to carbon dioxide and partly might be remained in the biomass. When the OLR increased to  $1.23 \text{ kg m}^{-3}\text{d}^{-1}$  (phase II),  $70.6\pm 3.5\%$  of the removed COD and  $55.7\pm 2.9\%$  added COD were converted to methane. The average value of amount of added and removed COD converted to methane at the OLR of  $1.52 \text{ kg m}^{-3}\text{d}^{-1}$  were  $47.9\pm 3.2\%$  and  $63.1\pm 4.1\%$ , respectively.

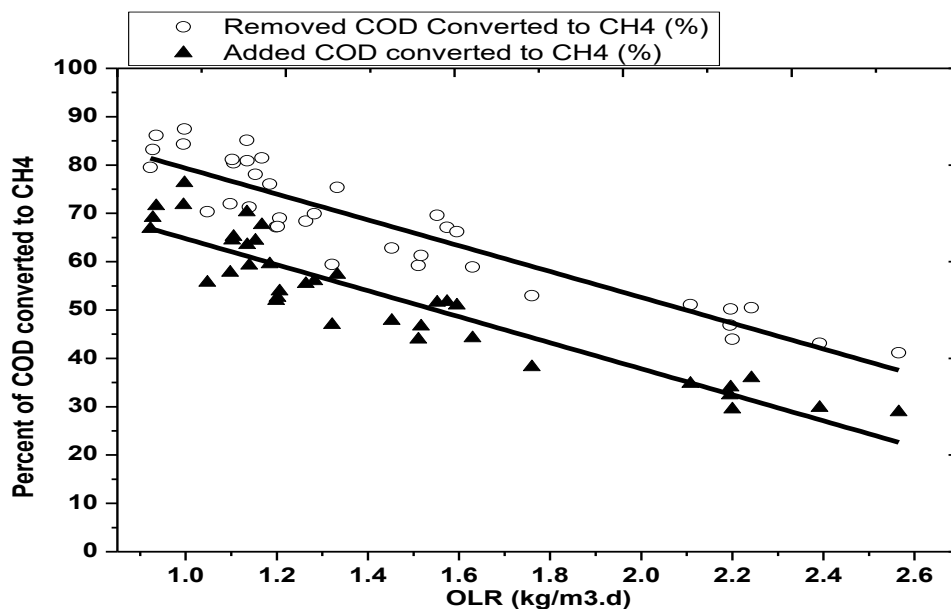


Figure 3: percent of added and removed COD converted to methane with OLR

When the OLR increased from  $1.52$  to  $2.21 \text{ kg m}^{-3}\text{d}^{-1}$  (phase IV),  $32.9\pm 3.4\%$  of the added COD and  $47.5\pm 4.3\%$  the removed COD were converted to methane (Table 2). The COD converted to methane (both the added and removed) was significantly highest at the OLR of  $1.03 \text{ kg m}^{-3}\text{d}^{-1}$  ( $p < 0.05$ ) and significantly lowest at the OLR of  $2.21 \text{ kg m}^{-3}\text{d}^{-1}$  ( $p < 0.05$ ).

## Kinetics Analysis

The first order model for COD removal is drawn in Figure 4. The value of the  $k$  was obtained from the slope of the line that was plotted  $(S_0 - S_e)/\text{HRT}$  versus  $S_e$ . The graph fit a straight line with regression coefficient

of ( $R^2 = 0.83$ ). This indicates that about 17% of the total variations were not explained in the first order regression model. The k value was determined as 0.99 per day.

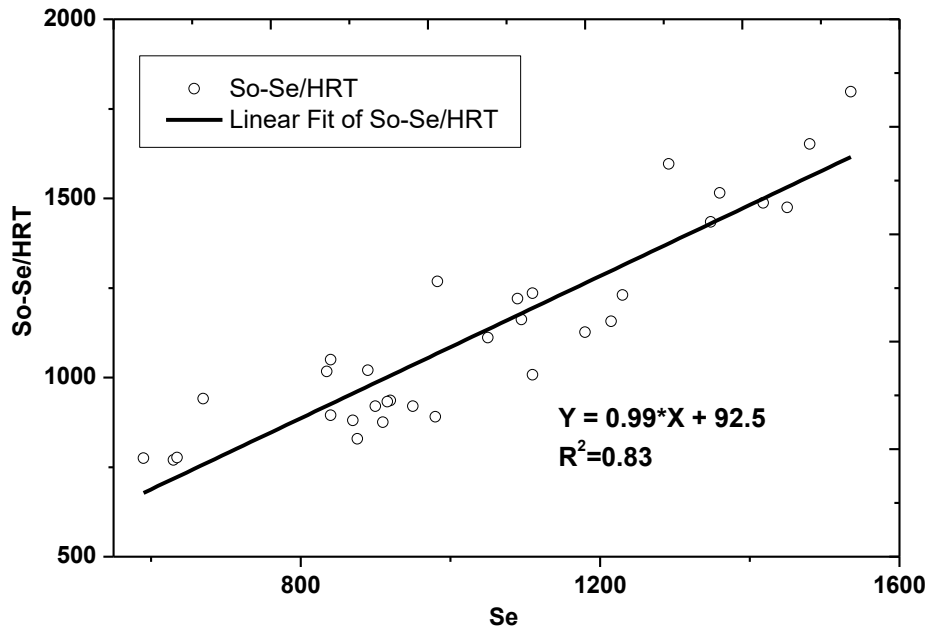


Figure 4: Substrate removal First order Model for ASBR

### Modified Stover-Kincannon Model

Figure 5 illustrates the graph drawn between the reciprocal of mass loading removal rate ( $V/(Q(So-Si))$ ) with the reciprocal of OLR to derive the values of  $U_{max}$  and  $K_B$  for the anaerobic sequencing batch reactor treating tannery wastewater.

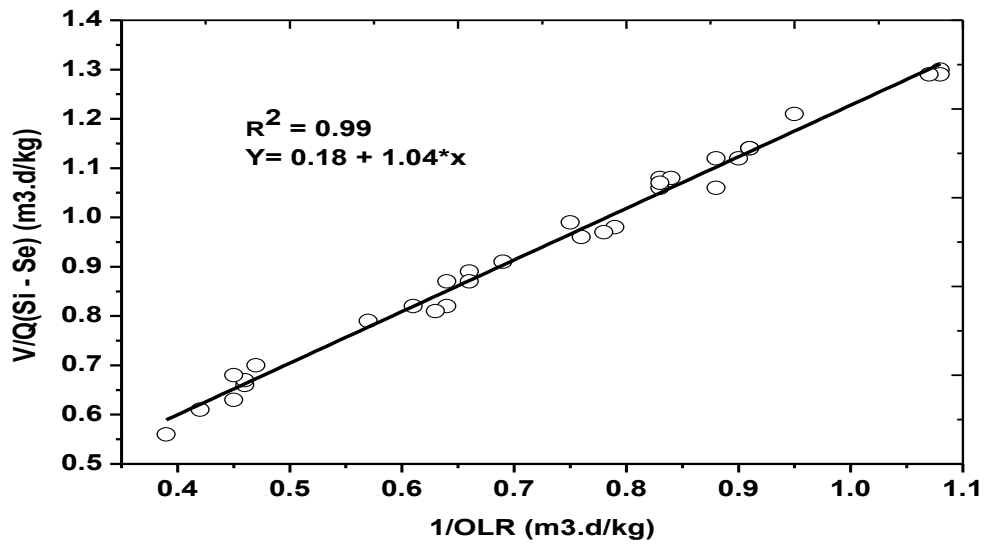


Figure 5: Modified Stover-Kincannon model for ASBR

The graph fit a straight line with regression coefficient of ( $R^2 = 0.99$ ). This indicates that only less than 1% of the total variations were not explained in the regression model. Hence, the regression coefficient supports strongly the validity of the linearized Stover-Kincannon model. It can be conclude that modified Stover-Kincannon model can be used to describe the performance of mesophilic ASBR treating tannery wastewater in this study. The maximum value for COD removal rate ( $U_{max}$ ) and saturation constant ( $K_B$ ) were determined as 5.56 and 5.78 kg of COD  $m^{-3} d^{-1}$ , respectively. The predicted  $U_{max}$  was higher than the maximum loading rate (2.21 kg  $m^{-3} d^{-1}$ ) used in this study. This revealed that ASBR has higher potential in withstanding high strength tannery wastewater. Moreover, the closeness of  $U_{max}$  and  $K_B$  values obtained indicate that increasing of organic loading rates would lead to reduction in the processes efficiency.

### 3.5. Estimated energy production and greenhouse gas emission mitigation

Table 3 illustrates the results obtained for the full scale system. At the OLR of 1.03 kg  $m^{-3} \cdot d^{-1}$ , the estimated methane production is 133,882  $m^3$  per year in the onetime feeding and 148,190  $m^3$  per year in the step feeding mode. This is equivalent to 4,779,587 and 5,290,383 MJ or 128739 and 142290 L diesel, respectively.

Table 3: The estimated methane production, energy content and greenhouse gas emission reduction

OLR	Methane (m <sup>3</sup> /y)	Energy (MJ)	kg CO <sub>2</sub> .yr <sup>-1*</sup> a	kg CH <sub>4</sub> . yr <sup>-1*</sup> a	kg N <sub>2</sub> O.yr <sup>-1*</sup> a	kg CH <sub>4</sub> .yr <sup>-1*</sup> b
1.03 (1)	133,882	4,779,587	338395	14.34	2.87	95592
1.03(2)	148,190	5,290,383	374559	15.87	3.18	105808
1.23	121,122	4,324,041	306142	12.97	2.59	86481
1.52	112,128	4,002,969	283410	12.01	2.40	80060
2.21	73,675	2,630,206	186219	7.89	1.58	52604

\*a=reduction from diesel replacement; \*b=reduction from CH<sub>4</sub> recovery ;(1)=one time feeding

(2)=step feeding and OLR=kg.m<sup>-3</sup>.d<sup>-1</sup>

The estimated methane production will be 121,122; 112,128 and 73,675 m<sup>3</sup> per year when the digester will be operated at OLR of 1.23, 1.52 and 2.21 kg.m<sup>-3</sup>.d<sup>-1</sup>, respectively. The estimated energy value 4,324,041; 4,002,969 and 2,630,206 MJ and this will replace 43, 40 and 26% of the diesel oil, respectively.

The capturing and utilization of biogas from the anaerobic digestion of tannery wastewater would contribute to the mitigation of greenhouse gas (GHG) emission. The amount of CO<sub>2</sub> emission reduced due to diesel oil burning displacement will be in the ranges from 186219kgper year (at OLR of 2.21kg.m<sup>-3</sup>.d<sup>-1</sup>) to 374559kgper year (at OLR of 1.03kg.m<sup>-3</sup>.d<sup>-1</sup> with step feeding). Moreover, there is reduction in CH<sub>4</sub>emission (in therange 7.89-15.87kgper year) and N<sub>2</sub>Oemission (in the range of 1.58-3.18kgper year). The highest gas reduction will be at OLR of 1.03kg.m<sup>-3</sup>.d<sup>-1</sup>and the lowest will be at OLR of 2.21kg.m<sup>-3</sup>.d<sup>-1</sup>. This directly associated with amount of diesel oil replaced by the biogas. As it is shown in Table 5, the estimated annual methane production decrease with increasing organic loading rate and this in turn reduce the amount of diesel oil to be replaced. The reduction of diesel oil displacement with increasing organic loading rate will result in reduction in the amount of green house gas emission mitigation. Moreover, the estimated amount of methane produced in the anaerobic digester would also reduce from 105,808 kg per year at the OLR of 1.03kg.m<sup>-3</sup>.d<sup>-1</sup> with step feeding to 52,604kg per yearat OLR of 2.21kg.m<sup>-3</sup>.d<sup>-1</sup>. The GHG reduction due to diesel replacement would range between 187 and 340 ton CO<sub>2</sub>-eqper year and it would be between 1315 and 2646 ton CO<sub>2</sub>-eqper year due to methane recovery. The total amount of GHG reduction can be in the range between 1500 and 3032 ton CO<sub>2</sub>-eqper year.The highest estimated reduction will be atOLR of 1.03kg.m<sup>-3</sup>.d<sup>-1</sup> when step feeding mode employed and the lowest will be at OLR of 2.21kg.m<sup>-3</sup>.d<sup>-1</sup>.This is mainly due to the reduction of the volume of methane produced with increasing of OLR.

## Conclusion

The results of this study showed that COD removal, methane yield and GHG reduction were decreased with increasing OLR or decreasing HRT. The highest energy value and GHG reduction was estimated at the OLR of  $1.03\text{kg.m}^{-3}.\text{d}^{-1}$  in the stepwise feeding mode and the lowest was obtained at OLR of  $2.21\text{kg.m}^{-3}.\text{d}^{-1}$ . It can be also conclude that ASBR is efficient on generating biogas and reducing GHG while treating strong wastewater like tannery.

## Reference

- IFC (2007) Environmental, Health, and Safety Guidelines Tanning and Leather Finishing. Washington, D.C.
- Jahan, M.A.A, Akhtar, N., Khan, N.M.S., Roy, C.K., Islam, R., & Nurunnabi. (2014). Characterization of tannery wastewater and its treatment by aquatic macrophytes and algae Bangladesh. *J. Sci. Ind. Res.* 49(4): 233-242
- Kaparaju ,P. & Rintala, J. (2011). Mitigation of greenhouse gas emission by adopting anaerobic digestion technology on dairy, sow and pig farms in Finland. *Renewable Energy* 36: 31-41
- Kavitha, K. & Murugesan, A.G., (2007). Efficiency of Upflow anaerobic granulated sludge blanket reactor in treating fish processing effluent. *Jr. of Industrial Pollution Control* 23 (1): 77-92
- LIDI (2010). Leather Industry Development Institute and United Nation Development Program (UNDP), July, 2010: proceeding of National workshop on enhancing the Ethiopian Leather Industry and its Market Competitiveness. Adama, Ethiopia.
- Pathak, H., Jain, N., Bhatia, A., Mohanty, S., & Gupta, N. (2009). Global warming mitigation potential of biogas plants in India. *Environ. Monit. Asses.* 157:407-418
- Seghezzi, L., Zeeman, G., Jules, B. V., Hamelers, H. V. M. & Lettinga, G. (1998). A Review: The anaerobic treatment of sewage in UASB and EGSB reactors. *Bioresour. Tech.* 65: 175-190
- Timur, H., & Oèzturk, I. (1999). Anaerobic sequencing batch reactor treatment of landfill leachate. *Water Research.* 33(15): 3225-3230
- Xiangwen, S., Dangcong, P., Zhaohua, T. & Xinghua, J. (2008). Treatment of brewery wastewater using anaerobic sequencing batch reactor (ASBR) *Bioresour. Tech.* 99:3182–3186
- Zhang, R. H., Yin, Y., Sung, S. & Dague, R. R. (1997). Anaerobic treatment of swine waste by the anaerobic sequencing batch reactor. *Transactions of the ASAE* 40(3):761-767

## **BIO-ENZYMES FOR ROAD CONSTRUCTION AND MAINTENANCE: AN INNOVATIVE APPROACH**

**Eshetu Mekonnen**

PhD Candidate in Microbiology at Haramaya University, (Soil Stabilizing Bio-Enzyme Project (Geo-Biotechnology) Researcher at Addis Ababa Science and Technology University)

**E-Mail: [eshetumicro@gmail.com](mailto:eshetumicro@gmail.com) Cell Phone: +251911399619**

### ***Abstract***

*Soil stabilization is the alteration of one or more soil properties, by mechanical or chemical means, to create an improved soil material possessing the desired engineering properties. It is an important part of any structure constructed on earth so that it becomes a vital aspect of any development and progress. Soils may be stabilized to increase strength and durability or to prevent erosion and dust generation. Cost effective soil stabilization has been an integral part of any construction and it is very important for economic growth in any country. In some cases construction has been challenged due to the high cost of soil stabilization because soil stabilization before any construction project is a crucial procedure. Besides, methods of stabilization using common stabilizing agents are getting costly. Currently, there is a growing interest to identify new and cost effective materials to improve construction techniques and to expand the road network. Therefore, the search for new materials and improved techniques to process the local materials has received an increased focus. For countries like Ethiopia bio-enzymes are now creating an opportunity to improve soil stability with an effective cost reduction in the overall process of soil stabilization. The use and production of bio-enzymes holds the most promising key for the advancement of a country by saving time, energy and finance. It also saves a big deal of hard currency which might be lost for purchase and shipping of commercial bioenzyme products. A better understanding of this emerging technology is of utmost importance to exploit any improvement it can offer to soil stability. With little research and practice it is possible to produce soil stabilizing bio-enzymes using local raw materials. This review paper tried to show the current technology of stabilizing soil with bio-enzymes, commercially available bio-Enzymes, mechanism of soil stabilization with Bio-Enzymes, the current opportunities and challenges of bio-enzyme production and application in our country, Ethiopia.*

**Keywords:** - Soil Stabilization, Bio-Enzyme, Engineering Properties, Fermentation, Clay

## **1. Introduction**

Soil stabilization is the permanent physical and chemical alteration of soils to enhance their physical properties (Breneman, 2011). It is an important part of any structure constructed on earth including road construction; so, it becomes a vital aspect of any development and progress. It is real that any structure constructed on the earth is as strong as its foundation. Cost effective road construction has been an integral part of construction since the bygone years. In some cases construction has been rendered in futile due to the high cost of soil stabilization. Common methods of soil stabilization using conventional stabilizing agents are getting costly due to the depletion of stabilizing materials (Nitin, 2011).

Cost effective road construction techniques are very vital for economical growth in any country. There is an urgent need to identify new and cost effective materials to improve construction techniques and to expand road network. Now days the search for new materials and improved techniques to process the local materials has received an increased impetus. When poor quality soil is available at the construction site, the best option is to modify the properties of the soil so that it meets the pavement design requirements. This has led to the development of soil stabilization techniques (Tingle *et al.*, 2007). Over the past 60 years, progress has been made in search of new soil stabilization techniques, but a “magic juice” has not yet been found that has the ability to convert a weak soil to a strong material with very little effort and in a matter of hours (Susan, 2006). In recent years, more attention has been given to the use of bio-enzymes for road construction due to expansion in manufacturing capacity, low cost, and relatively wide applicability compared to standard stabilizers (hydrated lime, portland cement, and bitumen) (LRRB, 2005).

Bioenzymes are chemical, organic, and liquid concentrated substances which are used to improve the stability of soil sub-grade for pavement structures. Bio-enzymes are convenient to use, safe, effective and dramatically improves road quality (Tingle *et al.*, 2007). They are natural, non-toxic, non-flammable, non-corrosive liquid enzyme formulation fermented from vegetable extracts. They are claimed to improve the engineering qualities of soil, facilitates higher soil compaction densities, and increases stability. Enzymes catalyze the reactions between the clay and the organic cations and accelerate the cationic exchange process to reduce adsorbed layer thickness. Unlike other chemical stabilization techniques, bio-enzymes are easy to use as they can be mixed with water at optimum moisture content and sprayed over soil for compaction (Tingle *et al.*, 2007).

## **2. Types of Soil Stabilization Techniques commonly used for Road Stabilization**

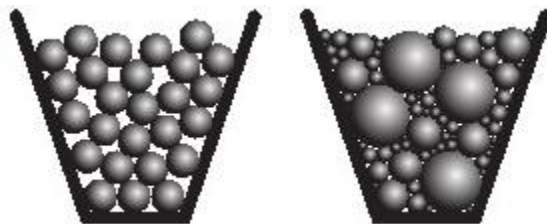
There are two general techniques of soil stabilization techniques used to modify the engineering properties of soil during road construction; i.e. Mechanical and Chemical addition (US Army Corps of Engineers, 1984). Nearly every road construction project utilizes one or both of these stabilization techniques.

Mechanical soil stabilization involves compaction of soil particles or addition of non-biodegradable reinforcement into the soil. While, chemical stabilization involves improving the engineering properties of soil by the addition of chemicals (Kestler, 2009). Generally, a chemical additive may be used to act as a binder, alter the effect of moisture, increase the soil density or neutralize the harmful effects of a substance in the soil (US Army Corps of Engineers, 1984). Most widely used chemical additives used for soil stabilization in road construction includes: Portland cement, Lime, Fly Ash, Calcium Chloride, Bitumen and Bio-Enzymes.

## **3. What is the need of Soil Stabilization in Road Construction**

During road construction, traditionally stable sub-grades, sub-bases and/or bases have been constructed by using selected, well-graded aggregates, making it fairly easy to predict the load-bearing capacity of the constructed layers. By using select material, the engineer knows that the foundation will be able to support the design loading (US Army Corps of Engineers, 1984).

It is desirable from an engineering standpoint to build a road upon a foundation of ideal and consistent density. Thus, the goal of soil stabilization is to provide a solid, stable foundation. “Density” is the measure of weight by volume of a material, and is one of the relied-upon measures of the suitability of a material for construction purposes. The more density a material possesses, the fewer voids are present. Voids are the enemy of road construction; voids provide a place for moisture to go, and make the material less stable by allowing it to shift under changing pressure, temperature and moisture conditions (Kestler, 2009).



**Less compacted Vs Compacted Soil**

With the increased global demand for energy and increasing local demand for aggregates, it has become expensive from a material cost and energy use standpoint to remove inferior soils and replace them with choice, well-graded aggregates. One way to reduce the amount of select material needed for base construction is to improve the existing soil enough to provide strength and conform to engineering standards. This is where soil stabilization has become a cost-effective alternative (US Army Corps of Engineers, 1984).

#### **4. Microbial Enzymes (Bio-enzymes)**

An enzyme is by definition an organic catalyst that speeds up a chemical reaction, that otherwise would happen at much slower rate, without becoming a part of the end product. Since the enzymes do not become the part of end product and are not consumed by the reaction, a very small amount of bio enzyme is required for soil stabilization (Scholen, 1982). They are organic molecules that catalyze very specific chemical reactions if conditions are conducive to the reaction they facilitate. For an enzyme to be active in a soil, it must have mobility to reach at the reaction site. The pore fluid available in the soil mass provides means for mobility of the molecules of bioenzyme, the specific soil chemistry provides the reaction site, and time is needed for the enzyme to diffuse to the reaction site. An enzyme would stay active in a soil until there are no more reactions to catalyze. Enzymes would be expected to be very soil specific (Tingle *et al.*, 2007).

Soil stabilizing bio-enzymes catalyze the reactions between the clay and the organic cations and accelerate the cationic exchange process to reduce adsorbed layer thickness. For other types of chemical stabilization, chemicals are mixed with soil, which is difficult to mix thoroughly, but bio-enzyme is easy to use as it can be mixed with water at optimum moisture content and then it is sprayed over soil and compacted. Microbial enzymes change the hydrophilic nature of lime material and clay to hydrophobic. Its application not only assists in the expulsion of water from the soils, but it also helps the lubrication of soil particles and increases the compatibility of many soils (Lim *et al.*, 2014).

#### **5. Bio-Enzymes as a Soil Stabilizer**

The idea of using enzyme stabilization for soil pavement was developed from the application of enzyme products used to treat soil in order to improve horticultural applications. A modification to the process produced a material, which was suitable for stabilization of poor ground for road traffic. When added to a soil, the enzymes increase the wetting and bonding capacity of the soil particles. The enzyme allows soil materials to become more easily wet and more densely compacted. Also, it improves the chemical bonding

that helps to fuse the soil particles together, creating a more permanent structure that is more resistant to weathering, wear and water penetration (LRRB, 2005).

## **6. Mechanism of Bio-enzyme soil stabilization**

An enzyme is by definition an organic catalyst that speeds up a chemical reaction, that otherwise would happen at a slower rate, without becoming a part of the end product. The enzyme combines with the large organic molecules to form a reactant intermediary, which exchanges ions with the clay structure, breaking down the lattice and causing the cover-up effect, which prevents further absorption of water and the loss of density. The enzyme is regenerated by the reaction and goes to react again. Because the ions are large, little osmotic migration takes place and a good mixing process is required. Compaction of aggregates near the optimum moisture content by construction equipment produces the desired high densities characteristic of shale. The resulting surface has the properties of durable “shale” produced in a fraction of the time (millions of years) required by nature (Scholen, 1982).

Organic cations generated by the growth of vegetation and microorganisms also have the capability to exchange position with other ions attracted to the clay platelet in the soil. In contrast with metal cations, the organic cations have large flat structures that approach the size of small clay particles. These organic cations can blanket the clay particle and effectively neutralize its negative charge in a short distance, thus greatly reducing the double layer thickness (Tingle *et al.*, 2007).

Because of the effect of the enzyme formulation in reducing the electric charge of the water molecule, there is sufficient negative charge to exert adequate pressure on the positively charged metal ions in the absorbed water film (Scholen, 1982). As a result of this, the existing electrostatic potential barrier is broken. When this reaction occurs, the metal ions migrate into the free water, which can be washed out or removed by evaporation. Thus, the film of absorbed water enveloping the particles is reduced. The particles thereby lose their swelling capacity and the soil as a whole acquires a friable structure. The hydrogen ions, which are liberated in the dissociation of the water molecules, can once again react with free hydroxyl ions and form water along the gaseous hydrogen. It is important to note that the moisture content of the soil affects the surface tension and is thus a factor affecting compaction. The enzyme reduces surface tension making the soil compaction easier to perform. After the absorbed water is reduced the soil particles tend to agglomerate and as a result of the relative movement between particles, the surface area is reduced and less absorbed water can be held, which in turn reduces the swelling capacity (The Carbon Group) (Mohd *et al.*, 2013).

## **7. Microbial Bio-enzyme production**

Certain soil micro organisms produce specific enzymes that catalyze the reactions between the clays and the organic cations, producing clods of stable soil among the roots of the vegetation. These soil-stabilizing enzymes accelerate the cationic exchange without becoming part of the end product (Tingle *et al.*, 2007).

By utilizing fermentation processes, specific microorganisms can produce stabilizing enzymes in large quantities. When exposed to the air, the microorganisms multiply rapidly and produce large organic molecules, which the enzyme attaches to the clay platelets. The negative charges on the clay platelets are neutralized through this process and the size of the electrical double layer shrinks. This limits further adsorption of water or the resultant swelling with loss of density (Scholen, 1982).

## **8. Commercially available Microbial Bioenzyme Products**

The idea of using enzyme for stabilization in pavement construction was developed from the application of enzyme products used to treat soil in order to improve horticultural applications. A modification to the process produced a material, which was suitable for stabilization of poor ground for road traffic. When added to a soil, the enzymes increase the wetting and bonding capacity of the soil particles (Vijay and Suneet , 2014).

Commercially available soil stabilizing enzyme formulations include:

- i. Renolith (Patented product developed in Germany)
- ii. Permzyme: (Patented Product in USA)
- iii. Fujibeton (Patented product in Japan)
- iv. Earthzyme (Patented in Canada)
- v. Terrazyme
- vi. Natural Crete
- vii. ClayPack / DuraPack: Soil Bond International, Texas
- viii. EMC<sup>2</sup>: Soil Stabilization Products Co.,Merced, California
- ix. PSCS-320: Alpha Omega Enterprises
- x. Leviev ECOroads®: Leviev Development PLC, USA
- xi. Zym-tec: ECOMAX , Israeli Company

## **9. Field Performance of Commercially available Bio-Enzymes in different Countries**

The enzyme products have been used in more than 40 countries in the construction of structures from rural roads to highways for the past 30 years. According to the manufacturers in the overwhelming majority of the cases enzyme stabilization provided a tool that enhanced the life-cycle and quality of the resulting product. A short review of some of the projects where enzymes were used as a road stabilizer is presented below (LRRB, 2005).

A World Bank study on soil stabilization using enzymes in Paraguay reported consistent road improvements and better performance from soil stabilizer treated roads compared to untreated roads (Brazetti and Murphy, 2005). Enzymes have been used successfully to stabilize roads in Malaysia, China and the Western USA at low cost (<http://www.terrazyme-europe.net>). In Mendocino County, California Department of Transportation has conducted several tests of a compaction additive based on enzymes. This natural product helped the road base to set very tightly, reducing dust and improving chip-seal applications. With air quality and water quality agencies requiring dust reduction, this is a potentially effective new product, cheaper than asphalt (<http://www.hals-pals.org/march-7-2003.html>.)

Emery County in Utah has more than 40 miles of surface-dressed roads treated with the product that has been in use for several years. Jerome County in Idaho is nearby and reported a similar experience (<http://www.permazymeusa.com>). Two city streets in Stillwater, Oklahoma were also treated with enzyme products. The clay had a plastic index of 20% and good performance was reported (<http://www.permazymeusa.com>). A number of projects have been completed in Panaji (India) with the use of enzymes. A rural road and a city road in Maharashtra have lasted for more than two years without any damage (<http://www.terrazyme-europe.net>).

Road sections placed in western Pennsylvania in the fall of 1992 passed subfreezing winters and over forty freeze-thaw cycles and required no maintenance for ruts, potholes or wash boarding during three years. The road sections then received chip-seal coats and asphalt surfaces with no requirement for repairs to the stabilized base (<http://www.terrazyme-europe.net>).

## **10. Application of Bio-Enzymes in Africa**

The well being and prosperity of most Africa countries is hampered by the ongoing poverty of its rural population. One of the major contributing factors is the all too often lack of proper communication between the rural and urban areas. Rural roads in general are of unacceptably low standards, which prohibited any form of transport during wet rainy conditions (Lyatuu *et al.*, 2000).

Some commercial bio-enzyme formulations are now being introduced into African market and started some experimental tests in some countries. Intensive study of permazyme was conducted in South Africa and

Uganda while currently experimental study is going in Ethiopia at Addis Ababa Science and Technology University. The Information regarding the application of other soil stabilizing bioenzymes in Africa is rare and not well organized.

## **11. Application, Opportunities and Challenges of Soil Stabilizing Bio Enzymes in Ethiopia**

In 2016, Ethiopia spent around 33 Billion birr for construction of new roads while 2.7 billion spent for maintenance and rehabilitation of new roads (ERA, 2016). There is no reported research performed on the application and identification of soil stabilizing enzymes in Ethiopia. But, Addis Fortune News paper published on December 12, 2010 reported that new road construction technology was imported from Israel, which involves changing the soil density by treating it with an enzyme. A demonstration section of 300m long and 7m width has been constructed adjacent to Imperial Hotel on principal Arterial Street in Addis Ababa by an Israeli company; I-Tec-W-Ltd in June 2009 which costs around 650,000 Br. (**Tesfahun**Ashuro,2010). In 2017, experimental 450m long road construction was conducted at Addis Ababa Science and Technology University using Permazyme where performance test is in progress.

According to Ethiopian Roads Authority, ERA, companies with road material stabilization chemicals and enzymes, geotechnical solutions, and other sort of technologies have contacted them and the research department tried to respond to this requests bearing in mind any technology which can enhance the road building and maintenance should be applied without affecting the environment and need to have value for money (ERA, 2015).

As part of the GTP, the government of Ethiopia is expanding roads in urban and rural areas of the country in faster rate. Despite the demand, the higher expense of construction materials and soil stabilizing techniques are the challenges that are hampering road quality and distribution in the country. This fact is a good opportunity for research organizations and other interested bodies to find for economical and easily produced soil stabilizing agents.

The other good opportunity for researchers is the possibility of producing soil stabilizing enzymes using locally available organic substrates like cereals, tubers, and industrial wastes like molasses. Molasses is believed to be substrate of choice in Ethiopia where food security is an issue for other substrates. The current molasses production in Ethiopia is 1,260 ton per day and in the coming 15 years the production is expected to rise about 31, 2300.00 ton per (Ethiopian Sugar Development Corporation, 2014).

Expected challenges in bioenzyme application includes the newness of the technology, lack of trained expertise and lack of research trials here and there for the development of bioenzyme of our own kind.

## **12. Future Prospects of Soil Stabilizing Enzymes**

Bio enzymatic soil stabilization is now gaining tremendous ground and now has a universal approval with institutions like WHO and UNESCO. The main feature of bio enzyme soil stabilization is that it uses no foreign stabilizing material. This very aspect opens a great opportunity to improve soil stabilization process with an effective cost reduction in the overall process. Bio enzyme holds the most promising key for a developing country like Ethiopia what we get is stupendous savings in time, energy and finances. A better understanding of this emerging technology is of utmost importance to exploit any improvement it can offer to better our well being and surroundings.

Relevant inventions must be identified and commercialized to suit the needs of Ethiopia. For example, the use of liquid enzymatic soil stabilization fits perfectly with Ethiopia's needs, budget, and geography. New innovations hold potential for being developed first in Ethiopia and exclusively exported to the world. To maximize incentive, the green economy should not be a government agency. However, it holds great promise for advantageous government support, job creation, new tax revenues, and development for a sustainable future.

## **13. Summary**

Soil stabilization is a very crucial procedure in road contraction projects and it needs complex technology which produces a stable base that can carry traffic loads. Enzymes as soil stabilizers have been used to improve the strength of sub-grades due to low cost and relatively wide applicability compared to standard stabilizers. The use of enzymes as stabilizer has not been subjected to any technical development and is presently carried out using empirical guidelines based on previous experience. Several commercial enzymes are available in the market and their production procedures and microbes used for fermentation are patent protected and they are not easily available on the internet. For developing countries like Ethiopia, the higher price of the chemical and mechanical stabilization techniques has created the need for safe, cheap and easily produced soil stabilization techniques. Due to this bio-enzymes produced by microorganism are the best choice where cost effective technologies are the primary interest of the economy. Because of variability in the nature of soil it becomes an important priority to study and determine the effects of the enzymes on the strength of different soils prior to being used. The production of low cost, easy and widely applicable, and environmentally friendly enzymatic formulations from locally available raw materials should be the interest of research and academic institutes of our country.

#### **14. REFERENCES**

- Addis Fortune; (2010). News paper, Vol 11 No 554, Dec 12, 2010
- Brazetti Rubens and Murphy Sheldon (2005). Results and Conclusions from a Comprehensive World Bank Study of the Performance of Roads Rehabilitated with Soil Stabilizers in Paraguay.
- Chandrasekhar, B.P (2006) A Critical reviews of innovative rural road construction techniques and their impact NRRDA, New Delhi.
- Civil Engineering Research Foundation/ International Institute of Energy Conservation. (2009). “Environmental and Toxicological Analysis Report for Permazyme™.”
- CON-AID User Manual (2002). CON-AID Liquid Chemical Stabilizer.
- Dallas roadway products Inc (1999). Highway construction road materials technical manual. Dallas, Texas.
- Daniel Nebro (2002). Stabilization of potentially expansive subgrade soils using lime and CON-AID. MSc Thesis, School of postgraduate studies, Addis Ababa University.
- Ethiopian Road Authority (2002). Assessment Report on CON-AID Chemical, ERA, Addis Ababa.
- Ethiopian Road Authority (2016), Budget report.
- Khan L.I. and M. Sarker.(1993) Enzyme Enhanced Stabilization of Soil and Fly Ash. Fly Ash for Soil Improvement. ASCE GSP 36. New York. 1993. 43-58.
- Lyatuu W, Swai MM & Haule HO: “The role of Road Transport in Poverty Reduction.” Proceedings Year (2000). Annual Roads Convention; Tanzania Roads Association Tanzania, pp165 – 174.
- Kestler, (2009). “Stabilization selection guide for aggregate and native-surfaces low volume roads,” U.S. Department of Agriculture.
- M. Lee, P. C. Tan, Daud, and D. Q. Wu, (2009). “Green approach to rural roads construction – Stabilization of in-situ soils and construction wastes,” Asia Pacific, in press.

Mohd Raihan Taha, Tanveer A. Khan, Tanveer A. Khan, Ali Akbar Firoozi and Ali Asghar Firoozi. (2013) Recent Experimental Studies in Soil Stabilization with Bio-Enzymes–A Review, EJGE, Vol. 18

Nitin Sreenivasan, (2011): BIO ENZYME FOR SOIL STABILIZATION: A simple and economical development using local resources. Blue Bonds 229, Rasta Peth, Pune 411011, Maharashtra, India.

NRG Technology International Ltd (2012) “NRGRenolith- Presentation-august 2011-updated-May-2012.

Perma-Zyme 11X. The Charbon Group, LLC Products Division, Huntington Beach, CA, Version: No. 5450, June 1998.

Preliminary laboratory Investigation of Enzyme Solutions as a Soil Stabilizer. Minnesota Department of Transport.

Permazyme Testing, Volume-I: Final Summary Report. (2010). California Pavement Preservation Center. 25 Main Street, Suite 202, California State University Chico, California: 98929-0930, (530) 898-5981

PURE ONE Environmental, Inc (2004). PURE CRETE Technical Manual. Pure One, USA.

S. M. Lim, D. C. Wijeyesekera, A. J. M. S. Lim, I. B. H. Bakar. (2014) Critical Review of Innovative Soil Road Stabilization Techniques. International Journal of Engineering and Advanced Technology (IJEAT) ISSN: 2249 – 8958, Volume-3 Issue-5.

Scholen, D.E. (1982). Nonstandard Stabilizers. Report FHWA-FLP-92-011 US Department of Transportation.

US Army Corps of Engineers (1984). Soil Stabilization for Pavements: EM 1110-3-137. Washington DC.

Sureka Naagesh and S. Gangadhara, (2010) Swelling Properties of Bio-enzyme Treated Expansive soil, International Journal of Engineering Studies, Volume 2, Number 2, pp. 155–159.

Sureka Naagesh and S. Gangadhara, (2010). Swelling Properties of Bio-enzyme Treated Expansive

soil, *International Journal of Engineering Studies*, Volume 2, Number 2 (2010), pp. 155–159.

Tesfahun *Ashuro*, (2010). “Performance of Unconventional Soil Stabilizers in Stabilization of Substandard Materials for Road Subgrade and Subbase”. MSc. Thesis Adis Ababa University.

Tingle J.S, *et al* (2007). Stabilization Mechanisms of Non-traditional Stabilizers. In *Transportation Research Record: Journal of the Transportation Research Board*, No. 1989, Vol.2, Transportation Research Board of the National Academies, Washington, D.C., pp. 59–67.

US Department of Labor: Occupational Health and Safety Administration (2001). “Material Safety Data Sheet: Permazyme.”

Velasquez R., M.O. Marasteanu, R. Hozalski & T. Clyne (2005). Preliminary Laboratory investigation of Enzyme solutions as a soil stabilizer. Research Report MN/RC-2005-25. University of Minnesota, USA.

Vijay Rajoria, Suneet Kaur (2014). Review on Stabilization of Soil using Bio-enzyme. *ijret: International Journal of Research in Engineering and Technology* EISSN: 2319-1163 | PISSN: 2321-730

Yohannes Argu (2008). Stabilization of light grey and red clay of subgrade soil using SA-44/LS-40 chemical and lime. MSc Thesis, School of postgraduate studies, Addis Ababa University

## Development of Innovative Integrated Treatment System for the Treatment of High Strength industrial Wastewater, in Ethiopia

Tadesse Alemu<sup>1,2</sup>, Eshetu Lemma<sup>2</sup>, Andualem Mekonen<sup>2</sup> and Seyoum Leta<sup>2</sup>

<sup>1</sup>Assosa University, College of Natural Sciences, Ethiopia.

<sup>2</sup>Center for Environmental Sciences, Addis Ababa University, Ethiopia.

Contact E-mail: [tadesse07@yahoo.com](mailto:tadesse07@yahoo.com), Mob. +251 09 11 74 99 41

### *Abstract*

*Agro-processing industrial sectors in Ethiopia are now the fastest growing sectors, and its growth is not accompanied with the right technology. Wastewaters from agro-processing industries are characterized by high level of organic and inorganic matter; nutrients, heavy metals, suspended and dissolved solids. Discharge of untreated wastewater creates substantial challenges for the public health and receiving environment. It causes eutrophication, lower oxygen in water bodies, and thus fish kills, generate methane and sulfide gas –which causes nuisance to peoples due to foul smelling. In addition to being expensive, existing traditional wastewater treatment practices often don't meet national wastewater discharge standards to protect the human population at risk. The objective of the present study was to develop an innovative biological wastewater treatment technology-taking tannery wastewater as a case study - through anaerobic reactor and a sequence batch reactor (SBR) connected to constructed wetlands to remove nutrients, organic matter and heavy metals to generate clean water for reuse by the industries and nearby communities. The performance of an anaerobic-SBR, integrated with CW systems, was assessed for selected parameters following standard methods (APHA). Heavy metals were analyzed using Atomic absorption spectrophotometer (AAS) following standard methods. The integrated pilot treatment system showed demonstrable treatment performance of tannery wastewater with overall removal efficiencies of 96% of COD, 90% of TN, 97% of NH<sub>4</sub>-N, 81% of SO<sub>4</sub><sup>2-</sup>, 99% of S<sup>2-</sup>, 95% of total Cr, 86% of EC and 99.9% of pathogens. The final treated effluent meets the acceptable minimum national environmental quality standards. The prototype is now not only turning the industrial wastes into value added products (energy and clean water) but also serving as a model prototype for public-private partnership in developing scalable innovations for the sustainable management of all other agro process wastewaters in the country.*

*Keywords: Innovative Technologies\* Anaerobic-SBR, Constructed wetlands\* Tannery wastewater*

## **1. Introduction**

Industrial expansion coupled with weak regulatory mechanisms, in developing countries, such as Ethiopia, have led to widespread pollution of environmental resources due to the discharge of high strength wastewaters. Many industries, in developing countries, did not afford investment costs in pollution remediation technologies, because of their low profit margin (EEPA 1997). It is estimated that only 10% of the existing industries treat their wastewaters to any degree, while the majority (90%) of the existing industries discharge their effluents directly into the nearby water bodies and open land without any form of treatment (EEPA 2003; Seyoum *et al.* 2004; Tadesse and Seyoum 2015). The agro-processing sector, in Ethiopia, generates a large quantity of highly loaded effluents, which if managed appropriately, can result in a perpetual source of energy and organic fertilizer.

At present there are twenty nine fully operating tanning companies in Ethiopia; eleven of them are found in Modjo town along Modjo River, the river which feeds into Koka reservoir dam (Seyoum *et al.* 2004; Tadesse and Seyoum 2015, Tadesse *et al.*, 2016). If the untreated wastewater is discharged into the environment it affects the water quality, causes eutrophication, lower oxygen in water bodies and thus harm aquatic life, which causes nuisance to people due to foul smell resulting from generation of sulfides. Different treatment technologies have been tested to treat tannery wastewater. However, the use of a single type of treatment system such as biological (Farabegoli *et al.* 2007) or physico-chemical (Song *et al.* 2004) for tannery wastewater still leaves pollutants above the legal discharge limits (Wang 1991; Alves *et al.* 1993; Rittiruk *et al.* 2011) or produce secondary pollutants due to the addition of metal coagulants. Advanced technologies such as ion exchange resins, reverse osmosis, membrane filtration and an electrolysis system (Vlyssides and Israilides 1997; Kocaoba and Akcin 2002; Scholz and Lucas 2003; Hafez *et al.* 2002) are expensive, need trained personnel and are inappropriate to apply in developing countries.

The challenge, therefore, is to develop reliable and appropriate technology that is within the economic and technological capabilities of the country. Treatment of such strong industrial wastewater is clearly favored by the combination of processes, such as anaerobic and aerobic reactors (Del Pozo and Diez 2003) integrated with tertiary treatment systems. The objective of this study was therefore to develop and evaluate a model innovative integrated agro-process wastewater treatment system (anaerobic -SBR reactor integrated with constructed wetlands) involving wastewater treatment, energy and treated water reuse in Ethiopia to serve as a prototype for wider application of the technology.

## 2. Materials and Methods

### 2.1 The Study area description

The integrated innovative pilot-scale biological wastewater treatment (WWT) system for treating tannery wastewater was established at the Modjo Tannery Share Company premises found in Modjo town, 75 km south of Addis Ababa. Modjo town is located South-East of Addis Ababa at 8° 35' N and 39° 10' E with an altitude of 1,825 m above sea level.

### 2.2. The Innovative Pilot-scale integrated treatment system

The pilot integrated biological wastewater treatment installed at Modjo Tannery for treating tannery wastewater is shown in Figure 1. The integrated biological treatment system consists of a primary screening and a grit removal tank, sedimentation tanks for sludge settling, two stage anaerobic reactors; two hydrolysis tank and and a sequence batch reactor (SBR) with a maximum working volume of 60 m<sup>3</sup> and sedimentation tank with a volume of 50 m<sup>3</sup>. These systems were connected with three horizontal subsurface flow (HSSF) constructed wetland (CW) connected in series with a total effective volume of 70.875m<sup>3</sup>. The CW was filled with medium- sized gravel ranging from 6 to 20mm size and vegetated with *Phragmites karka*. The performance of pilot WW treatment plant has been recorded for three years. The CWs system was then operated for three years under two hydraulic conditions. The flow rate in to the CW was 23.625 and 14.18 m<sup>3</sup>/day for 3 and 5 days of HRT, respectively.

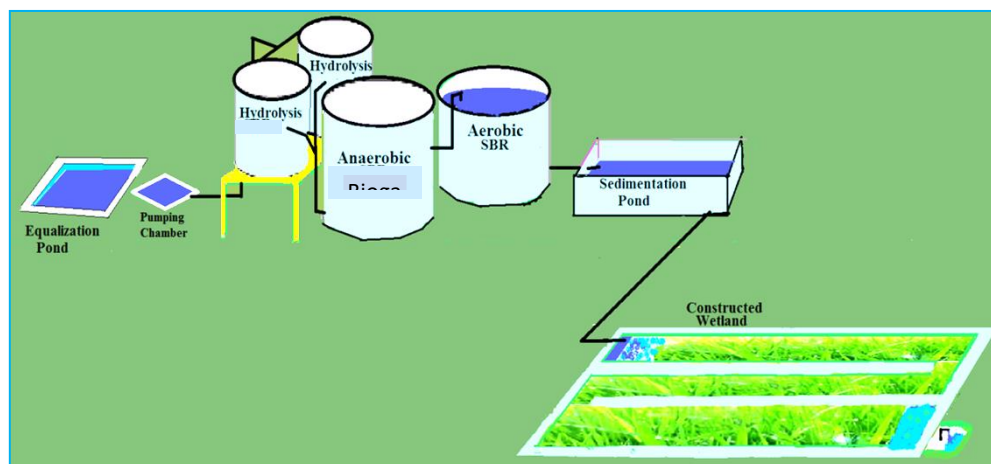


Fig 1: Pilot scale treatment system setup

### 2.3. Sample collection and Wastewater Characterization

Triplicate samples from the influent, supernatant at the end of each reactor and final effluent of CWs were collected in May 2013 to February 2015 and detailed tannery wastewater characterization was performed using standard methods (APHA) for selected parameters that are considered to be harmful to the receiving environment. COD, TN, NH<sub>4</sub>-N, NO<sub>3</sub><sup>-</sup>-N, S<sup>2-</sup> and SO<sub>4</sub><sup>2-</sup> were all measured using spectrophotometer (DR/2010 HACH, Loveland, USA) according to HACH instructions and APHA (1998). Total chromium, total suspended solids (TSS) Total dissolved solids (TDS) were also be measured according to the methods described in standard methods (APHA 1998). pH were measured using a pH meter (Model HI 9024 HANNA). TDS and conductivity were measured using conductivity meter (CC-401, ELMETRON). The Cr containing wastewater samples were digested using Mixed Nitric Acid Digestion (5ml) and hydrogen peroxide (2 ml) and analyzed using flame Atomic Absorption Spectrophotometer (model: analyticjena nova AA 400P, Germany). Percent of pollutant removal rates were calculated according to the following equation:

$$R = \frac{C_i - C_f}{C_i} \times 100$$

where,  $R$  is the removal rate,  $C_i$  is influent concentration (mg/L) and  $C_f$  is effluent concentration (mg/L)

### 2.4. Statistical data analysis

Data analysis was performed using Microsoft Excel XP version 2010, SPSS package 21.00 and Origin Lab 8 soft wear. The data was analyzed through one-way ANOVA (analysis of variance) to compare the performance of CWs for 3 day HRT and 5 day HRT concerning nutrient and organic matter removal to detect the statistical significance of difference ( $p < 0.05$ ).

## 3. Results and Discussion

### 3.1. Characteristics of tannery wastewater

Modjo tannery has shown that the tannery has a soaking capacity of 8,500 pieces of sheep and goat skins and 500 hides per day, producing semi-processed hides and skins and finished leather for domestic and export market with a discharge of 400m<sup>3</sup>/day wastewater. The tanning process generated three waste streams; general wastewater, chrome and sulphide containing wastewater, discharged in separate lines. The characteristics of tannery wastewater used in this study are presented in Table 1, demonstrating its variability and levels of COD, TN, TDS, TSS, S<sup>2-</sup>, SO<sub>4</sub><sup>2-</sup>, NO<sub>3</sub><sup>-</sup>-N and NH<sub>4</sub>-N. The average inflow values of

these pollutants to the integrated treatment system in terms of COD, TN, NH<sub>4</sub>-N, NO<sub>3</sub><sup>-</sup>-N, SO<sub>4</sub><sup>2-</sup> and S<sup>2-</sup> were 7273±536.97 mgO<sub>2</sub>/L; 545±12.7 mg/L; 261.5±68.51 mg/L; 112.2±24.36 mg/L; 583.7±170 mg/L and 148.5±6.18 mg/L, respectively. The mean influent concentration of TDS, TSS, EC and pH were 7035±42.52 mg/L, 2215.38±61mg/L, 15.5±1.99 ms/cm and 8.67±3.56, respectively. The high variable composition and high load of organic and inorganic matter of tannery wastewaters is due to the types of skins and hides (El-Bestawy *et al.* 2013) and various chemicals used at different stages and processes such as hide preparation, tanning and finishing processes (UNEP 1991; Reemtsma and Jekel 1997; Khan 2001; [Kongjiao \*et al.\* 2008](#)). The total Cr concentration in the influent wastewater for this study was ranging from 19 to 37 mg/L (28.47± 5.37mg/L). Similarly Cr and sulfur containing effluents were partly channeled in to the Cr recycling and sulfide oxidation reactor (built by the industry), respectively, which makes the concentrations lower in the present study compared with Seyoum *et al.* (2003).

The discharge of high strength tannery effluents from these clustered tannery industries in to Modjo River poses severe environmental and public health concerns (Seyoum *et al.* 2003) to the downstream community and receiving water bodies. As shown in Figure 2, the downstream pollution profile of Modjo river course varies from 30 to 390 mgO<sub>2</sub>/L COD, 1.25 to 2 mg/L S<sup>2-</sup>, 210 to 410 mg/L SO<sub>4</sub><sup>2-</sup>, and 110 to 191 mg/L NO<sub>3</sub><sup>-</sup>-N. The downstream Modjo river pollution profile study by Seyoum *et al.* (2003) also reported higher values of COD (15 to 475 mg O<sub>2</sub>/L), TN (35 to 100 mg/L), NH<sub>4</sub>-N (5 to 50 mg/L) and S<sup>2-</sup> (2 to 30 mg/L).

Table 2: Characteristics of influent and effluent concentrations of tannery WW for the 3 day HRT; (concentrations are in mg/l, except for pH and conductivity).

Parameters	Raw Wastewater	Effluent Conc.	EEPA/ US EPA Discharge limits
pH	8.67±3.56	6.53±0.12	6-9 <sup>a</sup>
EC ms/cm	15.5±2	2.23±0.17	100 <sup>b</sup>
Chloride	-	450±51	1000 <sup>a</sup>
TDS (mg/l)	7035.52±42	2.59±0.29	500 <sup>b</sup>
BOD (mg/l)	3120.6±172	56±18	200 <sup>a</sup>
COD (mg/l)	7273±536	169±26.85	500 <sup>ab</sup>
(SO <sub>4</sub> <sup>2-</sup> ) (mg/l)	488.7±71	88±120.65	-
S <sup>2-</sup> (mg/l)	268.5±76	0.4±0.44	1 <sup>a</sup>
NO <sub>3</sub> <sup>-</sup> -N(mg/l)	112.2± 24	22.75±20.66	50 <sup>a</sup>
NH <sub>3</sub> <sup>+</sup> - N (mg/l)	261.5±68	7.1±6.75	30 <sup>a</sup>

Total N (mg/l)	545±12	49.3±13.45	60 <sup>a</sup>
phenol (mg/l)	-	0.71	1 <sup>a</sup>
TCF/100ml	-	1	-
FCF/100ml	-	ND	-
Total Cr	28.47±5	0.73±0.068	2 <sup>ab</sup>

EEPA: Ethiopian Environmental protection Authority; US EPA: United States Environmental protection Authority, a=EEPA, b=US EPA limits

The present study also confirmed that Modjo River downstream pollution profile was above the WHO standards for river water quality for all measured parameters. Increased in downstream pollution profile, for measured parameters, were due to the discharge of high strength wastewater from the surrounding clustered tannery industries and slaughterhouse. Seyoum *et al.* (2003) reported that Modjo River and the reservoir, Lake Koka, were affected by eutrophication due to discharge of excess  $\text{NO}_3^-$ -N,  $\text{S}^{2-}$  and Cr toxicity are also the possible impacts of tannery wastewater in the receiving environments. The measured parameters, in the upper stream samples, were detected in small amounts; hence the source of these pollutants was not of agricultural or geological origin.

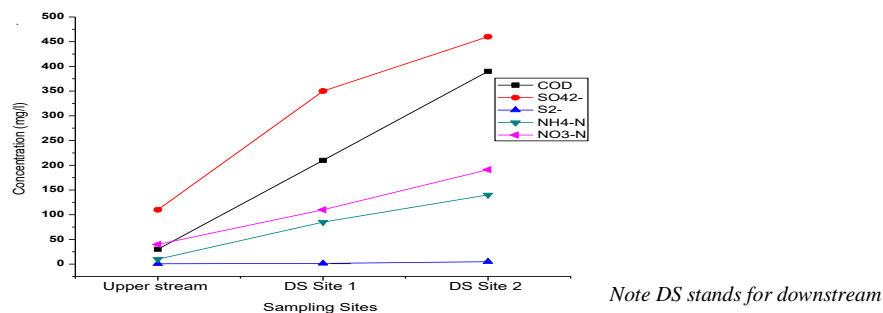


Figure 2: Modjo river upstream and downstream pollution profile

Despite its high pollution level, communities in downstream areas use the water from the Modjo River for a variety of purposes; such as drinking, irrigation, fishing, livestock watering, recreation and other domestic purposes (Seyoum *et al.* 2004). It should also be noted that farmers in the river basin use irrigation and the contaminants can easily get into the growing vegetables, posing a potential danger to humans and animal health. With these levels of pollution (Figure 2) the biological resources are at high risk due to toxicity of chromium, sulfide, and low oxygen content. Similarly the health of the downstream community was affected by the toxic effects of chromium and toxic microscopic algal blooms resulting from nutrient pollution.

### 3.2. Performance of Pilot integrated treatment system

The removal efficiency of pilot biological treatment system integrated with CWs in the removal of priority pollutants of tannery wastewater was high (ranges between 81- 99.9 %). The final effluent concentration of organic and inorganic parameters, namely; COD, TN,  $\text{SO}_4^{2-}$ ,  $\text{S}^{2-}$ ,  $\text{NO}_3^-$ -N,  $\text{NH}_4$ -N and total Cr, were in line with the Ethiopia EPA discharge limit values (Table 2) set for tannery effluents (EEPA 2003). In this study the average over all removal efficiencies of integrated treatment system were 96.6% COD for, 98.78% for TSS, 90.4 % for TN, 97% for  $\text{NH}_3$ -N, 95.98% for  $\text{NO}_3$ -N, 81.8% for  $\text{SO}_4^{2-}$ , 99% for  $\text{S}^{2-}$  and 95.9% for total Cr (Figure 3).

These results showed that the pollutant removal capacity of the treatment systems was found to be very high demonstrating that the biological system in the anaerobic and the SBR systems significantly reduced the organic compounds and the nutrients whereas the remaining residues (nutrients, residue organic matter and Cr have also been further removed using CWs to meet the required national environmental quality standards.

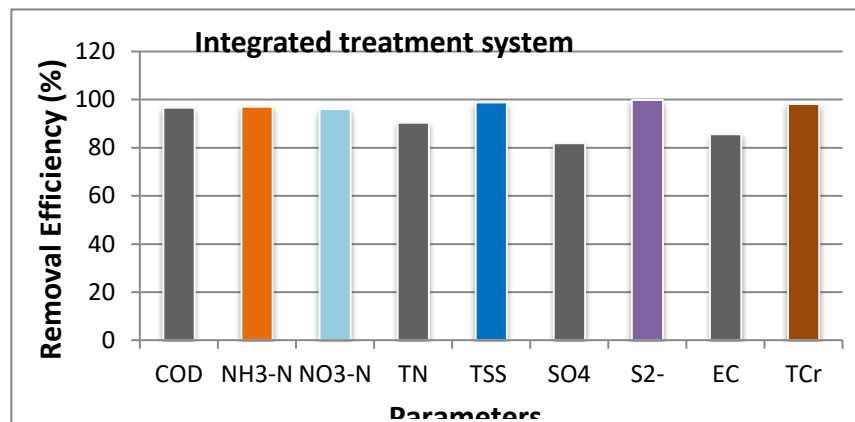


Figure 3: Performance of integrated biological treatment system

Comparing the integrated treatment systems, the CWs performed the highest removal efficiencies for all the measured parameters (ranging from 79.7 to 95% removal). The SBR performed well in terms of TN,  $\text{S}^{2-}$  and  $\text{NO}_3^-$ -N removal ranging from 55.3–99%. In an anaerobic reactor the  $\text{S}^{2-}$  and  $\text{NH}_4$ -N concentration were increased due to an anaerobic microbial process (sulfate reduction and ammonification). As shown in Figure 4, the  $\text{NH}_4$ -N and  $\text{S}^{2-}$  concentration were varying depending on the type of treatment systems.  $\text{NH}_4$ -N and  $\text{S}^{2-}$  concentration were increased in anaerobic system due to anaerobic decomposition of  $\text{NO}_3^-$ -N and organic matter to  $\text{NH}_4$ -N. The highest removal of  $\text{NH}_4$ -N and  $\text{S}^{2-}$  were obtained in aerobic SBRs effluent (89.2% and 97.5% respectively) due to the  $\text{NH}_4^-$ -N and  $\text{S}^{2-}$  oxidation. A constant decreased of TN

concentration, moving from aerobic reactor to CWs systems, were observed (Figure 4A). The aerobic SBR effluent contains higher concentrations of  $\text{SO}_4^{2-}$  due to the conversion of  $\text{S}^{2-}$  and digestion of sulfur containing organic matter in to  $\text{SO}_4^{2-}$ . However the concentration of nitrogen species at the end of aerobic SBR effluents were less due to high denitrification processes in the anoxic phases of SBR.

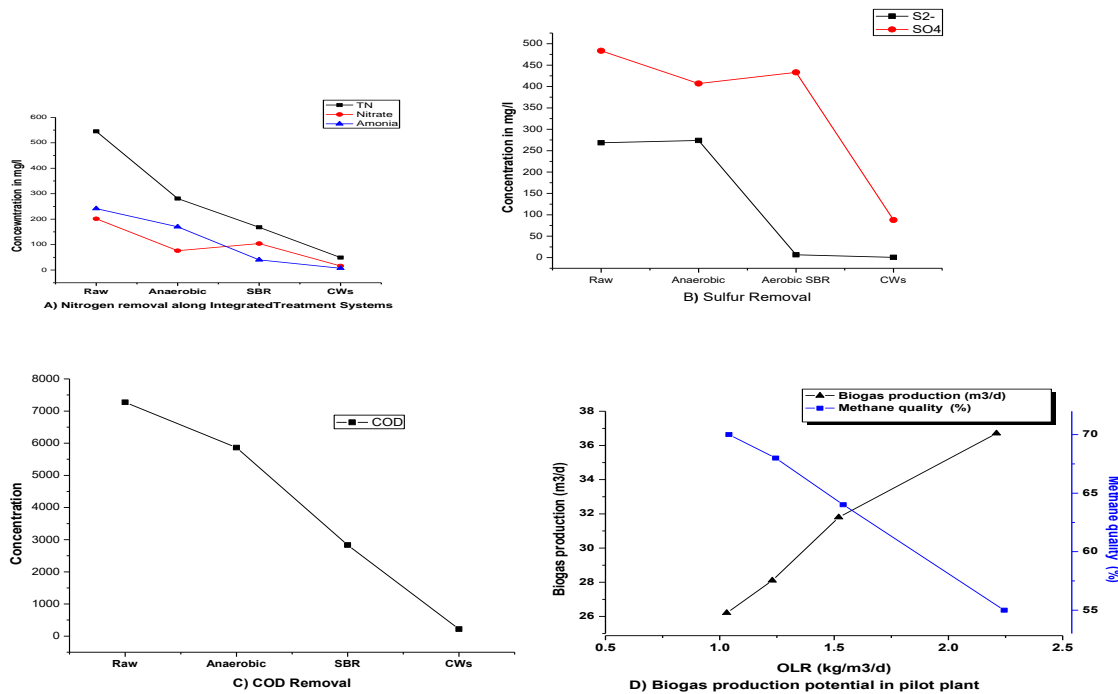


Figure 4: Organic matter, Cr and nutrient removal in anaerobic-SBR and CWs systems

The concentration of TN,  $\text{SO}_4^{2-}$  and  $\text{NO}_3^-$ -N were decreased in hydrolysis reactors may be due to  $\text{SO}_4^{2-}$  and  $\text{NO}_3^-$ -N reduction and anaerobic decomposition of organic matter by consortia of microbes. In anaerobic (hydrolysis) phase, microbes use  $\text{SO}_4^{2-}$  and  $\text{NO}_3^-$ -N as an electron acceptor to decompose organic compounds (Mburu *et al.* 2012). Microorganisms reduce the sulfate to sulfides ( $\text{H}_2\text{S}$  or  $\text{HS}^-$  or  $\text{S}^{2-}$ , depending on pH), as end product by dissimilatory sulfate reduction pathway, and inorganic carbon, (Ralf *et al.* 2006). Hence the concentration of  $\text{S}^{2-}$  was increasing in hydrolysis reactors (Figure 4 B). In this study sufficient HRT (24hrs) and aeration (12hrs) could contribute for high efficiency of nitrification in the SBR reactor. The concentration of  $\text{NO}_3^-$ -N in the aerobic stages of SBR was increased may be due to ammonium oxidation but reduced dramatically in the anoxic stages of SBR due to denitrification which results highest removal efficiency of  $\text{NO}_3^-$ -N (97%) (Figure 3). SBRs technology is reported as an efficient method for nutrients and organic matter removal (Ganesh *et al.* 2006; Farabegoli *et al.* 2007). The removal efficiency of the integrated system for  $\text{S}^{2-}$  and total Cr were 99.8% and 98.5%, respectively, for an influent value of  $268.5 \pm 6$  mg/L and  $28.47 \pm 5$  mg/L, respectively. The present study showed that the treatment efficiency of

the technology, for the treatment of tannery effluent, was higher than the existing conventional technology for organic matter, nutrients and total Cr. The technology is now not only turning the industrial wastes into value added products such as energy and clean water but also serving as a model prototype for public private partnership in developing scalable innovations for the sustainable management of all other agro process wastewaters in the country.

## **Conclusion**

The results show that the technical performance of the pilot integrated treatment processes were efficient to treat high strength tannery wastewater and the treated water meets the acceptable minimum national environmental discharge standards allowable by regulatory bodies. The treated water has a potential for reuse for irrigation. The release of treated effluent into the receiving Modjo River will also greatly reduce the pollution burden from the untreated tannery wastes being directly discharged into the river. The study revealed that the removal efficiency of the biological treatment systems alone was not in the acceptable limit for most pollutants. It was clearly observed that post-treatment of tannery effluent by HSSF CWs was achieved highest removal efficiencies (ranges between 81- 99.9 %) for BOD, COD, TSS, pathogens, heavy metal (Cr), and nutrients. The inflow fluctuations tolerance by the *Phragmites Karka*, including interruptions in the feeding, was found to be high. The study proved that the integrated treatment technology can turn industrial wastes in to value added products such as energy and clean for use for domestic purposes and irrigation. The innovative pilot scale integrated treatment system is environmental friendly, cost effective and efficient model for treating tannery effluent.

## **Acknowledgement**

The authors would like to thank Modjo Tannery Industry, for making possible the establishment of this pilot wastewater treatment project. We also greatly thanks to Swedish International Development Corporation (sida-Sweden) -Bio-innovate program- and Addis Ababa University for their continuous financial support.

## References

- Alemu, T., Lemma, E., Mekonnen, A., and Leta, S. (2016). Performance of Pilot Scale Anaerobic-SBR System Integrated with Constructed Wetlands for the Treatment of Tannery Wastewater. *Environmental Processes*, 3(4), 815–827. <http://doi.org/10.1007/s40710-016-0171-1>.
- Alves MM, Gonzalez, CG, Guedes D, Carvalho R, Castanheira JM, Sol Pereira MC, Vasconcelos LAT (1993). Chromium Removal in Tannery Wastewaters: ‘Polishing’, *Pinus Sylvestris* Bark. *Water Research*, 27(8), pp-1333-1338.
- APHA (1998). Standard Methods for the Examination of Water and Wastewater: 20<sup>th</sup> Ed. American Public Health Association/American Water Works Association/ Water Environment Federation, Washington DC, USA.
- Del Pozo R, Diez V (2003). Organic matter removal in combined anaerobic–aerobic fixed-film bioreactors. *Wat.Res.* 37, 3561–3568.
- EEPA (Federal Environmental Protection Authority of Ethiopia) (2003) Standards for industrial pollution control in Ethiopia, Part Three: Standards for Industrial effluents. ESIS project - US/ETH/99/068/ETHIOPIA, EPA/UNIDO, Addis Ababa, 46p.
- EEPA (1997). Environmental Protection Authority. Annual Report; Addis Ababa, Ethiopia.
- El-Bestawy E, Al-Fassi F, Amer, R, Aburokba, R (2013) Biological Treatment of Leather-Tanning Industrial Wastewater Using Free Living Bacteria. *Advances in Life Science and Technology*, Vol.12,
- Farabegoli G, Carucci A, Majone M, Rolle E (2007). Biological treatment of tannery wastewater in the presence of chromium. *J. Environ. Manage.* 71 (4): 345–349.
- Ganesh R, Balaji G, Ramanujam RA (2006). Biodegradation of tannery wastewater using sequencing batch reactor-respirometric assessment. *Bioresour. Technol.*, 97: 1815-1821.
- Hafez AI, El-Manharawy MS, Khedr MA (2002). RO Membrane Removal of Unreacted Chromium from Spent Tanning Effluent: A Pilot- Scale Study, Part 2.
- Khan A G (2001). Relationships between Chromium Biomagnification Ratio, Accumulation Factor, and Mycorrhizae in Plants Growing on Tannery Effluent-Polluted Soil. *Environmental International*. 26, 417-423.
- Kocaoba S, Akcin G (2002). Removal and Recovery of Chromium and Chromium Speciation with MINTEQA2; *Talanta* 57, 23-30.

- Kongjao S, Damronglerd S, Hunsom M (2008). Simultaneous removal of organic and inorganic pollutants in tannery wastewater using electro coagulation technique, *Korean Journal of Chemical Engineering*, pp. 703-709.
- Mburu N, Sanchez-ramos D, Rousseau DPL, Bruggen JJA Van, Thumbi G, Stein, OR, ... Lens PNL (2012). Simulation of carbon , nitrogen and sulphur conversion in batch-operated experimental wetland mesocosms. *Ecological Engineering*, 42, 304–315. <http://doi.org/10.1016/j.ecoleng.2012.02.003>
- Reemtsma T, Jekel M (1997). Dissolved organics in tannery wastewaters and their alteration by a combined anaerobic and aerobic treatment. *Water Res* 31: 1035–1046.
- Rittiruk U, Kangpanich C, Rakseree S (2011). Design and operation of a biological integrated system for wastewater of cattle farm treatment and utilization in circulated water fish culture. *J Agri Technol* 7: 215–224.
- Scholz W, Lucas M (2003). Techno-economic evaluation of membrane filtration for the recovery and re-use of tanning chemicals. *Advanced Journal of International Water Association* 37, 1859-1867.
- Seyoum Leta, Fassil Assefa, Dalhammar G (2003). Characterization of tannery wastewater and assessment of downstream pollution profiles along Modjo River in Ethiopia. *Eth J Biol Sci* 2: 157–168.
- Seyoum Leta, Fassil Assefa, Gumaelius L, Dalhammar G (2004). Biological nitrogen and organic matter removal from tannery wastewater in pilot plant operations in Ethiopia. *Applied Microbiol. Biotechnol.*, 66: 333-339.
- Song Z, Williams CJ, Edyvean RGJ (2004). Treatment of tannery wastewater by chemical coagulation. *Desalination* 164, 249-259.
- Tadesse A, Seyoum L (2015). Evaluation of Selected Wetland Plants for the Removal Efficiency of Chromium and Organic Pollutants from Tannery Wastewater in Constructed Wetlands at Modjo Tannery; *Journal of Environmental science and Technology*; Vol. 9(5), pp. 440-447.
- UNEP (United Nations Environment Program) (1991). *Tannery and the Environment: A Technical Guide to Reducing the Environmental Impact of Tannery Operations*. UNEP/IEO, UN Publication series III, Paris.
- Vlyssides A, Israilides CJ (1997). Detoxification of Tannery Waste Liquors with an Electrolysis System. *Environmental Pollution* 97(1-2), 147- 152.
- Wang B (1991). Ecological waste treatment and utilization systems on low - cost, energy - saving/ generating and resources recoverable technology for water pollution control in China. *Water Sci Technol* 24: 9–19.

## Computer-Aided Colonic Polyp Detection Using Convolutional Neural Networks

**Kinde A. Fante**

Assistant Professor, School of Electrical Engineering & Computer Engineering,  
Jimma Institute of Technology, Jimma university, P.O.Box 378, Jimma Ethiopia Email:  
kinde.anlay@Ju.edu.et

### ***Abstract***

*Colorectal cancer is the third leading cause of cancer-related deaths worldwide. Its incidence rate is increasing in developing countries. Its most effective prevention method is detection and removal of polyp before its advancement into cancerous stage using colonoscopy. The accuracy of polyp detection depends on experience, fatigue and attentiveness of the colonoscopist during the procedure. The polyp miss rate by human subject ranges from 4% to 12%. Computer-aided polyp detection system can assist the colonoscopist in order to reduce polyp miss rate. The aim of this research is to design computer algorithm which can help the colonoscopist during the colonoscopy procedure. Design of computer-aided polyp detection system is a challenging task due to the variation of polyp property in appearance, size, shape, color and texture. There is also a high similarity between colonic-polyp region and its surrounding. The artifacts of the imaging system such as motion blur and specular highlights pose additional challenges. To overcome these challenges, a polyp detection system which is based on data-driven approach using Convolutional Neural Networks (CNN) is proposed. We use the capability of CNN that it learns the optimal features that discern different classes of images from labeled images automatically. CNN model, with four convolution layers which are followed max-pooling layers and three fully-connected layers, for detecting polyp is trained on 3,713 images obtained from CVC-ColonDB and ASU-MayoClinic polyp image databases. Image preprocessing, data augmentation and CNN hyperparameter optimization methods are used to improve the performance of the system. The performance of the trained net model is tested on 9,758 images. The algorithm has a good detection performance of 86.09 % sensitivity, 90.21 % specificity, and 89.94 % accuracy. This research will have a significant impact for the improvement of our country's healthcare services as there is lack of experienced doctors in many of the hospitals.*

**Keywords:** *Polyp detection, convolutional neural networks, colonoscopy, colorectal cancer.*

## **INTRODUCTION**

Colon polyp is a protruding structure that appears from the colon wall. The most common type of cancer related to polyp is colorectal cancer (CRC). It is the third-leading cause of cancer related deaths globally (Sandouk et al., 2013). Its incidence rate is increasing in developing countries due to changes in diet and life style (Bishehsari et al., 2104). All polyps in color which are found in colon are not cancerous but it has a high possibility to develop into colorectal cancer unless it is detected early and removed. Hence, early detection and removal of colon polyp reduces the possibility of its advancement into cancerous stage. The most widely used screening method of polyp is colonoscopy. In a colonoscopy procedure, a tiny camera at the tip of flexible tube (flexible endoscope) is used for screening the inner wall of colon. The flexible endoscope is inserted via anus and is pushed until it reaches the end of the colon. As soon as it reaches the end of the colon, it is slowly withdrawn while the endoscopist carefully examines the presence of abnormalities such as polyp on the inner wall of the colon in real-time on the screen connected to the one end of the flexible tube (Bond, 2003). A polyp found during the procedure is removed regardless of its status.

Colonoscopy has contributed to decline of 30% in colorectal cancer (CRC) (Siegel et al., 2015). The accuracy of polyp detection depends on the experience, fatigue and attentiveness of the colonoscopist during the procedure. The polyp miss rate by human subject ranges from 4% to 12% (Young and Womeldorph, 2013). A polyp missed at early stage has high possibility to advance into cancerous stage and it can significantly reduce the survival rate of the patient.

The two main causes that lead to misses are (Ameling et al., 2008): (i) colonoscopist fails to cover all parts of the colon during the procedure, (ii) the polyp appears on the screen but missed by the colonoscopist during the procedure due lack of experience, fatigue or lack of attentiveness. The polyp miss due the first cause is difficult to deal with using computer systems. Computer-aided polyp detection algorithms can assist the colonoscopist during the procedure. Polyps in colon appear in different color, size, shape and texture as shown in Fig.1 which makes it quite challenging to detect using classical feature detection methods. One of the major challenge is that there is a high similarity between polyp region and non-polyp region. There may not exist strong boundary between the polyp region and its surrounding. A robust polyp detection algorithm must be able to be invariant to texture, shape, size and color of the polyp region or capture these varying features efficiently.

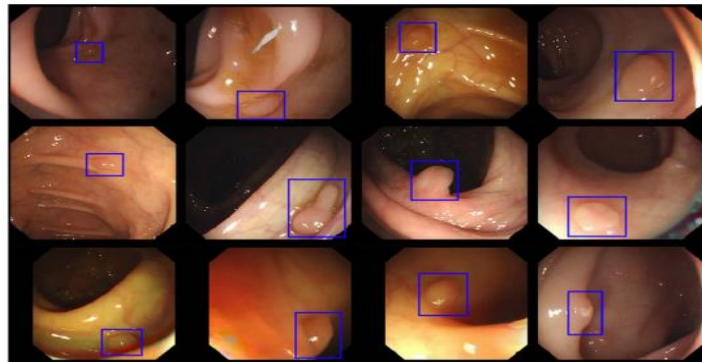


Fig. 1. Variation of polyp appearance in different videos (Bernal et al., 2012).

The polyp detection algorithms proposed in literature can be grouped as based on (i) image processing approaches, (ii) data-driven approaches, and (iii) hybrid approaches. Image processing based approaches employ image segmentation methods to detect the polyp regions in the image. The methods suffer from poor segmentation accuracy due to the high similarity between the interior region of polyp and its surrounding as well as the absence of strong boundary. In literature, polyp detection is done using depth of valley accumulation (Bernal et al., 2012), analysis of curvature profile of the boundary contours (Karargyris and Bourbakis, 2009), measure of the amount of protrudedness (Mamonov et al., 2014), and combination of both curvature and ellipse fitting (Hwang et al., 2007).

The data-driven approach is the least explored approach for polyp detection. In data-driven approaches both the feature extractor and classifier are learned through training. The polyp detection system in (Alexandre et al., 2007), support vector machine (SVM) is trained on color and position features.

In the hybrid approach, the classification is done through learning and feature extractor is designed manually. The features are texture, color, shape and temporal information. After feature extraction various classifiers such as SVM (Wang et al., 2014), Cascade adaboost (Silva et al., 2014) are used for classification. In the work (Tajbakhsh et al., 2016) three sets of patches based on color and texture, temporal features, and shape in context are generated. These three sets of patches are trained on three different CNN, each having two convolution blocks and two locally connected layers. The outputs of the three CNNs are aggregated for detection of a polyp. Sensitivity of 73.6% is reported. Even though, there is advancement, automatic polyp detection is still an unsolved problem.

In this paper, we explore the data-driven approach using CNN for detection of frames with polyp in optical

colonoscopy videos. The CNN architecture is a modified version of the popular architecture, AlexNet (Krizhevsky et al., 2012). We use the publicly available polyp image databases to train the CNN model, optimize its hyper-parameters and evaluate its performance. The remaining part of the paper is organized as follows. In section II, the methodology of the proposed research is presented. In section III, the experimental results and analysis is discussed. In section IV, the conclusion of the research output is given.

## Methodology

The proposed polyp detection algorithm uses convolutional neural network as a feature extractor and classifier. The block diagram of the algorithm is shown in Fig.3. It consists of image preprocessing algorithm for removing non-informative regions and specular highlight. The convolutional neural network (CNN) has multiple stage discriminating feature extractor and binary classifier. CNN learns the optimal features that discern different classes of images from labeled images automatically in hierarchical manner like human visual system. The algorithm is implemented using MATLAB scripts and C++ mex functions.

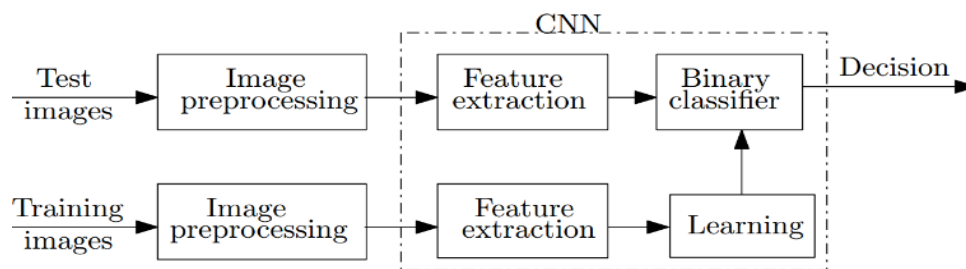


Fig.2 The block diagram of the proposed polyp detection system.

### Image Preprocessing

In this work, publicly available colon polyp image databases obtained from ASU-Mayo Clinic colon polyp database (Tajbakhsh et al., 2016) and CVC-ColonDB (Bernal et al., 2012) are used as training, validation and test datasets. The ASU-Mayo Clinic Polyp Database has 20 different colon short videos taken using optical colonoscopy. CVC-ColonDB has 380 frames with polyp extracted from 15 different videos.

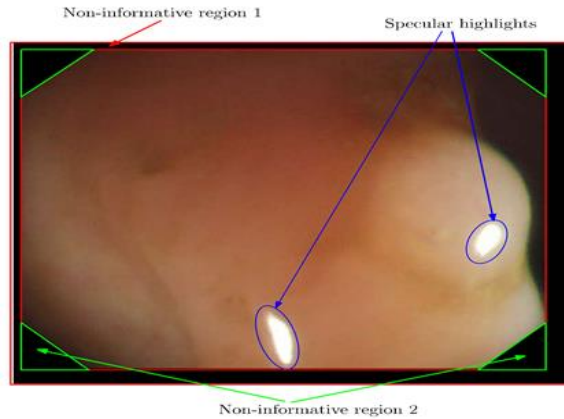


Fig.3. Colonoscopy video frame with non-informative regions (Bernal et al., 2012).

In addition to the original images, these databases have ground truth polyp mask which is suitable to train supervised machinelearning methods. The frames of these videos have non-informative region around the boundary and specular highlights in the interior region of the image as shown in Fig. 3. The region around the boundary of the images has a pixel values of zero. This region contains no important information. It can be cropped without any loss of information. As shown in Fig.5, the cropped image still contains non-informative regions around its four corners (the regions designed by non-informative region 2 in Fig.3. These regions could be inpainted but their sizes are relatively smaller than whole image. Their locations are also fixed and they have almost similar shape in all the frames. Due to this, it will have a negligible effect on the performance of the polyp detection algorithm.

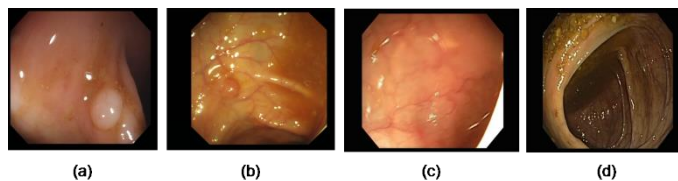


Fig.4 Examples of colonoscopy frames (Bernal et al, 2012, Tajbakhsh et al., 2016).

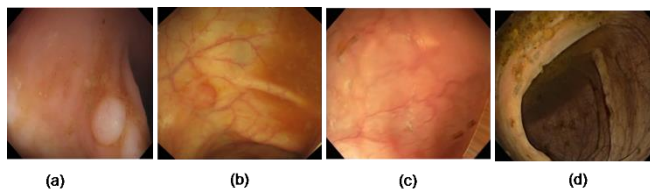


Fig. 5. The colonoscopy frames shown in Fig. 5 after image preprocessing.

Specular highlight appear in colonoscopy frames due to imperfections in the lighting system of the imaging device. The Specular highlight removal algorithm proposed by Bernal et al. (2013) uses two step

operations. In the first step, the specular highlight regions are segmented to generate their mask. Finally, by using the mask generated in the first step, the specular highlight regions are inpainted by diffusing the neighborhood pixels.

The colon polyp videos described in the above databases do not have equal size of frames. The videos have a spatial resolution of 480 x 712, 480 x 856, 574 x 500 and 1080 x 1920. The CNN architecture requires the size of all frames to be equal to the number of neuron in its input layer. Hence, we have rescaled all of the frames to a size of 451 x 451 which is equal to the size of the input layer of the nets we are going to use. This size is chosen since each side approaches the size of the smallest side of the low-resolution image in the dataset after applying the image preprocessing algorithms described above.

### **Convolutional Neural Network**

Let us describe the architecture of the CNN used in this work. We use the CNN architecture illustrated in Table 1. It is a modified version of the popular CNN architecture known as AlexNet (Krizhevsky et. al, 2012), a deep convolutional neural network used for classification of 1000-class images. After several experiments were done, the following CNN architecture is found to be suitable for this application. As shown in Table 1, the net is made up of five convolution layers, four feature pooling layers and three fully-connected layers including the output layer.

Table 1. The CNN architecture specification. The conv and max stand for convolution and max-pooling operations respectively.

Layer	1	2	3	4	5	6	7	8
Stage	conv + max	conv + max	conv	conv + max	conv + max	full	full	full
# channels	48	128	192	128	128	2048	2048	2
Filter size	11x11	5x5	3x3	3x3	3x3	-	-	-
Conv.stride	4x4	1x1	1x1	1x1	1x1	-	-	-
Pooling size	3x3	3x3	-	3x3	3x3	-	-	-
Pooling stride	2x2	2x2	-	2x2	2x2	-	-	-
Zero-padding size	-	2x2	1x1	1x1	1x1	-	-	-
Spatial input size	451x451	55x55	27x27	27x27	13x13	6x6	1x1	1x1

The feature pooling method used in this work is a max-pooling. And the non-linearity employed in this net is a rectifying linear unit (ReLU) (Krizhevsky et. al, 2012), and it is applied to all the outputs of convolutional and fully-connected layers. Four of the convolution layers are followed by max pooling layers whereas one convolution layer is sandwiched between two convolution layers. The arrangement of the layers and hyper-parameters of each layer are described in Table 1.

The output layer consists of two fully-connected neurons. They compute a classifier function. In this work a two-way Softmax classifier function is computed by these neurons. In image classification tasks using neural networks, the net performs both forward and backpropagation operation. In the forward pass, the class of the input image is predicted. In the backward pass the error of the prediction is backpropagated to reduce the prediction error by adjusting the network parameters. This net architecture has 610,203-dimensional input and two output neurons. The net consists of 14,253,570 parameters (weights and biases) that are learned by training the net on labelled images.

In addition to image preprocessing methods described above, different techniques have been proposed to aid generalization or improve the performance of CNNs. Some of the techniques can be incorporated in the CNN architecture and others in the learning algorithm. Among the algorithms that can be incorporated in the CNN architecture, dropout (Krizhevsky et. al, 2012) and local response normalization (Hinton et al., 2012) are used in this work.

## **Experimental Results and Analysis**

The training and validation dataset consists of 3,713 frames without polyp that are extracted from 10 different videos (Tajbakhsh et al., 2016) and 2,409 frames with polyp that are extracted from 20 different videos (Tajbakhsh et al., 2016, Bernal et al., 2012). The ASU-Mayo clinic Polyp database contains 20 short videos along with the ground truth information. Out of the twenty short videos, ten of them are used as a training and validation dataset. The remaining ten short videos are used as test dataset. All the frames from CVC-ColonDB database are used as training and validation dataset. The validation dataset consists of 100 randomly chosen frames and 6,022 frames are used as training dataset. The training data was augmented by rotating the frames with polyp. The frames with polyp are rotated by 90, 180 and 270 degrees which increases the total number of frames with polyp by a factor of four. Rotation of the frames is a level-preserving transformation. After data augmentation, the total number of training frames becomes 13,099.

### **Details of the Training**

The most widely used training method for neural networks is backpropagation algorithm (Werbos, 1988). In this work, we use stochastic gradient descent algorithm to train the CNN architecture described in Table 1 with a batch size of 125 frames. The weights of the neurons in each layer are initialized to small random numbers drawn from Gaussian distribution with a mean of zero and standard deviation of 0.01 (Krizhevsky et. al, 2012). The neuron biases in all the layers are initialized to zero. The backpropagation algorithm uses

gradient descent method and has the following form for updating the weights in each layer during training the net.

$$W_{i+1} = W_i - \lambda \left\langle \frac{\partial L}{\partial W} \right\rangle_{|W_i} D_i, \quad (1)$$

where  $i$  is the iteration index,  $\lambda$  is the learning rate and it is a hyper-parameter of the network.  $\left\langle \frac{\partial L}{\partial W} \right\rangle_{|W_i} D_i$  is the average over the  $i$ -th batch  $D_i$  of the derivative of the loss function with respect to weights  $W$ , evaluated at  $W_i$ . The learning rate in all the network layers was initially set to 0.01. An equal learning rate is used in all the net layers. It is manually adjusted during the training time. We followed the same heuristic approach used in (Krizhevsky et. al, 2012) that the learning rate is divided by 10 when the improvement in validation error stops with the current learning rate.

In order to increase the speed of convergence of a network or to avoid overfitting, modified versions of the standard backpropagation algorithms were proposed. The most common ones are the addition of momentum (Plaut,1986) and weight decay (Werbos, 1988) terms to original weight update formula given in equation (1). These two methods are used in this work.

The CNN model described above was trained on MATLAB platform using multi-core CPU which has 64GB RAM. MatConvNet function libraries (Vedaldi and Lenc, 2015) are used for implementation of the net. The net uses stochastic gradient descent method to minimize the objective function during the training. It is worth noting here that four different methods are used for combating overfitting. These methods are input noise removal, network parameter optimization, data augmentation and dropout. The mean of the training images is subtracted from all the training images. Examples of the learned 11x11 kernels of the first convolution layer of the net is shown in Fig. 7. The net has learned some meaningful features

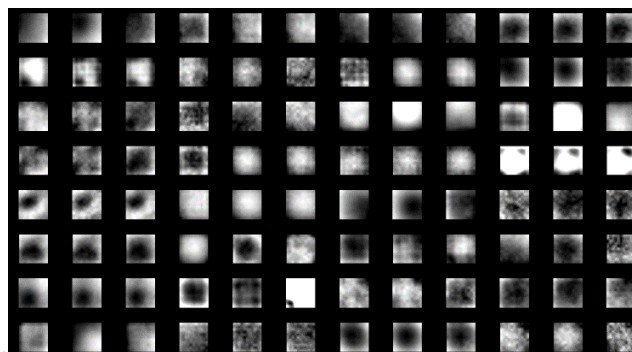


Fig.6.The weights of the learned kernels of the first layer of the convolutional neural network

The trained network model was tested on 9,758 frames extracted from 10 different video. Five of the videos have frames without polyp and the remaining 5 videos have both frames with polyp and normal frames. This test dataset consists of 8,011 normal frames extracted from 10 different videos and 1,747 frames with polyp extracted from 5 different videos. All the image preprocessing algorithms described in section II-A are also applied on the testing dataset, including the subtraction of the mean of the training image from every test frame.

#### Analysis of the Classification Results

During testing, the two output neurons of the CNN model described in Table 1 compute the class scores of the two classes of images, image with polyp and image without polyp. One neuron computes the probability that a given input frame,  $X_i$ , is a frame with polyp, denoted by  $P_p(X_i)$ , and the other neuron computes the probability that a given input frame is a frame without polyp, denoted by  $P_{np}(X_i)$ . The probability values calculated by the two neurons are related by equation (2).

$$P_{np}(X_i) = 1 - P_p(X_i) \quad (2)$$

Obviously, the two-way softmax classifier, which is used in this work, is a logistic regression classifier. The decision of the polyp detection system is taken based on the output values of these neurons. We interpret the hypothesis of the classification output as follows. The two-way softmax function use the logistic function, which has a continuous values ranging from 0 to 1, to represent the hypothesis in polyp classification. When the logistic function outputs a number for an input test image,  $X_i$ , we treat that value as the confidence level of detection that the image has a polyp.

The decision boundary on the output of the output neuron affects the performance of the polyp detection system. We have evaluated the performance of the net described above by changing the decision boundary from 0.01 to 0.95 as shown in Fig. 7.

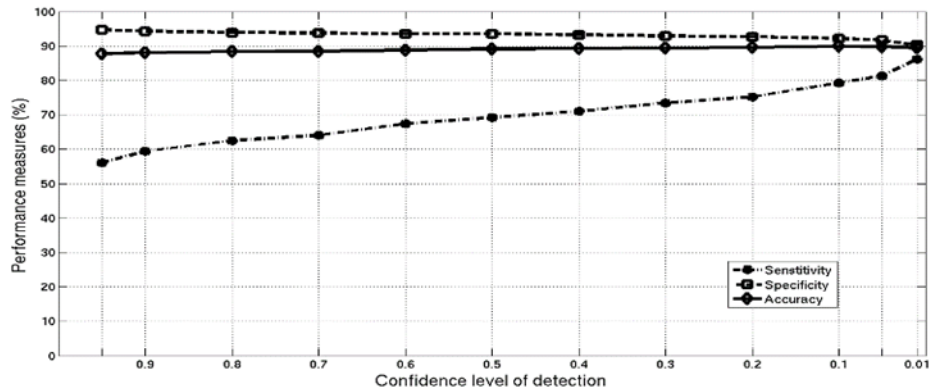


Fig.7. The overall sensitivity, specificity and accuracy of the CNN architecture versus decision boundary of confidence level of detection.

In many applications, a decision boundary of 0.5 confidence level is used by giving equal importance to both the classes for binary class problem. In polyp detection, the impact of false positive detection is not detrimental. However, false negative detection has a detrimental effect as the missed polyp can develop into cancer and reduce the survival rate of the patient. Therefore, the polyp detection system is required to achieve higher sensitivity than specificity. This can be done by shifting the decision boundary towards the lower confidence level of detection i.e. even if the system gives low confidence level of polyp detection for a given input image then it is classified as a polyp and further investigated by endoscopist.

The trained net has a sensitivity of 59.42 % and specificity of 94.28 % when the confidence level of detection threshold is set to 0.9. The specificity and sensitivity becomes 92.28 % and 79.28 % respectively when the threshold value is 0.1. The accuracy varies from 88.04 % to 89.94 % when the threshold value is reduced from 0.9 to 0.1. The algorithm achieves detection performance of 86.09 % sensitivity, 90.21 % specificity, and 89.94 % accuracy when the threshold value is set to 0.01.

Fig. 8 shows the detection latency of the trained net for each of the five test videos which have frames with polyp. As depicted in the figure, highest detection latency is obtained on video-8, about 0.73 millisecond and 0.2 millisecond at 0.9 and 0.1 threshold values respectively.

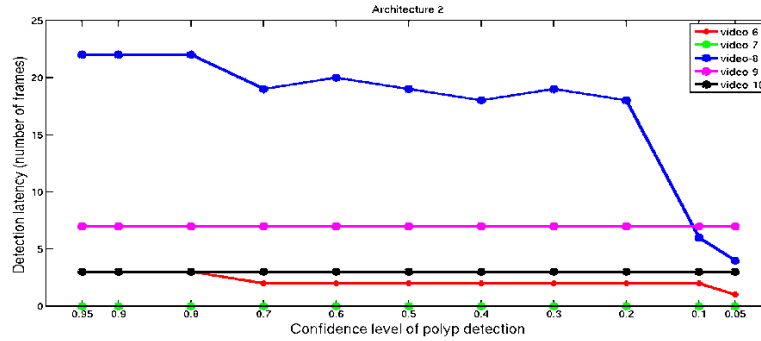


Fig.8 Detection latency of the detection algorithm on 10 test videos for different confidence level of polyp detection.

The lowest detection latency is obtained on video-7, with zero detection latency. At 30 frames per second and 0.2 confidence level of detection, the mean and median detection latency of this polyp detection net is 200 milliseconds and 100 milliseconds respectively. The proposed network has high polyp detection promptness in the sequence of colonoscopy frames.

The receiver operation characteristics (ROC) curve of the system is shown in Fig.9. As depicted in the ROC curve, the number of false positive frames is insignificant as compared to the number of true positive frames. This is an important metric as it shows the number of frames that are needed to be carefully examined by a colonoscopist.

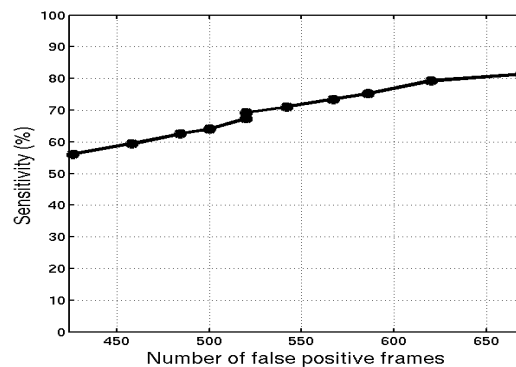


Fig. 9. The receiver operating characteristics (ROC) curve of the trained net. It is drawn by varying the confidence level of detection threshold value from 0.95 to 0.05.

The comparison of the proposed polyp detection system in terms of sensitivity with two existing systems in literature is given in Table 2. As shown in the table, the sensitivity of the proposed system is good as compared to the others. More accurate comparison between the algorithms can be performed by using the same training and test data for all them.

Table 2. Performance comparison of the proposed algorithm with existing systems.

Author	Feature	Dataset # images with polyp/without polyp	Sensitivity (%)
Bae et al., 2015	Discriminating Feature learning	1123/140	24
		300/0	70.6
Tajbkhsh et al., 2016	Shape and context information	5200/14200	48
		300/0	88
<b>Current work</b>	<b>Feature learning</b>	<b>1747/8011</b>	<b>86.09</b>

### Conclusion

A deep Convolutional Neural Network architecture has been trained on large polyp dataset and its performance has been evaluated. We have shown that high classification performance can be achieved by using convolutional neural networks for detection of polyps in colonoscopy frames. The trained nets classify the frames of the videos without poly with higher accuracy than the frames of the videos with polyp. Therefore, reducing the threshold value of confidence level of detection increases the sensitivity without a significant effect on specificity. Generally, the trained network gives high specificity on the videos which has no polyp and high sensitivity on the videos with polyp which is an acceptable characteristics for this application. This system can help the doctors to save more lives if it is deployed in hospitals.

The performance of the network can be improved by further tuning its parameters and hyper-parameters. More training data with different polyp appearance can also increase the system robustness. The CNN method can also be combined with other systems such as texture feature extractor or image segmentation method to localize polyps in frames of colonoscopy videos.

### REFERENCES

1. Alexandre, L. A., Casteleiro, J., & Nobreinst, N. (2007, September). Polyp detection in endoscopic video using svms. In *European Conference on Principles of Data Mining and Knowledge Discovery* (pp. 358-365). Springer Berlin Heidelberg.
2. Ameling, S., Wirth, S., & Paulus, D. (2008). Methods for polyp detection in colonoscopy videos: a review.
3. Bae, S. H., & Yoon, K. J. (2015). Polyp detection via imbalanced learning and discriminative feature learning. *IEEE transactions on medical imaging*, 34(11), 2379-2393
4. Bernal, J., Sánchez, J., & Vilarino, F. (2012). Towards automatic polyp detection with a polyp appearance model. *Pattern Recognition*, 45(9), 3166-3182.

5. Bernal, J., Sánchez, J., & Vilarino, F. (2013, July). Impact of image preprocessing methods on polyp localization in colonoscopy frames. In *Engineering in Medicine and Biology Society (EMBC), 2013 35th Annual International Conference of the IEEE* (pp. 7350-7354). IEEE.
6. Bishehsari, F., Mahdavinia, M., Vacca, M., Malekzadeh, R., & Mariani-Costantini, R. (2014). Epidemiological transition of colorectal cancer in developing countries: environmental factors, molecular pathways, and opportunities for prevention. *World J Gastroenterol*, 20(20), 6055-6072.
7. Bond, J. H. (2003). Colon polyps and cancer. *Endoscopy*, 35(01), 27-35.
8. Hinton, G. E., Srivastava, N., Krizhevsky, A., Sutskever, I., & Salakhutdinov, R. R. (2012). Improving neural networks by preventing co-adaptation of feature detectors. *arXiv preprint arXiv:1207.0580*.
9. Hwang, S., Oh, J., Tavanapong, W., Wong, J., & De Groen, P. C. (2007, September). Polyp detection in colonoscopy video using elliptical shape feature. In *Image Processing, 2007. ICIP 2007. IEEE International Conference on* (Vol. 2, pp. II-465). IEEE.
10. Karargyris, A., & Bourbakis, N. (2009, April). Identification of polyps in wireless capsule endoscopy videos using log gabor filters. In *Life Science Systems and Applications Workshop, 2009. LiSSA 2009. IEEE/NIH* (pp. 143-147). IEEE.
11. Krizhevsky, A., Sutskever, I., & Hinton, G. E. (2012). Imagenet classification with deep convolutional neural networks. In *Advances in neural information processing systems* (pp. 1097-1105).
12. Mamonov, A. V., Figueiredo, I. N., Figueiredo, P. N., & Tsai, Y. H. R. (2014). Automated polyp detection in colon capsule endoscopy. *IEEE transactions on medical imaging*, 33(7), 1488-1502.
13. Plaut, D. C. (1986). Experiments on Learning by Back Propagation.
14. Sandouk, F., Al Jerf, F., & Al-Halabi, M. H. D. (2013). Precancerous lesions in colorectal cancer. *Gastroenterology research and practice*, 2013.
15. Siegel, R. L., Miller, K. D., & Jemal, A. (2015). Cancer statistics, 2015. *CA: a cancer journal for clinicians*, 65(1), 5-29.
16. Silva, J., Histace, A., Romain, O., Dray, X., & Granada, B. (2014). Toward embedded detection of polyps in WCE images for early diagnosis of colorectal cancer. *International Journal of Computer Assisted Radiology and Surgery*, 9(2), 283-293.
17. Tajbakhsh, N., Gurudu, S. R., & Liang, J. (2016). Automated polyp detection in colonoscopy videos using shape and context information. *IEEE transactions on medical imaging*, 35(2), 630-644.
18. Wang, Y., Tavanapong, W., Wong, J., Oh, J., & De Groen, P. C. (2014). Part-based multiderivative edge cross-sectional profiles for polyp detection in colonoscopy. *IEEE journal of biomedical and health informatics*, 18(4), 1379-1389.
19. Werbos, P. J. (1988, January). Backpropagation: Past and future. Proceeding of international conference neural networks icann.

20. Young, P. E., & Womeldorph, C. M. (2013). Colonoscopy for colorectal cancer screening. *J Cancer*, 4(3), 217-226.

## SOFTWARE COMPLEXITY PREDICTION MODEL: A COMBINED MACHINE LEARNING APPROACH

<sup>1</sup>Ermiyas Birihanu (MSc.) and <sup>2</sup>Tibebe Beshah

<sup>1</sup>Software Engineering, Wolkite University, Wolkite

<sup>2</sup>School of Information System, Addis Ababa University, Addis Ababa  
[mymam21@gmail.com](mailto:mymam21@gmail.com) , [tibebe.beshah@gmail.com](mailto:tibebe.beshah@gmail.com)

### *Abstract*

*The necessity of computer grew rapidly. Consequently, the use of the software is enormous and complex. Software companies are building increasingly complex systems. At the same time, the market needs them to complete their project in less time while customers also require high quality. Software companies have various measurement methods some of them are customer feedback, after it delivered to customers and software testing, before the software delivered to customers or stakeholder.*

*The goal of this study is to apply combined machine learning methods for predicting the status of software faults from the NASA MDP data set. Especially, the researcher gives emphasize to build best prediction model, finally the researchers develop and evaluate the best model by building a prototype system.*

*In this Study, the methodology was considering both single and combined machine learning approach. This research work has a total of 498, 10885, 2109, 522 and 458 records and 22 attributes in order to predict software faults. Noise removal and handling of missing values was done to prepare the dataset for experiments. For the purpose of building the model machine learning algorithms such as decision tree, support vector machine, artificial neural network and combination of single classifiers using vote method is used. To evaluate the model accuracy 10-fold cross validation is used and*

*Accuracy, precision and Recall was used to evaluate the performance of the developed model. The evaluation of best performing methods is compared according to accuracy, sensitivity, specificity and execution time to build the model. Based on performance evaluator the best algorithms are found to be combination of J48 with SMO classifiers were SMO is followed by J48 classifier.*

*Information extraction from the source code should be done before the researcher an attempt to test or maintain the software is done; then the development model will be applied for determining the complexity of the software product.*

**Keywords:** Software Complexity, Prediction Model, Machine Learning, Software Metrics, Software Faults

## **I. Introduction**

Software companies are building increasingly complex systems. At the same time, the market needs to complete their project in less time while customers also require high quality.

Mostly the quality of the software could be measured by the number of faults or bugs that are searched in software products. A simple way to count or assess the quality of the software product might be from the customer feedback. However, these metrics create at least two problems. First, it does not provide actionable feedback about where improvement can occur, and second, it occurs too late to make any corrections. The purpose of using software fault classification is thus to prevent faults and find as many faults as possible, as early as possible.

Machine Learning is one of the most vital and motivating area of research with the objective of finding meaningful information from huge data sets. So, that, applying this area into software application systems is the recommended one. The basic purpose of machine learning is to extract useful pattern from the data, mining data may be structured format (example. Multiple database) or text mining: unstructured data (example, natural language document). Machine learning tasks can be classified in two categories, descriptive and predictive. The predicative task is used to infer the current data from data set to make predictions for the future.

The core of the machine learning process is identifying the Machine learning technique. There are a number of Machine Learning technique and algorithm such as classification, clustering, Regression, Artificial Intelligence, Neural Networks, Association Rules, Decision Trees, Genetic Algorithm, Nearest Neighbor Method etc....; All of these techniques and algorithm are used to extract knowledge from databases. The basic thing that the researcher is looking here is each technique has its own application.

The necessity of computer grew rapidly. Consequently, the use of software becomes enormous and complex. Software is computer programs that are used to instruct the computer to do a given task. Software Development Life Cycle (SDLC)(M. Saini & Kaur, 2014) describes the methodology by which the development of any software takes place. SDLC includes Feasibility Analysis, Requirement Analysis and Specification, Designing, Implementation, Testing, and Maintenance. In this study, the researcher was not going through each software phase in detail, but only on software testing and maintenance. Software testing(SHICHAOZHANG, 2003) provides a means to reduce errors, cut maintenance and overall software costs. Various software techniques are applied for testing the software; from being reduced error, but, it cannot possible error free. The systems that are taking an input such as character, number and file; it is easy to test for any small input, but what if the line of code is complex and large. Software testing is a means of determining the quality of the software.

Now a day, there is exist several data sets that could be mined in order to discover useful knowledge regarding defects. In this study, the researcher applies different machine learning techniques on several publicly available datasets of the National Aeronautics and Space Administration(NASA) software repository that is CM1, JM1, KC1, KC2 and KC3. The purpose is to classify the software modules into either fault prone or not fault prone modules.

## **II. Statement of Problem**

Software testing is one of the most critical and costly phases of software development. Project managers need to know “when to stop testing?” And “which parts of the code to test?”. The answers to these questions would directly affect defect rates and product quality as well as resource allocation (i.e. experience of test staff, how many people to allocate for testing) and the cost.

As the size and complexity of software increases, manual inspection of software becomes a harder task. In this context, alternative methods that are used to predict potential effects clearly are software defect prediction. Since testing typically consumes 40 - 50% of development efforts, and consumes more effort for systems that require higher levels of reliability, it is a significant part of the software engineering (SHICHAOZHANG, 2003)(Shivaji, 2013)(Chayanika S, Sangeeta S, & S, 2013). Software defect is not only the quality of software, but also increase costs and suspend the development schedule. In addition to above, there could be many reasons for the system to be faulty; most of them are because of the human factor, mistake and errors made in designing or coding by the peoples, data entry, documentation and communication failures. In order to solve the most common, human factors we shall use software fault prediction before us taking the software systems to test and maintains.

The objective of Software complexity predictions in this study used to solve the problem that we are mentioned above. This study helps the software project manager to predict and fix the bug before it is delivered to customers that assures the quality of software.

## **III. Objective of Study**

The general objective of this study is to design and develop software complexity predictive model.

## **IV. Literature Review**

Ezgi Erturk et al. (Chayanika S et al., 2013) The data set for the experiment are collected from the PROMISE Software Engineering Repository and applied McCabe software metrics. The algorithm they are using form experiment was SVM, ANN and ANFIS (new adaptive model proposed), the performance measure was 0.7795, 0.8685, and 0.8573 respectively.

Another successful paper was published by Surndha Naidu et al.(M. SURENDRA & GEETHANJALI, 2013), the primary goal of this paper were finding the total number of defects in order to minimize time and cost. The defect was classified into five parameters such as Volume, Program length, Difficulty, Effort and Time Estimator. They were using ID3 classification algorithm, to classify defects.

Saiqa Aleem et al.(Aleem, Capretz, & Ahmed, 2015), In this study, they were used around fifteen data sets (AR1, AR6, CM1, KC1, KC3 etc.) with various machine learning methods. Measured the performance of each method and finally conclude that SVM, MLP and bagging had high accuracy and performances.

## **V. Research Methodology**

This study is based on the data collected from NASA MDP (research purpose data set developed by NASA); in order to well understand the data, it needs a close relationship with Domain Experts such as software developers and software tester.

## **VI. Design of Software Complexity Prediction Model**

This research work focused with design and developing for the software complexity prediction model. First, we took the selected data from the NASA Promise MDP and it has trained data which include software metrics and corresponding values. Second, preprocessing of the input data was performed through noise removal and handling missing values. Third, applying the chosen methods (J48, MLP, SMO and Vote) with 10 –fold cross validation test mode. Finally, software complexity predictions are aligned to fault or non-fault one and performance report was explored. In order to assure the design and develop a model the researcher develop the prototype system that have an input form that automatically feed from the database when the user click on the load data button to determine whether its faults and non-fault. Figure 1shown below architecture of the software complexity prediction model.

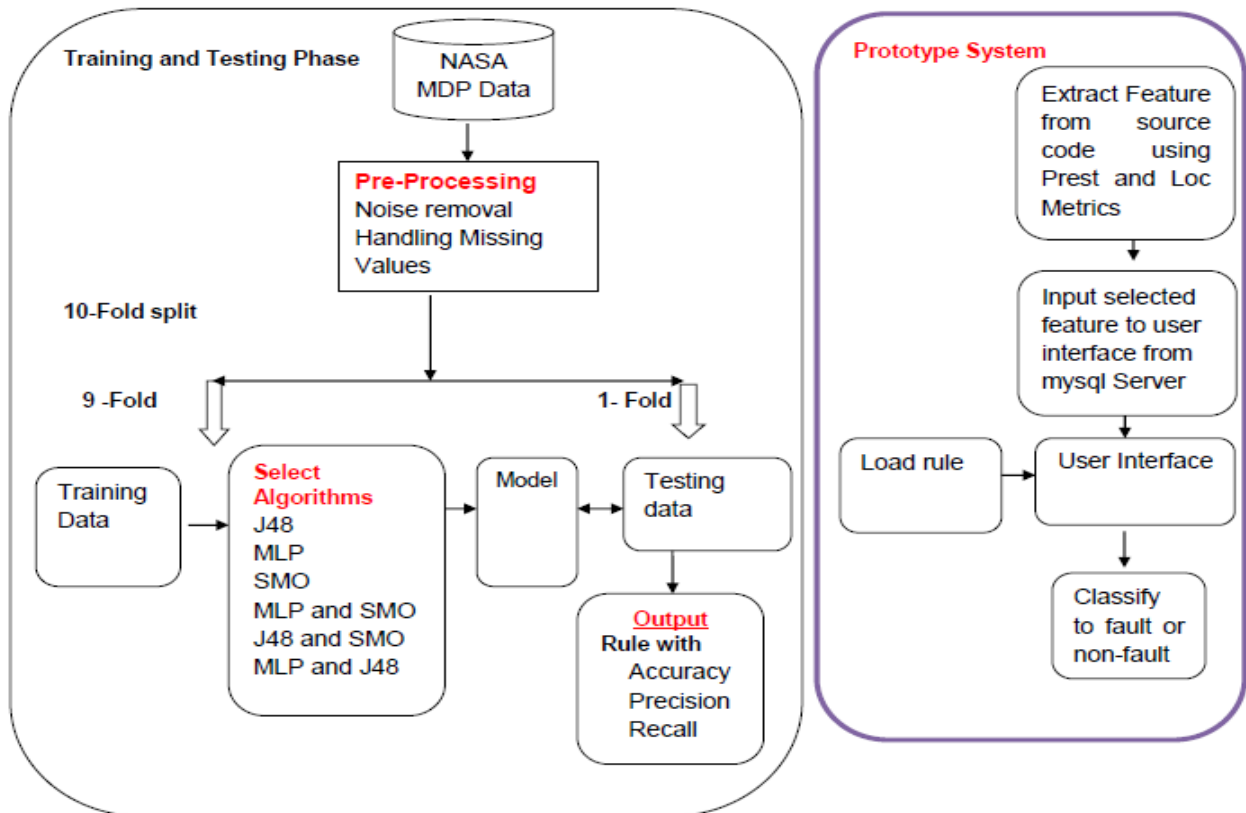


Figure 1: Proposed Architecture of Software Complexity Prediction Model

## VII. Data Understanding

Software fault data is not easy to acquire; commercial software development companies do not have a software fault measurement program and

Even the company having a fault measurement program do not goto publicizing fault data.

For this study, we were collecting and used from NASA MDP Promise due to its original version and 60 % of software fault studies were selecting it as a priority(Malhotra, 2015). We have various things that we considered about the data set information's before applying machine learning techniques, which are discussed as follows:

## VIII. Choosing and Collecting Data Set

Based on NASA Promise repositories(Gray, Bowes, Davey, Sun, & Christianson, 2012)("NASA ") currently consists 13 data set described intended for software metrics research. Among this 13-data set we have chosen five data sets (CM1, JM1, KC1, KC2 and KC3) because of it consisting different

programming language, code metrics (Halstead's complexity, code size and McCabe's Cyclomatic complexity) and time constraints.

### IX. Description of The Selected Dataset

The description of the data set and attributes we used is explained in Table 1 and Table 2 below:

**Table 1: - Data Set Information**

	<b>CM1</b>	<b>JM1</b>	<b>KC1</b>	<b>KC2</b>	<b>KC3</b>
<b>Language</b>	C	C	C++	C++	Java
<b>LOC</b>	20k	315k	43k	18k	18k
<b>Modules</b>	498	10885	2109	522	458

**Table 2: Attribute and Their description for CM1, JM1, KC1, KC2 and KC3 data set**

<b>No</b>	<b>Attribute Name</b>	<b>Data Type</b>	<b>Description</b>
1	Loc	Numeric	McCabe's line count of code
2	V(g)	Numeric	McCabe "Cyclomatic complexity"
3	ev(g)	Numeric	McCabe "essential complexity"
4	iv(g)	Numeric	McCabe "design complexity"
5	N	Numeric	Halstead total operators + operands
6	V	Numeric	Halstead "volume"
7	L	Numeric	Halstead "program length"
8	D	Numeric	Halstead "difficulty"
9	I	Numeric	Halstead "intelligence"
10	E	Numeric	Halstead "effort"
11	B	Numeric	Halstead
12	T	Numeric	Halstead's time estimator
13	IOCode	Numeric	Halstead's line count
14	IOComment	Numeric	Halstead's count of lines of comments

15	IOBlank	Numeric	Halstead's count of blank lines
16	IOCodeAndComment	Numeric	Line of code and comment
7	uniq_Op	Numeric	Unique operators
18	uniq_Opnd	Numeric	Unique operands
19	total_Op	Numeric	Total operators
20	total_Opnd	Numeric	Total operands
21	branchCount	Numeric	of the flow graph
22	Defects	Text	Module has not one or more reported defects

## X. FEATURE EXTRACTION

In this section, we took two sample code that is measured software metrics tools (Prest and Loc Metrics). In case of Prest and Loc Metrics we used Java source code, as we discussed in the following sections.

Code 1, the researcher extracted the feature from the source code based on mathematical methods. Based on the Halsted metrics researcher is extracted number of operands and operators.

## XI. Prest Based Extracting Attributes

In this study, we used remote method invocation for scientific calculator Java source code. The Prest can Parse all files that are written in C, C++, Java, JSP and SQL through different parser at the same time. One of the project like sample code that we in presenting for scientific Java source code is parsed and the metrics are presented as Figure 2 below. In Figure 1, only four metrics, i.e. Cyclomatic density, decision density, Essential density, branch count, is presented as the static code attributes that can be extracted by Prest, since we have page limitations. However, Table 3 provides a full set of extracting attributes with corresponding values.

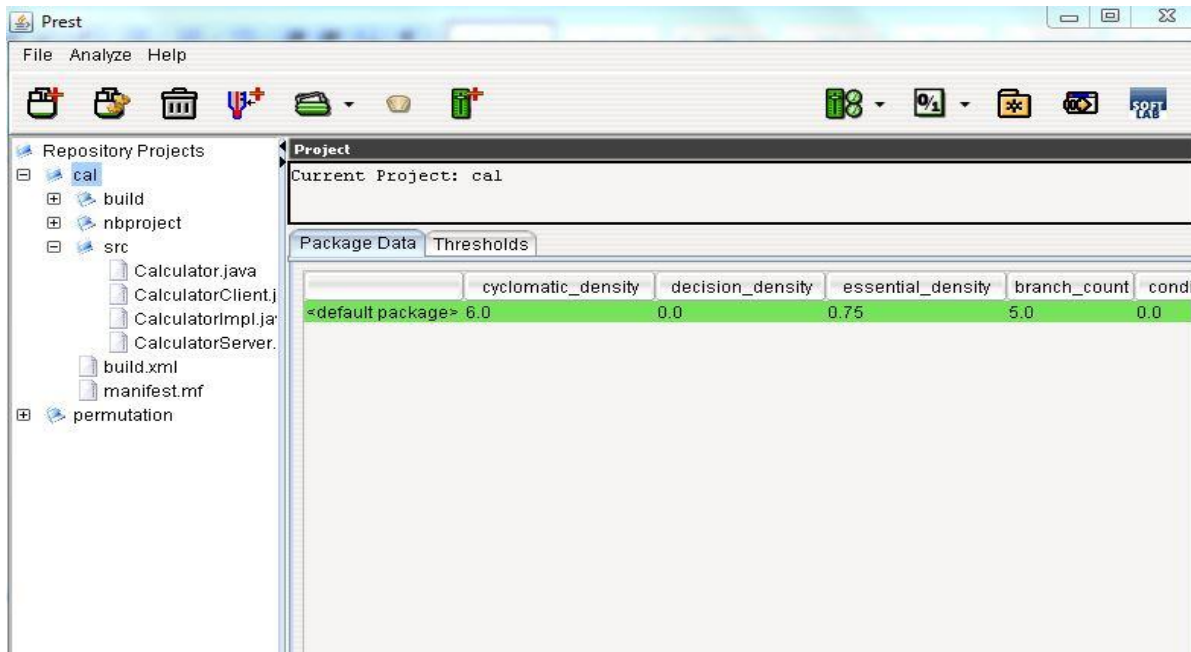


Figure 2: Software Metrics Attributes Extraction for RMI calculator source code

### XIII. Loc Metrics Based Extracting Attributes

Similarly, the researcher used remote method invocation source code to extract attributes. Loc Metrics computes physical lines, Logical lines, Blank Lines, Total line of code, Executable Physical, Executable Logical, McCabe VG Complexity, Comment, Header Comment. Among these we only considered IO code and Comment, Halsted Comment and Halsted Blank lines because of Prest cannot support these attributes. In Loc Metrics tool first the user's browser the source code to be extracted attributes, then click on Count LOC, the tool automatically puts the attributes with corresponding values as shown in figure 3 below.

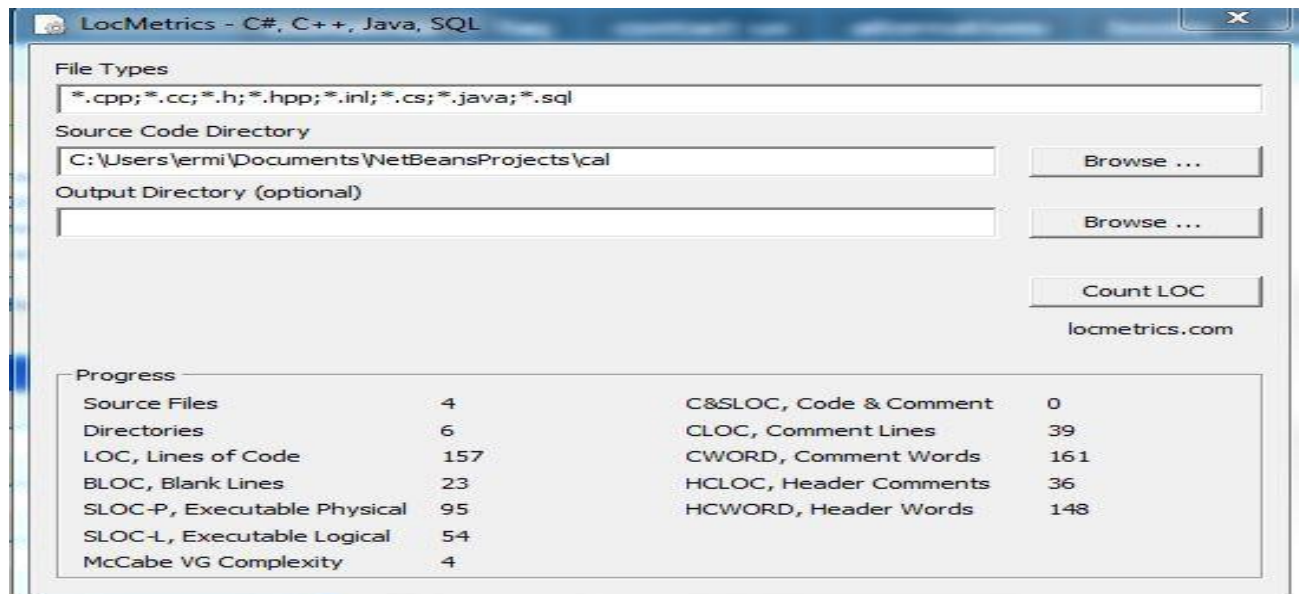


Figure 3: Software Metrics Attribute Extraction for RMI Calculator source code

Table 3: Static code Metrics Extracted by Prest and LOC metrics

Number	Software code metrics	Extracted feature values
1	Line of code	126.0
2	Cyclomatic complexity	21.0
3	Essential complexity	16.0
4	Design complexity	0.76
5	Total operators + operands	37.0
6	Halstead "volume"	0.23
7	Halstead "program length"	37.0
8	Halstead "difficulty"	5.88
9	Halstead "intelligence"	8.51
10	Halstead "effort"	1.35
11	Halstead	1
12	Halstead's time estimator	0.08
13	Halstead's line count	1
14	Halstead's count of lines of comments	39
15	Halstead's count of blank lines	23
16	IO Code and Comment	0

17	Unique operators	9.0
18	Unique operands	14.0
19	Total operators	19.0
20	Total operands	18.0
21	BranchCount	5.0

#### XIV. Experimentation and Discussion

As the main purpose of this study is to predict software fault using machine learning approach by single classifiers and combining of two classifications. Methods are adopted to develop a predictive model using WEKA 3.6.9 Machine Learning Software.

##### A. Model Building Using Single Classifiers

The main goals of this research were to improve the accuracy and performance of single classifiers, in order to do this, first we should measure the performance and accuracy of single classifiers and record it based on the method and performance measure that we were selected. We have chosen three algorithms, namely decision Tree, Artificial Neural Network, Support Vector Machine. Table 4 which discussed below is an experimental result summery for selected machine learning methods.

Table 4: Result Summery on single classifiers

Data set	Learning Method								
	J48			MLP			SMO		
	Correctly classified	Precision	Recall	Correctly classified	Precision	Recall	Correctly classified	Precision	Recall
CM1	87.95	0.90	<b>0.96</b>	87.55	0.901	0.969	89.56	0.903	0.993
JM1	79.7	0.83	0.93	80.95	0.841	<b>0.99</b>	80.73	0.807	<b>1</b>
KC1	84.54	0.88	0.93	85.91	0.872	0.978	84.78	0.996	0.85
KC2	81.41	0.87	0.89	84.67	0.873	0.945	82.76	0.828	0.98
KC3	<b>89.3</b>	<b>0.92</b>	<b>0.96</b>	<b>90.61</b>	<b>0.919</b>	0.983	<b>90.82</b>	<b>0.952</b>	0.90
<b>10- fold cross validation</b>									

## B. Model Building Using Combined Methods

Based on the researchers showed that combining of two methods, improve the performance and accuracy of single classifiers (Tao W, Weihua L, Haobin S, & Zun L, 2011 ) due to that in this study, we combined two classifiers in order to evaluate the performance and accuracy of combined classifiers using a vote algorithm with the average probability combinational method. Table 5 which discussed below is an experimental result summery for selected machine learning methods.

Table 5: Result summery on combined method

Data set	Learning Method								
	J48 and MLP			J48 and SMO			MLP and SMO		
	Correctly classified	Precision	Recall	Correctly classified	Precision	Recall	Correctly classified	Precision	Recall
CM1	88.5	0.903	0.978	89.5	0.901	0.993	89.5	<b>0.901</b>	0.998
JM1	80.7	0.808	<b>0.999</b>	80.72	0.807	<b>1</b>	80.72	0.807	<b>1</b>
KC1	85.4	0.881	0.957	84.6	0.848	0.997	84.6	0.845	<b>1</b>
KC2	81.8	0.874	0.901	82.7	0.828	0.998	79.5	0.795	<b>1</b>
KC3	<b>90.6</b>	<b>0.921</b>	0.981	<b>90.8</b>	<b>0.908</b>	<b>1</b>	<b>90.82</b>	0.906	<b>1</b>
<b>10- fold cross validation</b>									

## XV. Performance Evaluation

In section 4.1 and 4.2, the researcher observed the following basic research work outcomes:

- J48, When the size of dataset increased
  - The number of leaves, size of tree and time taken to build model were increased.
  - Recall, precision and accuracy of the model were decreased.
- MLP, SMO, J48 &MLP, J48 &SMO, SMO& MLP, when the size of the dataset is increased
  - Recall, precision, and accuracy of the models were decreased
  - Time taken to build model were increased

## XVI. Experimental Discussion

In order to develop the software fault predictive model single and combined classifier are used which includes six experiments separately for each classifier and data sets. A total of 30 experiments was conducted based on all attributes. The experiment designed to examine whether increasing data set size improves or reduced the performance of selected algorithms, to evaluate the effect of algorithms for performance and to compare the performance of algorithms in software fault prediction.

### A. Effect of Dataset Size

Experiment results show that increasing the data size has an impact on the performance of machine learning algorithms that we used. The researchers conducted additional experiments in order to determine why the performances of machine learning algorithms decreased while dataset size increased. We selected J48 classifiers with Pruned and un-pruned parameters for CM1, JM1, KC1, KC2 and KC3 data set. Table 6 shows that the effect of pruning on the performance of predictive models as the data size increases.

Table 6: Effect of Pruning

	Number of Instances	J48 with all attributes and pruned parameter			J48 with all attributes and Un-pruned parameter		
		Accuracy (%)	Precision	Recall	Accuracy (%)	Precision	Recall
<b>CM1</b>	498	<b>87.95</b>	0.904	0.969	<b>88.35</b>	0.919	0.955
<b>KC3</b>	458	<b>89.3</b>	0.924	0.961	<b>88.2</b>	0.925	0.947
<b>KC2</b>	522	<b>81.4</b>	0.873	0.896	<b>80.2</b>	0.88	0.87
<b>KC1</b>	2109	<b>84.5</b>	0.885	0.939	<b>83.8</b>	0.887	0.927
<b>JM1</b>	10885	<b>79.7</b>	0.837	0.919	<b>79.0</b>	0.837	0.919

From the experiments that we conducted and additional consideration by the researcher conclude that increasing data set decreases the performance of machine learning algorithms because of increasing dataset increases complexity of the model, increase number of rules generated and decreases the model accuracy, precision and recall. Table 7 shown below clearly illustrates.

Table 7: Effect of Dataset Size J48 Classifiers Model

J48 with all attributes	Instance Number	Number of Rules	Size of the Tree (size of complexity)	Recall	Precision	Accuracy
CM1	498	5	9	0.969	0.901	87.95
KC3	458	7	13	0.983	0.919	<b>89.3</b>

KC2	522	26	51	0.945	0.873	81.41
KC1	2109	56	111	0.978	0.872	84.54
JM1	10885	340	679	0.99	0.841	79.7

### B. Effect of Methods on Performance

Among all methods, the highest accuracy was performed for KC3 data that is 90.82 using combination of J48 with SMO method. Figure 4 depicted below shown the effect of algorithm on the performance for CM1 data set; from the Figure 4J48 and SMO register higher performance when we compared with other methods, the second performance was registered for MLP with SMO and SMO methods for CM1 data set.

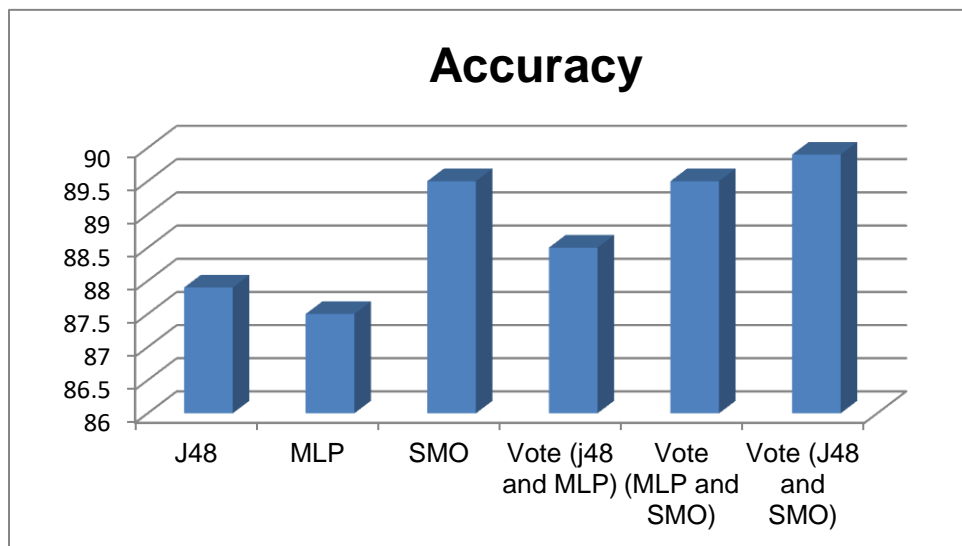


Figure 4: Model Comparison for CM1 Data set

### C. Rule Extraction from Decision Trees

In this research work, based on the performance evaluator like specificity and execution time took; J48 classifiers achieved relatively high performance when we compared with other five classifiers that we used. As we have seen in Experiment 1(J48 method) results, J48 decision tree generated 25 rules for predicting software fault. The researcher selected 7 rules that cover most of instances within the given data set, and then the researcher made deep discussion with domain experts in order to assure that the selected rules really works for all instances.

## XVII. Software Complexity Classification System: A Prototype

In this study, an attempt was made to design and develop an operational application prototype named software defect classification system that uses the classification rules generated from J48 classifiers. The

prototype is used to classify a software product into one of the software labels (fault or not-fault). The Software defect classification system includes the user to load extracted source code data from the database when the user clicks on the load data button, predict the user based on the trained in to defect or not defected one, if we click on predict button. From Figure 5 there are 22 inputs (attributes) and output is calculated by a click on the predict button. Inputs are given from extracted source code data. Predict button is used to categorizing the input data into fault or non-fault one. Exit button is used to close out from the graphical user interface

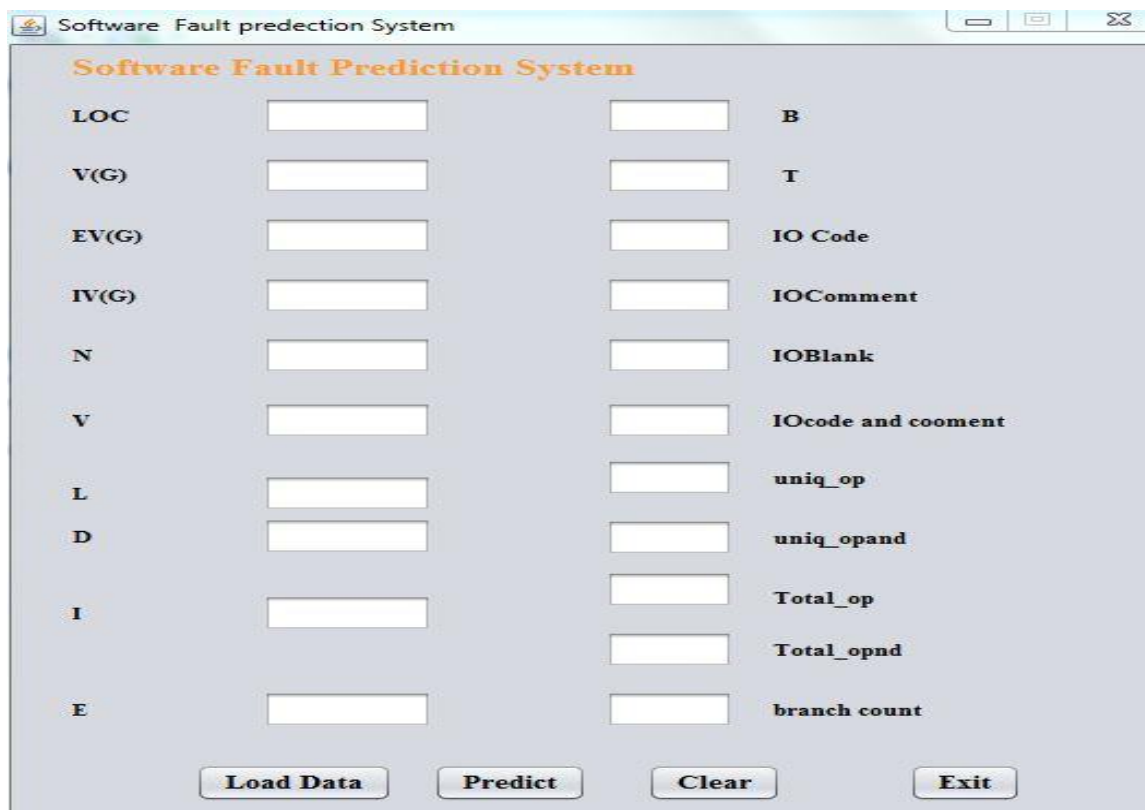


Figure 5: Software Complexity Classification System User Interface

As shown Figure 6 below, this prototype prediction model can be used for predicting software faults based on the rules generated by J48 classifier. We loaded the extracted source code, data into the prototype as we saw in Figure 6 to show the predicted result of software faults as TRUE based on rule 7 in Experiment one. We have used Java source code to predict software faults according to the selected rule that generated from J48 classifiers.

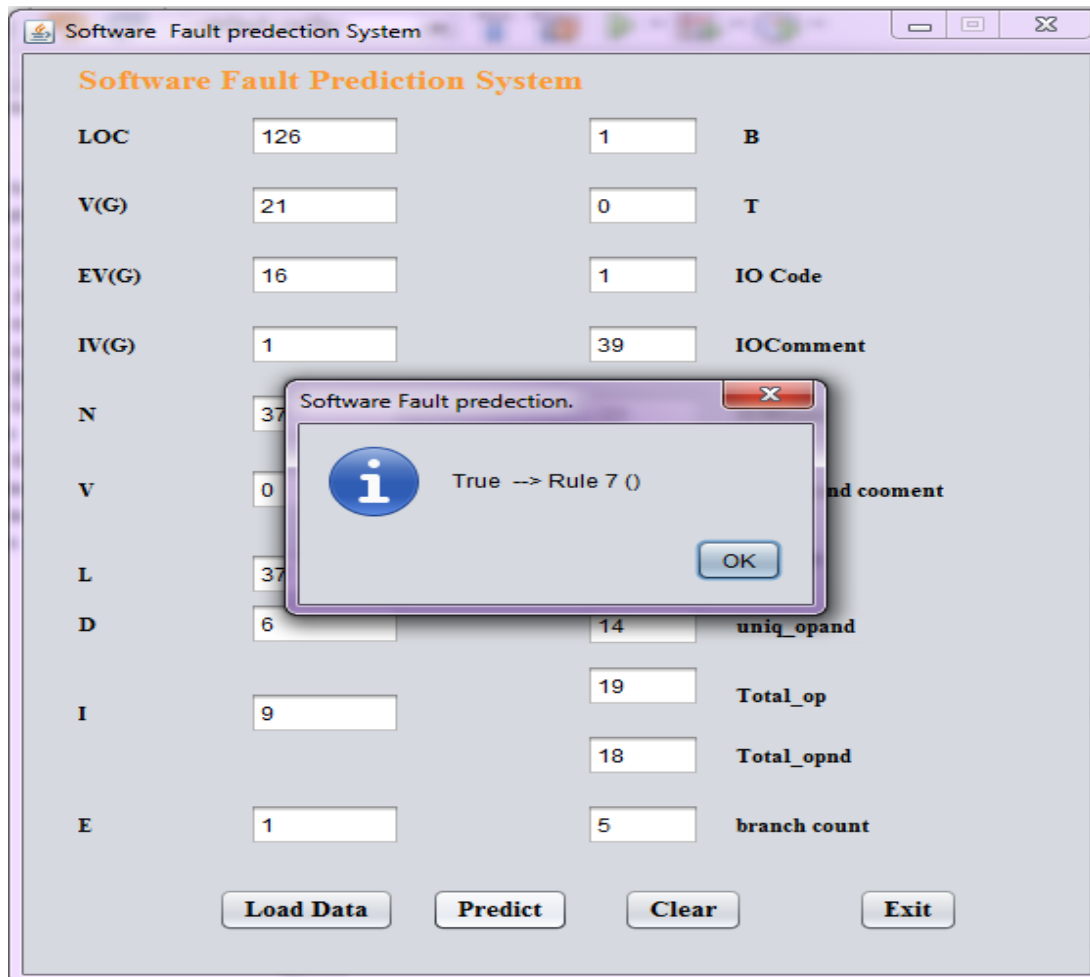


Figure 6: Software Complexity Prediction Prototype User Interface with sample result

## XVIII. Conclusion and Future Work

Now a day the development of software based system are increasing from the previous years due to its benefit. However, the quality of the system is required before it is delivered to end users. In order to enhance the software quality, we have various quality metrics such as software testing, CMM and ISO standards. Currently a Software testing becomes more and more important in the software reliability. Software defect prediction can effectively improve the efficiency of software testing and guide the allocation of resources. For the error-prone modules, we should spend more resource and time.

The primary objective of this study is to apply a combined machine learning algorithm for predicting software complexity in software products. This study attempted to extract useful predictive models from NASA MDP data set and developed graphical user interface for effective utilization of the developed model.

In this Study, the methodology was considering both single and combined machine learning approach. This research work has a total of 498, 10885, 2109,522 and 458 records and 22 attributes in order to predict software complexities. Noise removal and handling of missing values was done to prepare the dataset for experiments. For the purpose of building the model we were using machine learning algorithms such as decision tree, support vector machine, artificial neural network and combination of single classifiers using vote method. To evaluate the model accuracy 10-fold cross validation was used and rule with Accuracy, precision and Recall was used to evaluate the performance of the developed model.

J48 classifier generated model was selected as the best model that can predict the software faults. J48 decision tree generated 25 rules for predicting software Complexities data from which the researcher considered only 7 rules. The graphical user interface was designed using these seven selected rules. The development of graphical user interface in this study was using Java NetBeans IDE 8.0.2.

The model developed in this research work point out that extracting of the source code information before we test and maintains then applying the developed model in this research in order to determine whether the software product have faults or not.

The researcher recommends the following work for the future.

- Extend the model to more software repositories. During this study, we only used NASA Promise MDP data set and have not tested the performance of other repositories such as Eclipse, JEdit open source software data and AR data sets.
- Use more classifiers and more software metrics data set and maybe even better data pre-process method.
- Test the effect of attribute reduction on the performance of the selected machine learning algorithms and data sets.
- Experiment using other software metrics in addition to product metrics such as resource metrics.

## **References**

- Aleem, S., Capretz, L. F., & Ahmed, F. (2015). Benchmarking Machine Learning Techniques for Software Defect Detection. *International Journal of Software Engineering & Applications*, 6(3), 11-23. doi: 10.5121/ijsea.2015.6302
- Chayanika S, Sangeeta S, & S, R. (2013). A Survey on Software Testing Techniques using Genetic Algorithm. *International Journal of Computer Science*, 10, 381-393.

- Gray, D., Bowes, D., Davey, N., Sun, Y., & Christianson, B. (2012). Reflections on the NASA MDP data sets. *IET Software*, 6(6), 549. doi: 10.1049/iet-sen.2011.0132
- M. Saini , & Kaur, K. (2014). A Review of Open Source Software Development Life Cycle Models. *International Journal of Software Engineering and Its Applications*, 8, 417-434.
- M. SURENDRA , & GEETHANJALI, D. N. (2013). Classification of Defects In Software Using Decision Tree Algorithm. 5, 1332-1340.
- Malhotra, R. (2015). A systematic review of machine learning techniques for software fault prediction. *Applied Soft Computing*, 27, 504-518. doi: 10.1016/j.asoc.2014.11.023
- NASA from <http://promise.site.uottawa.ca/SERepository>
- SHICHAOZHANG, C. Z. a. Q. (2003). Data Preparation for Data Mining *Applied Artificial Intelligence*, 17, 375–381
- Shivaji, S. (2013). *Efficient Bug Prediction and Fix Suggestions* (PhD A dissertation ), UNIVERSITY OF CALIFORNIA
- Tao W, Weihua L, Haobin S, & Zun L. (2011 ). Software Defect Prediction Based on Classifiers Ensemble *Journal of Information & Computational Science*, 8(16), 4241–4254

## Potential Co-Targets of Isoniazid Identified through Proteome Interactome Network Analysis

<sup>1</sup>Tilahun Melak,<sup>2</sup>Sunita Gakkhar

<sup>1</sup>Department of Computer Science, Dilla University, Ethiopia, [the\\_melak@yahoo.com](mailto:the_melak@yahoo.com)

<sup>2</sup>Department of Mathematics, IIT Roorkee, India, [sungfma@gmail.com](mailto:sungfma@gmail.com)

### *Abstract*

*Tuberculosis (TB) continues to be a serious global public health problem by being the cause of morbidity and mortality of millions every year. This is mainly due to the emergence of drug-resistance varieties of TB. In spite of the implementations of several strategies, the resistance forms are still in rise and drug resistance remains the main threat. One approach to deal with the problem is preventing the emergence of resistance. Systematically integrated comparative genome, betweenness centrality measure and maximum flow approach have been used to identify potential co-targets of isoniazid. A drug-specific weighted proteome interaction network of Mycobacterium tuberculosis H37Rv has been used as interactome network dataset where drug targets of isoniazid were considered as source node and a curated list of set of genes involved in intrinsic and extrinsic drug resistance mechanisms as a sink node. Then, the flows from drug targets to resistance genes were calculated. The proteins were ranked according to their maximum flow value to the sink node. A subsequent of comparative genome and network centrality measures were carried out on the resulted proteins by aiming to obtain more reliable co-targets. List of proteins which have strong influence on the resistance genes were proposed as potential co-targets for isoniazid. These proteins are expected to be important input to experimental study which in the way could save considerable amount of time and cost of drug discovery.*

**Keywords:** *betweenness; drug-resistance; isoniazid; maximum flow; proteome network; resistance genes*

## Introduction

Tuberculosis (TB) is one of the main health threats by being the cause of death and illness for millions of people every year [1]. Isoniazid (INH) is a first line drug used to treat tuberculosis [2]. INH adducts (INH-NAD(P)) of the pyridine nucleotide coenzymes are the mycobactericidal agents of INH. These agents are generated in *vivo* after INH activation and they bind to inhibit essential enzymes. Isonicotinic acid hydrazide, the powerful and specific anti-tubercular effects of isoniazid, was discovered in 1952 and revolutionized the treatment of tuberculosis since then [2-5]. INH has continued to be one of the widely used drugs in the treatment of the disease. It is among the [World Health Organization's List of Essential Medicines](#) which contains a list of medications required for fulfilment of the bare minimum of a basic health system [6]. It has been used singly in prophylaxis or in a multi-drug combination with rifampicin, pyrazinamide and ethambutol for active infections. However, an eventual emergence of resistance has been a big challenge in the effectiveness of the drug for the treatment of the disease.

Various strategies ranging from rotation of antibiotic combinations to use of virulence factors as targets and 'phenotypic conversion', which aims to inhibit the resistance mechanism employed by the bacterium were implemented to counter the problem of resistance to TB [7]. But these methods are not effective enough to control its rise which indicates the requirements of new systematically designed strategies and more researches on the area [8]. As a new direction, understanding the ways by which resistance emerges upon during an exposure to a given drug and targeting the resistance mechanisms is believed to be an efficient approach to confront the problem at its source. Out of plenty of ongoing computational and experimental researches in tuberculosis, there are few which are focused on the emergence of resistance mechanisms and possible counter measures [8-10]. Raman et al. (2008), tried to identify possible pathways that may be responsible for generating drug resistance using proteome network of *Mycobacterium tuberculosis H37Rv* [8]. They identified controlling hubs within these paths and proposed potential co-target proteins as a new concept to counter the problem of resistance. Chen et al (2012), uses a random walk model on interactome network of *Mycobacterium tuberculosis* and

gene expression data to identify potential co-targets of Isoniazid and Ethionamide. The main drawback with the stated methods is that they are based on shortest paths without considering other paths that could be important in the communication of information between drugs and resistance genes.

In this analysis, systematically integrated comparative genome, betweenness centrality measure and maximum flow approaches have been used to identify potential co-targets of Isoniazid from protein-protein interaction network of *Mycobacterium tuberculosis H37Rv*. The comparative genome analysis was used to identify those proteins which are non-homologous to human to minimize host toxicity. The network centrality measure was used to filter out those proteins which are more central to the interactome network so that their inhibition would disrupt the communication among the proteins of the pathogen. Then, maximum flow approach was applied on the filtered list of proteins to prioritize them based on their flow in the maximum flow from targets of Isoniazid to resistance genes. The objective was to identify those proteins that are involved in mediating information between drug targets and resistance genes so that they can be inhibited through combination with primary targets to disrupt communication. This is believed to be a systematic way to prevent the emergence of resistance at the initial stage of drug discovery process.

## **Materials and Method**

### **Proteome network construction**

A weighted proteome interactome network of *Mycobacterium tuberculosis H37Rv* was constructed using a dataset retrieved from Search Tool for the Retrieval of Interacting Genes/Proteins (STRING) database [11]. Only a portion of the dataset with combined score value of pair of interactions greater than 770 were taken since it is more reliable [12]. The combined score value for the interacting pair of proteins was taken as the weight of the respective edge to quantify the possible flow [13]. For the purpose of understanding the general functional organization of interacting proteins, The resulted

proteome network were characterized by different network statistical measures such as; degree distribution, characteristic path length and clustering coefficient.

Drug targets of INH and resistance genes of *Mycobacterium tuberculosis H37Rv* were identified and connected to artificially created source and sink nodes respectively. Proteins involved in the whole pathway were taken as drug targets since metabolic adjustments often occur to minimize the effect of inhibition on the particular protein [8, 14, 15]. The list of proteins taken as drug targets is shown in Table 1. The curated list of genes, involved in both intrinsic and extrinsic drug resistance mechanisms of the pathogen, were identified from two published literatures [8, 10]. Out of the resulted list of resistance genes, only those which exist in the interactome network are considered (see Additional File 1).

Table 1. Drug Targets of INH

Isoniazid	Rv0340, Rv0341, Rv0342, Rv0343, Rv1483, Rv1484(InhA), Rv1592c, Rv1772, Rv1854c, Rv1908c(KatG), Rv1909c, Rv2243, Rv2245, Rv2247, Rv2428, Rv2846c, Rv3139, Rv3566c, Rv3795
-----------	--

### Maximum flow approach

The main objective of this analysis was to identify proteins that are involved in mediating information between drug targets of INH and resistance genes in the development of drug resistance so that these proteins can be used in a systematic combination with INH as co-targets to prevent the emergence of resistance. Maximum flow approach has been used as a main method to prioritize proteins based on their flow in the maximum flow between drug targets and resistance genes. The approach was effectively used by Yeh et al. (2012) to predict drug targets of prostate cancer from microarray data, disease genes and interactome network [16]. It has also been used in our recent work on further prioritization of potential drug targets of *Mycobacterium tuberculosis H37Rv* [17]. The classical combinatorial maximum flow problem has various methods of implementation including; network simplex, method of Dantzig [18,19], the augmenting path method of Ford and Fulkerson [20], the blocking flow method of Dinitz

[21], and the push–relabel method of Goldberg and Tarjan [22], [23]. We have used modified push–relabel method of Goldberg and Tarjan since it has practical superior computational time [24]. The modifications were applied to convert the problem into classical maximum flow problem [16]. Flows usually are uni-directional but edges in the protein-protein interaction network are bi-directional and the network is treated as undirected graph where there will be flow in both directions of an edge of interest. The weight of the edges connected to source and sink nodes is set to the number that exceeds the potential flow value which is the product of maximum degree and maximum capacity plus one instead of setting them to infinity for the sake of practicality.

Then, the weighted interactome network is redefined as graph  $G = (V, E, s, t, c)$  where  $V$  and  $E$  are node set and edge set respectively;  $s$  and  $t$  are distinguished source and sink node respectively; and  $c$  is non negative capacity of the edge. The flow  $f$  is defined as a real valued function on the edges which satisfies capacity constraints on all edges and conservation constraints on all nodes except the source and the sink [23, 24]. The flow  $f$  has to also satisfy skew symmetry constraint;  $f(v, u) = -f(u, v)$  for all  $(v, u) \in V \times V$ . The excess value  $e_f(v)$  is defined as the difference between the incoming and outgoing flows and a node  $v$  is said to be active if  $v \in V - \{s, t\}$ ,  $d(v) < n$  and  $e_f(v) > 0$ . An edge  $(v, w)$  is admissible if the distance  $d(v) = d(w) + 1$ . The residual capacity  $u_f$  of an edge  $(v, w)$  is the amount by which the edge flow can be increased without violating capacity constraint which is calculated as  $c(v, w) - f(v, w)$ .

The following four initializations have been made prior to computation of flows of proteins [23]:

$$f(v, u) = 0 \text{ for all } (v, u) \in (V - \{s\}) \times (V - \{s\})$$

$$f(s, v) = c(s, v) \text{ for all } v \in V$$

$$d(v) = n \text{ for } v = s \text{ and zero for all } v \in (V - \{s\})$$

$$e_f(v) = \begin{cases} \sum c(v, u) & \text{for } v = s \\ 0 & \text{for } v \in (V - \{s, t\}) \end{cases}$$

After initializations, repeated push and relabel operations were carried out on active nodes starting from the source node.

The *Push* ( $v, w$ ) and *Relabel* ( $v$ ) operations:

*Push* ( $v, w$ ).

Applicability:  $v$  is active,  $u_f > 0$  and  $(v, w)$  is admissible

Action: send  $\delta = \min(e_f(v), u_f)$  units of flow from  $v$  to  $w$ :

$$f(v, w) = f(v, w) + \delta; f(w, v) = f(w, v) - \delta$$

$$e_f(v) = e_f(v) - \delta; e_f(w) = e_f(w) + \delta$$

If  $w$  becomes active then add  $w$  to the rear of  $Q$

*Relabel* ( $v$ ).

Applicability:  $v$  is active and *push* ( $v, w$ ) can't be applied

Action: replace  $d(v)$  by  $\min\{d(w) + 1 | (v, w) \in E_f \text{ or by } n \text{ if } \nexists (v, w) \in E_f\}$

If  $v$  becomes active then add  $v$  to the rear of  $Q$

With gap relabeling heuristic, push and relabel operations have an enhanced performance because the problem of local relabel operation which makes the method to lose the global picture of the distances has been solved [24]. Gap relabeling heuristic is based on assumption stated as: let  $g$  be an integer whose value is between 0 and  $n$ , let us also assume at certain stages of the algorithm there are no nodes with distance label  $g$  but there are nodes  $v$  with  $g < d(v) < n$  [24]. This implies that there is no path from these nodes to the sink. So, the distance labels of these nodes are set to  $n$  and they will never be active.

The implementation contains a comprehensive iterative operation called discharge operation which consists of a repeated push-relabel and gap-relabel operations.

*Discharge* ( $v$ ) operation:

*Discharge* ( $v$ )

Applicability:  $v$  is active.

Action: let  $(v, w)$  be the current edge of  $v$ ;

$end - of - list \leftarrow \mathbf{false}$ ;

```
repeat
  if( $v, w$ )is admissible then  $push(v, w)$ 
  else
    if( $v, w$ ) is not the last edge on the edge list of  $v$ then
      replace( $v, w$ )as the current edge of  $v$  by the next edge on the list
    else begin
      make the first edge on the edge list of  $v$  the current edge;
       $end - of - list \leftarrow true$ ;
    end;
  until $e_f(v) = 0$ or  $end-of-list$ ;
if $end-of-list$ then gap relabel ( $v$ ) /  $relabel(v)$ ;
```

Queue Q was used to maintain active nodes and their order have been processed through First In First Out (FIFO) where the front node is selected for discharging and newly active node is added to the rear of the queue.

## Comparative genome

Through maximum flow approach, the maximum flow values of proteins were computed and those which have a flow value greater than zero were sorted. Subsequently, the sequence dataset of this ordered list of proteins was retrieved from Tuberculosis Database which is an integrated platform providing access to genome sequence, expression data and literature curation for tuberculosis research [25, 26]. BLASTp search of these proteins was carried out against the non-redundant database with an e-value threshold cut off set to 0.005 and restricted to *H. sapiens* [27]. The purpose was to filter out only those proteins, which do not have detectable human homology to prevent host toxicity.

## Network centrality

Betweenness centrality measure has been used to further filter the resulted list of proteins. This was carried out by aiming to numerically characterize the importance of proteins in

the biological system where the nodes that are more central in the network were expected to be distinguished.

Betweenness centrality is a measure of the total number of shortest paths between two nodes passing through the specified node. Therefore, betweenness of a node  $p$  is computed as;

$$B(p) = \sum_{s \neq p \neq t} \frac{\sigma_{st}(p)}{\sigma_{st}}$$

where  $\sigma_{st}$  is the number of shortest paths from  $s$  to  $t$  and  $\sigma_{st}(p)$  is the number of shortest paths from node  $s$  to node  $t$  passing through  $p$ .

Only proteins found at the centre of gravity of the proteome network were considered. For a protein to be said that it found at the centre of gravity of functional network of interest, its betweenness measure has to be above the total number of shortest paths expected to pass through it [28].

## **Data analysis and visualization**

The statistical property of the network was generated by Cytoscape 3.0.2 [29]. The betweenness centrality measure was computed by CytoNCA, a plug-in of Cytoscape [30]. The maximum flow approach was implemented using First In First Out (FIFO) push-relabel maximum flow with gap relabeling heuristic in c++. A graph obtained from an analysis by Schroeder et al. (2004) has been used for the purpose of proof of correctness [31].

## **Results and Discussion**

### **Interactome network**

Proteome scale interaction network of *Mycobacterium tuberculosis H37Rv* was constructed from a subset of SRING dataset consisting of protein-protein interactions

with a combined score  $\geq 770$  [11, 12]. Some adjustments have been made on the resulted network to convert it into drug (INH) specific weighted interactome network. The combined score values has been used as a weight of an edge between the interacting proteins. In STRING, combined score is computed using naïve Bayesian method by combining several pieces of evidence where higher score is assigned when an association is supported by different types of evidence, thus hypothesised as representing more flow between interacting proteins [32]. Sink node that connects drug targets of INH and source node which links all the drug resistance genes were artificially created. The redefined drug specific network contains 14,766 undirected interactions among 3,487 proteins. The statistical property of the network to depict its general characteristics has been computed and the result is shown in Table 2.

Table 2: Statistical Properties

Parameter	Value
Number of nodes (n)	3487
Connected components	106
Network diameter	15
Average number of neighbours	8.469
Network density	0.002
Characteristic path length	5.575
Clustering coefficient	0.379

Characteristic path length of the network, an average of shortest paths between interacting pairs of proteins, is small in spite of the network's size. It shows that the network is in compact form where the communication between any two vertices is possible through traversing only few steps. It is also smaller than  $\log(n)$ , where  $n$  is the network's size, which implies that the generated *Mycobacterium tuberculosis H37Rv* proteome interaction network is small world network. The shortest path length distribution of the network is shown in Fig.1. The network's clustering coefficient which shows local cohesiveness and internal structure of the given network is significantly higher than the *clustering coefficient* of a random graph with the same number of vertices

(0.002). Another important characteristic of a network is its degree distribution  $p(k)$  which is the measure of the proportion of nodes in the network having degree  $k$ . The network is a scale free network since its degree distribution approximately follows a power law  $p(k) \sim k^{-\gamma}$ , with  $\gamma=1.758$ . The corresponding degree distributions are shown in Fig. 2.

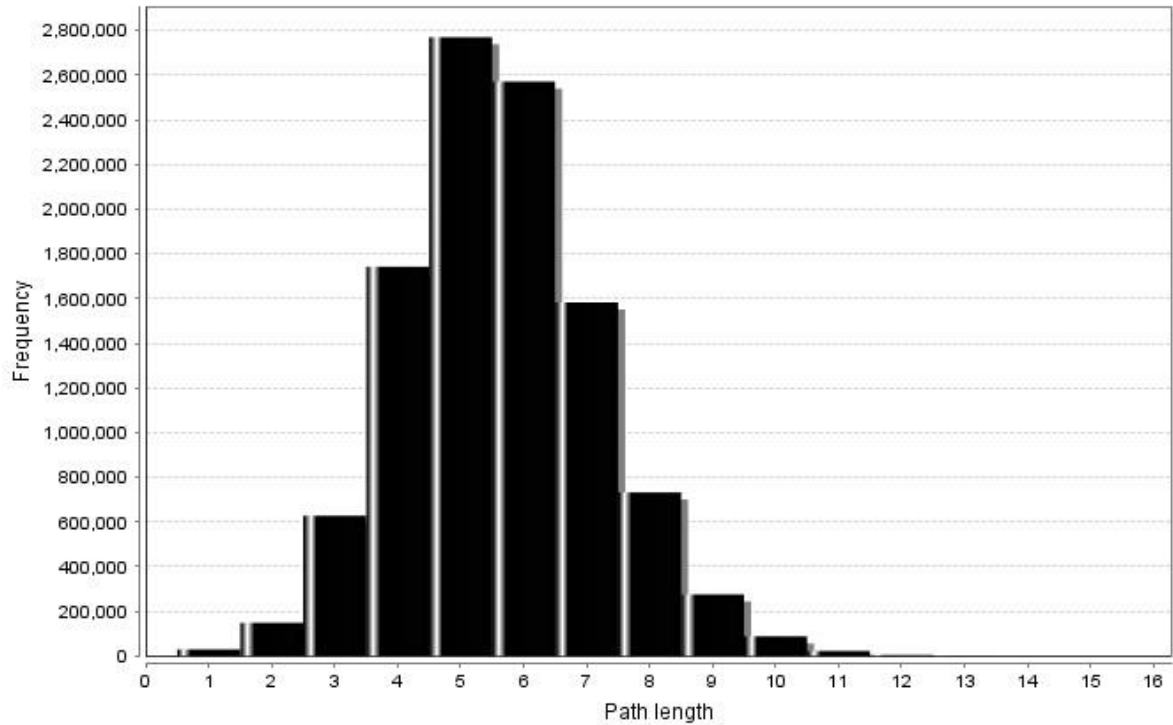


Figure 1. Shortest Path Length Distribution.

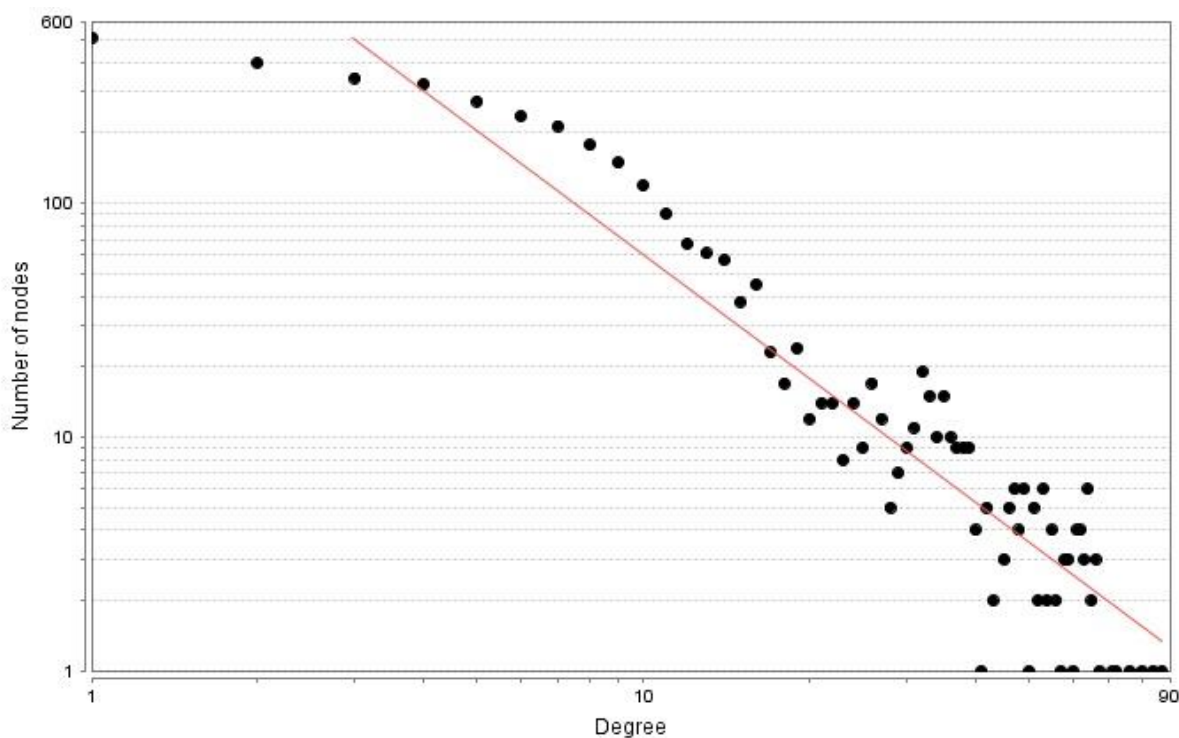


Figure 2. Node Degree Distribution.

### Potential co-targets

The main focus of this analysis is to identify and propose potential co-targets of INH through systematic combination of methods by aiming the inhibition of newly proposed targets with combination of INH will have a better success in dealing with drug resistance. Maximum flow approach is the main method used to identify and prioritize these proteins. The maximum flows of each protein in the flow from dummy source node to dummy sink node were computed to identify those proteins that are involved in the emergence of drug resistance. Flows are used to quantify structural and biochemical signals where a protein with a higher maximum flow value is hypothesized to be key in the development of drug resistance by being used as the main mediator of communication between drug targets and resistance genes. Proteins were sorted based on their maximum flow values. It has been observed that 2737 proteins have maximum flow value greater than zero. Only these proteins were considered for further analysis. A protein with

maximum flow value of zero means there is no flow that passes through these proteins to resistance genes, thus it is not involved in the development of resistance.

Even though the involvement of proteins in the development of resistance is the main criteria for identification of potential co-targets, comparative genome and betweenness centrality measure were carried out on the resulted list of proteins to increase their drugability. The comparative genome was used to filter out those proteins which are non-homologous to human where the possible side effects that will be caused by the proposed co-targets could be minimized. It is also more rational method than the common traditional drug discovery approach where the drug molecule is modified to avoid host toxicity. Subsequently, the betweenness centrality measures of the resulted filtered list of proteins were computed to identify those proteins that found at the center of gravity of interactome network. For a protein to be called it found at the centre of gravity of the interactome network of interest, its betweenness measure should be above the total number of shortest paths expected to pass through it, which is 19440.025. Proteins that found at the center of gravity of interactome network have been proposed as co-targets of INH to counter the problem of resistance. The list of these co-targets including detailed information of maximum flow values, essentiality, non-homologous and interaction with the host has been provided as Additional File 2. The top 10 potential co-targets are also shown in Table 3.

Table 3. Top 10 potential co-targets to counter drug resistance under the treatment of INH

<b>Rv number</b>	<b>Max-flow</b>	<b>Betweenness</b>	<b>Essentiality</b>
<b>Rv3316</b>	8639	42475.86	No-essential
<b>Rv0111</b>	6423	66460.61	No-essential
<b>Rv0033</b>	5682	76296.38	No-essential
<b>Rv0133</b>	5619	72768.63	No-essential
<b>Rv3552</b>	5333	47026.63	No-essential
<b>Rv1547</b>	5119	34472.22	Essential
<b>Rv2043c</b>	4439	100070.1	No-essential
<b>Rv3240c</b>	4099	20443.37	Essential

---

---

<b>Rv2938</b>	3825	34863.73	No-essential
<b>Rv2391</b>	3607	90561.54	Essential

---

## **. Conclusion**

Potential co-targets of INH have been identified and proposed through systematic integration of comparative genome, betweenness centrality measure and maximum flow approach. Comparative genome was useful for filtering out non-human homologous proteins at the drug identification phase so that possible side effects that can be caused by co-targets could be avoided in advance. Maximum flow approach is the main method used to identify and prioritize proteins that are involved in the mediation of information between the drug targets of INH and various resistance mechanisms. This has been done through computing the flow that can possibly pass through each protein in the possible communication between the stated two parties. The general idea is that if the mediator proteins could be identified effectively, they can be used to systematically design roadblocks for these communications, thus development of resistance could be prevented. Through betweenness centrality measure, proteins likely to be essential for the functioning of the system by serving as a bridge of communication between several other proteins in the network were filtered out to increase the success of identified co-targets. The final list of proposed proteins is hypothesised as reliable list that can be used in combination with INH to prevent the emergence of drug resistance.

## **References**

1. Chen et al.: Identifying co-targets to fight drug resistance based on a random walk model. *BMC Systems Biology* 2012, 6:5.
2. Argyrou A, Jin L, Siconilfi-Baez L, Angeletti RH, Blanchard JS. **Proteome-wide profiling of isoniazid targets in Mycobacterium tuberculosis.** *Biochemistry.* 2006 Nov 28;45(47):13947-53.
3. Bernstein J, Lott WA, Steinberg BA, Yale HL. Chemotherapy experimental tuberculosis. V. Isonicotinic acid hydrazide (nydrazid) and related compounds. *Am. Rev. Tuberc.* 1952;65:357–364. [PubMed]

4. Youatt J. A review of the action of isoniazid. *Am. Rev. Respir. Dis.* 1969;99:729–749. [PubMed]
5. Bloom BR, Murray CJ. Tuberculosis: commentary on a reemergent killer. *Science.* 1992;257:1055–1064. [PubMed]
6. World Health Organization: "[WHO Model List of Essential Medicines](#)". October 2013.
7. Tan YT, Tillett DJ, McKay IA. **Molecular strategies for overcoming antibiotic resistance in bacteria.** *Mol Med Today.* 2000;6:309–314. doi: 10.1016/S1357-4310(00)01739-1. [PubMed] [Cross Ref]
8. Raman K, Chandra N: **Mycobacterium tuberculosis interactome analysis unravels potential pathways to drug resistance.***BMC Microbiol* 2008; 8: 234. [PMC free article] [PubMed]
9. Chen et al.: Identifying co-targets to fight drug resistance based on a random walk model. *BMC Systems Biology* 2012, 6:5.
10. Padiadpu J, Vashisht R, Chandra N: **Protein-protein interaction networks suggest different targets have different propensities for triggering drug resistance.***Syst Synth Biol.* 2010, 4(4):311-22. doi: 10.1007/s11693-011-9076-5.
11. Jensen LJ, Kuhn M, Stark M, Chaffron S, Creevey C, Muller J, Doerks T, Julien P, Roth A, Simonovic M, Bork P, von Mering C: **STRING 8—a global view on proteins and their functional interactions in 630 organisms.***Nucleic acids research* 2009, 37: D412–D416. [PMC free article] [PubMed]
12. Zhou H, Wong L: **Comparative analysis and assessment of M. tuberculosis H37Rv protein-protein interaction datasets.***BMC Genomics.* 2011 Nov 30;12 Suppl 3:S20
13. Babaei S, Hulsman M, Reinders M, de Ridder J: **Detecting recurrent gene mutation in interaction network context using multi-scale graph diffusion.***BMC Bioinformatics* 2013, 14:29. doi: 10.1186/1471-2105-14-29.
14. Nguyen L, Thompson CJ: **Foundations of antibiotic resistance in bacterial physiology: the mycobacterial paradigm.***TRENDS in Microbiology* 2006, 14(7):304-312.

15. Mdluli K, Slayden RA, Zhu Y, Ramaswamy S, Pan X, Mead D, Crane DD, Musser JM, Barry CE III: **Inhibition of a Mycobacterium tuberculosis  $\beta$ - ketoacyl ACP Synthase by Isoniazid.***Science* 1998, 280:1607-1610.
16. Yeh SH, Yeh HY, Soo VW: **A network flow approach to predict drug targets from microarray data, disease genes and interactome network - case study on prostate cancer.***J Clin Bioinforma.* 2012, 13;2(1):1. doi: 10.1186/2043-9113-2-1.
17. Melak T, Gakkhar S. **Maximum flow approach to prioritize potential drug targets of Mycobacterium tuberculosis H37Rv from protein-protein interaction network.***Clin Transl Med.* 2015 Dec;4(1):61. doi: 10.1186/s40169-015-0061-6. Epub 2015 Jun 5.
18. G. B. Dantzig. Application of the Simplex Method to a Transportation Problem. In T. C. Koopmans, editor, *Activity Analysis and Production and Allocation*, pages 359–373. Wiley, New York, 1951.
19. G. B. Dantzig. *Linear Programming and Extensions*. Princeton University Press, Princeton, NJ, 1962.
20. L. R. Ford, Jr., and D. R. Fulkerson. *Flows in Networks*. Princeton University Press, Princeton, NJ, 1962.
21. E. A. Dinitz. Algorithm for Solution of a Problem of Maximum Flow in Networks with Power Estimation. *Soviet Math. Dokl.*, 11:1277–1280, 1970.
22. A. V. Goldberg. Efficient Graph Algorithms for Sequential and Parallel Computers. PhD thesis, M.I.T., Cambridge, MA, January 1987. (Also available as Technical Report TR-374, Laboratory for Computer Science, M.I.T., Cambridge, MA, 1987).
23. Goldberg A, Tarjan R: A new approach to the maximum-flow problem. *J. Assoc. Comput. Mach.* 1988;35(4):921–940. doi: 10.1145/48014.61051. [[Cross Ref](#)]
24. Cherkassky BV, Golderg AV. On implementing push-relabel method for the maximum flow problem. *Algorithmica.* 1997; 19:390–410.
25. Reddy TB, Riley R, Wymore F, Montgomery P, Decaprio D, Engels R, et al. TB database: **an integrated platform for tuberculosis research.** *Nucleic Acids Res.* 2009, 37: pp. D499–D508

26. Galagan JE, Sisk P, Stolte C, Weiner B, Koehrsen M, Wymore F, et al. **TB database 2010: overview and update.** *Tuberculosis*.2010, 90(4):225-35. doi: 10.1016/j.tube2010.03.010
27. Altschul SF, Thomas LM, Alejandro AS, Jinghui Z, Zheng Z, Webb M, et al. **Gapped BLAST and PSI BLAST: a new generation of protein database search programs.** *Nucleic Acids Res.* 1997, 25 (17):3389–3402.
28. Mazandu G, Nulder N: **Generation and analysis of large-scale data-driven Mycobacterium tuberculosis functional networks for drug target identification.** *Adv. Bioinformatics.* 2011; 2011: 801478.
29. Cline M, Nat P: **Integration of biological networks and gene expression data using Cytoscape.** 2007; 2:2366. [PMC free article] [PubMed]
30. Yu T, Min L, Jianxin W: **CytoNCA: a cytoscape plugin for centrality analysis and evaluation of biological network.** 2013.
31. Schroeder J, Guedes A, Duarte A: **Computing the minimum cut and maximum flow of undirected graphs.** Technical reports, Universidade Federal do Parana, 2004.
32. von Mering C, Jensen LJ, Snel B, Hooper SD, Krupp M, Foglierini M, Jouffre N, Huynen MA, Bork P: **STRING: known and predicted protein-protein associations, integrated and transferred across organisms.***Nucleic Acids Res.* 2005, 1;33:D433-7

## Demystifying the Nile Water Discourse

Wuhibegezer Ferede\*

\*Asst. Professor, Blue Nile Water Institute, Bahir Dar University, Ethiopia

E-mail: [wuhibegezerbdu@gmail.com](mailto:wuhibegezerbdu@gmail.com) Cellphone: +251-0989845211

### *Abstract*

*Historical linguistic and archeological evidences indicated that the Nile Basin had made rich contribution to world civilization. In addition to this advanced state of socio-economic development the basin is also dominated with tales and countless myths embedded in cultural core and the discourses of the society. Thus, this research had attempted to explore the epistemological foundations of the Nile water myths and their impact on the contemporary policy formulation and riparian dialogue for fair and equitable utilization of the river. Hence, the data collected from discourses such as ancient tales, archives, travel accounts, inscriptions, and decrees was analyzed using analytical and qualitative pluri-disciplinary approach through critical discourse analysis method. Accordingly, the basin was dominated with ethnocentric, creation, geographic, cartographic, migration and diversion myths which had direct impact on the Nile water utilization claims and counter claims. The impacts are manifested in the naming, the morphology, origin, discovery and in the quest of the ownership of the Nile water. The commutative effect of these myth driven assumptions are found as basic determinants of riparian dialogue. Thus, the demystification of the epistemological basis of the Nile water discourse by promoting water science is a demanding task for democratizing the utilization of the Nile water.*

**Keywords:** *Demystification, Discourse, Myths, Nile, Water*

## **1. Background**

### 1.1. Shared Past

Historical linguistic and archaeological studies have confirmed the **antiquity of the cultural and social diversities** in the Eastern Nile Basin (Ehret, 1995:236). There has been also **peaceful movement of population** within the region that resulted in population mixing, intercultural dialogue for mutual cultural enrichment/ synthesis, recognition and assimilation among Egyptians, Sudanese and Ethiopians (Erlich, 2000:305). Thus, on top of sharing similar physical space, the peoples in the region are linguistically and ethnically linked evincing a complex pattern of interrelationships and trans-state identity sharing. In short, all these states have shared social and cultural values emanating from centuries old tradition of interrelationships.

The commonalities entrusted from the veritable past are still surviving. However, the need of promoting what unites them in lieu of what sets them apart (Beshir, 1984:4) for addressing common challenges and competing needs has been a neglected concern because of the fenced mentality shaped by territorial states. Hence, the shared past should be taken as an opportunity for nurturing a spirit of mutual cooperation in the basin .

### 1.1. Synergetic Destiny

The fate of each state in the region has been inextricably intertwined with that of neighboring states. Indeed, no state in the Nile Basin and greater Horn of Africa has been insulated from the problems of the other states no matter how distant, no matter how strong or weak its. Hence, harnessing the shared values for promoting cooperation demands the revisiting of the preexisting socio-political fabrics which resulted in unceremonious relation specifically in the quest for democratizing the Nile question

## **2. Objectives**

### **2.1. General Objective**

Analyzing **structural and historical foundations** of the discourses obsessed with the nationalization of the **Nile water resources** as key determinant of riparian dialogue

## **2.2. Specific Objectives**

- Identifying how the **infusion of myths** in the Nile discourse impacted the riparian relation
- Indicating demystification strategies of the epistemological basis of the Nile discourse
- Explode vulgar **errors and weaken predispositions** to lay the foundation for change in the general way of thinking in the Nile water Basin.
- To indicate the significance of harnessing the shared veritable past for promoting cooperation among the Eastern Nile Basin States

## **3. Research Methodology**

### 3.1. Method

The method used in the research was plurali-disciplinary analytical interpolation, historical approach and discourse analysis.

### 3.2. Sources

Primary data: largely qualitative data was collected from archives, inscriptions, ancient coins, diplomatic correspondences, travel accounts, treaties, informants, public workshop, research reviews, conference papers, and magazine articles. Secondary data were also collected from conference papers, thesis works and journals.

## **4. Discussion of Results**

### **4.1: Invention of Pseudo-History**

The Nile Basin was the womb of some of Africa's oldest Civilizations such as Kemet, Meroe and Aksum that had left enduring legacies to the continent and the world at large. Out of these Civilizations, Egypt has often been mentioned as the progenitor of world civilization, the parent of the continent's history and the seat of ancient wisdom for ages (Browder, 1996:72; Beshir, 1984:3; Shavit, 2000:79&81). Consequently, many European scholars and statesmen used to refer Egypt as a book of history, one of God's great

monumental records, a birth place of literature, the cradle of science, the garden and garner of the world (Browder, 1996:72). According to Clarke the de-Africanization of the root of the Civilization of Egypt or Europeans' claim of the non-African origin of Egypt was deliberately designed order to downgrade the position of African people and annul their history in fear of revenge for their historic misdeeds (Clarke, 9 in Browder, 1996).

He further explained that disregarding the description and eyewitness account given by antique historians such as Herodotus, Homer, Plutarch and others confirming the blackness and nativity of Egyptian state to the continent, most European scholars branded it as a 'dark-skinned white' (Browder, 1996:16). This assertion had also won the heart of Egyptians who had consolidated the European painting through self-denial as it was manifested in the wordings of Aboul-ela during the Rameses II conference controversy in the US (Ibid). Therefore, in the words of Browder (1996:36), Egypt has mysteriously detached itself from the continent and floated off to a nebulous area of the Middle East.

Though the identification of the types of economic, social, and technological influences that have flown North or South wards is virtually incomplete, the myth that ancient Egyptian Civilization was white at best and mixed at least has dominated historical discussions about the continent for ages. Hence, counter arguments that claimed it as a pure African Civilization were discarded and branded as neurotic needs for inventing new pedigree (ibid, 17). Besides to racism, this assertion was clouded with a wrong assumption that narrowed the Nile Valley Civilization to the mouth of the Nile because the Nile Valley Civilization embraces a land mass that extends over 4000 miles into the body of Africa and touches multiple civilizations (Ibid, 9).

According to Clarke, the area which is designated as Egypt by the Greeks was a misnomer for it was rather a composite of a number of nations which used the Nile as the world's first cultural highway (Ibid). The other most often silent issue which falsifies the claim is the fact that the rehearsal for what's referred as Egypt by Europeans rooted from the South, from the presented states of Ethiopia, Sudanese

republic and the adjacent territories(Ibid). Therefore, the civilization at the mouth was the outgrowth of the culture that develops upstream (Ibid, 45).

Therefore, much recent archaeological evidences such as the finding at **Kerma** and Hadar in the Northern Sudan and Ethiopia respectively suggest that the pedigree of Egyptian civilization was evolving in the South (Browder, 1996:11). In this respect, Haggai Erlich (2000:305) argued about the process of intercultural dialogue for mutual cultural enrichment, misconceptions and conflicts among Egyptians, Sudanese and Ethiopians instead of identifying the primal center. But he didn't deny about the existence of multifaceted and complex intercultural relations among these states centering on the Nile River.

Clarke eloquently argued that the parent **of the Egyptian civilization came from the Southern** part of the Nile Valley Civilization (Browder, 1996:11). The primacy of the South in hosting the first organized society and as well the establishment of a mining complex which is older than even the appearance of Egypt itself are some of the basic evidences he mentioned to substantiate his argument (Ibid). Hence, this eminent scholar has shattered the fundamental precepts of the Nilotic Theory or the hyper African paradigm that posits Egypt as parent of the cultural and historical achievement of the peoples of the continent.

This finding is also supported by the US based researcher,Houston (1926). Quoting the work of Diodorus Siculus, she explained that 'Egypt was formed of the mud carried from Ethiopia, [the place where] the first men that ever lived, the only truly autochthonous race and the first to institute the worship of the gods and the rites of sacrifice found (Ibid: 17). She also mentioned that Ethiopia was mastering Egypt as its colonial possession. It's a very simple logic to talk about the primacy of the Southern/Upper Nile valley civilization over the downstream civilization of 'Black' Egypt having in mind the notion that 'water is mother of all things.' Nevertheless, the idea of having single root of human culture is highly contested by scholars who advance the idea of historical particularism.

However, this assertion in turn is strongly defended by Universalists who claim about single root of humanity as of the creation narratives (Noor Bergen, 1977: 10-30).

Moreover, scientific investigations highlighted that life originated in Aqua. In this regard, Ethiopia is source of Nile which is assumed as primal center of hydrolysis and root of humanity due to the presence of Lucy. This assertion and the various pre-historic paleoanthropology and archeological findings such as Lucy are suffice to identify Ethiopia as Cradle of humanity and world civilization.

In addition to the above mentioned findings, the genetic and fossil evidences discovered so far show that the Horn was the original homeland of human race (Browder, 1996:14; Bashir, 1984:3). Therefore, due to the availability of all mitochondrial lineage diversities, in fact, with the exception of the daughter of single lineage along with archaeological findings such as the 1974 discovery of the human skeleton of Lucy at Hadar in Ethiopia (Jean, 1959:222), the scientific community has designated Ethiopia as a cradle of humanity and its prehistory (Paulos, 2004:103-107; Munro-Hay, 2002:17; Pankhurst, 2000: 1; Isichei, 2000: 23&31).

This finding indicates that the peopling of the Nile valley was effectuated as a result of wave of migration from south (Shavit, 2000: 79 &81). Thus, it consolidates the down river theory and the prehistoric human migration, cultural diffusion and transmission from the South to the North (Ibid: 91). Therefore, it's safe to conclude that the Nile Basin was workshop of social and cultural engineering. In this regard, eminent local scholars such as Getachew Haile, Loraet Tsegaye Gebre Medhin, Teshale Tibebu, Milikias Paulos and Bahru Zewde identified the epistemological plunder committed by the West in reference to the preeminence of the Orientalists Semiticist intellectual tradition (Erlich, Ethiopia and Middle East, p.3) in the writing of the history of Ethiopia. They defended the normative explanations of this tradition, yet their contribution towards the identification of Ethiopia as primal incubating center of the Nile Valley Civilization is complicated with the divergent self-identification of the pioneering people in the respective geographic entity.

This prognosis doesn't mean that the works of these eminent scholars such as Haile W/Michael and Loraet Tsegaye is naïve as the works of some of their contemporaries who failed in the trap of a counterproductive task of ethnicization and reproduction of the

racist Euro-centric history at subsidiary level through further alienation of the subject from its history.

Hence, mentioning their works is worthy for consolidating the arguments of Noorbergen, Clark, Houston and for de-ethnicizing the works of the contemporary academic prostitutes. Though most of his ideas initially identified by Clarke, Haile W/Michael (1984:4-5) eloquently argued about the primacy of the Nile valley civilization in the historical development of world civilization. In fact, Haile borrowed ideas from Clarke's finding in enlisting the conception of religion, art of writing, domestication, irrigation and water transport as the primary innovations of the peoples of the Nile valley. Moreover, he didn't strictly indicate whether the origin or the pedigree of the Nile valley civilization is upstream or downstream. Unlike him, Clarke stated that the Nile valley civilization which embraces Egypt and the geographical region that extends over 4000 miles in to the body of Africa and touches multitude of civilizations at the present map of Sudan and Ethiopia.

According to the classic Egyptologist Tsegay<sup>1</sup>, Africa pioneered the world not only being cradle of humanity but also cradle civilization. The beginning of writing system, music, art, carving all goes to the content. This claim is basically supported due to the dependence of the antiquity historians who were writing about the world on the Cushitic Civilization before the rise of the Greco-Roman civilization. Unlike Haile, Tsegay has vividly indicated the very root of the continental and the global civilization. Therefore, the authors of this book share the findings of these two scholars that recognize Ethiopia as the parent of Black Egypt for it was the creation of Nile, Ethiopia's offspring. However, the contemporary Egyptologists and some Universalist might brand us as someone who is contracted with neo-neurotic need of inventing an ethno-centric civilization pedigree.

In the future, the decoding of the mysterious Meroitic writing and advanced archeological research around the source/s of the Nile could also enable us better understand about the direction of the flow of history and culture along the Nile River. However, the primacy of

---

<sup>1</sup>Tobia Vol.5 No.3, 1989

the Southern/Upper Nile valley civilization over the downstream civilization of Egypt would not be disputed unless another pioneering cradle of humanity is found in the southern part of the Nile valley

## **4.2. Infusion of Myths**

### **4.2.1. Water Myth**

Historical records indicated that the ancient Egyptians were worshiping the Nile, Hapi (Beshir, 1984: 2&55). As part of the ritualization ceremony, they composed rites. The hymn which is believed to be composed around 2100 B.C dedicated to the Nile shows the deep religious feeling it evoked (Long core *et'al*, 1999:119). Like the Egyptian sun-god this stream was revered in Meroe and Aksum. In Sudan, it was connected with beautiful Huri and Ginn devils (Beshire, 1984:3). Some Alexandrian Bishops invested their labor to turn myths into a core cultural identity of the Ethiopian society. They were serving as emissary for the enculturation of Ethiopian society with the veneration and fear of streams whose imprints felt everywhere in the country still today.<sup>2</sup> Still today, there are peoples who slaughter oxen, throw coins, pay tribute and provide sacrifice to rivers including Blue Nile, Abbay. The peoples living in Debre ziet and its vicinity believe in the existence of Lucifer in Hora and Besheftu lakes. There are lots of lakes and streams which are either reverend or feared in Tigray. In the city of Mekelle alone, at least four local small streams referred as the abodes of devil and no one fetches a droplet while the society is suffering from extreme shortage of water.

### **4.2.2. Creation Myths**

The ancient Egyptians had also creation myths that attribute the origin of the world to watery chaos. According to this myth, the sun is described as a god having risen from this chaos.

### **4.2.3. Osiris Myth**

The most celebrated Egyptian myth is related to the resurrection of the man-god Osiris (Shavit, 2000:80). The legend attributes Osiris to the spirit of the deceased pharaoh who

---

<sup>2</sup> However, this assertion needs further multidisciplinary study

had been murdered by a jealous brother called Seth. This myth attributes the origin of the Nile from the tears of Isis when she mourned the death of her husband (Beshire, 1984:2). The Nile is viewed as both earthly and divine in the cosmological explanation about its creation. These beliefs has sealed all forms of Egyptian life with myths as it's vividly depicted in the adoration dedicated to it (Thatcher, 1907; Shavit, 79; Hanscom *et al*, 1967:28-29).

Besides, the adoration for the Nile is very special reminder that turns the river in to a caring only for Egyptian. Due to this hegemonized, visible sacred being and politicized mythology embedded in to the cultural core, the Egyptian begin to misconceive the Nile as the sole gift and sacred husband of Egypt alone while its intrinsically polygamous husband that had concluded legal marriage with twelve riparians since time immemorial. The Egyptians were also celebrating the arrival of the Nile floods, the sign of their hope, through burning of frankincense, human and animal sacrifice (Beshir, 1984:2). It's vividly indicated in the last four lines of the adoration dedicated to the Nile as:

Oxen are immolated to thee,  
Great festivals are instituted thee,  
Birds are scarified to thee,  
Gazelles are taken for thee in the mountain,  
Pure flames are prepared for thee (Thatcher, 1907; Shavit, 2000:79; Hanscom *et al*, 1967:28-29)

#### **4.2.5. Geographic Myth**

The Egyptians also hold geographic myth which took the South to North flow of the Nile as natural course of all rivers (Shavit, 80). The flow of the Nile from the high mountains in the south to the Mediterranean in the North crossing the desert contrary to its bearing on a map has resulted in this geographic myth in the minds of Egyptians. Thus, Egyptians aspired to undo "wrong" flow of other rivers.

#### **4.2.6. Ethnocentric Myth**

Ancient Egyptians usually regard their neighbors as uncivilized forces threatening to overwhelm the Egyptian Nile Valley (Phillips, 1997: 423; Braines & Malek, 1980:36-37).

Besides, the adoration symbolizes Nile as inexhaustible creator of all good things, master of energy and life but docile to Egypt. Hence, Egyptians whose life is a gift of this symbolic hegemony, cultivated the sense of superiority through self-association. However, the production, reproduction and continuity of this position was demanding the accomplishment of two fundamental tasks. The first was process of camouflaged defilement followed by placing the self on the throne of the disillusioned entity. These two basic processes can be clarified by taking a comparative look of ‘historic Ethiopia’ and Black Egypt.’ Here I would like to pose some important questions:

- Was there Egypt before Lucy and the Nile?
- Was there a time where there were no both Nile and Egypt but historic Ethiopia?
- Is the annexation and the administration of the lower course of Nile by historic Ethiopia a pseudo-science or a genuine history?
- Does this mean that there was hegemon in the upper basin of the Nile before the rise of the hegemon downstream?

Therefore, myth driven hegemony and the asymmetric production-consumption relation has played significant role in figuring out the contemporary popular perception towards the Nile water sharing arrangements and the process of establishing an inclusive and efficacious water regime. Falling in the trap of this myth, any quest for water or benefit sharing arrangements that challenges hitherto water use arrangements over the Nile is often branded as an affirmation indiscriminate killing of all Egyptians. Accordingly, Egyptian hegemony over the history of the entire continent and as well in the appropriation of the Nile water was initially crafted using such symbolic mythologies.

This mindset refutes even to differentiating tolls of death caused by tangible acute starvation from the discourse of death due to allege thirsty. They had hardly observed the souls and the cries of the starved peoples of the Nile Basin in the floodplain on which they have been growing their cereals as it’s reflected in their popular poem (Petros, 2010:4). This myth constituted hydro hegemony and historical idiosyncrasy that favors the favored was not practically challenged in spite of some insights produced by eminent

water scientists. The explanations for such failures often go to the preoccupation of the upper basin states on the destructive legacies of colonialism.

#### 4.2.7. Hellenistic and Roman Myth

The early Greco- Roman expedition/conquest was inspired by the ‘Mount Everest of Rivers’. Before the great geographical discoveries Africa was ‘Darker Content’ to the outside world. Its peoples were represented as hydra headed monsters and strange creatures & map makers represent the continent with clouds. Early Greco-Roman expedition/conquest/ ended with the representation of the river as ‘male god’ and with wrong geographic location and cartographic representation. This myth made Nile the sole gift and sacred husband of sardonic Egypt. Therefore, for the Egyptian minds versed with theses mythologies, any request for water or benefit sharing arrangement was constantly nullified (Tesfaye, 2001:83).

### **4.3. Projecting Ideational Power using Social Institutions**

#### **4.3.1. Religious Institution**

##### **4.3.1.1. Contested Date of the Christianization of Ethiopia**

Egyptians were well aware of the role of religious institutions for realization of their hegemony over the Nile long before their imperialist military encroachment of the Horn of Africa. Religion has served for figuring out the Ethio-Egyptian relations since the 4<sup>th</sup> century A.D which is usually cited as the beginning of the Christianization of Ethiopia (Bahru, 2002:8; Munro-Hay, 1991:69).

However, the reason that made the psyche, the body and the mind of Ethiopians subordinate to the dictation of the Alexandrian Bishops for about 16 centuries is hardly examined due to the acceptance of the normative explanations about the date of the Christianization of Ethiopia as for granted. The normative historical dating of the Christianization of Ethiopia is bereft of empirical evidence and most often refuted by the contemporary traditional scholars.

Some scholars refer back to the first century arguing either on the basis of the conversion of Bacos, the treasurer of Queen Candace (Eusabius, 1887) and the two paintings in St. Mathew Church of Italy which narrates about the presence of St. Mathew in Ethiopia.

Historians usually cite the trilingual inscription of Ezana. Disregarding the debate on the issue of its credibility, the narratives produced out of it couldn't address the fallacy of generalization if we ask the question 'how could it be possible to talk about the Christianization of the entire state merely because of the conversion of its leader. In this regard, the date of the total conversion of the broad mass can't be perfectly the same as the date of the conversion of the imperial man.

The account of Rufinius is the second source of historical relevance but it's also dominated with self-contradicting narratives. Rufinius's description about the wrecked ship and the appointment

St. Frumentius as head of the Ethiopian Church by Egypt contradicts with Ezana's inscription and as well with his own account which narrates about the coming of St. Mathew to Ethiopia in the first century following the drawing of apostolic lots. Denying the then 'Ethiopia' an access to Christianity for about 300 years while its neighbor Nubia embrace it in the first century looks anomalous. This limit of historical reasoning is probably due to the epistemological plunder made Egypt for ensuring its ideational hegemony for securing a bargaining power, patriarchal authority.

#### **4.3.1.2. The Alexandrian Patriarchal Hegemony**

The development of religious nationalism was crippled and the quest for autocephaly silenced through the infusion of frightening myths and in few cases with the application of coercion and Nicaean Creed. Mandated by the Fetha Nagast and the apocryphal canon of the Nicaean Creed, every head Bishop of the Ethiopian Church was appointed by the Egyptian Patriarch in Alexandria until 1959. This claim is vividly indicated in Fetha Nagast as follows:

ወሰብእኢትዮጵያ እያህረው ላዕሌሆሎ ለቀዳሳ ሳንታኒም ራኒሆሎ ወኢበስም ረተርዕሰ ሙእስላም ጳጳሳ ሳንታኒም ረተርእሶ ሙእስላም ጳጳሳ ሳንታኒም ይኸውን እምታሕተእደሀለበአለእስክንድርያ ወደላቱ ዘይደልዋይህም ላዕሌሆሎ ቀእምሀቤሀዘደእቱ ሙትሕተሊ ቀዳሳ ሳንታኒም (Fetha Nagast, 1990:30)

(lit. trans.)

Ethiopians are not allowed to be assigned as Patriarchs from their own for they are under the suzerainty of the Alexandrian See, and therefore, it's only the Coptic fathers who can hold the position with exception of ranks below Arch Bishop.

In its earliest form, the Fetha Nagast predates the Nicaean apocryphal canon. This fact indicates that the prohibition of the appointment of Ethiopian citizens as heads of its Church is rooted in the original version of the Fetha Nagast than the Nicaean Creed (Mahoney 1994:77).

Astoundingly, the relaxation of some of the prerogatives and even the complete abrogation of the creed coincides with the signing of the two basic Nile water agreements of 1929 and 1959. In 1929, Egypt send three Bishops and in 1959 they acknowledged the sovereignty of EOTC. Why they breach the principles of the unbreakable creed, which was kept intact for 1600 years?

The grant of independence was designed to deafen the ears of the Ethiopian mass including the statesmen from hearing the news of the conclusion of 1959 Nile Water agreement by deflecting their attention to the joys of the spiritual independence.

#### **4.3.2. Political Institution: Politicization of Religious Authority**

Alexandrian Bishops were entitled with the ultimate power to decide on the legitimacy of the political figureheads that can rule the country. Ethiopian monarchs were anointed by Coptic Bishops who were even held sway in courts. The popes were also active in deposing kings.

They instigate a protest against rulers of the country such as Atse Lalibela, Tewodros IV and Leji Iyassu. They were serving both as political and spiritual representatives (Paulos, 2005:243) and as well as an important bargaining chip for Egypt in times of misunderstanding. Thus, disguising themselves in the question of the Church, the Egyptians were intervening in the internal political affairs of Ethiopia. For instance, after

the defeat of Dejjach Wube at the battle of Deresege, the captive Abune was affiliated with Tewodros IV and anointed him in his coronation in return for enforcing the Tewahido doctrine (Bahru, 2002). Though Tewodros IV came up with a strong belief of defeating the 'undefeatable' and attaining state power by crushing the squabbling noble of the era of princes by dint of his power, yet he couldn't escape the established trap for securing political legitimacy through the blessing of the Egyptian Abune.

Eventually this mutuality declined and ultimately Tewodros found himself beset in an opposition of priests spearheaded by the Abune. This can be inferred from the 'imprisonment of Abune Selama at Meqedela' (Paulos, 2005:46). Though in most cases the Church opposition against Tewodros IV narrated as internal contradiction between the modernization project of the state and the Church resistance against the program, the opposition was initially an outside driven and initiated by Abune Selama, the agent of the Egyptian policy, in response to Tewodros's obsession against them and suspicion about the damming of the Nile as part of his economic modernization program.

This engrained mentality of the reigning kings that valued anointment for the attainment of political legitimacy rather than the will and the aspiration of the people has cost the country high due to internal strife to capture the throne and the Abune. The horrific atrocities witnessed in such wrangling could inspire anyone to ask the question 'how spiritual father that works for the celestial kingdom legitimize political power secured by bloodshed? It's also perplexing why the Ethiopian rulers who were fighting Egyptians at the coast, allowed the Bishops to do whatever they want in the hinterland.

#### **4.3. 3. Influencing the Educational System**

Egyptians were the pioneering staffs and administrators of the Ethiopian modern/western education since its onset. Their involvement in the school system was facilitated due to EOTC's opposition of the European type of schooling under the auspice of white tutors on account of suspecting religious conversion/ proselytization of the students.

#### **4.3.4. Imposing Non-Efficacious Water Treaties**

The critical examination of the water treaties signed from 1890s to 1960s bring to light numerous legal defects associated with fraud, coercion, neglect of the relative effect, lack of reciprocity, exclusivity and the deficiency of many of the precepts of the international law (Wuhibegezer and Sheferawu, 2014). Moreover, the lower riparian states' advocacy for the succession of colonial treaties, which is branded as the re-affirmation of colonialism, is found to be incompatible with the principles of the clean-slate theory adopted by the upper riparian states (Ibid).

#### **4.3.5 Exogenous Factors**

The Egyptian hegemonic position in the Nile issue was facilitated by its greater ideational power, technical and bargaining capacity, military might, and access to international political and financial support. The combined effect of all of these elements in turn enabled Egypt to influence the knowledge production for shaping a hegemonic discourse. In addition to the internal situation, the global competition for patrolling the Red Sea traffic and the passage to the Indian Ocean /Suez Canal/ which made the Horn of Africa a bone of contention has also granted it preferential position in the power alignment

#### **Conclusions**

Egyptian hegemony over the history of the entire continent and as well in the appropriation of the Nile water was initially crafted using symbolic mythologies. This myth constituted hydro hegemony and historical idiosyncrasy that favors the favored was not practically challenged in spite of some insights produced by eminent water scientists. Therefore, unchaining or convincing the Egyptian mass from the disoriented and wrongly programmed mindset by power and academic elites through a continuous discourse of death toll due to alleged thirsty, needs heavy investment and neutral knowledge production. The ingrained thought patterns encoded in the minds of Egyptians and as well as Ethiopians entrusted from the antecedent to the subsequent through the cultural fabrics demands demystification. The myths can be fired by promoting positivism because it was positivism that had shaken the unquestionable ecclesiastic orthodoxy and nostalgic

love of mythology in medieval Europe. Thus, the emancipation of this mindset from the thralldom of past mythologies and prejudiced perspectives needs to get utmost priority.

Therefore, unchaining or convincing the Egyptian mass from the disoriented and wrongly programed mindset by power and academic elites through a continuous discourse of death toll due to alleged thirsty needs heavy investment and neutral knowledge production. Of course, it couldn't be as such difficult to differentiate pseudo death claims due to water stress when upper riparian's take a sip of water from a recurrent actual death due to acute starvation. These ingrained thought patterns encoded in the minds of Egyptians entrusted from the antecedent to the subsequent through the cultural fabrics demands a definite demystification for ensuring the de-politicization and re-Africanization of the issue of the Nile water. The myths can be fired by promoting positivism because it was positivism that had shaken the unquestionable ecclesiastic orthodoxy and nostalgic love of mythology in medieval Europe. Thus, the emancipation of this thought pattern from the thralldom of past mythologies and prejudiced perspectives needs to get utmost priority.

### **References**

A.M. Ibrahim (1984), Development of the Nile River System In: M.O. Beshir, *The Nile Valley Countries: Continuity and Change*. Institute of African and Asian studies: University of Khartoum, Sudanese Library Series No.12

Fetha Nagast (1990), Part One : Chapter ፲፮ /፲. Tensae Printing Press

Garretson, Albert (1967), "The Nile Basin," in: Albert H. Garretson et'al (eds.), *The Law of International Drainage Basins*. New York: Oceana

Haggai Erlich and Israel Gershoni (2000), *THE NILE: Histories, Cultures, Myths*. USA &UK: Boulder, London, Lynne Rienner Publishers

Haggai Erlich, (2000), "Identity and Church: Ethiopian-Egyptian Dialogue, 1924-1959." *International Journal of Middle East Studies*. Vol. 32, No.1, 2000

...(2002), *The Cross and the River: Ethiopia, Egypt, and the Nile*. Lynne Rienner Publishing, Inc

Kevin O'Mahoney, M Afro (1994), *The sprite and the Bride, Manual of Church History, Book One*. Ethiopia; United printers, AA

Mersea Hazen Wold Qirkose (1964), *Yethiopia Betkerstian: Ymejemerawu Patriyariik*. Berhanena Selam Printing Press, A.A, 1964

Oliver J. Thatcher (1907), *The Library of Original Sources*. Milwaukee Wisconsin University Research extension cac,

Omer Mohammad Ali Mohammad (1984), *Conflict and Cooperation*: In, M.O. Beshir (ed.), *The Nile Valley Countries; Continuity and Change*. Institute of African and Asian Studies, University of Khartoum, Sudanese Library Series No.12, V.2

Paulos Milkias (2004), *Shattering the Myth: Why Ethiopian Civilization is African not South Arabian*. *An Independent Journal of the Horn of Africa*, V. 23

Samuel Sharpe (1963), *Egyptian Mythology and Egyptian Christianity*. London

Yaacov Shavit (2000), *Up the River or Down the River? An Afro-centrist Dilemma* In: Haggai

## **Does Innovation improve the productivity of firms in least developed countries? Evidence from Ethiopia's Enterprise Survey**

**Abdi Yuya Ahmad**

Adama Science and Technology University, School of Humanities and Social Sciences

Email: [yuyabdi@gmail.com](mailto:yuyabdi@gmail.com) Cell phone: +251912290039

### ***Abstract***

*There appears to be an empirical regularity in literatures about the positive productivity effect of innovation, mainly, by firms in emerging and developed countries. This paper examines if the same holds for firms in Least Developed Countries (LDCs), specifically, in case of Ethiopia. The analysis is based on two waves of World Bank's enterprise survey (2011 and 2015) which include firms in the manufacturing, service and construction sectors. Due to the potential causalities between innovation and productivity, a combination of parametric (linear regressions with endogenous treatment effect) and non-parametric (Quantile regressions) methods are applied to analyze the data. Results show that both product and process innovation have strong positive effect on labor productivity after controlling for firm heterogeneities in terms of age, size, ownership, market orientation and sector affiliation. However, only the effect of product innovation remained robust when productivity is measured in terms of growth instead of level. Up on accounting for the likely impact of labor productivity on innovation, both the Average Treatment Effect (ATE) and the Average Treatment Effect on the Treated (ATET) turned to be similar with the baseline results. Investment in R&D and new fixed capital are the most important variables in raising the likelihood of firms to innovate. Results from the quantile regression indicate that the importance of innovation for labor productivity declines with the productivity quantile while the role of human capital increases with the productivity quantiles. Similar to the earlier, findings from this method are more robust for product innovation than process innovation when productivity is measured in terms of growth and level. The overall result suggests that the current dismal productivity of labor in Ethiopia would be improved if firms can manage to introduce new product and new process in their lines of operation.*

**Keywords:** Ethiopia, firms, productivity, innovation, treatment effect, quantile regression

## **1. Introduction**

The great challenge for least developed countries (LDCs) around the globe is to build a dynamic economy that can cope with the growing competition arising from globalization. This rests on the extent to which countries build local technological capabilities and transform their economies in a way that resources are moved from less productive to more productive sectors such as manufacturing and services. In other words, there is a need for structural change that eases countries' reliance on primary sector and building foundation for broad-based growth and economies that respond to incentives. McMillan and Rodrik (2011) indicated that countries that generate the largest proportion of export earnings from primary commodities (Latin America and Africa) were not successful in structural change. There are ample evidences that show East Asian countries have succeeded due to their capability in diversifying their economies away from primary products and improving their technologies in manufacturing and service sector (Wade, 2009). At the center of the success stories is innovation and technological progress which are also recognized by endogenous growth theorists (Romer, 1990, Aghion and Howitt, 1992; Grossman and Helpman, 1991) and Schumpeterian economists as the basis of cross-country differences in per capita income. Advancement in technology is the major driver of productivity growth in developing countries and increased opportunity to catch-up developed countries.

On this ground, Ethiopia is struggling to improve productivity growth through accelerating structural change that brings manufacturing industry at the forefront so that it would contribute the largest share to the national economy. However, the industry has never shown improvement while service sector has been growing over the last two decades. The main cause of the industry's poor performance has been associated with low labor productivity (World Bank, 2009, 2015). It was indicated that Ethiopia's high potential in attracting labor intensive manufacturing owing to the availability of cheap labor has been overshadowed by low labor productivity. Evidences suggest that innovation can solve the problem of low labor productivity through enhancing effective use of productive inputs, generating new ideas that can develop into new products, new

processes new management and new marketing techniques. Ample empirical evidences exist in support of this, mainly from advanced countries. For example, Griffith et al. (2006), Mairesse & Mohnen (2010), and OECD (2009) among others found positive strong relationship between R&D, innovation, and productivity of firms.

However, there are no adequate evidences in African context. Partly because of the widely prevailed believe that innovation does not exist in least developed countries and partly lack of appropriate data to conduct research. The first misunderstanding emanates from the very definition of innovation that assumes innovation to be the outcome R&D only (Bell & Pavitt, 1993). The type of innovation in LDCs differs from that of developed countries in that there is non-R&D type innovation which should include adoption and diffusion of technologies (Lundvall, 2010). According to Fagerberg and Verspagen (2002), firms in LDCs also do innovation through imitating and adapting foreign technologies to their context. Thus, imitation and technology acquisition whether disembodied or embodied in imported capitals and inputs are more important than R&D and radical innovation as a source of learning and local technological capabilities (Bell & Pavitt, 1993). Problem related to data deficiency is also detrimental to conducting research on the innovation productivity nexus. It is only recently that few countries have begun to conduct innovation surveys mainly based on OECD (2005) Oslo manual.

The case of Ethiopia is not different in the sense that it is more often than not to see any research analyzing the link between innovation and labor productivity. Therefore, this study was intended to fill the gap in literature in Ethiopia, particularly and in LDCs generally. Accordingly, this study was aimed at examining the impact of innovation on labor productivity, the impact of innovation on labor productivity growth, to see whether the effect of innovation varies with productivity, and to identify the main drivers of innovation by firms. Due to lack of proper innovation survey, the current paper utilizes two waves (2011 & 2015) of World Bank's Enterprise survey (ES) with some elaboration based on secondary data extracted from the report generated by Science & Technology Information Center (STIC) based on Ethiopia's innovation survey. Access to the raw data of this survey as well as adequacy of the data to support more comprehensive study is yet

to be explored. The analytical framework used to analyze the ES data to study the links between innovation and productivity is a variant of Heckman's (1976, 1978) control function framework designed to study models of endogenous treatment effects.

Compared to previous empirical studies, this paper contributed in four main ways. Firstly, it is the first ever study conducted in Ethiopia in this scale and one of the few empirical works in Sub-Saharan Africa that contributes to the thin literature. Secondly, it applied different estimation technique that is more capable to disentangle the effect of innovation on productivity. Thirdly, the effect of technologies embodied in imported fixed capital is included in the knowledge production function unlike other studies. Fourth, the role of human capital development is also accounted for which was indicated to be poorly studied (Guisado-Gonzalez, Vila-Alonso and Guisado-Tato, 2015).

The rest of this paper is organized as follows. Section two presents review of literatures. Section three will explain the methodology including the data and empirical estimation strategy. Section four discusses results from both descriptive and econometric estimation. Section five concludes and forwards recommendation.

## **2. Literature review**

The theoretical basis for the relationship between innovation and productivity goes back to the Solow (1957) where the main factor behind differences in total factor productivity (as a residual) was believed to be technology. Griliches (1979) advanced the idea by including R&D capital as a factor of production into the residual framework of Solow. R&D activities were shown to enhance firm-level knowledge accumulation leading to product or process innovation that would ultimately raise productivity. For Schumpeter (1942), technological innovation is the single most important factor for economic success or failure. Endogenous growth theories (Romer's, 1990; Aghion and Howitt, 1992) also recognized technology as endogenously determined factor that explains differential productivity growth between countries. From evolutionary theory (Nelson and Winter, 1982), technological capability (Kim, 1997; Lall, 1992) and national innovation systems

(Lundvall, 2010) perspectives, innovation and technological progress play a pivotal role for economic performance at all levels (national, sectoral and firm). Cohen and Levinthal (1989) indicated the role of R&D activities in fostering productivity growth through building the absorbing capacities of firms.

Empirical studies on the productivity effects of innovation involve difficulties due to the fact that both productivity and innovation are endogenous and they are interdependent. Moreover, problem with measuring innovation and endogeneity of innovative activities that give rise to innovation pose additional challenge. It is customary to model determinants of innovation in a knowledge production function and the productivity effect of innovation in an output production function (Griliches, 1979). Most of the empirical studies followed Crepon, Duguet and Mairesse (1998), often called CDM models, a framework that integrates the relationships between innovation and productivity. Applying CDM, numerous empirical works in developed countries established that product or process innovation leads to improved performance measured by labor productivity, total factor productivity, sales profit margin etc. (Janz, Loof, & Peters, 2004; Mohnen, Mairesse, & Dagenais, 2006; Hall & Mairesse, 2006; Mairesse & Mohnen, 2010; Mohnen and Hall, 2013). However, the effect of innovation on productivity varies with firm size, sector, and ownership. For instance Griffith et al. (2006) and OECD, (2009) found that product innovation has stronger effect on the productivity of larger firms. In terms of sector, the productivity effect of product innovation is larger in the manufacturing sector than in the services sector (OECD, 2009) in most countries. Similarly, using data from the BRICS countries and applying panel data and dynamic panel data methods, Kurt and Kurt (2015) found positive relationship between innovation and labor productivity.

In most developing countries, existing evidences on the relationship between innovation and productivity remained to be inconclusive for varying reasons. The main reason relates to lack appropriate indicator for innovation and innovative activities that inter into knowledge and output production functions. For instance, a study conducted by Mohnen

(2006) in case of Tanzania, using World Bank's Investment Climate Survey covering the years 2000 to 2002, showed that innovation (using R&D investment) did not have any effect on firm performance. Instead, he found institutional arrangements to be the most important factor for performance of firms. Crespi and Zuniga (2011) cited earlier studies in Latin America to show the inconclusiveness of results. In their effort to fill the underlying knowledge gap, they examined the innovation-productivity nexus in six Latin American countries. Their result appears to show more regularity in line with results in developed countries. In all the six countries, firms that invest in knowledge were found to be more innovative and those who innovate have higher labor productivity than the rest of firms (Crespi and Zuniga, 2011).

### **3. Methods and Data**

#### **3.1. Data**

Availability of appropriate data for studying the relationship between innovation and productivity is the primary challenge in LDCs. I only knew and accessed one innovation survey in Ethiopia conducted by the World Bank in 2011. However, the data lacks variables that are necessary to investigate determinants of innovation and the relationship between innovation and labor productivity. This paper, therefore, is based on two waves (2011 & 2015) of World Bank's Enterprise survey (ES) on Ethiopia. The data covers firms in the manufacturing, services and retail business and construction sectors. It constitutes variables that help analyze common performance indicators at firm-level. Most importantly, the fact that ES data collected after 2010 includes some basic innovation indicators made the data usable for this study. However, it is not an innovation survey; it does not allow in-depth analysis of innovation related issues. Particularly, since innovation indicators are entirely dichotomous, it is impossible to assess the intensities of innovation input and innovation outputs. Besides, since the variables refer to a three-year period (unlike the intensity that refers to the last year of this three-year period), it is difficult to know exact timing of innovation (Mohnen and Hall, 2013).

Nevertheless, these conditions are far from prohibiting the use of the data for the purpose at hand.

Lately, we came to know existence of innovation survey in Ethiopia conducted by Science & Technology Information Center (STIC) in 2015. However, nothing is clear about the data accessibility except the report generated out of it which is available on the homepage of STIC. The report was also used in this paper to show some descriptive aspects of innovation in Ethiopian firms which cannot be obtained from the ES data.

### **3.2. Empirical Strategy**

The usual way of analyzing the links between innovation and productivity is through estimating the CDM model introduced by Crepon, Duguet and Mairesse (1998). The model generally involves three step estimation procedure. In the first step, firms' decision to undertake formal R&D is estimated as a dichotomous outcome variable and for those with R&D projects the amount of investment on R&D activities is estimated either sequentially or applying Heckman selection model. In the second step, knowledge production function is estimated as a function of different innovation inputs and other firm and sector characteristics. In most cases the predicted value of R&D investment obtained in step one enters the knowledge production function instead of the actual R&D to account for the simultaneity that might result from the fact that innovation is measured over the past three years. It also enables inclusion of firms with missing R&D investment in the knowledge production function which can involve estimation of the probability of product, process, or organizational innovation using probit model or least square technique when innovation output is measured by the share of innovative sales. The final step in CDM model is estimation of output production function in which labor productivity is a function of the log capital intensity and the log of (predicted) innovation output (Hall, 2011).

Applying the above form of CDM model cannot be applied in this paper due to deficiency of the data used. Primarily, there is no R&D investment variable that is needed

in the first step of CDM. Second, there is no separate variable for innovative sales apart from total sales. Consequently, there should be other alternative strategy that would equally help in estimating the link between productivity and innovation with the capacity to overcome the endogeneity and reverse causality inherent in estimating such interrelated equations. For this purpose, applying instrumental variable approach or some variants of a control function approach motivated by Heckman (1976, 1978) can be the best alternative (Vella and Verbeek, 1998). Particularly, the maximum likelihood version of estimating linear equation with endogenous treatment effect derived by Maddala (1983) was applied in this paper. The primary regression equation of interest is given by

$$y_i = X_i\beta + \delta INN_i + \epsilon_i \quad [1]$$

where "X" is vector of control variables, "y" is outcome variable, sub-script "i" denotes a firm, "INN" is a binary-treatment variable (dummy for product or process innovation in the current case) that is assumed to stem from an unobservable latent variable:

$$INN_i^* = W_i\gamma + u_i \quad [2]$$

W is set of variables that explain the unobserved latent decision of firms to innovate. The decision to innovate is made according to the rule

$$INN_i = \begin{cases} 1, & \text{if } INN_i^* > 0 \\ 0, & \text{otherwise} \end{cases} \quad [3]$$

<i>Treatment effect Variables</i>	<i>Product</i> : Dummy for product innovation by a firm over three year period
	<i>Process</i> : Dummy for process innovation by a firm over three year period
<i>Outcome variables</i>	<i>lnlabp</i> : The natural logarithm of total sales of a firm per permanent employees at the end of a completed fiscal year
	<i>labpg</i> : Labor productivity growth computed as the difference between <i>lnlabp</i> and its value three years ago
<i>Independent Variables</i>	<i>lnage</i> : The natural logarithm of firm age as computed by the number of years since a firm started operation

	<i>lnsize</i> : the natural logarithm of total number of permanent employees of a firm
	<i>perempl</i> : Total number of permanent employees at the end of a completed fiscal year
	<i>Private</i> : Dummy for private ownership if the share of private owner is greater or equal to 90%
	<i>Foreign</i> : Dummy for Foreign ownership if the share of foreign owner of a firm is greater or equal to 50%
	<i>NEWAS</i> : Dummy for Spending on New fixed Capital(Machineries and Equipment)
	<i>RnD</i> : Dummy for spending on Research and Development (R&D) activities
	<i>humskil</i> : dummy for having 70% and above of permanent employees who completed high school
	<i>hschul</i> : The proportion of employees who completed high school
	<i>Train</i> : Dummy for firms which conducted formal training
	<i>EXP_D</i> : Dummy for exporting products

where  $\varepsilon$  and  $u$  are bivariate normal with mean zero and covariance matrix

$$\begin{bmatrix} \sigma^2 & \rho\sigma \\ \rho\sigma & 1 \end{bmatrix}$$

In order to see if there is any difference in the effects of innovation on firms at different productivity growth distribution as additional robustness check, quantile regression was also applied but only with respect product innovation. Process innovation has been ignored based on its insignificance on productivity growth when the above specifications are used. Definition of the variables that entered the above equations is given in table 3.1. To control for possible changes at the macroeconomic level and differences in sectoral characteristics, dummy for year 2015 and 24 dummies for two digit International Standard Industrial Classification (ISIC) of sectors were also included in estimating the regression equations.

Table 3.1: Definition of Variable

#### 4. Results and Discussion

In this section, results of the data analysis will be presented starting from descriptive analysis of the data and the prevailing characteristics of innovation in Ethiopian context. Results from Endogenous treatment regression and that of quantile regression will be presented one after the other.

##### 4.1. Descriptive analysis

Table 4.1 displays the descriptive statistics of continuous variables which are used in the analysis. The table shows that the mean number of permanent employees (perempl) hired by a firm in the data is about 96 with the standard deviation of about 362. The proportion of permanent employees who completed high school (hschul) averaged to about 0.68 with the corresponding standard deviation of 0.30. The mean labor productivity (in logarithm) and labor productivity growth of a given firm are about 12 and -0.02, respectively. The mean age and size of a firm are also estimated to be 2.32 and 3.24 log points, respectively.

Table 4.1: Descriptive statistics of continuous variables

Variable	Obs	Mean	Std. Dev.	Min	Max
perempl	1467	96.31	361.73	1	7600
hschul	1457	0.68	0.30	0	1
lnlabp	1270	12.10	1.54	5.94	18.22
labpg	1084	-0.02	2.18	-12	9.22
lnage	1471	2.32	0.78	0	4.49
lnsize	1467	3.24	1.43	0	8.94

Other variables related to firm-level knowledge accumulation which are measured at discrete scale are described in table 4.2. Of all the valid case with respect to spending on new fixed asset (NEWAS), 39% of firms responded to have spent positive amount at the end of last fiscal year with reference to survey year. Firms which conducted formal training for permanent employees account for 22% of all the valid cases. R&D spending

is also very low as only 14% of total firms reported positive spending. One of the important ways of acquiring knowledge among the Ethiopian firms is engagement in export market (Ahmad and Lee, 2016). As it has been the case, the current data also indicates that exporters account only for about 8% of the total sample. In terms of ownership, private owned firms constitute 90% of all valid cases (1405) while the remaining 10% are public firms. More than 85 firms in the data remained to be unidentified in this classification. These firms are likely to belong to what is called "endowment" owned conglomerates which are peculiar to and controversial form of business in the Ethiopia's context. Presence of foreign firms in a given sector is also beneficial as it would involve positive learning effect (Ahmad, 2015). However, it is evident that foreign firms account only 8% of the sampled enterprises while 92% of them are domestic firms.

In terms of innovation, 40% of firms in the total sample introduced new product, 37% introduced new way of logistics or distribution, 34% introduced new methods of production, 34% undertook marketing innovation and 30% conducted organizational innovation over three years periods. This shows that product innovation is the most common type of innovation among firms. The least is organizational innovation. This results differ from that of STIC (2015) which showed that product innovation is the least popular type of innovation (conducted by about 20% of firms) while marketing innovation is the most popular among Ethiopian firms (conducted by about 50% of firms).

Table 4.2: Frequency and percentage of dichotomous variables

Variables	Freq.	valid cases	%	innovation type	Freq.	valid cases	%
NEWAS	586	1,485	39	process	510	1,488	34
train	323	1,486	22	product	588	1,487	40
RnD	202	1,488	14	logistics or supply	556	1,485	37
EXP_D	117	1,484	8	organizational	448	1,485	30
private	1,268	1,405	90	marketing	505	1,488	34
foreign	107	1,405	8				

However, there appears to be differences in the rate of innovation between years and among sector of operation. Table 4.3 displays this sort of differences with respect to product and process innovation only which are often considered as technological innovation.

Table 4.3: Distribution of firms by sector, year and innovation

Sector	Year of Survey				Total	Type of innovation			
	2011		2015			Product		Process	
	Freq.	%	Freq.	%		Freq.	%	Freq.	%
Manufacturing	340	53	383	45	723	326	45	310	43
Services	284	44	412	49	696	239	34	184	26
Construction	20	3	53	6	73	23	32	16	22
<b>Total</b>	<b>644</b>	<b>100</b>	<b>848</b>	<b>100</b>	<b>1492</b>	<b>588</b>	<b>38</b>	<b>510</b>	<b>34</b>

The 2011 data is made of 53% manufacturing, 44% service and 3% construction firms. In 2015 data, the three sectors constitute 45%, 49% and 6%, respectively. In terms of innovation firms in the manufacturing sector seem to have the highest propensity to engage in both product (45%) and process (43%) innovation in line with STIC's (2015) findings. Firms in the service sector have slightly higher innovation than those in the construction sector. From all the sampled firms, 38% introduced product innovation while 34% have introduced new process over a three year period. If we see the differences in innovation between 2011 and 2015 (table 4.4), the former year witnesses more innovation propensities than the later year. Specifically, we can see that 43% of the total firms sampled in 2011 introduced new products while 37% of the sample firms in 2015 reported product innovation. Similarly, the number of firms who introduced process innovation in 2011 (44%) is higher than the number of firms with process innovation (27%) in 2015 data. This indicates that firm level innovations (both product and process) seem to have declined in 2015 as compared to 2011. This was stronger for process innovation.

Table 4.4 also displays a clear difference in the innovation propensity of firms within different size categories. Regardless of the representativeness of each size categories, microenterprises are the least innovators in terms of both product and process. Large

firms have relatively far higher probability to innovate new product (56%), new process (52%) than the rest of size categories. Medium sized firms follow with 42% of product innovation and 38% of process innovation. About 31% of small firms conducted product innovation while 25% introduced new process. The figures in the table generally indicate that innovation propensity increases with firm size. The same feature is observed from the recent innovation survey by STIC (2015).

Table 4.4: Innovation by year and size category

Innovation type	Survey year				Size category <sup>3</sup>							
	2011		2015		Micro		Small		Medium		Large	
	Freq	%	Freq	%	Freq	%	Freq	%	Freq	%	Freq	%
Product	274	43	314	47	6	9	213	31	191	28	178	26
Process	279	41	231	34	2	3	173	25	172	25	163	24
<b>total</b>	<b>640</b>		<b>848</b>		<b>26</b>		<b>690</b>		<b>456</b>		<b>316</b>	

Regarding the intended objectives and the actual effect of innovation, the current data does not give any descriptive information. STIC's report shed important lights in this regard. Firms engage in innovation activity for a number of objectives. Their objectives engaging in innovative activities relate to products, markets, efficiency, quality or the ability to learn and to implement changes. But the objective of improving quality of goods and service was the most important one followed by entry into new markets and increasing market share. Regarding the actual effect of innovation, improved quality of goods or services (55.4%), increased range of goods and services (45%), and entry to new market (40%) were reported to be the three most important effects. STIC's report also indicate that innovative firms employ more people and generate greater

<sup>3</sup>Categorized based on the number of permanent employees where Micro <5; Small >=5 and <=19; Medium >=20 and <=99; Large >=100

earnings which are interesting in view of the objective of the current paper. The effect of innovation on productivity is to be analyzed in sections that follow.

#### **4.2. Results from Endogenous treatment regression**

This section presents the full maximum likelihood estimation result of endogenous treatment regression. Results are displayed in four pairs of columns. The first two pairs of columns are estimates on the log of labor productivity (*lnlabp*) for the treatment variables of product and process innovations respectively while the remaining two pairs of columns show growth rates of *lnlabp* (*labpg*) over the two respective types of innovation. The second columns in each pair show robust standard errors (RSE). The Wald test at the bottom of the table indicates that we can reject the null hypothesis of no correlation between the treatment errors and the outcome errors implying dependence of the two equations (1&2). Except in case of the link between process innovation and labor productivity growth, the estimated correlation between the treatment-assignment errors and the outcome errors ( $\rho$ ) is -0.761, which indicates that unobservable factors that raise observed labor productivity appears to happen with unobservable variables that lower innovation. The overall fitness of the models also shows good fit.

Table 5A: Endogenous treatment regression with no interaction effect

	<i>lnlabp: Natural logarithm of labor productivity</i>				<i>labpg: labor productivity growth</i>			
	Coef.	RSE	Coef.	RSE	Coef.	RSE	Coef.	RSE
						0.10	0.236*	0.09
<i>lnage</i>	0.152**	0.062	0.192***	0.065	0.102	0	*	5
						0.35		0.36
<i>private</i>	-0.360*	0.211	-0.278	0.221	0.129	0	-0.268	4
						1.079*	0.26	1.313*
<i>EXP_D</i>	0.590***	0.179	0.615***	0.187	**	3	**	5
						0.28	0.574*	0.27
<i>hschul</i>	0.137	0.187	0.199	0.190	0.128	1	**	3

Product/					2.274*	0.84		1.19
process	2.295***	0.241	2.099***	0.292	**	9	-0.743	7
					-			
_cons	11.049***	0.283	11.022***	0.294	1.401*	0.48		0.55
					**	6	-0.563	2
					produ		proces	
	product		process		ct		s	
Inage	0.080	0.049	0.038	0.052	0.058	2	-0.017	9
Insize	0.059**	0.028	0.073**	0.028	0.069*	7	0.075*	3
private	-0.290	0.259	-0.413	0.268	0.490*	6	0.587*	6
Foreign	-0.281	0.269	-0.291	0.275	-0.491	2	-0.329	1
hschul	0.367***	0.137	0.388***	0.137	0.347*	0.16		0.16
					*	0	0.324*	8
RnD	0.653***	0.122	0.606***	0.121	0.687*	0.15	0.565*	0.25
					**	8	*	1
train	0.202**	0.098	0.103	0.089	0.389*	0.13		0.11
					**	9	0.220*	8
NEWAS	0.458***	0.074	0.470***	0.085	0.535*	0.12	0.566*	0.15
					**	3	**	3
					-			
_cons	-1.168***	0.345	-0.727**	0.345	1.286*	0.39		0.43
					**	0	-0.133	0
					-			
/athrho	-0.999***	0.142	-1.021***	0.169	0.619*	0.29		0.40
					*	6	0.309	2
/lnsigma	0.545***	0.042	0.555***	0.049	0.826*	0.07	0.777*	0.05

					**	7	**	7
						0.20		0.36
rho	-0.761	0.060	-0.770	0.069	-0.551	6	0.300	6
						0.17		0.12
sigma	1.725	0.073	1.741	0.085	2.283	6	2.175	4
						0.56		0.82
lambda	-1.313	0.151	-1.341	0.179	-1.258	2	0.652	8
no. obs	1147		1147		981		981	
					47.54*		40.48*	
lglikelihood	182.91***		133.3***		**		**	
Wald(chi2)	49.27***		36.60***		4.37**		0.59	

Note: 24 two-digit sector dummies and year dummies included but not reported

\*, \*\*, \*\*\* represent significance levels at 10, 5 and 1 percent, respectively

Results in table 5A indicate that the Average Treatment Effects (ATE) of product and process innovations on labor productivity at levels are about 2.30 and 2.10, respectively with strongly high statistical significances. This is in line with most of the findings in both developed and developing countries. The ATE on labor productivity growth, however, remained to be positive and strong (2.27) only in case of product innovation. The ATE of introducing new process on productivity growth turned to be negative but insignificant. Among the control variables, dummy for export participation is seen to have positive and strong effect on labor productivity which confirms findings in Ahmad and Lee (2016) for large and medium sized manufacturing sectors. Older firms seem to be more productive than younger counterparts in terms of both level and growth. Having higher proportion of high school complete among permanent employees also improves productivity though results are generally insignificant. The negative sign of "Private" dummy (though insignificant) imply better performance of public owned firms.

The proportion of employees who completed highschool (hschul), investment in R&D(RnD), investment in new fixed capital at the end of last fiscal year(NEWAS) have strong positive effect on the propensity of firms to introduce new process and new

product. However, R&D and new assets are the first and the second most important effects on both types of innovation. Among the control variables, only firm size appeared to have positive significant effect whereas firm age, private and foreign ownership have negative but insignificant effects. However, private owned firms tend to have significantly lower propensity to innovate than public owned firms. Regardless of the statistical insignificance of both Private and Foreign dummies, the negative coefficients suggest the fact that domestic and public owned firms have better propensity to innovate. Conducting formal training to permanent employees appeared to have positive and significant effect on product innovation while it is only marginally significant on process innovation with respect to results corresponding to productivity growth. In the above case, ATE is the same as ATET because the treatment indicator variables (product and process innovation) have not been interacted with any of the outcome covariates.

#### ***Case when labor productivity has effect on innovation***

The above result disregards the possibility of interaction between the outcome and treatment variables. Here estimation is extended to see the robustness of the findings taking the possible interaction effect into account. Interaction of outcome covariates with treatment indicator suggests the potential effect of outcomes (*lnlabp* and *labpg*) on treatment (innovation). To see this effect, factor-variablenotation was used to allow the coefficients of private dummy and dummy for export participation to vary over the two types of innovation. First interaction between Private and product innovation (product\_Pvt), interaction between process innovation and Private (process\_Pvt), interaction between product innovation and export dummy (product\_EXP), interaction between process innovation and export dummy (process\_EXP). Then notation of indicator variables was used to include the interaction variables in labor productivity and labor productivity growth regressions. Results are presented in table 5B. The likelihood tests at the bottom of the table show good fitness of all the models except in case of growth regression where the treatment variable is process innovation. Similar to results in

table 5B, process innovation appeared to be independent of the labor productivity growth equation.

Results show that the coefficients of private dummy are negative in both innovators and non innovators. But the variation is significant at 10% only in case of non-innovators of process. When labor productivity growth is an outcome variable, the coefficients of private dummy varies positively though statistically insignificant. However, coefficients of export dummy positively and significantly vary over both innovators and non-innovators of process and product innovations. This implies that export participation significantly increases the productivity and growth of both innovating and non innovating firms. It is interesting to see differences in the coefficients of exporters and non-exporters, particularly in case of productivity growth. It appears from the result that innovators reap higher productivity growth if engaged in export. This is true in case of both process and product innovations.

Table 5B. Endogenous treatment regression with interaction effect

<i>lnlabp: Natural logarithm of labor</i>								
<i>productivity</i>				<i>labpg: labor productivity growth</i>				
	Coef.	RSE	Coef.	RSE	Coef.	RSE	Coef.	RSE
						0.10	0.195**	0.09
lnage	0.151**	0.063	0.192***	0.065	0.203**	2	*	6
					-			
					0.207**	0.06		0.11
lnsize	-	-	-	-	*	7	0.091	0
product_Pvt/process_Pvt								
						0.37		0.36
	0	-0.384	0.235	-0.441*	0.255	-0.508	5	-0.598*
						0.43		0.51
	1	-0.335	0.299	-0.102	0.287	0.490	1	0.087
product_EXP/process_EXP								
	0	0.543**	0.237	0.677***	0.259	0.853**	0.36	1.117**
								0.33

							0	*	9
						1.466**	0.35	1.554**	0.38
	1	0.641**	0.271	0.557**	0.259	*	2	*	3
							0.27		0.28
hschul		0.136	0.188	0.198	0.190	0.015	4	0.649**	5
product/proce						1.800**	0.61		1.16
ss		2.246***	0.386	1.787***	0.423	*	8	-1.952*	1
							0.47		0.45
_cons		11.076***	0.298	11.176***	0.314	-0.474	7	-0.302	6
						produc		proces	
		product		Process		t		s	
							0.05		0.06
Inage		0.080	0.049	0.039	0.052	0.033	9	-0.019	7
						0.119**	0.03		0.04
Insize		0.059**	0.028	0.072**	0.029	*	8	0.084**	0
							0.26		0.30
private		-0.287	0.260	-0.417	0.266	-0.430	3	-0.543*	1
						-	0.27		0.36
Foreign		-0.277	0.270	-0.293	0.278	0.474**	5	-0.255	5
							0.15		0.16
hschul		0.366***	0.137	0.387***	0.137	0.363**	5	0.326**	6
						0.651**	0.14		0.26
RnD		0.654***	0.121	0.604***	0.121	*	9	0.486*	0
						0.345**	0.11		0.11
train		0.200**	0.098	0.110	0.090	*	5	0.218*	4
						0.484**	0.10	0.510**	0.17
NEWAS		0.457***	0.074	0.474***	0.085	*	2	*	5
						-			
						1.437**	0.37		0.39
_cons		-1.169***	0.345	-0.727**	0.345	*	0	-0.146	6
						-			
						0.777**	0.18		0.39
/athrho		-1.002***	0.144	-1.012***	0.172	*	5	0.483	5

					0.860**	0.06	0.803**	0.07
/lnsigma	0.546***	0.042	0.552***	0.050	*	0	*	6
						0.10		0.31
rho	-0.762	0.060	-0.767	0.071	-0.651	7	0.449	5
						0.14		0.16
sigma	1.726	0.073	1.736	0.086	2.363	1	2.232	9
						0.33		0.77
lambda	-1.316	0.152	-1.331	0.183	-1.538	6	1.002	4
no. obs	1147		1147		981		981	
					73.86**		44.23**	
lglikelihood	185.68***		135.16***		*		*	
					17.64**			
Wald(chi2)	48.64***		34.42***		*		1.5	

Note: 24 two-digit sector dummies and year dummies included but not reported here

\*, \*\*, \*\*\* represent significance levels at 10, 5 and 1 percent, respectively

Unlike the case where interaction between outcome covariates and treatment variables, the coefficients of treatment variables (product and process innovation) do not show the actual ATE and ATET due to inclusion of interaction terms. Moreover, ATE and ATET are no longer equal. To estimate ATE the "margins" post estimation option of stata was used. Besides, the *vce(unconditional)* option in stata was used to obtain the standard errors for the population ATE instead (reported as USE in table 5C) of the sample ATE. To obtain ATET the same post estimation option of "margins" was used but with specifying the "subpop(innovators)" option in order to restrict the sample used by margins to innovators (both process and product). Results are reported in table 5C.

Table 5C. ATE and ATET over product and process innovation

Outcome var.	lnlabp: <i>Natural logarithm of labor productivity</i>				labpg: <i>labor productivity growth</i>			
	Product		Process		Product		Process	
	Contrast	USE <sup>a</sup>	Contrast	USE	Contrast t	USE	Contrast t	USE
ATE	2.30	0.242	2.09	0.299	2.77	0.53 3	-1.28	1.18 7
ATET	2.30	0.244	2.07	0.301	2.76	0.53 0	-1.30	1.18 2

a: USE stands for unconditional standard error

The estimated ATET and ATE of product and process innovations are exactly the same indicating equality of the average predicted labor productivity and labor productivity growth for innovating firms with that of the whole population. The most important observation about the effect of including interaction of the treatment variable with outcome covariates is that there is no difference in the ATE and ATET (2.95 in table 5A and 2.30 in table 5B) when labor productivity is measured at levels. On the other hand, the differences seem to be high in case of labor productivity growth. That is the ATE and ATET of product innovation on growth is 2.47 in table 5A while the two values increased to about 2.77 up on including the interaction effects (table 5C). It is apparent from the above analysis that only product innovation has positive and stronger effect on labor productivity growth. However, it would be possible that the effect would vary with the growth quantiles which would involve important policy implication. The following section sheds some light on this aspect.

### 4.3. Result from Quantile Regression

We have seen that both product and process innovation exert significant effect on labor productivity at level. But only product innovation remains to be important for productivity growth. The question that would follow then is whether effect of innovation vary with productivity growth quantiles. As a result, it is important to further the analysis

to see the robustness of the above findings along different distribution of growth apart from the mean effect. To this end, quantile regression was applied up on controlling important variables. Results are reported in table 5D. The first column of the table displays mean regression to be compared with results of quantile regression.

Table 5D shows that on average product innovators' growth in labor productivity is 45% higher that of non innovators. However, if we look at outputs of quantile regression, product innovation has varying effect on the growth of firms at different productivity growth quantile. Firms at the lower productivity growth quantile generate the highest (60%) gain while those at the higher quantile benefit the least (about 32%). Thus, we can generally say that the effect of product innovation decreases with the growth quantile. Similar effects prevail with regard to firm age. This suggests that experience matters the most for improving the growth of firms at the lower age of the growth quantile. Dummies for ownership (Private and Foreign), dummy for investing in new fixed asset, and firm size do not seem to affect growth. Exporting and having endowed with skilled human labor (humskil) exert consistently increasing effect with increasing labor productivity growth. These could be due to the cumulateness of the learning effects of exporting and having more skilled labor which would improve the absorptive capacity of firms. The above patter can be seen on the following figure (Figure 5.1).

Table 5D: Output of Quantile Regression

<i>Dependent var.: Labor productivity growth</i>						
	Mean	10	25	50	75	90
	Coef.(RSE)	Coef.(SE)	Coef.(SE)	Coef.(SE)	Coef.(SE)	Coef.(SE)
product	0.452*** (0.144)	0.599* (0.314)	0.493** (0.233)	0.329* (0.182)	0.475** (0.189)	0.318 (0.248)
lnage	0.226** (0.091)	0.379** (0.171)	0.339** (0.151)	0.026 (0.122)	0.117 (0.120)	0.062 (0.132)
private	-0.196 (0.396)	-0.199 (0.841)	0.314 (0.833)	-0.313 (0.687)	-0.255 (0.351)	0.448 (0.353)
Foreign	-0.440	-0.425	0.214	-0.465	-0.354	0.349

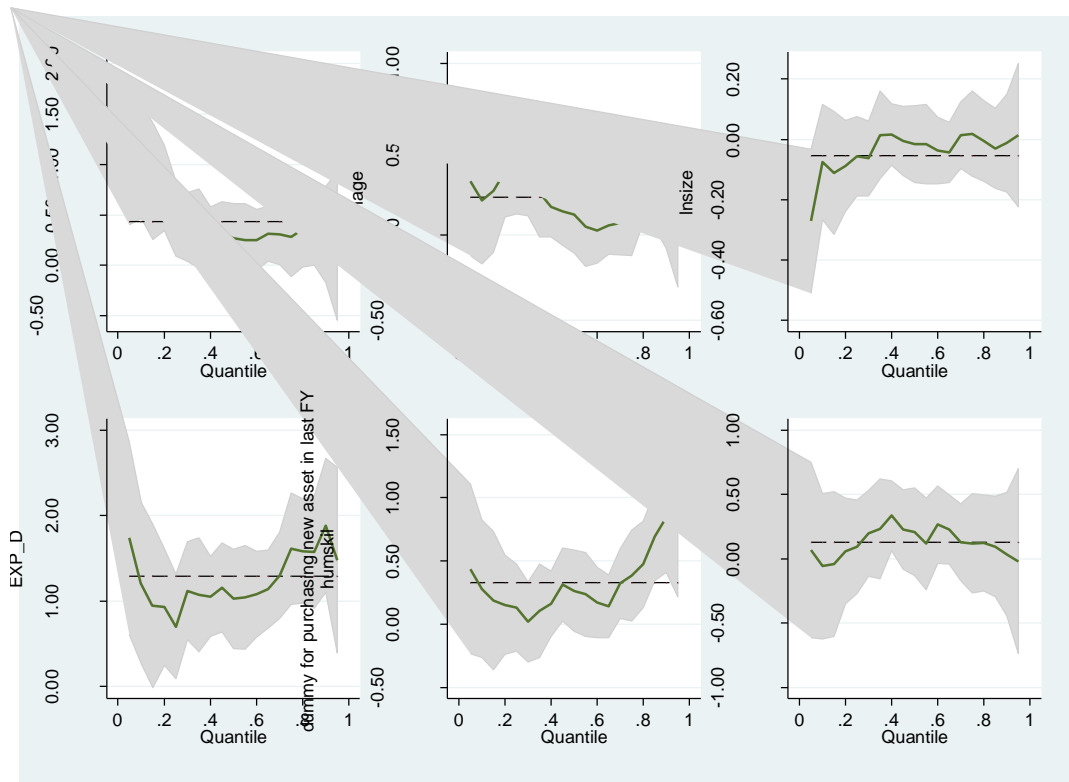
	(0.527)	(1.040)	(0.858)	(0.768)	(0.519)	(0.589)
Insize	0.012	-0.047	-0.017	0.027	0.072	0.081
	(0.056)	(0.121)	(0.087)	(0.066)	(0.080)	(0.075)
EXP_D	1.019***	0.663*	0.776**	1.004***	1.001***	1.293***
	(0.251)	(0.364)	(0.359)	(0.323)	(0.355)	(0.416)
humskil	0.238*	0.015	0.061	0.271*	0.385**	0.446**
	(0.131)	(0.253)	(0.187)	(0.145)	(0.167)	(0.187)
NEWAS	0.191	0.199	0.220	0.106	0.142	0.277
	(0.136)	(0.243)	(0.255)	(0.134)	(0.171)	(0.169)
_cons	-1.482***	-4.278***	-3.600***	-0.579	-0.048	0.763
	(0.558)	(1.111)	(0.997)	(0.791)	(0.681)	(0.747)
no. obs	984	984	984	984	984	984
R-squared	0.20	0.15	0.13	0.10	0.12	0.16

Note: 24 two-digit sector dummies and year dummies included but not reported here

\*, \*\*, \*\*\* represent significance levels at 10, 5 and 1 percent, respectively

The graphs in figure 5.1 show the actual effect of product innovation, age, exporting and human capital on growth. The dashed lines in all the graphs show the mean regression result. As one can clearly see there is clear deviation from the mean result. The effects of innovation and firm age tend to decline while the effects of export and human capital increase with the growth quantiles. Though insignificant, the effect of firm size also gets stronger with increasing growth. Buying new fixed capital, does not seem to have any significant effect (though positive) on labor productivity growth.

Figure 5.1: graphs of quantile regression



## 5. Conclusion and recommendation

This paper examined the links between innovation and productivity in the Ethiopian context using two waves of World Bank's enterprise survey. By pooling the data collected in 2011 and 2015, the researcher applied linear regression with endogenous treatment effect where labor productivity and labor productivity growth are outcome variables and product and process innovations are taken as treatment effect variables. Due to the fact that labor productivity growth is a more strict measure of performance, differences in the effect of innovation on growth were examined using quantile regression. Results show that both product and process innovation have positive significant effect on labor productivity at level. In terms of growth, however, only product innovation remained to have strong positive effect. Upon considering the potential effect of the outcome variables, no differences were observed in the ATE and ATET of innovation on labor productivity. However, there is some difference in ATE and ATET when growth is used as the outcome variable. New machineries and

equipment, R&D spending, training and the qualification of employees are the most important variables in driving both process and product innovation. The effect of innovation appears to decline with labor productivity growth quantiles.

Compared to previous empirical studies, this paper contributed in four main ways. Firstly, it is the first ever study conducted in Ethiopia in this scale and one of the few empirical works in Sub-Saharan Africa that contributes to the thin literature. Secondly, it applied new estimation technique that is more capable to disentangle the effect of innovation on productivity. Thirdly, focus is given to the effect of technologies embodied in imported capital asset which is more vital than R&D investment in case of LDCs. Finally, the importance firm - level training on innovation is also investigated.

As is the case in any empirical studies, it is important to indicate the weakness of this study. Firstly, the fact that the data does not have variables that measure all innovation investments limited the application of more incisive way of examining the relationship between productivity and innovation. Secondly, the fact that no variable measuring intensity of innovation also limited the paper to use innovation outputs in terms of binary variable which may not be adequate as it does not show the intensity of innovation. Particularly, the fact that the variables refer to a three-year period (unlike the intensity that refers to the last year of this three-year period), they do not show the exact timing of innovation (Mohnen and Hall, 2013). The fact that partial productivity is used as outcome variable would also raise a question as it would have been more interesting had total factor productivity also been used. Thus, future research would aim at addressing these issues.

Nevertheless, the study has significant benefit in informing policy making aimed at designing ways that help build local innovation capability. The result generally suggests that, there should be some incentive mechanisms to encourage innovation if the current dismal status of labor productivity in Ethiopia, especially in the manufacturing sector, has to be improved. Product innovation was found to generate greater reward than process

innovation in building the innovation capability and enhancing the competitiveness of firms. It is rewarding to make focused support for firms at the lower productivity growth quantiles as it generate higher positive effect.

## **References**

- Aghion, P., and Howitt, P. (1992). 'A model of growth through creative destruction.' *Econometrica*, 60(2), 323-351.
- Ahmad, A. and Lee, K. (2016). Embodied technology transfer and learning by exporting in the Ethiopian manufacturing sector. *Innovation and Development*, 1-23.
- Ahmad, A. Y. (2015). The impact of Foreign Direct Investment on the Productivity and growth of Ethiopian firms. Paper presented on the 13th Globelics International Conference, Havana, Cuba, 23rd–25th September 2015.
- Bell, M., & Pavitt, P. (1993). Technological accumulation and industrial growth: Contrasts between developed and developing countries. *Industrial and Corporate Change*, 2(2), 157–211.
- Cohen, W. and Levinthal, D. (1989). "Innovation and learning: The two faces of R&D". *Economic Journal*, 99: 569:596.
- Crepon, B., Duguet, E., & Mairesse, J. (1998). Research, innovation and productivity: An econometric analysis at the firm level. *Economics of Innovation and New Technology*, 7(2), 115–158.
- Crespi, G. and Zuniga, P. (2011). Innovation and Productivity: Evidence from Six Latin American Countries. *World Development*, 40 (2), 273–290.
- Fagerberg, J. and Verspagen, B. (2002). Technology-gaps, innovation-diffusion and transformation: an evolutionary interpretation. *Research Policy*, 31, 291–1304.
- Griffith, R., Huergo, E., Mairesse, J., & Peters, B. (2006). Innovation and productivity across four European countries. *Oxford Review of Economic Policy*, 22(4), 483–498.
- Griliches, Z. (1979). Issues in Assessing the Contribution of R&D to Productivity Growth, *Bell Journal of Economics*, 10: 92-116.
- Grossman, G. and Helpman, E. (1991). *Innovation and Growth in the Global Economy*. Cambridge, MA: MIT Press.
- Guisado-Gonzalez, M., Vila-Alonso, M., and Manuel Guisado-Tato, M. (2015). Radical innovation, incremental innovation and training: Analysis of complementarity, *Technology in Society*, 44, 48-54.
- Hall, B. (2011). Innovation and productivity. *Nordic Economic Policy Review*, 2, 168-195.
- Hall, B., & Mairesse, J. (2006). Empirical studies of innovation in the knowledge-driven economy. *Economics of Innovation and New Technology*, 15(4–5), 289–299.

- Heckman, J. (1976). The common structure of statistical models of truncation, sample selection and limited dependent variables and a simple estimator for such models. *Annals of Economic and Social Measurement*, 5, 475–492.
- Heckman, J. (1978). Dummy endogenous variables in a simultaneous equation system. *Econometrica*, 46, 931–959.
- Janz, N., Loof, H., & Peters, B. (2004). Innovation and productivity in German and Swedish manufacturing firms: Is there a common story? *Problems and Perspectives in Management*, 2, 184–204.
- Kim, L.(1997). *Imitation to innovation: the dynamics of Korea’s technological learning*. Boston, Harvard Business School Press.
- Kurt, S. and Kurt, Ü. (2015). Innovation and Labor Productivity in BRICS Countries: Panel Causality and Co-integration. *Procedia - Social and Behavioral Sciences*, 195, 1295 – 1302.
- Lall, S. (1992). Technological Capabilities and Industrialization. *World Development*, Vol. 20, No. 2, pp. 165-186.
- Lundvall, B.- Å. (ed.) (2010). *Post script: Innovation system research where it came from and where it might go*. London, Anthem Press.
- Maddala, G. S. (1983). *Limited-Dependent and Qualitative Variables in Econometrics*. Cambridge: Cambridge University Press.
- Mairesse, J., & Mohnen, P. (2010). *Using innovation surveys for econometric analysis*. NBER working paper 15857. Washington, DC, United States: National Bureau of Economic Research.
- Mohnen, P. (2006). What drives productivity growth in Tanzania: Technology or institutions? paper presented at the Blue Sky II Forum, Ottawa, Canada.
- Mohnen, P., and Hall, B. (2013). Innovation and productivity: an update. *Eurasian Business Review*, 3(1), 47-65.
- Mohnen, P., Mairesse, J., & Dagenais, M. (2006). *Innovativity: A comparison across seven european countries*. NBER working papers 12280. Washington, DC, United States: National Bureau of Economic Research, Inc.
- Mohnen, P and Hall B.H. (2013). Innovation and Productivity: An update. *Eurasian Business Review*, 3(1), 47-65.
- Nelson, R., Winter, S., (1982). *An Evolutionary Theory of Economic Change*. The Belknap Press of Harvard University Press, Cambridge.
- OECD (2009). *Innovation in firms: A microeconomic perspective*. Paris, France: Organization for Economic Cooperation and Development.
- Romer, D. (1990). Endogenous technological change. *Journal of Political Economy*, 98:71-102.
- Schumpeter, J. (1942). *Capitalism, Socialism and Democracy*. New York: Harper and Row.

- Science & Technology Information Center (STIC), Ethiopia (2015).Ethiopian Innovation Survey Report.Addis Ababa Ethiopia.
- Solow, R. M. (1957). Technical change and the aggregate production function, *Review of Economics and Statistics* 39, 312-320.
- Vella, F., and Verbeek, M. (1998).Estimating and Interpreting Models with Endogenous Treatment Effects.
- World Bank .(2009). Toward the Competitive Frontier: Strategies for Improving Ethiopia's Investment Climate. African Region Report No. 48472-ET.
- World Bank. (2015). Overcoming constraints in the manufacturing sector: 4th Ethiopia Economic Update. World Bank. Washington DC.

## **Production and Characterization of Biodiesel from *Citrullus colocynthis* seed oil**

**Solomon Girmay\* and Hikeal Tsade**

Applied Chemistry Program, Adama Science and Technology University

P.O.Box 1888, Adama, Ethiopia\*E-mail:[solochem2003@gmail.com](mailto:solochem2003@gmail.com)

### ***Abstract***

*Biodiesel production from oil-bearing plants have attracted the attention different scholars as a consequence of global issues such as depletion of fossil fuel reserves, global warming, and environmental pollution problems. Hence, this study focused on the production and characterization of biodiesel from *Citrullus colocynthis* oils using two step transesterification reactions. The raw oils were extracted from *Citrullus colocynthis* seeds, using soxhlet extractor with n-hexane as solvent. The effects of different parameters were studied; including reaction temperature, oil to methanol molar ratio, time of transesterification reaction, and amount of alkaline catalyst in order to achieve the optimum condition to obtain the highest conversion. The results indicate that 60°C reaction temperature, 6:1 methanol to oil ratio, 90 minutes reaction time and 1.00 wt % NaOH catalysts were taken as optimum conditions for transesterification to achieve the highest conversion of the raw oils to the corresponding biodiesel, which led to biodiesel yield of 98.53%. The physicochemical properties of the raw oil; acid value, saponification value, free fatty acid value, iodine value, PH value, peroxide value, density, specific gravity, calorific value, flash point, fire point, moisture content, and viscosity were characterized and compared with the reported standard values. Based on these finding, the raw oil of the plant was acceptable for prior transesterification reaction process. Therefore, the produced biodiesels and its blends were further analyzed to determine its fuel properties, such as kinematic viscosity, caloric value, flash and fire point, pour and cloud point, water content, moisture content, ash content, distillation temperature, PH, free fatty acid, acid value and others as per ASTM 6751 standard methods and compared with reported values. For comparison, commercially available petro-diesels fuels were analyzed using the same tests used for the produced biodiesels. The qualities of all the tested parameters of the biodiesel were found to be within international acceptable biodiesel and diesel standards. Hence, the produced biodiesel is used as alternative source of energy for petrodiesel engine without further modifications.*

**Keywords:** *Citrullus colocynthis* seeds, raw oil, transesterification, biodiesel, physicochemical parameters, characterization.

## 1. Introduction

Bitter apple (*Citrullus colocynthis* L.) a species of flowering plant in the family, Cucurbitaceae is selected for this study. *C. colocynthis*, commonly known as the bitter apple, bitter is a plant native to the Mediterranean Basin and Asia, but now days it is widespread throughout Arabia, Australia and Ethiopia(Oduvaldo, 2007). Biodiesel produced from *C. colocynthis* has a remarkable advantage regarding lubricity because of its high energy value and positive fuel properties (Berman *et al.*, 2011). The competition between edible oil and fuel needs may cause worldwide disproportion in the food industry and market demands. Therefore, there is a need for nonedible and inexpensive feedstock such as *C. colocynthis* oil for biodiesel production. The fatty acid in a *C.colocynthis* made up of triglycerides; 67-73% linoleic acid, 4-5% linoleic acid, 10-16% of oleicacid, 12% palmitic and 5-8% stearic acids (Taufiq-Yap *et al*, 2011).

Environmental concerns, production cost, associated hazards and sustainability issues have bedeviled fossils utilization. However, biodiesel usage is less affected by most of these factors as it's renewable, environmentally friendly and produced from varieties of feedstock in respective regions. Biodiesel is defined by American Societies and Test Materials (ASTM) internationally as a fuel composed of monoalkyl esters of long-chain fatty acids derived from renewable vegetable oils (ASTM, 2008). Biodiesel is an alternative and renewable bio-fuel that could help to diminish the dependency of the import from petroleum-producing countries (Van Gerpen, 2005). The most common way to produce biodiesel is the transesterification method, which refers to a catalyzed chemical reaction involving vegetable oil and alcohol to yield biodiesel and glycerol as by-product (Zhang *et al.*, 2003).

biodiesel has a high heat value, and contains higher amount of oxygen (10-11%) that ensures more complete combustion of hydrocarbons (Global Farmer, 2009) and it is essentially free of sulfur and polycyclic aromatic hydrocarbons. These properties reduce CO, CO<sub>2</sub>, SO<sub>x</sub>, NO<sub>x</sub>, hydrocarbons and particulate matter emissionswhen compared with petro-diesel.Therefore, the potential production of biodiesel from *C.colocynthis* seed oil

in Ethiopia is associated to the solution of economic, environmental, and social problems. To the best of the researchers' knowledge, there were no further studies on the production and characterization of biodiesel from *C. colocynthis* in Ethiopia. The overall objective of this work is to produce and characterize biodiesel from *C. colocynthis* seed oil and compare with conventional diesel and reported standard values.

## **2. Materials and Methods**

### **2.1. Materials and equipment**

The chemicals and equipment used were: solvents (99.5% methanol ACS grade, 99.5 % n-hexane ACS grade and 99.5% chloroform ACS grade Newdlihi, India, distilled water), anhydrous sodium sulphate (Techno pharmchem Dehi, India), sodium hydroxide pellets AR 99% (Breckland Scientific Supplies, Thetford Norfolk, UK), pH meter, distillation apparatus, viscometer, magnetic stirrer, digital weighing balance, separating funnel, oil test centrifuge, pycnometer bottles, flash point tester, soxhlet apparatus, water bath, rotary evaporator, polyethylene bags, and heating mantle.

### **2.2. Experimental methods**

#### **2.2.1. Sample collection and preparation**

The Dry seeds of *C. colocynthis* were collected from Awash, Oromia Regional State from October-November, 2015. The dried plant materials were chopped into small pieces and finally pulverized into fine powder using a sterile electric grinder and packed in polyethylene bags.

#### **2.2.2. Extraction of seed oil**

Air dried seeds of *C. colocynthis* (5 Kg) powder was extracted using Soxhlet apparatus with n-hexane as solvent for 8 hrs. 60 g of the ground sample was poured into the thimble and two third volume of the round bottom flask was filled with the solvent. An anhydrous sodium sulphate was added to the extracted oil to remove drops of water and filtered using whatman NO.1 filter paper. Rotary evaporator was used to separate the oil from the solvent under reduced pressure at 40°C. This extraction procedure was repeated for many

runs to obtain a reasonable oil quantity. The yield of the crude oil was weighted and recorded and it was kept in refrigerator at 4°C for further analysis.

### **2.2.3. Physicochemical Analysis of the crude oil**

Prior to the production of biodiesel from *C. colocynthis* seed oil, physicochemical analysis of the crude oil such as density, specific gravity, acid value, free fatty acid, saponification value, iodine value, peroxide value, viscosity, and moisture content were conducted according the standard procedure AOCS and ASTM D-6751 standards.

### **2.2.4. Two-step transesterification of the crude oils**

In order to avoid the problem of saponification, a two-step transesterification was used for synthesis of biodiesel from *C. colocynthis* seed oil.

#### **Acid catalyzed etherification**

The oil was heated in the reaction glass tube to 60°C and a solution of concentrated H<sub>2</sub>SO<sub>4</sub> acid in methanol (30% v/v) was heated to 45°C. The resulting mixture was stirred on a magnetic stirrer for 1 hr and the content was poured into a separating funnel and allowed to settle for 2 hrs. The methanol-water fraction at the top layer was removed and the oil was decanted to be used for transesterification reaction

#### **Base catalyzed transesterification reaction**

50 mL of oil was measured and poured into a 150 mL conical flask and heated to a temperature of 45°C using a water bath. A solution of sodium methoxide was prepared in a 500 mL beaker using 1.00 g of NaOH pellet and 150 mL of anhydrous methanol. Sodium methoxide solution was then poured into the warm oil and stirred vigorously for 90 minutes using a magnetic stirrer and the mixture was left to settle for 24 hr in a separating funnel. After settling, the upper layer biodiesel was decanted into a separate beaker while the lower layer comprises of glycerol and soap was collected from the bottom of the funnel.

### **2.2.5. Purification of the produced biodiesel**

#### **Washing and Drying**

Biodiesel should be washed to remove any remaining methanol, glycerin, catalyst, soaps and other impurities. The biodiesel washing sometimes leaves the biodiesel looking a bit cloudy. It was heated slowly to 90-100°C and held there until all moisture present was evaporated.

### **2.2.6. Characterization of the prepared biodiesel**

The physicochemical characterization analysis and comparative test were carried out according to the ASTM-D6751 specification standards. Specific gravity, density, acid value, free fatty acid, refractive index, iodine value, peroxide, moisture content, ash content, kinematic viscosity saponification values, flash and fire point, cloud and pour point were determined using the same procedure as the characterization of the extracted seed oil.

### **2.2.7. Preparation and Characterization of Blends of Biodiesel**

The biodiesel was blended with diesel by volume as B5 (5% biodiesel and 95% diesel fuel) was prepared as first 95% (95 mL) of diesel fuel was taken in reactor vessel then 5% (5 mL) biodiesel and introduced in the same vessel. The mixture was then stirred (300 rpm) at 40°C for 15 minutes. Other blends were prepared with the same method B10 (10% biodiesel and 90% diesel fuel), B20 (20% biodiesel and 80% diesel fuel), and B100 (100% biodiesel and 0.00% diesel fuel). The physicochemical properties of the blends of biodiesel were characterized according to the ASTM D6751 standard method and compared with the conventional diesel fuels.

### **2.2.8. Fatty Acid analysis using GC**

The fatty acid composition of *C. colocynthis* oil was determined by Gas Chromatography (Shimadzu GC-17A) equipped with capillary column BPX 70 (30 m × 0.25 mm × 0.25 μm) and FID detector. The column temperature was programmed at 120°C with an increment of 3°C per minute for 57 minutes whereas the injector and detector temperatures were set at 260°C and 280°C, respectively. Fatty acid methyl ester (FAME) was prepared

according to PORIM Official Test Method (1995) with some modifications. The identification of the peaks was performed by comparing the retention times with standard methyl linoleic acid and other individual fatty acid methyl ester.

### **3. Result and Discussion**

#### **3.1. Physicochemical properties of *C. colocynthis* oil**

The extracted crude oil was yellowish brown in color and it gets darkened during the storage, sweet odor and bitter taste. The percentage yield of the extracted oils was 52.06 %. This yield was higher than the values reported for *Jatropha* oil (52%) and lower than for *Castor* oil (56%) (Van Gerpen *et al.*, 2004). In order to utilize the crude oil as a feedstock for the production of biodiesel; the physicochemical properties characterization such as density, specific gravity, ash content, pH, viscosity, acid value, saponification value, free fatty acid, moisture content, peroxide value and iodine value were very important. The results obtained on the properties of oils were compared with that of AOCS and ASTM D6751 standard values. The physicochemical properties of the crude oil were reported and summarized in **Table 1**.

The moisture content of the oil was seen to be 3.5%; these agree with ASTM D6751 standard specification range (1.25 – 5.88%). The ash content of the crude oil was 5.83 %, it is within the specified standard value by ASTM. Ash content is important parameter for the determination of heating value; high heating value of oils is expected with lower ash content. Refractive index of the crude oil at 30°C was investigated to be 1.45 which is in agreement with the ASTM specified standard (1.245 and 1.675). Refractive index is widely used in quality control to check for the purity of materials and to follow hydrogenation and isomerization reactions. The iodine value shows the level of unsaturation of the oil and also influences the oxidation and deposition formed in diesel engines. Iodine value obtained for *C. colocynthis* was 102 gI<sub>2</sub>/100 g values fall within the acceptable AOCS limit. The saponification value obtained from the oil was 195 and it is within the range specified by AOCS standards. The saponification value of the oil is a measure of the tendency of the oil to form soap during the transesterification reaction.

The presented result (195 mgKOH/g) revealed a similar saponification value with *Prunus armeniaca*, *Prunus persica*, *Datura metel*, and *Hyptissuaveolens* seed oil (Indraet al., 2013).

Acid value of the crude oil was 1.85 mg KOH/g. This value showed an agreement with ASTM D664 specification standard (0.5-0.8 mgKOH/g). The high acid value indicates that more quantity of the base will be required to neutralize the acidity of the oil to be transestrified and it also indicates high free fatty acid content in the crude oil. The percentage free fatty acid content of the oils was also determined as 2.75 %. As the free fatty acid content is greater than 2.50%, it needs further pretreatment in order to remove the formation of soap which is a serious problem for the base catalyzed biodiesel production. The viscosity of the crude oil at 40°C was 28.70mm<sup>2</sup>/s which was higher than the ASTM specification standard. However, it is lower than to that reported for *Jatropha* oil 31.5mm<sup>2</sup>/s and *moringa* oil 33.50 mm<sup>2</sup>/s (Van Gerpen *et al.*, 2004). The high viscosity of the oils indicates that the oil cannot be used directly in diesel engines due to its low flow capability, thus there is need for further transesterification process.

**Table 1.** Physiochemical properties of *C. colocynthis* oils with ASTM D6751 standard values.

Parameter	Unit	Experimental Value	ASTM D6751	Remark
Yield	%	52.06	-	
Moisture content	%	3.5	1.25-5.88	
Density	g/cm <sup>3</sup>	0.874	0.86-0.90	
Ash content	%	5.83	4.5-10.00	
Acid value	mgKOH/g	1.85	0.80-1.00	
Free acid value	%	2.75	3.00-5.00	
viscosity	mm <sup>2</sup> /s	28.70	6.0 max	
saponification Value	mgKOH/g	195	-	
Iodine Value	gI <sub>2</sub> /100g	102	-	

Flash point	oC	157	90-130.00	
Cloud point	oC	8	-15-5.00	
Fire point	oC	183	-	
Pour point	oC	10	-15-10.00	
Refractive index	-	1.45	1.245-1.675	
pH value	-	6.35	5.5-6.8	

#### 4.2. Characterization of the prepared biodiesel and its blends

Biodiesel (FAME) yield obtained after the transesterification process was found to be 98.53 % using an optimal conditions of 6:1 methanol to oil molar ratio, 1.00 wt% NaOH reaction catalyst, 60 °C reaction temperature and 90 minute reaction time. According the data summarized in the **table 2** the fuel properties of the biodiesel and its blends were discussed. The kinematic viscosity value determined for the biodiesel at 40 °C was (5.75) mm<sup>2</sup>/s falls within the ASTM D445 specification standard. This value is in agreement with the international standard of China (1.9- 6.0); USA 1.9-6.0 and EU 3.5-5.0. The kinematic viscosity of the crude oil was 28.70mm<sup>2</sup>/s and reduced to within the ASTM limits for biodiesel after transesterification and blending with diesel fuels. The transesterification process principally works to reduce viscosity of raw oil and the result was compared with raw oil which was much reduced but higher than the conventional diesel fuel. High viscosity affects the atomization of a fuel upon injection into the combustion chamber and thus leads to the formation of engine deposits. Kinematic viscosity is influenced by factors such us increase of fatty acid chain length, increasing degree of saturation or oxygenated moiety, position, number, and nature of double bonds in the fatty acid methyl ester (Knothe *et al.*, 2003). Refractive index of the produced biodiesels at 30°C was 1.42 and is also in agreement with the ASTM D1500 specification standard. The refractive index was decreased tremendously after transesterification reaction as compared to that of their raw oils, which indicates that heavier molecules have been converted to lighter ones, enabling

interface detection, enhancing lubricity and increasing functionality of the fuel oil (Antony *et al.*, 2011).

The acid value (mgKOH/g) of the methyl esters was 0.68 mgKOH/g. This was in agreement to the ASTM D664 specification standard (0.5-0.8 max) mgKOH/g. This lower acid value of the biodiesel may be due to the absence of air and water contact with the biodiesel fuel. A lower acid value will also decrease % FFA which helps to protect the corrosion of engine parts as the amount of water is decreases in the fuel. The cloud point and pour point of the produced biodiesel was -6.5°C and -13 °C, respectively and this was in agreement with the ASTM D2500 specification standards. Cloud point and pour point have implications on the use of biodiesel in cold weather applications. The cloud point is the temperature at which wax first becomes visible when the fuel is cooled. The cloud point is the most common measure of the tendency of a fuel to crystallize. Pour point measures the lowest temperature at which the biodiesel is observed to flow easily.

The flash point is the lowest temperature at which an applied ignition source will cause the vapours of the fuel to ignite. The flash point and fire points of the produced methyl esters were 141°C and 175°C, respectively, but the flash point result was out of the ASTM D93 standard (90 -130°C). Biodiesel flash points higher than 90°C are safer than diesel in terms of storage and transportation from the standpoint of fire hazard. The flash point of raw oil decreases after transesterification processes that show improvement in its volatile characteristics. The fire points of the produced biodiesel value were lower than that reported for jatropha biodiesel having a firepoint of up to 296°C (Ullman *et al.*, 1990).

The distillation temperature of the raw oil and the produced biodiesel (B100) at 60°C were determined to be 296 °C and 293°C, respectively, which differs by 3°C. However; the temperature was reduced to 275 °C, 270 °C and 267°C for B20, B10 and B5, respectively, because diesel fuels contain much heavier components. The calorific value

of biodiesel was 70 MJ/L which indicates the energy available in it was very lower in comparisons with conventional diesel fuels. This lower energy content of biodiesel leads to higher consumption of biodiesel in order to achieve yield of diesel in the engine (Da-Silva, 2013). Biodiesel is also potentially subject to hydrolytic degradation caused by the presence of water. Fuel contaminated with water can cause engine corrosion and breakdown. From the results obtained, bitter apple has traces of bottom sediment and water with 0.04%vol values conforms to the ASTM D 6751 set of standard whose maximum allowable limit is 0.05%vol. Since *C.colocynthis* fatty acid methyl ester has a legible amount of bottom water and sediment, it has been taken as better quality of fuel and acknowledged as great advantage over fossil diesel.

Table 2: Comparison of physiochemical properties of *C. colocythis* biodiesel, blends and diesel with ASTM D6751 standard values.

Property	Unit	ASTM Test Method	Expt. Value of Biodiesel	Expt. Value of blends				Expt. Value Of petro diesel for Biodiesel	Remark
				B100	B20	B10	B5		
Yield	%	-	98.53	-	-	-	-	-	
FAME									
Density	g/cm <sup>3</sup>	ASTM D1298	0.890	0.850	0.84 2	0.830	0.832	0.860 – 0.890	
Specific Gravity	-	ASTM D287	0.880	0.863	0.84 5	0.834	0.825	0.860 – 0.890	
Kinemat c Viscosity at 40oC	mm <sup>2</sup> /s	ASTM D445	5.75	3.420	2.84 0	1.760	1.320	1.900 -6.00	

Acid value	mgKO H/ g	ASTM D664	0.68	0.57	0.39	0.26	0.189	0.50 -0.80 max
Water content	%	ASTM	0.04					0.05 max
Flash Point	oC	ASTM D93	141	96	89	83	67	130 -170.00max
Cloud Point	oC	ASTM D2500	-6.5	-	-	-	-	-3.00 to 12.00
Pour point	oC	ASTM D97	-13	-	-	-	-	-15 00 to 10.00
Fire point	oC	ASTM D 445	175	-	-	-	78	
Caloric value	MJ/L	ASTM D6751	70	216	254	295	310	-
Refractive index		ASTM D1500	1.42	1.46	1.48	1.51	1.53	1.33-1.55
Iodine	gI2/100	ASTM	96.02	91.07	88.2	80.40	-	-

value	g	D2075			6			
Peroxide	meq/kg		17.24	15.80	14.3	13.42	-	-
					5			
value								
Saponific	mgKO		202.30	165.49	162.	154.20	-	-
ati	H/g				60			
on value								
Distillati	oC	ASTM D86	293	275	270	267	260	-
on								
temperat		ASTM						
ure		D1160						

---

### 4.3. Optimization of Parameters

Transesterification is the reaction between triglycerides and methanol to produce fatty acid methyl ester (FAME) and free glycerol as byproducts. It involves reaction between the oil which is the feedstock and an alcohol, usually methanol in the presence of a basic catalyst sodium hydroxide to give corresponding methyl esters. The main factors influencing the transesterification reactions are the methanol to oil molar ratio, catalyst concentration, reaction temperature and reaction time. High amount of methanol to oil ratio which was used to drive the equilibrium to a maximum fatty acid methyl ester yields.

Results obtained on the effect of temperature on the yield of the produced biodiesel from *C.colocynthis* oil as the feed stock were presented in **Table 3**. The maximum FAME yields were obtained at the temperature of 60°C with the percentage of 98.53%. This is because the reaction temperature at 60°C, the molecules of the triglycerides of *C. colocynthis* had high kinetic energy and this thus increased the collision rate and therefore improved the overall process by favouring the formation of biodiesel while at the lower temperatures of 50°C and 55°C with corresponding percentage yielding 92.08% and 96.85%, respectively at 6:1 methanol to oil molar ratio, there was lesser collision of reacting molecules and thus, reduced biodiesel yield as reported in **Table 3**. The higher reaction temperature would favour endothermic reaction, thus increasing the rate of reaction as well as the methyl ester concentration. However; at 65°C, it was noticed that there was a drop in percentage of methyl ester yield which is because at the reaction temperature (65°C), there was increased vaporization of the methanol used in the transesterification process due to the proximity of the reaction temperature (65°C) to the boiling point of methanol (64.7°C).

Based on the investigated results on the effect of reaction temperature on the yield of biodiesel production, it can be realized that the optimum conditions for the production of fatty acid methyl ester from crude oil of *C. colocynthis* through two step transesterification process are methanol to oil molar ratio of 6:1, catalyst concentration of 1.00wt%, reaction time of 90 minutes and reaction temperature at 60°C. According the data reported in **table 3**, biodiesel yield with respect to time for 3:1, 4.5:1 and 6:1 methanol to oil molar ratio at different percentage of catalyst NaOH and reaction temperature were increased. It has been observed that there is higher yield in case of 6:1 molar ratio as compared to 3:1 and 4.5:1 molar ratio. It may be because of the amount of methanol using for 6:1 molar ratio was more

than that of 3:1 and 4.5:1 molar ratio. In all these reactions fatty acid methyl esters were produced. The stoichiometric relation between methanol and the oil was 3:1. However, an excess of methanol is usually more appropriate to improve the reaction towards the desired product side. The maximum yield of biodiesel produced at the highest catalytic reaction conditions was 98.53 for 6:1 molar ratio, at 60°C reaction temperature and 90 minutes reaction time. It can be seen that the conversion of *C.colocynthis* oil to biodiesel increased steadily in the first 90 minutes. The reaction temperature, catalyst, and molar ratio of methanol to oil at fixed reaction time were showed a linear relationship.

**Table 3** Yield (%) of biodiesel and time for different molar ratio, temperature and catalyst concentration

Temperature (°C)	%catalyst (NaOH)	Molar ratio 3:1		Molar ratio 4.5:1		Molar ratio 6:1	
		Tim(min)	Yield (%)	Tim(min)	Yield (%)	Tim(min)	Yield (%)
50	0.5	30	79.64	30	81.13	30	84.35
		45	80.38	45	82.18	45	85.46
		60	82.73	60	85.23	60	88.70
		75	84.14	75	87.44	75	90.05
		90	86.21	90	88.98	90	92.08
55	0.75	30	82.08	30	85.34	30	88.37
		45	84.26	45	87.46	45	91.25
		60	86.79	60	89.18	60	93.27
		75	88.42	75	91.29	75	95.68
		90	90.13	90	93.74	90	96.85
60	1.00	30	85.25	30	87.82	30	91.09
		45	87.15	45	89.53	45	94.16
		60	89.27	60	91.37	60	96.85
		75	91.06	75	93.41	75	97.42
		90	93.48	90	95.65	90	98.53

#### 4.4. Fatty acid methyl ester composition

Fatty acid methyl ester composition of *C. colocynthis* oil was determined using gas chromatography (GC) analyzer equipped with a flame ionization detector (FID). The sample of *C.colocynthis* seeds oil was esterified to bring them into a vaporous phase, transforming the fatty acid into fatty acid methyl esters using alkaline catalyzed

methanolysis process. Based on the GC chromatogram thirteen fatty acid methyl esters were determined in the esterified oil. The major component of oil found was linoleate (C18:2; 60.34), oleate (C18:1; 12.46), palmitate (C16:0; 10.59), stearate (C18:0; 8.73), linolenate (C18:3; 1.76) and myristate (C14:0; 1.42) methyl esters and other trace amount of fatty acid methyl esters were also determined. The fatty acid profile of biodiesel has strong influence on its physicochemical properties such as iodine value, saponification value, viscosity and cloud point (Ramadhas *et al.*, 2009). Blending biodiesel with the conventional diesel fuels has very little effect on the proportion of the fatty acids presented in the oil.

#### **4. Conclusion**

World biodiesel production is on the increase due to rising crude oil prices, decreasing fossil fuel reserves and environmental concerns. The current research focused on the production of biodiesel from non-edible oil as alternative energy that will replace the existing conventional diesel fuels. Hence, it is more desirable to use non-edible oils as a feedstock in the production of biodiesel, which is the focus of this study. Based on the physicochemical analysis results of the raw oil, it can be concluded that it is suitable feed stock for prior production of biodiesel. The raw oil was transesterified using methanol in the presence of sodium hydroxide to produce 98.53% biodiesel (FAME) at 6:1 methanol to oil molar ratio, 60°C temperature, 90 minute time and 1.00% NaOH catalyst reaction conditions. The properties of the biodiesel produced were tested and compared with conventional diesel fuel and found to be in confinement with the ASTM-D6751 specification standard for biodiesel fuels. According to the GC chromatogram the oil composition of *C. colocynthis* was found to be synonymous in chemical constituents with those of sunflower, groundnut, and soybean biodiesel which have been well established and widely published in international journals. *C. colocynthis* raw oil and its biodiesel confirm that the biodiesel promotes clean and environmental friendly, nontoxic, biodegradable and renewable bio-energy alternative fuels.

#### **Acknowledgement**

The authors would like to acknowledge Adama Science and Technology University research offices for undeserved financial support.

## References

- ASTM, (2008). Standard specification for biodiesel fuel (B-100) blend stock for distillate fuels. In: Annual Book of ASTM Standards, ASTM International, West Conshohocken, and Method D6751-08.
- Antony, S., Raja, Robinson, D.S. smart, C. Lindon and Robert Lee, 2011. Biodiesel production from *Jatropha* oil and its characterization. Research journal of chemical societies. **1(1)**:81-87.
- Berman, P., Nisri S., Wiesman, Z. (2011). Castor oil biodiesel and its blends as alternative fuel. Biomass Bioenergy, **35**:2861-2866.
- Global farmer, 2009. India Gives Biofuels a Chance to Grow. Available: <http://globalfarmer.com.au/>, accessed 23rd July 2009.
- Indra, R., Bachheti R.K., Archana, J. (2013). Chemical composition, mineral and nutritional value of wild *Bischofia javanica* seed. International Food Research Journal, **20(4)**:1747-1751.
- Knothe, G., Matheaus, A.C., Ryan, T.W. (2003). Cetane numbers of branched and straight-chain fatty esters determined in an ignition quality tester. Fuel, **82**:971-975.
- Oduvaldo, C.M.P.J., (2007). Comparison between Polyurethanes Containing Castor Oil (Soft Segment and Cancellous Bone Autograft in the Treatment of Segmental Bone Defect Induced in Rabbits". J. Biomater. Appl. **21(3)**: 283-297.
- Ramadhas, A.S, Jayaraj S., Muraleedharan C., (2009). Biodiesel Production from High FFA Rubber Seed Oil. Fuel. **84(4)**:335-340.
- Taufiq-Yap, Y.H., Lee, H.V.R. Yunus and Juan, J. C. (2011). Transesterification of non-edible *Jatropha curcas* oil to biodiesel using binary Ca-Mg mixed oxide catalyst: effect of stoichiometric composition. Chemical Engineering Journal. **178**:342-347.
- Ullman, T., Mason R., Montalvo D., (1990). Study of cetane number and aromatic content effects on regulated Emission from a heavy-duty engine. Southwest Research Institute Report 08-2940.
- Van Gerpen, J., (2005). Biodiesel processing and production. Fuel Processing Technology. **86(10)**:1097-1107.
- Van Gerpen, J.H., Shanks B., Pruszko R., (2004). Biodiesel Analytical Method". Iowa State University. National Renewable Energy Laboratory. **42(5)**:3041-3393.
- Zhang, Y., Dubé M. A, McLean D. D., Kates M., (2003). Biodiesel production from waste cooking oil: Process design and technological assessment. Bioresource Technology. **89(1)**:1-16.

## **Investigation on Pollution Caused by Gasoline& Diesel Fueled Vehiclesa Case of Adama Town**

**Solomon Neway<sup>1</sup>, Ramesh Babu Nallamothe<sup>2</sup>**

<sup>1</sup>Mechanical Engineering Department, Arba Minch University, Arba Minch, Ethiopia.

Mobile: +251 911093012 [solomonnewayjida@gmail.com](mailto:solomonnewayjida@gmail.com)

<sup>2</sup>Mechanical systems & vehicle engineering program, School of Mechanical Chemical and Materials Engineering, Adama Science and Technology University, Adama, PoBox: 1888, Ethiopia. Mobile:+251 912234395 [rbnallamothe@gmail.com](mailto:rbnallamothe@gmail.com), [ramesh.babu@astu.edu.et](mailto:ramesh.babu@astu.edu.et)

### ***Abstract***

*The transport sector has an important role to play in the effort to avert the dangerous effects of climate change because it heavily depends on fossil fuels. Currently, most transport related emissions are concentrated in urban areas which account for the largest share of on-road transport energy consumption. It is estimated that transport sources in developing countries contribute about 4% of the global fossil carbon dioxide versus 18% by industrialized countries. The cost of urban air pollution is estimated to be 2% of GDP in developed countries and more than 5% in developing countries. Adama is one of the old cities in Ethiopia and it is at a distance of 100 km from capital city of Addis Ababa, Ethiopia. Most of heavy duty truck vehicles in the country are across Adama because of it is corridor of import and export. With an annual vehicle registration and a population growth of over the year, the number of trucks continues to grow exponentially in Adama City. With the increasing urban population and there is an increasing demand for transportation vehicles in Adama necessitating increased air pollution around the city. Most of the minibus vehicles used in Adama has very low energy efficiencies, mainly because they are imported into the country when quite old. The general objective of this study is to investigate the pollution caused by gasoline and diesel fueled vehicles in Adama. The measured vehicle emissions have been analyzed in detail. It found that emissions like CO, NO<sub>x</sub>, HC, PM and CO<sub>2</sub> levels are higher than worldwide standards for human and environmental health. The findings indicate the level of pollution is high and will continue to grow if left unabated. Tailpipe emission findings estimated the highest level of NO<sub>x</sub> emissions at 3.44 g/km, HC emissions at 6.53 g/km, CO at 13.9 g/km, PM<sub>2.5</sub> at 1.3 g/km and 35.96 g/km of CO<sub>2</sub>. These amounts of*

*emission exceed the proposed draft NEMA ambient air quality emission data and the World Bank ambient air quality guidelines. This implies that persons exposed to these emissions on a daily basis are likely to develop health complications over time as the concentration levels increase. Several mitigation methods can be applied to reduce the emission level such as reduce consumption of fossil fuels and increase efficiency in transport usage of energy. This study confirms that exhaust gases from vehicles pollute Adama's air, and that improperly maintained vehicles contribute significantly to this pollution. It is recommended that a comprehensive motor vehicle pollution control program be designed to implement the proposed NEMA vehicle emission standards. Establishment of an integrated transport system should be made priority to enable the decongestion of Adama city.*

**Keywords:** *Greenhouse effect, climate change, mitigation, vehicle emissions standards.*

## **1. INTRODUCTION**

Emissions of many air pollutants have been shown to have variety of negative effects on public health and the natural environment. Emissions that are principal pollutants of concern include: hydrocarbons, carbon monoxide (CO), nitrogen oxides (NO<sub>x</sub>), particulate matter, sulfur oxide (SO<sub>x</sub>), volatile organic compounds (VOCs). Hydrocarbons are toxins. Hydrocarbons are a major contributor to smog, which can be a major problem in urban areas. Carbon monoxide poisoning is also a major killer (S.E. Institute, 2015).

Emission levels are dependent upon many parameter including vehicle-related factors such as model, size, fuel type, technology level and mileage, and operational factors such as speed, acceleration, gear selection, road gradient and ambient temperature (MOWAT, Uganda, 2006). The power to move a car comes from burning fuel in an engine. Pollution from cars comes from by-products of this combustion process (exhaust) and from evaporation of the fuel itself (S.E. Institute, 2015). In the last century, the level of CO<sub>2</sub> in the atmosphere has increased by more than 30% as a result of human activities. The effects of climate change are becoming more pronounced and they include droughts, floods, heat waves and changes in the weather patterns. Global temperatures have increased by almost 0.8°C over the past 150 years. Without any global action, it is expected that temperatures will increase further by 1.8 — 4 °C by 2100 (IPCC, 1996). It is anticipated that this rise will result in sea level increment of 15 to 95 centimeters. While the transportation sector is crucial to a nation's economy and personal mobility, it is also a significant source of GHGs. Nearly 50% of global CO, HCs,

and NO<sub>x</sub> emissions from fossil fuel combustion come from internal combustion engines (ICE). The contribution of the transport sector to total CO<sub>2</sub> emissions in developed nations is forecast to increase from 20% in 1997 to 30% in 2020 (Ken Gwilliam, 2004). The transport sector accounts for almost all the oil demand growth around the world. The world transportation oil demand has continuously risen with increasing Gross domestic product (GDP). World forecasts show that transport oil demand in developing nations will increase three times more than in developed nations. Increasing income will cause a tremendous increase in car ownership in developing countries, where the vehicle stock is expected to triple (Cozzi L, 2006). Developing countries account for about 10% of the global automobile population and a little over 20% of the global transport energy consumption. In comparison, the United States alone consumes about 35% of the world's transport energy (MOWAT Uganda, 2006).

Road vehicles are among the main consumers of world energy and they dominate global oil utilization, consuming up to 80% of transport energy. The transport sector's share of oil consumption has been increasing steadily at around 0.6% per year. Current policies are not sufficient to control road vehicle energy use. Even if governments implement all the measures that are currently being considered, projections by the international energy agency (IEA) show that road vehicle energy use would still rise between now and 2030 at 1.4% per annum respectively (Cozzi L, 2006). In developing nations, it is envisaged that with rising income and the rapidly rising mobility that accompanies it, the increase in automobile emissions will be even greater than the developed nations. Steady growth in vehicular populations has put environmental stress on urban centers in various forms particularly causing poor air quality. There is growing evidence that links vehicle pollutants to human ill health. Motor vehicles are major emission sources for several air pollutants, including NO<sub>x</sub>, CO, PM, and HCs (Weyn Chris, 1994). These pollutants have significant adverse effects on human beings and the environment. Vehicle emissions cause both short and long term problems associated with health effects. For example, HCs and NO<sub>x</sub> are the precursors of ozone gas, which has effects ranging from short term consequences such as chest pain, decreased lung function, and increased susceptibility to respiratory infection, to possible long-term consequences, such as premature lung aging and chronic respiratory illnesses (Weyn Chris, 1994).

The most affected group is the urban inhabitants especially the traffic policemen who are exposed to the fumes for a long period of time (Kean AJ, 2003). Steerenbeg et al, 2001 compared children attending a school located near a busy way in Utrecht, Netherlands (mean black smoke levels; 53 g/m<sup>3</sup>) with children attending a school located in the middle of a green area (mean black smoke levels; 18 g/m<sup>3</sup>) in a suburban area. It was discovered that respiratory diseases were more pronounced in the urban than suburban children. The severity of the problem increases when traffic flow is interrupted and the delays and start-stops occur frequently. These phenomena are regularly observed at traffic intersections, junctions and at signalized roadways. Emission rates depend on the characteristics of traffic, vehicles and type of road intersections (Gokhale S, 2009). The age of a vehicle and maintenance levels also contribute to the emissions of all classes of vehicles. Further, the fuel quality has a direct effect on the vehicular exhaust emissions (G. Perry, 1995).

Adama is exhibiting high social, economic, structural and change is found to be a fast growing city. Taking into account, Adama fast growth and to enable the transport sector to play its required role, the government has invested a huge resource to construct express way roads Addis to Adama so as to expand the road network. An effort has been made to improve the transport service provisions (C.S. Agency, 2014). There is no integrated planning between agencies of the environmental protection and transport sector. The absence of coordination and symbiosis in implementing the laws and regulations pertinent to environment protection and transport sectors, as well as gaps in improving quality of fuel used in the transportation sector is also a main problem.

A clear understanding of the looming dangers of increased vehicle numbers on the air quality needs to be established (AC Administration, 2015).

## **2. METHODOLOGY**

Measuring the levels of HC, CO, NO<sub>x</sub>, CO<sub>2</sub> and PM concentrations at three selected Adama sites for six days and conducting a roadside vehicle inspection by randomly pulling over in-use vehicles to inspect a representative sample of the Adama three wheelers and minibuses fleet are the two major steps in this study. The inspection included; visual inspections of the ECS a measurement of their tailpipe exhaust emissions, on selected vehicles. Interviewing the drivers and obtaining responses for questioners distributed. A questionnaire which was aimed at determining the age of vehicles and mileage and peoples' perceptions on the impact of

vehicle emissions was prepared and administered to 50 each minibuses and three wheelers operators. The interviewee sample size was selected based on the availability and co-operation of vehicles operators to respond to the study. The Vehicles were randomly selected based on the age, type and engine model. The experiment was conducted on- road at three areas namely Adama post office, Adama Bus station and Adama Mebrat Haile. By analyzing the advantage and disadvantages of the vehicle pollution measuring techniques, the researcher has chosen a direct on-road emission measurement technique.

### **3. RESULTS**

#### **Vehicle parc age and mileage**

A total of 240 unique vehicles were tested ranging from model year 1981 to model year 2015, of which 120 (50%) were gasoline-powered and 120 (50%) were diesel-powered. Among gasoline powered vehicles, 40 (33.33%) were minibuses taxi and 80 (66.67%) were three wheelers. And from a total of 120 diesel powered vehicles, 60 (50%) were minibus taxi and the remaining 50% were three wheelers taxi. In this study diesel powered vehicles were tested for only particulate matter (PM<sub>2.5</sub>). The vehicle mileage for minibuses ranged between 15,988 km and 695,910 km with an average of 294,703.32 km and standard deviation of 157,418.6 km. The vehicle mileage for the three wheeler vehicles ranged between 1,111km and 67,162km with an average of 25,736.1km and standard deviation of 16,112.64km. . Out of the 50 vehicle owners interviewed, 92% indicated that they had purchased their vehicles from other existing owners. 90% of the minibuses vehicles lie between 11-32 years indicating that the Adama vehicle parc is quite old but the age of three wheelers lie between 1-8 years. The most common emissions test in I/M programs is a measurement of hydrocarbon and carbon monoxide concentrations in the exhaust while the vehicle is idling. Many inspections in Finland, Germany, Sweden, and the United States supplement this measurement with a second measurement carried out with the engine running at 2500 rpm with no load. The analysis of the emissions from different vehicles showed that CO<sub>2</sub>, CO, HC and NO<sub>x</sub> are released during combustion of fossil fuels. The results obtained are a combination of all the vehicle types considered in the analysis. They cover vehicles with different engine types and sizes. This because of the difficulty involved in accessing vehicles for the experiments. The analysis was done on tail pipe emission

#### **HC Emissions**

As show from Figure 1 the level of HC emissions from all selected vehicle types. The level of HC emissions observed is highest both idle and 2500rpm operating condition in minibuses.

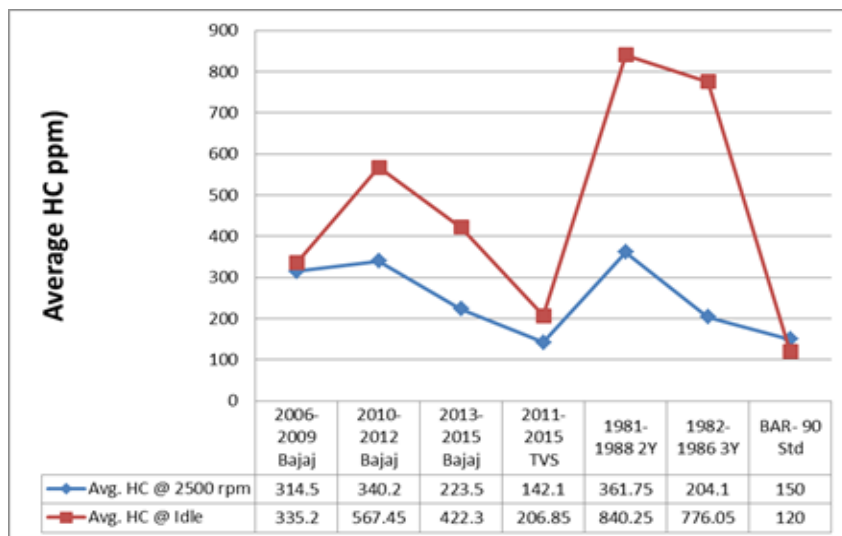


Figure 1: Average Idle/2500 rpm HC Emission

### CO Emissions

Emission of carbon monoxide is an indicator of incomplete combustion in the engine. Figure 2 shows the level of carbon monoxide emitted by the three vehicle types. The level of CO emissions observed is highest both Idle and at 2500 rpm operating condition in three wheelers than Minibuses.

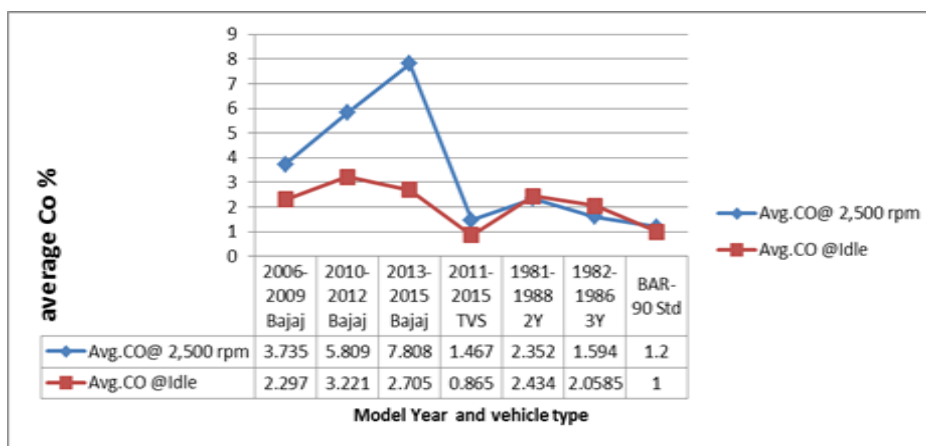


Figure 2: Average CO at Idle/2500 rpm Emission

### CO<sub>2</sub> Emissions

From Figure 3, it is observed that the maximum amount of CO<sub>2</sub> emitted at free acceleration from the three wheelers Bajaj 2013-15 models and minibus 3Y model, the rest were under the standards. Also, it is observed that the CO<sub>2</sub> emission level highest during idle rpm operating condition in the minibuses 3Y model, the remaining models were under the stated standards.

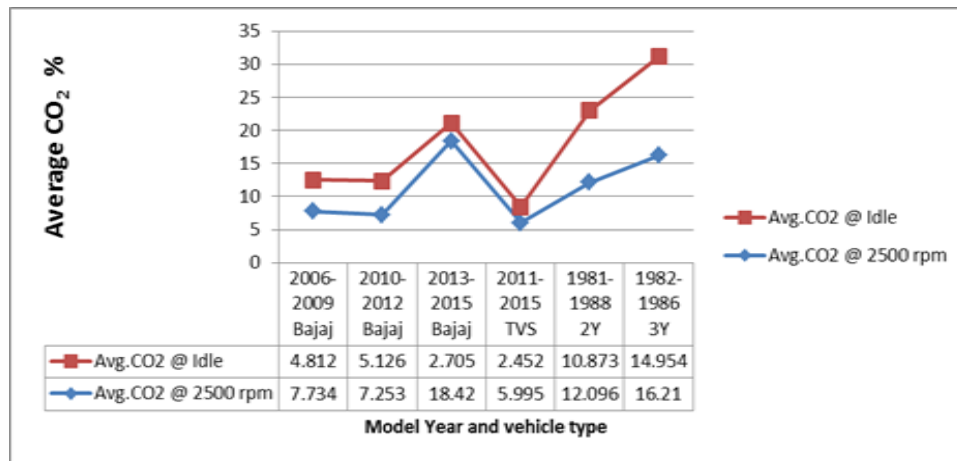


Figure 3: Average CO<sub>2</sub> at Idle/2500 rpm emission

### NO<sub>x</sub> Emissions

Figure 4 shows the NO<sub>x</sub> emissions for the different vehicles. The highest level of NO<sub>x</sub> observed was from the minibuses 3Y at 4.26 ppm, minibuses 2Y at 3.03 ppm, three wheelers Bajaj 2013-15 model at 1.32 ppm, three wheelers Bajaj 2010-12 at 1.24 ppm, and three wheelers Bajaj 2006-09 model at 1.01 ppm and TVS at 0.73 ppm.

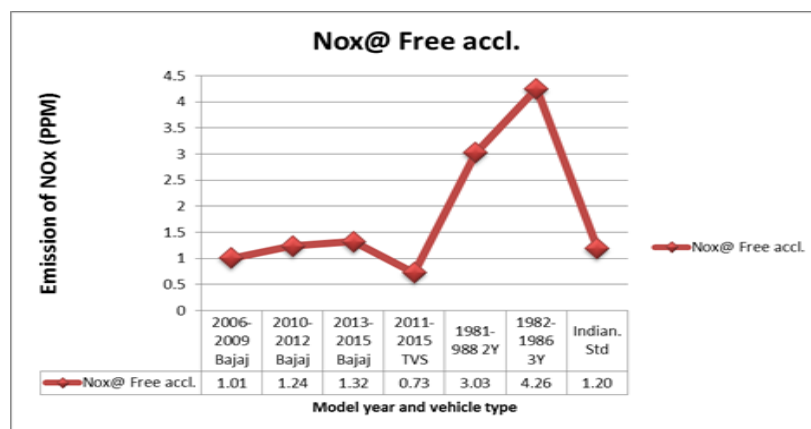


Figure 4: Average NO<sub>x</sub> at free acceleration emission

### Particulate Matter (PM)

Figures 5 show the particulate matter readings for three wheelers Force and minibuses (2L, 3L & 5L) model diesel vehicles, respectively. These graphs show several PM reading values for both vehicles. However, note that there are more emissions for 2L at 2.0145 times followed by, 1.74 times, 1.711 times and 1.0375 times 5L, 3L and three wheelers 2006-12 model higher than CARB standards, respectively.

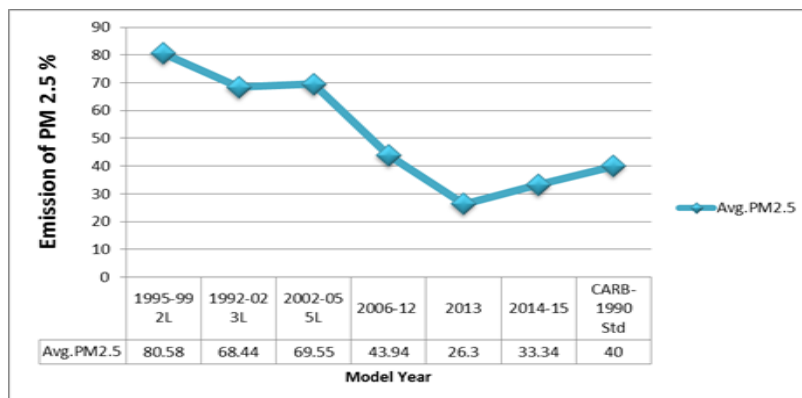


Figure 5: Average PM<sub>2.5</sub> at free acceleration

### Vehicular Emissions Control Systems (ECS's)

The inspection result shows the various ECS's and the number of vehicles which that have equipped with ECS. Based on the collected data 198 (82.5%) of the inspected vehicles have Positive Crankcase Ventilation (PCV) and 57 (23.75%) have Thermostatic Air Cleaners (TAC).

### 4. DISCUSSION

The field survey revealed that most of the minibuses taxis for public transport are imported into the county as second hand overhauled vehicles. The vehicle owners mentioned that at the time of purchase, some of the vehicle mileages were altered to reflect lower mileage indicating that there is a high level of uncertainty in the recorded vehicle mileage data. The impact of the dropping mileage with age is significant in assessing the environment impacts of transport and the potential impact of environment polices. NO<sub>x</sub> and PM emissions of passenger cars drop by more than 20% when a decreasing function of mileage with age is used, instead of a fixed mileage for each environment class. Also, the emission contribution from old vehicles decreases which worsens the cost-effectives of air related policy measures targeting such old vehicles(Stefano, 2013).

Generally, an excessively high hydrocarbon (due to incomplete combustion) causes carbon monoxide emissions to be high. Hydrocarbon emissions result from spark plug misfires, incorrect ignition timing, wrong air-fuel mixture, etc. These findings further suggest that the lack of regular vehicular preventive maintenance is one of the major aggravators of Adama air pollution.

Emission of carbon monoxide is an indicator of incomplete combustion in the engine. CO results from spark plug misfires, incorrect ignition timing, and wrong air-fuel mixture etc.

Incomplete combustion in the engine due to reduction in the level of oxygen may reflect in more CO emission. The overall weighted average vehicle tailpipe CO emissions were 2.7% and 7.8%, respectively, which is almost equal to the maximum allowable standards for the oldest vehicles (1966-1969) in the California BAR-90 Smog Check program for idle and for 2500 rpm.

In generally the tests indicating that CO<sub>2</sub> emission levels in three wheelers Bajaj is more compared to both the minibuses vehicles and TVS vehicles. The minibuses emitting more CO<sub>2</sub> compared to the TVS vehicles. This is supported by the findings from the survey where vehicles owners were asked how often they carried out maintenance work on their vehicles. Carbon Dioxide (CO<sub>2</sub>) - non-toxic gas but contributes towards acidification of oceans and one of the most important greenhouse gases. Governments around the world are pursuing policies to reduce CO<sub>2</sub> emissions to combat global warming.

The NO<sub>x</sub> is formed due to dissociation of molecules when the engine is running hot enough that the oxygen in the air combines with the nitrogen in the air, rather than burning the gasoline. NO<sub>x</sub> emissions were 3Y 4.26 times, 2Y 3.03, Bajaj 2013-15 model 1.1 and Bajaj 2010-12 model 1.033 times higher than the maximum allowable standards for gasoline/gasoline fueled engine in the Indian ARAI-2011 emission standards for passenger cars & light commercial vehicles respectively, which is almost equal to the maximum allowable standards for the oldest vehicles for fixed deterioration factors respectively (TARAO India, 2011).

The result shows that the vehicle age, mileage, and lack of inspection and regular maintenance were factor for increasing particulate matter emission for the minibuses.

Emissions benefits are only achieved if the PCV, TAC, and other emissions control devices function properly. Although functional checks of the ECS's were not done during the study, it is encouraging to note that most of the tested vehicles had these systems on their engines, which indicates that vehicle (owners) generally do not remove the factory-installed ECS's.

## **5. CONCLUSIONS**

The main aim of this research was to determine the level of pollution from vehicle exhaust gases in Adama. The analysis of emissions was done on three wheelers and public minibuses taxi vehicles which amount to 80% of the automobile population in Adama city. It was found

that emissions from both types of vehicles like CO, NO<sub>x</sub>, HC, PM and CO<sub>2</sub> levels are well above worldwide standards for human and environmental health. This indicates that improper functioning and maintenance of causes for pollution from vehicles in Adama. The emissions study has given basic information about emission and vehicle conditions from vehicles were tested. The findings indicate the level of pollution is high and will continue to grow if left unabated. Tail pipe emission findings estimated the highest level of NO<sub>x</sub> emissions at 3.44 g/km, HC emissions at 6.53 g/km, CO at 13.9 g/km, PM<sub>2.5</sub> at 1.3 g/km and 35.96 g/km of CO<sub>2</sub>. These amounts exceed the proposed draft NEMA ambient air quality emission data and the World Bank ambient air quality guidelines. This implies that persons exposed to these emissions on a daily basis are likely to develop health complications over time as the concentration levels increase. The potential diseases include lung cancer, bronchitis, cardiovascular diseases and neurobehavioral effects. The reduction in transport emissions can be achieved in two main ways that include reduced consumption of fossil fuels and increased efficiency in transport energy use.

## **REFERENCES**

- A.C. Administration, " Available [www.Adamacity.gov.et/](http://www.Adamacity.gov.et/)," 2015. [Online]
- Cozzi L, "Energy and Carbo dioxide Emission Trends in the Transport Sector," in *IEA World Energy Outlook*, London, 12th Januray, 2006.
- C. S. Agancy, "Population Projection Values of 2014 at Zonal and Wereds levels by Urban and Resident based," Addis Ababa, 2014.
- Gokhale S. and Ghoshal, "[www.elsevier.com/locate/trd](http://www.elsevier.com/locate/trd)," 2009. [Online]. [Accessed 04 09 2009].
- G. Perry R., Vehicle Emission in Relation to Fuel Composition, vol. 169, science of the Total Environment, 1995, pp. 149-156.
- IPCC, "Guidelines for National Greenhouse Gas Inventories," in *Inter-Governmental Panel on Climate change*, Barcknell, USA, 1996.
- Kean A.J, Effects of Vehicle Speed and Engines load on Motor Vehicles Emissions, Environmental Science and Technology, 2003.
- Ken Gwilliam., Reducing Air Emission from Urban Transport, USA: The International Bank for Reconstruction and Development, 2004.

M. O. W. A. T. Uganda, "National Transport Database," 2006.

S. E. Institute, 2015. [Online]

Stefano Caserini, "Impact of the dropping activity with vehicle age on air pollutant emissions",

Atmospheric Pollution Research, 2013.

T. A. R. A. O. India, "Indian Emissions Regulations, limits, Regulations & Measurement of Exhaust

Emissions and Calculation of Fuel Consumption," ARAI, 2011.

Weyn Chris and R. Klausmeier., Aircare I/M Program, Radian Corporation, 1994.



Solomon Neway obtained his first degree in 2011 from Adama Science and Technology University and MSc in Automotive Engineering in 2016 from Adama Science and Technology University. Currently he is working as lecturer in Mechanical Engineering Department, Arbaminch University.



Ramesh Babu Nallamothe did his masters from National Institute of Technology Warangal, India. He is pursuing PhD at Andhra University. Has 20 years of experience in teaching. He worked for 2 years in USA in the field of softwareEngineering. He has published around 25 research articles in national and international journals. At present he is working at Adama Science and Technology University, Ethiopia.

## **Productivity Improvement by using Statistical Process Control Tools: Case Study at Adama Garment Industry**

**Yeshareg Diresa<sup>1</sup>, Ajit Pal Singh<sup>2</sup>**

<sup>1</sup>General Metal Fabrication & Assembly Department Nekmte Polytechnic, Nekmte, Ethiopia

<sup>2</sup>Production Engineering Department, College of Engineering Defence University, Bishoftu,

Ethiopia E-mail: singh\_ajit\_pal@hotmail.com, Phone No. +251-921512436

### ***Abstract***

*The main purpose of this study is to improve quality and productivity as well as to enhance profit by minimizing defective products produced using statistical process control tools at Adama Garment Industry, Adama, Ethiopia. By using statistical process control (SPC) tools, the existing production system and the quality problems of garment industry have been assessed. The product selected for this study was olive green T-shirt due to high defects rate at final product. Pareto analysis reveals that there is high number of defective rate per month for punkered seam (397), broken stitches (240), size problem (184), misalign seam (121), staggered stitch (106), hole-and-cut (97), uneven stitch (96), fabric (93), thread break (78), color (68), and others (176). For punkered seam and broken stitches defects cause-and-effect diagram was constructed and remedies are recommended. Attribute u-control chart was constructed for one month data (out of control) before and after implementation of remedies again u-control chart was constructed for one month data (under control). Analysis was done after implementation again shows that most of the defects per month reduced as puckered seam (273) and broken stitches (175), only on these defects management has given attention. The annual production output increased from 1461.04 to 1517.8 shirts/year/operator, production line from 45292.24 to 47051.8 shirts/year and machine production output from 45284.4 to 47053.44 per line. Amount which can be saved by implementing the proposed improvement action scales up to 71442 ETB annually, because of two defects only considered. The finding of the study has shown that the industry has many problems; specifically there is high defect rate in the sewing production lines. Therefore it is recommended to implement SPC tools and continuously monitor the production process for visual defects to improve quality and productivity in the garment industry. The quality and productivity improvement can be done via these methods and could benefit to workers as well as to any Ethiopian companies.*

**Keywords:** *Quality, Productivity, Garment industry, Cause-and-effect diagram, Pareto analysis, Control chart.*

## **1. Introduction**

At today's competitive market place, there is a need for organizations to ensure continual improvement. Garment industries experience growing pressure to improve quality, increase productivity and reduce cost with limited resources. Industry needs to reduce response time, eliminate errors and improve customer satisfaction (Martinovic & Colovic, 2007). Statistical process control (SPC) tools are one of the methods used to control and improve productivity by many ways such as reducing repetitive mistakes. SPC tools are also important for timely signaling of unwanted variations in a process. The techniques used in carrying out productivity improvement programs are mostly collecting information, analyzing and increasing the effectiveness of work (Ott et al., 2000). SPC implementation is important as it could improve process performance by reducing product variability and improves production efficiency by decreasing scrap and rework which leads to productivity improvement.

## **1.2. Quality and Productivity Improvement**

In this highly competitive world, quality plays vital role as it leads to an improvement in productivity. Productivity, quality and cost of operation relatively dependent on each other. By improving the quality, the productivity also must be improved and hence lower the reject rates or defects (Jafri & Chan, 2001). Effective quality improvements should result in a future stream of benefits, such as: reduced failure costs, lower appraisal costs, increased market share, increased customer base and more productive workforce. Improved quality increases productivity (Fig. 1), hence, many world class industries use quality as a powerful competitive tool.

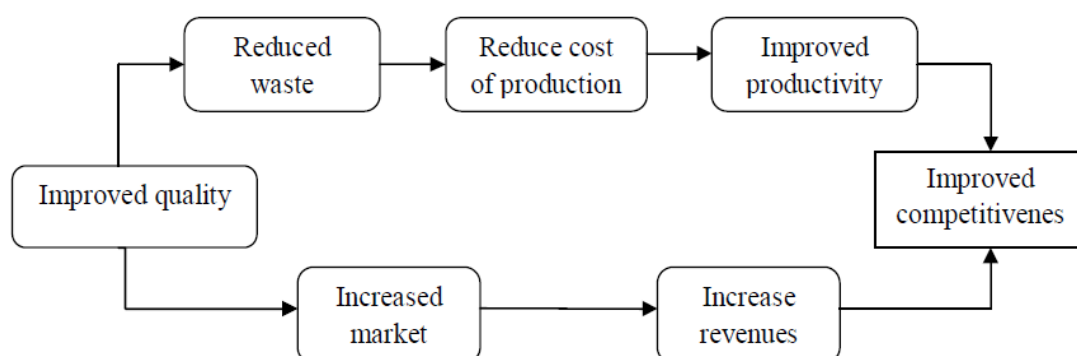


Fig. 1. Quality and competitiveness

There are many aspects of quality in garment operations including quality of garment design, quality of production, quality of inspections, and quality of sales as well as quality of

marketing of the final product which is as important as the quality of the garment itself. In garment industry, quality control should be practiced from the initial stage of sourcing of raw materials to the stage of finished garment (Mears, 1995).

### **1.3. Statistical Process Control**

SPC is a collection of problem-solving tools useful for achieving process stability through the reduction of variability. The major tools in SPC are SPC charts (Montgomery, 1996). They are charts of observations generated over time with a center line and control limits that help interpret performance and detect changes in the process. SPC is a powerful problem-solving technique used for monitoring, controlling, analyzing, managing and improving a process using statistical methods (Antony et al., 2000). Quality in manufacturing requires the practices of SPC for controlling and managing a process either manufacturing through the use of statistical methods. A point out that SPC's strength lies in its ability to monitor both process center and its variation about that center. It can be done by collecting data from samples at various points within the process; variations in the process that may affect the quality of end product can be detected and corrected. Thus, SPC will be able to reduce the probability of passing problems to the customers (Ishikawa, 1982).

### **1.4. Basic Tool for Statistical Process Control**

SPC tools can be through of as a filtration process/funnel for quality and productivity(Griffith, 1996). Seven SPC tools can be used in all process phases, starting from the beginning of a product development up to management of a process, on day to day basis, and in systematic manner. They form the fundamental foundation for all problem solving and quality control activities (Sultana et al., 2009). The seven QC tools are (Ishikawa, 1982): Check sheet, Scatter diagram/chart, Histogram, Flow chart, Cause-and-effect or fishbone diagram, Pareto chart and Control charts (Shewhart, 1931; International Standard-ISO 8258). SPC charts build on the principle of allocating the observed variation in performance to two categories of sources viz., common causes and special causes. Common-cause variation is that which can be expected to occur in a stable process or system-one which is 'under control'. Special-cause variation may derive from systematic or unexpected deviation from the norm and may highlight an area or an observation which is worthy of further investigation (Jafri & Chan, 2001; Shewhart, 1931). The different characteristics that can be measured by control charts can be divided into two group's viz., variables (X bar and R charts) and attributes (np-chart, p-chart, c-chart, and u-chart).

SPC is an important tool and leads to many process improvements and positive process results, such as (Panirchelvan, 2009): uniformity of output, reduced rework, fewer defective products, increased profit, lower average cost, fewer errors, higher quality output, less scrap, less machine downtime, less waste in production labor hours, increased job satisfaction, improved competitive position.

### **1.5. Statement of the Problem**

Adama Garment Industry (AGI), Adama, is an industry where this study was conducted. The existing subjective methods of quality control i.e. the quality decision is based on perception not based on data analysis using SPC tools. This does not guarantee the quality and productivity in garment processing.

AGI has the following shortcomings:

- High defect rate in manufacturing of garment is one of the problems. As a result, the industry is not able to provide its customers the necessary quality and quantity of garments.
- Lack of systematic quality control strategy in order to keep the production process in control. Quality control is done by using visual inspection which is not effective and mostly attention is given for detecting defects of the products rather than preventing it during production. Also no analysis was done by using quality control techniques, which lets the industry monitor their processes and determine whether they are in or out of control. For the entire problems indicated, an accurate and effective process control method is required.
- Other shortcomings are low skilled employees, shortage of adequate training, low employees satisfaction level, capacity underutilization, work in process, high rework and scrap rate, low product quality, low volumes of production, long lead time, setup time, absenteeism, and poor inventory management system are some of the specific problems.

#### **1.5.1. General Objective**

The main objective of this study is to apply SPC tools for improving quality and productivity on selected product (i.e. Olive green T-shirt) in Adama Garment Industry, Adama (Ethiopia).

#### **1.5.2. Specific Objectives**

The specific objectives are:

- Examine and identify the quality associated problems;
- Identify the highest frequency of defects occur at workstations;

- Identify the potential areas for quality and productivity improvement;
- Implementing of SPC tools to control the quality of the product (Olive green T-shirt) through which productivity improvement could be realized.

In this study garment manufacturing defects and their causes, and how to improve and control a process using SPC tools has been investigated. This study apply the SPC tools in the production processing line and on final garments (product) in order to improve productivity by identifying garment defects that causes the highest waste in the industry and to give suggestion/implementation for improvement. As per the sewing section/department manager suggestion, the specific product was selected based on high defects found in process and at finishing manufacturing stages.

## **2. Material and Methods**

By giving a focus to sewing section at AGI, the following types of defects were collected (30 observations) Olive green T-shirt from March 15-April 20 during 30 working days (Table 1) at sewing department of AGI. Having the observed data collected, data organization and analysis has been carried out using SPC tools such as Pareto chart (analysis), cause-and-effect diagram, and u-control chart for attributes. After analyzing the data, interpretation has been carried out.

Table 1. Types and number of defects

<b>Type of defects (Attributes)</b>	<b>Number of defects</b>	<b>Type of defects (Attributes)</b>	<b>Number of defects</b>
Puckered seam	397	Uneven stitch	96
Broken stitches	240	Fabric	93
Size problem	184	Thread breaks	78
Misalign seam	121	Color	68
Staggered stitch	106	Others	176
Hole and cut	97		

### **2.1. Pareto Chart Analysis**

Table 2 shows summarized form of the inspection sheet for March 15-April 20. As per Table 2, a Pareto chart was constructed. It revealed that the two major visually identified defects are puckered seam (23.97%) and broken stitch (14.49%), contribute about 38.46% defects

and followed by size problem (11.11%) (Fig. 2). All other minor defects are also shown in the Pareto chart. Taking into consideration that it is easier to reduce a high frequency than a low one, the diagram shows that it would be more useful that the improvement focuses on the first two causes which are puckered seam and broken stitch defects rather than on the low incidence ones.

Table 2. Data sheet for Pareto chart

Type of defects (Attributes)	Number of defects	Cumulative total	Percentage of overall total	Percentage cumulative total
Puckered seam	397	397	23.97	23.97
Broken stitches	240	637	14.49	38.47
Size problem	184	821	11.11	49.58
Misalign seam	121	942	7.31	56.88
Staggered stitch	106	1048	6.40	63.29
Hole and cut	97	1145	5.86	69.14
Uneven stitch	96	1241	5.80	74.94
Fabric	93	1334	5.62	80.56
Thread breaks	78	1412	4.71	85.27
Color	68	1480	4.11	89.37
Others	176	1656	10.63	100.00

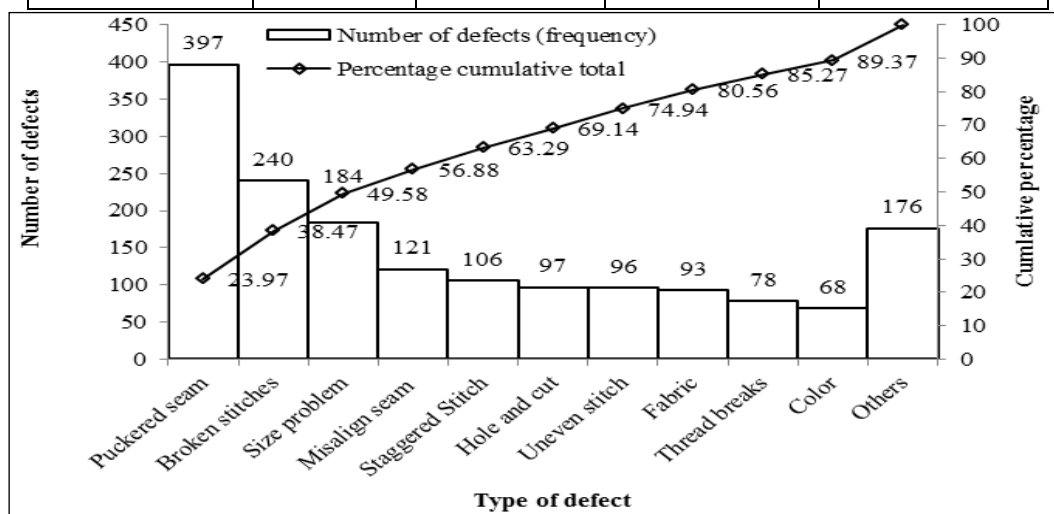


Fig. 2. Pareto chart for defects Olive green T-shirts observed

## **2.2. Cause-and-Effect Diagram**

Once the core problem has been identified, the cause of the core problem and the effect caused by the problem are stated from the organized information. Thus the next process is forming a diagram showing the cause-and-effect relationship in the form of a problem tree. This is done by restating all negative condition of the problem into positive condition that is desirable and realistically achievable.

(a) *Puckered seam defect*: It is the gathering of material resulting from improper tension adjustment, fittings selection and adjustment, needle selection. Figure 3 shows some possible causes of puckered seam defects.

(b) *Broken stitch defect*: Often times the fault of wrong type of stitch for specific seam construction could be caused by excessive tightness in machine tensions. Figure 3 shows some possible causes of broken stitch. Figures 3 and 4 reveals that the major causes of puckered seam and broken stitch defects are machine set up, low skill of workers, defective raw material, environment and lack of communication among different departments to avoid defects.

Sewing machine must have a daily check sheet and machine operator must check the machine set up and condition like its pressure, tightness, speed, and temperature every days to confirm that the machines are in good condition but operators doesn't check the conditions of machine which result a defects in products. Because the industry does not provide any training especially on how to avoid defect caused by human, no work instruction sheets used by operators that used as a guide for the proper work method and also poor quality management result the defects. Finally every incoming material doesn't go through quality checking to avoid defects. Hence, the combination of all factors result puckered seam and broken stitch defects and affects quality and productivity of the industry.

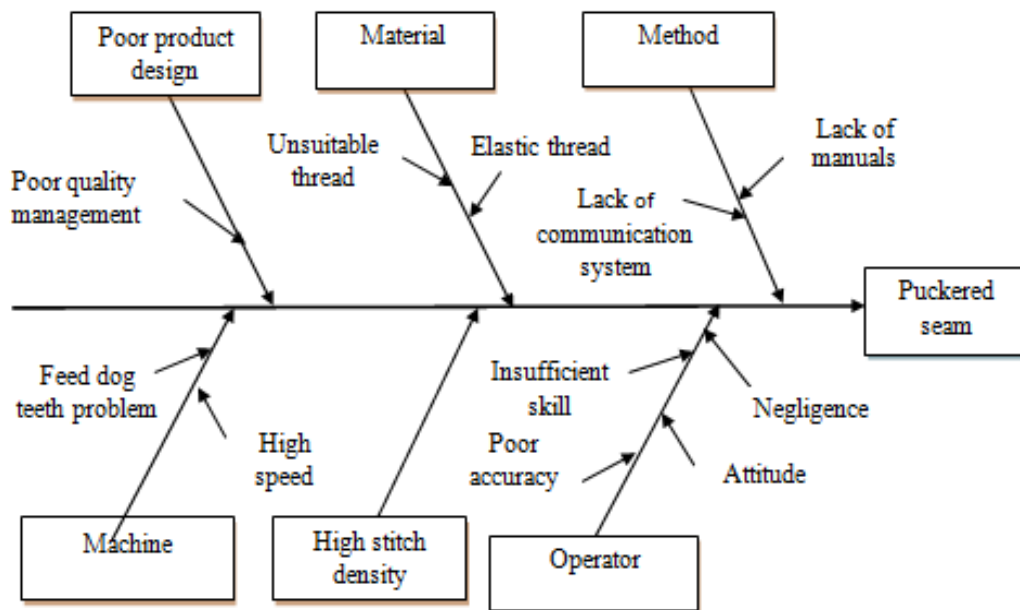


Fig. 3. Cause-and-effect diagram for puckered seam defect

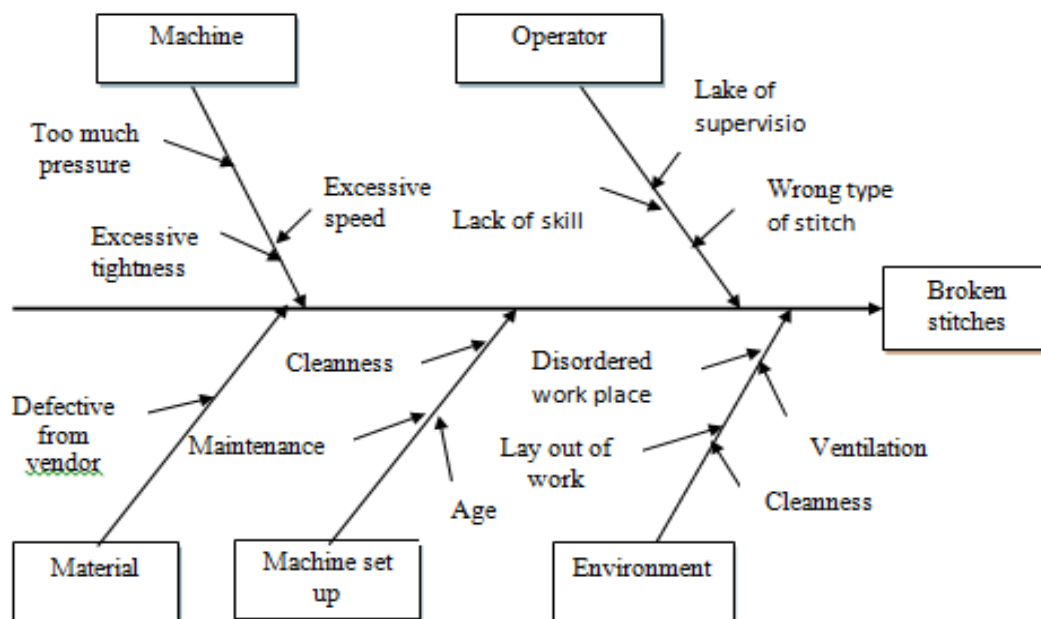


Fig. 4. Cause-and-effect diagram for broken stitch defect

### 2.3. u-Control Chart for Attributes

The data has been collected in March 15-April 20 production. Based on the data sheet in Table 3, attribute u-control chart with variable subgroup number has been used and constructed by using Microsoft Office Excel 2007, as shown in Fig. 5. The process average defect per Olive green T-shirt (product) is calculated as:  $\bar{u} = \sum c \div \sum n = 1656 \div 5497 = 0.3010$

(a) *Analysis of the Pattern of the u-Control Chart:* A u-chart has been constructed (as per Table 3) to understand the distribution of the number of defects per Olive green T-shirt during the 30 working days period and it indicates an out of control condition either when one or more points fall beyond the control limits, or when the plotted points exhibit some non-random pattern of behavior.

Table 3. Data sheet for the construction of u-control chart for defective T-shirts

Days	No. of T-shirts	Defective T-shirts (c)	Proportion defective ( $u=c \div n$ )	Standard deviation
<i>UCL</i>	<i>UWL</i>	<i>CL</i>	<i>LWL</i>	<i>LCL</i>
1	170	74	0.4353	0.0421
<i>0.4276</i>	<i>0.3855</i>	<i>0.3013</i>	<i>0.2171</i>	<i>0.1750</i>
...	...	...	...	...
30	200	56	0.2800	0.0388
<i>0.4177</i>	<i>0.3789</i>	<i>0.3013</i>	<i>0.2237</i>	<i>0.1849</i>
Total	5497	1656	-	-

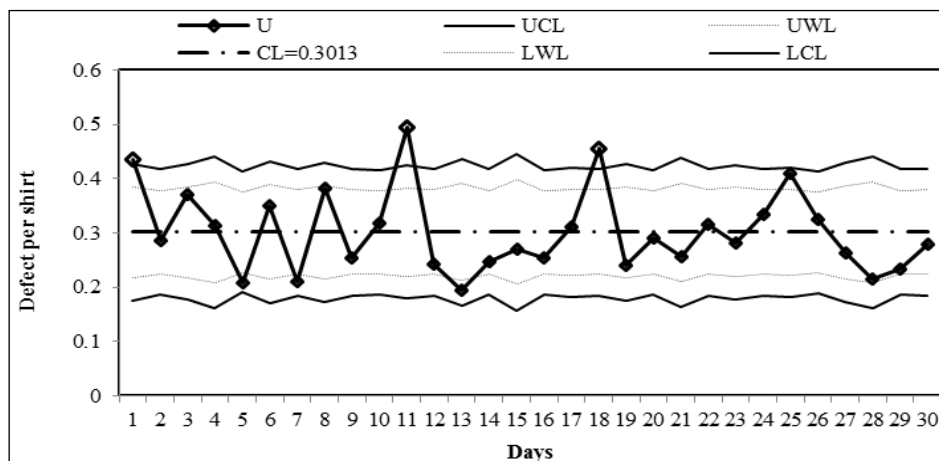


Fig. 5. u-control charts for defective Olive green T-shirt from March 15-April 20

(b) *Interpretation of the u-Control Chart:* Figure 5 presents, the point that lies within the warning limits (WL) in which the process assumed to be on target and if it lies outside the action limits the process is off target and the machines must be reset or other action have to be taken. However; points that lie between the warning and action limits are a signal that the process may be off target. Moreover, the points that lie on these zones needs appropriate

adjustment. Therefore after all these analysis has been done and process control chart indicate that the process was out of control at three points at subgroup numbers 1, 11, and 18 (Fig. 5) because of assignable cause (power interruptions and operator absent and new operator assigned). It confirms that improvement action must to be taken. Brain storming session has been carried out to find root causes. Based on these identified causes, improvement remedy suggestion has been made and provided to the industry quality control department.

The uneven upper control limit ( $UCL = \bar{u} + 3\sqrt{\bar{u} \div n}$ ), lower control limit ( $LCL = \bar{u} - 3\sqrt{\bar{u} \div n}$ ) and warning limits ( $UCL = \bar{u} \pm 2\sqrt{\bar{u} \div n}$ ) of the chart are due to different sample size taken due to daily production variation. For example, from calculation, the UCL for sample size of 170 is 0.4276 and 0.4177 for sample size of 200. By discarding the values for the subgroups 1, 11 and 18 (Table 3) the revised u-control chart has been constructed and it indicated that the process in control (Fig. 5).

The subgroups with assignable causes such as subgroup 1 with the value of 0.4353, subgroup 11 with the value of 0.4944 and subgroup 18 with the value of 0.4550 are not considered part of the natural variation and are discarded from the data, and new values of center line and control limits computed with remaining data. Thus the center line and control limits must be revised after discarding the out of control points as shown in Fig. 6. The sub groups are discarded to check the one which are available on the warning zones because they have a chance to be out of control. Hence Fig. 6 indicates all are under control.

*(c) Remedy Suggestion Forwarded to Industry:* Before correcting a defect, the following points must have to be remembered.

- How many of the particular defects are reject?
- If corrected what other types of defects may be produced as a result of the adjustment made?
- Only make adjustments when sure that it will produce non defect garments.

Tables 4 and 5 summarize the remedy suggestion for puckered seam defects and broken stitch defects respectively forwarded to industry.

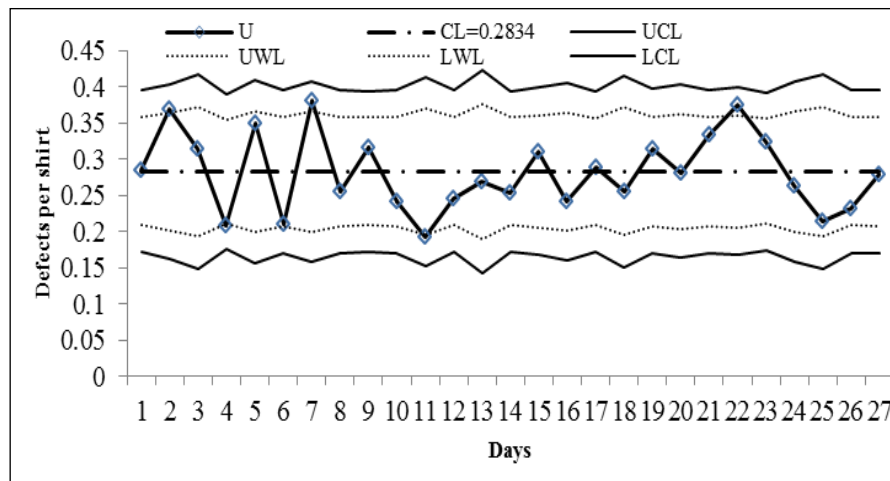


Fig. 6. Revised u-charts

Table 4. Remedy suggestion for puckered seam defect

Table 5. Remedy suggestion for broken stitch defect

<p><b>Type: Operator</b></p>	<p><b>Type: Operator</b></p>
<ul style="list-style-type: none"> <li>▪ Creation of awareness about defects and continuous follow up to avoid negligence,</li> <li>▪ The development of motivation scheme,</li> <li>▪ Pay full attention and avoid carelessness for minor mistakes,</li> <li>▪ Scaling up the proper attitude toward quality,</li> <li>▪ Enabling operators skillful/conducting training need assessment and provide appropriate training.</li> </ul>	<ul style="list-style-type: none"> <li>▪ Creation of awareness about defects,</li> <li>▪ Continuous follow up to avoid negligence,</li> <li>▪ Favor good attitude toward quality,</li> <li>▪ Capacitate their skill in identifying causes of defects before it occurs or provide training,</li> <li>▪ Safely handling of materials, tools and equipment's.</li> </ul>
<p><b>Type: Material</b></p>	<p><b>Type: Material</b></p>
<ul style="list-style-type: none"> <li>▪ Procurement of raw material with appropriate quality from appropriate source,</li> <li>▪ The practice of eligible raw material suppliers' selection process,</li> <li>▪ Provision of training on Fabric characteristics for procurement personnel.</li> </ul>	<ul style="list-style-type: none"> <li>▪ The use of raw material with appropriate quality,</li> <li>▪ Every incoming material needs to be inspected properly.</li> </ul>

<b>Type: Machine setup and operation</b>	<b>Type: Machine setup and operation</b>
<ul style="list-style-type: none"> <li>▪ Improve machine feed slippage and reduce incorrect machine operation,</li> <li>▪ Reduce feed dog teeth problem,</li> <li>▪ Implementation of preventive maintenance planning technique,</li> <li>▪ Improve a needle problem.</li> </ul>	<ul style="list-style-type: none"> <li>▪ Properly set minimizing tight tension,</li> <li>▪ Decrease the machine speed at the appropriate level,</li> <li>▪ Avoid sharp feeds or too much pressure.</li> </ul>
<b>Type: Design</b>	<b>Type: Machine and equipment</b>
<ul style="list-style-type: none"> <li>▪ Product design should incorporate customer requirements,</li> <li>▪ Compatible with process capability.</li> </ul>	<ul style="list-style-type: none"> <li>▪ Development of preventive maintenance to ensure machine always in a good condition,</li> <li>▪ Machine, must be clean all the time.</li> </ul>
<b>Type: Management</b>	<b>Type: Environment</b>
<ul style="list-style-type: none"> <li>▪ Has to be committed in provision of the necessary resources,</li> <li>▪ Committed in taking corrective actions,</li> <li>▪ Develop fact-based decision making process,</li> <li>▪ Develop leadership management style.</li> </ul>	<ul style="list-style-type: none"> <li>▪ Practicing clean work environment,</li> <li>▪ Creation of favorable working condition.</li> </ul>

(d) *Revised u-Control Chart*: u-Control chart after improvement was constructed to analyze the process and help to determine how to yield further improvement. To plot control chart, data has been collected again for 30 working days for the month of May month (Table 6). Table 6 reveals that improvement is made on both defects. The process average defect per Olive green T-shirt is calculated as follows:  $\bar{u} = \sum c \div \sum n = 1574 \div 5489 = 0.2869$

Based on the data sheet in Table 7, revised u-control chart was constructed for the month of May. After remedy suggestion recommended and implemented (for puckered seam and broken stitch defects) the revised u-control chart indicates that the process is in-control (Fig. 6). Within these limit the industry can continue their manufacturing process without any loss. After the implementation of the remedy suggestion for the identified defects, improvements have been observed on both defects. Tables 2, 8, Figs. 2 and 7, reveals that the puckered seam defect had reduced from 397 (23.97%) (March 15-April 20) to 240 (17.34%) (May month) broken stitch defect had reduced from 240 (14.49%) (March 15-April 20) to

175 (11.12%) (May month). Whereas other defects may increase or decrease as SPC tools are not implemented by the quality control department. Consequently, the change in defect reduction rate for the two months has been found to be  $397-273=124$  (6.63%). That is 6.63% Olive green T-shirts can be produced more per month only from defect caused by puckered seam. Where as in case of broken stitch defect, as a result an improvement of  $240-175=65$  (2.04%) Olive green T-shirts can be produced more per month.

Table 6.Type and number of defects after improvement

Type of Defects (Attributes)	Number of defects	Type of defects	Number of defects
Puckered seam	273	Uneven stitch	120
Broken stitches	175	Fabric	90
Size problem	196	Thread breaks	131
Misalign seam	110	Color	113
Staggered stitch	115	Others	181
Hole and cut	70		

Table 7. Data sheet for the construction of revised u-control chart for defective T-shirts

Days	Number of T-shirts	Defective T-shirts (c)	Proportion defective ( $u=c \div n$ )	Standard deviation
<i>UCL</i>	<i>UWL</i>	<i>CL</i>	<i>LWL</i>	<i>LCL</i>
1	200	58	0.2900	0.0379
0.4005	0.3626	0.2869	0.2112	0.1733
...	...	...	...	...
30	209	60	0.2871	0.0371
0.3981	0.3610	0.2869	0.2128	0.1757

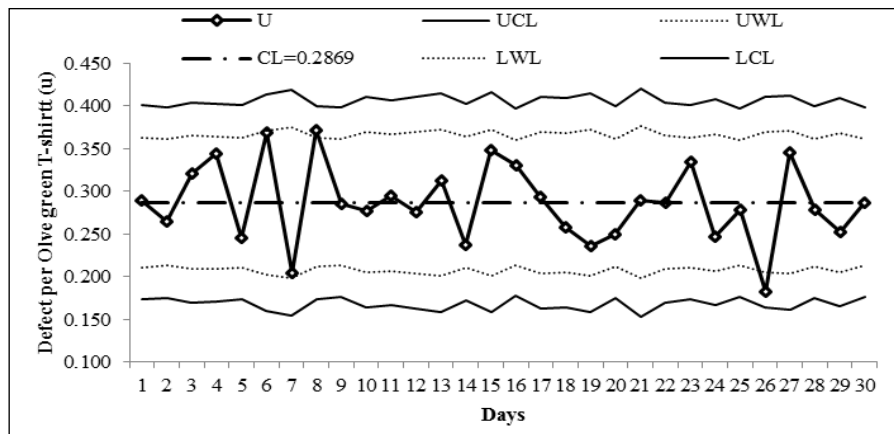


Fig. 7. Revised u-control chart for defective Olive green T-shirt after improvement for May month (Table 8)

Table 8. Data collected after improvement for broken stitch and puckered seam defects for May month

Type of defects (category)	Number of defects (frequency)	Cumulative total	Percentage of overall total	Percentage cumulative total
Puckered seam	273	273	17.34	17.34
Size problem	196	469	12.45	29.76
Broken stitches	175	644	11.12	40.91
Thread break	131	775	8.32	49.23
Uneven stitch	120	895	7.62	56.85
Staggered stitch	115	1010	7.31	64.16
Color	113	1123	7.18	71.34
Misalign seam	110	1233	6.99	78.33
Fabric	90	1323	5.72	84.05
Hole and cut	70	1393	4.45	88.50
Others	181	1574	11.5	100.00

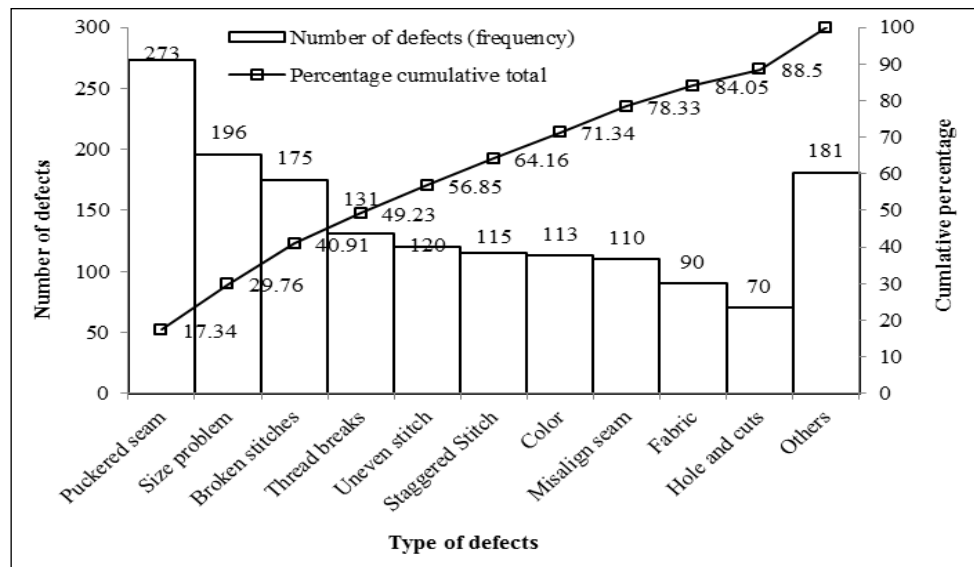


Fig. 7. Pareto chart for defect Olive-green shirt after improvement observed during May month (Table 6)

### 3. Productivity Measurements After Remedy Suggestion Implementation

As per the observation made on the industry the concentration is only given on final garments (product) inspection, daily activities and solving of the causes of defects but this is not the right way to minimize the causes of defects. The improvement achieved has been evaluated in terms of productivity, defect reduction rate and cost saving.

From the data average daily product of Olive-green T-shirt was 183 per production line. From these some of them were returned to reworks because of different defects. Among these defects major two which were puckered seam and broken stitch defects have been calculated. Before improvement made monthly puckered seam and broken stitch defects were (637). When calculating per day and average were 21.23 defects. However; daily production output was 183. Because of these two defects, the outputs were reduced to 161.77 Olive green T-shirts per day. Labor and machine productivity was calculated as follows (Shumon, 2010).

$$\text{Labor production output} = \frac{\text{Total number of output per day per production line}}{\text{Number of operators worked}} \quad (1)$$

$$\text{Machine production output} = \frac{\text{Total number of output per day per production line}}{\text{Number of sewing machines used}} \quad (2)$$

As per (1) the labor production output was  $161.77 \div 31 = 5.218$  Olive green T-shirts per day and per month were 156.54. After improvement, the defect were reduced to 448 during the study (15 April-20 May), and resulted 14.93 defects per day. Therefore, as per (1) the labor production output is equal to  $168.06 \div 31 = 5.421$  Olive green T-shirts per day and per month 162.64 Olive green T-shirts. Therefore, the labor production output was increased from 5.218 to 5.421 per day and from 156.4 to 162.66 per month. The average annual total working days in 2012 were 280, and hence, the annual production output grows from 1461.04 to 1517.8 Olive green T-shirts per year per operator. Total production output of the single production line grows from 45292.24 to 47051.8 Olive green T-shirts per year, where 31 are number of operators per line.

Machine production output before improvement as per (2) was  $161.77 \div 27 = 5.99$  Olive green T-shirt per day. After remedy suggestions given it become  $168.06 \div 27 = 6.224$  Olive green T-shirts per day. Therefore, machine production output increased from 5.99 to 6.224 per day per machine and for per year it was 45284.4 to 47053.44 per line, where 27 are number of machines per line. If the improvement achieved is equivalently converted to economic worth, the industry could save  $1190.7[(124 + 65) \times 6.30]$  ETB per month per production line (Jana and Singh, 2009) (where 6.30 ETB is average rework cost of Olive green T-shirt). This saving grows 5953.5 ETB per month for five production lines of the industry. Equivalently, the amount of money which can be saved by implementing the proposed improvement action scales up to 71442 ETB annually, because of two defects. This economic analysis clearly affirmed the fact that preventive measure assuming in the reduction of causes of defects help the industry in generating revenue.

#### **4. Conclusion**

The results obtained from the assessment of AGI shows low productivity due to poor quality control system. Major factors for low productivity are poor knowledge about SPC tools, lack of proper education and trainings, poor leadership, poor quality control, low technological level, lack of teamwork and lack of recognition activities. Though, most of these problems are potential areas for quality and productivity improvement, problems pertaining to technological upgrading and teamwork may not be feasible to the AGI for various reasons. This industry has financial constraints to renovate their technology in order to improve the quality of their products. On the other hand the current AGI dominant work culture does not encourage teamwork. Moreover, detailed analysis results the following points:

- The main problems observed are the problem of excessive rework of products due to defect outputs and there is no effective utilization of resources (material, manpower, machineries, time).
- There is no clear information exchange among different departments of the industry about the progress of job. For example the quality control inspection results is not prepared in such a manner that it could explain test request receiving time, result delivering date and time, causes of defect and possible remedial solution that have to be made by the concerning section.
- Training is required to reduce the defect rate of final products through SPC tools. In conclusion the industry should strive for reducing the defect rate of final products through SPC tools. SPC tools are important as it could improve process performance by reducing product variability and improves production efficiency by decreasing scrap and rework.

## **References**

1. Antony, J., Balbontin, A. & Taner, T. (2000). Key ingredients for the effective implementation of statistical process control. *Work Study*, 49(6), 242-247.
2. Griffith, G.K. (1996). *Quality Technicians*, 3rd Edition, Prentice-Hall, Inc., Englewood Cliffs, Handbook, New Jersey.
3. International Standard. ISO 8258, (1991-E) Shewhart Control Charts. International Organization for Standardization, Geneva, Switzerland.
4. Ishikawa, K. (1982). *What is Total Quality Control?* Prentice-Hall Inc. Cliffs, New Jersey.
5. Jafri & Chan (2001). Quality and Productivity Improvement. *International Journal for Quality Research*, 7(9), 293-303.
6. Jana, D.R. & Singh, A.P. (2009). Quality improvements at an automobile component manufacturing plant: A case study. *International Journal of COMADEM*, 12(3), 32-40.
7. Martinovic, M. & Colovic, G. (2007). System proof in garment industry. *Serbian Journal of Management*, 2(1), 77-85.
8. Mears, P. (1995). *Quality Improvement Tools and Techniques*. McGraw-Hill, Inc.
9. Montgomery, D.C. (1996). *Introduction to Statistical Quality Control*. John Wiley & Sons, Hoboken.

10. Ott, E.R., Schilling, E.G. & Neubauer, D.V. (2000). *Process Quality Control*, 3rd Edition, McGraw-Hill, New York.
11. Panirchelvan, R. (2009). Quality control in bearing manufacturing company using statistical process control. Master Thesis, University Malaysia Pahang, Malaysia.
12. Shewhart, W.A. (1931). *Economic Control of Quality of Manufactured Product*. D.Van Nostrand, Co., New York.
13. Shumon, Md. Rezaul Hasan (2010). Productivity Improvement through Line Balancing in Apparel Industries. Proceedings of the 2010 International Conference on Industrial Engineering and Operations Management, Dhaka, Bangladesh, January 9-10.
14. Sultana, F., Razive, N.I. & Azeem, A. (2009). Implementation of statistical process control (SPC) for manufacturing performance improvement. *Journal of Mechanical Engineering*, Transaction of the Mechanical Engineering Division, The Institution of Engineers, Bangladesh, ME 40(1), 15-21.

## **Exploring the Industrial Characteristics of Tef [*Eragrostis tef*(Zucc.) Trotter]: An Engineering Approach**

**Workineh Abebe**

Ethiopian Institute of Agricultural Research Email: workineh09@gmail.com,  
[worknaber@yahoo.com](mailto:worknaber@yahoo.com) Tel. +251 0983680300 (Mob.)

*Tef [*Eragrostis tef* (Zucc.) Trotter] is recently been receiving global attention due to its promising potential in nutrient-rich, gluten-free and functional food product formulations. As it is almost a new raw material for industrial scale modern processing, studying the bulk handling and processing characteristics of the grain and its intermediate and final products is compulsory. In this paper, the flowability and compaction, water sorption and thermal properties of flours from three Ethiopian tef varieties together with wheat (whole and refined) and rice flours (included as references) are discussed. Accordingly, the flowability of tef flours were inferior to the reference flours and their flow and compaction properties were more sensitive to flour moisture content change. The tef flours exhibited sigmoidal sorption isotherms which are similar to other common cereal flours and their computed monolayer water content were 0.053 (BET model) and 0.057 (GAB model) g water/g dry solids. Starch gelatinization enthalpy of the tef flours was independent on tef variety type and similar to rice, while it is higher than that of wheat flour. The amylopectin recrystallization extent after 7 days of storage at 4°C was significantly higher in tef than in wheat flour indicating the existence of higher retrogradation (staling) in tef products in the specified storage period. Therefore, the design and development of bulk handling and processing devices as well as product formulation should be considerate of such peculiarities of tef flour.*

### **Introduction**

Tef [*Eragrostis tef*(Zucc.) Trotter] is an indigenous to Ethiopia. It is one of the most dominant crops in Ethiopia that covers about 3 million ha and with 4.75 million tons of grain annual harvest (CSA, 2015) contributing around 4 billion Birr to the national GDP. In Ethiopia, tef is mainly consumed as injera (a staple food in the country) after it is whole floured with disc type cottage mills and traditionally processed at house hold level. Products from tef are well packed, rich in carbohydrate and fiber, with high iron, calcium and zinc. The grain proteins offer an excellent balance among the essential amino acids. It has no gluten and gluten-

like proteins, making it suitable for celiac disease patients (Dekking et al., 2005), and also due to other dietary advantages such as slow-release of carbohydrate constituents useful for diabetic patients (Abebe & Ronda, 2014). Hence, tef is recently receiving attention from the global modern food industry for its high potential in nutrient-rich food product formulation, especially in gluten-free and functional foods.

The great majority of tef consumers in Ethiopia traditionally prefer to buy the tef grain and get the grain milled rather than buying the flour or the baked injera. However, with the changing life styles in the urban areas, this traditional way of processing at each household is becoming a challenge and forcing people to buy tef flour and injera from household and micro level processors or some supermarkets (Abiyu et al., 2013). In addition, the demand for tef injera export is growing. Therefore, these factors are contributing to the proliferation of household, micro-level and cottage level processors making growth to industrial scale tef processing eminent in Ethiopia. Therefore, the local and international trend in tef utilization underlines industrial scale processing which requires bulk handling and processing of its flours.

Flour flow and compaction characteristics are the inherent behaviors of a flour system that affect different unit operations, such as flow from hoppers and silos, transportation, mixing, compression, processing and packaging (Knowlton et al., 1994). Controlling moisture content of a flour system through studying its moisture sorption characteristic is a critical activity for facilitation of flour handling during storage and processing. Studying sorption behavior of a flour system helps to determine flour monolayer content (which gives information about the minimal water content conferring food stability over time) and isotherm equation (a compulsory model for evaluating the water sorption kinetics in the flours) (Al-Muhtaseb et al., 2002). Furthermore, in cereal processing application of thermal treatment of different magnitude at varying moisture level is the most important unit operation. Hence, understanding the thermal transitions that the starch (which is the dominant component in cereal flours) undertakes in the presence of other components of the system (such as proteins, lipids and other nonstarch carbohydrates) is very important (Schiraldi et al. 2009).

Tef is a relatively new cereal for the modern food industry which perhaps has the smallest grain size among carbohydrate-rich kernels. Tef is consumed as a whole grain and its flours have different physical and chemical properties from other common cereal flours like wheat and rice (Abebe and Ronda, 2014). This may affect flour moisture sorption, flowability and

thermal behaviors which in turn dictate the bulk handling and thermal characteristics during handling (storage and conveying) and processing. Therefore, this paper focuses on the studies done on flowability and compaction, moisture sorption and thermal characteristics of tef flours from three Ethiopian tefcultivars.

## **2. Materials and Methods**

### **2.1. Materials**

Three tef varieties DZ-01-99 (brown tef), DZ-Cr-37 (white tef) and DZ-Cr-387 (white tef) obtained from the DebreZeit Agricultural Research Center were whole milled using Cyclotech Sample mill (Foss Tecator, Sweden) fitted with a 0.5 mm sieve. Rice, whole and refined wheat flours used as references were supplied by Emilio Esteban SA (Spain). The initial proximal compositions, mean particle diameter ( $D_{50}$ ), size dispersion ( $(D_{90}-D_{10})/D_{50}$ ), bulk density, true density, and damaged starch level and physical properties of tef, refined wheat and rice flours are reported in Abebe et al. (2014 & 2015).

### **2.2. Sorption isotherm**

Approximately 3g of flour samples were transferred to glass vials and dried in oven at 50°C for 24 h. and then the flours were further dehydrated in desiccators with  $P_2O_5$  at room temperature. This was taken as the weight of dry sample. The dried samples were equilibrated in evacuated desiccator over saturated salt solutions of LiBr,  $CH_3COOK$ ,  $MgCl_2 \cdot 6H_2O$ ,  $K_2CO_3$ , NaBr,  $NaNO_2$ , NaCl, KCl, and  $K_2SO_4$  at corresponding water activity ( $a_w$ ) of 0.07, 0.23, 0.33, 0.43, 0.59, 0.64, 0.76, 0.85 and 0.98 respectively, at  $20 \pm 2^\circ C$ . Equilibrium was acknowledged when three daily weight measurements varied less than 0.001g. Moisture content (MC) at each  $a_w$  was determined in triplicate. BET, Peleg, GAB, and modified GAB models (Equations 1 to 4 respectively), were fitted to experimental data of MC versus  $a_w$ . Linear and nonlinear regression statistical analyses were performed using Statgraphics Centurion XVI program. The quality of the fitting was evaluated by comparing the  $R^2$  and the root mean squared error (RMSE).

$$M = \frac{A \times B \times a_w}{[(1 - a_w) \times (1 + (B - 1) \times a_w)]} \quad (1)$$

$$M = A \times a_w^C + B \times a_w^D \quad (2)$$

$$M = \frac{A \times B \times C \times a_w}{(1 - C \times a_w) \times (1 - C \times a_w + B \times C \times a_w)} \quad (3)$$

$$M = \frac{A \times B \times C \times a_w}{(1 - C \times a_w) \times (1 - C \times a_w + B \times C \times a_w)} + \frac{A \times B \times C \times D \times a_w^2}{(1 - C \times a_w) \times (1 - a_w)} \quad (4)$$

Where:  $A$  in equation 1, 3, and 4 = the monolayer moisture content of the BET, GAB and modified GAB models,  $B$  in equations 1, 3 and 4 and  $C$  in equations 3 and 4 = energy constants related to the temperature.  $A$ ,  $B$ ,  $C$  and  $D$  = constants of Peleg model (Equation 2) as this model is purely empirical.

### 2.3. Flour flowability and compaction characteristics

This study was done at 2 moisture content levels adjusted by putting them in evacuated desiccators containing saturated salt solutions of NaBr or KCl, with  $a_w$  of 0.59 and 0.85 respectively at 20°C. A powder flow analyzer (PFA) coupled to a texture analyzer, TA-Xt 2 Plus (Stable Micro Systems, UK) was used to measure the flowability and the compaction properties of the flours as stated in Landillon et al. (2008) each with 4 replications. Cohesiveness is the tendency for particles of powder to cling together and agglomerate. The PFA measures this cohesion characteristic by moving the blade in such a way as to lift the powder. The negative area under the force versus distance curve while lifting is recorded as cohesion coefficient (g·mm). The cohesion index (mm) is calculated by dividing the cohesion coefficient by the initial weight of the sample. Powder flow speed dependence (PFSD) test which helps to assess if the flow properties of a powder change with increasing or decreasing flow speeds, was done as described in Janjatović et al. (2012) with 5 sets of 2 cycles each at increasing speeds (10, 20, 50, 100 mm/s and finally 10mm/s). The compaction coefficient (g·mm) is the work required to move the blade down through the powder column using a compacting action. The compaction coefficient at each speed is the positive area under the compaction curve averaged over the two cycles at each speed. An increase in the compaction coefficient as the test speed increases indicates increasing resistance to flow while a decrease would mean that the powder becomes more free flowing. Marginal or no change of the compaction coefficient with flow speed would show that the powder is flow speed independent. Caking properties, which indicate the potential of powder to form a compact mass, were determined as stated in Abu-hardan and Hill (2010). In this test 5 compression cycles were performed to form a powder bed and finally the blade sliced the

cake formed and the force required for cutting through the cake or bed was measured. The average force required to cut the cake was recorded as cake strength (g).

## **2.4. Thermal properties**

Thermal characteristics of flours were determined using a differential scanning calorimeter (DSC) (Mettler Toledo, SAE) on 12mg samples as described in Ronda and Roos (2008). For gelatinization scan the samples were scanned from 25 to 160°C using an empty pan as reference. The glass transition ( $T_g$ ) of maximally freeze-concentrated solutes and the onset of ice melting ( $T_m$ ) temperatures were obtained after annealing of samples (Ronda and Roos, 2008). The ice melting temperature of the maximally freeze-concentrated system was measured after annealing of samples for 15 min at a temperature slightly below  $T_m$ . Retrogradation scan was done on the samples previously gelatinized in the DSC oven stored in the pans at 4 °C for 7 days. These samples were scanned from 0 to 150 °C. The enthalpy ( $\Delta H$ ), the onset and endset temperatures ( $T_o$  and  $T_e$ ) and the peak temperature ( $T_p$ ) were established in both scans. The reported values are means of at least triplicate measurements.

## **3. Result and Discussion**

### **3.1. Flour moisture sorption characteristics**

All models presented a good fitting to the sorption data (with  $R^2 > 0.99$  and RMSE=0.002, data not shown). However, the GAB model showed the best fitting for all the samples. The estimated monolayer water content of the tef flours by the BET model ranged between 0.052–0.053 g water/dry solids, while the estimation by the GAB model was 0.057 g water/dry solids. The monolayer values of the tef flours had no important differences among themselves and with the reference flours and they are in the range normally reported for cereal products. The multilayer moisture capacities (GAB constants,  $C$  Eqn. 3) were identical for the three tef flours (0.84) but higher than rice (0.82) and lower than wheat (0.87 and 0.90 refined and whole respectively). Hence, at 20°C with increasing relative humidity the water uptake of the flours will vary accordingly.

Sorption isotherms of the flours of the different tef cultivars and the reference flours at 20°C are presented in Fig.1. In agreement with earlier reports on various starchy materials (Al-Muhstaseb et al., 2002), all flour types had type II sorption isotherm curves, which is characteristic of finely divided non-porous solids or macro-porous materials indicating the

occurrence of multi-layer adsorption (Hébrard et al., 2003). The flours of the three tef varieties led to identical isotherms and closer to the reference flours (Fig. 1). Marked differences among flours were observed at the highest relative humidity ( $a_w = 0.98$ ). At this point sorbed moisture by the tef flours was 32.1%, 31.4% and 32.4% for DZ-01-99, DZ-Cr-37 and DZ-Cr-387 respectively, which are notably lower than refined wheat (36.2%) and whole wheat (40.2%) and higher than rice (29.5%). Such higher hydration capacity of wheat flour can be mainly attributed to damaged starch, proteins and pentosans (Hebrard et al., 2003; Abebe et al., 2015).

### 3.2. Flour flowability and compaction characteristics

Flour MC adjustment by storing at  $a_w = 0.59$  and  $a_w = 0.85$  to get two moisture categories led to 13.7–14.3% and 19.1–20.3% on dry basis, respectively (Tab.1). The flow and packing properties of each flour type were strongly ( $p < 0.001$ ) influenced by the moisture level or category (Tab. 1 and Figs. 2a and 2b). The result corroborates earlier reports (Abu-hardan and Hill, 2010) stating flours with higher initial moisture content or stored at increased surrounding relative humidity (which absorbed more water molecules) had greater powder cohesion and reduced flowability.

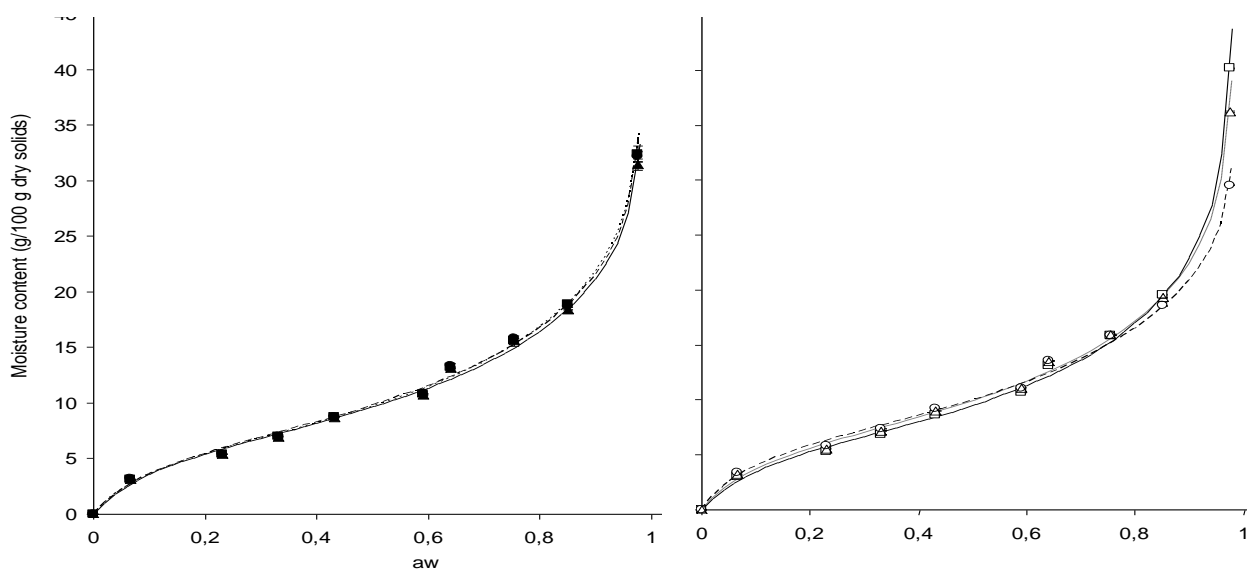


Figure 1: Sorption isotherms (GAB model fittings) of DZ-01-99 (□) DZ-Cr-37 (□) and DZ-Cr-387 (□) tef flours and rice (○), refined wheat (□) and whole wheat (□) flours at 20°C

The tef cultivar flours at  $a_w=0.59$  showed significant variations in their cohesive properties varied as: DZ-Cr-37 < DZ-01-99 < DZ-Cr-387, while their caking and flowability properties were equivalent. This could be associated with the crude fat content that promotes flour cohesion, in the tef flours which varied in the same order (Abebe and Ronda, 2014). Compared to the reference flours, at  $a_w=0.59$  tef flours were more cohesive than the whole wheat and rice flours and less cohesive than refined wheat flour. However, at  $a_w=0.85$ , DZ-Cr-387 flour was the most cohesive flour of all flours studied, including the refined wheat flour. At  $a_w=0.59$  the cake strengths exhibited by the tef flours were equivalent among themselves and with refined wheat flour, while they exhibited lower cake strength than whole wheat and rice flours. The cake strength variation among the flours of the tef cultivars became significant at  $a_w=0.85$  being DZ-Cr-387 variety which showed again the highest value.

**Table 1.** Packing and flow properties of the flours conditioned at the two  $a_w$

Cereal	Moisture content (%db)	Cohesion Coeff (g.mm)	Cohesion index(mm)	Mean Cake Strength(g)
Flours conditioned with saturated solution of NaBr with $a_w=0.59$ at 20°C				
DZ-01-99	14.2 <sup>bc</sup> ±0.1	348 <sup>d</sup> ±20	22.1 <sup>d</sup> ±1.3	140.9 <sup>a</sup> ±0.3
DZ-Cr-37	14.1 <sup>bc</sup> ±0.1	305 <sup>c</sup> ±6	19.3 <sup>c</sup> ±0.3	140.9 <sup>a</sup> ±2.3
DZ-Cr-387	14.2 <sup>bc</sup> ±0.1	390 <sup>e</sup> ±30	24.7 <sup>e</sup> ±1.9	145.3 <sup>a</sup> ±4.5
Refined wheat	14.0 <sup>b</sup> ±0.1	389 <sup>e</sup> ±14	30.2 <sup>f</sup> ±1.1	148.1 <sup>a</sup> ±5.6
Whole Wheat	13.7 <sup>a</sup> ±0.1	232 <sup>b</sup> ±21	16.0 <sup>b</sup> ±1.4	467.3 <sup>c</sup> ±30.1
Rice	14.3 <sup>c</sup> ±0.1	180 <sup>a</sup> ±10	11.1 <sup>a</sup> ±0.7	201.7 <sup>b</sup> ±7.9
Flours conditioned with saturated solution of KCl with $a_w=0.85$ at 20°C				
DZ-01-99	19.9 <sup>c</sup> ±0.1	583 <sup>b</sup> ±56	38.6 <sup>cd</sup> ±3.5	404.1 <sup>b</sup> ±11.9
DZ-Cr-37	19.7 <sup>b</sup> ±0.1	559 <sup>b</sup> ±22	36.0 <sup>c</sup> ±1.4	421.8 <sup>bc</sup> ±9.1
DZ-Cr-387	20.3 <sup>d</sup> ±0.1	686 <sup>c</sup> ±32	44.8 <sup>e</sup> ±2.1	432.6 <sup>c</sup> ±13.8
Refined wheat	19.1 <sup>a</sup> ±0.1	536 <sup>b</sup> ±20	41.5 <sup>d</sup> ±1.5	530.2 <sup>d</sup> ±14.3
Whole Wheat	19.6 <sup>b</sup> ±0.1	289 <sup>a</sup> ±36	19.6 <sup>b</sup> ±2.3	667.8 <sup>e</sup> ±42.5
Rice	20.0 <sup>c</sup> ±0.1	258 <sup>a</sup> ±8	16.4 <sup>a</sup> ±0.5	260.8 <sup>a</sup> ±13.3

Data are the mean ± standard deviation. Flours conditioned at  $a_w=0.59$  and  $a_w=0.85$  were compared separately and values with the same small letters in a column at each  $a_w$  level are not significantly different ( $p>0.05$ ).

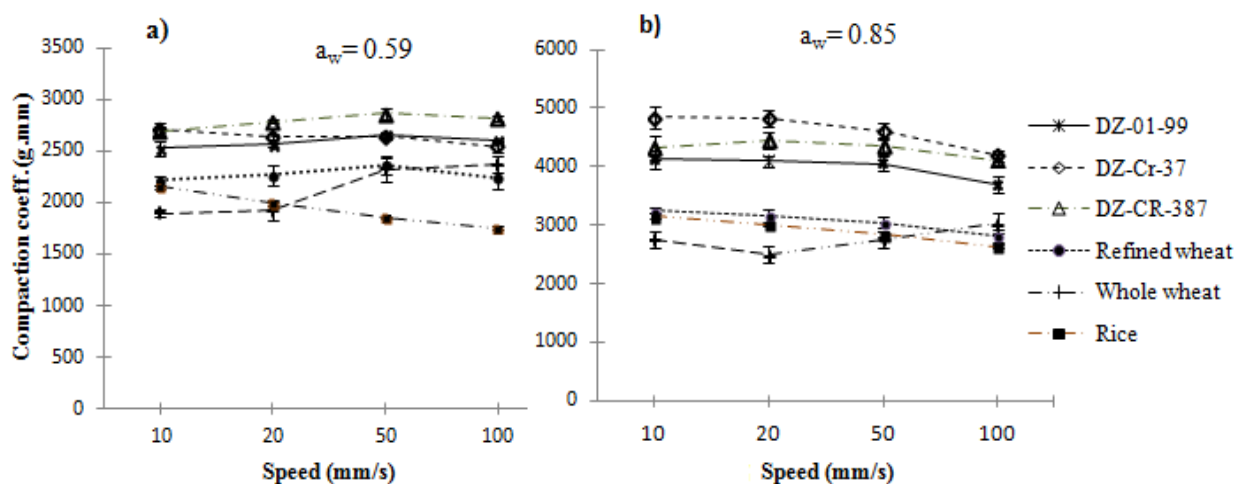


Figure 2. Speed dependence of compaction coefficient

The compaction coefficients of tef flours with  $a_w = 0.59$  were significantly higher than that of wheat and rice ones, independently of the blade speed applied during the test (Fig. 2). This indicates that tef flours have higher resistance to flow than the reference flours. The effect of speed on the compaction coefficients of tef flours and refined wheat flour were marginal which indicates that its flowability was practically independent on flow speed. However, the compaction coefficients, and consequently the flow resistance, of whole wheat flour increased appreciably with increasing speed while rice flour exhibited the opposite behavior. The compaction coefficients of the tef flours at  $a_w = 0.85$  were at least 36% higher than the reference flours indicating their higher resistance to flow at this level of moisture content. With the exception of whole wheat flour, the compaction coefficient of all the flours decreased with the increase in flow speed. Hence, at this moisture level the flow resistance of these flours decreased with the increasing flow speed while the whole wheat flour showed the opposite behavior. The effect of moisture content on packing and flow properties was more marked on tef flours than in the references (Fig. 2). The cohesion and compaction coefficient at 10 mm/s increased, as result of the moisture increase, around 75% and 67% respectively for tef meanwhile the reference flours increased only 35% and 45%. The cohesion and compaction coefficients of all the flours increased with moisture content. This could be due to the act of water as an adhesive between particles by creating liquid bridges that increases the powder cohesivity and packing behavior (Groger et al., 2003).

### **3.3. Thermal properties and Retrogradation**

The DSC thermograms obtained from gelatinization and retrogradation scans, showed two peaks for all flours (Fig. 3). The first peaks in the gelatinization (between 60–85°C) and retrogradation (between 40–63°C) scans were related to starch gelatinization/retrogradation while the second peaks (further endothermic signals) (between 90°–115°C) could be attributed to the fusion of amylose-lipid complexes. The gelatinization enthalpy ( $\Delta H_{gel}$ ) of tef flour starch was  $14.6 \pm 0.5$  J/g starch, without significant differences among the varieties. The mean gelatinization temperature of all tef flours was 4°C below that of rice flour and 8°C above the wheat flour (data not shown).

The melting peaks of recrystallized amylopectin obtained after storing the gelatinized flours (retrogradation scans) appeared at notably lower transition temperatures than initial gelatinization. The decrease in the melting temperatures suggested the formation of smaller and/or less perfect crystalline regions (Biliaderis et al., 1986). The melting enthalpies of the recrystallized amylopectin in tef flours were about 30% the gelatinization enthalpy with insignificant variations among varieties. However, melting enthalpies of the recrystallized amylopectin in wheat flour gel is significantly less than of tef showing amylopectin retrogradation in wheat gel was markedly higher than in tef. This was also confirmed in the gel hardening kinetics studies (Abebe & Ronda, 2014) where the hardening of tef flour gels stored for 9 days at 4°C was faster and markedly higher than wheat flour gels. However, opposite was confirmed with respect to amylose retrogradation from rapid viscoanalyzer tests (Abebe et al., 2015). Hence it could be concluded that staling in tef products could be slower in short term storage than wheat products and the vice versa could happen on long term storage.

The sub-zero temperature scans carried out on gelatinized samples led to the initial melting temperature of the maximally freeze-concentrated system ( $T_{m'}$ ) values reported in Fig. 2c. As expected for high molecular weight systems, the onset temperature of glass transition of the maximally freeze-concentrated system,  $T_g'$ , coincided with the  $T_{m'}$ . These data represent the maximum temperature we are able to store the flour gels without undesirable changes under frozen conditions. The  $T_{m'}$  value obtained for the tef gels was  $-15.4 \pm 0.4$  °C and it was independent of the variety. Wheat flour gels showed similar  $T_{m'}$  to tef gels, while rice flour gel had a  $T_{m'}$  four degrees above those of tef and wheat. Probably, the very low content of

soluble solids in rice flour, quantified from its water solubility index, with respect to tef and wheat flours could justify this fact (Ronda and Roos, 2008; Abebe et al., 2015) .

#### **4. Conclusions**

As tef is a relatively new material for industrial scale modern processing, this paper tried to cover the engineering properties (bulk handling and thermal characteristics) of tef flours obtained from three Ethiopian tef cultivars. Like other cereal products the tef flours had a sigmoidal shape sorption behavior with type II isotherms. The estimated monolayer water content of the tef flours were in the range normally reported for cereal products. Hence, similar precaution should be undertaken during handling of these flours. The measured flour flow and compaction characterises reveal the pronounced effect of air relative humidity on handling and packing properties of tef flours, higher than in the wheat and flours studied as reference. Slight variations were observed among flow and packing properties of the three tef cultivars themselves, while they had important differences with the reference flours. At both  $a_w$  levels the tef flours had more cohesive behaviour than rice and whole wheat flours and were less flowable than all the reference flours. At  $a_w=0.59$  the flowability of the tef flours was hardly dependent on the bulk flow speed while at  $a_w=0.89$  their flow resistance decreased with increasing bulk flow speed. Among the flours of the tef varieties DZ-Cr-387 was more cohesive and less flowable. In the thermal property study the starch gelatinization enthalpies of the three tef cultivar flour water suspensions were higher than wheat flour while they were equivalent among themselves and with rice flour. Retrogradation scan after storing the gels at 4°C for 7 days it could be concluded that retrogradation/stalling in tef flours is higher than wheat flour. Therefore, the design and development of bulk handling and processing devices as well as product formulation should be considerate of such peculiarities of tef flour.

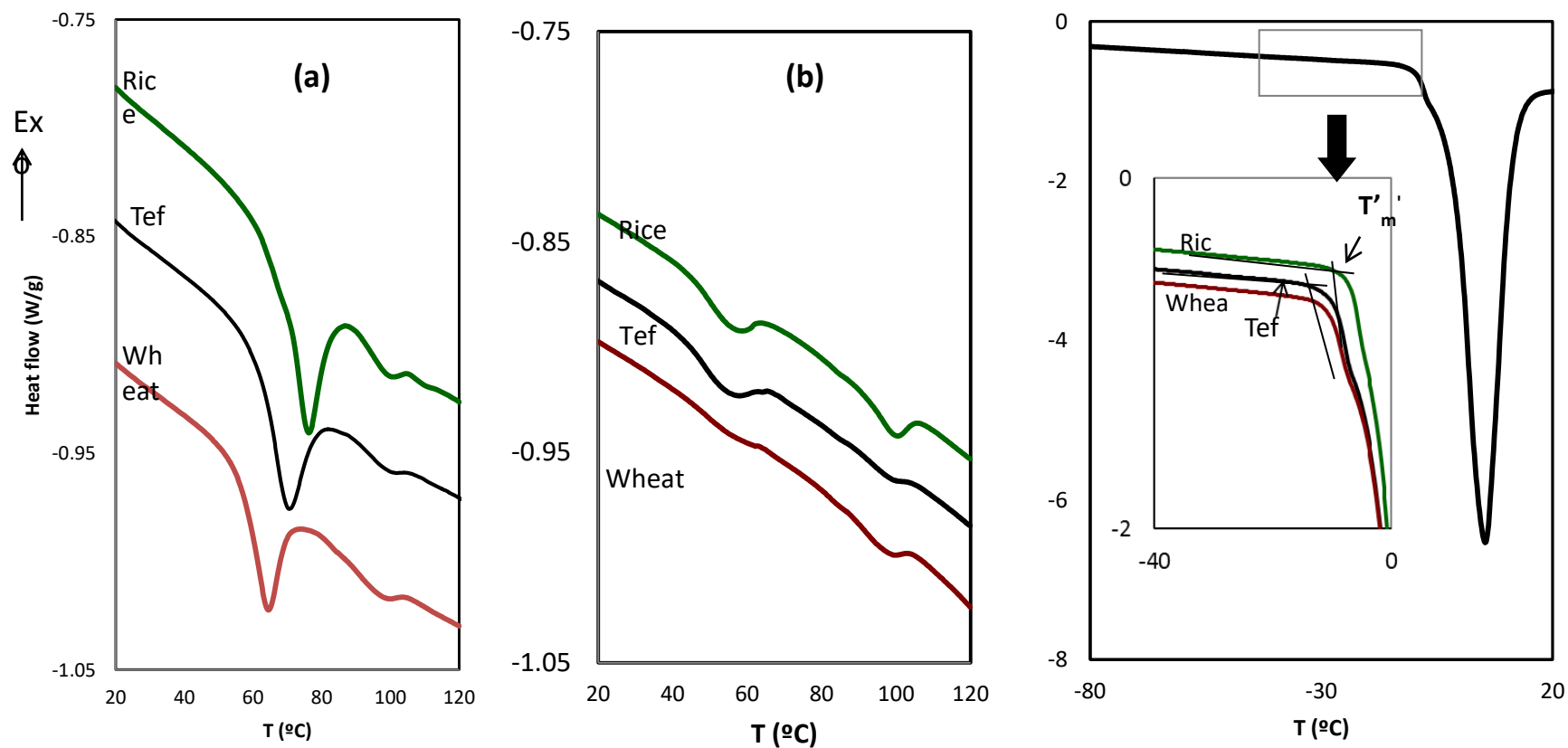


**Figure 3:** (a) Gelatinization scan thermograms; (b) retrogradation scan thermograms and (c) thermograms of the sub-zero temperature scan after annealing of gelatinized samples for the determination of the ice melting temperatures of the maximally freeze-concentrated systems

## **References**

- Abebe, W., & Ronda, F. (2014). Rheological and textural properties of tef [*Eragrostis tef* (Zucc.) Trotter] grain flour gels. *Journal of Cereal Science*, 60(1), 122-130.
- Abebe, W., Collar, C., & Ronda, F. (2015). Impact of variety type and particle size distribution on starch enzymatic hydrolysis and functional properties of tef flours. *Carbohydrate polymers*, 115, 260-268.
- Abiyu, H. T., Woldegiorgus, A. Z., & Haki, G. D. (2013). Preparation of injera pre-fermented flour: nutritional and sensory quality. *International Journal of Science Innovations and Discoveries*, 3, 165-175.
- Al-Muhstaseb, A.H., McMinn, W.A.M., Magee, T.R.A., 2002. Moisture sorption isotherm characteristics of food products: A review. *Trans IChemE 80 Part C*, 118-128.
- Biliaderis, C. G., Page, C. M., Maurice, T. J., Juliano, B. O., 1986. Thermal characterization of rice starches: a polymeric approach to phase transitions of granular starch. *Journal of Agricultural and Food Chemistry* 34, 6-14.
- CSA 2015. Central Statistical Agency, Agricultural Sample Survey 2014/15), Volume I, Report on Area and Production of Major Crops, Statistical Bulletin 278, May 2015, Ethiopia.
- Groger, T., Tuzun, U., Heyes, D.M., 2003. Modeling and measuring of cohesion in wet granular materials, *Powder Technology* 133, 203–215.
- Hébrard, A., Oulahna, D., Galet, L., Abecassis, J., Fages, J., 2003. Hydration properties of durumwheat semolina: influence of particle size and temperature. *Powder Technology* 130, 211–218.
- Janjatović, D., Benković, M., Srećec, S., Ježek D., Bauman, I., 2012. Assessment of powder flow characteristics in incoherent soup concentrates. *Advanced Powder Technology* 23, 620–631.
- Landillon, V., Cassan, D., Morel, M.-H., Cuq, B., 2008. Flowability, cohesive and granulation properties of wheat powders. *Journal of Food Engineering* 86, 178-193.
- Ronda, F., Roos, Y.H., 2008. Gelatinization and freeze-concentration effects on recrystallization in corn and potato starch gels. *Carbohydrate Research* 343, 903–911.

## Conducting polymer and polymer/carbon nanotube composites for electrochemical determination of biologically active compounds

Alemnew Geto<sup>a,b\*</sup>, Merid Tessema<sup>a</sup> and Shimelis Admassie<sup>a</sup>

<sup>a</sup>Department of Chemistry, Addis Ababa University, P. O. Box 1176, Addis Ababa, ETHIOPIA

<sup>b</sup>Ethiopian Biotechnology Institute (EBTi), P.O.Box 2490, Addis Ababa, ETHIOPIA

\*E-mail: [alemnew\\_geto@yahoo.com](mailto:alemnew_geto@yahoo.com); Tel: +251911742341

### Abstract

*Quinine, nicotine and histamine are naturally occurring biologically active compounds with the potential to affect the human health. Quinine has been used as an important anti-malarial drug for more than 300 years despite its potential to cause health impairments. Nicotine is also considered as the major stimulant in cigarette smoke and suspected to contribute to various cancer related health problems. Histamine, a metabolic product of histidine decarboxylation, is a major causative agent of sea food intoxication. Therefore, the development of a simple, inexpensive, sensitive and accurate analytical method for the determination of these compounds is an important topic.*

*Though several analytical methods have been reported, most of them usually suffer from limitations such as need for sample pre-treatment, necessity of derivatization, long analysis time and high cost of operation. Electrochemical methods have been of great interest in this regard due to the advantages of high sensitivity, selectivity, easy procedures, low cost and rapid response. However, the direct electrochemical detections at conventional electrodes usually show practical drawbacks such as high over-potential, slow kinetics, electrode fouling, poor selectivity and sensitivity. But, most of these problems could be minimized by treating the electrode surface by a suitable modifier.*

*In this work, glassy carbon electrode was modified by electrodeposition of poly(4-amino-3-hydroxynaphthalene sulfonic acid). Cyclic voltammetric studies in phosphate buffer solution showed higher current response for plant alkaloids, quinine and nicotine at the modified electrode than the bare glassy carbon electrode. Under optimized conditions, calibration curves were drawn for the alkaloids with detection limits of  $1.42 \times 10^{-8}M$  and  $8.66 \times 10^{-7}M$  for quinine and nicotine, respectively. The method was successfully applied for the determination of nicotine*

in cigarette tobacco and quinine in pharmaceutical products and human urine. The polymer modified electrode was also coated with multi-walled carbon nanotubes and studied for the determination of histamine, an important fish spoilage indicator. A synergistic catalytic effect was observed at the polymer/multi-walled carbon nanotube composite modified electrode for the oxidation of histamine. Experimental conditions were optimized and the method was successfully applied for the determination of histamine in fish muscle with a detection limit of  $7.62 \times 10^{-8}$  M. The developed modified electrodes showed excellent performance in terms of repeatability, reproducibility, sensitivity, selectivity and stability which make them promising alternatives for practical analytical purpose.

**Keywords:** Conducting polymer; Carbon nanotube; Modified electrode; Voltammetry; Biologically active

## Introduction

A biologically active or bioactive compound is defined as one that has a direct physiological effect on plants, animals, or other microorganisms. Physiological effects of such compounds vary broadly from acute fatality to curative or medicinal (A. Bernhoft, 2010) depending on the compound, the dose or the bioavailability. Many known compounds with biological activity are found both in natural and manufactured products.

Nicotine (NIC) (3-(1-methylpyrrolidin-2-yl)pyridine) (Fig.1a) is a colorless to pale yellow oily liquid (A. Hannisdal & K. H. Schroder, 2007) and a toxic plant alkaloid belonging to the genus *Nicotiana* (L. Campanella & M. Tomassetti, 2001). *Nicotianatabacum* is cultivated throughout the world for the preparation of cigars, cigarettes, pipe and chewing tobacco (E. F. Domino, 1999). Nicotine has also been suspected to contribute to various human diseases such as lung cancer, atherosclerotic vascular disease and chronic obstructive pulmonary disease (G. Bastida & B. Beltran, 2011).

Quinine (QN) ((6-methoxyquinolin-4-yl-8-vinylquinuclidin-2-yl)methanol) (Fig.1b) is also an important plant alkaloid isolated from the bark of *Cinchona*, a plant of South American origin. Historically, it has been used as an important anti-malarial drug for more than 300 years (C. E.

Song, 2009). In spite of this broad and centuries long uses, QN is potentially toxic and its overuse has been observed to complicate health conditions. The therapeutic plasma concentration range of QN is 9 to 21  $\mu\text{M}$  and its presence in plasma higher than 30  $\mu\text{M}$  can cause adverse effects and might be lethal (S. Zaugg & W. Thormann, 2001).

Histamine (Fig.1c) is a biologically active compound playing important roles in a number of physiological processes (S. L. Taylor, 1986). Naturally, it is found in all human tissues acting as a chemical mediator in inflammation, gastric acid secretion and neural modulation (J. S.-Gajic & Z. Stojanovic, 2010; K. Yamamoto & T. Ikeda, 2001). The consumption of foodstuffs that contain high levels of histamine results in a food-borne chemical intoxication called histamine poisoning (S. L. Taylor, 1986).

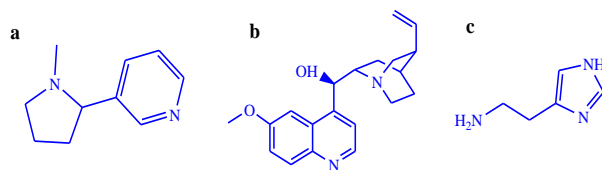


**Figure 1.** The chemical structure of (a) Nicotine, (b) Quinine and (c) Histamine

The successful detection and quantification of these biologically active compounds in samples of various origin is vital for their proper use by humans while avoiding the hazardous effects they might cause. Reported analytical methods for the determination of these chemicals include: chromatographic spectrophotometric and electrochemical techniques. However, most of the reported techniques are usually expensive, laborious, time consuming, need sample pre-treatment and involve toxic reagents. Thus, the design and development of quick, simple, inexpensive and effective methods are of great importance. Electroanalytical techniques have been considered simple, cheap and reliable when compared to other analytical methods (C.-T. Wu & K.-C. Ho, 2009). Therefore, the general objective of this study is to develop new conducting polymer modified electrodes and conducting polymer/carbon nanotubes composite modified electrodes and apply for the electrochemical determination of selected biologically active compounds.

## **Experimental**

### **Chemicals and reagents**

All chemicals and reagents used in this study are of analytical grade and were used as received without any further purification. Quinine sulphate and standard nicotine (98%) were obtained from BDH chemicals Ltd., England. Phosphate buffer solutions (PBS) (0.1 M) were prepared using  $K_2HPO_4$  and  $KH_2PO_4$  (both from FlukaChemika, Switzerland) for quinine and nicotine experiments while  $Na_2HPO_4$  and  $NaH_2PO_4$  (BDH Chemicals Ltd., England) were used in the electrochemical study of histamine. The monomer, 4-amino-3-hydroxynaphthalene sulfonic acid (AHNSA) and histamine dihydrochloride were purchased from Sigma-Aldrich. All aqueous solutions were prepared in doubly distilled water and supporting electrolyte used was 0.1 M phosphate buffer solution. Stock solutions of  $50.0 \times 10^{-3}$  M each for nicotine and quinine and  $1.0 \times 10^{-3}$  M histamine were prepared in doubly distilled water and stored in refrigerator. Nicotine solution was kept in dark condition until analysis.

Two brands of locally produced cigarette samples (Nyala and Delight from National Tobacco Enterprise, Ethiopia), and the fish sample, origin from Lake Tana (near Bahir Dar, Northwest Ethiopia) were purchased from a local supermarkets. The fish sample was carefully kept in a refrigerator until analysis. Quinine sulphate tablets (Ipca Laboratories Ltd., India) and quinine dihydrochloride injections (Intas Pharmaceuticals Ltd., India) were purchased from a drug store in Kombolcha (Northeast Ethiopia). The human urine sample was collected from a male volunteer and stored in the refrigerator until analysis.

### **Instruments**

The pH of buffer solutions were measured using Jenway 3345 ion meter. Electrochemical measurements were performed using CHI760D Electrochemical Workstation (CH Instruments, Austin, Texas, USA) (for quinine and histamine), BAS-CV 50W voltammetric analyzer (Bioanalytical Systems Inc., USA) (for nicotine). All voltammetric measurements were conducted in electrochemical cell with conventional three electrode system. The working electrodes used were: glassy carbon electrode (3 mm), poly(4-amino-3-hydroxynaphthalene sulfonic acid)-modified glassy carbon electrode [*p*-(AHNSA)/GCE], or multi-walled carbon nanotubes coated poly(4-amino-3-hydroxynaphthalene sulfonic acid)-modified glassy carbon electrode (MWCNTs/*p*-(AHNSA)/GCE). The reference electrode used was silver/silver chloride

(Ag/AgCl, KCl, saturated) except for nicotine in which saturated calomel electrode (Hg/Hg<sub>2</sub>Cl<sub>2</sub>) was employed. Platinum wire was used as the auxiliary (counter) electrode in all measurements.

## **Preparation of modified electrodes**

### **Polymer modified electrode**

Prior to surface modification, the glassy carbon electrode (GCE) was polished with 1.0, 0.3 and 0.05 µm alumina powders on polishing cloth and rinsed with distilled water. The polymer film was then deposited on the polished electrode by electrochemical polymerization of  $2.0 \times 10^{-3}$  MAHNSA in 0.1 M HNO<sub>3</sub> solution. The polymerization was performed using cyclic voltammetry by scanning the potential between -0.8 V and +2.0 V for 15 cycles at 0.1 V s<sup>-1</sup>. Following polymerization, the electrode was placed in monomer free 0.5 M H<sub>2</sub>SO<sub>4</sub> solution and stabilized by sweeping the potential between -0.8 V and +0.8 V until a stable voltammogram was obtained. The acid activated glassy carbon electrode, used for comparison, was prepared and stabilized in a similar way in the absence of the monomer in 0.1 M HNO<sub>3</sub>.

### **Multi-walled carbon nanotubes coated polymer modified glassy carbon electrode**

First, the polymer modified electrode was prepared following the previous procedure and stabilized. Then, this *p*-(AHNSA)/GCE was coated with 10 µL of the MWCNTs suspension and allowed to dry in room temperature. The MWCNTs suspension was prepared by dispersing 2 mg of MWCNTs in 2 mL of DMF and then immersed in an ultrasonic bath for 30 min. The polymer modified (*p*-(ANHSA)/GCE) and nanotubes modified (MWCNTs/GCE) electrodes were prepared in similar procedures without the nanotubes coating and electropolymerization steps, respectively.

### **Sample preparation**

The sample extraction procedure to determine NIC in tobacco was carried out with a slight modification of the previous report (H. B. Suffredini et al., 2005). Briefly, ten cigarettes were taken and the tobacco content was collected and kept in an oven for 30 minutes at 40 °C. Then, the dried tobacco was powdered using a mortar and pestle, 0.15 g of the powder was taken and dissolved in 25 mL distilled water in conical flask. The mixture was then sonicated for 2 h and

30 min at room temperature and filtered. A 500  $\mu\text{L}$  of the filtrate was diluted with 0.1 M phosphate buffer solution (pH 7.5) in 10 mL volumetric flask for the voltammetric measurement.

For QN analysis, human urine sample was collected from a healthy volunteer and stored in the refrigerator until the analysis. 5 mL aliquot of the urine sample (before and after filtration using 0.45  $\mu\text{m}$  pore size filter paper) was transferred to 50 mL flask. An appropriate amount of standard QN was added and diluted in phosphate buffer solution (pH 7.0) to make the concentration  $2.5 \times 10^{-6}$  M. Final quantification was performed similar to the standard solutions.

In QN pharmaceuticals, ten Quinine sulphate tablets were weighed, finely powdered and the amount of sample required to prepare  $1.0 \times 10^{-3}$  M QN solution was transferred to a 100 mL flask and filled to the mark with distilled water. The content of the flask was stirred with a magnetic bar for 1 h and the mixture was filtered. Then, an aliquot of the clear filtrate was diluted with phosphate buffer (pH 7.0) and analyzed. For quinine dihydrochloride injections, ten ampoules were mixed and a procedure similar to tablet samples preparation was followed.

The sample extraction to determine histamine in fish muscle was based on previous reports with slight modifications (C. M. Keow et al., 2007; M. A. A.-Lomillo & M. J. A.-Martinez, 2010; R. Draisci et al., 1998). Briefly, fish muscle of 10.0 g was homogenized with 100 mL of 0.1 M phosphate buffer solution of pH 7.0. The homogenate was ultrasonicated for 10 min and filtered through a Whatman filter paper. An aliquot of 100  $\mu\text{L}$  was transferred to a 10 mL volumetric flask and diluted with PBS of the same pH to make the final determination.

## **Results and discussion**

### **Electrochemical Behavior of Nicotine, Quinine and Histamine**

Cyclic voltammograms (CVs) of  $1.0 \times 10^{-3}$  M NIC in PBS (pH 7.0) were recorded at bare and poly(4-amino-3-hydroxynaphthalene sulfonic acid)-modified glassy carbon electrode (p-(AHNSA)/GCE). Results (curves 'a' and 'b' of Fig. 2) show that NIC undergoes an irreversible electrochemical oxidation at both electrodes. At the bare GCE, the oxidation signal is poorly resolved and the peak is diffused over a broad potential region with a weak current response. Whereas, at the p-(AHNSA)/GCE, the oxidation of NIC yielded a well resolved peak at about +0.99 V (vs. SCE) with a peak current of  $5.15 \times 10^{-5}$  A. Compared to the bare GCE, a peak potential shift to a lower positive direction is observed at the modified electrode. The significant

increase in peak current together with a decrease in the oxidation peak potential is an indication of the electrocatalytic oxidation of NIC at the modified electrode.

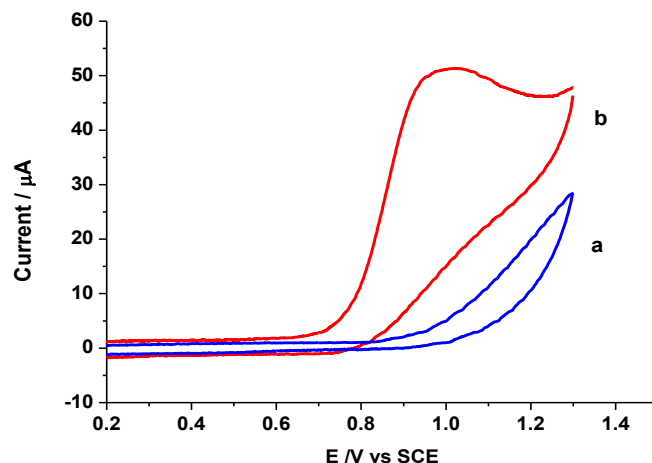


**Figure 2.** CVs of  $1.0 \times 10^{-3}$  M NIC in PBS (pH 7.0) at (a) bare GCE and (b)  $p$ -(AHNSA)/GCE. Scan rate:  $0.1 \text{ V s}^{-1}$

The electrochemical behavior of  $10 \times 10^{-6}$  M QN in 0.1 M PBS of pH 7.0 was investigated by CV. The voltammograms at bare,  $p$ -(AHNSA)-modified GCE are shown in Figure 3 (a) and (b), respectively. When scanned in the potential window from +0.5 to +1.4 V, a weak and diffused peak around +1.2 V was observed at the bare glassy carbon electrodes. However, a well resolved and highly pronounced oxidation peak was obtained at the  $p$ -(AHNSA)/GCE at +1.1 V. The absence of reduction peaks on the reverse potential scan suggests the irreversibility of QN oxidation reaction at the two electrodes. The better performance of the polymer modified electrode can be explained by the electrostatic interaction due to the charges on QN and the polymer film functional units. Since QN has two  $pK_a$  values ( $pK_{a1} = 4.13$  and  $pK_{a2} = 8.53$ ), it exists predominantly as monoprotonated cation ( $\text{QNH}^+$ ) in pH 7.0 solution (F. G. Thomas & L. Gierst, 1983; M. M. Zareh & K. Kasiura, 2001). Whereas, the  $p$ -(AHNSA) film has a dissociable  $\text{R-SO}_3\text{H}$  group ( $pK_a$  value between 3 and 4) (A. A. Ensafi & T. Khayamian, 2010) which bears a negative charge at the specified pH favoring the electrostatic attraction between the analyte and the polymer film.

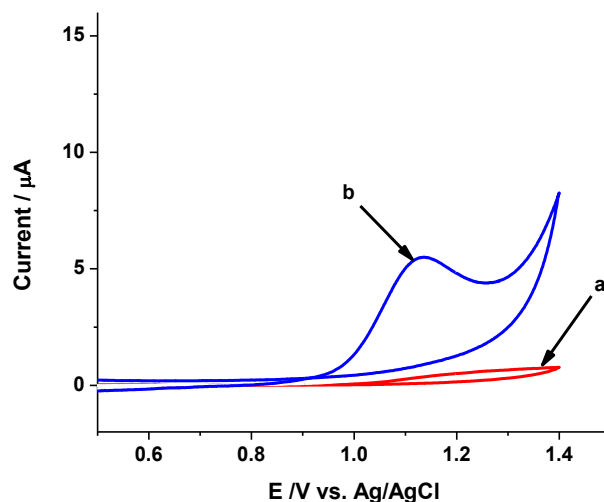


**Figure 3.** CVs of  $10.0 \times 10^{-6}$  M QN in PBS (pH 7.0) at (a) bare GCE and (b) *p*-(AHNSA)/GCE, Scan rate:  $0.1 \text{ V s}^{-1}$

CV was used to study  $1.0 \times 10^{-3}$  M histamine in 0.1 M PBS (pH 7.0) at bare GCE, *p*-(AHNSA)/GCE, MWCNTs/GCE and the composite MWCNTs/*p*-(AHNSA)/GCE. In all the voltammograms (Fig. 4), a single oxidation peak was observed with no corresponding reduction peak in the reverse potential scan indicating the irreversibility of the electrode reaction. The oxidation peak is observed at +1.37 V at the bare electrode which shifted negatively by about 0.16 V at the modified electrodes. Moreover, both the *p*-(AHNSA)/GCE and MWCNTs/GCE showed significant enhancement in peak current response of over 13-fold and 34-fold of the bare electrode response, respectively. This indicates the electrocatalytic role of the polymer and nanotube modifiers for the electrochemical oxidation of histamine. The better performance at the polymer modified electrode can be explained by the existence of electrostatic interaction between the protonated histamine and the charged polymer film functional unit. While, the catalytic effect of MWCNTs stems from the unique structure and properties they possess: such as larger specific surface area, strong adsorption ability and subtle electronic properties (E. Katz & J. Wang, 2004; H. Xiong & S. Wang, 2010; S. Iijima, 1991). The result at the MWCNTs/*p*-(AHNSA)/GCE showed a further enhancement in peak current responses about 40-times the current obtained at the bare electrode. It is also much higher than the responses obtained at the

individual polymer and nanotubes modified electrodes. This clearly showed the synergistic effect of the composite modified electrode in the electrocatalytic oxidation of histamine.

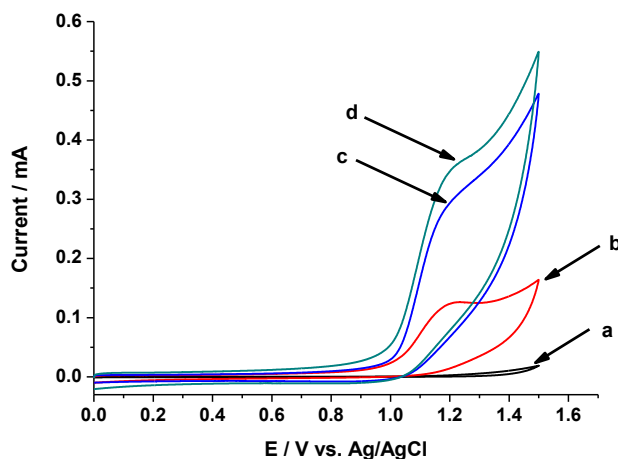


**Figure 4.** CVs of  $1.0 \times 10^{-3}$  M histamine in 0.1 M PBS (pH 7.0) at (a) bare GCE, (b) *p*-(AHNSA)/GCE, (c) MWCNTs/GCE and (d) MWCNTs/*p*-(AHNSA)/GCE at a scan of  $0.1 \text{ V s}^{-1}$

## Calibration Curves

Measurement parameters that may affect the final results including solution pH, potential scan rate, accumulation potential, accumulation time and polymer film thickness were optimized. Under the optimized conditions, a calibration curve was constructed using a series of NIC standard solutions over the concentration range of  $1.0 \times 10^{-6}$  to  $2.0 \times 10^{-4}$  M. The method showed a linearly increasing peak current response at +0.88 V for NIC over the concentration range. The linear relationship followed the regression equation:

$$I_{pa}(\mu A) = 2.80 + 0.127 C (\mu M) (R^2 = 0.9987)$$

The limit of detection (LOD) was calculated using the equation:  $LOD = \frac{3s}{m}$ ; where,  $s$  is the standard deviation of the response of the blank solution at the peak potential ( $n=10$ ) and  $m$  is the slope of the calibration curve. The calculated LOD was  $8.66 \times 10^{-7}$  M.

Similarly, the relationship between the peak current and QN concentration was studied by square wave voltammetry (SWV) under optimum conditions. The current response was proportional to the concentration of QN in the range of  $1.0 \times 10^{-7}$  to  $1.0 \times 10^{-5}$  M (Fig. 5). The linear regression equation was:

$$I_{pa}(\mu A) = 6.26 C (\mu M) + 0.2997 (R^2 = 0.9991)$$

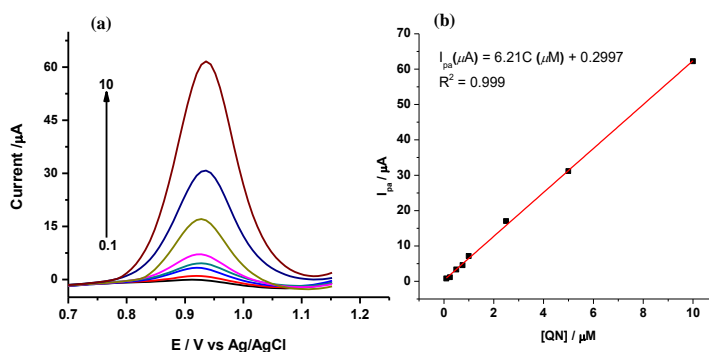


**Figure 5.** (a) Square wave voltammograms obtained for various concentrations of QN in the range of 0.1–10.0 μM and (b) the plot of peak current against QN concentration in PBS (pH 7.0)

In order to plot the calibration curve, differential pulse voltammograms were recorded using the MWCNTs/*p*-(AHNSA)/GCE for different concentrations of histamine in PBS (pH 7.0). Under the optimized experimental conditions, the peak current increased with increasing histamine concentration from  $1.0 \times 10^{-7}$  M to  $1.0 \times 10^{-4}$  M (Fig. 6) and the linear relationship is expressed by the regression equation:

$$I_p(\mu A) = 0.776 C (\mu M) + 5.14 (R^2 = 0.9985)$$

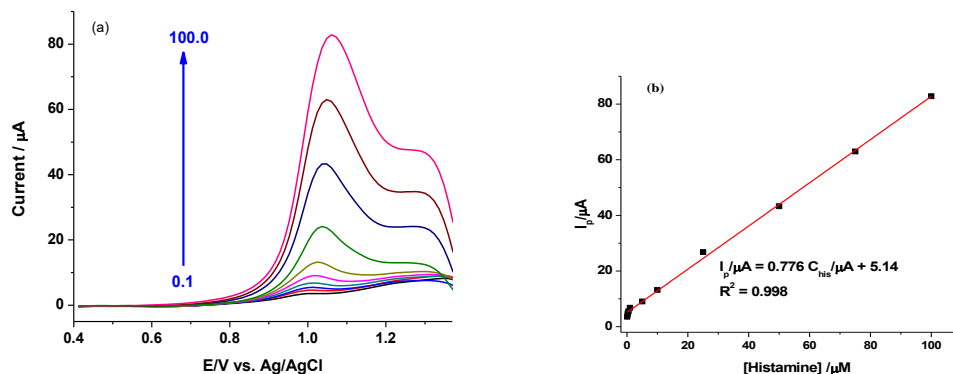


**Figure 6.** (a) Differential pulse voltammograms (DPV) obtained at MWCNTs/*p*-(AHNSA)/GCE in 0.1 M (PBS) (pH 7.0) for different concentrations of histamine in the range 0.1–100.0 μM and (b) the corresponding linear calibration curve

## Applications

In order to check the potential application of the proposed method for NIC determination in real samples, two locally produced cigarette samples were analyzed. The results obtained in the study are summarized in Table 1. The total NIC content of cigarette-I (C-I) and cigarette-II (C-II) were 3.84 (w/w%) and 4.26 (w/w%), respectively. Due to the absence of declared NIC content in the products analyzed, comparison of experimental results with labeled values was not possible. However, our results fall in the range where NIC is usually available in cured tobacco leaves which is 2–8% of the dry weight (E. F. Domino, 1999).

**Table 1.** NIC contents of cigarette samples obtained using SWV at *p*-(AHNSA)/GCE

Cigarette sample	<sup>a</sup> NIC content (w/w%) ± SD
C-I	3.84 ± 0.065
C-II	4.26 ± 0.117

<sup>a</sup>mean value ( $n = 3$ )

The *p*-(AHNSA)/GCE was used to determine QN in spiked human urine, quinine sulphate tablets and quinine dihydrochloride injections. The QN contents and recoveries on spiked

samples were measured and the results were calculated using the calibration equation (Table 2). The analysis of QN in pharmaceutical formulations exhibited the mean recovery of 97% and 95% for tablet and injection formulations, respectively. The measurement results are in good agreement with the declared content of the products.

**Table 2.** Determination of QN in tablet, injection and spiked urine samples

Sample	Declared	Found* (%RSD)	% Detected*	Added/ $\mu\text{M}$	Found/ $\mu\text{M}$ (%RSD)*	%Recovery*
Tablet (2.5 $\mu\text{M}$ )	300 mg/tablet	291.3 (1.9) mg/tablet	97.1	5.0	4.81 (0.7)	96.2
Injection (2.5 $\mu\text{M}$ )	300 mg mL <sup>-1</sup>	285.1 (1.0) mg mL <sup>-1</sup>	95.0	5.0	4.87 (0.4)	97.5
Urine Filtered	–	–	–	5.0	4.79 (1.2)	95.8
Urine Unfiltered	–	–	–	5.0	4.54 (1.5)	90.8

\* mean value ( $n = 3$ )

The effect of sample matrix on the response of the electrode was examined by adding  $5.0 \times 10^{-6}$  M standard QN to human urine and the pharmaceutical samples. Recovery values of 95.8% and 90.8% were obtained for filtered and unfiltered spiked human urine samples, respectively. Similarly, recoveries of 96.2% and 97.5% were obtained in tablet and injection formulations, respectively. This shows the excellent potential of the *p*-(AHNSA)/GCE for accurate determination of QN in real samples in the presence of other matrix components.

The developed method was applied for the determination of histamine in fish muscle. Measurements were performed by DPV under the optimum conditions. The calibration curve was used to calculate the concentrations of histamine in the sample and spiked solutions. The results of the analysis are summarized in Table 3. The amount of histamine in the fish sample was found to be 0.382 mg g<sup>-1</sup> (382 ppm) which is above the permissible level of 50 ppm, for human consumption according to the FDA regulation (“Fish and fishery products hazards and controls guidance,” 2011) and probably may cause histamine poisoning. In addition, recovery measurements were conducted spiking the sample at  $5.0 \times 10^{-6}$  M,  $10.0 \times 10^{-6}$  M and  $25.0 \times 10^{-6}$  M standard histamine. Results obtained ranged from 96.6% to 102.9%. This demonstrated the

potential of the developed method for the determination of histamine in fish and other samples rich in histamine content.

**Table 3.** Determinations of histamine in fish muscle extract and spiked sample solutions using MWCNTs/*p*-(AHNSA)/GCE

Sample	Added ( $\mu\text{M}$ )	Expected ( $\mu\text{M}$ )	<sup>a</sup> Found ( $\mu\text{M}$ ) (RSD)	Recovery (%)
	–	–	2.08 (0.42)	–
Fish muscle	5.0	7.08	7.16 (0.30)	101.1
	10.0	12.1	12.4 (0.19)	102.9
	25.0	27.1	26.2 (0.05)	96.6

<sup>a</sup>mean value of three measurements

## Conclusions

In this study, new conducting polymer and multi-walled carbon nanotubes-based chemically modified electrodes were developed for the determination of selected biologically active compounds. The modified electrodes were prepared by a simple electropolymerization technique and casting carbon nanotubes suspension on a clean glassy carbon electrode. A poly(4-amino-3-hydroxynaphthalene sulfonic acid)-modified glassy carbon electrode was used to study the electrocatalytic oxidation of quinine and nicotine. In both cases, the modified electrode showed reduced overpotentials and higher oxidation peak currents, compared to the unmodified electrode. The findings demonstrate the excellent electrocatalytic activity of the polymer film towards quinine and nicotine oxidation. The electrode was successfully applied for the analytical determination of nicotine in cigarette tobacco and quinine in pharmaceutical products and human urine without extensive sample preparation requirement. The analysis result for quinine in pharmaceutical formulations was in good agreement with the declared amount on the products. A new sensitive electrochemical method for the determination of histamine was also developed based on multi-walled carbon nanotubes coated conducting polymer modified glassy carbon electrode. The composite use of carbon nanotubes and conducting polymer improved the performance of the bare electrode and modified electrodes using the polymer or the MWCNTs separately. The catalytic effect of the composite significantly reduced the calculated detection

limit of histamine to  $7.62 \times 10^{-8}$  M. In addition, it is also below the chemical index for fish spoilage indicator level of 50 ppm set by the FDA, which shows the suitability of the method for the assessment of fish product quality. The developed method was also successfully applied for the determination of histamine in fish muscle after simple sample preparation steps and very good results were obtained.

## **References**

- A. A. Ensafi, M. Taei, & T. Khayamian. (2010). Simultaneous determination of ascorbic acid, epinephrine, and uric acid by differential pulse voltammetry using poly(p-xylenolsulfonephthalein) modified glassy carbon electrode, *79*, 480–487.
- A. Bernhoft. (2010). A brief review on bioactive compounds in plants. In A. Bernhoft (Ed.), *Bioactive compounds in plants—benefits and risks for man and animals* (pp. 11–17). Novus forlag, Oslo, Norway: Det Norske Videnskaps-Akademi.
- A. Hannisdal, O. Mikkelsen, & K. H. Schroder. (2007). Analysis of nicotine in antismoking pharmaceutical products by differential pulse polarography and voltammetry, *72*, 1207–1213.
- C. E. Song. (2009). An overview of cinchona alkaloids in chemistry. In C. E. Song (Ed.), *Cinchona alkaloids in synthesis and catalysis* (pp. 1–10). Weinheim, Germany: Wiley-VCH Verlag GmbH & Co. KGaA.
- C. M. Keow, F. A. Bakar, A. B. Salleh, L. Y. Heng, R. Wagiran, & L. S. Bean. (2007). Anamperometric biosensor for the rapid assessment of histamine level in tiger prawn (*Penaeus monodon*) spoilage, *105*, 1636–1641.
- C.-T. Wu, P.-Y. Chen, J.-G. Chen, V. Suryanarayanan, & K.-C. Ho. (2009). Detection of nicotine based on molecularly imprinted TiO<sub>2</sub> modified electrodes, *633*, 119–126.
- E. F. Domino. (1999). Pharmacological significance of nicotine. In J. W. Gorrod & P. Jacob III (Eds.), *Analytical determination of nicotine and related compounds and their metabolites* (pp. 1–11). Amsterdam, The Netherlands: Elsevier.

- E. Katz, I. Willner, & J. Wang. (2004). Electroanalytical and bioelectroanalytical systems based on metal and semiconductor nanoparticles, *16*(1–2), 19–44.
- F. G. Thomas, & L. Gierst. (1983). On the electrochemical behaviour of quinine at the mercury electrode in aqueous solutions, *154*, 239–260.
- Fish and fishery products hazards and controls guidance. (2011). U.S. Department of Health and Human Services Food and Drug Administration Center for Food Safety and Applied Nutrition.
- G. Bastida, & B. Beltran. (2011). Ulcerative colitis in smokers, non-smokers and ex-smokers, *17*(22), 2740–2747.
- H. B. Suffredini, M. C. Santos, D. De Souza, L. Codognoto, P. H.-de-Mello, K. M. Honorio, ... L. A. Avaca. (2005). Electrochemical behavior of nicotine studied by voltammetric techniques at boron-doped diamond electrodes, *38*, 1587–1599.
- H. Xiong, Y. Zhao, P. Liu, X. Zhang, & S. Wang. (2010). Electrochemical properties and the determination of nicotine at a multi-walled carbon nanotubes modified glassy carbon electrode, *168*, 31–36.
- J. S.-Gajic, & Z. Stojanovic. (2010). Electrocatalytic determination of histamine on a nickel-film glassy carbon electrode, *22*(24), 2931–2939.
- K. Yamamoto, K. Takagi, K. Kano, & T. Ikeda. (2001). Bioelectrocatalytic detection of histamine using quinohemoprotein amine dehydrogenase and the native electron acceptor cytochrome c-55, *13*(5), 375–379.
- L. Campanella, G. Favero, & M. Tomassetti. (2001). Direct determination of nicotine in antismoking pharmaceutical products and in tobacco using an inhibition biosensor, *34*(6), 855–866.
- M. A. A.-Lomillo, O. D.-Renedo, P. Matos, & M. J. A.-Martinez. (2010). Disposable biosensors for determination of biogenic amines, *665*, 26–31.
- M. M. Zareh, E. Malinowska, & K. Kasiura. (2001). Plasticized poly(vinyl chloride) membrane electrode for the determination of quinine in soft drinks, *447*, 55–61.

R. Draisci, G. Volpe, L. Lucentini, A. Cecilia, R. Federico, & G. Palleschi. (1998).

Determination of biogenic amines with an electrochemical biosensor and its application to salted anchovies, *62*, 225–232.

S. Iijima. (1991). Helical microtubules of graphitic carbon, *354*, 56–58.

S. L. Taylor. (1986). Histamine food poisoning: Toxicology and clinical aspects, *17*(2), 91–128.

S. Zaugg, & W. Thormann. (2001). Capillary electrophoretic separation, immunochemical recognition and analysis of the diastereomers quinine and quinidine and two quinidine metabolites in body fluids, *24*, 785–799.

## **Prosopis Juliflora Pods Mash for Biofuel Energy Production: an Opportunity from the Invasive Species**

**Mebrahtu Haile<sup>\*1</sup> Hadgu Hishe<sup>1</sup>, Desta Gebremedhin<sup>2</sup>**

<sup>\*1</sup>Department of Land Resource Management and Environmental Protection, College of Dryland Agriculture and Natural Resources, Mekelle University, Ethiopia

<sup>2</sup>Department of Chemistry, College of Natural and Computational Sciences, Mekelle University, Ethiopia

### **ABSTRACT**

*The aim of this study was to investigate the potential of Prosopis juliflora pods mash for bioethanol production and its hydrolysis solid waste for solid fuel. The role of some hydrolysis and fermentation parameters like acid concentration (0.5 - 3 molar), hydrolysis times (from 5 min up to 30 min), fermentation times (6-72h); temperature (25 °C - 40 °C) and pH (4 - 8) on ethanol production using Saccharomyces Cerevisiae yeast were evaluated. The effect of acid concentration on sugar contents estimated was found that the content of sugars increases as the concentration of H<sub>2</sub>SO<sub>4</sub> was increased up to 1 molar and decreases beyond 1 molar. The maximum sugar content of 94.98 % was obtained at 1 molar of H<sub>2</sub>SO<sub>4</sub> concentration. Followed the sugar content determination, the parameters which affect the bioethanol production was determined for their optimum conditions. The investigation revealed that the optimum conditions for bioethanol production were found at 1 molar of H<sub>2</sub>SO<sub>4</sub> concentration (4.2 %v/v), 48 h fermentation time (5.1%v/v), 20 min hydrolysis time (5.57 %v/v), fermentation temperature at 30 °C (5.57 %v/v) and pH 5 (5.57 %v/v). Under these optimum conditions the maximum yield of ethanol (5.57%v/v) was obtained. Furthermore, the solid waste remaining after bioethanol production was evaluated for solid fuel application (18.22 MJ/kg). The results show that, Prosopis juliflora pods mash has the potential for bioethanol production. In addition, the preliminary analysis on the solid waste after hydrolysis suggests that it can be used as solid fuel hence alleviating major disposal problems.*

**Keywords-** *Prosopis juliflora pods mash, bioethanol, hydrolysis, fermentation, Saccharomyces cerevisiae, solid fuel*

## 1. INTRODUCTION

One of the greatest challenges for the growing society in this century is to meet the energy demand for transportation, heating, lighting and industrial processes, which have significant impact on the environment. World population and increased urbanization have directly or indirectly influenced the energy demand (Akpan et al, 2008). Presently, in most countries of the world energy is derived from crude oil and fossil fuels. However, the problems associated with continuously use petroleum and fossil fuel sources increasing concentration of CO<sub>2</sub> in the atmosphere and concerns over global warming and cannot be renewed, hence deplete on usage(Akpan et al, 2008). In developing countries, especially in rural areas, 2.5 billion people rely on biomass, to meet their energy needs for cooking (Zuzarte, 2007). As in many other countries in the region, fuel supply in Ethiopia is mainly biomass-based (94.3 % of total energy supply) (Minister of Mines and Energy, 2011).

Modern fuels are those that are controlled to provide consistent energy, efficient and clean when combusted, such as biofuels or electricity (Zuzarte, 2007). Ethanol (ethyl alcohol) is a biofuel which has long been recognized as a fuel suitable for a variety of applications, including transportation and cooking (Prasad et al., 2009). It is one of the safe and environmentally friendly energy, since it is made from plants; it does not release any new carbon dioxide (CO<sub>2</sub>) into the air, unlike fossil fuels which return carbon that was stored beneath the surface for millions of years. Ethanol presents the advantage of not only being a clean fuel, but also a sustainable one, in terms of reduction of greenhouse gases, use of renewable sources and contributing to rural development. It can be made from any sugary or starchy and from cellulosic biomass such as wood, paper pulp or agricultural waste (Pikūnas et al., 2003).Now a day research on non- food crops and cellulosic materials getting great attention worldwide because they are cheap, easily available, and profitable as compared to food crops and also reduces inflation of the cost of food crops used for bioethanol production (Choge et al., 2007).

One of the fast growing trees which have the potential to substitute food crops for bioethanol production is *Prosopis juliflora*. It is a tree species native to Northern Mexico and the Southern

U.S. that survives droughts and thrives in sunny arid regions. The plant fixes its own nitrogen, requires no seeding, fertilization or irrigation, and grows on dry, nutrient-poor soils. It is a truly promising tree for droughts, because of its multiple and important potential and actual uses, as well as of its remarkable resistance to drought, heat, and poor soils. Most often, the tree grows only to become a thorny shrub, but its complex and deep-ranging root system allows it to tap different water tables, both at the surface and deep underground, which makes it a very hardy crop. The roots also act as an energy storage mechanism, because once a tree is cut down, new shoots spring up rapidly from the existing roots (Pasicznik et al., 2001).

The fruit produced by *Prosopis* species are legume pods, high in sugars, carbohydrates and protein. Pods have been a historic source of food for human populations where *Prosopis* species are found, increasingly becoming less important as a human food and more important as a livestock feed during the last few centuries. Pods vary considerably in size between species and even between populations and individual trees of some species. Pods of all *Prosopis* species are composed of an exocarp, a sometimes fleshy mesocarp, fibrous endocarps and hard seeds. The form and relative amounts of each varies widely between species, with several *Prosopis* species having a high percentage of mesocarp favored as a source of food and feed (Choge et al., 2007). *P. juliflora* grows in Ethiopia mainly in arid and semi-arid areas of the Rift Valley. It is a highly invasive exotic tree, introduced to Ethiopia in the 1970s, that is spreading in the pastoralist areas of Ethiopia, making vast areas of land unavailable for grazing and it is becoming difficult to remove it. When the plant is cut new off-springs are grown from the root in a short period. This makes the removal of the weed difficult. The invasiveness of the species has been aggravated in Afar by animals which feed on it, such as camel, goats and cattle (Hailu Shiferaw et al., 2004).

*P. juliflora* is a fast growing tree species and it will be a good source of bioethanol production to reduce dependence on the rapidly increase price of petroleum crude and products and other problems related to environmental pollution and increase in cost of food crops. In addition, using the challenge as an opportunity serve communities by creating job and services and the farmers will be benefited from it by supplying the feed-stock for the producers of bioethanol besides its

controlling from invasion. The main objective of this research work is to evaluate the potential of *P. juliflora* pods for bioethanol production and its solid waste by-product as solid fuel.

## 2. MATERIALS AND METHODS

### 2.1. Collection of samples

This study was conducted in a laboratory in Mekelle University, Adigrat medical laboratory and Geological survey of Ethiopia central laboratory. The pods were collected from *P. Juliflora* plant in Amibara among the severely invaded woredas of Afar region, Ethiopia. They were collected in plastic bags and dispatched to the laboratory (MU) for further work. The following methods were followed (Onuki, 2005).

### 2.2. Dry and Milling

The *P. juliflora* pod was sun dried, and broken down to fine powder using a hammer mill process. Grinding increased surface area of the pods and enhance the contact between starch and acid or water. The seed of *p. juliflora* was hard to mill by hammer milling and only the pod (cover of the seed) was used for this experiment. Compared to the amount of pod, the amount of seed obtained from large collection of pod was very small in amount/content and not economical to use alone for bioethanol production.

### 2.3. Determination of Moisture Content

The *P. juliflora* pod was dried using an oven at 105 °C followed by cooling in a desiccator over silica gel (0% relative humidity) and weighing until a constant weight. The moisture content was determined as in equation 1;

$$\text{Moisture content (\%)} = \frac{w_1 - w_2}{w_1} \times 100 \quad 1$$

Where  $w_1$  and  $w_2$  are weights of the sample before and after drying, respectively

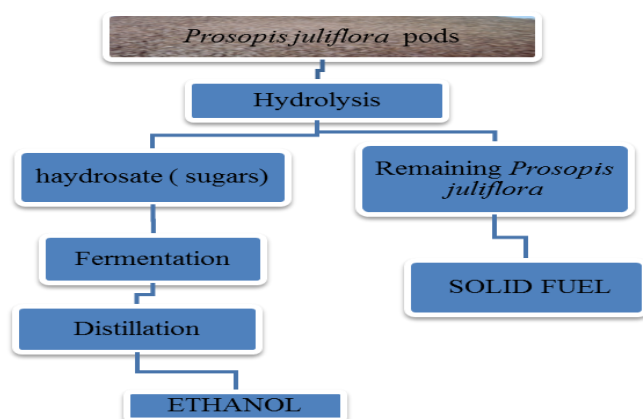


Fig.14. The path for the production of bioethanol and its value added from *P. juliflora* pods

## 2.4. Hydrolysis

The *P. juliflora* pod powder (25g) was hydrolyzed (pretreated) employing different concentrations of sulfuric acid (each of 0.5, 1, 1.5, 2, 2.5 and 3 molars) and with 250 ml of distilled water in 500 ml Erlenmeyer flask and separately heated at 90 °C for 15 and 30 minutes. After hydrolysis the liquid fraction was cooled, filtered and determined for glucose concentration. The distilled water and acid hydrolysates were adjusted to pH 5-6 by adding concentrated sulfuric acid and 2N sodium hydroxide, and the solutions were filtered and prepared for fermentation (Dawson and Boopaty, 2008).



Fig. 2. Hydrolysis process

## 2.5. Fermentation

### 2.5.1. Source of Microorganism for fermentation

*S. cerevisiae*, purchased from local market was used in the experiments. The yeast were first dissolved in warm water and left for 10 min before being used. Then the prepared solutions were taken in to the flask containing hydrolysate sample. Each fermentation of hydrolysates were carried out in 500 ml Erlenmeyer flask incubated with 5 g/l *S. cerevisiae* at 30 °C as described in

the literature (Thuesombat et al, 2007). The hydrolysates of water (Treatment 1), 0.5M sulfuric acid treated hydrolysate (Treatment 2), 1M sulfuric acid treated hydrolysate (Treatment 3), 1.5M sulfuric acid treated hydrolysate (Treatment 4), 2M sulfuric acid treated hydrolysate (Treatment 5), 2.5M sulfuric acid treated hydrolysate (Treatment 6) and 3M sulfuric acid treated (Treatment 7) was taken.



**Fig. 3. Samples prepared for fermentation.**

### **2.5.2. Ethanol Fermentation**

After scarification, the substrates were allowed to ferment with yeast (*S. cerevisiae*). The set up was left under anaerobic condition for 24 h with the different  $H_2SO_4$  concentrations (0, 0.5, 1, 1.5, 2, 2.5 and 3M) to select the best treatment type for ethanol production. Then substrate with the best ethanol yield was subjected for optimization with different period of fermentation times (12, 24, 48 and 72 h), hydrolysis times (5, 10, 15, 20, 25, 30 min), and fermentation temperatures (25 °C, 30 °C, 35 °C and 40 °C).

### **2.5.3. Ethanol Recovery**

#### ***2.5.3.1. Distillation method***

The known volume of fermented *P. juliflora* was distilled. Fermented solution was heated to force the lowest boiling material into the vapor phase. The vapors were passed over fractional column and the bulb of a thermometer at which point vapor was determined. The vapor was condensed to a liquid in the horizontal condenser that was cooled with a flow of cold water. The distillate was collected in a receiver. The weight of the distillate was measured.

#### 2.5.4. Yield calculations

$$\text{Gram of ethanol (g)} = \frac{(\text{Conc. of ethanol} \times \text{amount collected (g)})}{100} \quad 2$$

$$\text{Yield of ethanol (\%)} = \frac{\text{Gram of ethanol (g)}}{\text{Sample (g)}} \times 100 \quad 3$$

### 2.6. Analytical Methods

#### 2.6.1. Determination of Sugar Contents

The sugar contents in the samples during saccharification of the substrates were estimated as per the method described as in (Ayele Kefale et al., 2012). The reducing sugar concentration was determined using Fehling method. 50 mL of hydrolyzed sample solution was taken and dissolved in 10 mL of distilled water and mixed with 2 mL of conc. HCl acid and is heated for a period of 10 min. The obtained sample was neutralized by adding NaOH and it was prepared to 300 mL and taken into burette. The 10 mL of Fehling solution were taken and mixed with 90 mL of distilled water in 250 mL Erlenmeyer flask and Methyl blue indicator was added. The conical flask solution was titrated with burette solution in boiling conditions until disappearance of blue color and the volume at which brick red color observed were recorded. For each sample the sugar content was calculated by using the formula given below:

$$\text{Sugar content} = \frac{300 \text{ mL} \times f}{v} \times 100 \quad 4$$

Where  $f$ -Fehling factor (0.051);  $v$ -volume used in the titration (titrate value) (mL)

#### 2.6.2. Determination of Bioethanol Concentration

The Fourier Transform Infrared (FTIR) (65, PerkinElmer, UK) response was calibrated using different concentrations of pure ethanol. The measurement was carried out in reflectance mode where ZnSe (Zinc selenide) window was used as a sample holder. After the absorbance of pure ethanol was recorded the calibration curve was constructed first in weight-to-weight and then converted to volume-to-volume concentration units. The concentrations of ethanol were determined using the absorbance obtained for each sample from the calibration curve.

### 2.6.2.1. Standard Solution of Ethanol

Using the absorbance values obtained for the different ethanol concentrated solutions the calibration curve was constructed (Figure 4).

The data points were fitted a second order polynomial fit of the form

$$y = ax^2 + bx + c$$

Where  $y$  and  $x$  represent the absorbance and the concentration, respectively, and  $a$  and  $b$  are fit values and represent second and first order slope, respectively, and  $c$  is the absorbance bias where the concentration is 'zero'.

From the fit  $c = 0.00159$ ,  $a = -0.00064 \text{ mol}^{-2} \text{ L}^2$  and  $b = 0.05363 \text{ mol}^{-1} \text{ L}$  were at  $p$  value  $< 0.0001$ ).

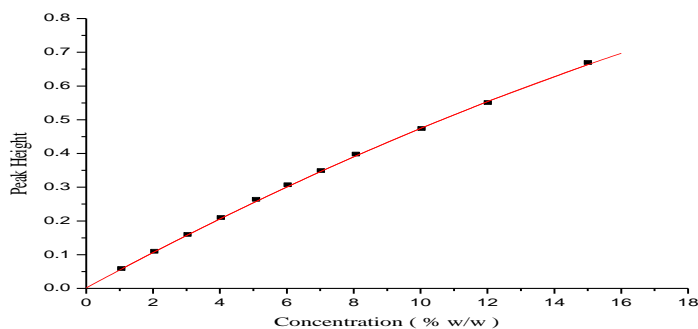


Fig. 4. Calibration curve of ethanol standard solution

The value of  $b$  is more than one order of magnitude greater than  $c$  indicating the absorbance residual bias is very small leading to the high sensitivity of the method with a standard deviation of  $SD = 0.00334$ . The regression value of  $R^2 = 0.99972$  further confirms the reliability of the fit. The calibration curve revealed excellent accuracy and sensitivity, and therefore, was used for determining the concentrations of the samples from the absorbance reading.

### 2.7. Determination of *P. juliflora* pod Calorific Value after Hydrolysis

The solid waste after hydrolysis of *P. juliflora* was characterized for solid fuel. The sample waste after hydrolysis was taken for calorific value determination with bomb adiabatic calorimetric instrument and calculated by using the formula given below:

$$Hg = \frac{TW - e_1 - e_2 - e_3}{m} \times 6$$

Where, Hg=Gross Heat Combustion

T= Difference temperature(°C)

W=energy equivalent of calorimetric in cal/ °C (2420 cal/ °C)

$e_1$  = correction in calories for heat of formation of HNO<sub>3</sub> (24.2 cal)\* titrate volume (mL)

$e_2$ = correction in calories for heat of formation of H<sub>2</sub>SO<sub>4</sub> (13.7 cal) \* content of sulphur (negligible)

$e_3$ = correction in calories for heat of formation of fuse wire (2.3) \* length of fuse wire combusted (cm)

m= weight of sample

### 3. RESULTS AND DISCUSSION

#### 3.1.Effect of Acid Concentration on Sugar Content

The values of sugar contents obtained from *P. juliflora* in this study were shown in the figure below. This *P. juliflora* reducing sugars were saccharified with different H<sub>2</sub>SO<sub>4</sub> concentrations and distilled water at 90 °C and 15 min hydrolysis time after determination of moisture content (15.65%).

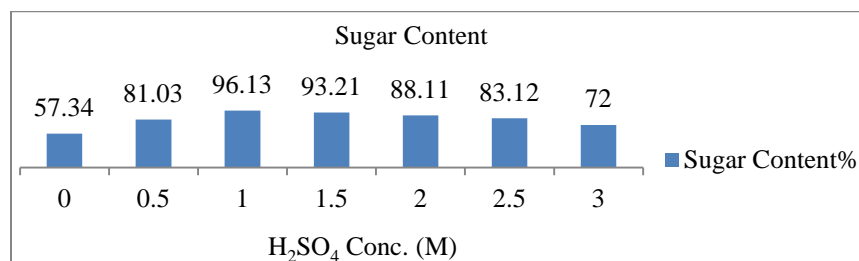


Fig. 5.The effect of acid concentrations on sugar content

The result shows that the *P. juliflora* recorded the value of 57.34% sugar content after it was saccharified with distilled water. The sugar content increased with an increase in acid concentration up to 1 M, and at this concentration the highest value of 96.13% sugar content was obtained. Further increase in acid concentration beyond 1 M led to a decrease in sugar content (Fig.5). The Increase of sugar contents in acid treated samples with increasing of acid concentration may be due to a complete and fast conversion of cellulose to glucose and hemicelluloses to C<sub>5</sub>-sugars (Nutawan et al., 2010) and as the solution was more concentrated, the monomeric sugars (xylose, glucose) may further be oxidized to undesirable by-products such

as furfural, hydroxyl methyl furfural (HMF), etc. by sulphuric acid on glucose (Nutawan et al., 2010, Joshi et al., 2011).

### 3.2. Parameters affecting Bioethanol Production

#### 3.2.1. Acid Concentration

For determining the optimum acid concentration for bioethanol production, distilled water and different concentrations of  $H_2SO_4$  were prepared, while keeping all the other parameters constant, *i.e.* 90 °C hydrolysis temperatures, 15 min hydrolysis time, pH 5, 24 h fermentation time and 30°C fermentation temperature were applied for all concentration samples.

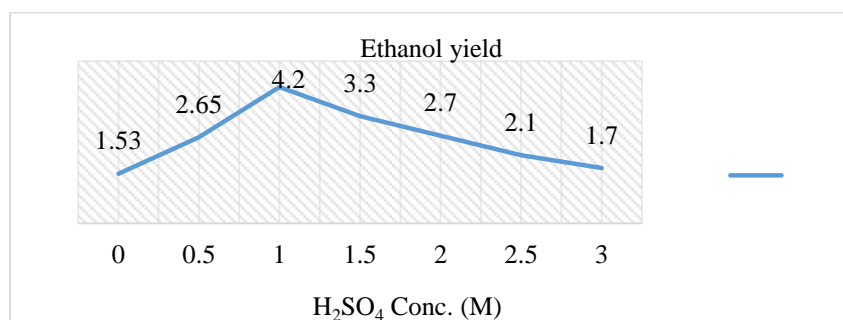


Fig. 6. The effect of acid concentration on bioethanol production

Figure 6 shows that, the ethanol yields obtained in distilled water and 0.5 M  $H_2SO_4$  concentrations were 1.53% and 2.65% *v/v* respectively and the maximum ethanol yield of 4.2% *v/v* was obtained in 1 M of  $H_2SO_4$  concentrations. Further increase in acid concentration resulted in a decrease in ethanol yield (1.5, 2, 2.5 and 3 M  $H_2SO_4$  concentrations resulted in the ethanol yields 2.73% and 1.22% *v/v* respectively). The decreasing of ethanol yield at higher acid concentration may be due to degradation of monomeric sugars to undesirable by-products or may be derived from dehydrating or oxidizing by sulphuric acid on glucose instead of forming ethanol (Nutawan et al., 2010).

#### 3.2.2. Fermentation Time

To determine the optimum fermentation time for bioethanol production, the fermentation times were adjusted ranged from 6-72 h, at the same time as keeping rest of the parameters constant (1 M  $H_2SO_4$  – optimum acid concentration obtained from the previous experiment, 90 °C hydrolysis temperature, 15 min hydrolysis time, pH 5 and 30 °C fermentation temperatures).

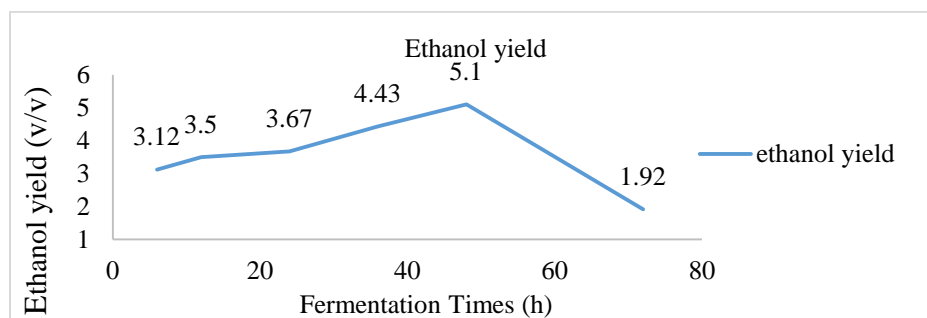
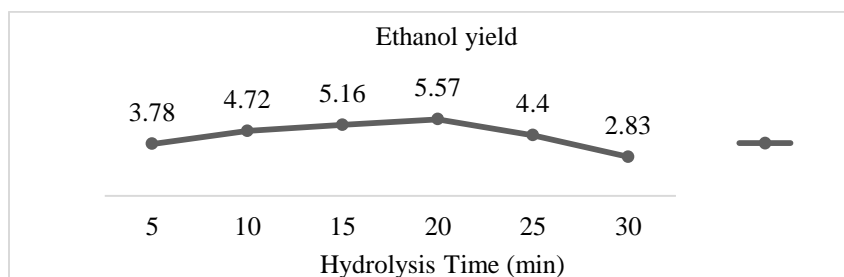


Fig. 7. The effect of fermentation time on bioethanol production

Figure 7 highlights ethanol yield obtained at 6, 12, 24 and 36 h fermentation times were 3.12%, 3.5%, 3.67% and 4.43% v/v respectively. The fermentation time of 72 h resulted in ethanol concentration of 1.92% v/v was the minimum value. The maximum ethanol yield of 5.1% v/v was obtained at 48 h fermentation time. The result revealed that the amount of ethanol increases as the increases of fermentation time and reaches maximum at 48 h fermentation times and decreased at the end of fermentation time. This may be due to the consumption of sugar by the microorganisms or the hydrolysate does contain significant levels of metabolic inhibitors (e.g., furfural and HMF) that can interfere with fermentation (Weil et al., 2002).

### 3.2.3. Hydrolysis Time

Hydrolysis time was taken as another parameter for bioethanol production optimization. To make out the optimum hydrolysis time for bioethanol production, the solutions were kept for 5, 10, 15, 20, 25 and 30 min, while keeping others parameters constant such as 1 M H<sub>2</sub>SO<sub>4</sub> solution concentration, 48 h fermentation times (both values are optimized previously), 90 °C hydrolysis temperature, pH 5 and 30 °C fermentation temperature. The result showed that ethanol yield in 5, 10, 15, 20, 25 and 30 hydrolysis times which were gave 3.78%, 4.72%, 5.16%, 5.57%, 4.4% and 2.83% v/v respectively. The maximum ethanol yield (5.57% v/v) was obtained at 10 min hydrolysis time as shown in Figure 8. The result showed that the ethanol yield increases as the increases of hydrolysis time and reaches optimum at 10 min hydrolysis duration. The result obtained is in agreement with the reference (Ayele Kefale et al., 2012).



**Fig. 8. The effect of hydrolysis time on bioethanol production** The reason for decreases of ethanol production as increases hydrolysis time may be due to the fact that longer residence time makes the sugars further oxidize to form inhibitors (furfural) (Nutawan et al., 2010).

### 3.2.4. Fermentation Temperature

To optimize the fermentation temperature for bioethanol production, fermentation was carried out at 25, 30, 35 and 40 °C, whereas all the optimized as well as hydrolysis temperature (90 °C) and pH 5 was kept constant.

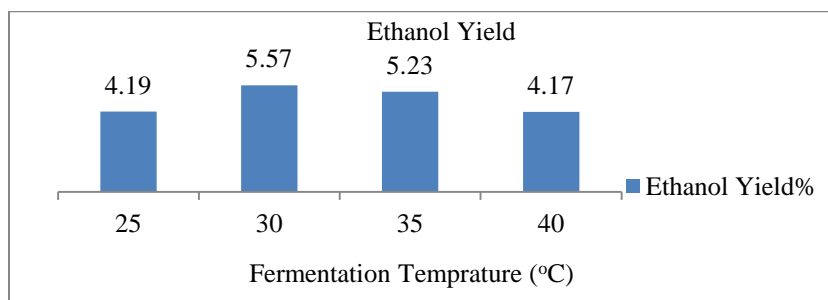


**Fig. 9. The effect of fermentation temperature on bioethanol production**

Figure 9 shows that ethanol yields obtained with fermentation temperatures of 25, 30, 35 and 40 °C were 4.19%, 5.57%, and 5.23% and 4.17% v/v respectively. According to these results, ethanol yield increases from 25 °C - 30 °C, however increasing the temperature beyond 30 °C decreased the ethanol yield of *P. juliflora*. As the result shows at 30 °C ethanol yield was optimum and decrease was pronounced at 35 °C. Temperature is one of the major constraints that determine the ethanol production. At very low temperatures, the yeast is deactivated and thus the reaction slows down or stops altogether. According to reference (Hoi, 2003) however, too high temperature kills yeast, and low temperature slows down yeast activity.

### 3.2.5. PH Value

Besides the other parameters, the PH value of the ethanol production was optimized keeping all the optimized parameters constant. As figure 10 shows, the PH from 4-8 were taken and the result revealed that 4.5%, 5.57%, 5.31%, 2.7% and 2.2% v/v respectively. The maximum ethanol yield was found at PH 5.

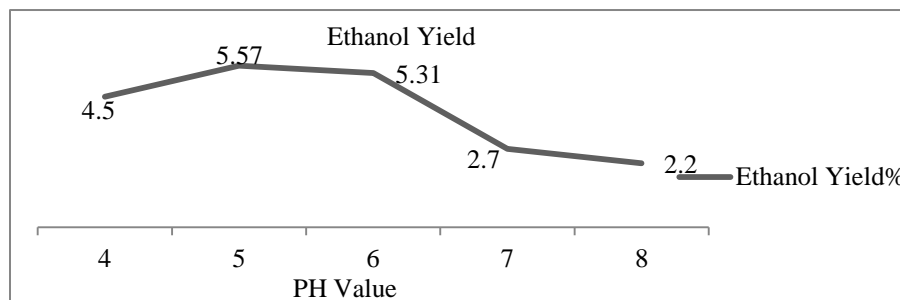


Fig.10. the effect of PH value on bioethanol production

### 3.3.P. juliflora as a solid fuel potential after Hydrolysis

Measurement of the calorific value of *P. juliflora* after bioethanol production provided the result of 18.22 MJ/kg. In particular, It has high calorific value compared to the conventional biomass as in (Hoi, 2003), like bagasse (7.7-8 MJ/Kg), rice husks (14 MJ/Kg), coffee husk (16 MJ/Kg) and wood (8.4- 17) but less than the calorific value of spent coffee ground (20.8 MJ/kg) after hydrolysis and spent coffee ground and glycerin ratio (glycerin content from 20-40%) was found (19.3-21.6 MJ/Kg) as in [Mebrшту Haile et al., 2013, Mebrшту Haile, 2014] respectively . This result showed that utilization of *P. juliflora* after hydrolysis as a raw material for solid fuel production has the potential to serve as the energy instead of disposed as a waste.

## 4. CONCLUSIONS

The aim of this work was to evaluate *P. juliflora* pods as a potential alternative feedstock for bioethanol production and its by-product as a solid fuel. In this work *P. juliflora* pods was used as a substrate and *S. cerevisiae* as a fermentative agent to study the importance of some hydrolysis and fermentation parameters in improving the alcoholic fermentation and to determine the calorific value of *P. juliflora* after hydrolysis. It was further found that the effect of different hydrolysis and fermentation parameters on ethanol yield. From the present results, it

was concluded that *P. juliflora* has potential for ethanol production, as well for solid fuel after hydrolysis. The maximum amount of ethanol yield (5.57% v/v) was obtained after 1 M H<sub>2</sub>SO<sub>4</sub>, 48 h of incubation. Hydrolysis (20 min.), pH (5) and temperature (30 °C) were optimized. However, the quantity of bioethanol production is not proportion to the amount of sugar content in the samples due to *S. Cerevisiae* yeast can ferment only C6 sugars. Additionally the calorific value of *P. juliflora* after hydrolysis (18.22 MJ/kg) was determined to ensure the potential of hydrolysis *P. juliflora* as the source of energy. Generally, using biomass, such as fuel wood, charcoal, dung cakes, agricultural residues and fossil fuel as the energy source, causes for environmental negative effects and global warming. Additionally rising ethanol production from first generation feed-stocks (directly use crop and use crop land for feedstock) are reasons for food security problem. Based on these facts, *P. juliflora* which is a promising alternative feedstock for bio-ethanol production to reduce environmental degradation and the global warming arising from combustion of fossil fuel and could also contribute to the solution of fossil fuel replacement in Ethiopia.

#### **ACKNOWLEDGMENTS**

We would like to acknowledge Mekelle University for the recurrent financial support that allowed us to undertake the research work.

#### **REFERENCE**

- Akpan, U.G., Alhakim, A. A. and Ijah, U. J.J., (2008), "Production of Ethanol Fuel from Organic and Food Wastes", Leonardo Electronic Journal of Practices and Technologies ISSN 1583-1078.
- Ayele Kefale , Mesfin Redi and Araya Asfaw (2012). Potential of Bioethanol Production and Optimization Test from Agricultural Waste: The Case of Wet Coffee Processing Waste (Pulp), International journal of renewable energy research, vol.2, no.3.
- Choge, S.K., Pasiecznik, N.M., Harvey, M., Wright, J., Awan, S.Z., and Harris, P.J.(2007). *Prosopis pods* as human food, with special reference to Kenya. Nairobi, Kenya Forest Research Institute 33 (3): 419-424. (<http://www.wrc.org.za>)
- Dawson, L. and Boopaty, R. (2008). Cellulosic Ethanol production from sugarcane bagasse without enzymatic saccharification. *Bioresources* 3: 452-460.
- Hailu Shiferaw, Demel Teketay, Sileshi Nemomissa and Fassil Assefa, (2004). Some biological characteristics that foster the invasion of *P. juliflora* (Sw.) DC. At Middle Awash Rift Valley, North-eastern Ethiopia. *Journal of Arid Environment* 58: 34-153.

- Hoi, W. (2003). Potential of biomass utilization for energy in asia pacific experience of philippine situation, Forest Research Institute. Kepong, Kuala Lumpur Malaysia.
- Joshi, B., Raj Bhatt,M., Sharma, D., Joshi, J., Malla, R. and Sreerama, L.,(2011). Lignocellulosic ethanol production: Current practices and recent developments, *Biotechnology and Molecular Biology Review* Vol. 6(8), pp. 172-182.
- Mebrahtu Haile (2014). Integrated volarization of spent coffee grounds to biofuel. *Biofuel Research Journ al* 2: 65-69.
- Mebrahtu, H.; Araya, A. and Nigist, A. (2013). Investigation of Waste Coffee Ground as a Potential Raw Material for Biodiesel Productio, *international journal of renewable energy research*: vol.3, No.4.
- Minister of Mines and Energy, (2011),” Energy Policy of Ethiopia”, Japan International Cooperation Agency (JICA) Tokyo international center.
- Nutawan, Y., Phattayawadee, P., Pattranit, T. and Mohammad, N., (2010), “Bioethanol Production from Rice Straw”, *Energy Research J.* 1: 26-31.
- Onuki, S., (2005), “Bioethanol, Industrial production process and recent studies.USA organic and food wastes”, *Journal of Practices and Technologies* 13:1-11.
- Pasiecznik, N.M., Felker, P., Harris, P.J., Harsh, L.W., Cruz, G., Tewari, J.C., Cadoret,K.and Maldonado, L.J. (2001). *The Prosopis juliflora – Prosopis pallida Complex: A Monograph*. HDRA, Coventry, UK,pp 162.
- Pikūnas, A., Pukalskas,S. and Grabys, J., (2003), “Influence of composition of gasoline – ethanol blends on parameters of internal combustion engines”, *Journal of kones internal combustion Engines* 2003, vol. 10, 3-4.
- Prasad, M.P., Rekha, S., Tamilarasan, M. and Subha, K.S., (2009), “Production Of Bioethanol Using Various Agricultural Raw Materials By Two Step Enzymatic Process”.
- Thuesombat, P., Thanonkeo ,P., Laopaiboon ,L., Laopaiboon ,P., Yunchalard ,S.,Kaewkannetra, L. and Thanonkeo ,S. (2007). The batch ethanol fermentation ofjerusalem artichoke using *saccharomyces cerevisiae*.*Journal of scince and Technology* 7:93-96.
- Weil, J., Dien, B., Bothast, R., Hendrickson, R., Mosier, N. and Ladisch, M., (2002), “Removal of fermentation inhibitors formed during pretreatment of biomass by polymeric adsorbents”, *Ind. Eng. Chem. Res.* 41: 6132–6138.

Zuzarte, F., (2007), “Ethanol for Cooking - Feasibility of Small-scale Ethanol Supply and its Demand as a Cooking Fuel: Tanzania Case Study”, KTH School of Energy and Environmental Technology, Heat and Power Technology, Stockholm, Sweden.

## Microstructures and Electrical Properties of B-Site Modified Bismuth Sodium Titanate Ferroelectric-Ceramic

<sup>1</sup>E.A. ZEREFFA, <sup>2</sup>A.V. PRASAD RAO

<sup>1</sup>Adama Science and Technology University, School of Applied Natural Science, Applied Chemistry Program, P.O. Box: 1888, Ethiopia. E mail: enyewama@yahoo.com, Mobile: 0912063504, Fax: 0221100038

<sup>2</sup>Department of Inorganic and Analytical Chemistry, College of Science and Technology, Andhra University, Visakhapatnam – 530003, E mail: pasadraoav@Rediffmail.com

### **Abstract:**

*In recent years, ferroelectric ceramic capacitors have attracted considerable attention of scientists, engineers and technologist worldwide, due to their potential application in energy storage devices. These advanced materials are also good at converting vibration (mechanical energy) into electricity. They have become one of the most promising materials for vibration energy harvesters, with the advantages of simple configuration, miniaturized size, higher efficiency and cost-effective fabrication. Lead containing perovskite type mixed metal oxides at phase boundaries have been found to be extensively useful because of their excellent ferroelectric and piezoelectric properties. However, in order to minimize the use of toxic lead, several other materials have been investigated, of which bismuth sodium titanate (BNT) was found to be promising as an environmentally friendly alternative to lead zirconate titanate (PZT). The effects of sintering temperature and doping on structure, microstructure, electric, phase transition temperature and piezoelectric properties of  $0.94(\text{Bi}_{0.5}\text{Na}_{0.5})\text{TiO}_3\text{-}0.06\text{BaTiO}_3$  (BNT6BT) ceramics prepared by solid sintering technique at 1050-1200°C were investigated. The X-ray diffraction patterns showed that of the BNT6BT modified ceramics at low concentration exhibited a single perovskite structure with monoclinic phase. A fine and homogeneous grains were observed for samples sintered at 1100 and 1150°C and the increase of the sintering temperature up to 1180 & 1200°C induces significant grain growth with the appearance of coarse grains. Co-doping of Mg and Nb with 1% raised the dielectric constant while single doping with Nb lowered at different frequencies. Increase in  $(\text{Mg}_{1/3}\text{Nb}_{2/3})^{4+}$  concentration up to 15% increased the transition temperature from 275°C to 339°C and lowered the dielectric constant.*

**Keywords:** Ceramic, Dielectric, Ferroelectric, Sintering and Microstructure

## **1. Introduction**

Perovskite type oxides like  $\text{Pb}(\text{Mg}_{1/3}\text{Nb}_{2/3})\text{O}_3$ ,  $\text{Pb}(\text{Zn}_{2/3}\text{Nb}_{1/3})\text{O}_3$  and  $\text{Pb}(\text{Zr,Ti})\text{O}_3$  have been shown to be extremely useful for a variety of applications in ferroelectric and piezoelectric devices [1]. Most of these materials are lead based with more than one cation occupying the octahedral lattice sites. The presence of heterovalent ions with different ionic radii, valence states and varying polarizabilities in the octahedral site were found to be effective in enhancing the dielectric, electrical and electromechanical properties. However, the toxicity of lead and volatilization of toxic PbO during processing of these ceramics materials have resulted in an increasing demand for alternate environmental friendly materials.

Dielectric properties of perovskite type compounds can be modified by suitable dopants at A-site or B- site in the crystal lattice. A number of reports are taken on the effects of doping on  $\text{BaTiO}_3$ (BT) that improve their dielectric permittivity, Curie temperature and influence the diffuse phase transitions of ceramic materials. The room temperature resistivity of  $\text{BaTiO}_3$ , can also be reduced to a much lower value by introducing small amounts of trivalent ions (such as  $\text{Bi}^{3+}$ ,  $\text{La}^{3+}$ ,  $\text{Y}^{3+}$ , etc.) in the place of Ba or pentavalent ions (such as  $\text{Nb}^{5+}$ ,  $\text{Ta}^{5+}$  etc.) in the Ti-site to produce n-type semiconductor[2-3]. Many commercial BT-based multilayer capacitors contain a certain amount of bismuth because of its significant effect on lowering the sintering temperatures [2]. Bismuth is also found to be able to enhance the magnitude of positive coefficients of resistance and dielectric properties [3]. The additives for  $\text{BaTiO}_3$  transducers,  $\text{Sr}^{2+}$ , lower  $T_c$  downward from  $130^\circ\text{C}$ ,  $\text{Pb}^{2+}$  used for varying the  $T_c$  upward,  $\text{Ca}^{2+}$  for increasing the temperature range of stability of the tetragonal phase, and  $\text{Co}^{2+}$  for decreasing the high-electric-field losses without affecting the piezoelectric constants. Depressors, such as  $\text{Bi}_2(\text{SnO}_2)_3$ ,  $\text{MgZrO}_3$ ,  $\text{CaTiO}_3$ ,  $\text{NiSnO}_3$ , as well as Curie point shifters are added in small (1–8 wt%) quantities to the base  $\text{BaTiO}_3$  composition to lower or depress the sharpness of the dielectric constant peak at the  $T_c$ , thus giving a flat dielectric constant–temperature profile [4]. In some cases suitable solid solutions leads to the formation of morphotropic phase boundary (MPB) which exhibits enhanced properties compared to the separate components on either side of the compositions. Thus for instance,  $\text{PbTiO}_3$  and  $\text{PbZrO}_3$  show morphotropic phase boundary around  $\text{Pb}(\text{Ti}_{0.48}\text{Zr}_{0.52})\text{O}_3$  which shows a  $T_c$  of  $230^\circ\text{C}$ , compared to  $495^\circ\text{C}$  for  $\text{PbTiO}_3$ [5]. Any ferroelectric material is therefore amendable to changes with proper doping.

Bismuth sodium titanate (BNT), a perovskite material with Curie temperature  $T_C = 320^\circ\text{C}$ , remanent polarization  $P_r = 38 \mu\text{C}/\text{cm}^2$  and coercive field  $E_C = 73 \text{ kV}/\text{cm}$  reported by (Smolenskii et al 1961) has been projected as a potential candidate in place of lead based piezoelectric ceramics [6]. Nevertheless, the electrical properties of the BNT ceramics are not as good compared to lead-based piezoelectric ceramics. Therefore, several studies have been made to enhance its ferroelectric properties by forming solid solutions with  $\text{BaTiO}_3$  [7],  $\text{NaNbO}_3$  [8],  $\text{KNbO}_3$  [9],  $\text{K}_{0.5}\text{Bi}_{0.5}\text{TiO}_3$  [10],  $\text{Ba}(\text{Ti},\text{Zr})\text{O}_3$  [11],  $\text{Bi}(\text{Mg}_{2/3}\text{Nb}_{2/3})\text{O}_3$  [12],  $\text{BiFeO}_3$  [13] as well as with cations of rare earth and transition metal ions like  $\text{Ce}^{4+}$  [14],  $\text{Mn}^{4+}$  [15],  $\text{La}^{3+}$  [16],  $\text{Fe}^{3+}$  [17] and  $\text{Nb}^{5+}$  [18]. Among the various systems that have been reported, bismuth sodium barium titanate  $(\text{Bi}_{0.5}\text{Na}_{0.5})_{1-x}\text{Ba}_x\text{TiO}_3$  (BNBT) solid solution was found to exhibit a morphotropic phase boundary (MPB) near  $x = 0.06$  and showed relatively enhanced piezoelectric properties [19]. Hence, the present work is undertaken to investigate the effect of simultaneous substitution of Mg and Nb at B site of BNBT, on the dielectric properties and phase transition Temperatures.

## **2. Experimental Materials and Methods**

The starting materials were A.R. grade  $\text{Bi}_2\text{O}_3$ ,  $\text{BaCO}_3$ ,  $\text{TiO}_2$ ,  $\text{Na}_2\text{CO}_3$ ,  $\text{MgO}$  and  $\text{Nb}_2\text{O}_5$ . All compositions were prepared by conventional solid-state reaction. Stoichiometric amounts of precursor powders corresponding to the compositions  $\text{BNBT}(\text{MN})_x$  where  $x = 0.0, 0.01, 0.05, 0.15, 0.20$  were mixed in ethanol media and well ground in an agate mortar. In the initial stages of the research, small samples of pure BNBT, about 10 g, of the dried mixed powders were calcined at temperatures ranging from  $700$  to  $900^\circ\text{C}$  for 2-3 hours. The samples were ground up using a Zircona mortar and pestle, and prepared for X-Ray Diffraction (XRD) analysis to set the optimum calcination temperature that yield a single perovskite phase. Then, the mixed powders were calcined at  $900^\circ\text{C}$  for 3h. The Phase formation is followed by using X-ray diffractometer (PANalytical- X' Pert PRO, Japan) with  $\text{CuK}\alpha$  radiation and a Ni filter. The scan range for all of the powders was from 20 to 80 degrees.

For the systems under investigation after the phase formation, the calcined powders were mixed and ground with 1 wt% aqueous poly vinyl alcohol (PVA) solution which acts as a binder amongst the granules of the powders. The green compacts with a diameter of about 12 mm and thickness of 1mm were pressed using uniaxial stress of 6MPa with the help of tungsten carbide

dye. The pellets were taken on a platinum foil and covered by platinum crucible to minimize evaporation of materials and sintered at 1150°C for 2hrs in a programmable furnace at 5°C per minute heating and cooling rate with an intermediate soaking time 1hr at 500°C for organic binder removal in the initial heat treatment. For dielectric measurements, silver paste was coated on the both sides of polished surface pellets and fired at 600°C for 30 min. Phase sensitive multi meter (N4L PSM 1700) was used to measure the complex impedance, capacitance, quality factor, resistance, dielectric loss, phase angle and inductance in series and parallel as function of temperature at frequencies ranging from 100 Hz to 1 MHz using 3°C per minute heating and cooling rates from room temperature to 400°C.

In this work the microstructures investigations of the sintered ceramic samples were made on the fractured surface of the sample using SEM (JEOL-JSM-6610LV, Tokyo, Japan) after a thin layer of gold was coated by using Auto Fine Coater (JFC-1600) for 90 second. Energy Dispersive X-ray Spectroscopy (EDS) with conjunction of SEM was used to characterize the elemental composition of the analyzed volume.

Phase transition temperatures for powder samples calcined at 900°C for 3hrs were obtained while heating at the rate of 3°C per minute from room temperature to 600°C using DSC 823e (METTLER TOLEDO, Japan). Compositions with  $x = 0.0, 0.01, 0.05, 0.15$  and  $0.20$  in  $(\text{Bi}_{0.5}\text{Na}_{0.5})_{0.94}\text{Ba}_{0.06}(\text{Ti}_{1-x}(\text{Mg}_{1/3}\text{Nb}_{2/3}))\text{O}_3$  will be denoted in subsequent discussion as BNBT, BNBT(MN)1, BNBT(MN)5, BNBT(MN)15 and BNBT(MN)20.

### **3. Results and Discussion**

XRD patterns of pure BNBT and  $(\text{Bi}_{0.5}\text{Na}_{0.5})_{0.94}\text{Ba}_{0.06}\text{Ti}_{1-x}(\text{MN})_x\text{O}_3$  with  $x = 0.01, 0.05, 0.15, 0.20$  samples where MN refers to  $(\text{Mg}_{1/3}\text{Nb}_{1/3})$  are shown in figure 1. From the figure, it can be seen that the XRD pattern of  $x = 0.0$  are in good agreement with that of rhombohedral  $(\text{Bi}_{0.5}\text{Na}_{0.5})\text{TiO}_3$  (JCPDS file number 36-0340) and XRD patterns for  $0 < x \leq 0.15$  samples are in good agreement with XRD pattern of monoclinic BNT (JCPDS file No.46-0001) indicating the formation of phase pure samples. Sample BNBT(MN) $x$  for  $x = 0.20$  showed two extra peaks of very small intensity at  $2\theta \sim 28^\circ$  and  $30^\circ$ . The extra peaks observed could not be assigned to any phase at this point of time. The lattice parameters of BNBT(MN) $x$  materials with  $x = 0.01, 0.05, 0.15$  and  $0.20$  have been calculated by using a standard computer program “POWD”, and

tabulated in table 1 with densities of the samples.. The apparent crystallites size and lattice strain of BNBT(MN)<sub>x</sub> samples for x = 0.0, 0.01,0.05, 0.15 and 0.20 were estimated by analyzing the x-ray diffraction peak broadening. The corresponding crystallite sizes and lattice strains were obtained as 44.2 nm, 28.96nm, 26.7nm, 27.6nm and  $1.6 \times 10^{-3}$ ,  $2.3 \times 10^{-3}$ ,  $2.2 \times 10^{-3}$ ,  $1.5 \times 10^{-3}$  respectively.

Table 1.Lattice parameters and densities of  $(\text{Bi}_{0.5}\text{Na}_{0.5})_{0.94}\text{Ba}_{0.06}\text{Ti}_{1-x}(\text{Mg}_{1/3}\text{Nb}_{2/3})_x\text{O}_3$  samples, where x values refers to a dopant concentration of 0.01, 0.05, 0.15 and 0.20 respectively

Composition	Lattice Parameters in Å			Density	
	a	b	c	Experimental	% Theoretical
BNBT(MN)01	4.1595	2.7607	5.8818	5.684g/cm <sup>3</sup>	99.5%
BNBT(MN)05	4.1692	2.7560	5.8759	5.587g/cm <sup>3</sup>	98.7%
BNBT(MN)15	4.140	2.7006	5.7719	5.57g/cm <sup>3</sup>	96.1%
BNBT(MN)20	4.1352	2.7506	5.6352	5.52g/cm <sup>3</sup>	92.2%

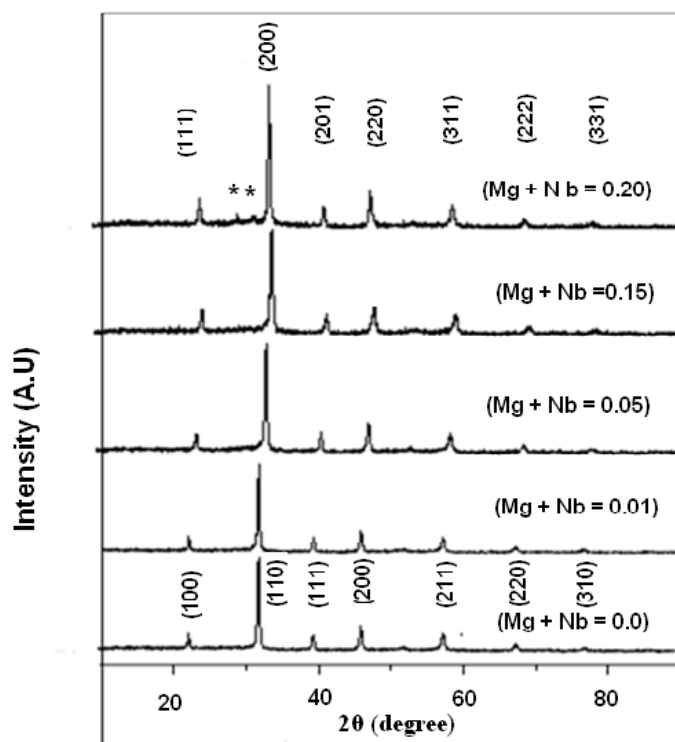


Figure 1 x-ray diffraction patterns of BNBT(MN)<sub>x</sub> for x = 0.0, 0.01, 0.05, 0.15 and 0.20  
Powders heat treated at 900°C for 3 hr.

### 3.1 Thermal Analysis

Differential scanning calorimeter measurements taken on calcined powder samples showed a significant influence on magnesium and niobium co-doping on the two anomalous transition temperatures of bismuth sodium barium titanate as depicted on Fig.2. The phase transformation temperatures determined for the base material BNBT ( $T_d = 88^\circ\text{C}$  and  $T_c = 275^\circ\text{C}$ ) is relatively close to the results reported by (Xu et al., 2008) [20]. Each DSC curve of BNBT(MN)<sub>x</sub> sample showed two small endothermic peaks and assigned to an antiferroelectric to the ferroelectric (AFE- FE) and ferroelectric to paraelectric (FE-PE) phase transitions respectively. The figures show that the substitution of  $\text{Mg}^{2+}$  and  $\text{Nb}^{5+}$  in the place of  $\text{Ti}^{4+}$  in the host compound increases the transition temperature ( $T_c$ ) from  $275^\circ\text{C}$  to  $304^\circ\text{C}$ ,  $333^\circ\text{C}$  and  $339^\circ\text{C}$  for  $x = 0.0$ ,  $0.1$ ,  $0.05$  and  $0.15$  respectively. This increase in the  $T_c$  may be explained in terms of variations in ionic sizes. The ionic radius of  $\text{Mg}^{2+}$  ( $0.72\text{\AA}$ ) and  $\text{Nb}^{5+}$  ( $0.64\text{\AA}$ ) are larger than that of  $\text{Ti}^{4+}$  ( $0.62\text{\AA}$ ), that may

causes a lattice distortion or expansion, and resulted in an increase of dielectric constant and transformation temperature ( $T_C$ ) which is consistent with the x-ray studies.

### **3.2. Dielectric Studies**

Temperature dependence of dielectric constant  $\epsilon'$  and dielectric loss at 1KHz, 10KHz and 50KHz for compositions BNBT(MN) $_x$  with  $x = 0.0, 0.01, 0.05, 0.15, 0.20$  samples sintered at 1150°C for 2hrs are shown in figure 3. In the measured frequency range of 1, 10 and 50 KHz all samples exhibited highest dielectric constant at 1 KHz. According to (Srivastava et al 1979) [20], the increase of  $\epsilon'$  at lower frequencies for polar materials is attributed from the contribution of multi component polarization mechanisms (i.e. electronic, ionic, orientation and space charge). At higher frequency the dipoles cannot rotate rapidly, so that their oscillations lag behind those of the field. As the frequency is further raised the dipole will be completely unable to follow the field and the orientation polarization ceases, so  $\epsilon'$  decreases and attain a constant value at high frequencies. BNBT(MN)01 showed relatively higher  $\epsilon_{max}$  values 8225,6270 and 5592 compared to 6510, 5429 and 4340 values for pure BNBT at 1, 10 and 50KHz respectively. The variation in  $\tan\delta$  is also less for BNBT(MN)01 compared to BNBT up to 300°C. As the concentration of Mg-Nb increased above 0.05,  $\epsilon'$  values decreased below that of pure BNBT. The temperatures of maximum dielectric constant and dielectric loss tangent are shifted to higher temperature with both increasing frequency and also increasing concentration of (Mg, Nb). The increase in dielectric loss tangent at temperatures above 300°C might be due to the formation of higher concentration of charge carriers. All BNBT(MN) $_x$  samples showed relaxor behavior in terms of variation of  $\epsilon'$  with frequency as shown in figure 3. This may be due to the heterogeneity caused by  $Na^+$ ,  $Ba^{2+}$ ,  $Bi^{3+}$  and  $Ti^{4+}$ ,  $Mg^{2+}$   $Nb^{5+}$  cations in the A and B lattice sites respectively.

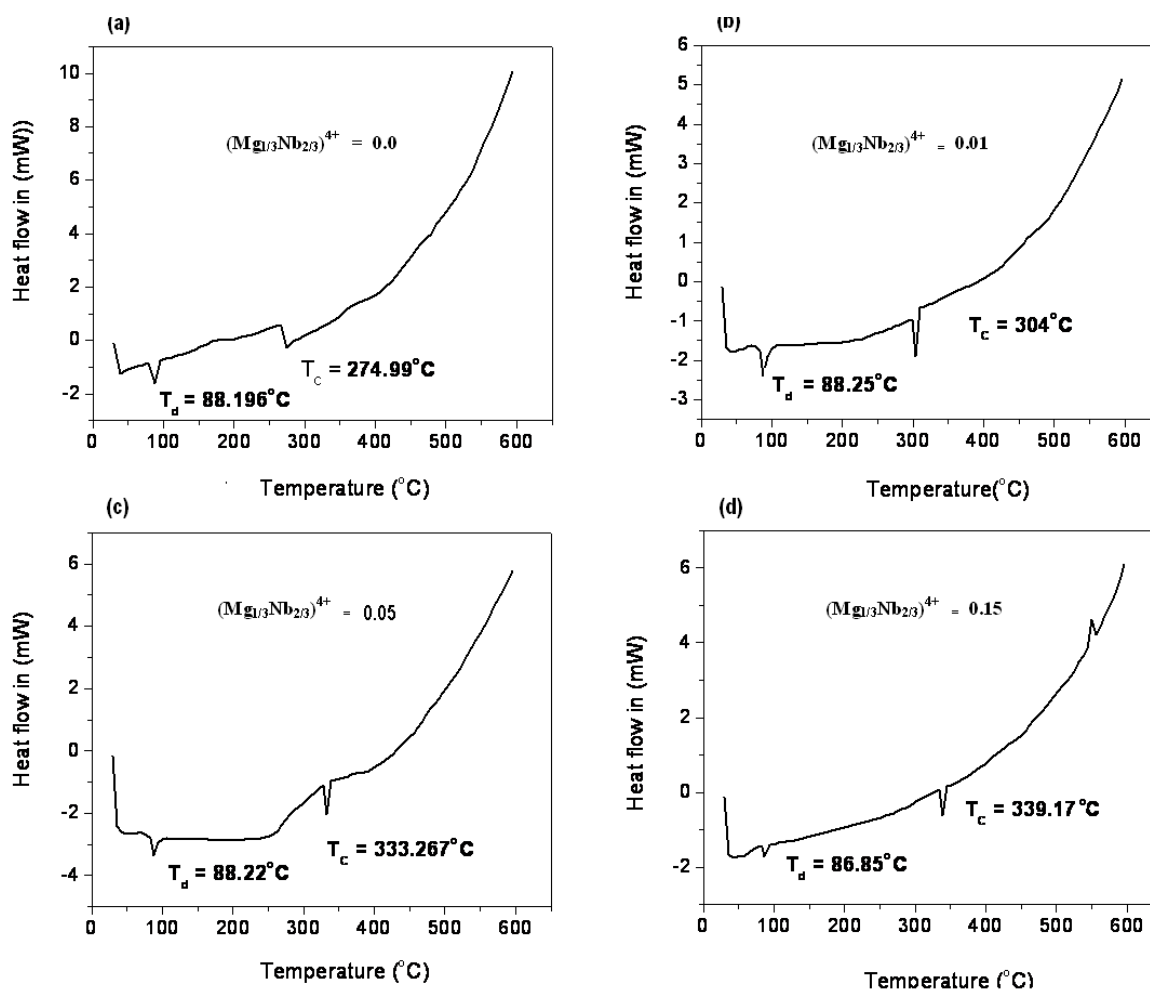


Fig.2 DSC curves of powder ceramic samples of  $\text{BNBt}(\text{MN})_x$  with  $x = 0.0, 0.01, 0.05$  and  $0.15$  from room temperature to  $600^\circ\text{C}$  up on heating.

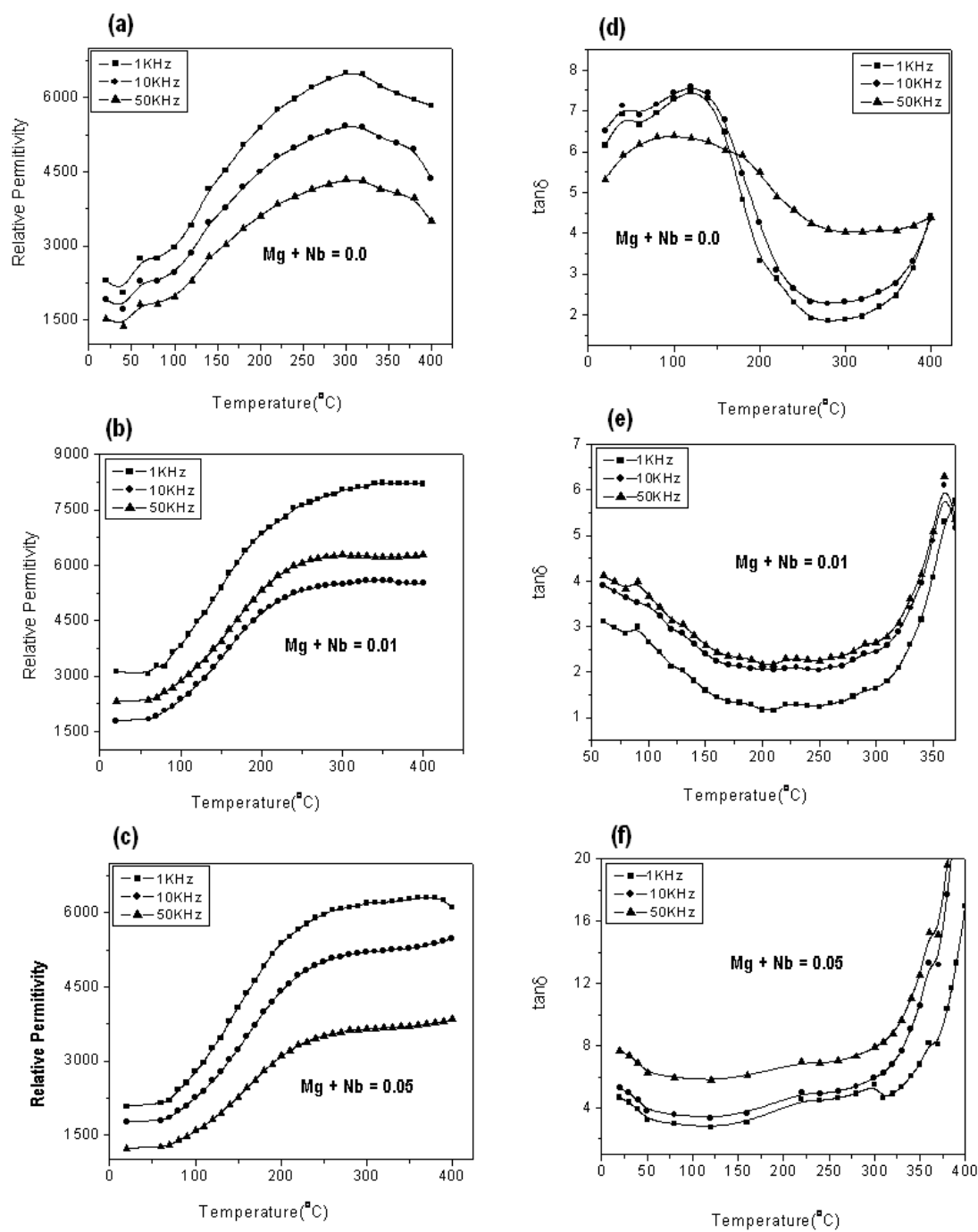


Fig. 3(a-e) variation of permittivity (a-c) and dielectric loss( d-f) as a function of temperature measured at 1, 10 and 50 KHz for BNBT(MN)<sub>x</sub> where x = 0.0, 0.01 and 0.05 samples sintered at 1150°C.

### **3.3 Microstructure**

SEM micrographs of fractured surfaces of pure and  $(\text{Mg}_{1/3}\text{Nb}_{2/3})^{4+}$  doped BNBT sintered pellets are shown in the Fig.4. All samples showed grain sizes in the range of 1  $\mu\text{m}$  and microstructure with porosity less than 3%. The decrease in grain size with doping might be due to the partial substitution of grain growth inhibitor  $\text{Nb}^{5+}$  for  $\text{Ti}^{4+}$  [21].

However, from the grain size variations observed in SEM micrographs, it may be noticed that there is a slight decrease in grain size for niobium & manganese content = 0.01. This decrease in grain size can be explained by cation vacancies created by substitution of  $\text{Nb}^{5+}$  in  $\text{Ti}^{4+}$  sites in the lattice. According to (Yi et al.,2001) [22] the cation vacancy in the grain boundaries would attract positively charged cations through columbic interactions and restrain the mobility of grain boundaries thus resulting in small grains. The observed increase in densification from SEM micrographs for BNBTMNx corresponding to  $x = 0.01$ , as compared with pure sample might be due to increased mass transportation ability to B-site vacancies. The energy dispersive spectroscopy (EDS) analysis of BNBT(MN)x revealed the presence of  $\text{Na}^+$ ,  $\text{Bi}^{+3}$ ,  $\text{Ba}^{+2}$ ,  $\text{Ti}^{+4}$ ,  $\text{Mg}^{+2}$ ,  $\text{Nb}^{+5}$ , and  $\text{O}^{-2}$  ions in the respective compositions as depicted in figure 5(a-c).

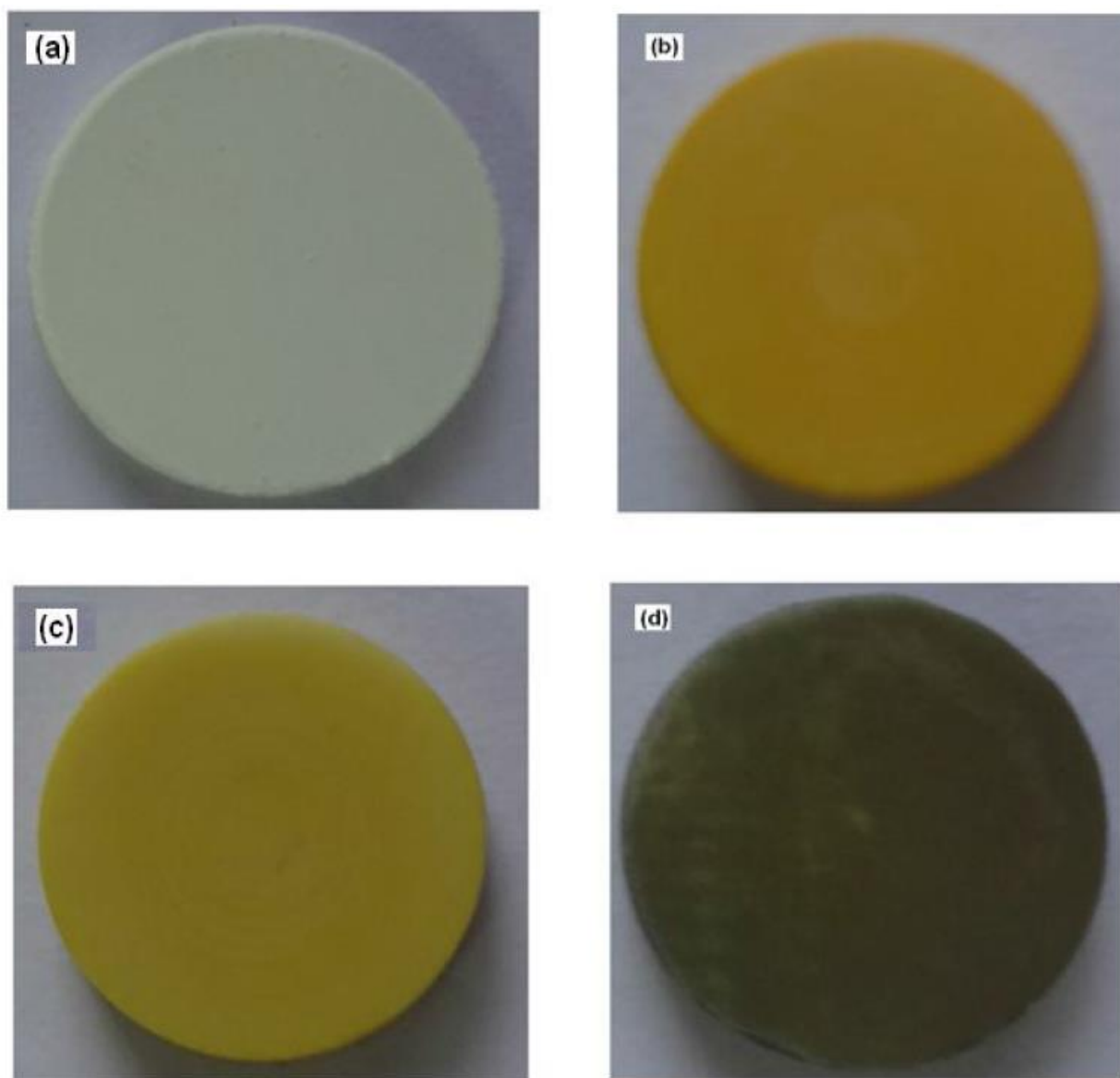


Figure 4a. ceramic pellets at different processing stages: (a) green body, (b and c) sintered pellets with different dopant (d) conductor coated sintered ceramic

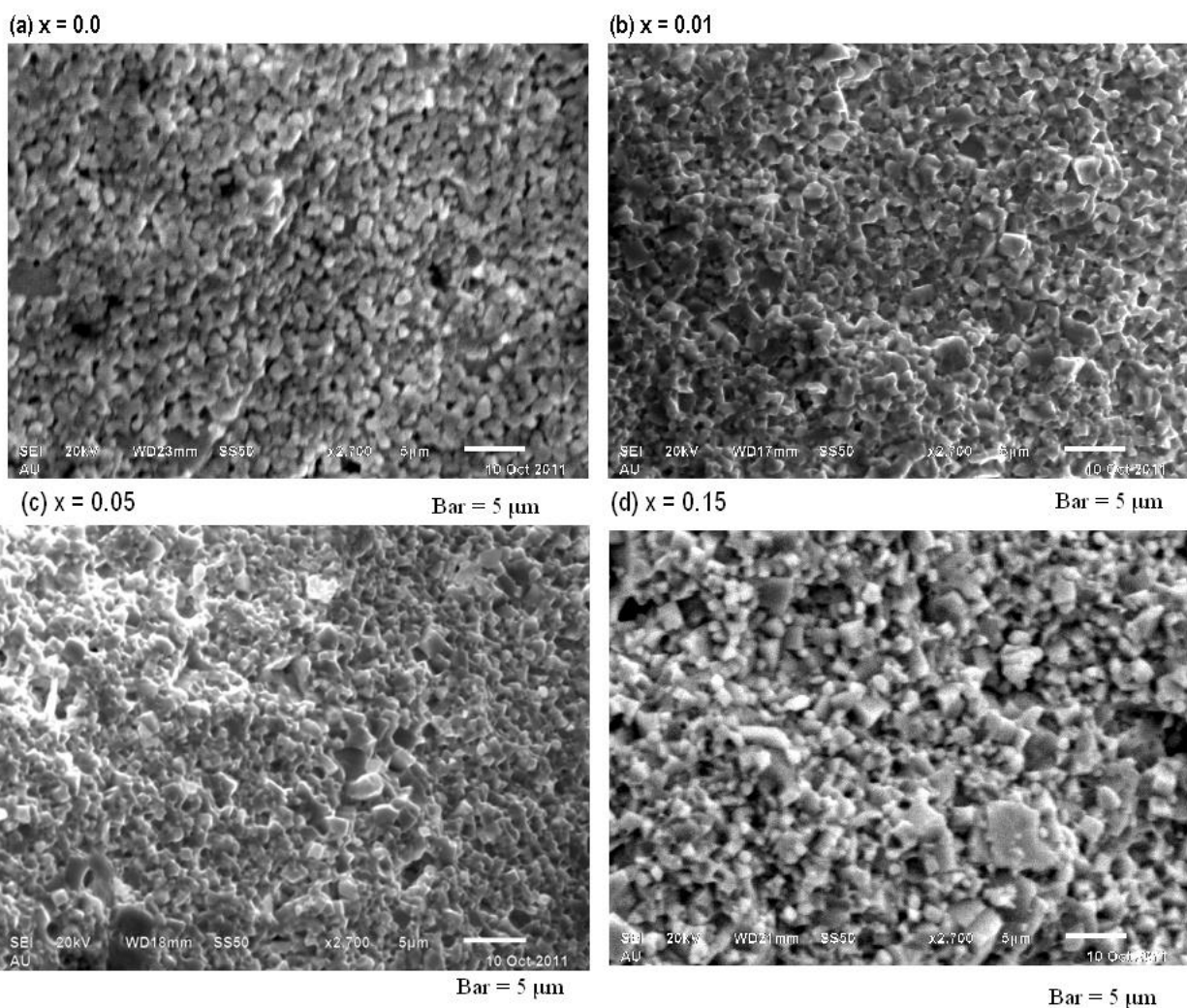


Fig.4b SEM micrographs of  $\text{BNBT}(\text{NM})_x$  fractured surfaces of sintered pellets (a)  $x = 0.0$  (b)  $x = 0.001$ , (c)  $x = 0.05$  and d)  $x = 0.15$

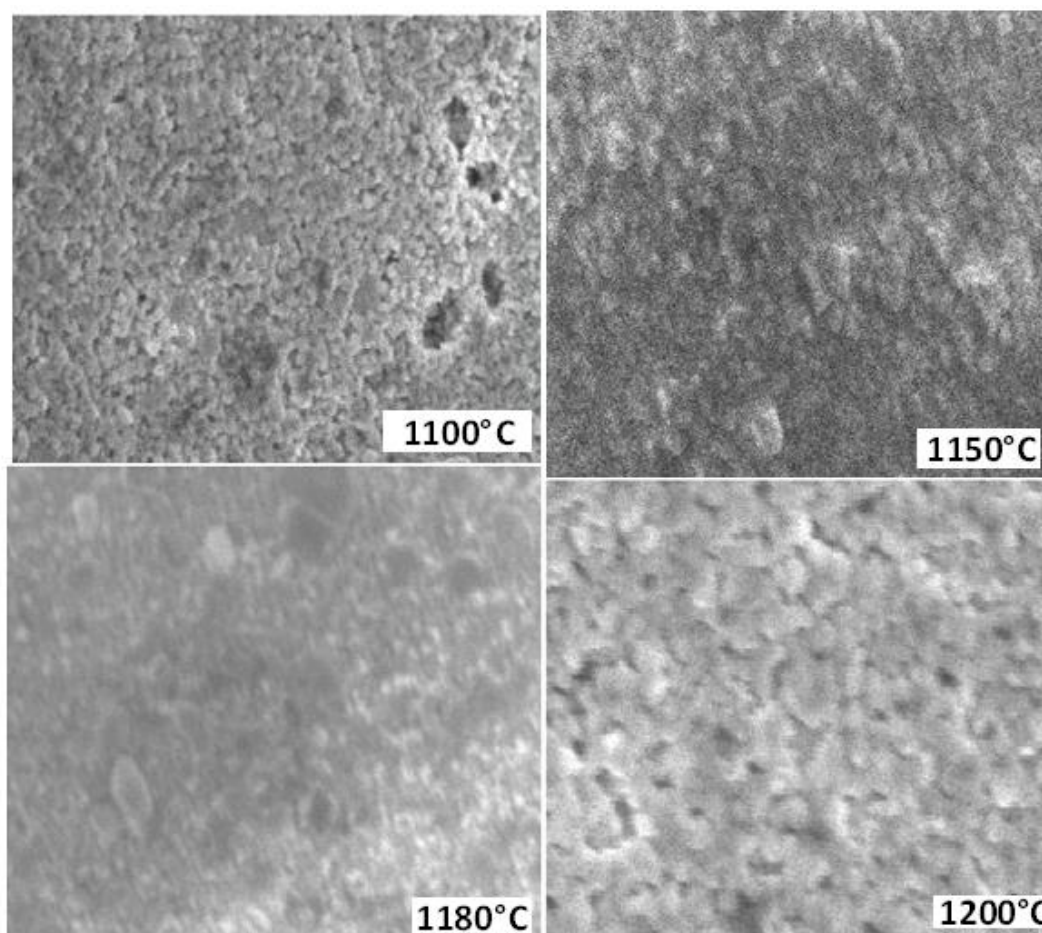


Fig.4C Backscattered SEM images of BNBT(MN)<sub>x</sub> fractured surfaces of sintered pellets for  $x = 0.01$  at different sintering temperature for 2hrs.

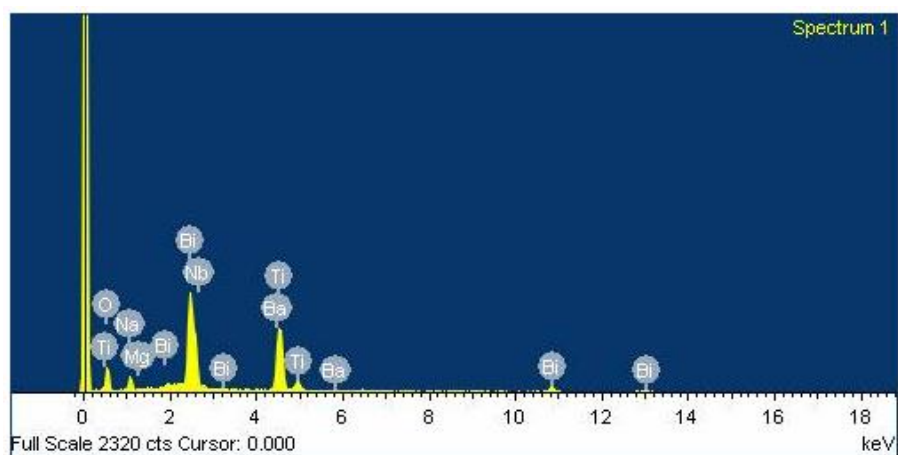


Figure.5 EDS Spectra of BNBT(MN)<sub>x</sub> for  $x = 0.01$

### 3.4 Impedance Spectroscopy

Fig.6a. Depicts Cole-Cole plot of BNBTMN15 sample at different temperatures in the frequency range (100Hz-1MHz) which shows a linear response in  $Z''$  at lower temperature indicating the insulating behavior in the sample. As the temperature increases the linear response gradually changes to semicircular which become smaller and shifts towards lower  $Z'$  values, indicating a reduction in grain ( $R_g$ ) resistance. The spikes are observed in the impedance at higher temperatures. In this case the capacitance value has been obtained from the high frequency semicircle and low frequency spikes that corresponding to the bulk and electrode polarization effect respectively. The centre of semi-circles lies below the x-axis which indicates non-Debye type relaxation process in the material [23]. The value of grain resistance ( $R_g$ ) at different temperature (310-400) has been obtained from the intercept of the semicircular arc on the real axis ( $Z'$ ) for BNBT(MN)15 is depicted on Fig.6b. From the figure it is clear that the value of  $R_g$  in the sample decreases with rise in temperature which indicates a negative temperature coefficient behavior of resistivity like that of semiconductor [21, 24].

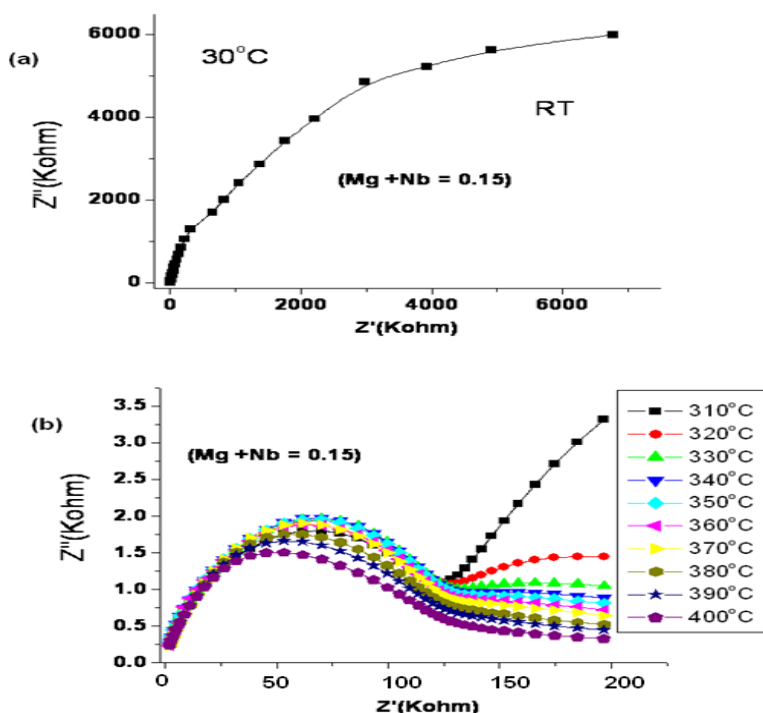


Fig.6a impedance plots of BNBTMN15 at different temperatures

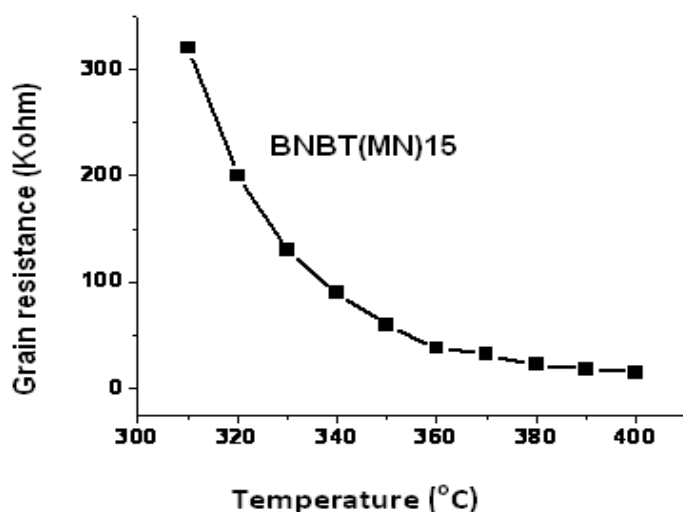


Fig.6 (b) Temperature dependence of grain resistance of BNBT (MN)15

### 3.5. Conductivity studies

The patterns of the conductivity graphs of BNBT(MN) $x$  where  $x = 0.01, 0.05$  and  $0.15$  at the same measuring temperatures in the studied frequency range are similar as it is indicated on figure 7. As it is seen from figure.7 the conductivity curves of BNBT(MN) $x$  that displayed as an example increased with increasing frequency and merged at high temperature. The conductivity curves merged at higher temperature region due to the release of space charge [25-26]. The electrical conduction in dielectrics is due to the motion of weakly bound charged particle under the influence of the external electric field. The conduction process is always dominated by the type of charge carriers like electrons/holes or cations/anions. In all ferroelectrics, electrical conductivity is very important since the associated properties like piezoelectricity, pyroelectricity and poling depends on it. In BNBT(MN) $x$  ceramics, the electronic conduction in the grains is expected to result mainly from the defects present in the lattice. Being an ionic compound, the BNBT solid solutions may have high energy gap between valence band and conduction band, so that electrons could not be thermally activated until at higher temperatures. Therefore, the conductivity of the system is expected to result mainly from the presence of defects that come from the volatilizations of  $\text{Bi}_2\text{O}_3$  during material processing, which could results in oxygen vacancies. All the mechanisms of conduction in ferroelectric

material are temperature dependent phenomena and follows Arrhenius behavior in a particular temperature range. The variation of a.c. conductivity with temperature shows maxima around the ferroelectric-paraelectric phase transition temperature for all frequencies. This behavior can be attributed to the relaxation process associated with the domain reorientation, domain wall motion, and the dipolar behavior [27].

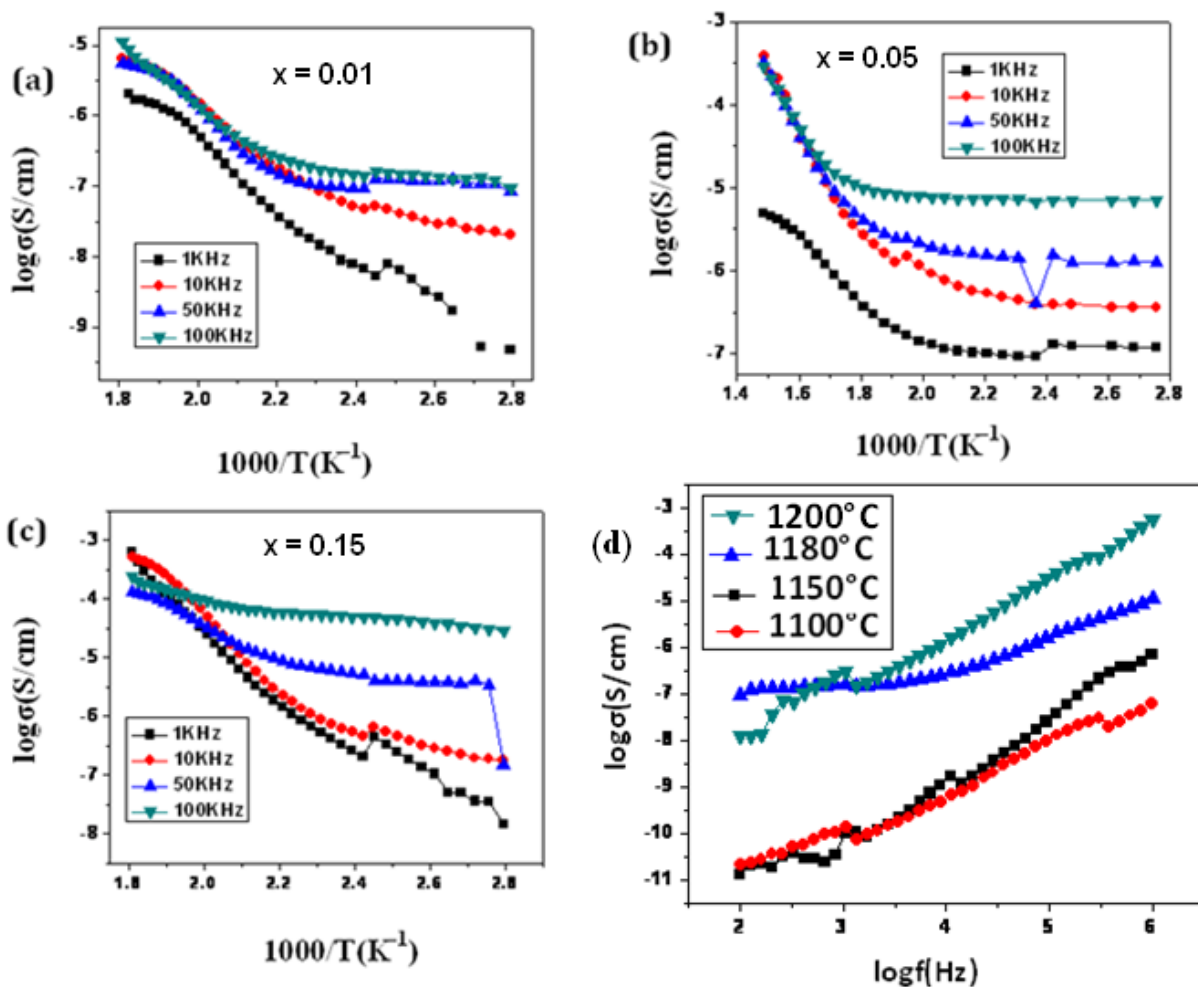


Fig.7. Conductivity versus inverse of absolute temperature for BNBT(MN)<sub>x</sub> (a)  $x = 0.01$  (b)  $x = 0.05$  (c)  $x = 0.15$  at the frequencies of 1, 10, 50, 100 KHz. (d) room temperature conductivity of BNBT(MN)<sub>x</sub>,  $x = 0.01$  sintered at 1000°C, 1150°C, 1180°C, 1200°C.

#### 4. Conclusions

Lead-free ferroelectric ceramics with composition BNBT(MN)<sub>x</sub> for  $x = 0.0, 0.01, 0.05, 0.15, 0.20$  have been prepared by conventional solid-state method. X-ray diffraction patterns showed formation of single phase rhombohedral structure for pure BNBT and pure monoclinic phase for  $x \leq 0.15$  investigated compositions. The powder samples were pressed into discs and sintered at 1150°C for 2 h for densification. Microstructure studies on the fractured surface of the sintered pellet revealed that niobium & magnesium doping inhibits grain growth and improves densification behavior of the material at low dopant concentration. The dielectric investigation on the silver coated sintered pellets also showed that niobium & magnesium substitution has enhanced the dielectric properties of BNBT polycrystalline ceramic materials at low dopant concentration. Differential Scanning Calorimetric studies indicated a progressive shift of ferroelectric phase transition to paraelectric phase to higher temperature compared to the undoped BNBT. The bulk resistance ( $R_b$ ) was shown to decrease with increasing temperature indicating a negative temperature coefficient of resistance (NTCR) behavior.

#### Acknowledgements

One of the authors, Enyew Amare Zereffa, gratefully acknowledges the financial support from the Ministry of Education of The Federal Democratic Republic of Ethiopia, through Embassy of Ethiopia in New Delhi.

#### References

- [1] Lines, M.E., Glass, A.M., Principles and Applications of Ferroelectrics and Related Materials, Clarendon Press, Oxford, (1977).
2. Zhou, L., Vilarinho, P.M., & Baptista, J.L., Bol. Soc. Esp. Cerám. Vidrio, 38 [6] (1999) 599-602.
3. Moulson, A.J., and Herbert, J.M., *Electroceramics: Materials, Properties, Applications*, Chapman and Hall, New York, 1990.
4. Heartling, G. H., J. Am. Ceram. Soc, 82[4] (1999) 797-818
5. Cohen, R. E., Relaxors go critical, Nature (London), 441 (2006) 941-942
- [6] Smolenskii, G.A., Isupov, V.A., Agranovskaya, A.I., Kraink, N.N., Sov. Phys. Solid State., 2 (1961), 2651.
- [7] Takenaka, T., Sakat, K., Ferroelectrics., 95 (1989), 153.

- [8] Li, Y.M., Chen, W., Zhou, J., *Mater. Sci. Eng.B.*, 112(2004,) 5.
- [9] Nagata, H., Takenaka, T., *Jpn. J. Appl. Phys.*, (1997), 366055.
- [10] Li, Y.M. , Chen, W., Zhou, J., *Ceram. Int.*, 31 (2005), 139.
- [11] Peng, C., Li J. F., Gong, W., *Mater. Let.* 59 (2005),1576.
- [12] Zhou, C., Liu, X., *J. Mater. Sci.*, (2008),431016.
- [13] Nakada, H., Koizumi, N., Takenaka,T., *J. Ceram. Soc. Japan.*, (1999), 37.
- [14] Wang, X., Chan h. L., Choy, C., *Solid-state. Commun.*, 125(2003) 395.
- [15] Hao, J. J., Wang, X. H., Gui z. L., Li, L. T. ,*Rare Metal Mater and Eng .*, (2003),32438.
- [16] Herabut ,A. , Safari, A., *J. Am, Ceram. Soc.*, 80 (1997),2954.
- [17] Watcharapasorn, A., Jiansirisomboon. S., Tunkasiri, T.,*Mater Let.*, 61[14-15] (2007),2986.
- [18] Wang, H., Zuo, R., Liu ,Y., Fu, J.,*J. Mater. Sci.*, (2010),453677.
- [19] Takenaka, T., Maruyama, K., Sakata, K., *Jpn. J. Appl. Phys.*, 30 (1991), 2236.
- [20]. Srivastava, K. K., Kumar, A., Panwar ,O.S., and Lakshminarayan, K. N., *J. Non-Cryst. Solids*, 33(1979)205-211.
- [21] Fan, C. L ., Ciardullo ,D., Huebrier, W., *Mater. Sci.Eng.*,B1009 (2003), 1.
- [22].Yi, J. Y., Lee, J. K. & Hong, K. S., *J. Am.Ceram. Soc*, 85(2002)3004-3010.
- [23]. Rao ,K.S., Krishna, P.M., Prasad, D.M., Latha ,T.S., Hussain, M. ,*Phys. J.*
- [24] Bauerle, J. E.,*J. Phys. Chem. Solids.*, 30(1969),2657.
- [25]. Sundarkannan, S., Kakimoto, K., Ohsato, H., *Journal of Applied Physics.*,9(2003), 5182.
- [26]. Lu, Z., Bonnet, J.P., Ravez, J., Hagenmullar, *Solid- State Ionics.*,57(3-4)(1992), 235.
- [27] Cross, L. E. *Relaxor ferroelectrics,Ferroelectrics*, 76 (1987) 241-267.